



TECHNISCHE
UNIVERSITÄT
WIEN

Dissertation

**CONTINUOUS FLOW CHEMISTRY IN SYNTHESIS:
FROM IONIC LIQUID PRODUCTION TOWARDS
CARBON DIOXIDE VALORISATION**

Ausgeführt zum Zwecke der Erlangung des akademischen Grades eines Doktors
am Institut für Angewandte Synthesechemie unter der Leitung von

Univ.Prof.ⁱⁿ Dipl.-Ing.ⁱⁿ Dr.ⁱⁿ techn. Katharina Schröder
Institutsnummer: 163
Institut für Angewandte Synthesechemie

eingereicht an der Technischen Universität Wien
Fakultät für Technische Chemie

von

MSc. Kristof Andras Stigel
Matrikelnummer: 12002108

Wien, im November 2023

Acknowledgements	IV
Abstract	V
Kurzfassung.....	VI
List of abbreviations	VII
1. Introduction	1
1.1 Flow chemistry	1
1.2 Ionic liquids	5
1.2.1 Structure and properties	5
1.2.2 Historical overview	7
1.3 Synthesis of ionic liquids	11
1.3.1 State-of-the-art synthesis of ionic liquids	11
1.3.2 Halide-free synthesis of ionic liquids.....	13
1.3.3 Continuous-flow synthesis of ionic liquids	17
1.4 Application of ionic liquids in continuous catalytic processes	20
1.4.1 Ionic liquids as reaction media in continuous catalytic processes.....	20
1.4.2 Ionic liquids as supported catalyst in continuous processes	25
2. Aim of the thesis.....	31
3. Halide-free continuous synthesis of hydrophobic ionic liquids.....	32
4. Supported ionic liquid phase (SILP) allylic alkylation of amines in continuous flow	49
5. Continuous synthesis of carbamates from CO₂ and amines	57
6. Online coupling high-temperature electrolysis with carbonylation reactions: a powerful method for continuous carbon dioxide utilisation	78
7. Conclusions	111
8. Appendix A.....	114
8.1 General remarks	115
8.2 Representative protocol for the synthesis of alkyl bistriflimides.....	116
8.3 General procedure for the batch-wise synthesis of ionic liquids	117
8.4 General procedure for the continuous-flow synthesis of ionic liquids	118
8.5 Analysis of alkyl bistriflimides	119
8.6 Analysis of bis(trifluoromethanesulfonyl)imide-based ionic liquids	121
8.7 Kinetic analysis of ionic liquid formation	126
8.8 Optimisation of the alkyl bistriflimide synthesis.....	128
8.9 Batch and continuous-flow synthesis of 2b	129
8.10 Ion chromatography measurement parameters, halide- and water content.....	130
8.11 E-factor calculations.....	132
8.12 NMR spectra of alkyl bistriflimides	134
8.13 NMR spectra of ionic liquids	142
9. Appendix B.....	165
9.1 General remarks	166
9.2 Substrate synthesis for the non-enantioselective allylic alkylations (1a-d)	167
9.3 Substrate synthesis for the enantioselective allylic alkylations (1e-i)	169
9.4 Continuous-flow synthesis of allylic amines (3a-h)	172
9.4.1 Synthesis of non-chiral supported ionic liquid phases (SILPs)	172
9.4.2 General procedure for the synthesis of allylamines 3a-h	172
9.5 Procedures for the synthesis of chiral ligands L1-L4.....	176

9.6 General procedure for the continuous-flow asymmetric allylation – synthesis of allylic amines 3d, 3i-m	179
9.6.1 General procedure for the synthesis of racemic diphenyl-propenyl pyrrolidine derivatives	179
9.6.2 Synthesis of chiral supported ionic liquid phases (chiral SILPs)	179
9.6.3 General procedure for the synthesis of allylamines 3a, 3i-m	180
9.7 TGA measurements of the SILP catalysts	183
9.8 SEM images of the chiral SILP catalyst	185
9.9 NMR spectra of allyl acetate derivatives	186
9.10 NMR spectra of amines 3a-h	195
9.11 NMR spectra of chiral ligands	202
9.12 NMR spectra of amines 3d, 3i-m	206
9.13 Chiral HPLC traces	213
10. Appendix C	219
10.1 General remarks	220
10.2 Set-up of the continuous-flow experiments	221
10.3 General procedure for the continuous synthesis of carbamates.....	222
10.4 General procedure for the synthesis of aziridines.....	227
10.5 General procedure for the continuous synthesis of oxazolidinones.....	228
10.6 NMR spectra of 3a-5b	229
10.7 Chiral HPLC traces	254
11. Appendix D	257
11.1 General remarks	258
11.2 Set-up of the continuous-flow experiments	259
11.3 Solid-oxide electrochemical cell.....	260
11.4 Optimisation of the aminocarbonylation reactions in continuous mode	261
11.5 Procedure for the synthesis of ethyl nonanoate	262
11.6 Procedure for the batch-wise synthesis of phenyl benzoate	263
11.7 General procedure for the continuous synthesis of benzoic acid ester derivatives.....	264
11.8 Procedure for the batch-wise synthesis of <i>N</i> -(benzoyloxy)-succinimide	266
11.9 General procedure for the continuous synthesis of redox-active esters	267
11.10 Procedure for the batch-wise synthesis of diphenylpropynone.....	269
11.11 General procedure for the continuous carbonylative Sonogashira coupling	270
11.12 General procedure for the continuous aminocarbonylations	272
11.13 NMR spectra of 1a-5c	274
12. Bibliography	294

Acknowledgements

First and foremost, I would like to thank my supervisor, Prof. Dr. Katharina Bica-Schröder, for the opportunity to join her research group and for all her support and advice during the years of my doctoral studies. Furthermore, I would like to acknowledge the support of my co-supervisor, Prof. Dr. Michael Schnürch, especially in the first year of my Ph.D.

I am very grateful to all my former and current lab colleagues: Aitor Sainz Martinez, Olga Lanaridi, Prasad M. Kathe, Cornelia S. Büttner, Philipp Miksovsky, Lisa Eisele, Julia A. Piotrowska, Bletë Hulaj, and Michael Weiser for creating an exceptionally pleasant and professional atmosphere in the lab. I would like to give special thanks for all the scientific- and practical advice to Ádám M. Pálvölgyi and Fabian Scharinger.

I am very thankful to Irena Jelenkovic-Didic for her assistance with the chiral HPLC and HRMS measurements. I would also like to acknowledge the help of all scientific and non-scientific employees of the Institute of Applied Synthetic Chemistry.

I would like to take this opportunity to thank the professors of my former universities for their quality teaching in the field of organic chemistry, especially Prof. Dr. Rita Skoda-Földes and Prof. Dr. Péter Huszthy.

Last but not least, I would like to thank my family and friends, especially my beloved Anna, for all their support.

And finally, thanks are due to the majestic Ludwig van Beethoven, who filled the well of delights to overflowing, providing an endless source of magnificence.

Abstract

Developing alternative, environmentally benign synthetic strategies to replace conventional approaches in the light of sustainability has become a key challenge in the 21st century chemical industry. It is the chemical society's responsibility to solve problems such as enormous solvent consumption and the utilisation of carbon dioxide, which is considered the primary reason for global warming.

This thesis is dedicated to the continuous synthesis of hydrophobic ionic liquids and their catalytic application in continuous chemical transformations. Additionally, this work focuses on the utilisation of carbon dioxide in the continuous synthesis of carbonyl compounds and carbamates. In total, four different sub-projects have been carried out.

1. In the first part of this work, the halide-free, continuous synthesis of bistriflimide-based hydrophobic ionic liquids is demonstrated. After successfully employing the new precursors, the alkyl bistriflimides, the continuous process provided the corresponding ionic liquids with excellent yields in just 7.5 minutes.
2. The second project focuses on the application of the previously synthesised hydrophobic ionic liquids as supported phases for the immobilisation of palladium complexes on silica. The catalyst system was utilised in the continuous allylic alkylation of *N*-nucleophiles. The novel method requires neither an additional base nor an inert atmosphere for the reaction. The developed catalyst system proved suitable for an extended period as only marginal leaching of the ionic liquid was observed within an operation time of 3.5 hours.
3. The third part focuses on the continuous utilisation of carbon dioxide in the synthesis of organic urethanes. The established method does not require any catalyst or additive and provides a significantly faster and safer alternative for synthesising carbamates. The modified approach was successfully utilised in the continuous synthesis of oxazolidinones from aziridines.
4. The last part is dedicated to the valorisation of carbon dioxide in continuous carbonylation reactions. The CO₂ was utilised either mixed with carbon monoxide or partially reduced to CO by employing a solid oxide electrochemical cell. The generated mixtures contained low CO amounts and were successfully utilised in phenoxy- and aminocarbonylations, in the synthesis of redox-active esters, and carbonylative Sonogashira cross-couplings.

Kurzfassung

Die Entwicklung alternativer, umweltfreundlicher chemischer Prozesse als Ersatz für konventionelle Verfahren ist zu einer zentralen Herausforderung für die chemische Industrie des 21. Jahrhunderts geworden. Es liegt in der Verantwortung der chemischen Gesellschaft, Probleme wie den enormen Lösungsmittelverbrauch zu lösen oder die Verwendungsmöglichkeiten für Kohlendioxid das als Hauptgrund für die globale Erwärmung gilt, zu entwickeln. Diese Arbeit widmet sich der kontinuierlichen Synthese von hydrophoben ionischen Flüssigkeiten und ihrer katalytischen Anwendung bei kontinuierlichen chemischen Umwandlungen. Weiters konzentriert sich diese Arbeit auch auf die Anwendung von Kohlendioxid in der kontinuierlichen Synthese von Carbonylverbindungen und Carbamaten. Insgesamt wurden vier verschiedene Teilprojekte durchgeführt:

1. Im ersten Teil dieser Arbeit wird die halogenidfreie, kontinuierliche Synthese von hydrophoben ionischen Flüssigkeiten auf Bistriflimidbasis demonstriert. Durch den Einsatz der neuen Vorstufen, der Alkylbistriflimide, lieferte der kontinuierliche Prozess die entsprechenden ionischen Flüssigkeiten mit ausgezeichneten Ausbeuten in nur 7,5 Minuten.
2. Das zweite Projekt befasst sich mit der Anwendung der zuvor synthetisierten hydrophoben ionischen Flüssigkeiten als geträgerte ionische Flüssigphasen für die Immobilisierung von Pd-Komplexen auf Kieselgel. Das Katalysatorsystem wurde für die kontinuierliche allylische Alkylierung von *N*-Nukleophilen eingesetzt. Die neue Methode erfordert weder eine zusätzliche Base noch eine inerte Atmosphäre für die Reaktion. Das entwickelte Katalysatorsystem erwies sich als geeignet für einen längeren Zeitraum, da innerhalb einer Betriebszeit von 3.5 Stunden nur ein geringes Auslaugen der ionischen Flüssigkeit beobachtet wurde.
3. Der dritte Teil befasst sich mit der kontinuierlichen Valorisierung von Kohlendioxid in der Synthese von organischen Urethanen gewidmet. Die hier entwickelte Methode benötigt keinen Katalysator oder Zusatzstoff und stellt eine wesentlich schnellere und sichere Alternative für die Synthese von Carbamaten dar. Das modifizierte Verfahren wurde erfolgreich für die kontinuierliche Synthese von Oxazolidinonen aus Aziridinen eingesetzt.
4. Der letzte Teil ist der Valorisierung von Kohlendioxid in kontinuierlichen Carbonylierungsreaktionen. Das CO₂ wurde entweder durch seine Vormischung mit Kohlenmonoxid oder durch seine Teilreduktion zu CO unter Verwendung einer elektrochemischen Festoxidzelle verwertet. Die erzeugten Gemische enthielten geringe CO-Mengen und wurden erfolgreich bei Phenoxy- und Aminocarbonylierungen, bei der Synthese redoxaktiver Ester und bei carbonylativen Sonogashira-Kreuzkupplungen eingesetzt.

List of abbreviations

(<i>Sa,Rc</i>)-(1-Nph)-Quinaphos	(<i>R</i>)-2-(1-naphtyl)-8-diphenylphosphino-1-[(<i>S</i>)-3,5-dioxa-4-phosphacyclohepta[2,1- <i>a</i> :3,4- <i>a'</i>]dinaphthalen-4-yl]-1,2-dihydroquinoline
[C ₁ m ₂ im]	1,2,3-trimethylimidazolium
[C ₂ mim]	1-Ethyl-3-methylimidazolium
[C ₄ mim]	1- <i>n</i> -Butyl-3-methylimidazolium
[C ₈ mim]	1- <i>n</i> -Octyl-3-methylimidazolium
AAA	Asymmetric allylic alkylation
ATR	Attenuated total reflectance
BASIL™	Biphasic Acid Scavenging utilising Ionic Liquids
BINAP	2,2'-bis(diphenylphosphino)-1,1'-binaphtyl
Bistriflimide, NTf ₂	Bis(trifluoromethanesulfonyl)imide
BOX	Bis(oxazoline)
BPR	Back-pressure regulator
CBILS®	Carbonate-based ionic liquid synthesis
COD	1,5-Cyclooctadiene
CSTR	Continuous stirred tank reactor
DABCO	1,4-Diazabicyclo[2.2.2]octane
DBU	1,8-Diazabicyclo[5.4.0]undec-7-ene
DIPEA	<i>N,N</i> -Diisopropylethylamine
dppf	1,1'-Bis(diphenylphosphino)ferrocene
dppp	1,1'-Bis(diphenylphosphino)propane
dtbpm/ dtbpx	1,2-Bis-(di- <i>tert</i> -butylphospinomethyl)-benzene
EDG	Electron donating group
ESI-TOF	Electrospray ionisation time-of-flight
EWG	Electron withdrawing group
FID	Flame ionisation detector
FTIR	Fourier-transform infrared spectroscopy
GC-MS	Gas chromatography-mass spectrometry
HOMO	Highest occupied molecular orbital
HRMS	High-resolution mass spectrometry
HSQC	Heteronuclear single quantum coherence
IC	Ion chromatography
IL	Ionic liquid
LUMO	Lowest unoccupied molecular orbital
MOF	Metal-organic framework
NHC	<i>N</i> -heterocyclic carbene
NMR	Nuclear magnetic resonance
PFA	Perfluoroalkoxy alkanes
PTFE	Polytetrafluoroethylene
RTIL	Room temperature ionic liquid
scCO ₂	Supercritical carbon dioxide
SILLP	Supported Ionic Liquid-Like Phase
SILP	Supported Ionic Liquid Phase
S _N 2	Bimolecular nucleophilic substitution
STT(R)	Spinning tube-in-tube (reactor)
STY	Space-time yield
Sulfoxantphos	Sodium 4,5-bis(diphenylphosphino)-9,9-dimethylxanthen-2,7-disulfonate
TEA	Triethylamine

TOF	Turnover frequency
TON	Turnover number
tppti	Tri(<i>m</i> -sulfonyl)triphenylphosphine tris(1-butyl-3-methyl-imidazolium)
tppts	Tri(<i>m</i> -sulfonyl)triphenylphosphine trisodium salt
Xantphos	4,5-Bis-(diphenylphosphino)-9,9-dimethylxanthene

1. Introduction

1.1 Flow chemistry

There are two fundamentally different ways to conduct a chemical transformation concerning technical implementation. The conventional approach, known as batch processing, relies on placing all the reactants and solvent(s) into a container, typically a flask, pressure vessel, or vial. The mixture is then stirred, heated, or cooled, depending on the required conditions. While reaction mixtures in small vessels can be efficiently heated or stirred, this becomes more challenging with increasing container size. It is not just more time-consuming to heat a large reaction vessel but also unfavourable from a safety point of view when highly reactive or hazardous reactants are employed. The need for several adjustments of the reaction parameters also renders the scale-up of these reactions very challenging (Figure 1).

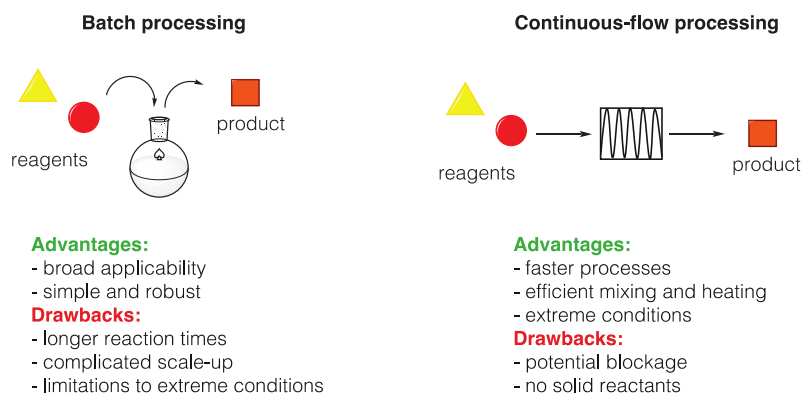


Figure 1. Batch versus flow processing

These problems can be circumvented by employing continuous-flow technologies. This methodology had already been employed in the industrial-scale gas-phase synthesis of bulk chemicals in the early 1900s.^[1] Still, in the liquid phase on a laboratory scale, it only started to receive significant scientific attention in the mid-90s. This approach aims to perform the chemical reactions directly in the tubes through which the reactants are continuously pumped. The synthetic reactions occur inside the tube in a continuously flowing stream (Figure 2).

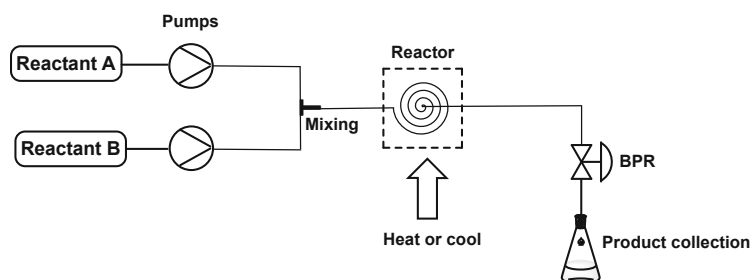


Figure 2. Schematic representation of a typical continuous-flow system (BPR: back-pressure regulator)

The tubes have a much higher surface area-to-volume ratio, typically 40-50 times higher than that of the corresponding batch reactor or flask, thus leading to the rapid and effective heating of the components. This eliminates temperature gradients and allows for fast heat dissipation and effective heat removal, which is extremely useful in exothermic reactions.

While working under continuous conditions, the most critical interrelated parameters are flow rate and residence time. For example, if a batch reaction takes 20 minutes at a specific temperature, the corresponding flow approach would require 20 minutes of residence time, i.e., the time reactants spent passing through the tube at the same temperature. Additionally, if the tube had a total volume of 10 mL, the reaction mixture should have a flow rate of 0.5 mL/minute to complete a residence time of 20 minutes. Naturally, the flow rate goes hand in hand with the residence time when batch conditions are transferred to continuous mode; an increased flow rate leads to a decrease in residence time, and *vice versa*. In practice, the same reactions can often be performed faster in continuous mode than under batch-wise conditions due to the aforementioned advantages. These processes provide straightforward scale-up, as the products can be collected for an extended period, and the increase of the tube diameter is also uncomplicated in its implementation. Additionally, multiple reactors can be employed in sequence, thus resulting in increased product formation.

Mixing is also a key parameter in continuous-flow chemistry. Unlike batch processes where the reactants are mixed by stirring, in continuous-flow mode, the easiest way to combine two streams is to employ so-called cross-, T-, or Y-pieces. Once the reactants enter the tube and react, diffusion is most of the time sufficient to provide efficient mixing in a small flow cross-section. Laminar flow occurs in pipes and tubes when the fluid flows in parallel layers without any mixing between the layers. At low flow rates, the fluid flows without any lateral mixing. There are no cross-currents perpendicular to the flow direction, nor are there any fluid swirls. In laminar flow, all particles move in straight lines parallel to the pipe walls. Any lateral mixing that does occur in laminar flow is due to diffusion between the fluid layers. Laminar flow allows for efficient mass and heat transfer and, thus, good mixing due to the parallel flow of fluids. Unlike laminar flow, turbulent flow does not have distinct layers, and the fluid mixes freely across the tube, causing a disordered flow of the fluid, which does not allow for uniform mixing of reactants (**Figure 3**). If a chemical transformation is performed in continuous reactors, it can be assumed that laminar flow occurs.

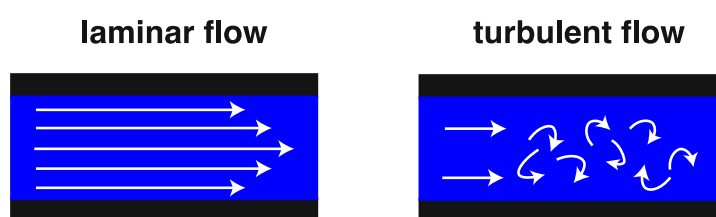


Figure 3. Laminar *versus* turbulent flow^[2]

Continuous processing also allows for integrating micro-analytics into the chemical process; thus, essential information can be obtained about the reaction progress in real time. This possibility significantly decreases the time required for parameter screening and allows for immediate intervention should the reaction proceed in an undesired reaction.

Another advantage of the continuous-flow technology is that only a tiny amount of the reaction mixture is in the tube at any given time, which renders the process much safer, allowing operation at elevated temperatures or pressures. If a reaction must be performed at a temperature above the solvent's boiling point, elevated pressure is required to keep the solvent in the liquid phase. This can be maintained with a back-pressure regulator (BPR) device placed after the reactor at the end of the tube. This device acts as a valve with a spring holding it closed. The pump has to push the valve open to release the reaction mixture from the tube. Most commonly, peristaltic-, HPLC-, or syringe pumps are employed for the reagent supply.

Depending on the reaction requirements, many different reactors can be employed in a continuous process (**Figure 4**).

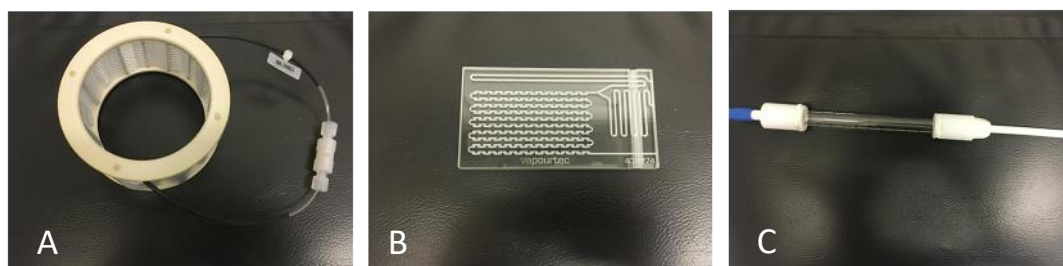


Figure 4. Continuous-flow reactors: (A) coil-based (10 mL, Vapourtec), (B) chip-based (1 mL, Vapourtec), (C) fixed bed reactor (Vapourtec)

The simplest type of flow reactor is the tube reactor (**Figure 4. A**), which is generally coiled to save space and provide efficient temperature control. The internal diameter can vary from less than 0.5 mm to several centimetres, depending on the scale of the chemical process. PFA is the most commonly used material, but stainless steel- or PTFE tubes can also be employed depending on the reaction parameters. Micro-reactors (**Figure 4. B**) featuring tiny passageways in a glass, metal, ceramic, or plastic slice are typically employed in small-scale chemical reactions. These may feature specific internal channels designed to promote mixing and have passageways as small as 0.1 mm in diameter. Column reactors (**Figure 4. C**) are valuable tools for heterogeneous catalytic reactions. They can be filled with solid catalyst support (packed-bed reactors); thus, when the reagents pass through the column, they are surrounded by the supported catalyst, which provides a high local catalyst loading and quick reactions. The supported catalyst is held in place while the reagent mixture moves on to collection, allowing the catalyst to be recycled.

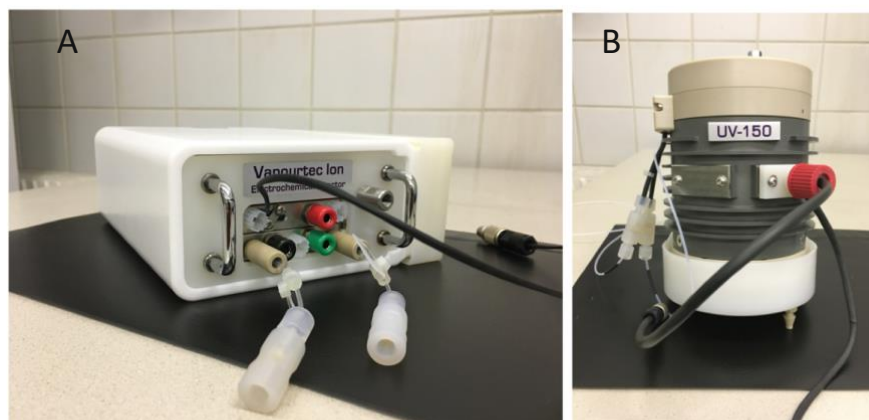


Figure 5. Reactors (Vapourtec) employed in (A) electro- and (B) photochemistry

Reactors designed to conduct electro- (**Figure 5. A**) or photochemistry (**Figure 5. B**) can be considered a newer generation of continuous-flow reactors. The former utilises flat electrodes and provides variety in electrode area, spacing, and reactor volume. The photochemical reactor features several light sources, a space-saving design, and interlock safety.

As discussed before, flow chemistry proved to be a valuable alternative for performing chemical transformations; however, some drawbacks of the approach are worth considering. It is not compatible with solids; if either a reagent or the product is solid, they can block the tubes and cause obstruction, especially as they build up at the BPR unit. Therefore, choosing a solvent in which all the reactants and products are known to be soluble is essential. If a solid product is formed as the reaction mixture cools down, the entire length of the tube, including the exit orifice, must be kept above the product's melting point. These concerns can be eliminated by employing continuous stirred tank reactors (CSTR). CSTR is a reaction vessel in which reagents and solvents flow while formed products concurrently exit the vessel. The efficient mixing allows for working in the slurry phase or employing solid catalysts, which can be recycled *via* filtration. Reactions not amenable to being performed fast at elevated temperatures are unsuitable for flow chemistry. As a rule of thumb, if a residence time of more than one hour is required, there is no advantage in employing flow chemistry. Additionally, the exorbitant prices of commercial flow equipment deserve some consideration from an economic point of view.

Thanks to their modular nature, continuous flow technologies provide a versatile approach, allowing for the facile integration of new conditions and equipment. These continuous transformations are drastically faster, which results in reduced energy costs, rendering the method more efficient and cost-effective. Moreover, carrying out a reaction in a continuous manner provides a safer and more precise synthetic route toward many invaluable chemical compounds, as the reaction parameters are more straightforward to regulate.^[3]

1.2 Ionic liquids

1.2.1 Structure and properties

Ionic liquids (ILs) are salts with a melting point below 100 °C. The Latvian-German chemist Paul Walden described the first room-temperature IL in 1914.^[4] He prepared ethylammonium nitrate, a salt with a melting point of 12 °C. However, the earliest organic salt with a melting point below 100 °C was reported by Gabriel back in 1888; ethanolanmonium nitrate, the salt he described, melts at 52-55 °C.^[5]

The low melting point of these compounds can be explained by the modest local order in their crystal structure. Common salts, such as sodium chloride, melt above 1000 K. At room temperature in the solid state, NaCl has a cubic crystal symmetry, where six counterions surround each ion. The Coulomb interaction between the sodium and chloride ions determines the strong local order. The disruption of this proper local order leads to the lowering of the melting point. For example, by replacing the chloride anion with a trifluoromethanesulfonate ion, the melting point decreases from 1074 K to 526 K. It is a combination of size and distributed charge effects responsible for the lowered melting point. The size of the relatively large trifluoromethanesulfonate anion lowers the crystal symmetry by frustrating the packing. Because of the anion size, the negative charge is distributed over a larger molecular volume, which leads to a reduced attraction with its cationic neighbours. Suppose the sodium cation is replaced with 1-ethyl-3-methylimidazolium ion. In that case, the melting point is further lowered to 262 K since this cation is roughly 40 times larger than sodium. It is also anisotropic, thus making the ion packing less efficient and disrupting crystallisation.^[6]

Concerning their structure, many IL cations contain heterocycles, e.g., imidazolium, pyridinium, pyrrolidinium, while different ammonium, phosphonium, or sulfonium derivatives have been used as well. Typical anions are halides, alkyl sulfates, various tetra- and hexafluoro derivatives, and, in particular, bis(trifluoromethanesulfonyl)imide (**Figure 6**).

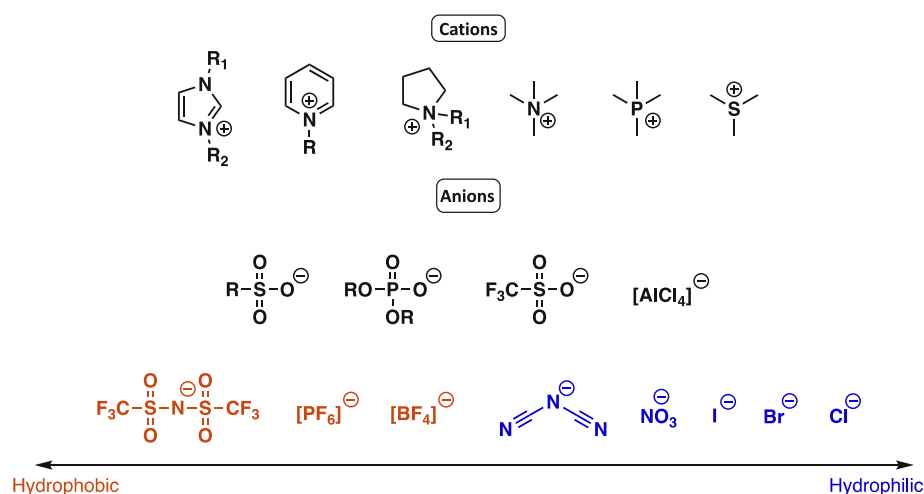


Figure 6. Common IL cations and anions

The plethora of cation/anion combinations imparts variation in the ILs' physicochemical properties over a broad range. The hydrophobicity of an IL mostly depends on its anion, but the cation can also influence it. ILs consisting of halides, nitrates, acetates, trifluoroacetates, or chloroaluminates are considered hydrophilic, whereas hexafluoro derivatives are hydrophobic.^[7] It is worth noting that certain species, such as the Lewis acidic chloroaluminate-containing ILs are not just moisture-sensitive, but incompatible with aqueous media as they react with water to form a chlorooxoaluminate(III) species and HCl.^[8] This type of ILs featuring the chlorometallate anion represents the Lewis acidic class of ionic liquids, which have found widespread application in catalysis, e.g., Friedel-Crafts chemistry and oil refinery.^[9] Introducing a longer alkyl side chain on the cation can increase hydrophobicity, while viscosity can be manipulated by modification on the side chains.^[10] A change in viscosity will cause changes in such properties such as conductivity or diffusion coefficient.^[11]

ILs can have numerous advantageous properties, such as low vapour pressure, non-volatility, high thermal stability, wide liquid range, and high electrical conductivity, although these properties must not necessarily apply to all potential candidates.^[12]

While ionic liquids initially raised interest as alternative to conventional solvents, their application has spread into other fields, such as analytics,^[13] extractions,^[14] catalysis,^[15] lubrication technologies,^[16] and various electrochemical applications.^[17] Their utilisation as liquid crystals^[18] and thermal fluids has also been reported.^[19] Some of their properties made them exceptionally popular in organic synthesis: they are suitable solvents for a broad range of organic and inorganic compounds, allowing us to bring an unusual combination of reagents into the same phase. Additionally, they are immiscible with many organic solvents and provide a non-aqueous but polar alternative for biphasic systems. Thanks to their non-volatility, they can be easily contained and may be used in high-vacuum systems.^[20]

1.2.2 Historical overview

Although over 100 years have passed since ionic liquids were discovered, their intensive investigation only started in the late 90s/early 2000s (**Figure 7**), thanks to the attraction their unique properties pose to the scientific community.

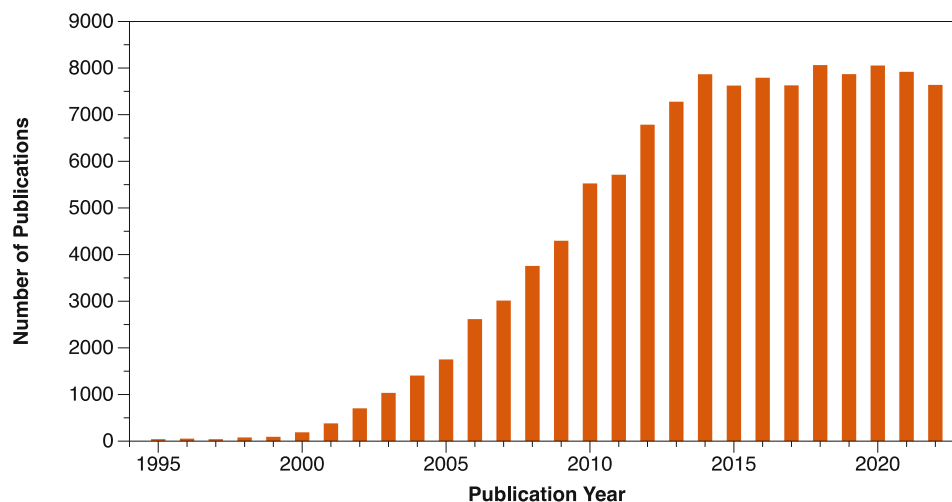


Figure 7. Ionic liquid-related publications provided by SciFinderⁿ (search term: ionic liquids, 12.01.2023)

After the first published report on room-temperature ionic liquids in 1914, ILs remained neglected and received marginal scientific interest for almost 70 years. In the 1980s, ILs slowly began to receive more attention, followed by their explosive spread in the late 90s.^[21] However, some examples of their early synthetic applications exist. Parshall and his co-workers investigated tetraethylammonium salts as solvents for the platinum-catalysed transformation of olefins.^[22] One of the employed ILs, tetraethylammonium trichlorostannate(II) demonstrated high reactivity and decent selectivity in the hydrogenation of 1,5,9-cyclododecatriene. Some other early studies focused on the ILs toxicity and antimicrobial activity^[23] or their effect on the rates of organic reactions,^[24] whereas others investigated their electrochemical properties.^[25]

In the 80s, ethylammonium nitrate started to attract more interest as different studies discovered its potential to be used as non-aqueous reaction medium for enzymatic reactions^[26] or as stationary phase in gas chromatography.^[27]

In the same decade, 1,3-dialkylimidazolium cations were introduced into ILs for the first time by Wilkes *et al.* as a new class of room-temperature ILs (RTILs).^[28] The research group described the synthesis of dialkylimidazolium chloroaluminate ILs and suggested their use in electrochemistry, spectroscopy, and catalysis. Later on, this class of cations became a popular choice in ionic liquid structures. Around this time, interest was also focused on the chloroaluminate species of these ILs. In 1989, Smith and co-workers discovered that solutions of HCl in 1-ethyl-3-methylimidazolium chloroaluminates are superacids capable of protonating arenes to a degree similar to that of liquid

HF.^[29] This discovery became essential for the application of ILs in the oil refining industry.^[30] Subsequently, the Lewis acidity of these chloroaluminate ILs allowed them to be utilised in Friedel-Crafts reactions as a combination of solvent and catalyst.^[31]

As the interest in ILs grew in the late 80s and during the 90s, air- and water-stable 1-ethyl-3-methylimidazolium-based ionic liquids have been reported,^[32] which demonstrated high thermal and hydrolytic stability. Around that time, the bistriflimide (NTf_2^-)^[33] and the $[\text{PF}_6]^-$ anions^[34] were introduced, which allowed to broaden the range of ILs.^[35] By the end of the 20th century, ILs became commercially available at high quality and affordable prices, therefore accessible to researchers in higher quantities. This led to an increased number of participants in the ionic liquid field and an explosion of interest in their potential application.^[21] Since then, many ILs have been successfully employed in fields such as biomass processing,^[36] biocatalysis,^[37] energy generation and storage,^[38] extraction technologies,^[14b, 39] fuel cells,^[40] separation agents,^[13a, 41] and the pharmaceutical industry.^[42]

The utilisation of ethylaluminium chloride-containing room-temperature ILs in Ni-catalysed dimerisation of alkenes in 1990^[43] led to the development of one of the earliest industrial methods which utilise ILs. The so-called biphasic Difasol process (**Figure 8**) relies on the catalyst's solubility and the product's insolubility in the IL. The easier separation of the products from the catalyst allows recycling, thus reducing catalyst disposal and cost. On the other hand, decreased reaction time, better dimer selectivity, and higher yields were observed during the oligomerisation process.^[44]

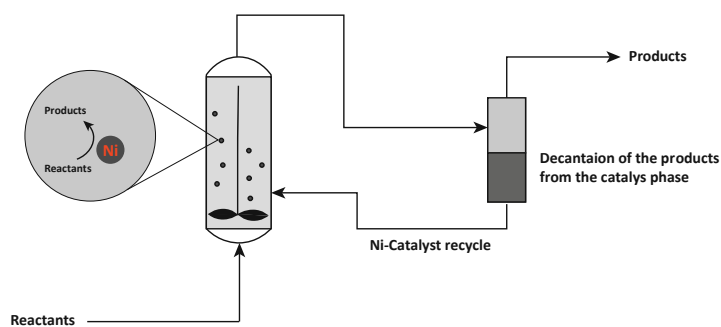


Figure 8. The biphasic Difasol process^[45]

As another example of the commercial application of ionic liquids, BASF's BASILTM process is worth mentioning. The original method used by BASF relied on triethylamine as a proton scavenger in the synthesis of diethoxyphenylphosphine (**Figure 9**). The formed salt precipitated from the reaction mixture, forming a solid-liquid emulsion, thereby hampering the mixture's stirring. Hence, the formed salt had to be removed *via* filtration. The new concept replaced triethylamine with methylimidazole, which led to the formation of the protic ionic liquid methylimidazolium chloride during the process, a by-product that is liquid at the temperature of the reaction. The formed liquid-liquid biphasic system enabled straightforward phase separation. Moreover, the formed IL could be regenerated upon alkali

treatment with NaOH, resulting in reduced waste formation. Eliminating the formation of solid by-products allowed for utilising smaller, continuously operated reactors and, thus, a tremendous increase in the space-time yield (STY).^[46]

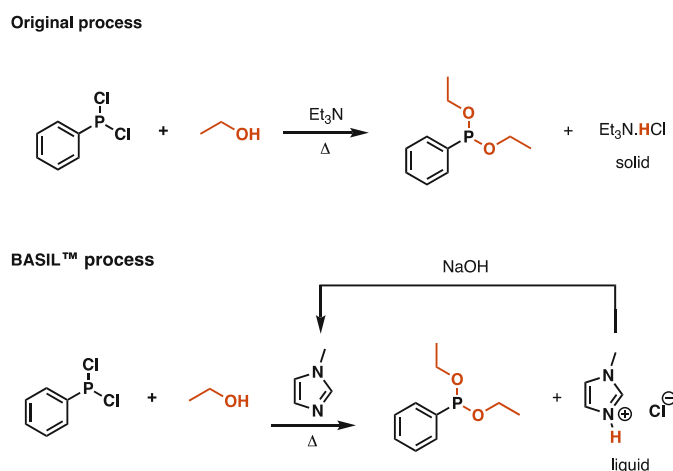


Figure 9. The BASIL™ process

As another industrial-scale application of ionic liquids, a synthetic process with significant relevance in the oil industry can be mentioned. In this approach, isobutene is alkylated to form trimethylpentanes, desirable components of high-quality gasoline (Figure 10).

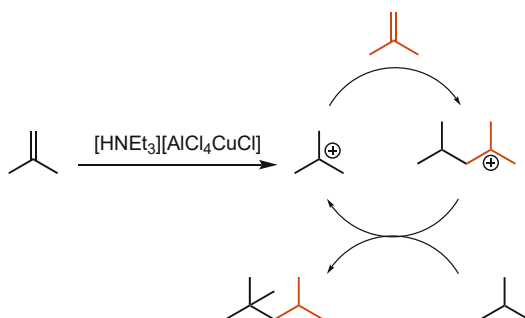


Figure 10. Isobutene alkylation by employing ILs in the oil industry

The conventional alkylation process utilises mineral acids, which has significant concerns since handling large quantities of H_2SO_4 or HF . In order to avoid problems associated with mineral acids, a process relying on Lewis acidic ILs was developed by Chevron. The so-called ISOALKY process utilised ammonium- and phosphonium-based chloroaluminate ILs for improving the reaction selectivity. Another similar example of applying ILs in the oil industry is the so-called Ionikylation process developed by Petrochina. The Ionikylation process employs a Lewis acidic IL-based liquid composite as catalyst, significantly reducing the corrosion rate in the process. The addition of CuCl to $[\text{HNEt}_3][\text{AlCl}_4]$ inhibits side reactions such as isomerisation, polymerisation, or cracking by the formation of the composite anion $[\text{AlCl}_4\text{CuCl}]^-$, which acts as an acceptor of carbenium-ion. Employing the composite anion increases the hydride transfer rate, which results in a better selectivity toward the desired compound in the continuous biphasic process (Figure 11).^[47]

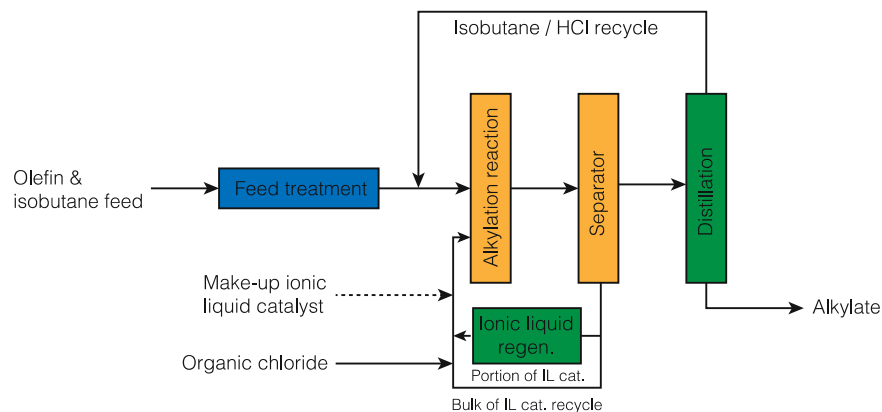


Figure 11. Continuous processing for isobutane alkylation^[48]

The application of ILs as supported catalysts in pilot-scale processes are also known. Evonik Industries employed supported ILs for immobilising a metal catalyst for hydroformylations. Ultimately, a Rh-complex containing an anthracene-based ligand demonstrated long-term stability over 2000 h, allowing for its consideration for commercialisation.^[49]

Another approach utilising supported ionic liquids was commercialised by Petronas and Clariant.^[50] The strategy employs supported chlorocuprate(II)-based ILs for capturing mercury from gas streams. The concept relies on the oxidative dissolution and complexation of elemental mercury into the IL as a stable mercurate(II) species. Since its fundamental chemistry does not change with the scale of the process, the method provided a convenient approach for continuous mercury removal in the natural gas industry.

As discussed in this chapter, ionic liquids can contribute to sustainable chemistry in many ways. As the first two parts of the conducted experimental work were dedicated to developing alternative synthetic routes for producing hydrophobic ionic liquids and their catalytic application, these fields will be discussed in the following chapters.

1.3 Synthesis of ionic liquids

1.3.1 State-of-the-art synthesis of ionic liquids

Until today, there is a conventional method for the preparation of ILs, which comprises two steps: the initial is the alkylation - also called quaternization - of a nucleophile, e.g., an amine or a phosphine, and this is followed by subsequent metathesis to exchange the anion (**Figure 12**).

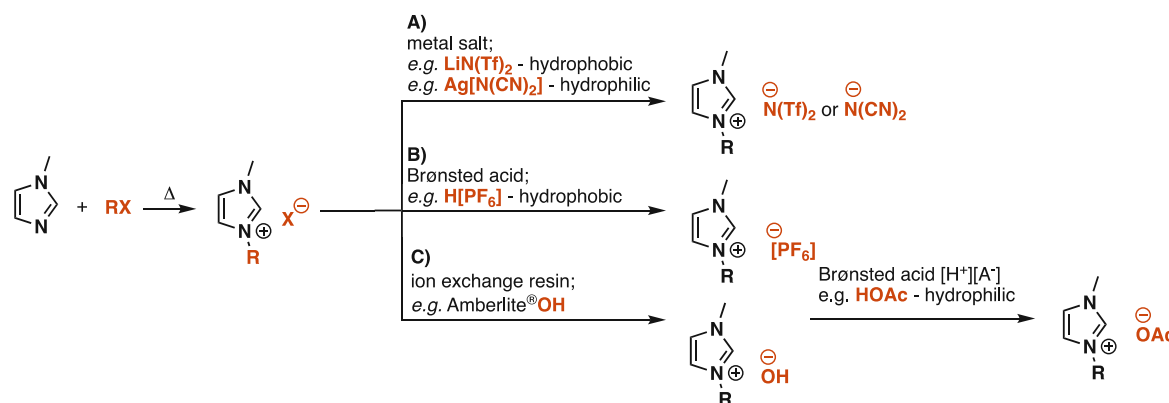


Figure 12. State-of-the-art synthesis of ILs

Concerning the second step, there are different paths to vary the anion. On the one hand, the halide derivative can be reacted with a metal salt; in this case, the metal halide (e.g., when working with silver salts in aqueous solutions) or the IL (e.g., when working with lithium salts in aqueous solutions) can precipitate from the solution (**Figure 12**, Path A). Such a method has been reported by Bonhôte *et al.* for the synthesis of dialkylimidazolium bistriflimides. The corresponding halide or triflate was reacted with lithium bistriflimide in an aqueous solution to form the desired product.^[33] Alternatively, the halide can also be treated with a Brønsted acid with the release of the halide's corresponding acid (**Figure 12**, Path B and C). As an example, the synthesis of $[\text{C}_2\text{mim}][\text{PF}_6]$ was described in 1994.^[34] The halide precursor was reacted with an aqueous solution of HPF_6 in water to obtain the product with a melting point of 60 °C. These two-step methods for producing hydrophobic and hydrophilic ILs were described in detail in the late 90s, and since then, they have remained almost unaltered.^[20, 51]

Although this state-of-the-art method is well established and broadly used, several challenges exist for the production of ionic liquids of high quality. Some of the significant discrepancies in the reported physicochemical properties of ILs are associated with their halide and metal contamination and variations in their water content.

In the initial step, where the organic halide precursor is formed, low-volatile alkyl halides are used, rendering the first step time-consuming. Alkyl chlorides are cheaper but less reactive than alkyl bromides and -iodides, so a compromise must be made concerning the precursor price and reactivity. The reaction time for the complete alkylation can reach several days; therefore, alternative activation strategies such as microwave irradiation^[52] or ultrasound treatment^[53] might be needed instead of

conventional conductive heating. During the alkylation process, problems arising from elevated temperature and local overheating still occur, leading to discoloured salts due to the formation of still unidentified chromophores. By-products obtained *via* temperature-induced S_N2 dealkylation, carbene formation, or cross-alkylation^[54] due to local overheating are even more problematic (**Figure 13**).

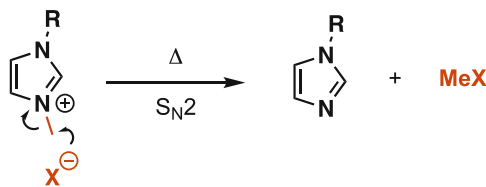


Figure 13. Temperature-induced dealkylation of imidazole-based ILs

To eliminate all the impurities after alkylation, exhausting and expensive purification procedures such as zone melting, filtration over activated charcoal, or crystallisation are required.^[55] If future applications demand high purity, repeated crystallisation of the intermediate halide salts from organic solvents is recommended until the solvent remains colourless.

The arduous removal of halide and metal residues complicates the subsequent anion metathesis step. These residues can drastically influence the chemical and physical behaviour of the ILs. Moreover, alkali salts such as LiCl, NaCl, and KCl are stoichiometrically formed as a by-product, which is unacceptable in the light of sustainable and environmentally benign manufacturing of ionic liquids. In the case of hydrophobic ionic liquids, e.g., bistriflimides, after adding an aqueous solution of $\text{Li}(\text{Tf})_2$ to the corresponding water-soluble halide precursor, a biphasic mixture is formed immediately. After the metathesis, residual metal and halide contamination, such as LiCl, are present in the obtained hydrophobic IL. For example, when the ILs are employed as oil additive, the presence of residual halides is unacceptable since they can cause corrosion. These contaminants must be removed by excessive washing steps with water, which generates a large amount of wastewater until a high-purity ionic liquid is obtained. These consecutive washing steps after anion metathesis become difficult, if not impracticable, with increasing hydrophilicity: ILs bearing the tetrafluoroborate anion, but particularly those based on anions such as dicyanamide, carboxylate, or nitrate, suffer from incomplete anion exchange, therefore from metal and halide impurities. A reliable anion metathesis with cheap alkali salts is usually impossible in the case of very hydrophilic ionic liquids. The metathesis has to be forced with the silver salt of the corresponding anion, so this strategy is definitely limited to small-scale synthesis due to economic concerns.^[56]

Although the state-of-the-art strategy is well established if the application of the ILs demands high purities, alternative synthetic routes are needed to circumvent problems associated with residual halide- or metal contaminations. Since the halide content is responsible for undesirable properties such as increased corrosion potential,^[57] there is a demand for developing halide-free synthetic approaches for the reliable production of ILs.

1.3.2 Halide-free synthesis of ionic liquids

An approach to circumvent the problems associated with ion metathesis and eliminate contamination by residual halides and metals was published in 2002.^[58] That strategy provides an entirely halide-free, straightforward synthetic method for producing sulfate-based ionic liquids. Direct alkylation of imidazole derivatives with the corresponding dialkyl sulfate led to the formation of the desired IL in just one step (**Figure 14**).

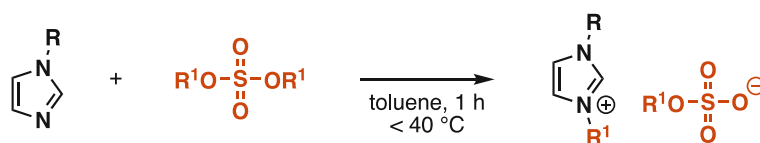


Figure 14. Halide-free synthesis of sulfate ILs

The reaction was performed in toluene, and the mixture was cooled with an ice bath to maintain the temperature below 40 °C due to the reaction's exothermic nature. The alkylating agent's high reactivity significantly reduced the time and energy demand of the alkylation step, as the product was obtained in 1 hour. However, these benefits are outweighed by the enormous toxicity of the alkylating agents, such as dimethyl sulfate.

Kuhlmann and co-workers reported a similar strategy for preparing alkylimidazolium dialkyl phosphates (**Figure 15**).^[59]

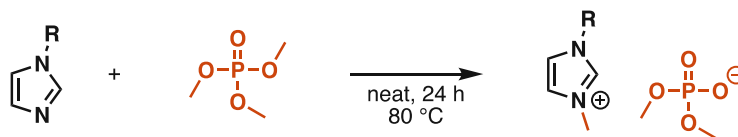


Figure 15. Synthesis of dimethyl phosphate ILs

The employed alkylating agent, trimethyl phosphate, proved less reactive as elevated temperature and extended reaction time were required to obtain the desired products with excellent yields. The decreased reactivity allowed it to work under solvent-free conditions, rendering the process environmentally more benign. Both the sulfate- and the phosphate-based ILs can serve as a precursor for further modifications toward more hydrophobic esters *via* transesterification.^[60] This two-step procedure provides hydrophobic ILs by replacing the dimethyl phosphate anion with a Brønsted acid derived from a more hydrophobic acid.

Another way to circumvent problems associated with the state-of-the-art method is an approach relying on dimethyl carbonate as a relatively cheap methylating agent. In this commercialised strategy, a methyl carbonate intermediate is formed, which is further reacted either with equimolar amounts of acid or the ammonium salt of the anion, forming the desired IL upon release of CO₂ and methanol (**Figure 16**).^[61]

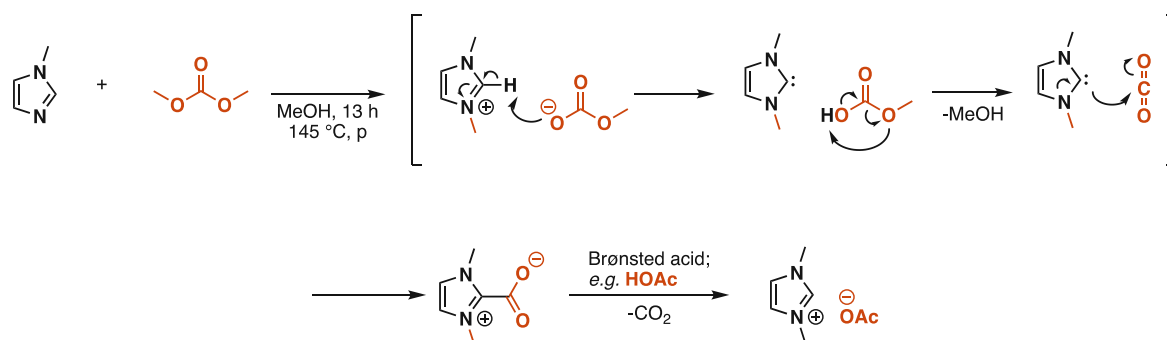


Figure 16. Halide-free IL synthesis relying on dimethyl carbonate

The formation of the zwitterion product is linked to the initial methylation of methylimidazole followed by a reaction of methyl carbonate anion with the imidazolium cation. The formed dialkylimidazolium cation's acidic C2-hydrogen is abstracted by the methyl carbonate anion, forming an NHC and carbonic acid monomethyl ester. The latter is naturally unstable, especially at this reaction temperature, and decomposes to methanol and CO₂. The heterocarbene, as a nucleophile, attacks carbon dioxide and leads to the formation of the zwitterionic species.^[62] This process provides access to a plethora of mainly hydrophilic ionic liquids, but the exact neutralisation of methyl carbonate salts can be challenging, and the excess reagent can cause contaminations. The approach provides the desired products in quantitative yields and high purity and provides a versatile strategy for synthesising various ILs. This strategy has been commercialised and is known as the CBILS[®] process.^[63]

Zhang *et al.* announced the direct methylation and trifluoroethylation of *N*-nucleophiles to form ILs in 2003.^[64] The concept relies on trifluoroethyl phenyliodonium bistriflimide and *N*-methyl bis((perfluoroalkyl)sulfonyl)imides as alkylating agents. Concerning the latter, a new synthetic pathway is described in the manuscript. Refluxing trimethyl orthoacetate with the corresponding fluorinated sulfonimide generates the corresponding alkylating agents with acceptable yields. The alkylating agent is further reacted with an *N*-nucleophile in chloroform for 5 hours, affording the corresponding IL in excellent yields (**Figure 17**).

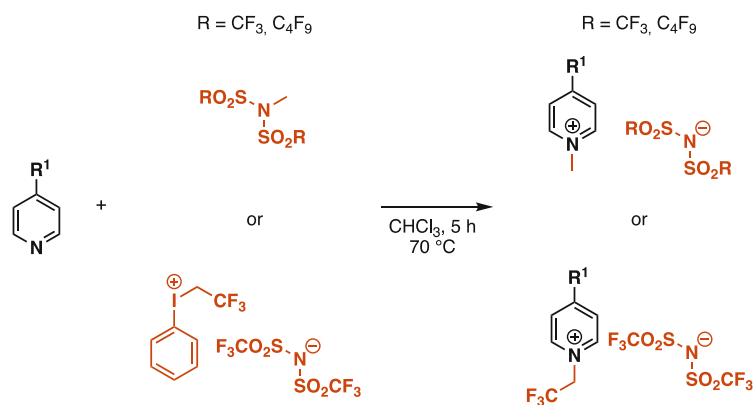


Figure 17. Toward ILs containing fluorinated anions

Takao and Ikeda have described a methodology for the halide-free synthesis of tetrafluoroborate ILs.^[65] The approach employs trialkyloxonium salts as alkylating agents, forming dialkyl ethers as a by-product (**Figure 18**).

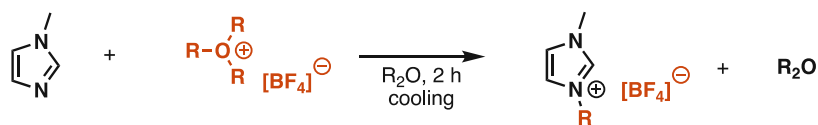


Figure 18. The halide-free route toward $[\text{BF}_4]^-$ ILs

The components are reacted in anhydrous etheric suspensions in an inert atmosphere. Typically, the same dialkyl ether is employed as solvent as the one which is formed as a by-product. The volatile ether residues are then removed under reduced pressure, thereby allowing access to ILs with excellent yields. However, treatment with activated charcoal is required to obtain the desired high-quality products, rendering the simple process more tedious. Regardless, any by-product formation is undesirable according to the corresponding principle of green chemistry.

For the production of nitrate-containing imidazolium-based RTILs, a silver- and halide-free method has been communicated by Smith *et al.*^[66] The one-step approach utilises alkyl nitrates for the alkylation of *N*-nucleophiles (**Figure 19**).

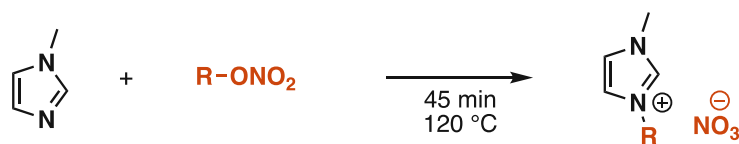


Figure 19. Silver- and halide-free synthesis of nitrate ILs

The excessive alkyl nitrate was decanted, followed by the addition of water and treatment with charcoal; the products were obtained after removing solvent- and charcoal residues. As an alternative strategy, microwave irradiation has enabled access to the desired products in just 45 minutes in quantitative yields. This approach proved to be limited to imidazole derivatives, as employing other nucleophiles led to poor conversion or complex mixtures.

Most recently, Kim and co-workers described the direct alkylation of imidazole and pyridine derivatives employing orthoesters as alkylating agents in the presence of an acid (**Figure 20**).^[67]

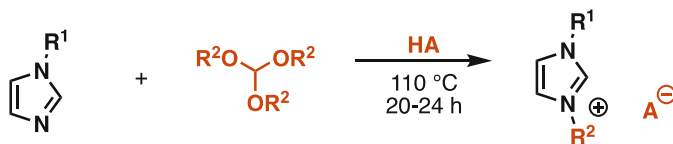


Figure 20. Employing orthoesters as alkylating agents

The process demonstrated widespread applicability for preparing a plethora of ILs with good yields. On the other hand, methanol and the corresponding formic acid monoalkyl ester are formed in equimolar amounts, which is undesirable.

Although various methods already exist for the halide-free synthesis of ILs, these methods have certain limitations. Complicated purifications hamper some; others require significantly toxic reagents or long reaction times. The still-growing application of ILs demands an entirely halide-free preparation strategy for hydrophobic ILs that eliminates the necessity of anion metathesis or the formation of by-products. Because of the demand for halide-free ILs, more attention should be paid to the direct synthesis of bistriflimide-based hydrophobic ionic liquids; hence, this particular anion provides superior physical properties such as low viscosity and high thermal stability.

1.3.3 Continuous-flow synthesis of ionic liquids

Recent trends focus on preparing ILs with microfluidic devices, combining the advantages of high throughput capacity and efficient temperature control. These reactors provide large interfacial contact areas for the alkylating agent and nucleophile, resulting in significant heat- and mass transfer improvements compared to conventional batch processes.^[68]

One of the first continuous approaches for IL production was reported in 2005 by Große Böwing *et al.*^[69] The study focuses on synthesising chloride- and sulfate-containing methylimidazole-based ionic liquids in continuously operated tube reactors. The group claims that cooling might be necessary during the mixing of methylimidazole and diethyl sulfate under neat conditions, as discolouration may occur upon mixing at 40 °C. The established approach can produce up to 4 kg [C₂mim][EtSO₄] per day without employing any solvent by pumping the corresponding reagents into a cooled tube reactor.

Waterkamp *et al.* presented a strategy for enhancing the synthesis of [C₄mim][Br] by employing a continuous micro-reactor.^[70] The system consisted of a vortex-typed micro-mixer and a tubular reactor with 2 to 6-mm inner diameters. Experiments at three different temperatures were carried out to determine the reaction's kinetic parameters. The reactor system allowed precise temperature control for the alkylation, even at elevated temperatures. Therefore, solvents could be avoided, leading to high productivity (9.3 kg/day) in a solvent-free process. Compared to the conventional batch process, more than a twenty-fold increase in the STY was achieved.

In 2009, a continuous method for synthesising 1,3-dimethylimidazolium triflate was described by Löwe and co-workers (**Figure 21**).^[71] The employed micro-reactor combined with a pipe for cooling allowed access to the desired IL with a production rate of up to 1.24 kg/h.

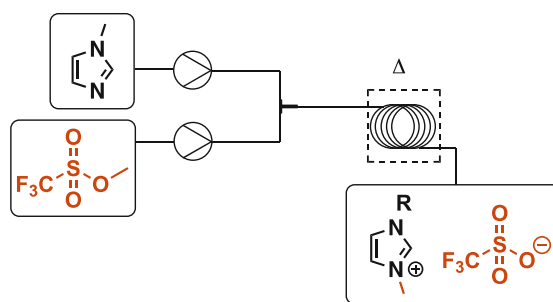


Figure 21. Continuous synthesis of triflate ILs

Ionic liquids bearing new imidazolium-based cations have been prepared with a continuous device consisting of HPLC pumps and a micro-mixer.^[72] The research group introduced various alkyl chains to the imidazole ring, thus broadening the range of available ILs. The excellent heat-transfer properties of the continuous system allowed it to work safely at high temperatures without thermal overrun and loss of control over the reaction. Moreover, the residence time and temperature could be adjusted to the various substrates without modifying the experimental setup. By employing additional reactors in

parallel operation mode, a production rate of multi-kilogram per hour can be achieved without the necessity of employing a more complex system. The strategy developed by Wilms and co-workers provided highly pure ILs without requiring subsequent purification.

Gonzalez *et al.* reported an alternative continuous process relying on a spinning tube-in-tube (STT) reactor to produce imidazolium-based ILs.^[73] Upon the reactants' introduction to the STT reactor, they create a thin film on the surface of a rotor inside a stationary shell. Applying high rotation rates allows for increased mixing efficiency, rendering the STT reactor an attractive tool for continuously synthesising ILs. The system could achieve large throughput rates (up to 16 kg/day) with minimal purification requirements and without using any solvent. Moreover, it provided easy optimisation and real-time analytical monitoring (**Figure 22**).

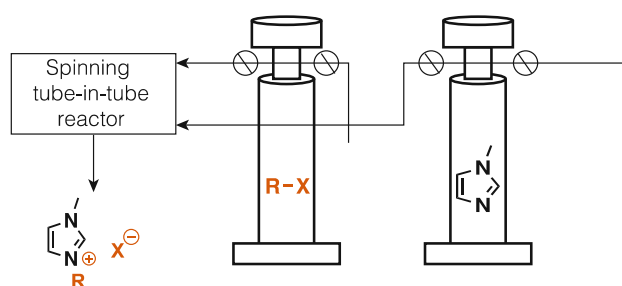


Figure 22. Continuous IL synthesis in a tube-in-tube reactor^[73]

Zimmermann *et al.* announced the synthesis of ILs relying on the modified continuous Radziszewski reaction for the formation of the imidazolium ring system.^[74] The process employs butylamine, glyoxal, formaldehyde, and a Brønsted acid to synthesise imidazole-based ILs. After screening parameters, such as reactant ratio or reactant addition sequence in batch mode, the process was adapted to the continuous micro-reactor to synthesise hydrophilic ILs. The reaction times for producing acetate- and chloride ILs were significantly decreased compared to the batch-wise approach. Moreover, ILs such as 1,3-dibutylimidazolium chloride and -acetate were obtained with excellent yields: 70% (STY: 0.12 g h⁻¹ L⁻¹) and 91% (STY: 0.35 g h⁻¹ L⁻¹), respectively. The process is only suitable for symmetric ILs, since two equivalents of the corresponding amine needs to be employed. Working with amines containing different alkyl chains would lead to the formation of a statistical mixture.

Nokami and co-workers reported the use of a micro-reactor system for the continuous production of a plethora of ionic liquids.^[75] The group successfully introduced various alkoxy groups as side chains on the cations. Moreover, the pyrrolidine-, imidazole-, and piperidine-based ionic liquids were obtained with excellent yields in a reaction time of 1 minute.

Most recently, Cao *et al.* have reported a microwave-assisted continuous method for the water-free synthesis of ILs (**Figure 23**).^[76]

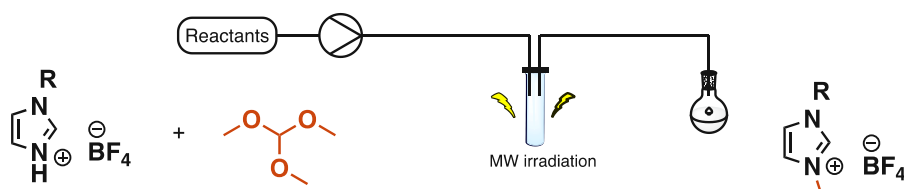


Figure 23. Microwave-assisted continuous synthesis of ILs

After optimising the microwave settings, the ILs were synthesised in batch mode prior to the fine-tuning of the continuous-flow parameters. Once the optimal parameters were determined, the continuous process provided various imidazole-, pyridine-, and triethylamine-based ILs in quantitative yields in just 10 minutes.

The carbonate-based halide-free synthetic route discussed before was successfully implemented in continuous mode.^[77] In this process, the starting materials are reacted in methanolic solutions with dimethyl carbonate to form the desired product $[\text{C}_2\text{mim}][\text{MeCO}_3]$ with a STY of $2.5 \text{ g min}^{-1} \text{ L}^{-1}$.

Continuous-flow systems proved more efficient than the corresponding batch process for synthesising various ionic liquids. The simple and precise control of the reaction parameters provided a safer and more rapid overall process and allowed access to many ILs with high qualities and yields. The straightforward scale-up and applicability of alternative heating strategies, such as MW irradiation, are also favourable from an engineering point of view. Continuous processes for IL synthesis decrease the energy requirements by the shortened reaction times and allow the reactions to be carried out under solvent-free conditions. Therefore, these approaches provide an environmentally benign synthetic route for a plethora of ionic liquids.

However, keeping all the compounds in the synthetic approach liquid during the entire process can be challenging. Neat conditions can only be employed if the desired IL is liquid at room temperature. For producing ILs such as tetraalkylammonium halides, there is a need for employing solvents in the process, rendering it environmentally less benign. Often, high temperature is required for obtaining good yields and overcoming drawbacks arising from high viscosity, which increases the energy demand of continuous processes.

1.4 Application of ionic liquids in continuous catalytic processes

1.4.1 Ionic liquids as reaction media in continuous catalytic processes

Ionic liquids have been widely exploited in liquid-liquid biphasic systems to immobilise a reagent or a catalyst *via* dissolution.^[78] Immobilising a catalyst in the IL phase provides several advantages. The tuneable miscibility of ILs with other solvents can facilitate the separation of the catalyst or the reaction medium from the product, allowing easier catalyst recycling. This strategy does not require modifications of the homogeneous catalyst for the immobilisation, and the IL phase can contribute to activating or stabilising the catalyst. Moreover, the large variety of available cations and anions allows the fine-tuning of the catalytic system.^[79] Concerning transition metal catalysis, transition metal complexes are generally polarisable enough to be soluble in ILs. However, it is worth considering that the ILs can interact with the coordination sites of the catalyst complex, thus blocking the catalytic cycle. ILs are likely to form catalytically active solutions with a metal complex if the latter is neither too electrophilic nor highly nucleophilic. An extremely nucleophilic catalyst complex can react with the IL's cation, whereas immensely electrophilic catalytic centres are likely to strongly coordinate even anions that are considered weakly coordinating.^[80]

Taking advantage of these principles, Liu and co-workers established a system for performing a continuous Heck reaction.^[81] Iodobenzene as substrate and butyl acrylate as reagent were used to form butyl cinnamate. Conducting such reactions in ionic liquids has previously been reported.^[82] However, for a continuous process, employing ILs with lower viscosity is beneficial. The group used $[C_4mim][NTf_2]$ as a non-viscous solvent and a Pd-NHC complex soluble in the IL as the catalyst (**Figure 24**).

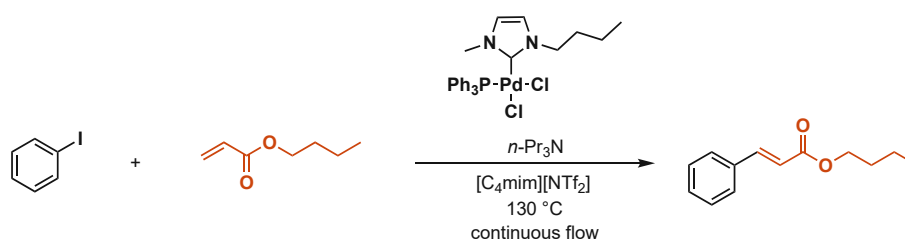


Figure 24. Continuous Heck reaction in ILs

The reactants were mixed, and the catalyst was dissolved in the IL. The mixtures were loaded in two syringes, respectively. A reaction temperature of 150 °C and a residence time of 50 minutes was employed. In order to involve the work-up step in the continuous process, additional micromixer units were used. This allowed the separation of the product from the IL phase upon extraction with hexane. The formed ammonium salts were extracted with water from the IL phase in the other unit. The method provided the desired product with excellent yields (80% overall yield, 10 g/h productivity).

Moreover, the recovered IL could be recycled and used in consecutive runs without losing catalytic activity.

Fukuyama *et al.* have described a similar method for synthesising a key intermediate of an active pharmaceutical ingredient.^[83] The intermediate of the so-called matrix metalloproteinase inhibitor was synthesised *via* copper-free Sonogashira coupling in $[C_2mim][NTf_2]$ as solvent (**Figure 25**). The process implemented reaction work-up and proved suitable as the target molecule was isolated with excellent yield, and the palladium-containing IL phase was successfully recycled.

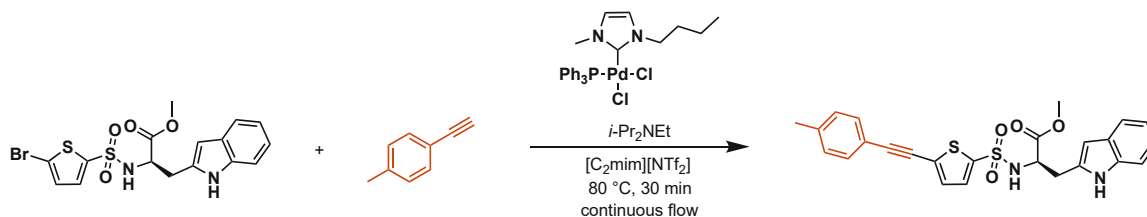


Figure 25. Continuous Sonogashira coupling in ILs

A method for an industrial IL-based process employing continuous stirred-tank reactors has been developed by the Eastman Chemical Company.^[84] The concept relies on tetraalkylphosphonium ILs as liquid phase and Lewis base for the isomerisation of 3,4-epoxybut-1-ene to 2,5-dihydrofuran, which can serve as a precursor for other valuable products.

Glasnov and co-workers reported a continuous method for methylating various *N*-, *O*-, and *S*-nucleophiles with the aid of dimethyl carbonate.^[85] The process employed the basic IL, tributylmethylammonium methyl carbonate, as a catalyst in the reaction. After optimising the conditions for the methylation of indole under batch-wise conditions, the process was successfully translated into a continuous approach (**Figure 26**). The employed IL was generated *in situ*, transforming an ineffective base, Bu_3N , into an efficient catalyst for these reactions. The reactions were carried out at 285 °C and 150 bar in 3 minutes and allowed access to many methylated derivatives with excellent yields.

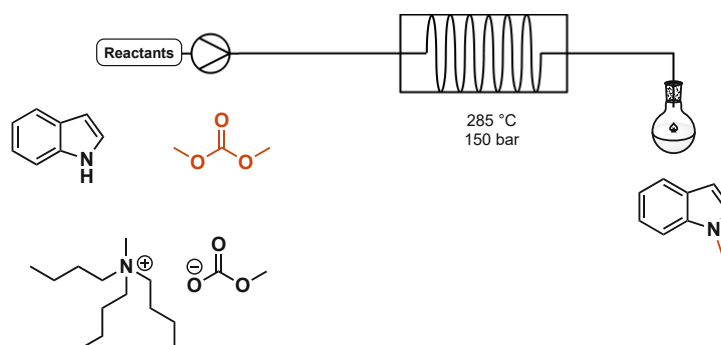


Figure 26. Employing basic ILs for continuous methylations

A continuous electrochemical system for anodic substitution reactions was described by Horii *et al.* in 2007.^[86] Combining ILs with continuous-flow technologies allowed for overcoming restraints such as

the stability of carbocations and the oxidation potential of nucleophiles. The reaction of *N*-(methoxycarbonyl)pyrrolidine with allyltrimethylsilane was investigated by employing different ILs as solvents. Using *N,N*-diethyl-*N*-methyl-*N*-(2-methoxyethyl)ammonium bistriflimide provided the product with an excellent yield of 91%. Based on the results, ILs showed excellent stabilising ability for the carbocation and allowed it to react with allyltrimethylsilane before its decomposition.

Ionic liquids proved to be suitable solvents in continuous biocatalytic processes as well. This is remarkable, as microorganisms usually only tolerate physiological conditions and water as solvent.^[87]

Wang and co-workers reported the continuous esterification of various alkyl caffeates with 2-phenylethanol by employing a packed-bed microreactor with an immobilised enzyme (Novozym 435) and [C₄mim][NTf₂] as solvent (**Figure 27**).^[88]

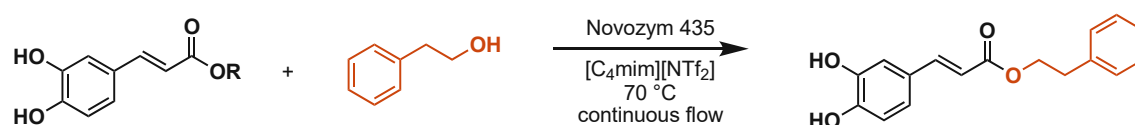


Figure 27. Continuous enzymatic catalysis in ILs

The method provided the desired product, caffeic acid phenylethyl ester, with an excellent yield of 93% within 2.5 hours. The system proved stable as the biocatalyst could be recycled without losing its catalytic activity.

A continuous biocatalytic process has been reported by Gubicza *et al.* for the esterification of acetic acid with ethanol in [C₄mim][PF₆] as solvent.^[89] The formed ethyl acetate and water were removed by a double pervaporation system using hydrophobic and hydrophilic membranes, respectively. The membrane process allowed a safe and environmentally benign product removal with low energy demand. Moreover, no loss in the catalytic activity was observed during a 72-hour operation of the system.

Other biphasic systems derived from an ionic liquid phase and a supercritical fluid, particularly supercritical carbon dioxide (scCO₂) can also be employed in continuous mode.^[90] These systems are harvesting the knowledge that scCO₂ is highly soluble (up to 60 mol%) in some ILs, whereas the ILs have no measurable solubility in scCO₂.^[91] The catalyst is typically immobilised in the IL phase, whereas the scCO₂ delivers the substrates in the IL phase, thus enhancing the separation of the products (**Figure 28**).^[92]

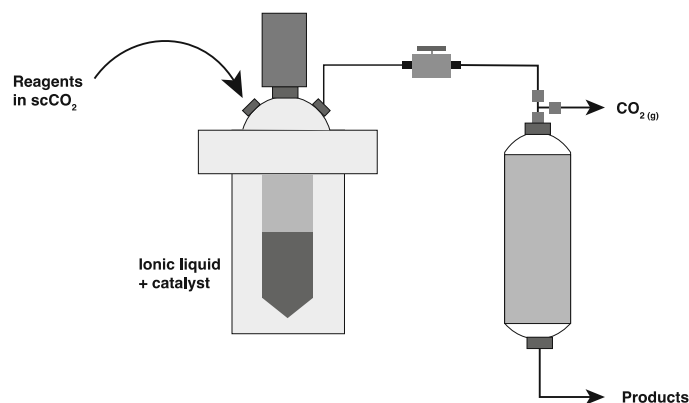


Figure 28. Continuous processing by combining ILs with scCO_2 ^[93]

Based on these principles, Sellin and co-workers developed a strategy for the hydroformylation of 1-octene employing Rh-complexes as a catalyst.^[94] The catalyst complex was dissolved in $[\text{C}_4\text{mim}][\text{PF}_6]$, and the substrates, the hydrogen, and the carbon monoxide were dissolved in scCO_2 and carried with its aid to the reactor. At the optimal conditions, the method provided excellent yields and selectivity for the desired linear aldehyde. Moreover, a high turnover frequency was obtained as the system proved stable for more than 20 hours, while negligible metal leaching was observed during the process.

Similar concepts relying on scCO_2 and ionic liquids can be applied in continuous asymmetric transformations. In 2013, Theuerkauf and co-workers announced a strategy for the asymmetric hydrogenation of methyl propionylacetate.^[95] Hydrophobic ILs were used for immobilising the chiral Ru-BINAP complex, whereas the supercritical CO_2 was used as a mobile phase carrying the reactants in and products out of the reactor. The system provided excellent conversion (>90%) and good enantioselectivity (82%) in the first 80 hours. A maximal STY of $180 \text{ gh}^{-1}\text{L}^{-1}$ was obtained, while neither IL- nor catalyst leaching was observed.

Ionic liquids can also facilitate continuous gas-liquid phase reactions, providing an excellent strategy for catalyst immobilisation. Rahman *et al.* developed a superior strategy for the Pd-catalysed multiphase carbonylation of aryl iodides with the aid of the hydrophobic IL $[\text{C}_4\text{mim}][\text{PF}_6]$.^[96] Yet again, the IL was used for catalyst immobilisation, allowing for easier separation and recycling. Various C- and N-nucleophiles were utilised as reactants to perform carbonylative Sonogashira couplings (**Figure 29**) and aminocarbonylations, respectively.

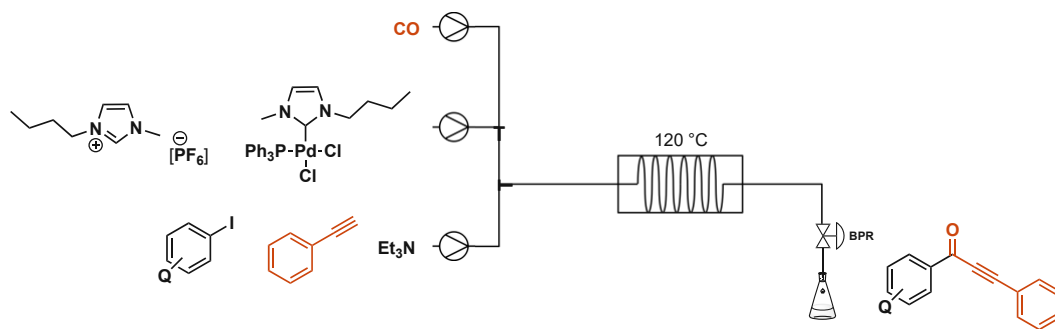


Figure 29. Continuous carbonylations with the aid of ILs^[96]

The carbonylative Sonogashira coupling showed increased activity and selectivity toward the desired product compared to the corresponding batch reactions. In most reactions, the batch process favoured the formation of the corresponding non-carbonylative Sonogashira product. The continuous aminocarbonylation reactions demonstrated increased selectivity toward the double-carbonylated products and provided them with increased yields. The method proved versatile as the desired products were obtained with excellent yields.

The strategies mentioned above clearly demonstrate the widespread applicability of IL in continuous processes, mainly for immobilising catalysts. However, there are some concerns regarding the industrial scale-up of a process relying on ILs. Using ILs in bulk quantities can be economically unfavourable as ionic liquids are typically 10-50 times more expensive than the organic solvents they aim to substitute. Handling ILs in large quantities can be challenging as they can cause corrosion or embrittlement to commonly used plant materials or pump sealings. In addition, IL proper disposal is a topic that requires careful consideration. ILs with high viscosity are often unsuitable for continuous processes as their use can lead to operational obstructions. Additionally, the high viscosity of ILs restricts mass transfer rates; thus, it can lead to mass transfer limitations when employed in liquid-liquid biphasic catalysis.^[15b, 97]

Consequently, there is a demand for new strategies that circumvent the problems associated with using ILs in large quantities.

1.4.2 Ionic liquids as supported catalyst in continuous processes

In the last two decades, attempts to minimize the risk of applying ILs for various practical approaches led to the development of IL thin-film technologies. Using ILs as thin films reduces all potential concerns regarding IL-specific financial investment. Supported ionic liquid phase (SILP) catalysis was developed to exploit the advantages of IL thin film technologies for catalysis. The SILP technology involves surface modification of a mesoporous solid material by an ionic liquid coating. It allows for tailor-made catalysts by confining a catalytically active, IL-transition metal complex solution onto the surface (**Figure 30**).^[15b]

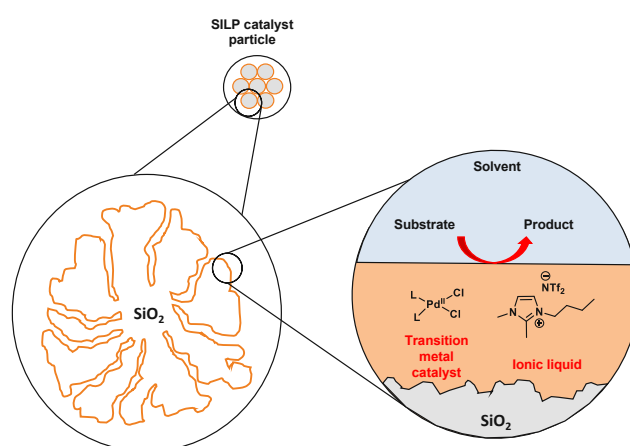


Figure 30. The principle of SILP catalysis

This coating constitutes a thin film, which is confined on the surface of a solid material by physisorption, tethering, or covalent anchoring of IL fragments. Most commonly, silica is used as supporting solid materials for ILs, but alumina and carbon nanofibers have also been reported.^[98] Typically, ILs are held on the porous support by electrostatic interactions, capillary forces, or hydrogen-bond interactions. The SILP concept allows for transferring specific properties of the fluid to the surface of a solid material. SILP technologies provide a high IL-fluid interfacial area, i.e., close proximity of the whole IL volume close to the fluid-fluid phase boundary (diffusion layer). The strategy circumvents mass transfer limitations due to the short diffusion length in the IL film. In contrast, mass transfer limitations are often encountered in liquid-liquid biphasic catalysis as the high IL viscosity restricts mass transfer rates. During the catalytic process, only the IL and the catalyst present in the diffusion layer are utilised. Thus, only a minor part of the IL and the catalyst participate in liquid-liquid biphasic reactions. The SILP strategy can circumvent these problems by effectively combining the advantages of classical homogeneous catalysis (high activity and selectivity) and heterogeneous catalysis (straightforward product separation and catalyst recycling).^[15b, 80] One possible drawback of SILP catalysis is leaching, which means the removal of IL or metal catalyst from the support's surface. This

can be avoided by the proper selection of solvents or by employing supported catalysts containing covalently bound moieties.

An early example of a continuous process employing SILP catalysts was announced by Riisager *et al.*^[99] The catalyst system was utilised in hydroformylation reactions in a continuous manner. [C₄mim]-based ILs with different anions have been employed to immobilise the Rh-Sulfoxantphos complex in the transformation of propene to the corresponding linear aldehyde, *n*-butanal (**Figure 31**). The catalyst system provided the desired product in excellent regioselectivity and proved suitable for the continuous fixed-bed process.

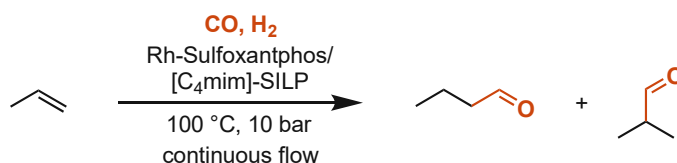


Figure 31. Continuous hydroformylation with SILP catalysis

The same research group established a similar method for the continuous carbonylation of methanol.^[100] The SILP catalyst was prepared from the corresponding alkylimidazolium iodide and [Rh(CO)₂I]₂; their methanolic solution was then impregnated on silica. The developed system provided a shorter reaction time and high activity.

Schneider *et al.* described the utilisation of a chirally modified rhodium complex-containing SILP catalyst in asymmetric hydrogenations.^[101] Pyridinium- and alkylimidazolium-based ILs provided excellent activities in the continuous transformation of methyl pyruvate to methyl lactate, as 84% yield was obtained for more than 50 h on-stream. However, the system provided inferior enantioselectivity.

The application of a Rh-Xantphos-containing SILP catalyst in hydroaminomethylation reactions followed this work.^[102] The reaction involves the one-pot cascade hydroformylation of an alkene followed by reductive amination (**Figure 32**).

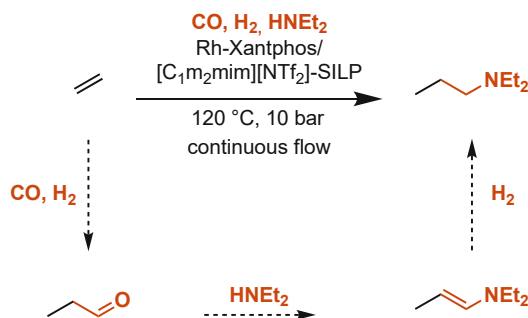


Figure 32. Hydroaminomethylation employing SILPs

Various supporting materials were examined, such as calcinated silica, neutral alumina, or activated carbon. The highest selectivity toward the desired product, *N,N*-diethylpropan-1-amine was achieved on the highly porous carbon support. Among the investigated ILs, trimethylimidazolium bistriflimide provided the highest selectivity toward the product. After experimentation in the optimal conditions,

the bistriflimide-containing SILP catalyst proved to be stable against thermal decomposition, as the catalyst provided a high yield (70%) and turnover frequency (450 h^{-1}) for an extended period of 18 hours.

Shortly afterwards, the continuous gas-phase oxycarbonylation of methanol employing SILPs was reported.^[103] Copper(I) bromide was dissolved in various ILs and dispersed on polymer-based spherical activated carbon as supporting material. The presence of ILs significantly improved the activity and stability of the copper halide catalyst. Trioctylmethylammonium bromide yielded the best result among all ILs investigated in the study. With the optimised conditions, high catalytic activity ($\text{TOF} = 10\text{--}14 \text{ h}^{-1}$) and high stability over more than 50 h time on stream could be realised.

SILPs can also catalyse continuous Friedel-Crafts alkylations. Joni and co-workers reported the continuous gas-phase isopropylation of toluene and cumene by employing Lewis acidic ILs for the SILP catalyst preparation (**Figure 33**).^[104] The moderate IL-loading and relatively high aromatic-to-propylene ratio (7:1) suppressed consecutive alkylation reactions, whereas highly acidic ILs enhanced the selectivity toward monoalkylated products. Moreover, the selectivity toward the monoalkylated products could be maintained for an extended period of 210 hours.

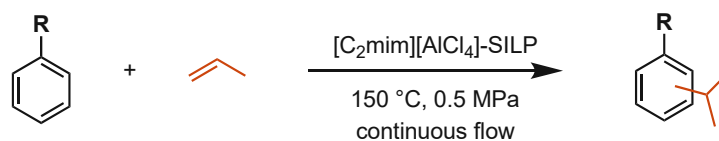


Figure 33. Continuous Friedel-Crafts alkylation with SILPs

The SILP-catalysed dimerisation of ethene employing supported Ni-catalyst has been reported.^[105] The use of ILs improved the catalyst's stability and reduced the deactivation behaviour of the metal catalyst in the reaction mixture.

Other strategies combine the advantages of supercritical carbon dioxide (scCO_2) and SILP catalysis in continuous processes. In these processes, ILs are used for catalyst immobilisation, and the scCO_2 is employed as a mobile phase that carries the reactants. Hintermair and co-workers reported applying SILP/ scCO_2 systems for the continuous hydroformylation of 1-octene.^[106] The employed Rh-catalyst was immobilised with the aid of $[\text{C}_8\text{mim}][\text{NTf}_2]$, and parameters such as pressure and substrate flow rate proved critical for the reaction. Under optimised conditions, the system allowed continuous operation over 40 hours with good rates ($\text{TOF} = 500 \text{ h}^{-1}$) and negligible catalyst leaching (0.2 ppm).

Supercritical CO_2 combined with SILP catalysts was also successfully employed in asymmetric hydrogenations.^[107] The process relies on a chirally modified cationic Rh-complex, dissolved in $[\text{C}_2\text{mim}][\text{NTf}_2]$ and deposited on dehydroxylated silica. The SILP catalyst was utilised in the chemoselective asymmetric hydrogenation of dimethyl itaconate (**Figure 34**).

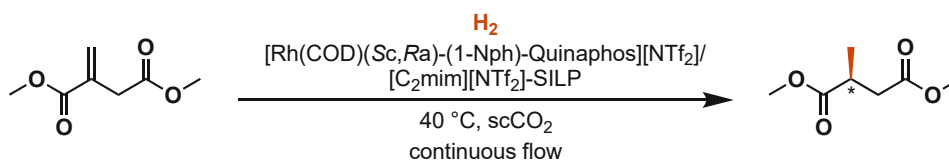


Figure 34. Continuous asymmetric hydrogenations with SILPs

The process proved efficient, as complete conversion and remarkable enantioselectivity (>99%) for the desired alcohol were achieved. The catalyst's TON reached an outstanding value of 115000, and a high STY of 0.3 kg^h⁻¹L⁻¹ was achieved.

Combining the advantages of scCO₂ and SILPs in continuous enzymatic reactions is also possible. Lozano *et al.* reported the immobilisation of a lipase enzyme, Novozyme 525L, by adsorption onto functionalised silica supports for the kinetic resolution of 1-phenyl ethanol.^[108] Bistriflimide-based ILs were employed for coating, and the coated catalyst showed increased activity already under batch conditions. The stabilising effect of the IL was evident since the enzyme maintained excellent activity at 95 °C. As mentioned, enzymes usually prefer physiological conditions, such as room temperature; therefore, the enzyme's activity at this temperature is remarkable. Working in the continuous scCO₂ system resulted in a six-fold higher synthetic activity than that obtained in hexane/IL media.

Supercritical carbon dioxide can serve as a solvent and reagent in continuous SILP-catalysed processes. Sainz Martinez and co-workers described the continuous utilisation of scCO₂ for synthesising cyclic carbonates in the presence of SILPs (**Figure 35**).^[109]

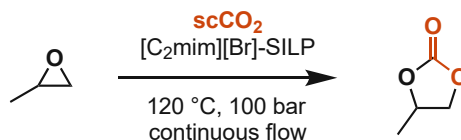


Figure 35. Continuous synthesis of cyclic carbonates by employing SILPs

Various tetraalkylammonium-, -phosphonium-, and imidazolium-based ILs have been examined in the study. Parameters such as temperature, pressure, or IL-loading have also been investigated. Physisorbed ILs such as [C₂mim][Br] showed high catalytic activity in the process. However, long-term experiments showed a rapid loss in yield due to the formation of undesired polypropylene carbonate, which agglomerated in the IL layer. On the other hand, when the ILs were covalently bound to the supporting material, they demonstrated improved long-term stability.

An alternative for immobilising the IL on a solid surface is to covalently attach IL structural fragments related to ILs to functional groups on the support's surface. The resulting materials have been termed supported ionic liquid-like phases (SILLPs). Both organic (crosslinked polymers) and inorganic (silica or metal oxides) supports have been used to prepare SILLP catalysts. Leaching can be avoided if the IL-like fragment is covalently bound to the support. On the other hand, the transfer of the IL properties to the solid phase needs to be guaranteed, which can be achieved by adequate

selection of the different design elements involved. The resulting materials feature the advantages of ILs but can overcome drawbacks associated with leaching.^[79]

The first catalytic process employing a SILLP catalyst in slurry-phase reactions was reported by Mehnert in 2002.^[110] The imidazolium-based, Rh-containing ionic liquid was covalently bound to silica (**Figure 36**) and utilised in the hydroformylation of 1-hexene. Transition metal-catalysed hydroformylations have found widespread industrial application; hence, the formed aldehydes are important precursors for plasticizers and detergent alcohols. The catalyst's selectivity can be improved by employing various ligands.^[80] The heterogeneous system provided high activity and decent selectivity toward the desired linear aldehyde.

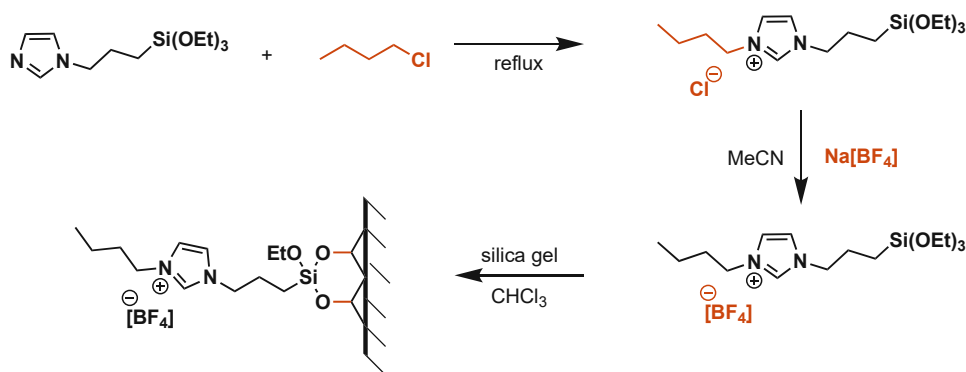


Figure 36. Catalyst preparation *via* covalent bonding

Urbán and co-workers reported the use of Pd-containing SILLPs with covalently grafted IL moieties in continuous Heck-reaction of aryl iodides (**Figure 37**).^[111]

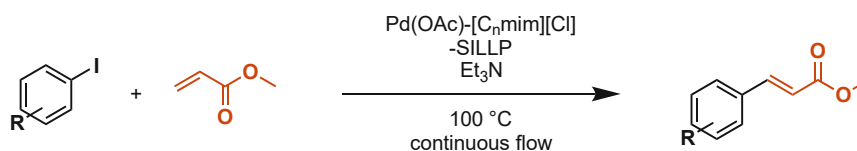


Figure 37. Continuous Heck-reactions employing SILLPs

SILP catalysts relying on various preparation methods have been examined in the study. Using ethanol as solvent in the presence of a strong base proved suitable for preparing the supported catalyst, as good yields and stable performance were achieved for several hours on stream. Moreover, the palladium leaching was negligible and did not exceed 0.46 %.

Polymer-supported SILLPs proved an efficient catalyst in the continuous cyanosilylation of carbonyl compounds under solvent-free conditions.^[112] First, different solvents were examined batch-wise; the solvent-free conditions provided the highest yield and TON. The counterion's relative activity was also determined; chloride-containing SILLPs proved the most efficient. The catalyst was then implemented in a continuous approach, where it demonstrated high activity and remarkable long-term stability. The

process proved to be highly efficient, as no by-product- or waste formation was observed, and the catalyst could be recycled without a significant drop of activity.

The same group reported the utilisation of Merrifield-supported SILLPs in continuous Henry reactions (**Figure 38**).^[113]

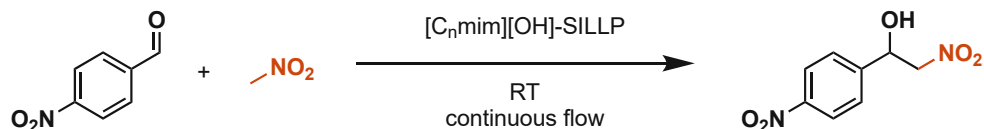


Figure 38. Continuous Henry reaction with SILLPs

The employed SILLPs contained basic anions, such as hydroxide or acetate. Complete conversion was obtained with a short residence time of 1-3 minutes. Moreover, the system provided excellent activity at room temperature, and the catalyst was successfully recovered.

These examples demonstrate the widespread applicability of ILs in continuous catalytic processes. Supported catalysts relying on physisorbed or covalently bound ILs proved efficient for many organic transformations. These SILP/SILLP catalyst systems provide high activity and easy recyclability; therefore, they are suitable alternatives for conventional catalysts in continuous approaches.

2. Aim of the thesis

The 21st-century chemical industry demands not just efficient chemical transformations but also processes that fulfil environmental principles as well. The enormous solvent consumption and carbon dioxide emission are just two examples of the main challenges that the chemical society has to address.

The application of modern flow-chemistry technologies can contribute to more sustainable synthetic approaches in many ways. Continuous processes are typically faster and, therefore, less energy- and time-demanding due to the efficient heating and mixing properties. Additionally, the precise dosage of the reactants often allows for omitting excessive reactants or solvents, rendering the strategy beneficial from an economic point of view.

This thesis focuses on developing novel continuous-flow processes in liquid state, with a particular focus on the synthesis of or catalysis with ionic liquids. The first two parts of the thesis are dedicated to the continuous synthesis of hydrophobic ionic liquids and their catalytic application in continuous allylic aminations. Initially, we aimed to develop a novel halide-free synthetic route for the continuous production of bistriflimide-based ionic liquids in high purity. After that, we sought to establish an environmentally more benign process for allylic amination of amine nucleophiles by utilising the previously synthesised ionic liquids for catalyst immobilisation.

In the second part of this work, continuous processes relying on carbon dioxide were investigated, optionally in the presence of ionic liquid-like additives. We initially aimed for the direct utilisation of CO₂ in the synthesis of urethanes, preferentially by decreasing the number of the employed catalysts or additives. In the last part of the thesis, we focused on employing carbon dioxide in carbonylation reactions. We aimed for its partial reduction with the aid of a solid oxide electrochemical cell and, subsequently, the *in situ* utilisation of the generated mixture towards the continuous formation of high-value carbonyl products.

3. Halide-free continuous synthesis of hydrophobic ionic liquids

If an ionic liquid application requires high purity, without metal and halide ions present, the halide-free synthetic route can provide a suitable alternative for its synthesis. Various halide-free methods have been previously reported, employing carbonates,^[61b] dialkyl sulfates,^[58] dialkyl phosphates,^[59] or orthoesters.^[67] These methods provide versatile strategies for the alternative preparation of ILs. However, these approaches have certain limitations. Some are hampered by the long reaction times or complicated removal of contaminants associated with excess reagents, while others require enormously toxic reagents. There is clearly a need for an entirely halide-free approach for hydrophobic ILs that eliminates any by-product formation or the necessity of anion metathesis with its exhaustive extraction steps.

In this chapter, halide-free methods for preparing bistriflimide- or dimethyl phosphate-based ionic liquids will be presented. We have developed a new way to perform allylic alkylation of N-nucleophiles in a continuous flow reactor using palladium-complex-containing supported ionic liquid phases (SILPs). We have developed a halide-free method for producing hydrophobic ionic liquids in a continuous-flow reactor. The process involves two steps: first, alkyl bistriflimides are formed, which are utilised in the quaternisation of amine nucleophiles. This produces the desired ILs in high yields and purities without forming by-products. The process provides broad flexibility, as different alkyl chain lengths and a wide range of amine nucleophiles can be employed. The quaternisation step can be performed without using solvents, and because the reactions are homogeneous, they can be carried out in a continuous flow reactor. ILs produced are also halide-free, which makes them suitable for a broader range of applications, especially in materials science.

In the second manuscript, phosphonium-based ILs are utilised as oil additives for lubrication. If an ionic liquid is employed as an additive in lubricants, the potential halide traces can lead to corrosion.^[57] Therefore, it is essential to prepare the utilised ionic liquids in a halide-free manner. We used phosphines as nucleophiles and various trialkyl phosphates as alkylating agents, thus circumventing the problems associated with alkyl halides. Moreover, the reaction's homogeneous nature allowed for the application of continuous-flow technologies that was previously developed in the framework of this thesis.

I.) The first sub-project focused on developing a halide-free synthetic method for producing bistriflimide-based ionic liquids (**Figure 39**). The applicability of continuous-flow technologies was investigated as well.

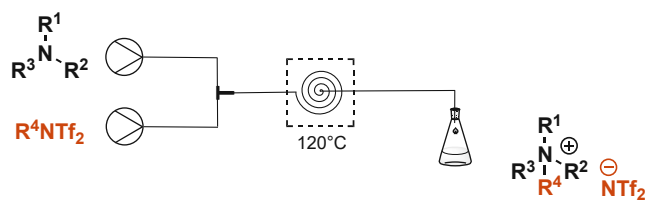


Figure 39. Halide-free continuous synthesis of bistriflimide ILs

II.) The second sub-project aimed to utilise hydrophobic ILs as MXene additives for improving their load-carrying capacity under boundary lubrication.

The following manuscripts will be presented in this chapter:

I.) K. Stigel, A. Szepecht, D. Zielinski, M. Smiglak, M. Schnürch, K. Bica-Schröder: Halide-Free Continuous Synthesis of Hydrophobic Ionic Liquids. *ACS Sustainable Chem. Eng.* **2022**, 10, 11215-1122.

As a first author, the experimental work was planned and performed by me, and I wrote the original draft.

II.) P. G. Grützmacher, R. Neuhauser, K. Stigel, K. Bica-Schröder, G. Boidi, C. Gachot, A. Rosenkranz: Combining Tailored Ionic Liquids with $Ti_3C_2T_x$ MXenes for an Enhanced Load-Carrying Capacity Under Boundary Lubrication. *Adv. Eng. Mater.* **2023**, 2300721.

As a co-author, I prepared the employed ionic liquids in batch and continuous mode, and I contributed to the manuscript preparation.

Halide-Free Continuous Synthesis of Hydrophobic Ionic Liquids

Kristof Stagel, Andrea Szpecht, Dawid Zielinski, Marcin Smiglak, Michael Schnürch, and Katharina Bica-Schröder*



Cite This: ACS Sustainable Chem. Eng. 2022, 10, 11215–11222



Read Online

ACCESS |



Metrics & More



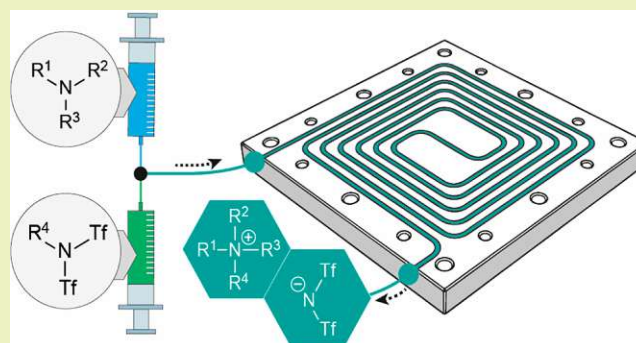
Article Recommendations



Supporting Information

ABSTRACT: Herein, we present a novel approach for the halide-free, continuous-flow preparation of hydrophobic ionic liquids (ILs) relying on the bis(trifluoromethanesulfonyl)imide (bistriflimide, NTf_2^-) anion. The simple yet fast two-step synthetic route, which involves the formation of different alkyl bistriflimides (R^4NTf_2), followed by the quaternization with an amine nucleophile, led to the desired ILs in high yields and excellent purities without any byproduct formation. The variable alkyl chain (R^4) length and the broad range of the applicable nucleophiles ($\text{R}^1\text{R}^2\text{R}^3\text{N}$) offer considerable flexibility to the synthetic protocol. The quaternization can be performed under solvent-free conditions; moreover, the homogeneous nature of these reactions allows the application of modern continuous-flow technologies. Given these advantages, the methodology can afford not just a fast and efficient alternative for the conventional synthesis of such compounds with reduced waste water production but their negligible halide content might provide a significantly broader application range of the IL products, especially for the field of materials science.

KEYWORDS: alkyl bistriflimide, triflic anhydride, ionic liquid, bis(trifluoromethanesulfonyl)imide, solvent-free



INTRODUCTION

Within the past decades, the application of ionic liquids (ILs) has spread into various fields, including analytics,¹ catalysis, extractions, various electrochemical applications,^{2–6} and lubrication technologies.⁷ While some applications do not call for high purity, others are extremely sensitive with regard to their metal and halide content, which can cause several problems such as corrosion when they are used as lubricants⁸ or catalyst poisoning in organic synthesis.^{9–12}

Until today, the preparation of hydrophobic ILs has mostly relied on a two-step process; the initial quaternization of a nucleophile with an alkyl halide is followed by anion metathesis. Although this state-of-the-art strategy has been described in detail and is well established,¹³ several challenges still exist for the reliable production, and large discrepancies observed in the reported properties of ILs can be traced to metal and halide residuals of the ILs.^{14,15}

The initial formation of the organic halide precursor can be challenging as the use of low-volatile alkyl halides as alkylating agents, for example, chloroalkanes in the first step, is time-consuming and might lead to preparative issues on both laboratory and industrial scale. Similarly, the anion metathesis step is problematic due to the onerous removal of metal and halide residues that decidedly influence the physical and chemical behavior of the ILs. Additionally, the stoichiometric formation of an alkali salt, for example, LiCl, as a byproduct is yet another issue in the light of sustainability as exhaustive

extractive work-up is required to suppress the residual halide content to a minimum.¹⁶

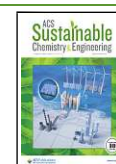
These problems with ion metathesis and residual metal and/or halide content can be circumvented in the synthetic route that relies on dimethyl carbonate as a cheap methylating agent.¹⁷ The method is based on the formation of a methyl carbonate intermediate which is further reacted with equimolar amounts of acid to form the IL upon release of CO_2 and methanol.¹⁸ Although this methodology provides access to a broad range of hydrophilic ILs, the complete neutralization of the methyl carbonate salts can cause contamination with excess reagents.

In 2002, Holbrey et al.¹⁹ reported a method that eliminates the anion metathesis step; direct alkylation of imidazole derivatives with the corresponding dialkyl sulfate led to the formation of the desired IL in one step. A similar strategy has been reported by Kuhlmann and co-workers²⁰ for the preparation of imidazolium dialkyl phosphates. The obtained methyl sulfate- or dimethyl phosphate-based ILs can serve as a

Received: May 13, 2022

Revised: July 18, 2022

Published: August 16, 2022

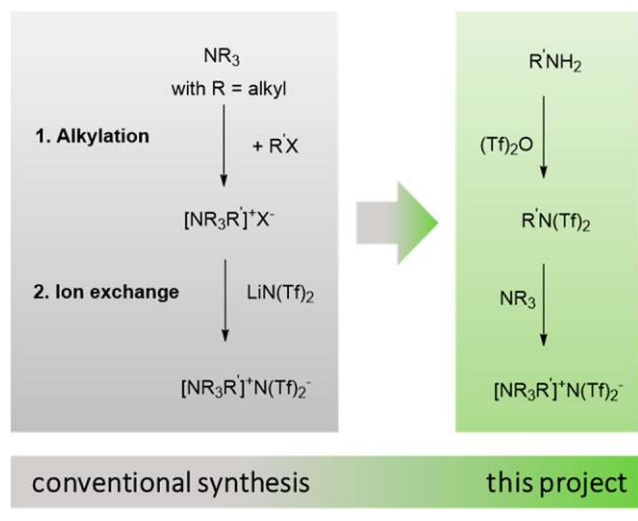


precursor for further modifications, for example, acid-catalyzed transesterification toward the more hydrophobic esters. The high reactivity of the dialkyl sulfates drastically reduces the time and energy demand of the alkylation step; however, these benefits are outweighed by their enormous toxicity as is the case of dimethyl sulfate. Kim et al.²¹ have developed a synthetic method for halide-free ILs using orthoesters in the presence of an acid. Even though they obtained outstanding yields and a broad range of ILs could be produced with this method, the relatively long reaction time required and the formed byproducts are unfavorable from an environmentally benign perspective.

Although strategies already exist for the halide-free preparation of ILs, unfortunately, these methods have certain limitations. Some of them require significantly toxic reactants, while others are hampered by the complicated removal of contaminants associated with excess reagents. There is clearly a need for an entirely halide-free preparation method for hydrophobic ILs that eliminates either the necessity of anion metathesis with its exhaustive extraction steps or the formation of byproducts in the final step.

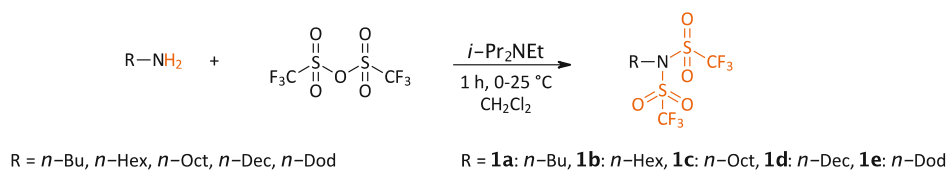
The present research focuses on the development of a halide-free approach for the synthesis of bistriflimide-based hydrophobic ILs *via* formation of alkyl bistriflimides, thus circumventing the problems associated with the state of the art (Scheme 1). The strategy we present offers a benign synthetic

Scheme 1. Toward the Halide-Free Synthesis of Hydrophobic ILs



route and considerable flexibility in the design of sulfonamide-based ILs, starting from cheap and easily accessible nucleophile precursors. The formation of undesirable byproducts is effectively eliminated, while the application of the continuous-flow method significantly decreases the reaction time, providing a rapid and efficient synthesis of hydrophobic ILs.

Scheme 2. Synthesis of Alkyl Bistriflimides as Precursors for IL Synthesis



RESULTS AND DISCUSSION

Initially, we focused on the optimization of the first step of our synthetic route toward the alkylating agents, that is, the formation of various alkyl bistriflimides in a batchwise fashion. The general strategy²² involves the reaction of a primary amine with trifluoromethanesulfonic anhydride (triflic anhydride, Tf₂O) in the presence of a base. As a primary amine as the substrate, butylamine was selected for the optimization of the reaction parameters. Subsequently, the optimized conditions were applied to the synthesis of a range of alkyl bistriflimides with various alkyl chain lengths (C₄–C₁₂, Scheme 2) in order to introduce a broader diversity with regard to the quaternization step. Short-chained amines were not considered in the preparation process due to their gaseous nature. Since ILs bearing an alkyl chain with odd carbon numbers are less frequently mentioned in the literature, we included only even-numbered alkyl groups in this study. However, based on the experimental work, similar results in terms of yield and purity can be expected with odd-numbered alkyl bistriflimides.

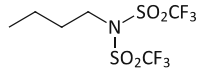
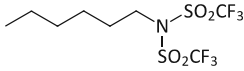
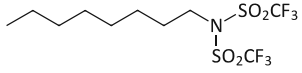
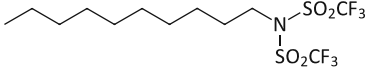
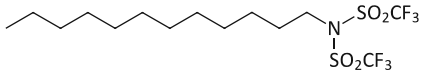
Based on our previous experiments,²³ we used *N,N*-diisopropylethylamine as an acid scavenger and dichloromethane as a solvent.^{24a} Increasing the amount of the reagent by 0.05 equiv (2.00–2.05 equiv) had a significant influence on the reaction rate; 97% conversion was observed after 1 h, while 3 h were required to obtain the same conversion using 2.00 equiv of triflic anhydride. A further increase in the amount of Tf₂O did not significantly favor the reaction rate (see Figure S3, Supporting Information); therefore, a reagent excess of 2.05 equiv was chosen as optimum. It is important to realize that these components—in comparison to the final IL—can be readily purified via distillation, a key advantage compared to the conventional synthesis of bistriflimide-based ILs that only allow for extractive purification. Consequently, after vacuum distillation, the alkyl bistriflimides could be obtained in high purities (see Figures S7–S21, Supporting Information) and with excellent yields (Table 1).

Following the parameter optimization for the synthesis of these alkyl bistriflimide IL precursors, the quaternization step was investigated in detail. All alkylations were first carried out in the batchwise mode, under solvent-free conditions, in glass screw cap vials.

As a model reaction, the synthesis of 1-butyl-3-methylimidazolium bis(trifluoromethylsulfonamido)imide was selected and studied in detail (Scheme 3).

Initially, we investigated the effect of the alkyl bistriflimide's ratio to the nucleophile on the reaction (Figure 1) at 80 °C. None of the ILs yielded full conversion after 24 h when conventional heating was applied; only approximately 90% conversion could be observed, supposedly due to the volatile nature of the alkyl bistriflimides. An increase in the amount of alkyl bistriflimide from 1.00 to 1.30 equiv exerted a pronounced positive effect on the reaction rate, but any further increase of the reactant beyond this did not

Table 1. Batchwise Synthesis of Alkyl Bistriflimides as Precursors for the Halide-Free Preparation of NTf₂⁻-Based ILs^a

entry	structure	isolated yield /%
1a		74
1b		81
1c		74
1d		88
1e		86

^aPerformed with 40.00 mmol (1.00 equiv) primary amine, 82 mmol (2.05 equiv) *i*-Pr₂NEt, and 82.00 mmol (2.05 equiv) trifluoromethanesulfonic anhydride in 110 ml CH₂Cl₂. Reaction time: 1 h. After the addition of the reactant dropwise, the temperature was slowly increased from 0 °C to RT. Products were obtained as slightly yellowish liquids after vacuum distillation.

Scheme 3. Halide-Free Synthesis of 1-Butyl-3-methyl-imidazolium Bistriflimide (2a)

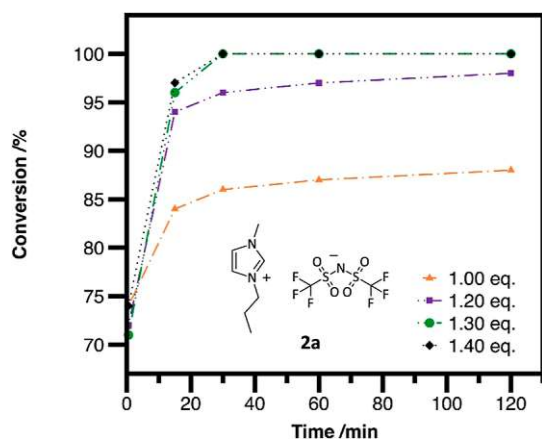
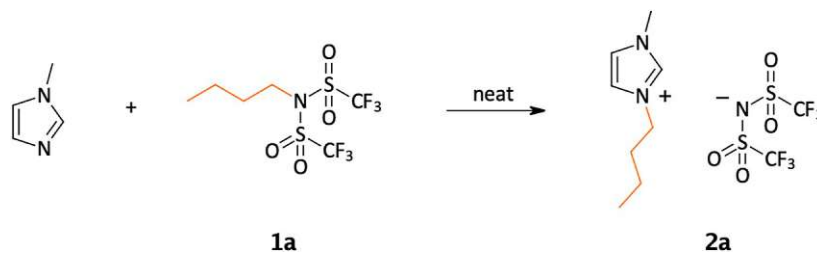


Figure 1. Effect of the alkylating agent equivalents on the reaction rate.

significantly accelerate the reaction further. Using 1.30 equiv of the alkylating agent, full conversion could be reached within 30 min.

To determine the optimal temperature for the quaternization, experiments were carried out at room temperature, 50 and 80 °C. In order to see a more pronounced difference between the results, an increased butyl bistriflimide loading of

1.30 equiv was applied for this optimization stage. The conversion was monitored by ¹H NMR spectroscopy over time; the first sample was taken 30 s after the addition of the reagent, and subsequently, samples were collected at 5 min intervals until the 30th minute and then after 45, 60, 90, 120, and 180 min.^b As expected, the reaction was significantly faster at 80 °C than at 50 °C; after 30 min, full conversion was observed at 80 °C, whereas at 50 °C, 3 h were not sufficient to obtain full conversion (Figure 2, green vs purple). At room temperature, only 49% conversion was observed after 3 h (Figure 2, orange).

The reactivity of the selected alkylating agents was additionally compared, using 1-methylimidazole as a nucleophile, at 80 °C. Since the reaction proceeds fast when 1.30 equiv of the alkylating agent is used, in order to uncover the difference between the reactivities, a 1:1 molar ratio was maintained. No significant difference was observed between the reactivities of butyl bistriflimide (1a) and dodecyl bistriflimide (1e): in the case of the shorter alkyl bistriflimide, 91% conversion was obtained after 24 h, while 82% conversion could be reached using dodecyl bistriflimide. Presumably, the reason for that is that in every case, a primary carbon atom is attacked by the nucleophile, which has a similar steric hindrance in every alkyl bistriflimide. On the other hand, in the case of dodecyl bistriflimide, the moderate hindering

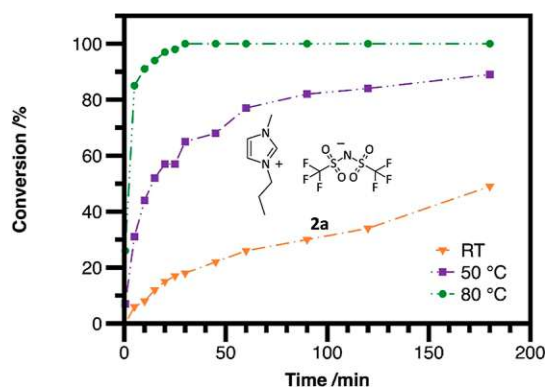


Figure 2. Reaction rate at different temperatures using 1.30 equiv of butyl bistriflimide for the synthesis of **2a**.

influence of the C₁₁ chain connected to the primary carbon atom eventually still exerts a minor influence on the reactivity.

Having optimized the alkyl bistriflimide loading and temperature, we sought to screen different nucleophiles. We focused on ILs that are derived from N-nucleophiles, such as 1-methylimidazole, 1-vinylimidazole, and pyridine, all of which are commercially available at low costs. The vinyl derivatives are of particular interest for the formation of polymeric ILs as conductive polymers; thus, a halide-free protocol is of particular importance.^{25–27}

Gratifyingly, the procedure was found to be quite versatile, as 15 different ILs (**2a–4e**) could be prepared in excellent yield and purity (Scheme 4); furthermore, no undesired polymerization was observed during the alkylation of vinylimidazole-derived species.

We further aimed to reduce the excess of the relatively expensive alkyl bistriflimides since using only 1 equiv is

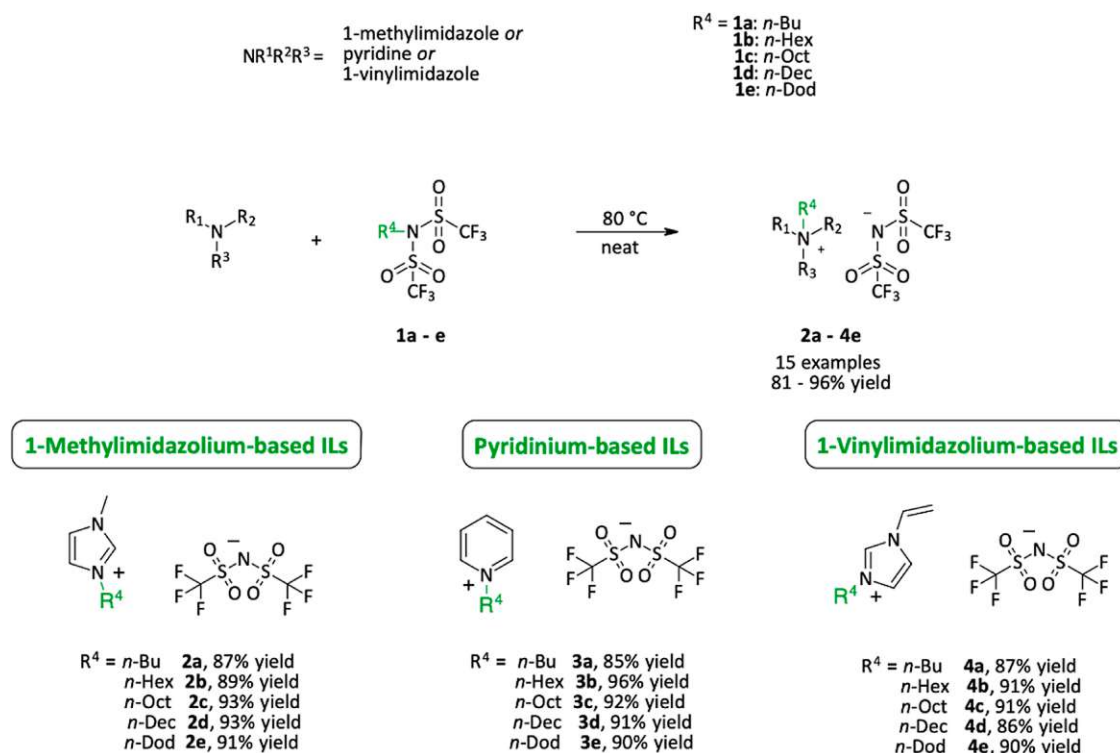
favorable not just from an environmental but also from an economic point of view. Apart from losses due to volatility, the low surface-to-volume ratio of the batchwise process might also limit the reactivity.^{28,29} We therefore investigated the IL synthesis under continuous-flow conditions by using a custom-made microreactor, whose setup is presented in Scheme 5.

As a model reaction, we examined the synthesis of 1-hexyl-3-methylimidazolium bis(trifluoromethylsulfonyl)imide (Scheme 6); in these experiments, an equimolar ratio of the nucleophile and the alkylating agent was maintained.

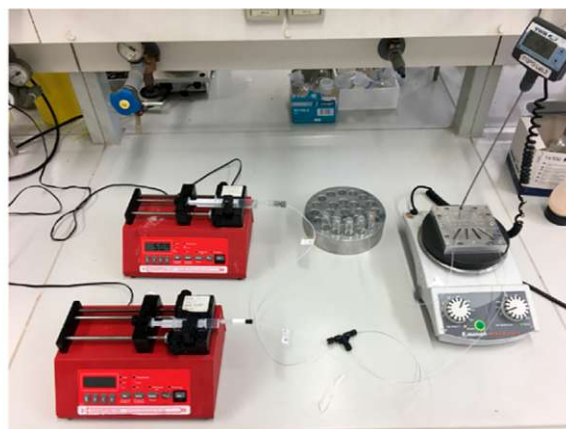
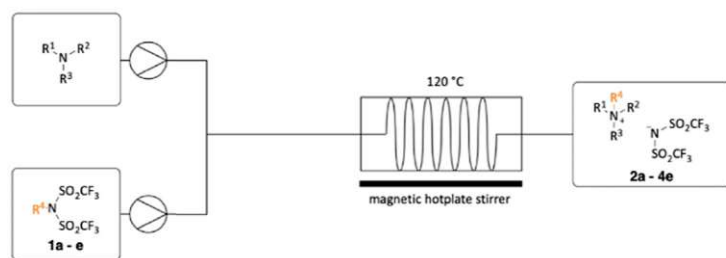
Initially, the influence of the temperature on the reaction was investigated. The flow rates were calculated to maintain a residence time of 15 min in order to provide sufficient mixing. At 80 °C, 79% conversion was observed (entry 1, Table 2), which increased to 90% at 100 °C (entry 2, Table 2), and full conversion could be earned when the temperature was set to 120 °C (entry 3, Table 2). Thereafter, the residence time was varied by increasing the flow rate of the reactants. By doubling the flow rate of the reactants, still full conversion could be observed at 120 °C (entry 6, Table 2), which means that the potentially negative impact of the decreased residence time was outweighed by the better mixing achieved at the increased flow rate. Nevertheless, by a further decrease of the residence time to 5 min, this is not the case anymore: only 92% conversion was observed (entry 7, Table 2).

As it is shown in Figure S4 in the Supporting Information, 7.5 min at 120 °C in the continuous mode yielded full conversion by using only 1.00 equiv from the hexyl bistriflimide. Using the same conditions in the batchwise mode, full conversion was not possible to be reached even when the reaction time was extended to 24 h. This clearly indicates the beneficial effect of the enormous surface-to-volume ratio, which results not just in full conversion but also leads to high productivity. Moreover, while this methodology

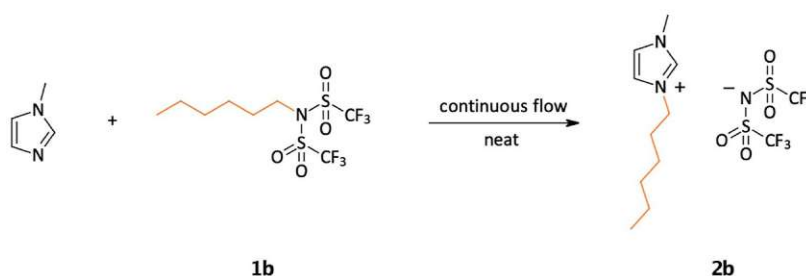
Scheme 4. Scope for the Halide-Free Synthesis of Various NTf₂⁻-Based ILs; Yields Reported Corresponding to Isolated Yields



Scheme 5. Scheme and Setup of the Continuous-Flow Experiments



Scheme 6. Model Reaction for the Continuous-Flow Experiments

Table 2. Parameter Optimization of the Continuous-Flow Experiments for the Synthesis of IL 2b^a

entry	residence time/min	flow rate/ $\mu\text{L min}^{-1}$		temperature/ $^{\circ}\text{C}$	conversion ^b /%
		substrate	reagent (1b)		
1	15	16	51	80	79
2	15	16	51	100	90
3	15	16	51	120	100
4	15	16	51	140	100
5	7.5	32	102	100	89
6	7.5	32	102	120	100
7	5	47	153	120	92

^aReactions were carried out in a 1000 μL reactor fitted with a PTFE capillary tube, and the reagents were supplied with the aid of one—syringe pumps, respectively. Performed with 7.00 mmol 1-methylimidazole and 7.00 mmol hexyl bistriflimide under solvent-free conditions. ^bThe conversion was monitored by ^1H NMR spectroscopy from the crude products. No byproduct formation was observed.

was developed for the synthesis of bistriflimide-based ILs, the microreactor setup and optimized conditions could be used in many other halide-free synthetic approaches, for example, in an orthoester-based or a trimethyl phosphate-based process.

After the initial optimization of the reaction parameters, the continuous-flow synthesis of all the other RTILs (2a–4e) was accomplished. As it can be seen in Table 3, all ILs were obtained with very good yields.

After the NTf_2^- -based ILs have been synthesized both batchwise and in the continuous mode, they were characterized by NMR spectroscopy and high-resolution mass spectrometry (HR-MS). Their water content was determined by Karl Fischer titration. All ILs have a water content of less

than 400 ppm, and the pyridine-based ILs (3a–3e) have less than 300 ppm (Table S1, Supporting Information).

Concerning purity, the synthesized ILs have been analyzed by ion chromatography,³⁰ and a purity of >99.1% was obtained for all ILs synthesized in a continuous flow (Table S1, Supporting Information).

Compared to the halide content of the conventionally synthesized butyl-methylimidazolium bistriflimide ILs, our alternatively developed alkyl bistriflimide-based, halide-free route shows a significant improvement in this regard. The state-of-the-art method requires multiple extraction steps and >200 mL of water to decrease the chloride content to a value below 200 ppm, which is—apart from a considerable workload—yet again unfavorable from an environmentally benign perspective (Table 4). Ultimately, the option for distillation in the case of alkyl bistriflimides can suppress extractive work-up to a minimum compared to the conventional anion metathesis of Cl^- against $\text{N}(\text{Tf})_2^-$ is also favorable in terms of waste generation. Based on the *E*-factor calculations (Figures S5 and S6, Supporting Information), this method generates approx. 15 kg less waste pro kg product.

Concerning energy requirements, the first step of the conventional route involves the alkylation of the desired nucleophile with an alkyl halide at elevated temperature, which can take up to 7 days; therefore, it is unfavorable from an energy efficiency point of view. In comparison, the reaction time for alkyl bistriflimides is 1 h only, without the need of heating but under moderate cooling. Elevated temperature is applied in the second step, but the reaction is carried out in 7.5 min, so the overall process is less energy-consuming. Ultimately, in terms of the financial aspects, the halide-free approach is currently less favorable: assuming that the chemicals are bought from the same provider, and working

Table 3. Continuous-Flow Synthesis of ILs in a 1000 μL Microreactor^a

entry	product	residence time/min	flow rate/ $\mu\text{L min}^{-1}$		temperature/ $^{\circ}\text{C}$	yield/%	productivity/g day ⁻¹
			substrate	reagent (1a–1e)			
1	2a	7.5	35	102	120	90	238
2	2b	7.5	31	102	120	94	241
3	2c	7.5	28	105	120	99	239
4	2d	7.5	25	108	120	98	222
5	2e	7.5	24	110	120	92	211
6	3a	7.5	35	98	120	90	236
7	3b	7.5	32	102	120	92	230
8	3c	7.5	28	105	120	86	205
9	3d	7.5	25	108	120	95	215
10	3e	7.5	24	109	120	90	203
11	4a	7.5	38	95	120	92	243
12	4b	7.5	35	99	120	92	232
13	4c	7.5	31	103	120	98	235
14	4d	7.5	28	106	120	93	212
15	4e	7.5	26	107	120	91	208

^aReactions were carried out in a 1000 μL reactor fitted with a PTFE capillary tube, and the reagents were supplied with the aid of one–one syringe pumps, respectively. The unreacted starting materials were removed under high vacuum (0.3 mbar) at 90 $^{\circ}\text{C}$.

Table 4. Halide Content of IL 2a Produced by Our Method and *via* Anion Metathesis

IL	purity/%	Cl^{-} content/ppm		
		bistriflimide-based method ^a	conventional method ^b	washing step
2a	>99.9	910	#1	40
		840	#2	80
		790	#3	120
		680	#4	140
		520	#5	180
		360	#6	220
		190	#7	240
		160	#8	280

^aIL 2a synthesized *via* the bistriflimide-based method, no removal of chloride residues *via* aqueous extraction required. ^bIL 2a produced by reacting the corresponding chloride IL precursor (1.00 equiv) with LiNTf_2 (1.20 equiv) in water as a solvent. The mixture was stirred for 4 h, IL 2a was extracted with dichloromethane (3 \times 30 mL). Then, the combined organic phases were washed 8 times with 40 mL of distilled water. After each washing step, an aliquot of 2 mL was taken from the organic phase. These samples were concentrated, and their halide content was quantified by ion chromatography.

on the same scale, our method is certainly more expensive as the price of the trifluoromethanesulfonic anhydride drastically increases the costs. However, it should be noted that this estimation refers to high-purity trifluoromethanesulfonic anhydride (>99%) purchased on a small scale and that prices are always subject to the demand. Especially in the case of trifluoromethanesulfonic anhydride, prices vary significantly, and other suppliers, scales, and purities render the cost difference significantly smaller.

CONCLUSIONS

A new synthetic method for the halide-free synthesis of bis(trifluoromethanesulfonyl)imide-based, hydrophobic ILs has been developed. The simple, two-step procedure could give straightforward access to a wide variety of NTf_2 -based ILs with good yields and excellent purities. The quaternization step could be carried out under solvent-free conditions and

provided high atom efficiency without additional waste formation. The reported method is intrinsically halide free, which offers many benefits for the development of new IL-based technologies that are sensitive to halide content. The overall process is significantly less time-consuming than most reported halide-free methods, and due to the reactions' homogeneous nature, it could be successfully performed not just in the batchwise application but also in the continuous-flow operation mode. This provided an even more rapid, safe, and easily scalable synthesis of these ILs, allowing them to be obtained in high yields (86–99%) and productivity, with a residence time of 7.5 min only. The high purity renders this process not just only safe and efficient but eventually also makes the IL products suitable for a significantly broader application range, especially for materials science.

EXPERIMENTAL SECTION

Representative Protocol for the Synthesis of Alkyl Bistriflimides. After transferring 40 mmol (1.00 equiv) of the corresponding amine and *N,N*-diisopropylethylamine (82 mmol, 2.05 equiv) to a three-neck round-bottom flask, 90 mL of anhydrous dichloromethane were added under an argon atmosphere. The mixture was stirred and cooled down *via* a NaCl /ice bath. Then, trifluoromethanesulfonic anhydride (82 mmol, 2.05 equiv) was dissolved in 20 mL of anhydrous dichloromethane, and it was added to the mixture dropwise, while the temperature was maintained below 5 $^{\circ}\text{C}$. Once the triflic anhydride was added, the NaCl /ice bath was removed, and the mixture was stirred at room temperature for 1 h. After that, the mixture was washed with saturated NaHCO_3 solution, 2 N HCl solution, and distilled water. The aqueous phases were back-extracted with dichloromethane. The combined organic layers were dried over Na_2SO_4 , filtered, and concentrated. The residuals were transferred in a round-bottom flask and distilled under vacuum using a Vigreux column. The products were obtained as colorless to slightly yellowish liquids.

General Procedure for the Batchwise Synthesis of ILs. The corresponding nucleophile (2 mmol, 1.00 equiv) was transferred to an 8 mL vial, then it was heated up to 80 $^{\circ}\text{C}$. Once the temperature reached 80 $^{\circ}\text{C}$, 2 mmol (1.00 equiv) alkyl bistriflimide was added, and the mixture was stirred for 24 h. Then, the mixture was transferred into a round-bottom glass flask, and it was dried under high vacuum at elevated temperature overnight (0.3 mbar, 90 $^{\circ}\text{C}$).

General Procedure for the Continuous-Flow Synthesis of ILs. The continuous-flow experiments were performed in a 1000 μL

reactor. The nucleophile and the reagent were supplied with the aid of one–one syringe pumps, respectively. The reactor was heated up to the desired temperature with the aid of a magnetic hotplate stirrer, and the syringes were filled with the reagents (7.00 mmol from both the nucleophiles and the alkyl bistriflimides). After starting the pumps, the dead volume of the reactor was allowed to pass. The products were then collected into tared round-bottom flasks for a calculated amount of time. The unreacted starting materials were removed under high vacuum (0.3 mbar) at 90 °C overnight.

■ ASSOCIATED CONTENT

SI Supporting Information

The Supporting Information is available free of charge at <https://pubs.acs.org/doi/10.1021/acssuschemeng.2c02871>.

Detailed characterization of the alkyl bistriflimides and ILs via ^1H -, ^{13}C -, and ^{19}F NMR spectroscopies, HR-MS spectroscopy, and infrared spectroscopy; halide and water content of the ILs; and kinetic analysis of IL formation (PDF)

■ AUTHOR INFORMATION

Corresponding Author

Katharina Bica-Schröder – Institute of Applied Synthetic Chemistry, TU Wien, Vienna 1060, Austria; orcid.org/0000-0002-2515-9873; Phone: +43 1 58801 163601; Email: katharina.schroeder@tuwien.ac.at

Authors

Kristof Stagel – Institute of Applied Synthetic Chemistry, TU Wien, Vienna 1060, Austria

Andrea Szpecht – Poznan Science and Technology Park, Adam Mickiewicz University Foundation, Poznan 61-612, Poland; orcid.org/0000-0003-3865-3878

Dawid Zielinski – Poznan Science and Technology Park, Adam Mickiewicz University Foundation, Poznan 61-612, Poland; Faculty of Chemistry, Adam Mickiewicz University in Poznan, Poznan 61-614, Poland; orcid.org/0000-0002-8372-6581

Marcin Smiglak – Poznan Science and Technology Park, Adam Mickiewicz University Foundation, Poznan 61-612, Poland

Michael Schnürch – Institute of Applied Synthetic Chemistry, TU Wien, Vienna 1060, Austria; orcid.org/0000-0003-2946-9294

Complete contact information is available at:

<https://pubs.acs.org/doi/10.1021/acssuschemeng.2c02871>

Funding

Open Access is funded by the Austrian Science Fund (FWF).

Notes

The authors declare no competing financial interest.

■ ACKNOWLEDGMENTS

Financial support by the Austrian Science Fund (FWF, grant P 32882-N) is gratefully acknowledged. The authors would like to thank Olga Lanaridi, Ádám Márk Pálvolgyi, and Fabian Scharinger for the scientific support.

■ ADDITIONAL NOTES

^aIn the literature, most room-temperature reactions with triflic anhydride are carried out in dichloromethane, while other solvents such as diethyl ether or THF are mostly used at extremely low (−78 °C) temperatures. Importantly, it is only

CH_2Cl_2 that is inert enough against triflic anhydride at room temperature, as even solvents such as THF react with TF_2O under such conditions. To avoid the necessity of cooling, we decided to use dichloromethane but kept the required amount to a minimum due to its unfavorable environmental footprint.^bTo suppress the progression of the reaction after the sampling, all samples were immediately cooled to room temperature and diluted with CDCl_3 after their collection.

■ REFERENCES

- (1) Jork, C.; Seiler, M.; Beste, Y.-A.; Arlt, W. Influence of Ionic Liquids on the Phase Behavior of Aqueous Azeotropic Systems. *J. Chem. Eng. Data* **2004**, *49*, 852–857.
- (2) Endres, F.; Zein El Abedin, S. Air and water stable ionic liquids in physical chemistry. *Phys. Chem. Chem. Phys.* **2006**, *8*, 2101–2116.
- (3) Lu, Q.; Wang, H.; Ye, C.; Liu, W.; Xue, Q. Room temperature ionic liquid 1-ethyl-3-hexylimidazolium-bis(trifluoromethylsulfonyl)-imide as lubricant for steel–steel contact. *Tribol. Int.* **2004**, *37*, 547–552.
- (4) Kawano, R.; Matsui, H.; Matsuyama, C.; Sato, A.; Susan, M. A. B. H.; Tanabe, N.; Watanabe, M. High performance dye-sensitized solar cells using ionic liquids as their electrolytes. *J. Photochem. Photobiol., A* **2004**, *164*, 87–92.
- (5) Yasuda, T.; Watanabe, M. Protic ionic liquids: Fuel cell applications. *MRS Bull.* **2013**, *38*, 560–566.
- (6) Zhang, H.; Liang, J.; Xia, B.; Li, Y.; Du, S. Ionic liquid modified Pt/C electrocatalysts for cathode application in proton exchange membrane fuel cells. *Front. Chem. Sci. Eng.* **2019**, *13*, 695–701.
- (7) Xiao, H. Ionic Liquid Lubricants: Basics and Applications. *Tribol. Trans.* **2017**, *60*, 20–30.
- (8) Seddon, K. R.; Stark, A.; Torres, M.-J. Influence of chloride, water, and organic solvents on the physical properties of ionic liquids. *Pure Appl. Chem.* **2000**, *72*, 2275–2287.
- (9) Dyson, J.; Welton, J.; Parker, T.; Parker, G. Arene hydrogenation in a room-temperature ionic liquid using a ruthenium cluster catalyst. *Chem. Commun.* **1999**, 25–26.
- (10) Gallo, V.; Mastroilli, P.; Nobile, C. F.; Romanazzi, G.; Suranna, G. P. How does the presence of impurities change the performance of catalytic systems in ionic liquids? A case study: the Michael addition of acetylacetone to methyl vinyl ketone. *J. Chem. Soc., Dalton Trans.* **2002**, 4339–4342.
- (11) Dyson, P. J. Transition metal chemistry in ionic liquids. *Transition Met. Chem.* **2002**, *27*, 353–358.
- (12) Davies, D. L.; Kandola, S. K.; Patel, R. K. Asymmetric cyclopropanation in ionic liquids: effect of anion and impurities. *Tetrahedron: Asymmetry* **2004**, *15*, 77–80.
- (13) Wasserscheid, P.; Keim, W. Ionic Liquids—New “Solutions” for Transition Metal Catalysis. *Angew. Chem., Int. Ed.* **2000**, *39*, 3772–3789.
- (14) Lévêque, J.-M.; Estager, J.; Draye, M.; Cravotto, G.; Boffa, L.; Bonrath, W. Synthesis of Ionic Liquids Using Non Conventional Activation Methods: An Overview. *Monatsh. Chem.* **2007**, *138*, 1103–1113.
- (15) Del Sesto, R. E.; McCleskey, T. M.; Macomber, C.; Ott, K. C.; Koppisch, A. T.; Baker, G. A.; Burrell, A. K. Limited thermal stability of imidazolium and pyrrolidinium ionic liquids. *Thermochim. Acta* **2009**, *491*, 118–120.
- (16) Bonta, M.; Anderl, T.; Cognigni, A.; Hejazifar, M.; Bica, K.; Limbeck, A. Determination of residual chloride content in ionic liquids using LA-ICP-MS. *RSC Adv.* **2016**, *6*, 90273–90279.
- (17) Smiglak, M.; Holbrey, J. D.; Griffin, S. T.; Reichert, W. M.; Swatoski, R. P.; Katritzky, A. R.; Yang, H.; Zhang, D.; Kirichenko, K.; Rogers, R. D. Ionic liquids via reaction of the zwitterionic 1,3-dimethylimidazolium-2-carboxylate with protic acids. Overcoming synthetic limitations and establishing new halide free protocols for the formation of ILs. *Green Chem.* **2007**, *9*, 90–98.

- (18) Maton, C.; Van Hecke, K.; Stevens, C. V. Peralkylated imidazolium carbonate ionic liquids: synthesis using dimethyl carbonate, reactivity and structure. *New J. Chem.* **2015**, *39*, 461–468.
- (19) Holbrey, J. D.; Reichert, W. M.; Swatloski, R. P.; Broker, G. A.; Pitner, W. R.; Seddon, K. R.; Rogers, R. D. Efficient, halide free synthesis of new, low cost ionic liquids: 1,3-dialkylimidazolium salts containing methyl- and ethyl-sulfate anions. *Green Chem.* **2002**, *4*, 407–413.
- (20) Kuhlmann, E.; Himmler, S.; Giebelhaus, H.; Wasserscheid, P. Imidazolium dialkylphosphates—a class of versatile, halogen-free and hydrolytically stable ionic liquids. *Green Chem.* **2007**, *9*, 233–242.
- (21) Kim, D. J.; Oh, K. H.; Park, J. K. A general and direct synthesis of imidazolium ionic liquids using orthoesters. *Green Chem.* **2014**, *16*, 4098–4101.
- (22) Arvai, R.; Toulgoat, F.; Langlois, B. R.; Sanchez, J.-Y.; Médebielle, M. A simple access to metallic or onium bistrifluoromethanesulfonimide salts. *Tetrahedron* **2009**, *65*, 5361–5368.
- (23) Bica, K.; Schön, M.; Gärtner, P.; Mihovilovic, M. Method for Producing Ionic Liquids. WO 2017112972 A1, 2017.
- (24) Tezuka, Y.; Goethals, E. J. Synthesis and reactions of poly-tetrahydrofuran with azetidinium salt end-groups. *Eur. Polym. J.* **1982**, *18*, 991–998.
- (25) Bozkurt, A.; Meyer, W. H. Proton conducting blends of poly(4-vinylimidazole) with phosphoric acid. *Solid State Ionics* **2001**, *138*, 259–265.
- (26) Arslan, A.; Kiralp, S.; Toppare, L.; Bozkurt, A. Novel Conducting Polymer Electrolyte Biosensor Based on Poly(1-vinylimidazole) and Poly(acrylic acid) Networks. *Langmuir* **2006**, *22*, 2912–2915.
- (27) Mecerreyes, D. Polymeric ionic liquids: Broadening the properties and applications of polyelectrolytes. *Prog. Polym. Sci.* **2011**, *36*, 1629–1648.
- (28) Souza, J. M.; Galaverna, R.; Souza, A. A. N.; Brocksom, T. J.; Pastre, J. C.; Souza, R.; Oliveira, K. T. Impact of continuous flow chemistry in the synthesis of natural products and active pharmaceutical ingredients. *An. Acad. Bras. Cienc.* **2018**, *90*, 1131–1174.
- (29) Lapkin, A. A.; Plucinski, P. K. Engineering Factors for Efficient Flow Processes in Chemical Industries. *Chemical Reactions and Processes under Flow Conditions*; The Royal Society of Chemistry, 2009; Chapter 1, pp 1–43.
- (30) Szepecht, A.; Zajac, A.; Zielinski, D.; Maciejewski, H.; Smiglak, M. Versatile Method for the Simultaneous Synthesis of Two Ionic Liquids, Otherwise Difficult to Obtain, with High Atom Economy. *ChemistryOpen* **2019**, *8*, 972–983.

Combining Tailored Ionic Liquids with $Ti_3C_2T_x$ MXenes for an Enhanced Load-Carrying Capacity Under Boundary Lubrication

Philipp G. Grützmaier, Roman Neuhauser, Kristof Stigel, Katharina Bica-Schröder, Guido Boidi, Carsten Gachot,* and Andreas Rosenkranz*

To improve the efficiency and lifetime of mechanical components, new lubrication systems are needed. Two complementary material classes, which have demonstrated a promising tribological performance, are ionic liquids and MXenes (2D transition metal carbides and nitrides). Herein, $Ti_3C_2T_x$ MXenes are used as additives in ionic liquids (ILs) to improve their load-carrying capacity under boundary lubrication. The specifically synthesized ILs share the same cation (trioctyl(methyl)phosphonium) but different anions (dimethyl phosphate and dibutyl phosphate for IL1 and IL2, respectively) to assess the effect of the anion's alkyl chain length. The wear reduction performance is tested with a cylinder-on-ring contact in a standardized Brugger tester, which is suitable to study boundary lubrication and to assess the antiwear ability of the IL/MXene lubricant blends. MXenes indicate an excellent dispersibility in both ILs over 24 h. It is found that, irrespective of the used IL, the addition of MXenes always increases the load-carrying capacity. Particularly, significantly reduced wear and thus a high load-carrying capacity are observed for the combination IL2/MXenes, which also outperform fully formulated commercially available lubricants such as turbine oils.

1. Introduction

The ongoing climate crisis demands for more energy-efficient mechanical systems, which will reduce the consumption of resources and emission of greenhouse gases. Consequently, this requires the development of new lubricants, which minimize friction and wear, are ecofriendly, and above all not based on crude oil.^[1,2]

Two material classes, which have great potential to be used as future lubricants due to their extraordinary tribological behavior, are ionic liquids (ILs) and 2D materials.^[3–5] ILs are molten salts in liquid state containing an organic cation and an anion, which can be either organic or inorganic.^[5,6] There are numerous different cations and anions available, making the properties of ILs tunable.^[5] Furthermore, they possess an excellent thermal stability, high heat capacity, good electrical conduc-


tivity, and are often considered as ecofriendly materials due to their low volatility and nonflammability.^[7,8] These properties give ILs various advantages over conventional liquid lubricants (oils and greases). The superior tribological performance has been first reported for an IL (1-methyl-3-hexylimidazolium tetrafluoroborate) by Ye et al.^[7] Subsequently, numerous ILs have been synthesized and their excellent tribological behavior as base lubricant or lubricant additive was systematically studied.^[9] Several studies have also verified superlubricious states, that is, a coefficient of friction (COF) below 0.01, when using ILs.^[10,11] The lubricating mechanism of ILs is based on the formation of thin films (as thin as a monolayer) on the involved rubbing surfaces.^[5] These films are either adsorbed layers with a layered structure possessing a low shear strength^[12] or protective layers induced by tribochemical reactions between the IL and the rubbing material surfaces.^[6] The load-carrying capacity and antiwear properties of ILs can be further enhanced by the addition of 2D layered materials, such as graphene,^[13] graphene oxide,^[14] or MoS_2 ,^[15] thus improving the ILs' tribological performance particularly under severe conditions. The ionic nature of ILs often allows for a good dispersibility of nanomaterials in the IL base liquid, which is crucial for their tribological performance.^[13] The 2D materials can be adsorbed onto the contacting surfaces, where they form low-shear tribolayers, thereby protecting the surfaces from wear.^[16]

P. G. Grützmaier, R. Neuhauser, C. Gachot
Institute for Engineering Design and Product Development
Research Unit Tribology E307-05
TU Wien
1060 Vienna, Austria
E-mail: carsten.gachot@tuwien.ac.at

K. Stigel, K. Bica-Schröder
Institut für Angewandte Synthesechemie (IAS)
Sustainable Organic Synthesis and Catalysis research group
TU Wien
1060 Vienna, Austria

G. Boidi
AC2T research GmbH
Viktor-Kaplan-Straße 2/C, 2700 Wiener Neustadt, Austria

A. Rosenkranz
Department of Chemical Engineering
Biotechnology and Materials (FCFM)
Universidad de Chile
Santiago 8370448, Chile
E-mail: arosenkranz@ing.uchile.cl

 The ORCID identification number(s) for the author(s) of this article can be found under <https://doi.org/10.1002/adem.202300721>.

DOI: 10.1002/adem.202300721

A rather new member of the 2D material family are MXenes, which are 2D layered transition metal carbides, nitrides, and carbonitrides based on MAX phases.^[17] The structure of MXenes (general formula $M_{n+1}X_nT_x$) is composed of alternating layers of transition metal atoms (M) and carbon or nitrogen atoms (X), whereby the outer layers are always X atoms, which are terminated with functional groups (T_x), such as -O, -OH, and -F.^[18] MXenes have been used in energy storage,^[19] sensing,^[20] or catalysis.^[21] However, their layer structure with reduced bonding strength between the layers renders MXenes also interesting for tribological applications.^[22] MXenes' interlayer binding energy and, therefore, the friction between the layers are significantly influenced by the surface terminations,^[23,24] making it possible to tailor their tribological properties. MXenes have already demonstrated their promising tribological performance on the nano-scale,^[25,26] the laboratory scale,^[27,28] and even when used for lubricating machine elements.^[29] They can be used as solid lubricant coatings,^[27,30] lubricious phase in composites,^[31] or lubricant additives.^[32] Recently, it has been shown that synergistic effects are induced by combining lithium hexafluorophosphate-based ILs and molybdenum carbide (Mo_2CT_x) MXenes as lubricating additives.^[33] In ball-on-disk tests, a protecting tribolayer with low shear strength consisting of molybdenum and phosphorous oxides intermixed with as-deposited MXenes was formed, which resulted in macroscale superlubricity (COF of 0.004) at contact pressures up to 1.42 GPa. While MXenes as solid lubricant coatings have been found to work well under medium contact pressures below 1 GPa, they are easily degraded when the contact pressures are too high, leading to reduced wear life.^[34] Therefore, for severely loaded contacts, the combination with ILs can be beneficial, as MXenes are embedded into the IL-based tribolayers, leading to a slower degradation and improved tribological performance.

Based on the presented state of the art, it becomes evident that MXenes have been scarcely tested as lubricant additives in ILs. Considering the chemical diversity and tunability of both ILs and MXenes, we anticipate significant potential to optimize the resulting tribological performance when combining ILs with MXenes. Therefore, in this study, we investigate the tribological behavior of $Ti_3C_2T_x$ MXenes as additives in two different ILs (P8881(MeO)₂PO₂ (IL1) and P8881(BuO)₂PO₂ (IL2), which are prepared in a halide-, chlorine-, and fluoride-free manner to avoid tribocorrosion issues in the respective metal contacts. In this regard, multilayer $Ti_3C_2T_x$ has been chosen since it is the most explored MXene in tribology and, therefore, serves as an excellent benchmark. The experiments are performed on a Brügger lubricant tester (DIN 51347-1), which is particularly suitable for studying boundary lubrication, thus allowing to assess MXenes' effect on the load-carrying capacity and antiwear ability of IL-based lubricants. The results demonstrate that MXenes can improve the load-carrying capacity of ILs under extreme conditions. This is a crucial step for using the tunability of both involved materials to create tailored lubricants.

2. Experimental Section

2.1. Synthesis and Characterization of MXene Nanosheets

Multilayer $Ti_3C_2T_x$ nanosheets were fabricated by selective etching of 2 g of MAX- Ti_3AlC_2 powder (purchased from Forsman

Scientific Co. Ltd., Beijing, China) in 20 mL of highly concentrated hydrofluoric acid (HF) with a concentration of 40 wt%. The mixture of Ti_3AlC_2 powder and HF was stirred at a speed of 60 rpm and a temperature of 35 °C for 24 h. After etching, the mixture was centrifuged at 3500 rpm and washed with deionized water in several washing cycles until a final pH of 6 was obtained and the residue was collected. Finally, the suspension was vacuum filtrated and freeze dried for 24 h at -60 °C (pressure below 30 Pa).

The structure, quality, and interlayer distance of the as-synthesized multilayer $Ti_3C_2T_x$ nanosheets were characterized by transmission electron microscopy (TEM, Tecnai F20, FEI) using an acceleration voltage of 200 kV. To characterize their surface chemistry, Raman spectra were obtained applying a Witec Alpha 300 RA in backscattering geometry and an excitation wavelength of 532 nm. The spectra were acquired between 80 and 1000 cm^{-1} with an acquisition time of 128 s for each spectrum and a spectral resolution of 3 cm^{-1} using a 300 $L\ mm^{-1}$ grating.

2.2. Synthesis of Ionic Liquids and Preparation of Lubricants

Two ILs, P8881(MeO)₂PO₂ (IL1) and P8881(BuO)₂PO₂ (IL2), were synthesized from the corresponding phosphines and alkyl phosphates in batch or continuous mode for optional scale-up. They share the same cation (trioctyl(methyl)phosphonium), while having dimethyl phosphate (DMP) anions and dibutyl phosphate (DBP) as anions in case of IL1 and IL2, respectively (Figure 1).

2.2.1. P8881(MeO)₂PO₂ (IL1)

As-synthesized and distilled trioctylphosphine (1.0 equiv.) were transferred to a round-bottomed flask under argon atmosphere. Subsequently, trimethyl phosphate (1.2 equiv.) was added to the flask under continuous stirring. The temperature was increased stepwise to 140 °C, and the mixture was stirred under inert atmosphere for 72 h. After completion of the reaction, the excess trimethyl phosphate was removed under vacuum

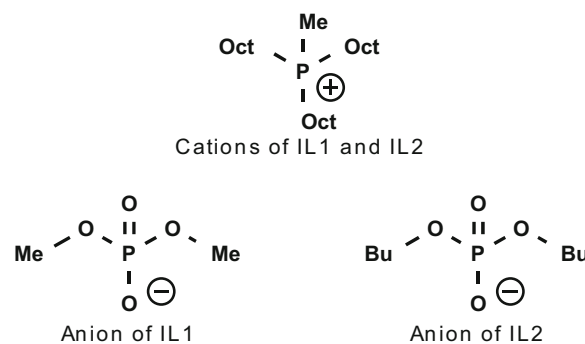


Figure 1. Chemical structures of the synthesized ionic liquids, namely P8881(MeO)₂PO₂ (IL1) and P8881(BuO)₂PO₂ (IL2). Both ionic liquids share the same cation (trioctyl(methyl)phosphonium (P8881)) but possess different anions, dimethyl phosphate (DMP) and dibutyl phosphate (DBP) for IL1 and IL2, respectively.

(0.2 mbar, 95 °C). The desired product ($\text{P8881}(\text{MeO})_2\text{PO}_2^-$) was obtained as an orange, viscous liquid at a yield of 98%.

In the future, ILs can be synthesized in a continuous manner (Vapourtec E-Series Flow Chemistry System) for scale-up. In this method, a tube reactor was used, which is designed for high-temperature reactions. In the continuous process, a 25 mL Vapourtec high-temperature tube reactor was used, operating at 240 °C. The two reactants were supplied to the reactor in a manner where an equimolar ratio was maintained during the reaction, with flow rates of $0.129 \text{ mL min}^{-1}$ for trimethyl phosphate and $0.496 \text{ mL min}^{-1}$ for trioctylphosphine, respectively. This corresponded to a residence time of 40 min. With the continuous method, a conversion of 75% as reached, and work-up can be performed accordingly.

2.2.2. $\text{P8881}(\text{BuO})_2\text{PO}_2$ (IL2)

$\text{P8881}(\text{BuO})_2\text{PO}_2$ was obtained in a subsequent synthesis step using IL1 as reaction product. A round-bottomed flask was charged with ($\text{P8881}(\text{MeO})_2\text{PO}_2$) (1.0 eq.) and dibutyl phosphate (1.2 eq.) under argon atmosphere. Afterward, triethylamine (1.4 eq.) was added dropwise under cooling in an ice bath. After the addition was complete, the reaction mixture was stirred for 20 min at 0 °C and overnight at room temperature. Distilled water was then infused to the mixture, before vigorously stirring it for 16 h at room temperature. The mixture was transferred in a separatory funnel and washed one time with a mixture of triethylamine and distilled water ($10:90 \text{ v v}^{-1}$) and four times with distilled water. Finally, the residual water was removed under vacuum (0.2 mbar, 95 °C). The desired ionic liquid $\text{P8881}(\text{BuO})_2\text{PO}_2$ was obtained as a slightly yellowish, viscous liquid with a yield of 97%.

The viscosities of IL1 and IL2 were evaluated at 40 and 100 °C (Table 1). For 40 °C, IL1 showed a kinematic viscosity of 496 cSt.

Table 1. Kinematic viscosities of the ionic liquids (IL1 and IL2) measured at 40 and 100 °C.

Ionic liquid	Viscosity @ 40 °C [cSt]	Viscosity @ 100 °C [cSt]
IL1	496	32
IL2	223	20

At 100 °C, the viscosity drastically dropped to 32 cSt. IL2 had a lower kinematic viscosity of 223 cSt at 40 °C and 20 cSt at 100 °C, respectively.

For the tests with MXene additives, dispersions with MXene concentration of 0.5 wt% in the ILs were prepared, which was a concentration typically used for solid lubricant additives.^[35] The dispersions were mixed using a magnetic stirrer for 15 min followed by ultrasonication for 20 min to ensure a homogeneous dispersion. The dispersion stability was controlled by visual inspection in time intervals of 15, 30, 60, and 120 min as well as after 1440 min (24 h).

2.3. Tribological Experiments

The tribological performance of the ILs **with** and **without** $\text{Ti}_3\text{C}_2\text{T}_x$ under boundary lubrication was studied using a standardized Bruggen tribometer according to the aforementioned DIN 51347-1. The test provided information on the lubricant's load-carrying capacity under pure sliding conditions at room temperature. The experimental conditions allowed for the suitability of the used lubricant system under severe test conditions and due to the use of a standardized test the results could be compared to those available in the literature. The contact was established between a fixed cylinder (AISI 52100) with a diameter of 18 mm and a rotating ring (AISI D6) with an outer diameter of 25 mm (Figure 2). Prior to the test, 8 mL of the test lubricant was poured onto the ring surface. Due to the high viscosity of the ILs, a thick film formed on the entire surface of the ring. Afterward, a constant load F_N of 400 N was applied (equivalent to an initial Hertzian contact pressure of 1.4 GPa) and the ring rotated with a constant speed of 960 r min^{-1} for 30 s, being equivalent to 1.2 m s^{-1} . After a lubricant-dependent run-time period, steel–steel contact occurred, simulating an oil starvation period. As a result, a well-defined elliptical wear scar was generated on the fixed cylinder with the major axis a and minor axis b in x - and y -direction (Figure 2). The performance of a lubricant was evaluated by analyzing the contact area that expanded linearly with time and was inversely proportional to the load-carrying capacity of the tested lubricants.^[36] To determine the contact area and the dimensions of the major and minor axis (a and b), a laser scanning confocal microscope (Keyence VK-X1000 3D) was used. Equation (1) was used to calculate the Bruggen load-carrying capacity B (N mm^{-2}) of

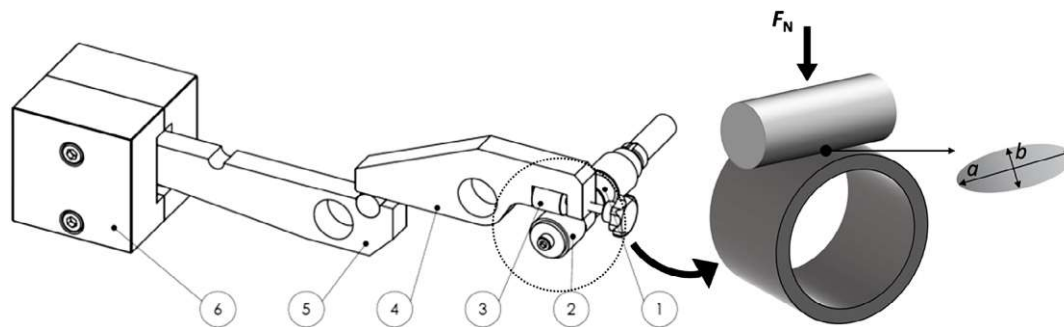


Figure 2. Schematic representation of the contact configuration of the Bruggen tests and the resulting elliptical wear track on the cylinder with the major and minor axes a and b . (1) drive shaft, (2) rotating ring, (3) clamped cylinder, (4) sample lever, (5) load lever, and (6) "dead" weight.

the tested lubricants. Three repetitions were carried out under the same test conditions to calculate an average load-carrying capacity.

$$B = \frac{4 \cdot F_N}{a \cdot b \cdot \pi} \quad (1)$$

3. Results and Discussion

As confirmed by TEM, the used synthetic approach resulted in multilayer $\text{Ti}_3\text{C}_2\text{T}_x$ flakes with an interlamellar spacing of 0.91 ± 0.09 nm (Figure 3a,b). These values align well with published data in literature.^[27] The selected-area electron diffraction (SAED) pattern (inset in Figure 3b) confirmed the hexagonal structure of the multilayer $\text{Ti}_3\text{C}_2\text{T}_x$.^[37] Raman spectroscopy (Figure 3c) was conducted to obtain more information about their surface chemistry. The Raman spectrum of the as-synthesized $\text{Ti}_3\text{C}_2\text{T}_x$ showed vibrational modes at 160, 220, and 707 cm^{-1} , as well as broader peaks around 285, 376, and 600 cm^{-1} , which are associated with the respective $-\text{O}$, $-\text{OH}$, and $-\text{F}$ surface terminations. The obtained Raman peaks correlate well with data published in literature.^[38]

Prior to tribological testing, the stability of the dispersions was inspected (Figure 4) since this aspect has been shown to significantly affect the tribological properties of lubricants with MXenes.^[39] Visual inspection of the as-prepared ILs and MXene dispersions did not show any sign of MXene precipitation or sedimentation neither in IL1 nor in IL2 up to 24 h (1440 min). Therefore, it can be concluded that the compatibility between $\text{Ti}_3\text{C}_2\text{T}_x$ and the used ILs is excellent. Although the used ILs are hydrophobic, their intrinsic ionic nature results in strong

electrostatic interactions with the polar MXenes.^[40] Moreover, MXenes contain reactive $-\text{OH}$ groups on their surface. Negatively charged ions are known to interact with H-containing bonds, resulting in the formation of a charge-induced hydrogen bond.^[41] The IL's anion may interact with the MXenes' polar $\text{O}-\text{H}$ bond in such a manner, thus enhancing the interaction between ILs and MXenes, leading to enhanced dispersibility. Additionally, both ILs are highly viscous, which prevents reagglomeration and sedimentation of MXenes after dispersion, thus also contributing to their excellent dispersibility.^[42] Overall, we conclude that an influence of reagglomeration and reduced dispersion stability over time on the tribological behavior of the ILs with MXene additives is negligible.

The tribological properties of the ILs with and without MXenes are studied on a Brugger tester, simulating high-pressure conditions (boundary lubrication). The elliptical wear scars formed during the tests on the upper cylinders are shown in Figure 5. Apart from the dimensions of the wear scars, their appearance is similar independent of the lubricant used with signs of abrasive and adhesive wear. The high load applied during the tests results in boundary lubrication conditions with predominant solid–solid contact, which is clearly demonstrated by the significant wear of the cylinder surfaces. However, based on the reduced dimensions of the wear scar, a higher wear resistance can be observed for IL2 compared to IL1, while the addition of MXenes also positively influenced the resulting performance.

The wear resistance under high-pressure conditions is further evaluated with respect to the Brugger load-carrying capacity (Figure 6). As the load-carrying capacity is determined by dividing the applied normal load by the area of the wear scar, a higher load-carrying capacity implies a better wear resistance. The average load-carrying capacities for the pure IL1 and IL2 are 25.7 and

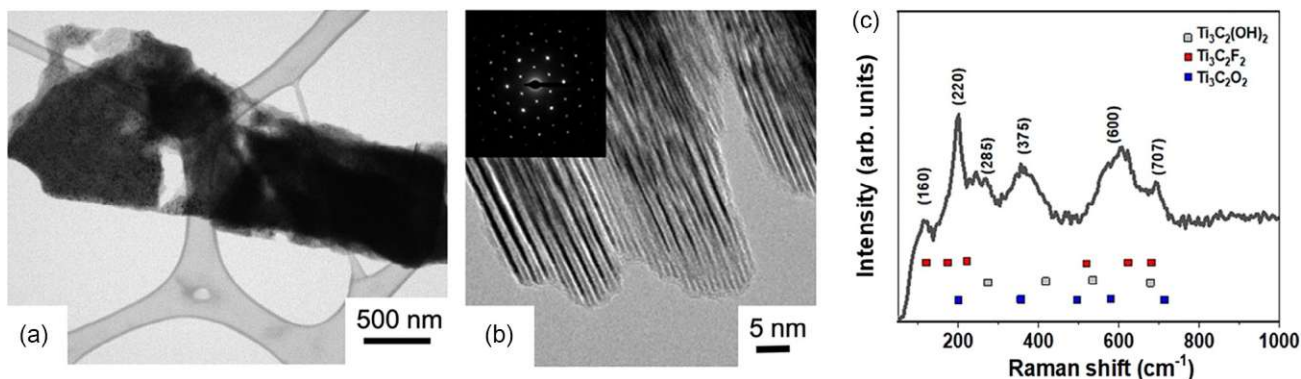


Figure 3. TEM micrographs in a) low and b) high resolution c) with the corresponding Raman spectrum of the as-synthesized multilayer $\text{Ti}_3\text{C}_2\text{T}_x$.

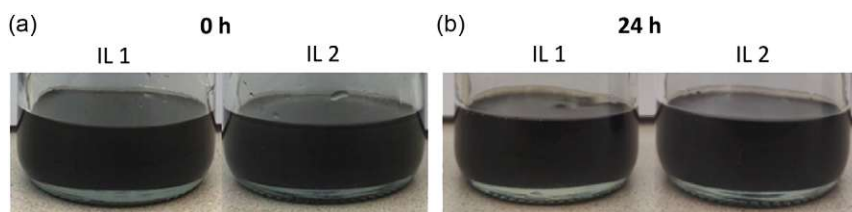


Figure 4. MXene dispersion in the ionic liquids IL1 and IL2 a) directly after stirring and ultrasonication and b) after 24 h.

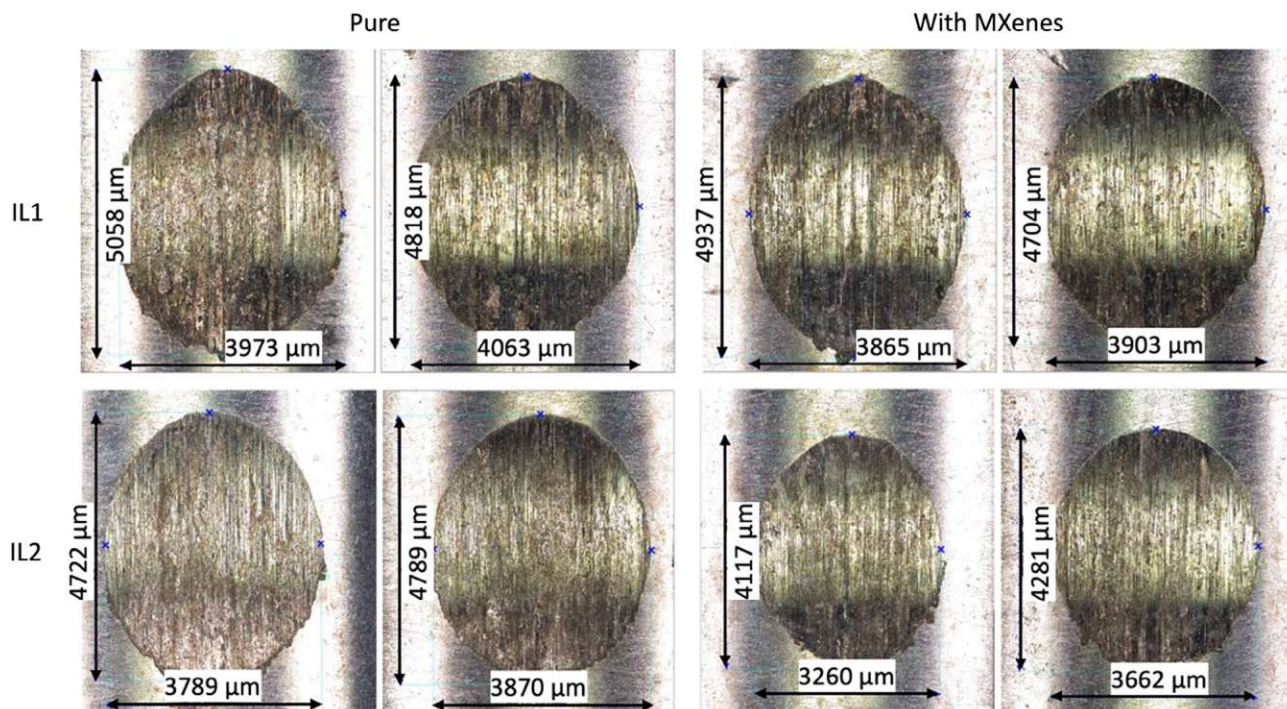


Figure 5. Wear scars on the cylinders after the Brugger test with the ionic liquids IL1 and IL2 with and without $Ti_3C_2T_x$ additives (pure, images on the left). From the dimensions a and b of the wear scars, the Brugger load-carrying capacity is determined according to Equation (1). Two different wear scars are shown for all lubricant formulations, showing a good reproducibility of the tests.

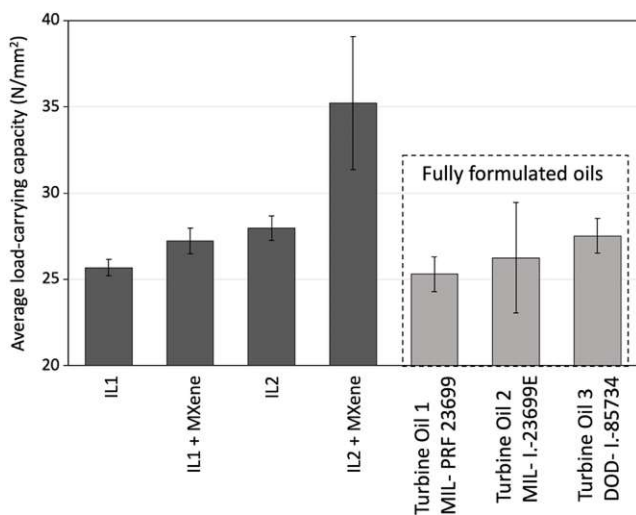


Figure 6. Average Brugger load-carrying capacity for the pure ILs 1 and 2 as well as the ILs additivated with 0.5 wt% of MXenes. As a comparison, the average Brugger load-carrying capacity of fully formulated turbine oils is provided.^[36]

28.0 N mm^{-2} , respectively. These values are substantially higher than that of a non-additivated FVA2 base oil as well as comparable to fully formulated and commercially used turbine oils measured using the same test setup.^[6,36] We already demonstrated the effectiveness of ILs to improve the antiwear properties of a FVA2 base oil when used as additives with a concentration

of 5 wt%, which was attributed to the formation of a phosphate-rich tribolayer.^[6] The pure ILs slightly increased the load-carrying capacity compared to the IL additivated base oils. We trace this observation back to their high viscosity promoting a thicker lubricant film as well as the greater availability of phosphorous-based compounds to form beneficial tribolayers. This is supported by the fact that ILs have shown to readily form tribolayers due to their inherent polarity, which facilitates self-adsorption.^[43]

Based on our results, IL2 containing the anion with the butyl groups performs better than IL1 (anion with methyl groups). This contradicts previous studies with these ILs showing better performance for anions having shorter alkyl chain lengths due to quicker reactions of these anions with the surface leading to the formation of tribolayers.^[6,44] However, the applied load in another study^[44] was also by two orders of magnitudes lower than in our study and, therefore, cannot be easily compared to our study. Consequently, we anticipate that the potentially lower reactivity of IL2 is advantageous under the high applied load in our study, thus promoting a slower degradation of the IL and a longer lifetime (wear life). Additionally, it has been shown that the thickness and compactness of the formed IL-based tribolayers mainly depend on the alkyl chain lengths of the ions.^[43,45,46] Therefore, we hypothesize that IL2 can form a thicker and more compact tribolayer on the steel surface, which protects the underlying surface from wear and results in a higher load-carrying capacity. This is somewhat counterintuitive since the viscosity of IL2 is significantly lower than that of IL1 (Table 1), basically suggesting a thinner lubricant film for IL2. However, under high-load

conditions inducing locally high temperatures, the predominant lubrication regime for both ILs is boundary lubrication irrespective of their viscosity. Due to the expected low film thicknesses, the different viscosities only play a minor role regarding the resulting tribological performance.

For both ILs, the addition of multilayer $Ti_3C_2T_x$ further improved the load-carrying capacity to 27.2 and 35.3 N mm⁻² for IL1 + MXene and IL2 + MXene, respectively. For IL2 in particular, this corresponds to values that are significantly higher than those of some fully formulated turbine oils used in helicopter applications.^[36] We anticipate that this improvement is due to the additional formation of MXene-rich tribolayer, which protects the steel surface from wear. The addition of MXenes had a greater effect for IL2, for which the load-carrying capacity increased by 26% compared to a rather marginal improvement of 6% for IL1. To understand this aspect, several elements have to be taken into consideration. As discussed above, we assume that IL2 has the capability to form a thicker and more compact wear-resistant tribolayer. Therefore, the acting mechanical stress on the MXenes, which are an integral part of this layer, is reduced, leading to a slower MXene degradation (structural and chemical) and, thus a better performance. In this context, it has been shown that MXene tribolayers degrade rapidly under high contact pressures of 1.47 GPa,^[34] which are close to the initial contact pressure of 1.4 GPa in our experiments, reducing their beneficial effects. Additionally, MXenes' mobility in the liquids depends on their viscosity.^[47] The lower viscosity of IL2 (Table 1) could benefit the mobility of MXenes in the ionic liquid. Therefore, the tribological contact is provided more easily with MXenes, which are embedded into the hybrid IL/MXene tribolayer to reduce wear.

4. Conclusion

In this work, we presented a new lubrication system consisting of ILs and $Ti_3C_2T_x$ acting as additive (concentration of 0.5 wt%) with the overall purpose to enhance the load carrying capacity and thus finally wear resistance under boundary lubrication at relatively high loads of 400 N. The specifically synthesized ILs share the same cation (trioctyl(methyl)phosphonium) but anions with different alkyl chain lengths (dimethyl phosphate and dibutyl phosphate for IL1 and IL2, respectively).

MXenes showed an excellent dispersibility in both applied ILs over 24 h, which was attributed to the intrinsic ionic nature of the ILs favoring electrostatic interactions with the polar MXenes, possible formation of hydrogen bonds between the negatively charged ions and OH-containing terminations of MXenes, as well as the high viscosity of the ILs preventing reagglomeration.

The produced IL/MXene dispersions always resulted in a higher average load-carrying capacity in standardized Brugger tests compared to the pure ILs. The combination IL2/MXene demonstrated the highest average load-carrying capacity, corresponding to an increase by 26% compared to the pure IL. The excellent tribological performance induced by the IL/MXene dispersion was explained by the formation of hybrid tribolayers on the rubbing surfaces, which protects the surfaces from wear. Anions with longer alkyl chain lengths are known to form thicker tribolayers, which explains the better performance of IL2,

especially in combination with MXenes. The MXenes in the IL2 tribolayer are exposed to less stress compared to IL1, resulting in a slower degradation and, consequently, improved wear resistance. It is worth to emphasize that the combination IL2/MXene even outperformed fully formulated turbine oils regarding their load-bearing capacity and wear resistance under contact pressures of 1.4 GPa. The results of our work point toward the suitability of ecofriendly IL/MXene lubricants with high thermal stability for high-load applications.

Acknowledgements

A.R. gratefully acknowledges the financial support given by ANID-CONICYT within the projects Fondecyt (grant no. 11180121) and Fondecip EQM (grant no. 190057). G.B. thanks the "Austrian COMET-Programme" Project InTribology1 (grant no. 872176) for financial support.

Conflict of Interest

The authors declare no conflict of interest.

Author Contributions

P.G.G., C.G., and A.R. conceptualized the work. K.S. fabricated the ionic liquids. R.N. performed the tribological experiments and the wear analysis. P.G.G., C.G., A.R., and K.B.-S. analyzed the data. P.G.G., R.N., G.B., and A.R. visualized the data. P.G.G. and A.R. prepared the first draft of the manuscript. P.G.G., K.S., K.B.-S., C.G., and A.R. edited the manuscript. All authors provided suggestions for the final discussion, have reviewed, edited, and read the final version of the manuscript.

Data Availability Statement

The data that support the findings of this study are available from the corresponding author upon reasonable request.

Keywords

2D materials, ionic liquids, MXenes, tribology, wears

Received: May 16, 2023

Revised: June 14, 2023

Published online:

- [1] *Environmentally Friendly and Biobased Lubricants* (Eds: B.K. Sharma, G. Biresaw), CRC Press, London, UK **2016**.
- [2] K. Holmberg, A. Erdemir, *Friction* **2017**, *5*, 263.
- [3] S. Zhang, T. Ma, A. Erdemir, Q. Li, *Mater. Today* **2019**, *26*, 67.
- [4] I. Minami, *Molecules* **2009**, *14*, 2286.
- [5] H. Xiao, *Tribol. Trans.* **2017**, *60*, 20.
- [6] A. Anifa Mohamed Faruck, P. G. Grützmaier, C.-J. Hsu, D. Dworschak, H.-W. Cheng, M. Valtiner, K. Stägel, P. Mikšovsky, A. R. Sahoo, A. Sainz Martinez, K. Bica-Schröder, M. Weigand, C. Gachot, *Friction* **2023**, *11*, 1057.
- [7] C. Ye, W. Liu, Y. Chen, L. Yu, *Chem. Commun.* **2001**, *21*, 2244.
- [8] M. D. Avilés, N. Saurín, T. Espinosa, J. Sanes, J. Arias-Pardilla, F. J. Carrión, M. D. Bermúdez, *Express Polym. Lett.* **2017**, *11*, 219.
- [9] Y. Zhou, J. Qu, *ACS Appl. Mater. Interfaces* **2017**, *9*, 3209.

- [10] X. Ge, J. Li, C. Zhang, Y. Liu, J. Luo, *ACS Appl. Mater. Interfaces* **2019**, *11*, 6568.
- [11] X. Ge, J. Li, C. Zhang, Z. Wang, J. Luo, *Langmuir* **2018**, *34*, 5245.
- [12] S. Perkin, T. Albrecht, J. Klein, *Phys. Chem. Chem. Phys.* **2010**, *12*, 1243.
- [13] V. Khare, M. Q. Pham, N. Kumari, H. S. Yoon, C. S. Kim, J. Il Park, S. H. Ahn, *ACS Appl. Mater. Interfaces* **2013**, *5*, 4063.
- [14] X. Ge, J. Li, H. Wang, C. Zhang, Y. Liu, J. Luo, *Carbon N Y* **2019**, *151*, 76.
- [15] K. Gong, W. Lou, G. Zhao, X. Wu, X. Wang, *Friction* **2020**, *8*, 674.
- [16] P. C. Uzoma, H. Hu, M. Khadem, O. V. Penkov, *Coatings* **2020**, *10*, 897.
- [17] B. C. Wyatt, A. Rosenkranz, B. Anasori, *Adv. Mater.* **2021**, *33*, 2007973.
- [18] A. VahidMohammadi, J. Rosen, Y. Gogotsi, *Science* **2021**, *372*, abf1581.
- [19] B. Anasori, M. R. Lukatskaya, Y. Gogotsi, *Nat. Rev. Mater.* **2017**, *2*, 1.
- [20] S. J. Kim, H. J. Koh, C. E. Ren, O. Kwon, K. Maleski, S. Y. Cho, B. Anasori, C. K. Kim, Y. K. Choi, J. Kim, Y. Gogotsi, H. T. Jung, *ACS Nano* **2018**, *12*, 986.
- [21] A. Liu, X. Liang, X. Ren, W. Guan, M. Gao, Y. Yang, Q. Yang, L. Gao, Y. Li, T. Ma, *Adv. Funct. Mater.* **2020**, *30*, 2003437.
- [22] D. Zhang, M. Ashton, A. Ostadhossein, A. C. T. Van Duin, R. G. Hennig, S. B. Sinnott, *ACS Appl. Mater. Interfaces* **2017**, *9*, 34467.
- [23] E. Marquis, M. Cutini, B. Anasori, A. Rosenkranz, M. C. Righi, *ACS Appl. Nano Mater.* **2022**, *5*, 10516.
- [24] Q. Yang, S. J. Eder, A. Martini, P. G. Grützmacher, *Npj Mater. Degrad.* **2023**, *7*, 6.
- [25] A. Rodriguez, M. S. Jaman, O. Acikgoz, B. Wang, J. Yu, P. G. Grützmacher, A. Rosenkranz, M. Z. Baykara, *Appl. Surf. Sci.* **2021**, *535*, 147664.
- [26] P. Serles, M. Hamidinejad, P. G. Demingos, L. Ma, N. Barri, H. Taylor, C. V. Singh, C. B. Park, T. Filletter, *Nano Lett.* **2022**, *22*, 3356.
- [27] P. G. Grützmacher, S. Suarez, A. Tolosa, C. Gachot, G. Song, B. Wang, V. Presser, F. Mücklich, B. Anasori, A. Rosenkranz, *ACS Nano* **2021**, *15*, 8216.
- [28] J. Y. A. Hurtado, P. G. Grützmacher, J. M. Henríquez, D. Zambrano, B. Wang, A. Rosenkranz, *Adv. Eng. Mater.* **2022**, *24*, 2200755.
- [29] M. Marian, S. Tremmel, S. Wartzack, G. Song, B. Wang, J. Yu, A. Rosenkranz, *Appl. Surf. Sci.* **2020**, *523*, 146503.
- [30] P. Tian, G. Yu, K. Wei, Z. Zhang, N. Wang, *Ceram. Int.* **2021**, *47*, 30722.
- [31] H. Zhang, L. Wang, Q. Chen, P. Li, A. Zhou, X. Cao, Q. Hu, *Mater. Des.* **2016**, *92*, 682.
- [32] X. Zhang, M. Xue, X. Yang, Z. Wang, G. Luo, Z. Huang, X. Sui, C. Li, *RSC Adv.* **2015**, *5*, 2762.
- [33] S. Yi, Y. Guo, J. Li, Y. Zhang, A. Zhou, J. Luo, *Friction* **2023**, *11*, 369.
- [34] M. Marian, G. C. Song, B. Wang, V. M. Fuenzalida, S. Krauß, B. Merle, S. Tremmel, S. Wartzack, J. Yu, A. Rosenkranz, *Appl. Surf. Sci.* **2020**, *531*, 147311.
- [35] H. Xiao, S. Liu, *Mater. Des.* **2017**, *135*, 319.
- [36] A. A. Mohamed Faruck, C. J. Hsu, N. Doerr, M. Weigand, C. Gachot, *Tribol. Int.* **2020**, *151*, 106390.
- [37] M. Nalguib, M. Kurtoglu, V. Presser, J. Lu, J. Niu, M. Heon, L. Hultman, Y. Gogotsi, M. W. Barsoum, *Adv. Mater.* **2011**, *23*, 4248.
- [38] A. Sarycheva, Y. Gogotsi, *Chem. Mater.* **2020**, *32*, 3480.
- [39] J. Gao, C.-F. Du, T. Zhang, X. Zhang, Q. Ye, S. Liu, W. Liu, *ACS Appl. Nano Mater.* **2021**, *4*, 11080.
- [40] S. Chen, Y. Xiang, M. K. Banks, C. Peng, W. Xu, R. Wu, *Nanoscale* **2018**, *10*, 20043.
- [41] E. I. Izgorodina, D. R. MacFarlane, *J. Phys. Chem. B* **2011**, *115*, 14659.
- [42] Y. Li, Q. Zhang, W. Zhou, Y. Huang, J. Han, *Lubricants* **2023**, *11*, 147.
- [43] H. Fang, Y. Li, S. Zhang, Q. Ding, L. Hu, K. Lu, *J. Colloid Interface Sci.* **2022**, *623*, 257.
- [44] S. Kawada, S. Watanabe, C. Tadokoro, S. Sasaki, *Tribol. Lett.* **2018**, *66*, 1.
- [45] M. Cai, Q. Yu, W. Liu, F. Zhou, *Chem. Soc. Rev.* **2020**, *49*, 7753.
- [46] R. Kreivaitis, M. Gumbytė, A. Kupčinskis, K. Kazancev, V. Makarevičienė, *Tribol. Int.* **2020**, *141*.
- [47] R. K. Upadhyay, A. Kumar, *Colloids Interface Sci. Commun.* **2019**, *31*, 100186.

4. Supported ionic liquid phase (SILP) allylic alkylation of amines in continuous flow

Transition metal-catalysed allylic alkylations provide a powerful tool for forming C-C or C-X bonds.^[114] The strategy was first pioneered by Tsuji^[115] and later adapted by Trost,^[116] introducing phosphine ligands. In this field, the nucleophilic substitution of an activated allylic acetate or carbonate electrophile provides the most straightforward strategy. The method has numerous advantages, such as mild conditions, variable ligands and nucleophiles, good functional group tolerance, and simple implementation. Since the strategy is mainly utilised in asymmetric transformations, the employed transition metal complex is typically modified with chiral ligands.^[117] For non-enantioselective reactions, achiral ligands, such as dppp or dppf can be employed.^[118] The reaction proceeds through the catalytic cycle presented below (Figure 40).^[119]

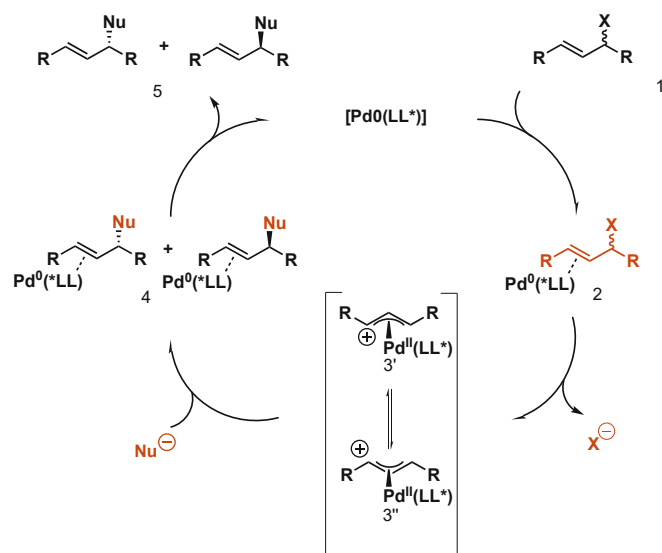


Figure 40. The mechanism of the Tsuji-Trost reaction

The cycle starts with the coordination of a zerovalent Pd-species to a substrate, which contains a good leaving group (X) in the allylic position (1). This results in the formation of η^2 - π -allyl-Pd⁰ complexes (2). This step is followed by an oxidative addition in which the leaving group (X) is expelled in an intramolecular S_N2 substitution, forming η^3 - π -allyl-Pd^{II} cationic complexes (3). The nucleophile attacks one of the allylic group's terminal C-atoms, which is activated by the Pd^{II} species. This results in the regeneration of the η^2 - π -allyl-Pd⁰ complexes *via* reductive elimination (4). Finally, the palladium species releases the product (5), and the catalytic cycle can start again.

The use of allylic alkylations for synthesising alkyl amines has attracted significant interest; hence, in contrast to classical alkylations with alkyl halides, such reactions provide better product selectivity and require milder reaction conditions.^[120] These reactions are mainly carried out batch-wise, relying

on homogeneous catalysis. Therefore, they are hampered by difficult catalyst separation, recycling, or reuse. Continuous methods relying on palladium-containing SILP catalysts can provide a suitable alternative for the sustainable production of allylic species.

This chapter presents an approach relying on a Pd-containing SILP catalyst for producing various allylic amines without employing any additional base, relying on the previously synthesised hydrophobic ionic liquids for catalyst immobilisation. The simple method provides straightforward access for both achiral and chiral compounds. Under optimal conditions, the flow reaction could run for 3.5 hours without a significant decrease in the conversion. Only a small amount of ionic liquid (0.7 wt%) leached out of the catalyst, and no leaching of the palladium complex was detected. The novel catalysts proved air-tolerating and provided the chiral and achiral *N*-allylation products in continuous mode in only 30 minutes.

The following manuscript will be presented in this chapter:

K. Stigel, Á. M. Pálvölgyi, C. Delmas, M. Schnürch, K. Bica-Schröder: Supported Ionic Liquid Phase (SILP) Allylic Alkylation of Amines in Continuous Flow. *ChemCatChem* **2023**, *15*, e202300381.

As a first author, the experimental work was planned and performed by me, and I wrote the original draft.

Supported Ionic Liquid Phase (SILP) Allylic Alkylation of Amines in Continuous Flow

Kristof Stagel,^[a] Ádám Márk Pálvölgyi,^[a] Clémence Delmas,^[a] Michael Schnürch,^[a] and Katharina Bica-Schröder^{*,[a]}

We present the use of Pd-complex-containing supported ionic liquid phases (SILPs) as a novel approach for continuous-flow allylic alkylation of *N*-nucleophiles. This immobilization strategy gave simple access to air-tolerating catalyst frameworks, providing rapid and convenient access to various achiral and

chiral *N*-allylation products. Under optimized conditions, the flow-reaction could be maintained for 3.5 hours with constant product output; meanwhile, only a marginal 0.7 wt% of ionic liquid leaching and no detectable palladium-complex leaching could be observed.

Introduction

Transition metal-catalyzed allylic alkylation reactions provide a versatile tool for various C–C and C–X bond formations and play an important role in synthesizing numerous biologically active compounds.^[1] Their use for synthesizing alkyl amines became particularly attractive: in contrast to classical alkylations with alkyl halides, such reactions require not just much milder reaction conditions but also results in significantly better product selectivity.^[2] In this field, the nucleophilic substitution of an activated allylic acetate or carbonate electrophile represents the most straightforward and widely investigated alkylation strategy. Apart from palladium-catalyzed *Tsuji-Trost*-type reactions,^[3] other advances, including iridium^[4]- or ruthenium-catalysis,^[5] have also been reported.

The allylic alkylation of amines is mostly carried out *via* homogeneous catalysis and therefore hampered by the difficult catalyst separation, recycling, or reuse. However, most catalyst immobilization strategies require tedious multi-step synthetic procedures, which might also lead to decreased catalytic efficiency. These issues can be effectively overcome with supported ionic liquid phase (SILP) catalysis:^[6] as such, a homogeneous catalyst is dissolved in an ionic liquid (IL), which is impregnated on a porous solid support. This concept efficiently combines the advantages of classical homogeneous and heterogeneous catalysis. Moreover, the thin impregnation of a highly porous surface with the liquid/catalyst also leads to significantly decreased ionic liquid and catalyst loadings

compared to classical organic solvent/ionic liquid biphasic catalysis.^[7]

Valkenberg and co-workers summarized various methods for immobilizing ionic liquids.^[8] The synthesized Lewis-acidic catalysts demonstrated good activities in Friedel-Crafts alkylations. The concept of SILP catalysis is already applied on larger scales in gas- or supercritical phase reactions, including hydroformylations, hydrogenations, carbonylations,^[9] as well as continuous CO₂ conversion.^[10] In terms of asymmetric catalysis, an approach from 2013 employs supercritical carbon dioxide as mobile phase in a continuous process for the asymmetric hydrogenation of dimethyl itaconate. The SILP catalyst system contains a chiral rhodium complex core and showed excellent reactivity and enantioselectivity in the asymmetric transformation.^[11] Additionally, Rufete-Beneite *et al.* established a methodology that relies on the immobilization of a chiral complex, RhDuphos, with the aid of the SILP strategy. This catalyst system provided high conversions and with increased IL loadings, also excellent enantioselectivities in asymmetric hydrogenations.^[12]

In comparison to reactions in gas or supercritical phase, the adaptation of the SILP concept to liquid-phase reactions was found to be more challenging as the catalyst and/or the ionic liquid might be leached into the organic reaction media.^[13] However, some approaches successfully combine transition metal catalysis and SILPs in liquid-phase reactions. In 2014, Urbán and his co-workers reported the utilization of a SILP-Pd catalyst framework in continuous Heck reactions, which demonstrated stable performance for several hours, providing high conversions.^[14] More *et al.* developed a Pd-SILP-system immobilized on Merrifield resin, which proved to be efficient and stable for Suzuki coupling reactions, and provided the corresponding products with excellent yields.^[15]

Based on our previous work on asymmetric allylations,^[16] we report herein the use of the SILP concept for the continuous-flow allylic alkylation towards various achiral and chiral *N*-allylation products. The simple physisorption of a palladium-complex in hydrophobic ionic liquid onto silica surface provided straightforward access to air-tolerant catalyst frameworks (Figure 1), which were successfully employed for allylic alkylation of

[a] K. Stagel, Á. M. Pálvölgyi, C. Delmas, Prof. M. Schnürch, Prof. K. Bica-Schröder
Institute of Applied Synthetic Chemistry
TU Wien
Getreidemarkt 9/163, 1060 Wien (Austria)
E-mail: katharina.schroeder@tuwien.ac.at

Supporting information for this article is available on the WWW under <https://doi.org/10.1002/cctc.202300381>

© 2023 The Authors. ChemCatChem published by Wiley-VCH GmbH. This is an open access article under the terms of the Creative Commons Attribution License, which permits use, distribution and reproduction in any medium, provided the original work is properly cited.

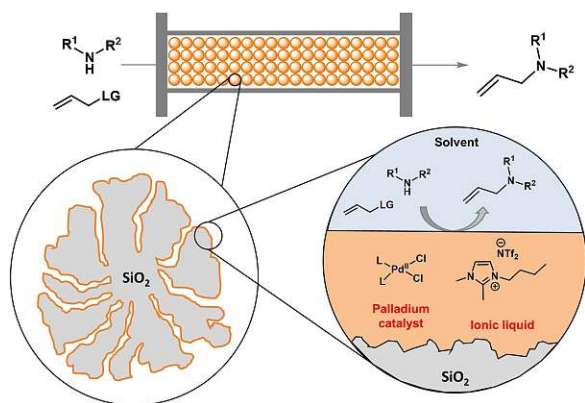


Figure 1. The concept of palladium-based SILP catalysis for continuous-flow allylation of *N*-nucleophiles.

N-nucleophiles. This methodology requires neither an additional base nor an inert atmosphere and provides fast access to various achiral and chiral allylic amines.

Results and Discussion

Based on our previous experiences with SILP-catalysis for liquid-phase reactions,^[13a,17] we aimed for a fast and simple preparation of the heterogeneous catalysts relying on hydrophobic ionic liquids. Because of the general insensitivity of palladium-catalysts towards mildly acidic environment such as the OH groups of the silica gel,^[18] no deactivation or pre-coating of the silanol groups was required. Using the cheap and readily available $[\text{Pd}(\text{C}_3\text{H}_5)_2\text{Cl}]_2$ catalyst precursor, 1,3-bis(diphenylphosphino)propane (dppp) and three different ionic liquids (IL1–3); a series of SILPs (SILP 1–3) with 10, 15, 20, and 30 wt% IL-loading was prepared by simple physisorption of the IL/PdLn on the silica surface, respectively.

With these SILPs in hand, we initially tested their catalytic efficiency in the achiral continuous-flow allylic substitution of cinnamyl acetate (**1a**) with pyrrolidine (**2a**) (Table 1). For this purpose, a continuous flow set-up consisting of a cartridge employed as a fix-bed reactor (0.707 mL) and a syringe pump was used (Supporting Information, Figure S5). A flow rate that corresponds to a residence time of 30 minutes was chosen. The crude product was directly analyzed to determine conversion *via* GC-MS. The leaching of the ionic liquid was further quantified by ^{19}F NMR spectroscopy with 2,2'-difluorobenzophenone as internal standard, allowing a limit of detection in the order of > 0.05 wt%.

The choice of an appropriate solvent is a key issue for liquid-phase reactions with supported catalysts. On the one hand, the polarity needs to be sufficiently high to dissolve starting materials and maintain homogenous conditions through the reaction. On the other hand, polarity needs to be balanced in order to avoid leaching of the ionic liquid – an aspect that would rather favor apolar conditions.^[19] Keeping environmental aspects in mind, we decided to use a mixture of

Table 1. Parameter screening for the continuous-flow synthesis of **3a**.

Entry	Solvent	Ionic liquid	Conv. [%] ^[b]
1 ^[a]	<i>n</i> -heptane/2-MeTHF 4/1	IL1	83
2 ^[c]	<i>n</i> -heptane/2-MeTHF 4/1	IL1	73
3 ^[d]	<i>n</i> -heptane/2-MeTHF 4/1	IL1	78
4	<i>n</i> -heptane/2-MeTHF 7/3	IL1	81
5 ^[e]	toluene/2-MeTHF 4/1	IL1	n. d.
6	<i>n</i> -heptane/2-MeTHF 4/1	IL2	77
7	<i>n</i> -heptane/2-MeTHF 4/1	IL3	69
8 ^[f]	<i>n</i> -heptane/2-MeTHF 4/1	IL1	0
9 ^[g]	<i>n</i> -heptane/2-MeTHF 4/1	IL1	83
10 ^[f]	<i>n</i> -heptane/2-MeTHF 4/1	IL2	0

[a] Reaction was performed on a 0.6 mmol scale using cinnamyl acetate (**1a**, 1.0 equiv.), pyrrolidine (**2a**, 2.0 equiv.) with 450 mg SILP1 (15 wt% IL, 0.5 wt% $[\text{Pd}(\text{C}_3\text{H}_5)_2\text{Cl}]_2$ and 1.13 wt% dppp). The residence time was 30 minutes. [b] Determined by GC-MS analysis. No side-product was observed. [c] Performed with 30 wt% IL. [d] 45 min residence time. [e] Leaching of the ionic liquid was observed (3 wt% of total IL amount), determined by ^{19}F NMR spectroscopy (limit of detection: > 0.05 wt%). [f] No *P*-ligand for SILP preparation. [g] dppf as *P*-ligand for SILP preparation.

n-heptane with ether-type solvents as polar modifier. When using 20 V/V% of 2-MeTHF, – a bio-based solvent – in *n*-heptane with the SILP1, the allylation product 1-cinnamylpyrrolidine (**3**) was formed in 83% conversion within 30 minutes of residence time (Table 1, entry 1); meanwhile, SILP1 with higher IL-loading or a longer residence time did not improve the conversion (Table 1, entries 1 vs. 2–3). Using an increased amount of 2-MeTHF led to a similar conversion (Table 1, entry 4), whereas using toluene as the apolar component resulted in leaching (Table 1, entry 5). Furthermore, a SILP with 1-butyl-2,3-dimethyl-imidazolium bis(trifluoromethylsulfonyl)imide ($[\text{bm}_2\text{im}][\text{NTf}_2]$, IL1) was indeed beneficial, as the SILPs with $[\text{bmim}][\text{NTf}_2]$ (IL2) or with the quaternary ammonium-based IL3 both resulted in slightly lower conversions (Table 1, entries 6–7). Imidazolium-based ILs are known to form carbenes, as their C2 atom can undergo deprotonation under basic conditions.^[20] Such a species can coordinate to the Pd-atom, resulting in the decoordination of the original ligand, which can lead to slightly decreased activity. If the C2 atom is protected with an alkyl group, deprotonation can be prevented. This can explain the slightly decreased activity of the SILP with IL2 compared to IL1. While a phosphine ligand was indeed found to be crucial (Table 1, entry 8); no difference between dppp and 1,1'-bis(diphenylphosphino)ferrocene (dppf) was observed (Table 1, entries 1 vs. 9); leaving the cheaper dppp as a preferential option. To further investigate the possibility of a Pd-NHC strategy, the catalytic effect of the IL2-based SILP in the

absence of a *P*-ligand was also investigated; however, no conversion was observed (entry 8).

After identifying SILP1 as the best-performing catalyst and with improved reaction conditions in hand, we investigated the longer-term usability of the SILP-system. After equilibrating the reaction mixture for 30 minutes as previously optimized, the system was stabilized. A constant product output could be observed for a total of 3.5 hours, thus corresponding to seven reaction cycles (Figure 2) without any loss of catalytic activity. Furthermore, only a marginal 0.7 wt% ionic liquid leaching, and no palladium-complex leaching could be observed.

We then explored the scope and limitations of the continuous-flow *N*-allylation reaction. A small set of allylic acetate electrophiles with different sterics were investigated, and the corresponding products **3a–d** were obtained in good to excellent yields (Scheme 1). It is worth mentioning that the reaction with cinnamyl alcohol instead of cinnamyl acetate (**1a**) still provided product **3a** in 10% yield, indicating that the

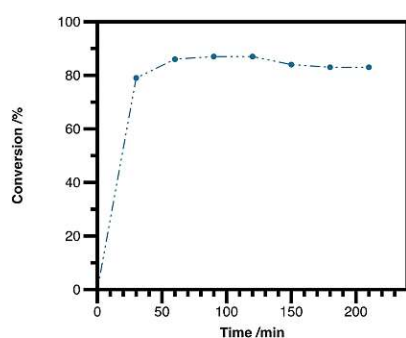
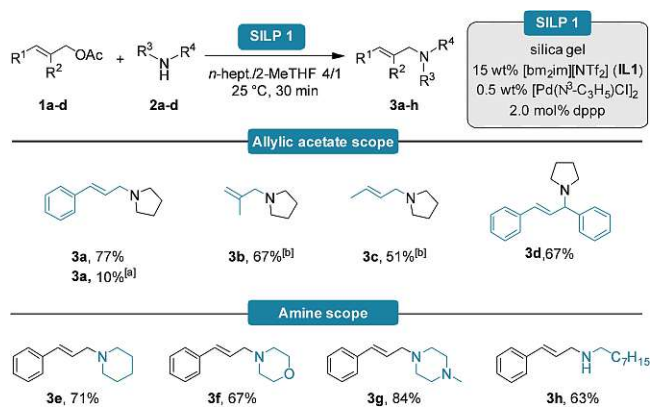


Figure 2. Long-term stability of the developed SILP-system. Reactions were carried out on a 3.2 mmol scale using 1.0 equiv. cinnamyl acetate (**1a**) and 2.0 equiv. pyrrolidine (**2a**) with 470 mg of SILP1 (15 wt% IL1, 0.5 wt% $[\text{Pd}(\text{C}_3\text{H}_5)_2\text{Cl}]_2$ and 1.13 wt% dppp) in *n*-heptane/2-MeTHF 4/1. The residence time was 30 minutes.



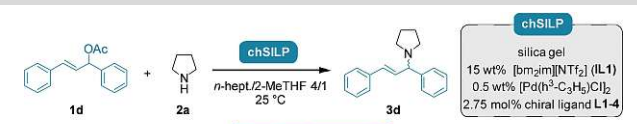
Scheme 1. Substrate and reagent scope for the continuous-flow allylic alkylation. Reactions were carried out on a 0.6 mmol scale using 1.0 equiv. allylic acetate (**1a–d**) and 2.0 equiv. amine (**2a–d**) with 450 mg of SILP1 (15 wt% IL1, 0.5 wt% $[\text{Pd}(\text{C}_3\text{H}_5)_2\text{Cl}]_2$ and 1.13 wt% dppp) in *n*-heptane/2-MeTHF 4/1. The residence time was 30 minutes. Yields refer to isolated products after column chromatographic purification. [a] Reaction was performed with cinnamyl alcohol, GC-MS conversion. [b] GC-MS conversion due to the extremely volatile nature.

silanol OH-groups might have a moderate co-catalytic effect on increasing the leaving group ability through H-bonding. Despite this moderate and non-optimized result, it could still be an important aspect, as the direct functionalization of allylic alcohols mostly requires harsh reaction conditions and/or strong Lewis or Brønsted acidic additives.^[21] Besides screening different allylic electrophiles, a few different *N*-nucleophiles, including primary and secondary amines, have also been tested and the corresponding *N*-allylated products (**3e–h**) could be isolated in good to excellent yields (Scheme 1). Meanwhile, slightly higher yields could be achieved in the literature in batch mode; these methods mostly rely on exotic reagents and/or harsh reaction conditions.^[22] In comparison, this method uses common reagents, applies mild reaction conditions, and results in short reaction times in continuous-flow operation.

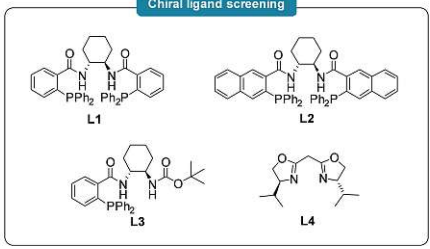
Aiming to adapt the established SILP-system to asymmetric allylic alkylations, we further envisioned expanding the system for the continuous-flow asymmetric allylic alkylations of pyrrolidines. In general, palladium-catalyzed enantioselective allylic alkylations have emerged as versatile and powerful chemical reactions for asymmetric carbon-carbon and carbon-heteroatom bond formation.^[23] Due to its numerous advantages, such as mild conditions, variable chiral ligands or nucleophiles, simple implementation, and good functional group tolerance; such allylations have found wide application in the synthesis of valuable optically active compounds. Since the seminal examples of Trost,^[24] a wide range of chiral ligands, including phosphinooxazolines,^[25] amino-acid derivatives,^[26] amino-phosphinites,^[27] phosphoramidites,^[28] and aminoalkyl-phosphines^[29] have been developed for the asymmetric allylation of stabilized C-nucleophiles. Despite the large number of advancements, up until today, the Trost-type ligands still have maintained a privileged position among the chiral modifiers in the field of asymmetric allylations.^[30] Although Trost-type ligands are well suited for unhindered substrates, they have proven less efficient for the alkylation of hindered substrates, such as *rac*-1,3-diphenylallyl acetate.^[30] Hitchcock's group^[31] circumvented these problems by introducing various ester groups to the ligand, using a series of *tert*-leucinol-derived diphosphines, which provided good yields in the allylation of the previously mentioned hindered substrate. In 2000, Kim *et al.*^[32] reported the synthesis of various *P,N*-type monophosphine ligands with (*R,R*)-diaminocyclohexane (*R,R*-DACH) backbone, which showed good reactivities and moderate enantioselectivities in asymmetric allylic alkylation of more hindered substrates. With most of the recent advancements being indeed reported for C–C bond formation, the asymmetric allylations of *N*-nucleophiles attracted significantly less attention.

In accordance with the findings for the non-asymmetric *N*-allylations, we initially screened different chiral SILPs (**chSILPs**) for the asymmetric *N*-allylations of pyrrolidine (**2a**) with (*rac*)-1,3-diphenylallyl acetate (**1d**) both in heterogeneous batch slurry phase, as well as in continuous flow (Table 2). By using the same ionic liquid IL1 and palladium-precursor $[\text{Pd}(\text{C}_3\text{H}_5)_2\text{Cl}]_2$ as before, a small set of **chSILP** catalysts were prepared using different chiral ligands (**L1–4**), and their catalytic efficiency was investigated in the same solvent mixture as for the non-

Table 2. Screening of different chiral ligands for the continuous-flow asymmetric *N*-allylation of pyrrolidine (**2a**) with **1d** using **chSILP** catalysts.



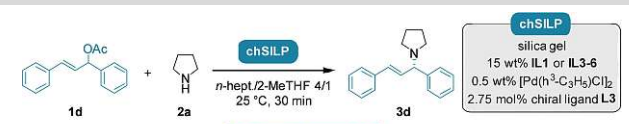
Chiral ligand screening



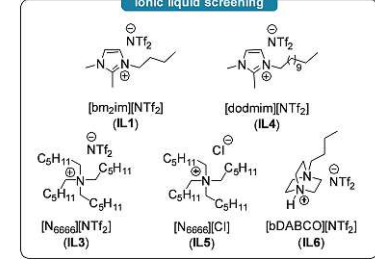
Entry	Chiral ligand	Reaction in slurry phase Conv. [%] ^[a]	Reaction in slurry phase ee [%] ^[b]	Reaction in flow Conv. [%] ^[a]	Reaction in flow ee [%] ^[b]
1	L1	44	44	39	30
2	L2	17	52	62	54
3	L3	70	65	81	74
4	L4	52	36	n.r.	n.d.

Reactions were carried out on 0.6 mmol scale using 1.0 equiv. allylic acetate **1d** and 2.0 equiv. pyrrolidine (**2a**) with 450 mg of **chSILP** (15 wt % **IL1**, 0.5 wt % [Pd(C₃H₅)Cl]₂ and 2.75 wt % chiral ligand **L1–4**) in *n*-heptane/2-MeTHF 4/1. Slurry-phase reactions were carried out in 8 mL screw-cap vials at 25 °C for 24 hours. Continuous-flow reactions were carried out at 25 °C with a residence time of 30 minutes. [a] Determined by GC-MS analysis, no side-product formation was observed. [b] Determined by chiral HPLC analysis using Daicel Chiralpak® IA-3 column.

Table 3. Effect of different ionic liquids for the continuous-flow asymmetric *N*-allylation of pyrrolidine (**2a**) with **1d** using **chSILP** catalysts.



Ionic liquid screening



Entry	Ionic liquid for chSILP preparation	Conv. [%] ^[a]	ee [%] ^[b]
1	IL1	81	74
2	IL3	54	68
3	IL4	76	73
4 ^[c]	IL5	n.d.	n.d.
5	IL6	36	74

Reactions were carried out on 0.6 mmol scale using 1.0 equiv. allylic acetate **1d** and 2.0 equiv. pyrrolidine (**2a**) with 450 mg of **chSILP** (15 wt % **IL1** or **IL3–6**, 0.5 wt % [Pd(C₃H₅)Cl]₂ and 2.0 wt % chiral ligand **L3**) in *n*-heptane/2-MeTHF 4/1 at 25 °C with a residence time of 30 minutes. [a] Determined by GC-MS analysis, no side-product formation was observed. [b] Determined by chiral HPLC analysis using a Daicel Chiralpak® IA-3 column. n.d.: not determined. [c] Leaching of the ionic liquid (5 wt % of total IL amount) was detected by ¹⁹F NMR spectroscopy (limit of detection: > 0.05 wt %).

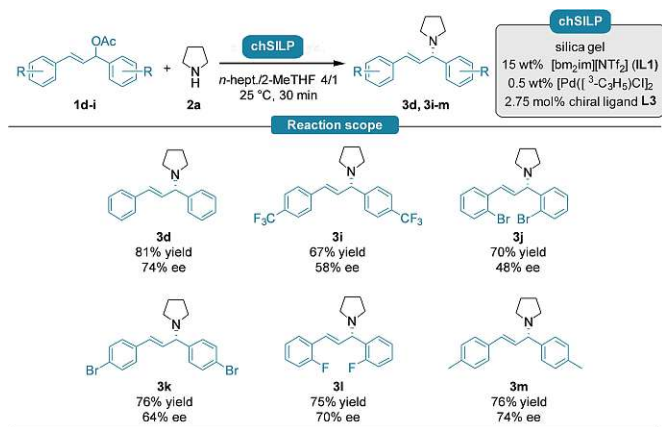
asymmetric *N*-allylations (*n*-heptane/2-MeTHF 4/1). The **chSILP** with the traditional Trost-ligand **L1** and bis(oxazoline) **L4** provided comparable reactivities and ee in slurry-phase, whereas **L4** proved inactive in the continuous-flow process (Table 2, entry 4). **L4** – as the only non-Trost-type ligand- differs from the other employed ligands in its structure, as it does not contain a strongly coordinating *P*-atom. This might result in the ligand's different coordination properties and its loss in the continuous process due to leaching. On the other hand, the allylation product **3d** could be obtained in continuous flow with moderate conversion and enantioselectivity when using the more sterically demanding Trost-type ligand **L2**. The introduction of a *tert*-butyl-carbamate-modified Trost-ligand **L3** led to a further improved conversion and to good ee in flow; yielding the product **3d** in a promising 81% conversion and 74% ee within 30 minutes of residence time.

We then investigated the possible catalytic effect of the ionic liquid matrix. Using the palladium-precursor [Pd(C₃H₅)Cl]₂ and the chiral ligand **L3**, we prepared a series of **chSILP** catalysts featuring various hydrophobic ionic liquids. The introduction of **IL4** could not outperform the result with **IL1**, indicating that the ionic liquid chain length has basically no effect on the reactivity and on the level of stereodiscrimination (Table 3, entries 1 vs. 3). Inspired by the findings of Trost and co-workers on the beneficial effect of tetraalkyl ammonium salts for *C*-allylations, we also probed different quaternary ammonium salt-based ILs (**IL3** and **IL5–6**). The **chSILP** catalysts prepared with the tetrahexylammonium- and DABCO-based hydrophobic ionic liquids **IL3** and **IL6** could not improve the

enantioselectivity; meanwhile, only moderate conversion was observed (Table 3, 1 vs. entries 2 and 5). When using the hydrophilic **IL5**, the corresponding **chSILP** catalyst leached entirely during the continuous-flow pre-conditioning phase (Table 3, entry 4), further underlining the importance of highly hydrophobic, NTf₂-based ionic liquids to tackle leaching issues efficiently.

With the optimized reaction conditions in hand, we investigated the asymmetric *N*-allylation of pyrrolidine (**2a**) with symmetrically substituted (*rac*)-1,3-diphenylallyl acetate derivatives featuring different steric and electronic properties (**1d–i**). The corresponding enantioenriched *N*-allylated products **3d** and **3i–m** were obtained in good to high yields and in good enantioselectivities (Scheme 2).

In order to uncover the role of the silica and the ionic liquid in the catalytic system, control experiments for the reaction of pyrrolidine (**2a**) with **1d** have been carried out in batch mode using a **chSILP** with Pd/**L3** (Figure 3). The homogeneous phase allylation (black line) was very slow, providing only 25% conversion within 3 hours. When performing the reaction in homogeneous phase in the presence of **IL1**, the reaction rate increases drastically (purple line). As the reaction proceeds *via* ionic mechanism, a polar co-solvent, such as an ionic liquid might increase the reaction rate. Similarly, the addition of silica (blue line) also significantly accelerates the reaction. This might be explained by the acidity of the silanol groups, which can catalyze the cleavage of the acetate group. When using a **chSILP** (with **L3** and **IL1**, orange line); a slightly lowered reaction



Scheme 2. Reactions were carried out on 0.6 mmol scale using 1.0 equiv. substituted allylic acetate **1 d-i** and 2.0 equiv. pyrrolidine (**2a**) with 450 mg of **chSILP** (15 wt% **IL1**, 0.5 wt% $[\text{Pd}(\text{C}_3\text{H}_5)\text{Cl}]_2$ and 2.0 wt% chiral ligand **L3**) in *n*-heptane/2-MeTHF 4/1 at 25 °C with a residence time of 30 minutes. Yields refer to pure products isolated by column chromatography. The enantioselectivities were determined by chiral HPLC analysis using a Daicel Chiralpak® IA-3 column.

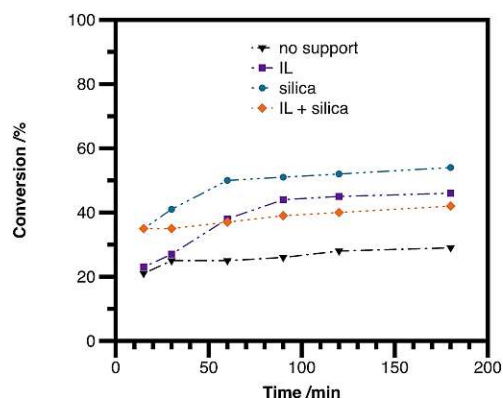


Figure 3. Effect of silica and ionic liquid on the *N*-allylation of pyrrolidine (**2a**) with **1 d** under batch conditions. Reactions were carried out on 0.6 mmol using 0.5 wt% $[\text{Pd}(\text{C}_3\text{H}_5)\text{Cl}]_2$ and 2.0 wt% chiral ligand **L3** in *n*-heptane/2-MeTHF 4/1 at 25 °C.

rate compared to the addition of pure IL and pure silica could be observed. The thin layer of ionic liquid on the silica surface might decrease the number of free silanol group sites, leading to a minor decrease in the activity of the catalyst system in batch mode. Nevertheless, using SILPs is crucial for continuous-flow operations, as only the combination of these components can lead to efficient catalyst immobilization, therefore circumventing catalyst leaching.

In order to quantify the possible catalyst leaching for continuous-flow reactions with chiral SILP-systems, ^{19}F NMR measurements were again carried out. When performing the *N*-allylation of pyrrolidine (**2a**) and **1 d** with the **chSILP** featuring the hydrophobic ionic liquid **IL1** and the chiral Pd/**L3** palladium complex, only a marginal 0.7 wt% of ionic liquid leaching (related to the total IL amount) and no detectable palladium-

complex leaching could be observed within an extended operation time of 3.5 hours.

Conclusion

Herein we reported the use of palladium-containing supported ionic liquid phases for the continuous-flow allylic amination of various allylic acetate electrophiles. Apart from the fast and straightforward catalyst immobilization, this novel approach requires neither an additional base, nor inert atmosphere for efficient *N*-allylation. Furthermore, the reactions could be carried out under mild conditions in benign reaction media. The optimal SILP catalyst could provide easy access to *N*-allylation products within short reaction times (30 minutes). By extending the reaction time to 3.5 hours, such a SILP catalyst could maintain stable conversions, whereas only a marginal ionic liquid- and no palladium complex leaching could be observed. Furthermore, this approach could be used for the simple immobilization of chiral palladium complexes, enabling asymmetric *N*-allylation reactions in continuous flow with good yields and enantioselectivities.

Experimental Section

Representative preparation of a chSILP catalyst

Allylpalladium(II)-chloride dimer (0.055 mmol, 20 mg, 0.5 wt%), ligand **L3** (0.22 mmol, 110 mg, 2.75 wt%) and 1-butyl-2,3-dimethylimidazolium bis(trifluoromethylsulfonyl)imide (**IL1**, 1.38 mmol, 600 mg, 15 wt%) were dissolved in anhydrous dichloromethane (1 mL) under argon atmosphere in a screw-cap vial. The mixture was stirred for 30 minutes, and it was poured into a silica gel (3270 mg, 81.75 wt%) containing flask. The vial was rinsed with dichloromethane, and the suspension was stirred for 24 hours at room temperature under inert atmosphere. Then, the solvent was removed *in vacuo*, and the resulting fine powder was dried on high vacuum (0.4 mbar) at room temperature for several hours.

Representative procedure for the continuous-flow synthesis using chSILP catalysis

The corresponding diphenyl-propenyl acetate derivative (**1 d-i**, 1.0 eq.) and pyrrolidine (**2a**, 2.0 eq.) were dissolved in a mixture of *n*-heptane: 2-methyltetrahydrofuran (4:1) and it was stirred for 15 minutes. A cartridge was filled with the solid catalyst and was pre-conditioned with the same solvent mixture. The reaction mixture was taken up with a syringe and pumped through the cartridge with the aid of a syringe pump. A flow rate which corresponds to 30 min residence time was chosen. The product was collected in a vial. After the whole volume was pumped through, the column was re-washed with the solvent. The collected mixture was concentrated *in vacuo* and purified by flash column chromatography.

Supporting Information

Additional references cited within the Supporting Information.^[33–46]

Acknowledgements

Financial support by the Austrian Science Fund (FWF, grant P 32882-N) is gratefully acknowledged.

Conflict of Interests

The authors declare no conflict of interest.

Data Availability Statement

The data that support the findings of this study are available in the supplementary material of this article.

Keywords: ionic liquid · chiral catalyst · SILP · Tsuji-Trost reaction · continuous flow

- [1] a) B. M. Trost, D. L. Van Vranken, *Chem. Rev.* **1996**, *96*, 395–422; b) B. M. Trost, M. L. Crawley, *Chem. Rev.* **2003**, *103*, 2921–2944.
- [2] a) T. C. Nugent, M. El-Shazly, *Adv. Synth. Catal.* **2010**, *352*, 753–819; b) A. Armstrong, *Org. Process Res. Dev.* **2001**, *5*, 457–457.
- [3] a) B. M. Trost, M. D. Spagnol, *J. Chem. Soc.-Perkin Trans.* **1995**, 2083–2097; b) J.-C. Hierso, A. Fihri, R. Amardeil, P. Meunier, H. Doucet, M. Santelli, *Tetrahedron* **2005**, *61*, 9759–9766.
- [4] R. Takeuchi, N. Ue, K. Tanabe, K. Yamashita, N. Shiga, *J. Am. Chem. Soc.* **2001**, *123*, 9525–9534.
- [5] B. L. Ashfeld, K. A. Miller, A. J. Smith, K. Tran, S. F. Martin, *J. Org. Chem.* **2007**, *72*, 9018–9031.
- [6] A. Riisager, R. Fehrmann, M. Haumann, P. Wasserscheid, *Eur. J. Inorg. Chem.* **2006**, *2006*, 695–706.
- [7] A. Wolny, A. Chrobok, *Molecules* **2022**, *27*, 5900.
- [8] M. H. Valkenberg, C. deCastro, W. F. Hölderich, *Green Chem.* **2002**, *4*, 88–93.
- [9] a) C. P. Mehnert, R. A. Cook, N. C. Dispenziere, M. Afeworki, *J. Am. Chem. Soc.* **2002**, *124*, 12932–12933; b) A. Riisager, B. Jørgensen, P. Wasserscheid, R. Fehrmann, *Chem. Commun.* **2006**, 994–996; c) M. Haumann, K. Dentler, J. Joni, A. Riisager, P. Wasserscheid, *Adv. Synth. Catal.* **2007**, *349*, 425–431.
- [10] a) P. Lozano, E. García-Verdugo, R. Piamtongkam, N. Karbass, T. De Diego, M. I. Burguete, S. V. Luis, J. L. Iborra, *Adv. Synth. Catal.* **2007**, *349*, 1077–1084; b) B. García, S. Lavallée, G. Perron, C. Michot, M. Armand, *Electrochim. Acta* **2004**, *49*, 4583–4588; c) A. Sainz Martinez, C. Hauzenberger, A. R. Sahoo, Z. Csendes, H. Hoffmann, K. Bica, *ACS Sustainable Chem. Eng.* **2018**, *6*, 13131–13139; d) P. Mikšovsky, E. N. Horn, S. Naghdi, D. Eder, M. Schnürch, K. Bica-Schröder, *Org. Process Res. Dev.* **2022**, *26*, 2799–2810.
- [11] U. Hintermair, G. Franciò, W. Leitner, *Chem. Eur. J.* **2013**, *19*, 4538–4547.
- [12] M. Rufete-Beneite, M. Haumann, M. C. Román-Martínez, *J. Mol. Catal.* **2018**, *453*, 31–38.
- [13] a) J. Brünig, Z. Csendes, S. Weber, N. Gorgas, R. W. Bittner, A. Limbeck, K. Bica, H. Hoffmann, K. Kirchner, *ACS Catal.* **2018**, *8*, 1048–1051; b) R. Kukawka, A. Pawlowska-Zygarowicz, J. Dzialkowska, M. Pietrowski, H. Maciejewski, K. Bica, M. Smiglak, *ACS Sustainable Chem. Eng.* **2019**, *7*, 4699–4706.
- [14] B. Urbán, D. Srankó, G. Sáfrán, L. Úrge, F. Darvas, J. Bakos, R. Skoda-Földes, *J. Mol. Catal. A* **2014**, *395*, 364–372.
- [15] S. More, S. Jadhav, R. Salunkhe, A. Kumbhar, *J. Mol. Catal.* **2017**, *442*, 126–132.
- [16] Á. M. Pálvölgyi, M. Schnürch, K. Bica-Schröder, *Tetrahedron* **2020**, *76*, 131246.
- [17] R. Castro-Amoedo, Z. Csendes, J. Brünig, M. Sauer, A. Foelske-Schmitz, N. Yigit, G. Rupprechter, T. Gupta, A. M. Martins, K. Bica, H. Hoffmann, K. Kirchner, *Catal. Sci. Technol.* **2018**, *8*, 4812–4820.
- [18] a) C. C. R. Allen, C. J. Boudet, C. Hardacre, M. E. Migaud, *RSC Adv.* **2014**, *4*, 19916–19924; b) M. Opanasenko, P. Štěpnička, J. Čejka, *RSC Adv.* **2014**, *4*, 65137–65162.
- [19] a) K. Machanová, J. Jacquemin, Z. Wagner, M. Bendová, *Procedia Eng.* **2012**, *42*, 1229–1241; b) L.-S. Wang, X.-X. Wang, Y. Li, K. Jiang, X.-Z. Shao, C.-J. Du, *AIChE J.* **2013**, *59*, 3034–3041.
- [20] C. J. Mathews, P. J. Smith, T. Welton, A. J. White, D. J. Williams, *Organo-metallics* **2001**, *20*, 3848–3850.
- [21] a) V. Chandrasekhar, R. Boomishankar, K. Gopal, P. Sasikumar, P. Singh, A. Steiner, S. Zacchini, *Eur. J. Inorg. Chem.* **2006**, *2006*, 4129–4136; b) B. Sreedhar, V. Bhaskar, C. Sridhar, T. Srinivas, L. Kótai, K. Szentmihályi, *J. Mol. Catal. A* **2003**, *191*, 141–147; c) H. Hu, H. Ota, H. Baek, K. Shinohara, T. Mase, Y. Uozumi, Y. M. A. Yamada, *Org. Lett.* **2020**, *22*, 160–163.
- [22] a) B. Emayavaramban, M. Roy, B. Sundararaju, *Chem. Eur. J.* **2016**, *22*, 3952–3955; b) A. Volkov, F. Tinnis, T. Slagbrand, I. Pershagen, H. Adolfsson, *Chem. Commun.* **2014**, *50*, 14508–14511; c) D.-Y. Wang, X.-M. Peng, G.-Z. Wang, Y.-J. Zhang, T. Guo, P.-K. Zhang, *Asian J. Org. Chem.* **2018**, *7*, 875–878.
- [23] B. M. Trost, G. M. Schroeder, *J. Org. Chem.* **2000**, *65*, 1569–1573.
- [24] a) B. M. Trost, L. S. Kallander, *J. Org. Chem.* **1999**, *64*, 5427–5435; b) B. M. Trost, M. Osipov, P. S. J. Kaib, M. T. Sorum, *Org. Lett.* **2011**, *13*, 3222–3225.
- [25] B. Wiese, G. Helmchen, *Tetrahedron Lett.* **1998**, *39*, 5727–5730.
- [26] J. C. Anderson, R. J. Cubbon, J. D. Harling, *Tetrahedron: Asymmetry* **2001**, *12*, 923–935.
- [27] G. Chen, X. Li, H. Zhang, L. Gong, A. Mi, X. Cui, Y. Jiang, M. C. K. Choi, A. S. C. Chan, *Tetrahedron: Asymmetry* **2002**, *13*, 809–813.
- [28] M. Majdecki, J. Jurczak, T. Bauer, *ChemCatChem* **2015**, *7*, 799–807.
- [29] Z. Császár, G. Farkas, A. Bényei, G. Lendvay, I. Tóth, J. Bakos, *Dalton Trans.* **2015**, *44*, 16352–16360.
- [30] O. Pàmies, J. Margalef, S. Cañellas, J. James, E. Judge, P. J. Guiry, C. Moberg, J.-E. Bäckvall, A. Pfaltz, M. A. Pericàs, M. Diéguez, *Chem. Rev.* **2021**, *121*, 4373–4505.
- [31] G. S. Mahadik, S. A. Knott, L. F. Szczepura, S. J. Peters, J. M. Standard, S. R. Hitchcock, *J. Org. Chem.* **2009**, *74*, 8164–8173.
- [32] Y. K. Kim, S. J. Lee, K. H. Ahn, *J. Org. Chem.* **2000**, *65*, 7807–7813.
- [33] M. Nascimento de Oliveira, S. Arseniyadis, J. Cossy, *Chem. Eur. J.* **2018**, *24*, 4810–4814.
- [34] A.-M. Carroll, M. McCarthy, P. M. Lacey, C. P. Saunders, D. J. Connolly, A. Farrell, B. V. Rokade, R. Goddard, P. Fristrup, P.-O. Norrby, P. J. Guiry, *Tetrahedron* **2020**, *76*, 130780.
- [35] N. Boufroua, E. Dunach, F. Fontaine-Vive, S. Achouche-Bouzroua, S. Poulain-Martini, *New J. Chem.* **2020**, *44*, 6042–6052.
- [36] H. Jin, X. Jiang, H. Yoo, T. Wang, C. G. Sung, U. Choi, C. R. Lee, H. Yu, S. Koo, *ChemistrySelect* **2020**, *5*, 12421–12424.
- [37] P.-S. Gao, F. Ye, X.-Y. Dong, Y. Chen, Z.-W. Gao, W.-Q. Zhang, L.-W. Xu, *RSC Adv.* **2015**, *5*, 33818–33822.
- [38] J. Jing, X. Huo, J. Shen, J. Fu, Q. Meng, W. Zhang, *Chem. Commun.* **2017**, *53*, 5151–5154.
- [39] K. N. Gavrilov, S. V. Zheglov, M. N. Gavrilova, I. M. Novikov, M. G. Maksimova, N. N. Groshkin, E. A. Rastorguev, V. A. Davankov, *Tetrahedron* **2012**, *68*, 1581–1589.
- [40] T. H. West, D. S. B. Daniels, A. M. Z. Slawin, A. D. Smith, *J. Am. Chem. Soc.* **2014**, *136*, 4476–4479.
- [41] D. Krishnan, M. Wu, M. Chiang, Y. Li, P.-H. Leung, S. A. Pullarkat, *Organometallics* **2013**, *32*, 2389–2397.
- [42] T. Ohshima, Y. Miyamoto, J. Ipposhi, Y. Nakahara, M. Utsunomiya, K. Mashima, *J. Am. Chem. Soc.* **2009**, *131*, 14317–14328.
- [43] D. Banerjee, R. V. Jagadeesh, K. Junge, H. Junge, M. Beller, *ChemSusChem* **2012**, *5*, 2039–2044.
- [44] B. M. Trost, D. L. Van Vranken, C. Bingel, *J. Am. Chem. Soc.* **1992**, *114*, 9327–9343.
- [45] Y. K. Kim, S. J. Lee, K. H. Ahn, *J. Org. Chem.* **2000**, *65*, 7807–7813.
- [46] M. Marinova, M. Torres-Werlé, G. Taupier, A. Maise-François, T. Achard, A. Boeglin, K. D. H. Dorkenoo, S. Bellemin-Laponnaz, *ACS Omega* **2019**, *4*, 2676–2683.

Manuscript received: March 9, 2023
 Revised manuscript received: April 6, 2023
 Accepted manuscript online: April 6, 2023
 Version of record online: May 11, 2023

5. Continuous synthesis of carbamates from CO₂ and amines

The excess of carbon dioxide in the atmosphere is considered the main contributor to global warming; therefore, its valorisation has become a key challenge in the 21st century.^[121] The magnitude of the crisis caused by climate change is gigantic, as approximately 36.6 gigatonnes of CO₂ are emitted into the atmosphere yearly, demanding urgent actions.^[122] It is the chemical society's responsibility to provide solutions for this issue, and so far, chemists have come up with some suitable approaches for CO₂ utilisation in chemical transformations. Using CO₂ as a C1 building block is an attractive strategy and has received significant scientific interest in recent years.^[123] Using carbon dioxide would be a direct way to harvest nature's carbon resources; therefore, its capture from flue gases is a field that has recently received a dynamic increase in interest.^[124]

The CO₂ molecule's low reactivity and high chemical stability render its utilisation in chemical reactions extremely challenging. Additional energy is required to activate the molecule to overcome its thermodynamically low level. Therefore, CO₂ is often reacted with high-energy starting materials, such as epoxides or aziridines (**Figure 41**).^[125]

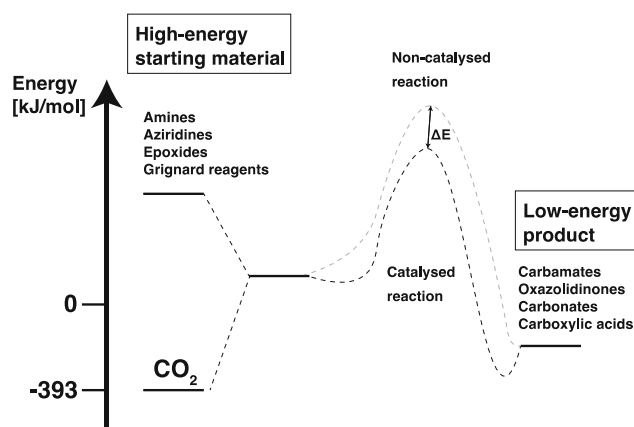


Figure 41. Schematic illustration of the energy balance for transforming CO₂ into low-energy products^[126]

The linear CO₂ molecule consists of 2 nucleophilic oxygen atoms and an electrophilic carbon centre with a π -electron system, thus providing various options for its chemical transformation. It has been successfully valorised in the synthesis of carboxylic acids,^[127] alcohols,^[128] cyclic- and non-cyclic carbonates,^[129] carbamates,^[130] and various polymers^[131] among many chemically invaluable species (**Figure 42**).

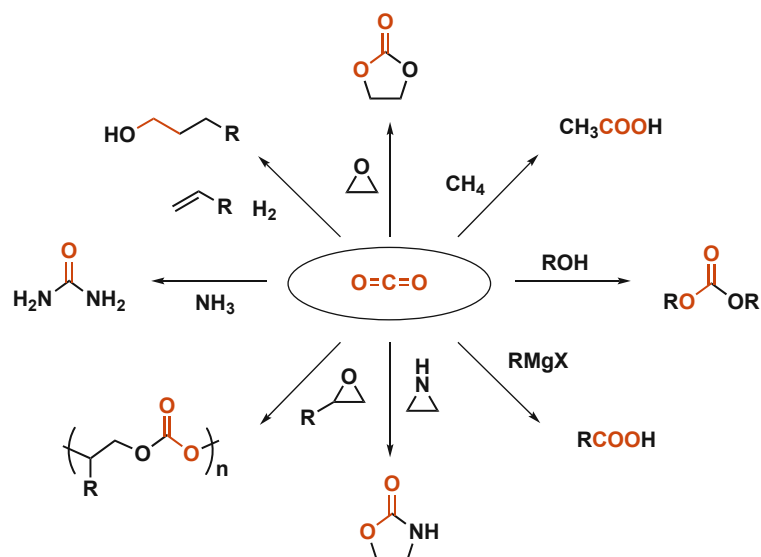


Figure 42. Selected examples for CO₂ utilisation in synthetic chemistry

Urethanes are considered essential structural moieties of many bioactive compounds, such as therapeutic agents or agricultural chemicals, and they are also utilised in the synthesis of polyurethanes. Carbamates have found widespread application in synthetic chemistry; many of the most popular protecting groups are introduced as carbamate moieties.^[132]

Methods relying on the direct fixation of CO₂ in the synthesis of carbamates became more relevant in the past decade and provide a suitable alternative to circumvent the problems associated with conventional strategies. Simultaneously, these approaches utilise an abundant C1 source and building block, which is favourable from an environmental perspective.^[130b, 133]

This chapter presents a continuous approach that employs no additional catalyst, performs under mild conditions, and provides the desired carbamates in just 50 minutes (**Figure 43**).

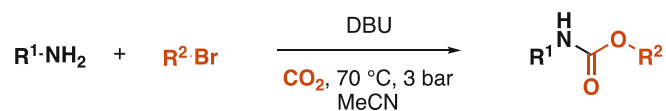


Figure 43. Continuous CO₂-based synthesis of urethanes

We investigated tetraalkylammonium salts as additives, but employing them did not have a positive influence on the reaction rate or selectivity. The simple and fast approach only uses DBU as additive, and the strategy offers synthetic flexibility as a wide range of amines can be employed. The continuous set-up significantly reduces the reaction time compared to other CO₂-based synthetic methods. The reaction conditions are mild, and the products can be obtained in 45 to 92% yields, often without subsequent purification *via* column chromatography. This makes the process less time-consuming and more environmentally friendly. The modified procedure can also be used for the selective synthesis of oxazolidinones from aziridines.

The following manuscript will be presented in this chapter:

K. Stigel, L. Ielo, K. Bica-Schröder: Continuous Synthesis of Carbamates from CO₂ and Amines. *ACS Omega* **2023**, submitted.

As a first author, the experimental work was planned and performed by me, and I wrote the original draft.

Continuous Synthesis of Carbamates from CO₂ and Amines

Kristof Stagel,^a Laura Ielo,^{a,b} and Katharina Bica-Schröder^{a,}*

^aInstitute of Applied Synthetic Chemistry, TU Wien, Getreidemarkt 9/163, Vienna, 1060, Austria

^bDepartment of Chemistry, University of Turin, Via P. Giuria 7, Torino, 10125, Italy

*Corresponding author: Katharina Bica-Schröder. E-mail: katharina.schroeder@tuwien.ac.at, Tel.: +43 1 58801 163601

Abstract

We present a novel approach for the CO₂-based continuous preparation of carbamates. The simple yet fast synthetic route relies on directly utilizing carbon dioxide and, in contrast with the literature-known methods, only employs DBU as additive. The applicable amines' diversity offers considerable flexibility to the synthetic protocol. Additionally, the continuous method's applicability significantly decreases the reaction time typically required for CO₂-based carbamate synthesis and allows for straightforward and precise gas introduction. The mild reaction conditions and omission of the need for column chromatography render the process less time-demanding and environmentally more benign, providing the desired compounds in yields of 45 to 92%. Moreover, the modified procedure can potentially be applied in the selective synthesis of oxazolidinones from aziridines.

Introduction

Since carbon dioxide is considered the primary contributor to global warming, its valorization has become the most severe task the chemical society faces in the 21st century.^{1,2} The annual CO₂ emission reached approximately 36.6 gigatonnes, demanding urgent actions to avoid an irreversible disaster.³ So far, chemists have developed suitable approaches for utilizing carbon dioxide, among which its use as a C1 building block provides an attractive strategy.⁴⁻⁷ Using CO₂ in chemical transformations has received significant scientific interest in the past decade since it is a direct way to harvest nature's carbon resources and simultaneously utilize non-toxic starting materials.⁸⁻¹⁰ Carbon dioxide has been successfully valorized in synthesizing chemically invaluable species, such as alcohols,^{11, 12} carboxylic acids,¹³ carbonates,¹⁴ or carbamates.¹⁵

Urethanes are considered essential structural moieties of a plethora of bioactive compounds, such as agricultural chemicals or therapeutic agents.^{16, 17} Moreover, organic carbamates are utilized in the synthesis of polyurethanes.¹⁸ Carbamates have found widespread application in synthetic chemistry; for example, many of the most popular protecting groups in peptide synthesis are introduced as carbamate moieties.^{19, 20}

The industrial synthesis of organic carbamates relied on reacting alkyl isocyanates with alcohols.²¹ Isocyanates are considered highly toxic reagents, as evidenced by the disastrous chemical accidents in the past;²² thus, they are often formed *in situ* to avoid safety hazards associated with handling large amounts of isocyanates. Other strategies react alkyl chloroformates with amines, thus generating at least stoichiometric amounts of HCl as a waste by-product. Additionally, the chloroformate-based synthetic route is also hampered by long reaction times, and a large excess of base is required to acquire an acceptable conversion.¹⁷ Methods relying on the direct fixation of CO₂ have become more relevant in the past decade

and provide an attractive alternative synthetic route that circumvents toxic alkyl isocyanates or costly metal catalysts while simultaneously utilizing an abundant C1 source and building block.

The first method employing carbon dioxide, amines, and alkyl halides in the presence of a base was reported by McGhee and co-workers.¹⁵ The group investigated the influence of different bases on the reaction selectivity and yield, and they also conducted mechanistic studies. Based on their research, the reaction proceeds through the formation of an ionic intermediate, and it can be accelerated by adding strong non-nucleophilic bases.

Dindarloo and co-workers utilized deep eutectic solvents (DESs) to synthesize carbamates.²³ The choline chloride-based DES was found to be suitable for the process, as less reactive alkyl chlorides were successfully utilized, and the desired carbamates were isolated in good yields.

Yoshida *et al.* investigated different quaternary onium salts for synthesizing carbamates using supercritical carbon dioxide as solvent and reagent.²⁴ Employing tetraalkylammonium halides, in particular tetrabutylammonium bromide, had a positive influence on the reaction yield.

In 2011, a PEG-promoted method for carbamate synthesis was reported by Kong.²⁵ The approach effectively suppressed the formation of the undesired by-products and provided the desired products under mild conditions.

As the application of zeolites in chemical transformations has emerged, a zeolite-assisted synthetic method for producing carbamates was reported in the early 2000s. Srivastava employed metal complex-containing zeolite catalyst frameworks, and the optimal conditions provided the desired products with good selectivity.²⁶

In recent years, various zinc-based catalyst systems have been described. Biswas *et al.* established a method relying on a polymer-bound zinc(II) complex to synthesize benzimidazole derivatives and carbamates.²⁷ The recyclable heterogeneous catalyst system proved effective and enabled the reaction to proceed under environmentally benign conditions,

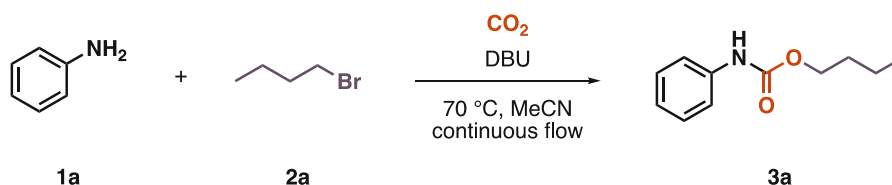
such as low pressure and temperature. The same research group reported a graphene oxide-based zinc composite as an efficient catalyst for CO₂ fixation through the synthesis of carbamates.²⁸ The group also described a method relying on titanium phosphate to convert epoxides and amines to carbonates and carbamates, respectively.²⁹

Evidently, various methods for the fixation of CO₂ through carbamate synthesis are available. However, they have certain limitations: some require elevated pressures or temperatures, whereas others are hampered by long reaction times, low reactivity, or reproducibility. Almost all the developed methods require additional catalysts, some of which are non-commercial and require a multistep synthetic pathway. Moreover, all the reported strategies have been developed for batch reactions, and none of the above-mentioned approaches were investigated in continuous mode.

In here, we report for the first time a continuous approach that employs no additional catalyst, performs under mild reaction conditions, and provides the desired carbamates in just 50 minutes. Additionally, the synthesized carbamates are, with few exceptions, analytically pure after an acidic workup, and no further purification was needed, which renders the approach more environmentally benign.

Results and discussion

Based on the results of McGhee in the CO₂-based synthesis of carbamates,¹⁵ we initially investigated the synthesis of *N*-phenyl butylcarbamate, starting from aniline and butyl bromide, employing DBU (1,8-Diazabicyclo[5.4.0]undec-7-ene) as a base (**Scheme 1**). DBU's liquid nature is beneficial for the continuous process; hence its employment provides a homogeneous mixture. Economically more viable alternatives, such as triethylamine and *N,N*-diisopropylethylamine, were investigated as well, but no conversion was observed when these bases were employed.

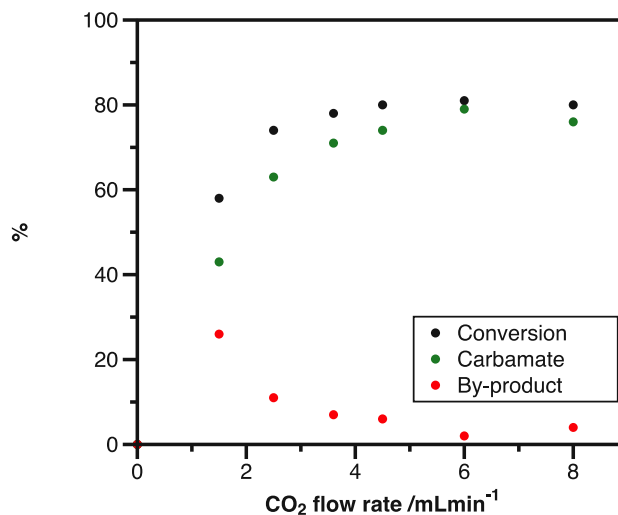


Scheme 1. Continuous synthesis of *N*-phenyl butylcarbamate

Initially, an excess of two equivalents of alkyl halide and DBU were employed. All the reactants were dissolved in acetonitrile. Carbon dioxide was introduced directly from a gas bottle using a mass flow controller. The bottle was connected to the flow chemistry device with metal tubing; the V3 pumps efficiently mixed CO₂ with the reaction mixture in a 10-mL coil reactor.

It is worth mentioning that there was no need to employ a gas-liquid tube-in-tube reactor; hence dynamic mixing can be achieved in the standard coil reactor if enough residence time is allowed for the reaction to be depleted. Therefore, the reaction mixture's flow rate was set to 250 μL/min. The reactions were carried out at 70 °C, and the back-pressure regulator was set to 3 bars.

First, we sought to investigate the influence of CO₂ flow rate on the conversion (**Scheme 2**); the samples were analyzed by GC-MS.



Scheme 2. The influence of CO₂ flow rate on conversion and by-product formation

A CO₂ flow rate of 1.5 mL/min yielded 58% conversion, which reached 78% with an increase of the flow rate to 3.6 mL/min, but any further rise did not have any significant influence. However, an increased flow rate of 6 mL/min yielded a favorable outcome as the formed by-product (*N*-butylaniline) amount decreased significantly. We assume that the sizeable volumetric excess of carbon dioxide accelerates the formation of the desired carbamate instead of the *N*-alkylated by-product. Therefore, a CO₂ flow rate of 6 mL/min was chosen for the following experiments.

Subsequently, the reaction mixture flow rate was varied. Neither its decrease nor its increase had any influence on the reaction. In fact, a flow rate of 125 μL/min led to a minor increase in the by-product amount. Similarly, varying the concentration of the substrate did not affect the conversion.

Further parameters, such as temperature and pressure, were evaluated after determining the ideal volumetric ratio of the reaction mixture and carbon dioxide (

Table 1).

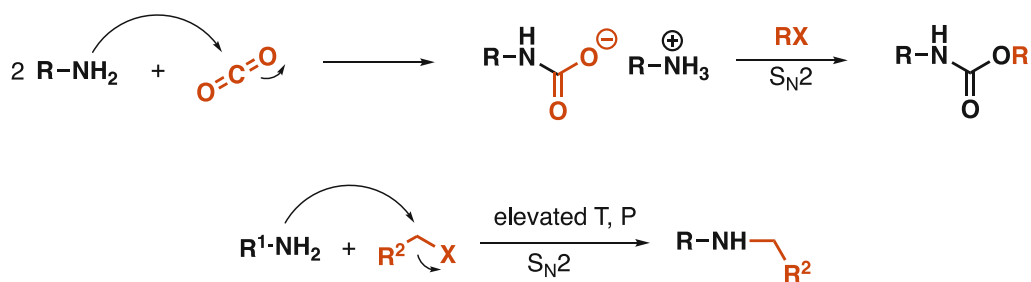
Table 1. Effect of temperature and pressure on the conversion

Entry ^[a]	Temperature /°C	Pressure /bar	Conversion /% ^[b]	Carbamate /% ^[b]	By-product /% ^[b]
1	60	3	70	67	3
2	70	3	83	81	2
3	80	3	88	79	9
4	70	1	56	51	5
5	70	3	92	88	4
6	70	5	98	91	7
7	70	7	96	83	13

[a] Performed with 4.3 mmol (1.0 eq.) aniline, 8.6 mmol (2.0 eq.) DBU and 8.6 mmol (2.0 eq.) butyl bromide in 5 mL MeCN in a 10-mL coil reactor. Reaction mixture flow rate: 250 μ L/min, CO₂ flow rate: 6 mL/min. The product was collected for 50 minutes. [b] Determined by GC-MS analysis.

As can be seen, lowering the temperature to 60 °C had an undesirable outcome, as the conversion decreased by almost 15% (entry 1). On the other hand, an elevated temperature of 80 °C favored the *N*-alkylated by-product formation (entry 3). Similarly, when maintaining the temperature at 70 °C, a decrease in pressure led to a drop in the conversion by 37% (entry 4), whereas its rise to 5 or 7 bars yielded 7% (entry 6) and 13% (entry 7) by-product, respectively. Presumably, in the 1st step of the reaction, CO₂ is attacked by the amine nucleophile, leading to a formation of a carbamate anion, which attacks the alkyl halide to form the alkyl carbamate.^{15, 26}

Strong organic bases are known to stabilize the carbamate intermediate.^{15, 24} Supposedly, if the reactor operates at harsher conditions when the reaction mixture enters, the *N*-alkylated by-product formation is significantly faster than the formation of the carbamate anion. Acetonitrile's polar and aprotic nature might also favor the S_N2 substitution of the halide, leading to the formation of *N*-butylaniline (**Scheme 3**).



Scheme 3. Proposed mechanism of carbamate- and by-product formation

Based on these results, 70 °C and 3 bar provide good conversion with only negligible formation of the corresponding by-product.

After identifying the optimal temperature and pressure, we investigated the alkyl halide's and the DBU's influence on the reaction (**Table 2**). First, the DBU amount was varied while the halide amount was maintained constant (entries 1-5), and an excess of 2.0 equivalents yielded the best conversion (entry 3). Any further increase did not positively affect the reaction. After that, we examined the alkyl halide's influence on the reaction (entries 6-9). Using 2.5 equivalents yielded 91% conversion (entry 8); however, an excess above 2.0 equivalents can significantly increase the by-product amount, as we discovered by testing other nucleophiles.







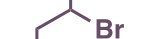



Table 2. Influence of the alkyl halide on the reaction

Entry ^[a]	BuBr eq.	DBU eq.	Conversion /% ^[b]	Carbamate /% ^[b]
1	2.0	1.0	62	55
2	2.0	1.5	76	69
3	2.0	2.0	81	79
4	2.0	2.5	81	76
5	2.0	3.0	77	73
6	1.0	2.0	59	57
7	1.5	2.0	71	66
8	2.5	2.0	91	87
9	3.0	2.0	87	84

[a] Performed with 4.3 mmol (1.0 eq.) aniline and 8.6 mmol (2.0 eq.) DBU in 5 mL MeCN in a 10-mL coil reactor. Reaction mixture flow rate: 250 $\mu\text{L}/\text{min}$, CO_2 flow rate: 6 mL/min. The product was collected for 50 minutes. [b] Determined by GC-MS analysis.

Having these optimal conditions at hand, we sought to screen different alkylating agents and additional alkyl bromides. The results are presented in **Table 3**.

Table 3. Screening results for alkylating agents

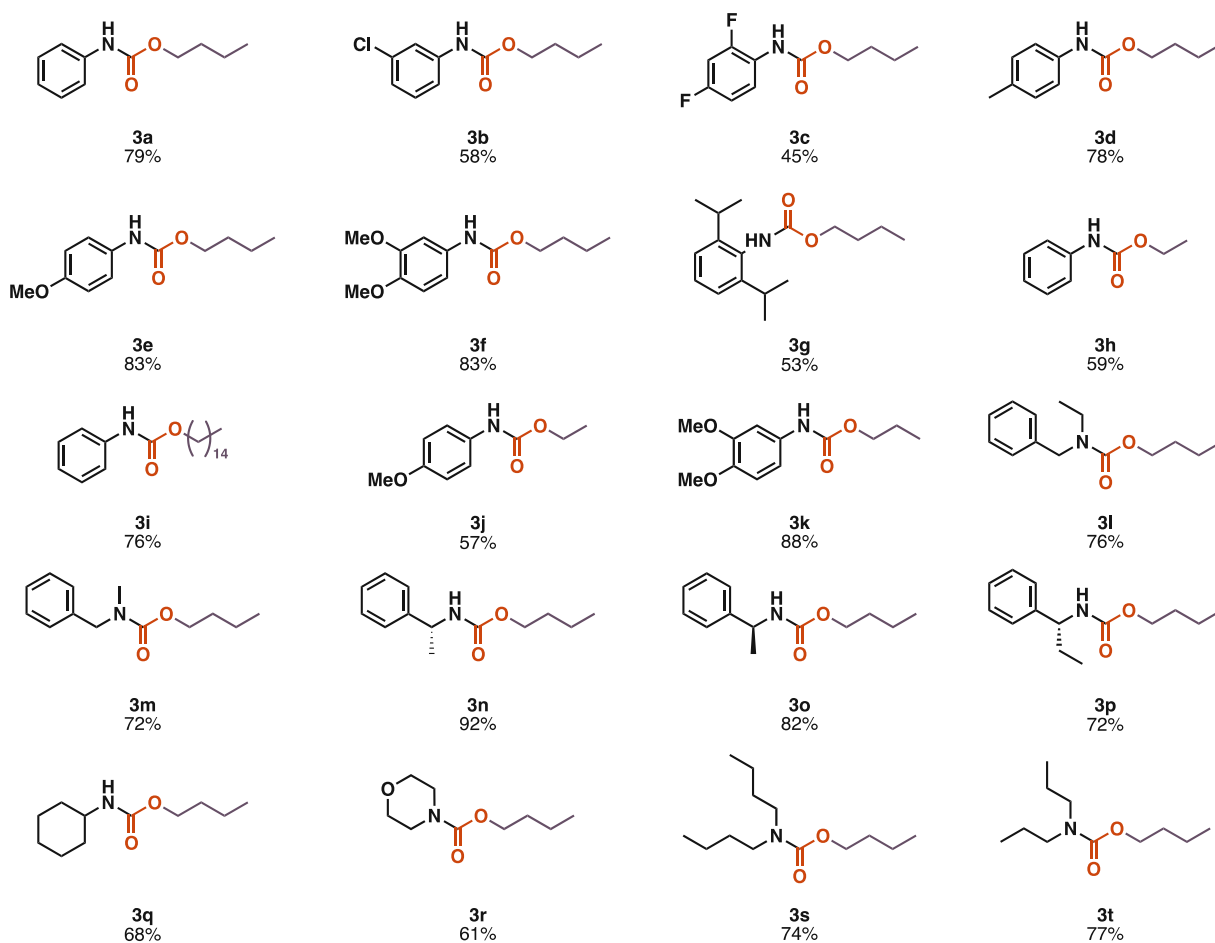
Entry ^[a]	Reagent	Reagent structure	Conversion /% ^[b]	Carbamate/% ^[b]	By-product /% ^[b]
1	2a		86	82 (79) ^[c]	4
2	2b		n.d.	n.d.	n.d.
3	2c		44	36	8
4	2d		92	48	44
5	2e		57	57	n.d.
6	2f		41	41	n.d.
7	2g		n.d.	n.d.	n.d.
8	2h		n.d.	n.d.	n.d.
9	2i		74	68 (59) ^[c]	6
10	2j	$\text{C}_{11}\text{H}_{23}$ 	93	83 (76) ^[c]	10

[a] Performed with 4.3 mmol (1.0 eq.) aniline, 8.6 mmol (2.0 eq.) alkylating agent, and 8.6 mmol (2.0 eq.) DBU in 5 mL MeCN in a 10-mL coil reactor. Reaction mixture flow rate: 250 $\mu\text{L}/\text{min}$, CO_2 flow rate: 6 mL/min. The product was collected for 50 minutes. [b] Determined by GC-MS analysis. [c] Isolated yields.

Surprisingly, the employment of 1-iodobutane (entry 3) did not provide sufficient conversion and demonstrated an overall lower reactivity compared to 1-bromobutane (entry 1). 1-Chlorobutane (entry 2) as alkylating agent proved completely inactive under the developed

conditions. When working with butyl tosylate (entry 4), 48% of the carbamate product was obtained. However, the by-product amount almost reached the same value (44%). Isobutyl bromide (entry 5) and *sec*-butyl bromide (entry 6) yielded low conversions, 57% and 41%, respectively. Theoretically, these primary and secondary bromides should undergo S_N2 substitution under these reaction conditions, but the steric hindrance of these halides complicates the reaction. The unsuccessful substitution of *tert*-butyl bromide can be explained by its tertiary nature, which would favor protic polar solvents to undergo S_N1 substitution. Its inactivity can also be explained by steric hindrance. By adding benzyl bromide (entry 8) to the vial containing the substrate and DBU in acetonitrile, we observed an immediate increase in temperature, indicating that instant *N*-alkylation probably occurred. Ethyl bromide (entry 9) provided slightly worse conversion, whereas dodecyl bromide (entry 10) proved almost as efficient alkylating agent as butyl bromide.

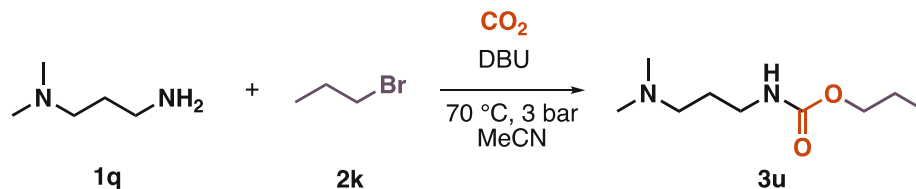
After testing a series of alkylating agents, we investigated various amines to extend the scope of our developed method; the results are presented below (**Scheme 4**).



Scheme 4. Scope of the continuous carbamate synthesis

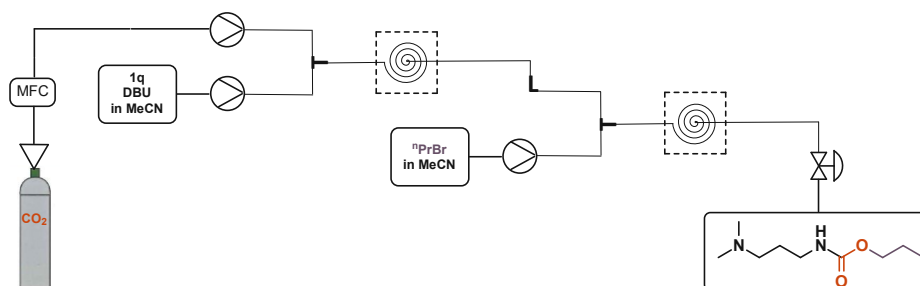
Aniline derivatives bearing electron-withdrawing groups, such as chloro- and fluoro substituents, as well as sterically hindered derivatives, proved less reactive as the corresponding carbamates (**3b**, **3c**, and **3g**) were isolated with lower yields. Anilines substituted by electron-donating groups provided similar reactivities to the unsubstituted aniline, as the corresponding carbamates (**3d**, **3e**, **3f**, **3k**) were isolated with good yields. The cyclic secondary amine derivative **3r** was obtained in a slightly lower yield than other non-cyclic secondary amine derivatives (**3s**, **3t**). To exclude the possibility of racemization, chiral HPLC analysis was performed in the case of compounds **3n** and **3o** (SI, Figure S57-59), which confirmed that the stereocenter remained intact during the reaction.

After successfully expanding the scope of our reaction, we employed our newly developed approach for a practical application. The synthesis of a pesticide commercially known as propamocarb (**3u**) was investigated (**Scheme 5**).



Scheme 5. Synthesis of propamocarb with our developed approach

We initially observed the formation of the *N*-alkylated carbamate as the main product while applying the previously developed conditions. Hence a second alkylation after forming the desired compound **3u** is unlikely; we suppose that the substrate initially reacted with the alkylating agent forming a secondary amine, which further reacted with CO₂ to form the undesired by-product. Therefore, we employed two reactors; in the first one, the reaction between the substrate and CO₂ took place to form the ionic intermediate, and this was further reacted in the second coil reactor with a solution of 1-bromopropane in acetonitrile to form the desired product (**Scheme 6**).



Scheme 6. System set-up for continuous synthesis of propamocarb

GC-MS analysis of the crude sample indicated complete conversion of propamocarb; however, it should be noted that the separation of remaining by-products was not successful with conventional chromatographic methods (Figure S46-S47, Supporting Information).

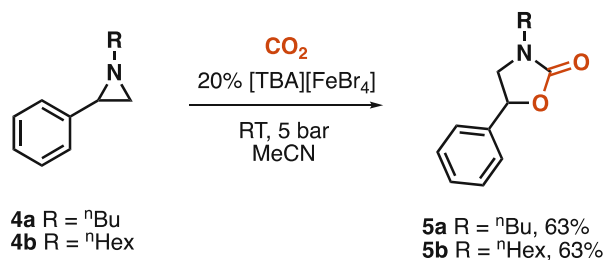
Finally, we expanded the developed method in the synthesis of oxazolidinones from aziridines. After testing several catalysts reported in the literature (**Table 4**),³⁰ we identified the Lewis acidic tetrabromoferrate ionic liquid formed from TBAB (tetrabutylammonium bromide) and FeBr₃ as the most suitable catalyst for continuous-flow formation of oxazolidinones (entry 8).³¹

Table 4. Toward the continuous synthesis of oxazolidinones

Entry	Catalyst /Conditions	CO ₂ flow rate /mL min ⁻¹	Conversion /% ^[a]	Oxazolidinone /% ^[a]	By- product /% ^[a]
1	10% L-threonine, 110 °C, 0.86 M	6	n.d.	n.d.	n.d.
2	10% TPPH ₂ Cl ₂ , 70 °C, 0.86 M	6	n.d.	n.d.	n.d.
3	10% TBAB, 70 °C, 0.86 M	6	98	3	95
4	10% [TBA][FeBr ₄], 70 °C, 0.86 M	6	1	1	n.d.
5	10% [TBA][FeBr ₄], 50 °C, 0.43 M	8	78	36	42
6	10% [TBA][FeBr ₄], 30 °C, 0.15 M	8	96	63	33
7	10% [TBA][FeBr ₄], 25 °C, 0.15 M	8	88	62	26
8	20% [TBA][FeBr ₄], 25 °C, 0.15 M	8	>99	95	5

[a] Determined by GC-MS analysis.

The reaction was carried out at room temperature, and the back-pressure regulator was set to 5 bar. Under these conditions, we successfully isolated the desired compounds with acceptable yields (63%, **Scheme 7**).



Scheme 7. Continuous synthesis of oxazolidinones from aziridines

It is worth mentioning that this method demonstrated high selectivity, as we only observed marginal amounts of the corresponding piperazine dimer by-products. The isolated oxazolidinones were found analytically pure, and the phenyl group position was confirmed by HSQC NMR analysis (Figure S54, Supporting Information).

Conclusions

Herein, we reported an approach for continuously utilizing CO₂ in the synthesis of carbamates without employing any catalyst or additive. To the best of our knowledge, this is the first continuous methodology that employs amines and alkyl halides in the presence of DBU and CO₂ to form urethanes. The process provides a faster and safer alternative for synthesizing carbamates from both primary and secondary amines. The desired compounds were obtained in just 50 minutes, with good to excellent yields, rendering our method a faster alternative for synthesizing urethanes from CO₂. Column chromatography could be avoided in many cases since an acidic treatment proved sufficient to obtain the products in high purities. We successfully demonstrated the method's applicability in synthesizing a commercial pesticide, propamocarb, providing excellent conversion. Moreover, the modified method was

tested in the aziridine-based synthesis of oxazolidinones and demonstrated high selectivity toward the desired compounds.

Experimental Section

General procedure for the continuous-flow synthesis of carbamates

The continuous-flow experiments were performed with the aid of a Vapourtec E-series flow chemistry device in a 10-mL coil reactor. A 30-mL vial with septum was charged with the corresponding amine (1.0 eq., 4.29 mmol), the corresponding alkyl bromide (2.0 eq., 8.58 mmol), and DBU (2.0 eq., 8.58 mmol). The reactants were dissolved in 5 mL acetonitrile. The solvent bottle was charged with MeCN. The reactor was heated up to the desired temperature (70 °C). Pump A was used as a back-pressure regulator (BPR, 3 bar). Pump B was connected to the vial with the reaction mixture; pump C was connected to the gas tube, where the CO₂ was introduced. Carbon dioxide was supplied from a cylinder. The gas flow rate was adjusted with a mass flow controller (6 mL/min). The tubes were primed with the reagent mixture and acetonitrile, respectively. The reactor (10-mL coil reactor) was initially rinsed by a CO₂/MeCN flow for several minutes. Then, the reaction mixture was supplied to the reactor (pump B: 0.25 mL/min; pump C: 6 mL/min). After the whole volume of the reaction mixture was pumped through the reactor, the vial was rinsed with pure MeCN, and the residue was pumped through the reactor. The product was collected for 50 minutes. Rotary evaporation of the solvent gave the crude product, which was bound to silica and subjected to column chromatography. Alternatively, the products could be purified *via* acidic treatment: the crude residue was taken up in dichloromethane, washed thrice with 1.5 M HCl solution, dried over anhydrous Na₂SO₄, filtered, and concentrated.

Acknowledgments

Financial support by the Austrian Science Fund (FWF, grant P 32882-N) is gratefully acknowledged. This project has received funding from the European Research Council (ERC) under the European Union's Horizon 2020 research and innovation programme (Grant agreement No. 864991).

Supporting Information

Detailed characterization of the synthesized carbamates via ^1H -, ^{13}C -, and ^{19}F -NMR spectroscopy, infrared spectroscopy, and high-resolution mass spectrometry. The data underlying this study are available in the published article and its Supporting Information.

Synopsis

A CO_2 -based method is applied for the continuous-flow production of carbamates without employing catalysts.

References

- (1) Kerr, R. A., How Hot Will the Greenhouse World Be? *Science* **2005**, *309* (5731), 100-100.
- (2) Montzka, S. A.; Dlugokencky, E. J.; Butler, J. H., Non-Co₂ Greenhouse Gases and Climate Change. *Nature* **2011**, *476* (7358), 43-50.
- (3) Bettenhausen, C., The Case for Direct Air Capture. *C&EN* **2022**, *100* (10), 22-24.
- (4) Aresta, M., Carbon Dioxide as Chemical Feedstock. In *Carbon Dioxide as Chemical Feedstock*, Aresta, M., Ed. John Wiley & Sons: 2010; p 394.
- (5) Bertau, M.; Offermanns, H.; Menges, G.; Keim, W.; Effenberger, F., Methanol Needs More Attention as a Fuel and Raw Material for the Future. *Chem. Ing. Tech.* **2010**, *82* (12), 2055-2058.
- (6) Saravanan, A.; Senthil kumar, P.; Vo, D.-V. N.; Jeevanantham, S.; Bhuvaneshwari, V.; Anantha Narayanan, V.; Yaashikaa, P. R.; Swetha, S.; Reshma, B., A Comprehensive Review on Different Approaches for Co₂ Utilization and Conversion Pathways. *Chem. Eng. Sci.* **2021**, *236*, 116515.
- (7) Kim, C.; Yoo, C.-J.; Oh, H.-S.; Min, B. K.; Lee, U., Review of Carbon Dioxide Utilization Technologies and Their Potential for Industrial Application. *J. CO₂ Util.* **2022**, *65*, 102239.
- (8) Ghiat, I.; Al-Ansari, T., A Review of Carbon Capture and Utilisation as a Co₂ Abatement Opportunity within the Ewf Nexus. *J. CO₂ Util.* **2021**, *45*, 101432.
- (9) Dubey, A.; Arora, A., Advancements in Carbon Capture Technologies: A Review. *J. Clean. Prod.* **2022**, *373*, 133932.
- (10) Chen, H.; Dong, H.; Shi, Z.; SenGupta, A. K., Direct Air Capture (Dac) and Sequestration of Co₂: Dramatic Effect of Coordinated Cu(Ii) onto a Chelating Weak Base Ion Exchanger. *Sci. Adv.* **2023**, *9* (10), eadg1956.
- (11) Marlin, D. S.; Sarron, E.; Sigurbjörnsson, Ó., Process Advantages of Direct Co₂ to Methanol Synthesis. *Front. Chem.* **2018**, *6*.
- (12) Zeng, F.; Mebrahtu, C.; Xi, X.; Liao, L.; Ren, J.; Xie, J.; Heeres, H. J.; Palkovits, R., Catalysts Design for Higher Alcohols Synthesis by Co₂ Hydrogenation: Trends and Future Perspectives. *App. Catal. B: Environ.* **2021**, *291*, 120073.
- (13) Ran, C.-K.; Liao, L.-L.; Gao, T.-Y.; Gui, Y.-Y.; Yu, D.-G., Recent Progress and Challenges in Carboxylation with Co₂. *Curr. Opin. Green Sustain. Chem.* **2021**, *32*, 100525.
- (14) Sainz Martinez, A.; Hauzenberger, C.; Sahoo, A. R.; Csendes, Z.; Hoffmann, H.; Bica, K., Continuous Conversion of Carbon Dioxide to Propylene Carbonate with Supported Ionic Liquids. *ACS Sustainable Chem. Eng.* **2018**, *6* (10), 13131-13139.
- (15) McGhee, W.; Riley, D.; Christ, K.; Pan, Y.; Parnas, B., Carbon Dioxide as a Phosgene Replacement: Synthesis and Mechanistic Studies of Urethanes from Amines, Co₂, and Alkyl Chlorides. *J. Org. Chem.* **1995**, *60* (9), 2820-2830.
- (16) Wang, L.; Qi, C.; Xiong, W.; Jiang, H., Recent Advances in Fixation of Co₂ into Organic Carbamates through Multicomponent Reaction Strategies. *Chinese J. Catal.* **2022**, *43* (7), 1598-1617.
- (17) Ghosh, A. K.; Brindisi, M., Organic Carbamates in Drug Design and Medicinal Chemistry. *J. Med. Chem.* **2015**, *58* (7), 2895-2940.
- (18) Takeuchi, K.; Matsumoto, K.; Fukaya, N.; Osakada, K.; Sato, K.; Choi, J.-C., Synthesis of Organic Carbamates as Polyurethane Raw Materials from Co₂: The Quest for Metal Alkoxides as Regenerable Reagents. *Dalton Trans.* **2022**, *51* (41), 15631-15643.
- (19) Chankeshwara, S. V.; Chakraborti, A. K., Catalyst-Free Chemoselective N-Tert-Butyloxycarbonylation of Amines in Water. *Org. Lett.* **2006**, *8* (15), 3259-3262.
- (20) Bergmann, M.; Zervas, L., Über Ein Allgemeines Verfahren Der Peptid-Synthese. *Ber. Dtsch. Chem. Ges.* **1932**, *65* (7), 1192-1201.

- (21) Chaturvedi, D., Recent Developments on the Carbamation of Amines. *Curr. Org. Chem.* **2011**, *15* (10), 1593-1624.
- (22) Varma, R.; Varma, D. R., The Bhopal Disaster of 1984. *Bull. Sci. Technol. Soc.* **2005**, *25* (1), 37-45.
- (23) Dindarloo Inaloo, I.; Majnooni, S., Carbon Dioxide Utilization in the Efficient Synthesis of Carbamates by Deep Eutectic Solvents (Des) as Green and Attractive Solvent/Catalyst Systems. *New J. Chem.* **2019**, *43* (28), 11275-11281.
- (24) Yoshida, M.; Hara, N.; Okuyama, S., Catalytic Production of Urethanes from Amines and Alkyl Halides in Supercritical Carbon Dioxide. *Chem. Commun.* **2000**, (2), 151-152.
- (25) Kong, D.-L.; He, L.-N.; Wang, J.-Q., Polyethylene Glycol-Enhanced Chemoselective Synthesis of Organic Carbamates from Amines, Co₂, and Alkyl Halides. *Synth. Commun.* **2011**, *41* (22), 3298-3307.
- (26) Srivastava, R.; Manju, M. D.; Srinivas, D.; Ratnasamy, P., Phosgene-Free Synthesis of Carbamates over Zeolite-Based Catalysts. *Catal. Lett.* **2004**, *97* (1), 41-47.
- (27) Biswas, I. H.; Biswas, S.; Islam, M. S.; Riyajuddin, S.; Sarkar, P.; Ghosh, K.; Islam, S. M., Catalytic Synthesis of Benzimidazoles and Organic Carbamates Using a Polymer Supported Zinc Catalyst through Co₂ Fixation. *New J. Chem.* **2019**, *43* (36), 14643-14652.
- (28) Khatun, R.; Biswas, S.; Islam, S.; Biswas, I. H.; Riyajuddin, S.; Ghosh, K.; Islam, S. M., Modified Graphene Oxide Based Zinc Composite: An Efficient Catalyst for N-Formylation and Carbamate Formation Reactions through Co₂ Fixation. *ChemCatChem* **2019**, *11* (4), 1303-1312.
- (29) Chowdhury, A. H.; Chowdhury, I. H.; Islam, S. M., Titanium Phosphate with Flower-Like Morphology as an Effective Reusable Catalyst for Chemical Fixation of Co₂ at Mild Reaction Conditions. *Ind. Eng. Chem. Res.* **2019**, *58* (27), 11779-11786.
- (30) Dank, C.; Ielo, L., Recent Advances in the Accessibility, Synthetic Utility, and Biological Applications of Aziridines. *Org. Biomol. Chem.* **2023**, *21* (22), 4553-4573.
- (31) Panza, N.; Alberti, M.; Galiè, S.; Damiano, C.; Cargnoni, F.; Italo Trioni, M.; Caselli, A., Ammonium Ferrate-Catalyzed Cycloaddition of Co₂ to Aziridines for the Synthesis of 1,3-Oxazolidin-2-Ones. *Eur. J. Org. Chem.* **2022**, *2022* (40), e202200908.

6. Online coupling high-temperature electrolysis with carbonylation reactions: a powerful method for continuous carbon dioxide utilisation

The reduction of CO_2 to a much more reactive, and thus, chemically more invaluable species, carbon monoxide, provides a suitable strategy for its utilisation.^[134] Since its applicability in synthetic organic chemistry has been demonstrated,^[135] carbon monoxide has found widespread utilisation in various chemical transformations.^[136]

In organic synthesis, CO is mainly used in carbonylation- or hydroformylation reactions, often in the presence of a transition metal catalyst.^[137] Although it is considered a subclass of carbonylation, hydroformylation means introducing a formyl group (CHO) to an unsaturated compound, mainly to a carbon-carbon double bond, forming aldehydes. In contrast, carbonylation reactions exclusively introduce the CO moiety to an organic substrate.

From the reaction intermediates' point of view, four different subcategories of carbonylation can be distinguished: (i) transition-metal-catalysed carbonylation, relying on the CO's subsequent coordination and insertion into the metal-carbon bond, (ii) cationic carbonylation initiated by strong acids, (iii) anionic carbonylation initiated by strong bases, and (iv) free-radical carbonylation, where organic free radicals capture the CO to form acid radicals. Carbonylation reactions are mainly based on transition-metal catalysts.^[138] The following figure shows how carbon monoxide coordinates to a metal atom (**Figure 44**).

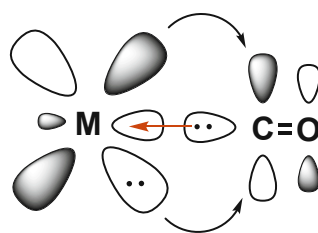
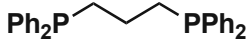
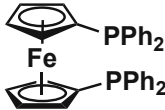
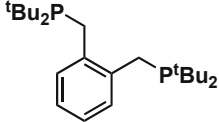
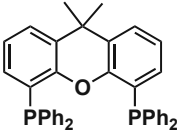
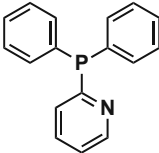
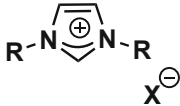
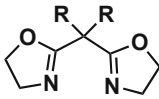


Figure 44. Bonding of CO with transition metal atoms

The electrons from the CO molecule's HOMO orbitals are donated to an empty d-orbital of the metal centre (σ donating, represented by the orange arrow), forming a synergetic M-CO bond. Subsequently, electrons are partially transferred from one of the metal's d-orbitals to the CO molecule's anti-bonding LUMO (relatively low-energy π^*) orbital (π back bonding, represented by the black arrows). This interaction strengthens the metal-carbon bond, shortens its length, and weakens the carbon-oxygen bond, resulting in its activation *via* π back bonding. Most of the transition metals are capable of forming complexes with CO and catalysing carbonylative transformations.^[134, 139]

Most frequently, noble metals such as Pd, Rh, or Ir are used,^[140] but the applicability of non-noble transition metals in carbonylation reactions is known as well.^[141] The catalyst reactivity and selectivity can be further improved by employing ligands, from which a plethora of which is available: various *P*-, *N*-, or *C*-based ligands can all be used (**Table 1**).^[142]

Table 1. Ligands employed in various carbonylation reactions

Ligand name/type	Structure
dppp	
dppf	
dtbpm/dtbp	
Xantphos	
PPh ₂ Py	
NHC	
BOX	

The typical mechanism of a carbonylation reaction employing an alkyl halide as a substrate is presented below (**Figure 45**).

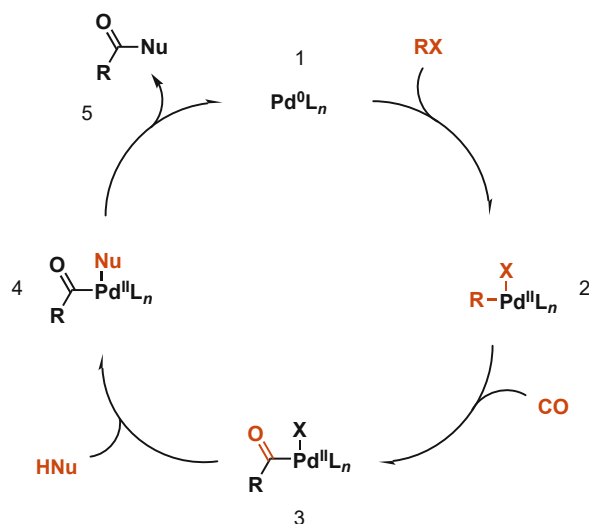


Figure 45. Reaction mechanism of carbonylation

Initially, the Pd-C species (2) is formed, which can be realized either by oxidative addition of Pd^0 (1) to a C-X bond or by nucleophilic palladation of Pd^{II} to an unsaturated compound (alkene, alkyne, or arene). This is followed by the coordination of CO and its subsequent insertion into the Pd-C bond to form the corresponding acyl palladium complex (3). After that, the nucleophile attacks, and the leaving group (X) is substituted (4). Finally, the product (5) is released by the Pd-complex, and the latter is regenerated, allowing the cycle to start again.^[142]

Over the past decades, a plethora of ligands and catalyst precursors have been tested, providing excellent activities and regioselectivities.^[143]

These processes can be further improved by implementing efficient catalyst regeneration strategies. Attaching water-soluble moieties to the employed ligand provides a feasible strategy for catalyst recycling. The biphasic method allows for straightforward recyclability, but bringing the water-soluble catalyst into contact with the hydrophobic substrate and reagents renders this approach challenging.^[144] Applying surfactants can improve the interaction between the catalyst and substrate molecules, providing a good solution.^[145]

Carbonylation reactions have found applications in continuous-flow processes as well. Fukuyama *et al.* reported a continuous carbonylation method relying on radical initiation.^[146] The desired carbonylated products were obtained with good to excellent yields in short residence times.

Gross and co-workers reported a continuous method for Pd-catalysed carbonylations by employing a tube-in-tube gas-liquid reactor.^[147] These reactors consist of a semipermeable membrane tube through which the reaction mixture passes. This inner tubing is covered by an outer, connected to a C cylinder; this allows the pressurised CO gas to surround the inner tube. A reverse arrangement of this setup is also possible. In that case, the gas flows in the inner-, and the reaction mixture through the outer tube (**Figure 46**).

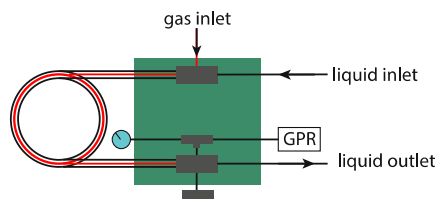


Figure 46. Tube-in-tube reactor^[147]

Reaction parameters, such as temperature, CO pressure, and metal-to-ligand ratio, have been optimised. With the optimal conditions in hand, different alkoxy-, hydroxyl-, and amino nucleophiles were employed in the carbonylation of aryl iodides and bromides to form the corresponding esters, carboxylic acids, and amides with excellent yields. Additionally, intramolecular reactions allowed the formation of lactones and lactams.

Carbon monoxide can be successfully utilised in continuous carbonylations; however, its intrinsic and tremendous toxicity renders its use severely risky. Its conventional substitutes, such as metal carbonyl or formates, are unavailable at affordable prices and suffer from low atom efficiency. To minimise the risk associated with CO and simultaneously utilise renewable sources, using CO₂ as its surrogate is worth considering. Due to its extreme thermodynamic stability, carbon dioxide needs to be activated to participate in a chemical transformation. Its partial/complete reduction to CO can provide a suitable basis for its utilisation in carbonylation reactions. Typically, harsh reaction conditions are required to reduce carbon dioxide, but its photo- or electrocatalytic reduction provides an attractive route for its activation under milder reaction conditions.

Jensen *et al.* announced a versatile strategy for electrochemically reducing carbon dioxide to CO with the aid of an iron porphyrin catalyst.^[148] Subsequently, the generated CO was utilised in various Pd-catalysed carbonylation reactions (**Figure 47**). The electrochemical reduction of CO₂ is performed with a galvanostat/potentiostat combined with stainless-steel electrodes, thus reducing the process costs. Many biologically active compounds have been synthesised and obtained with excellent yields. On the other hand, the approach was developed for batch-wise conditions; thus, longer reaction times were needed. Moreover, the generation of CO₂ on a 6 mmolar scale requires 24 hours, which is also undesirable.

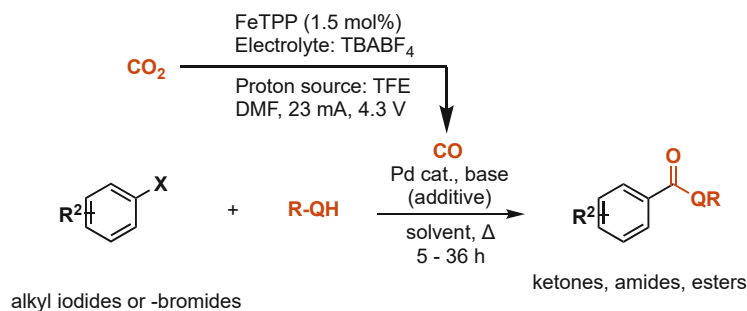


Figure 47. Electrochemical reduction of CO₂

In 2018, a photocatalytic strategy was reported for CO₂ reduction and subsequent utilisation in carbonylative transformations.^[149] The research group used a rhenium-based photocatalyst, which is easy to prepare, provides high selectivity toward CO production, and simultaneously acts as a photosensitiser and catalyst. The conditions were optimised for carbonylative Suzuki couplings, PdCl₂ and PPh₃ proved suitable for the reaction. After that, various substrates and reagents were screened, and the corresponding products were isolated with excellent yields (**Figure 48**).

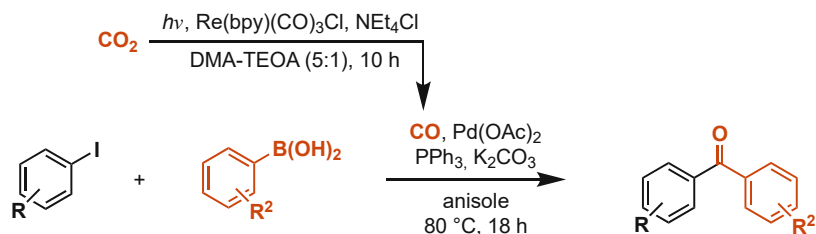


Figure 48. Carbonylative Suzuki couplings with CO₂

The method was implemented in alkoxy- and aminocarbonylations; the respective products were isolated with good yields. The corresponding experiments have been carried out under batch-wise conditions, which renders the process time-wise less efficient.

Another photocatalytic strategy relying on MOFs as photosensitisers was described in 2021.^[150] The method employs a cobalt single-site catalyst, ultrafine CuPd nanoclusters, and light-absorbing materials integrated into a MOF platform to construct a suitable catalyst for carbonylative couplings (**Figure 49**).

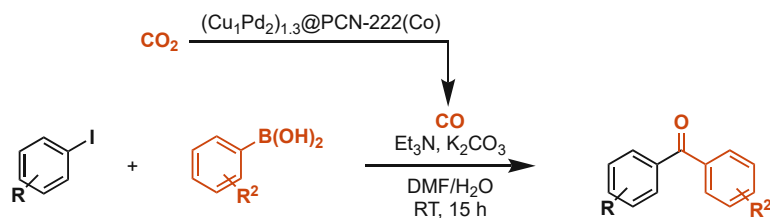


Figure 49. Photocatalytic CO₂ reduction with the aid of MOFs

The visible-light-drive transformations provided the corresponding products from the respective Suzuki- and Sonogashira couplings with excellent yields. The employed mild conditions are favourable from a sustainability point of view, but the reaction times could eventually be shortened by employing continuous-flow technologies.

Another MOF-based photoreductive strategy states that Ni-containing catalyst systems have higher selectivity toward CO formation than the corresponding cobalt-containing systems.^[151] A carbonylation reaction cycle was coupled to the photoreductive CO formation, resulting in the formation of amines, which were isolated with excellent yields.

Carbon dioxide has been successfully employed in oxidative carbonylative transformations for synthesising lactams and lactones.^[152] The strategy has emerged as a versatile tool for synthesising carbonyl-containing heterocycles under redox-neutral conditions. The redox-neutral pathway refers to the successive nucleophilic attack on CO₂ with the substrate possessing two nucleophilic sites. Often a carbonate is generated as a by-product in the presence of a base, facilitating the arduous C=O bond cleavage. Although these methods provide suitable alternatives for synthesising carbonyl-containing heterocycles, the harsh reaction conditions required for the transformation are undesirable in the light of sustainability.

Another technology employs a copper-containing supported catalyst for reducing carbon dioxide and, subsequently, utilises the formed CO in carbonylative reactions.^[153] The method proved suitable for amino-, alkoxy-carbonylations, and hydroformylations, providing the desired products with exquisite yields. However, the system did not reach the complete conversion of CO₂ to CO, which renders the process less efficient.

Continuous strategies relying on carbon dioxide as C1 source for carbonylations are known as well.^[154] The approach relies on the decomposition of CO₂ into CO by plasma. The generated carbon monoxide was subsequently utilised in a continuous aminocarbonylation reaction (**Figure 50**).

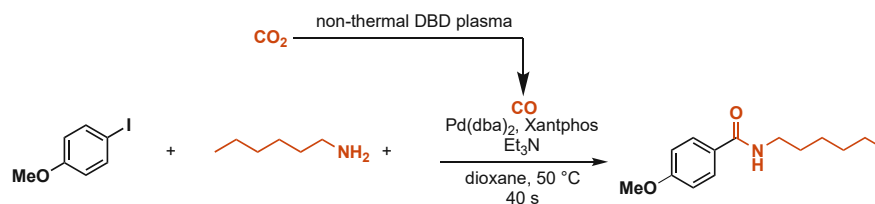


Figure 50. CO₂ decomposition and subsequent utilisation

The rapid method gave access to the desired product in just 40 seconds; however, the method seems to be limited to aminocarbonylations.

Although strategies already exist for utilising carbon dioxide in carbonylative transformations, these concepts have certain limitations. There are methods whose diverse applicability in carbonylations has yet to be proved, while others are hampered by long reaction times.

Our work focuses on the development of a continuous approach for the valorisation of abundant, non-toxic carbon dioxide in carbonylation reactions (**Figure 51**).

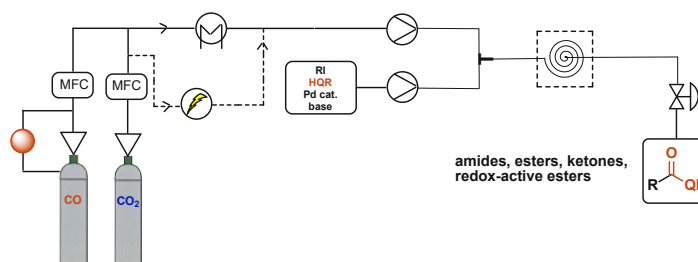


Figure 51. Continuous carbonylations with CO/CO₂ mixtures

The established methodology employs CO₂ in continuous carbonylation reactions by partially reducing it to carbon monoxide in a solid oxide electrochemical cell (SOEC). The unique aspect of this approach is that the partial reduction of CO₂ can easily be controlled by simply changing the current in the cell, allowing for the fine-tuning of reaction conditions for the desired carbonylation process. The generated CO was continuously converted into the desired product, avoiding concerns arising from its storage in bulk quantities. This approach provides a new platform for producing carbonyl compounds, such as aromatic esters, amides, redox-active esters, and carbonylative Sonogashira cross-coupling products.

The following manuscript will be presented in this chapter:

K. Stigel, K. Rath, P. M. Kathe, M. Schnürch, A. K. Opitz, K. Bica-Schröder: Online Coupling High-Temperature Electrolysis with Carbonylation Reactions: A Powerful Method for Continuous Carbon Dioxide Utilisation. **2023** (manuscript in preparation)

As the main author, I planned and performed the synthetic experimental work and contributed majorly to writing the original draft.

Online Coupling High-Temperature Electrolysis with Carbonylation Reactions: A Powerful Method for Continuous Carbon Dioxide Utilisation

Kristof Stagel,^a Kirsten Rath,^b Prasad M. Kathe,^a Michael Schnürch^a, Alexander K. Opitz,^{b,} and Katharina Bica-Schröder^{a,*}*

^aInstitute of Applied Synthetic Chemistry, TU Wien, Getreidemarkt 9/163, Vienna, 1060, Austria

^bInstitute of Chemical Technologies and Analytics, TU Wien, Getreidemarkt 9/164, 1060 Wien, Austria

*Corresponding authors:

Katharina Bica-Schröder. E-mail: katharina.schroeder@tuwien.ac.at;

Alexander K. Opitz. E-mail: alexander.opitz@tuwien.ac.at

Keywords: aminocarbonylation, carbonylative Sonogashira coupling, phenoxy carbonylation, redox-active ester, solid-oxide electrochemical cell, CO₂ electrolysis

Abstract

Despite its wide availability from matured capture technologies, the broad utilisation of CO₂ for bulk and fine chemical production is just in its starting blocks. Herein, we demonstrate the application of CO₂ in continuous carbonylation reactions through its partial reduction to carbon monoxide in a solid-oxide electrochemical cell (SOEC). The unique aspect of this strategy lies in a partial CO₂ reduction by simply varying the cell's current in combination with

continuous flow conversion of the formed CO, thus allowing tunable conditions for the desired carbonylation process. The streamlined conversion of *in situ* generated CO thus avoids the necessity of its use in bulk quantities. The approach provides a novel platform strategy for carbonyl components production, with broad applicability in phenoxy-, alkoxy-, and aminocarbonylations, in synthesis of redox-active esters, and carbonylative Sonogashira cross-couplings.

Introduction

Since its first industrial applications,^[1] carbon monoxide as a C1 building block has found widespread utilisation in transition metal-catalysed carbonylation reactions on both industrial and laboratory scales.^[2] However, its intrinsic and tremendous toxicity renders the use of carbon monoxide a severe risk, especially when it comes to an industrial application, where large amounts of this gas have to be stored and ultimately transported to the place of its use.^[3] Furthermore, its low solubility^[4] in many solvents hampers reaction kinetics. To cope with solubility issues, most of the reactions can be carried out at elevated pressure, which conversely introduces complexities in the required instrumentation and poses safety concerns.

The replacement of CO with less toxic and easier to manage alternatives is thus highly desirable, and several CO sources, including formates^[5] or even stoichiometric amounts of metal carbonyls,^[6] have been used. However, these costly options suffer from low atom efficiency, making them less attractive from an application point of view. Most recently, considerable attention has been drawn to the utilisation of carbon dioxide (CO₂) as a non-toxic, abundant, and low-cost replacement of CO in the formation of valuable products. However, while the reactivity of CO₂ is generally modest, its conversion to the desired

precursor often requires an additional reaction step, thereby increasing the complexity of the synthesis. A viable compromise would be to rely on CO₂ as a storage and transport form but to produce CO locally at the reaction site in exactly the required quantity so that it can be immediately converted again and thus consumed. This would allow for making use of the advantages of CO as a versatile reactant without the disadvantages associated with the provision and storage of large quantities of this dangerous gas.

Indeed, some authors already employed this approach and studied carbonylation reactions using CO produced by reverse water gas shift reaction (rWGSR) from CO₂,^[7] enabling the direct formation of alcohols, amines, aldehydes, carboxylic acids, or esters from olefins. This on-site chemical reduction of CO₂ via rWGSR presents a suitable method to supply CO for certain reactions locally. In 2022, Sang *et al.*^[7b] introduced a practical concept that relies on the Cu-catalysed reduction of CO₂ to carbon monoxide with H₂. The CO generated by the heterogeneous catalyst system was utilised in amino- and alkoxy-carbonylations and hydroformylations and provided exquisite yields. However, the presence of hydrogen and the water formed in rWGSR, limits the broad applicability and hamper the formation of sensitive products. Especially when moisture-sensitive catalysts or substrates containing reducible functionalities are employed, the feed gas needs to be free of H₂O and H₂, therefore practically excluding this pathway.

To circumvent the problems associated with the use of H₂ as CO₂ reductive agent, a novel approach has been developed by Gaudeau and co-workers^[8] for the fast aminocarbonylation of *p*-iodoanisole with hexylamine. The implemented technology relies on decomposing carbon dioxide into CO by plasma and provides the corresponding amide with excellent yield (95%) in just 40 seconds. However, this unique technology for carbonylation, providing rapid access to amides, is limited to aminocarbonylation.

He *et al.*^[9] reported a photoreductive strategy for utilising carbon dioxide in carbonylation reactions. A Re-based photocatalyst system was used for the *in situ* reduction of CO₂ to CO, which was further employed in aminocarbonylations, alkoxycarbonylations, and carbonylative Suzuki couplings. Although the products were obtained with excellent yields, the reduction of the CO₂ proved to be kinetically sluggish, and relatively long reaction times were required to form the corresponding products.

A completely different approach is based on the electrochemical reduction of CO₂, which has the advantage of not requiring the chemical reducing agent H₂ and thus also eliminating water impurities in the CO stream. Jensen and co-workers^[10] described a versatile strategy for the electrochemical reduction of CO₂ to CO with an iron porphyrin catalyst and its subsequent exploitation of several carbonylation reactions. While a broad range of carbonylation products, including the pharmaceutically active derivatives butoxycaine, olaparib, and moclobemide, could be formed in a specifically designed two-chamber reactor with outstanding yields, the system suffered from slow CO release due to low current densities and thus long reaction times. Such slow CO₂ electrolysis kinetics are a common issue in the case of the respective electrochemical cells operating at ambient temperatures.^[11]

High-temperature electrolysis of CO₂ in solid oxide electrolysis cells (SOECs) is currently the most efficient method available to reduce CO₂ to CO,^[12] which also meets the requirement of carbonylation reactions that the desired components in the gas stream, leaving the cell are only CO and CO₂. In an SOEC, the electrochemical reduction of CO₂ proceeds at the cell's cathode via the reaction in Eq. 1.



The oxide ions are taken up by the cathode, transported through the oxide ion conducting electrolyte, and released at the anode as O₂, while leaving two electrons behind



thus closing the electric circuit.

Even though dry CO₂ reduction in SOECs with state of the art electrodes is possible in principle, it poses a major challenge for them. Currently common SOEC cathodes are typically composites of ceramic ion conductors and Ni metal,^[13] which catalyses the formation of carbon deposits by the Boudouard reaction if the CO content is too high. Especially at higher overpotentials, this can lead to degradation and, in the worst case, to the destruction of the electrode since very high CO activities can be effective locally in the porous structure of the electrode close to the electrolyte. A common coping strategy is to add steam to the feed gas, thus operating the SOEC in so-called co-electrolysis.^[14] However, for the reasons already explained above, this is not an option for the application aimed at this work. In contrast, our approach makes use of the fact that Gd-doped ceria (GDC), due to its reducibility, shows a distinct mixed ionic and electronic conductivity under the strongly reducing conditions of a SOEC cathode, thus providing sufficient current collection even without Ni as a second phase. The strongly reducing conditions in electrolysis operation also cause high Ce³⁺ surface concentrations, making GDC a catalytically very active material for electrochemical CO₂ reduction.^[15] Moreover, the remarkable feature of CeO₂-based SOEC cathodes is that carbon deposition on their surfaces is strongly kinetically inhibited,^[16] which makes this material an excellent candidate for the dry high-temperature splitting of CO₂ in an SOEC.

While tremendous progress was made in CO₂ utilisation in carbonylation reactions (**Fig. 1**), as discussed above, these concepts still have some limitations. Among the aforementioned disadvantages, the CO₂-based carbonylative strategies reported in the literature are mainly carried out in a batch-wise fashion and are hampered by long reaction times. Moreover,

precisely controlling the gas dosage can also be challenging, and if gas mixtures are employed, the exact composition is complicated to determine and maintain.

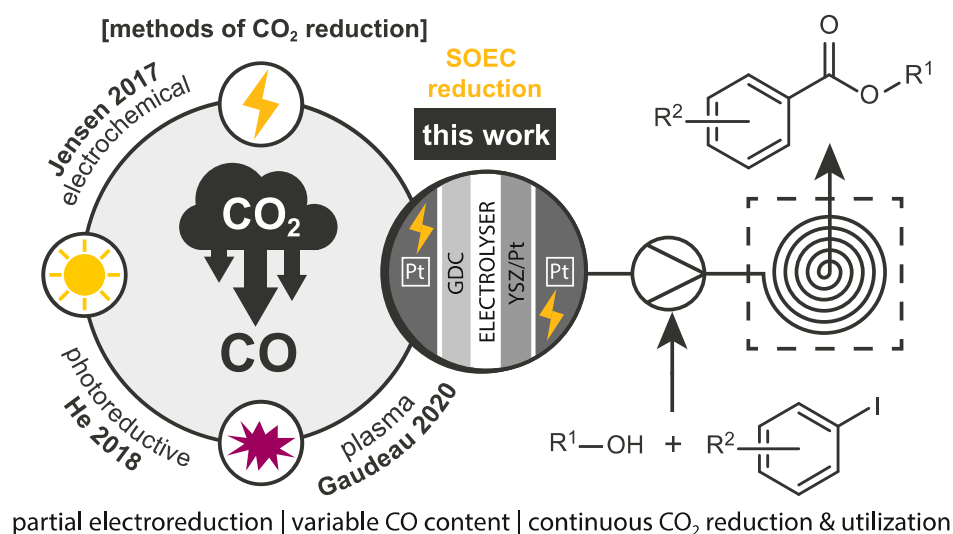


Figure 1. Various strategies for CO₂ utilisation in carbonylation reactions

In the present work, we utilise a SOEC with an optimized Ni-free GDC cathode to generate CO *in situ* through high-temperature electrolysis of CO₂, which serves as a reactant for various carbonylation reactions. Employing a SOEC offers the advantage of easily adjusting the CO content in the feed gas for downstream specific carbonylation processes by varying the cell's current, enabling continuous valorisation of abundant, non-toxic CO₂. In addition, in-situ conversion of the generated CO in a continuous flow coil reactor overcomes diffusion-related challenges and slow CO release, providing a versatile, scalable, and safe route for synthesizing amides, esters, ketones, and redox-active esters with short reaction times.

Results and discussion

Performance tests of pure GDC electrodes for dry CO₂ electrolysis

In order to demonstrate the performance as well as the coking resilience of the GDC cathode without the risk of damaging the actual SOEC – e.g., by irreversible processes that

can occur when the coking threshold is exceeded – these measurements were performed on model-type cells.

Characterization and Operation of the SOEC

Before using the SOEC for in-situ CO production, its electrochemical behavior was basically characterized. Therefore, the SOEC was heated to 750°C in a tube furnace, and as feed gas, a mixture of ca. 20 mbar H₂, 25 mbar H₂O, and 950 mbar Ar was supplied to the GDC cathode. Under these conditions, an open cell voltage OCV of 0.971 V was measured, which is in good agreement with the theoretical voltage of 0.982 V expected from Nernst's equation, indicating that the cell is gas-tight and both electrodes equilibrate with their gas atmospheres.

After this test, the atmosphere at the cathode was switched to CO₂, and the faradaic efficiency of the electrolysis was determined at two different gas fluxes of 10 and 100 ml CO₂/min. This was done by stepwise increasing the applied voltage to the SOEC and measuring the gas composition of the product gas by means of a micro gas chromatograph (Inficon Micro GC Fusion 4-Module System). The comparison of the recorded I-V-curve and the resulting CO concentration for feeding 10 ml CO₂/min to the SOEC is depicted in **Fig. 2(a)**, and the resulting faradaic efficiency is shown in **Fig. 2(b)**. Thereby, the relationship between the electrochemical current I and the flux \dot{V} of the product CO is given by Faraday's law

$$It = nzF \quad (3)$$

which, by inserting the ideal gas equation ($pV = nRT$) and substituting $\dot{V} = V/t$ reads

$$I = \dot{V} \frac{p}{RT} zF \quad (4)$$

In Eqs. 3 and 4, t denotes the time, n the number of moles, z the number of transferred charges (which is 2 for the reaction in Eq. 1), p the pressure, V the volume, and T the

temperature. R and F are the ideal gas constant and Faraday's constant, respectively. The faradaic efficiency FE is given by the ratio of the product flux (converted to a current I_{calc} by Eq. 4) and the measured respective DC current I_{DC} :

$$FE = \frac{I_{calc}}{I_{DC}} \quad (5)$$

As can be seen from **Fig. 2(a)**, the current that can be calculated from the feed gas flux (10 ml CO₂/min) and the measured CO concentration via Eq. 4 (I_{calc}) nicely follows the electrical current passing through the cell (I_{DC}). This, in turn, means that the faradaic efficiency is virtually 1, which is also depicted in **Fig. 2(b)**. The same type of experiment was also repeated for a higher feed gas flux of 100 ml CO₂/min, and the resulting plots are shown in the supporting information. Under these conditions, an excellent agreement between product gas composition and electrical current was found. The somewhat smaller error bars are due to the relatively higher accuracy of the mass flow controller at higher flow rates.

From these results of CO₂ electrolysis shown in **Fig. 2**, we can conclude that the SOEC with a pure GDC electrode excellently meets the requirements to be online coupled with carbonylation reactions.

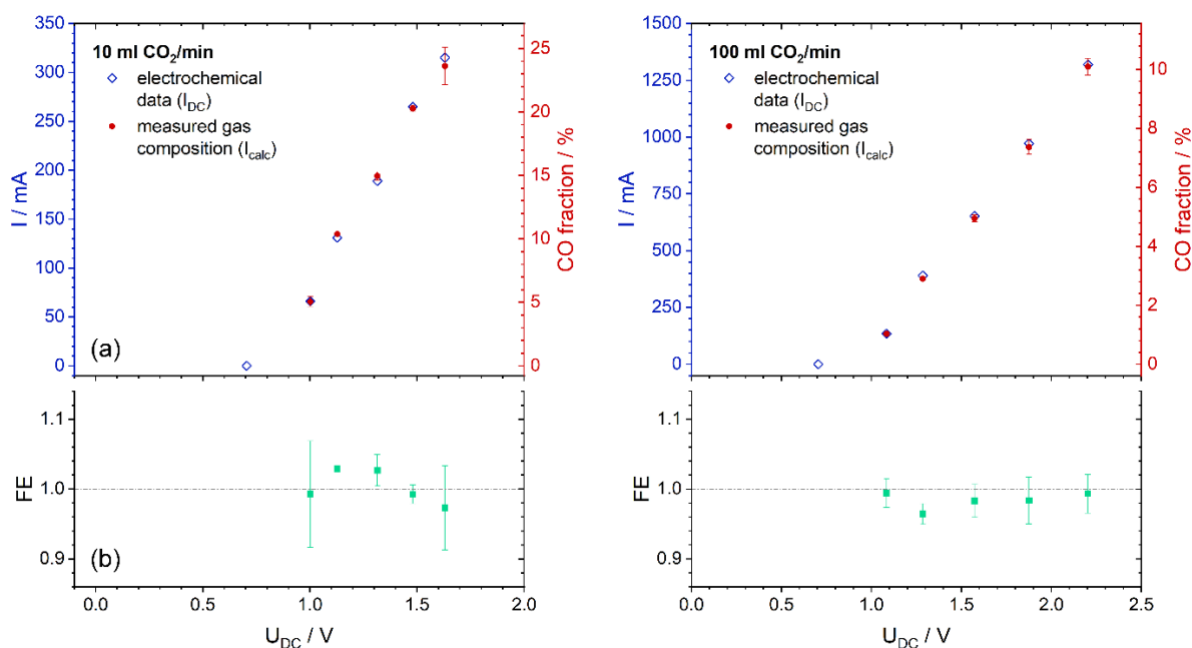
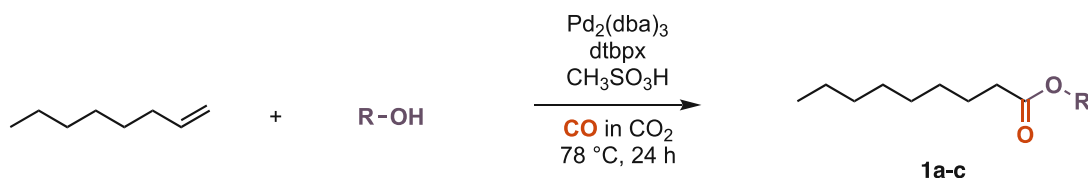


Figure 2. Electrochemical characteristics of the SOEC at a feed gas flux of 10 ml CO₂/min. (a) Current-voltage curve (I_{DC} vs. U_{DC}) together with the current I_{calc} obtained from the measurement of the CO concentration in the product gas. The two y-axes are linked by Faraday's law (Eq. 4) – hence, the measured gas composition is proportional to I_{calc} . (b) Faradaic efficiency FE plotted as a function of the voltage applied to the cell.

Studying the suitability of CO in CO₂ as a feed gas for carbonylations

In order to know the operating point of the SOEC, the optimal CO/CO₂ ratio for the carbonylation reactions was determined ex-situ by using CO/CO₂ mixtures generated with mass flow controllers (MFC). Among the known transition metal-catalysed carbonylation reactions, alkoxy-carbonylation has emerged as a versatile tool for converting unsaturated compounds, alcohols, and carbon monoxide into the corresponding esters.^[17] The obtained products and their derivatives are of great significance as they provide valuable intermediates in organic synthesis.^[18] We initially worked on the alkoxy-carbonylation of 1-octene under batch-wise conditions in alcoholic solutions, employing Pd₂(dba)₃ as precursor complex, 1,2-bis(di-*tert*-butylphosphinomethyl) benzene (dtbpx) as ligand, and methanesulfonic acid as proton source (Scheme 1).^[19]



Scheme 1. Synthesis of nonanoic acid esters; R = Et (**1a**), n-Pr (**1b**), i-Pr (**1c**)

Several bottlenecks may arise in a conventional batch-wise process involving gas bubbling into a reaction mixture with <10 mL solvent over an extended period. Obvious issues could be loss of solvent through gas saturation or the volatility of the product ester. While screening different reaction conditions, it was found that the concentration of 1-octene played a critical role in getting higher yields (**SI Table S1**). Eventually, a substrate concentration of 1.66 M in ethanol as solvent and nucleophile at a gas flow rate of 11 ml/min was found as optimum, allowing to isolate ethyl nonanoate (**1a**, **Scheme 1**) in a high yield of 80%. Once the experiments were optimized to overcome all practical bottlenecks, the concentration of CO in CO₂ was varied to resolve the ideal composition of the employed gas mixture (**Fig. 3**). The volume percentage of CO in CO₂ was set with a MFC with a total flow rate adjusted to 11 mL/min. The reactions were conducted at a 7 mmol scale, and the yields were determined by gas chromatography employing dodecane as internal standard.

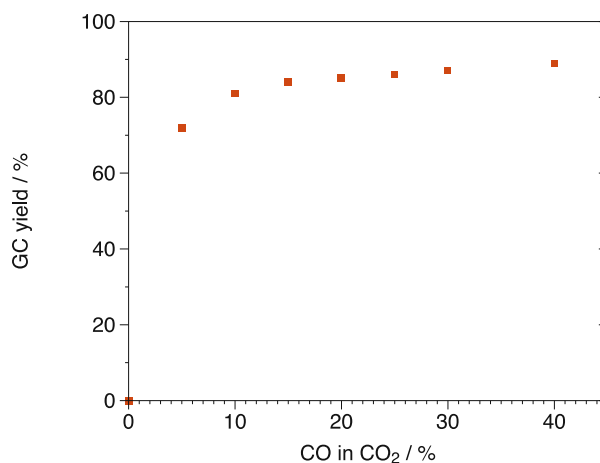


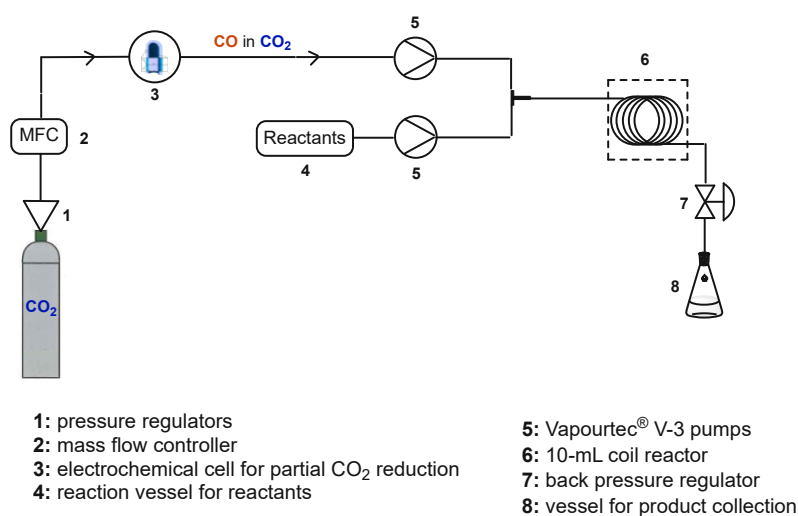
Figure 3. Resulting yield of ethyl nonanoate with varying CO concentrations. The reaction was performed with 7.0 mmol 1-octene, 0.8 mol% Pd₂(dba)₃, 4.0 mol% dtpbx, 12.0 mol% MeSO₃H at 78 °C for 24 hours (compare Scheme 1). The yield was determined by GC analysis using dodecane as internal standard.

When the CO content was varied, we found that a comparatively small content of CO in CO₂ is sufficient to reach complete conversion; in fact, an increase of CO in CO₂ beyond 15 % caused only negligibly increased the yield of the obtained ester. Moreover, this behavior is not limited to aliphatic alkoxy-carbonylations but has also been shown for the carbonylative synthesis of aromatic esters starting from aryl halides and phenols that are essential building blocks for a plethora of pharmaceuticals or agrochemicals.^[20] The carbonylative synthesis of these compounds, starting from aryl halides and phenols, has previously been reported in the literature.^[21] Nevertheless, our goal was to repeat a phenoxycarbonylation procedure reported in the literature^[22] under slightly modified parameters; working in DMF, phenyl benzoate could be isolated in 52% using 15% CO in CO₂ only (**SI Fig. S6**). This is a powerful and promising finding in the light of a future continuous process, as it allows a reaction design with partial CO₂ reduction and in-situ consumption of the formed CO in a streamlined carbonylation process.

Online coupling of CO generation in the SOEC with carbonylation reactions

Once the optimal conditions and the ideal set-up for the continuous CO supply have been identified by maintaining a constant and stable high-temperature electrolysis of CO₂ to CO, the process was combined with the previously optimized carbonylation reaction. While some authors have successfully demonstrated the use of photo- or electrochemically generated CO/CO₂ mixtures, these reactions are still hindered by long reaction times, often due to mass transfer limitations identified in studies on gas-liquid reactions, which issue becomes less significant when working in continuously operated reactors. Due to the larger interfacial surface area in continuous mode, the gas availability in the liquid phase can also be improved, potentially enhancing the gas solubility.^[23] When working with carbon monoxide on a laboratory scale, the gas is often supplied from balloons, rendering the precise control of gas dosage impossible.

To overcome the inherent limitations associated with batch processes, we opted for a continuous-flow reactor with a high surface-to-volume ratio for shorter reaction times and improved yields, as shown in **Scheme 3**.



Scheme 2. Schematic set-up of the continuous-flow experiments.

The continuous-flow experiments were carried out with the aid of a Vapourtec® E-Series flow chemistry device in a 10-mL coil reactor. The coil reactor's geometry is very similar to the so-called gas-liquid tube-in-tube reactor, typically used in continuous reactions for gas introduction. However, the gas-liquid reactor was originally designed for hydrogenation, and molecules such as CO, CO₂, or O₂ are too big to pass the reactor's membrane. Additionally, the electrochemical cell operated with a gas output of about 10 mL/min; therefore, a coil reactor with the highest available volume, 10 mL, seemed reasonable to employ in our reactions. The gas mixture and the reactants were introduced using the E-Series' V-3 pumps, respectively, allowing for precise gas introduction.

At first, we sought to investigate the phenoxycarbonylation reaction in continuous mode by employing iodobenzene as substrate and phenol as nucleophile. With respect to the product's polarity, in order to avoid obstruction, acetonitrile was used as solvent.

Table 1. Optimization of the phenoxycarbonylation of iodobenzene in continuous mode.

Entry ^[a]	CO content /%	Temperature /°C	Reaction mixture flow rate / μLmin^{-1}	Gas mixture flow rate / mlmin^{-1}	Conversion ^[c] /%
1 ^[b]	15	90	500	2.0	23
2	50	95	500	3.0	>99
3	40	95	500	3.0	>99
4	30	95	500	3.0	89
5	20	95	500	3.0	69
6	30	110	500	3.0	93
7	30	95	500	3.5	97
8	30	95	333	3.0	>99
9	15	100	250	3.6	>99
10	15	100	333	3.0	66
11	15	100	333	4.5	92

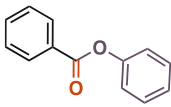
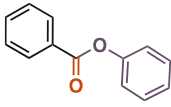
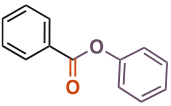
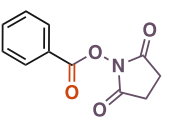
[a] The reactions were performed with 1 mmol iodobenzene, 2 mmol phenol, 0.03 mmol Pd(OAc)₂, 0.03 mmol Xantphos, and 3 mmol Et₃N in 10 mL acetonitrile; the BPR was set to 3 bar. [b] Performed in 10 mL toluene with 5 mmol iodobenzene. The gas mixture was generated with the aid of the electrochemical cell. [c] Determined by GC-MS analysis.

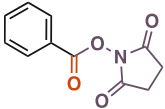
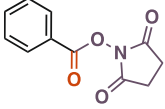
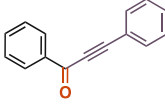
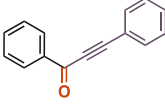
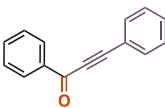
We initially worked with a relatively high carbon monoxide content of 50%, which resulted in complete conversion under 20 min reaction time. Excited by these promising results, we further aimed to reduce the carbon monoxide content to a possible minimum. 40% CO content still provided complete conversion under 20 minutes (**Table 1**, entry 3), but the reactivity dropped when mixtures with lower CO content were employed (**Table 1**, entries 4, 5). The temperature proved to be a less influential parameter of the reaction; hence, its increase by 15 °C only improved the conversion by 4% (**Table 1**, entry 4 vs. 6). With an extended reaction time and increased gas mixture flow rate, a carbon monoxide content of 15% proved sufficient to provide complete conversion (**Table 1**, entry 9), which is in excellent agreement with the results from our batch-mode screening reactions shown above. Ultimately, the product, phenyl benzoate (**2a**) was isolated with a high yield of 88% (see **Table 2**, entry 3).

After establishing the continuous process for esterifications, we employed the gained experience for other reactions to broaden the scope of the process and take full advantage of the tunability and variable CO content produced by the electrochemical cell. Most recently, many strategies have been reported for using of redox-active esters (RAEs) as radical precursors in the emerging field of radical chemistry.^[24] Carboxylic acid esters of *N*-hydroxysuccinimide (NHS) have been utilised as invaluable intermediates in the synthesis of peptides^[25] and nucleotides.^[26] Their synthesis via carbonylative cross-coupling was reported by Lou and co-workers in 2003.^[27] Under the standard optimized literature conditions, at a 3

mmol scale, employing a pre-formed CO/CO₂ mixture and iodobenzene as substrate, the transformation gave an excellent yield of 84% in batch mode, although a long reaction time of 17 hours was required (**Table 2**, entry 5, **SI Figure S8**). Gratifyingly, the developed continuous process was found to be quite versatile and equally applicable to RAE synthesis; in fact, the online coupling of the SOEC with a coil reactor yielded the desired product with 82% in 40 minutes only (**Table 2**, entry 6). Similarly, shortened reaction times and high yields were found for carbonylative Sonogashira couplings, thus demonstrating the advantages and versatility of the streamlined electrochemical set-up with the continuous conversion of CO generated by the electrochemical cell (**Table 2**, entry 9).

Table 2. Phenoxyacylation, carbonylative Sonogashira coupling, and synthesis of redox-active esters.

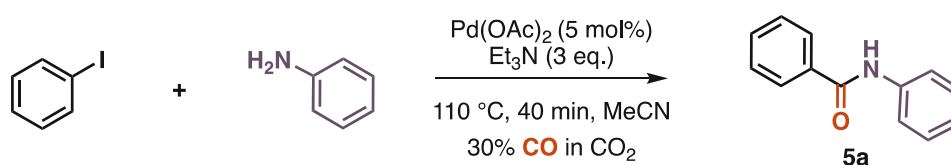
Entry	Product structure	Conditions	Set-up	Isolated yield /%
1 ^[a]	 2a	100% CO, 80 °C, DMF, 24 h	batch	90
2 ^[a]	 2a	15% CO, 80 °C, DMF, 24 h	batch	52
3 ^[d]	 2a	15% CO, 100 °C, MeCN, 40 min	continuous flow	88
4 ^[b]	 3a	100% CO, 70 °C, DMSO, 17 h	batch	86

5 ^[b]		10% CO, 70 °C, DMSO, 17 h	batch	84
6 ^[d]		15% CO, 100 °C, MeCN, 40 min	continuous flow	82
7 ^[c]		100% CO, 95 °C, DMF, 24 h	batch	86
8 ^[c]		15% CO, 95 °C, DMF, 24 h	batch	47
9 ^[d]		20% CO, 100 °C, MeCN, 40 min	continuous flow	77

[a] The reaction was performed with 3.00 mmol iodobenzene, 6.00 mmol phenol, 0.09 mmol Pd(OAc)₂, 0.09 mmol Xantphos, and 9.00 mmol Et₃N. [b] The reaction was performed with 3.00 mmol iodobenzene, 4.20 mmol NHS, 0.15 mmol Pd(OAc)₂, 0.15 mmol Xantphos, and 4.50 mmol Et₃N. [c] The reaction was performed with 2.00 mmol iodobenzene, 3.50 mmol phenylacetylene, 0.03 mmol Pd(OAc)₂, 0.06 mmol Xantphos, and 6.00 mmol Et₃N. [d] Reactions performed according to the corresponding batch procedure on a 1.00 mmol scale.

The developed continuous process proved suitable for *C* and *O* nucleophiles; however, we further aimed to construct the much more challenging amide bond via carbonylation. The importance of these bonds cannot be accentuated enough; hence, the amide motif can be found in countless biologically active molecules, agrochemicals, or physiologically essential peptides.^[28] After carrying out several preliminary experiments, an approach similar to the

previously utilised methods was identified for aminocarbonylations relying on Pd(OAc)₂, Xantphos in the presence of Et₃N (**Table S2**). Initially, harsh conditions, such as 120 °C and a CO content of 50%, were required to force the reaction. Interestingly, the conversion did not drop significantly when the CO content was decreased to 30%, and the reaction was carried out at 110 °C. Moreover, the continuous method could be performed without employing any ligand, and the product, benzanilide (**5a**), could be isolated with a good yield of 72% (**Scheme 4**).

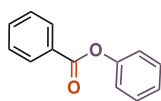


Scheme 3. Continuous synthesis of benzanilide.

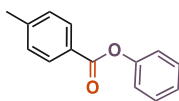
After demonstrating the applicability of our method in several reactions, we sought to uncover the scope and limitations of our approach (**Scheme 5**).

Phenoxycarbonylation

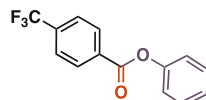
Performed with 15% CO in CO₂



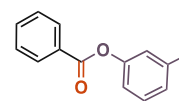
2a
88%



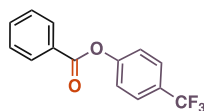
2b
88%



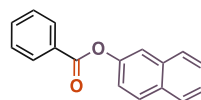
2c
72%



2d
91%



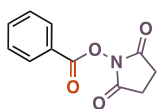
2e
93%



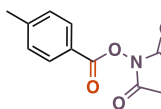
2f
86%

Redox-active esters

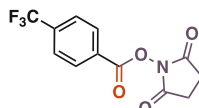
Performed with 15% CO in CO₂



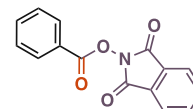
3a
82%



3b
78%



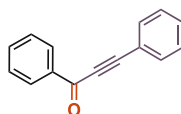
3c
65%



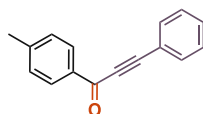
3d
77%

Sonogashira coupling

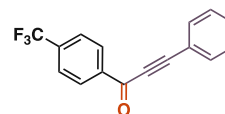
Performed with 20% CO in CO₂



4a
77%



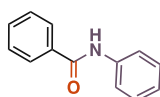
4b
76%



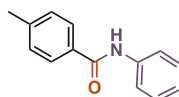
4c
20%

Aminocarbonylation

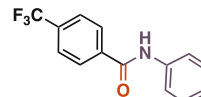
Performed with 30% CO in CO₂



5a
72%



5b
67%



5c
40%

Scheme 4. Scope of the continuous carbonylations with CO/CO₂ mixtures. The phenoxycarbonilations were performed with 1.00 iodobenzene derivative, 2.00 mmol phenol derivative, 0.03 mmol Pd(OAc)₂, 0.03 mmol Xantphos, and 3.00 mmol Et₃N dissolved in 10 mL MeCN at 100 °C, CO content: 15%. The redox-active esters were synthesized starting from 1.00 mmol iodobenzene derivative, 1.40 mmol N-hydroxiimide, 0.05 mmol Pd(OAc)₂, 0.05 mmol Xantphos, and 1.50 mmol Et₃N in 10 mL MeCN at 100 °C, CO content: 15%. Carbonylative Sonogashira couplings were carried out with 1.00 mmol iodobenzene derivative, 2.00 mmol phenylacetylene, 0.03 mol Pd(OAc)₂, 0.06 mol Xantphos and 3.00 mmol Et₃N in 10 mL MeCN at 100 °C, CO content: 20%. The aminocarbonylations were performed with 1.00 iodobenzene derivative, 3.00 mmol aniline, 0.05 mmol Pd(OAc)₂, and 4.00 mmol Et₃N in 10 mL MeCN at 110 °C, CO content: 30%. Reaction mixture flow rate: 0.25 mL/min, gas mixture flow rate: 3.6 mL/min (MFCs) or 8.0 mL/min (electrochemical cell), reaction time: 40 minutes.

Overall, the corresponding products were isolated with good to excellent yields in short reaction times, which is a significant improvement compared to the results from the experiments conducted in batch mode. The lower yields obtained in the aminocarbonylations can be explained by an additional acidic workup step. Due to the products' and the aniline's similar eluting properties, the excessive nucleophile had to be removed by acidic extraction, and product loss may occur during that step. It is worth mentioning that 2-naphthyl benzoate (**2f**), which is also known for its intestinal antiseptic property, could be isolated with an excellent yield of 86%. Substrates bearing the electron-withdrawing trifluoromethyl group proved much less reactive, as the corresponding products (**2c**, **3c**, **4c**, **5c**) were isolated with lower yields. The inferior yield of compound **4c** can be explained by the formation of the corresponding non-carbonylative Sonogashira product.

Conclusions

We successfully employed a solid-oxide electrolysis cell to perform dry CO₂ reduction; online coupling it with a continuous flow set-up allowed for the streamlined utilisation of the formed CO in carbonylation processes. One key factor for this success is the introduction of a

pure GDC cathode into the high-temperature cell, delivering high performance without the need for otherwise state-of-the-art nickel. This configuration allows dry electrolysis of CO₂ without degradation due to the coking of the SOEC cathode and without the addition of water. The developed process demonstrated widespread applicability in amino-, alkoxy-, and phenoxy-carbonylations, in the synthesis of redox-active esters, and in carbonylative Sonogashira couplings. The applicability of flow chemistry technologies renders the overall process less time-consuming and provides a tunable and easily scalable synthesis of these carbonyl compounds. Ultimately, the streamlined conversion of in-situ generated CO in CO₂ avoids the use of CO in bulk quantities and provides an entirely novel platform strategy for carbonyl components production, able to circumvent problems associated with the current state of the art.

Experimental Section

Fabrication of the Solid Oxide Electrolyser

For preparing the SOEC employed for the in-situ supply of CO, a dense sintered tube made of yttria-stabilized zirconia, which was closed on one side, was used as electrolyte. On the outer side of the tube, the cathode was applied as a three-layer electrode by depositing pastes of GDC, GDC/Pt, and Pt, similar to the electrodes in Ref.^[15a]. Located directly adjacent to the electrolyte, the electrochemically active layer consisted of porous pure GDC (Treibacher, AT). The topmost porous Pt layer acts as an electronic current collector, and it has already been proven in Ref.^[15a] that this layer does not contribute any catalytic activity to the electrode, owing to its distance to the electrode/electrolyte interface. In between the GDC and Pt layers, a GDC/Pt composite layer was applied, which ensures a gradual transition between the two

materials and thus provides good adhesion. (Please note that for commercial applications, Ni instead of Pt would be a much more suitable choice, but for the lab-based application here, Pt paste was used for convenience.)

For the air electrode, Pt/YSZ paste was applied to the inner side of the tube. After both electrodes were applied in the form of pastes, the whole assembly was sintered in air at 1200°C for 3 h. In order to be able to operate the cell obtained in this way as SOEC, the tube was bonded with the open side into a brass KF40 flange. The air electrode was contacted with a thick silver wire and the CO₂ splitting electrode with a Ni wire. The entire SOEC was capped with a one side closed quartz tube that fits as closely as possible to minimize dead volume. In order to bring the SOEC to its operating temperature of 750°C, the entire set-up was heated with a tube furnace. A sketch of the entire assembly is shown in **Fig. 4(a)**.

For in-situ production of CO, the outer compartment of the SOEC was supplied with CO₂ via a mass flow controller, and the GDC electrode was cathodically (i.e. negatively) polarized. The resulting CO concentration at the SOEC outlet is a result of the gas flux and the electrochemical current. For example, a gas flux of 10 ml CO₂/min and an electrochemical current of 195 mA result in a gas composition of 15 vol% CO and 85 vol% CO₂. For the examination of the Faraday efficiency of the cell please refer to the results section.

Model-type cells for studying the kinetics of pure GDC electrodes

In order to be able to explore the electrochemical behaviour of the GDC cathode alone and to demonstrate their coking resilience, additional model-type samples were prepared. In particular, three slightly different types of these GDC model samples were studied:

- (i) Type 1, which consists of a single crystalline YSZ electrolyte and porous spin-coated pure GDC working electrode with a porous Pt current collector on top, which is identical to the cathodes used in the SOEC described above and the Ni-free GDC electrodes in Ref. ^[15a].
- (ii) Type 2, where the Pt current collector is a patterned thin film grid buried under a GDC thin film (grown by pulsed laser deposition as described in Refs. ^[29], ^[15a]) at the interface to the YSZ single crystal electrolyte. On top of the Pt/GDC thin film sandwich, a porous GDC layer was applied by the same procedure as for model sample type 1.
- (iii) Type 3 carries the Pt/GDC model composite as the working electrode, like type 2, to study the reaction at the well-defined GDC surface of the thin film electrode. Thus, it differs from type 2 by the absence of the porous GDC functional layer.

As a counter electrode on all three model cells, a Pt/Pr_xCe_{1-x}O_{2-δ} (PCO) composite was applied to the bottom side of the electrolyte. This material combination was chosen to have maximum flexibility in terms of gas composition at the counter electrode as PCO shows good electrochemical activity both in oxidizing and reducing atmospheres. Sketches of these model-type samples are depicted in **Fig. 4(b)**.

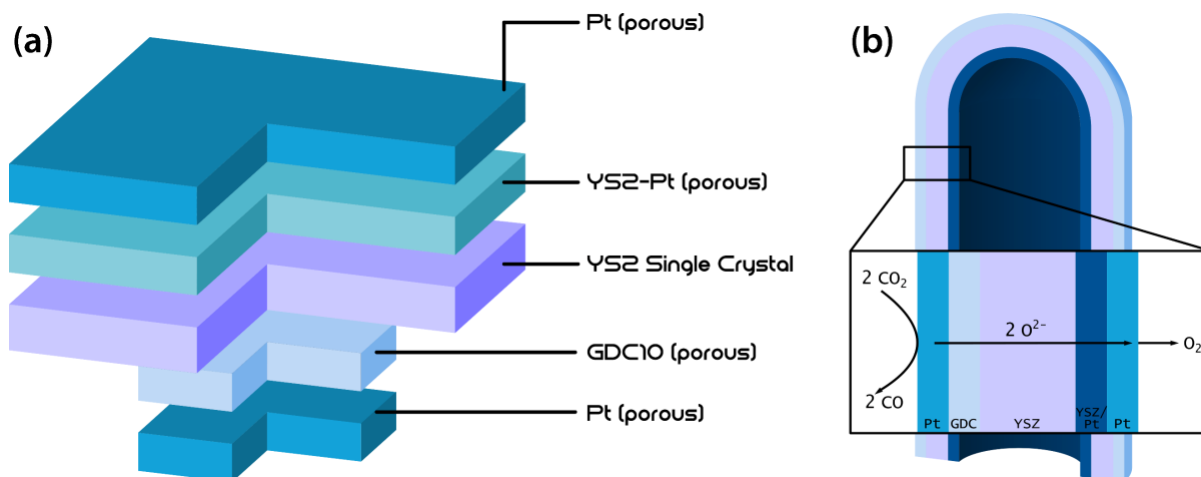


Figure 4: Sketches of the solid oxide cells used in this study. **(a)** Model-type cells on which the kinetics and catalytic properties of the GDC cathode were investigated. The GDC10 electrode is smaller than the counter electrode to leave space for the gasket in the 2-gas measurement set-up. **(b)** Cross section of a tubular SOEC consisting of GDC cathode, Pt/YSZ anode, and YSZ electrolyte, which was used for online CO production via high-temperature CO₂ electrolysis with carbonylation reactions.

Representative procedure for the continuous process relying on aryl iodides

A 30-mL vial with septum was charged with the corresponding aryl iodide and nucleophile, Pd(OAc)₂, Et₃N, and optionally Xantphos. The reactants were dissolved in 10 mL acetonitrile. The reactor was heated up to the desired temperature. The gas mixture was supplied from the solid-oxide electrochemical cell. The cell was connected to a CO₂ cylinder equipped with a low-pressure regulator, outputting 2 bar. The electrolyser was heated up to 750 °C, and the current was set according to the required carbon monoxide content (for 15% CO and a gas flux of 10 (8) mL/min: 195 (155) mA). After approximately 20-25 minutes, the feed gas flow has displaced the dead volume of the piping, and thus, the gas flowing into the reactor has reached the desired composition. Two pumps of the Vapourtec[®] E-series device were connected to the vial with the reaction mixture and to the gas line, respectively. The third

pump was used as a back-pressure regulator (BPR). The 10-mL coil reactor was initially rinsed by a CO/CO₂/MeCN flow for several minutes. Then, the pumps were set to the corresponding flow rates (gas mixture: 8.0 mL/min; reaction mixture: 0.25 mL/min), and the reaction mixture was supplied to the reactor. After the whole volume of the reaction mixture was pumped through the reactor, the vial was rinsed with MeCN, and the residue was pumped through. The product was collected for 50 minutes. Rotary evaporation of the solvent gave the crude products, which were bound to silica gel and subjected to column chromatography.

Acknowledgment

This project has received funding from the European Research Council (ERC) under the European Union's Horizon 2020 research and innovation programme (grant agreement no. 864991). Moreover, this research was funded in part by the Austrian Science Fund (FWF); Grant number I 5478-N. The authors thank Fabian Scharinger for his assistance in designing the graphical abstract.

Synopsis

A continuous process for carbonylation reactions based on online coupling of dry high-temperature CO₂ electrolysis with a coil reactor has been reported. The strategy relies on CO/CO₂ mixtures with low CO content, thus, providing a safe and fast concept for the synthesis of several carbonyl compounds. The method demonstrated widespread applicability in amino-, alkoxy-, and phenoxycarbonylation, in carbonylative Sonogashira couplings, and in the synthesis of redox-active esters. The corresponding products were isolated with excellent yields in just 40 minutes.

References

- [1] a) L. Gattermann, J. A. Koch, *Ber. Dtsch. Chem. Ges.* **1897**, *30*, 1622-1624; b) F. Fischer, H. Tropsch, *Ber. Dtsch. Chem. Ges.* **1926**, *59*, 830-831.
- [2] a) R. Skoda-Földes, K. Kollár, *Curr. Org. Chem.* **2002**, *6*, 1097-1119; b) A. Haynes, P. M. Maitlis, G. E. Morris, G. J. Sunley, H. Adams, P. W. Badger, C. M. Bowers, D. B. Cook, P. I. P. Elliott, T. Ghaffar, H. Green, T. R. Griffin, M. Payne, J. M. Pearson, M. J. Taylor, P. W. Vickers, R. J. Watt, *J. Am. Chem. Soc.* **2004**, *126*, 2847-2861; c) A. Brennführer, H. Neumann, M. Beller, *Angew. Chem. Int. Ed.* **2009**, *48*, 4114-4133; d) X.-F. Wu, X. Fang, L. Wu, R. Jackstell, H. Neumann, M. Beller, *Acc. Chem. Res.* **2014**, *47*, 1041-1053; e) S. Sumino, A. Fusano, T. Fukuyama, I. Ryu, *Acc. Chem. Res.* **2014**, *47*, 1563-1574.
- [3] a) R. J. Levy, *Anesth. Analg.* **2016**, *123*, 670-681; b) A. Dubey, D. Chouksey, *Neurol. India.* **2017**, *65*, 672-673.
- [4] a) R. Koelliker, H. Thies, *J. Chem. Eng. Data* **1993**, *38*, 437-440; b) A. Henni, A. E. Mather, *J. Can. Pet. Technol.* **1999**, *38*; c) Liu, F. Takemura, A. Yabe, *J. Chem. Eng. Data* **1996**, *41*, 589-592.
- [5] a) H. W. Lee, A. S. C. Chan, F. Y. Kwong, *Chem. Commun.* **2007**, 2633-2635; b) B. Gatlik, W. Chaładaj, *ACS Catal.* **2021**, *11*, 6547-6559.
- [6] T. Morimoto, K. Kakiuchi, *Angew. Chem. Int. Ed.* **2004**, *43*, 5580-5588.
- [7] a) R. M. Bown, M. Joyce, Q. Zhang, T. R. Reina, M. S. Duyar, *Energy Technol.* **2021**, *9*, 2100554; b) R. Sang, Y. Hu, R. Razzaq, G. Mollaert, H. Atia, U. Bentrup, M. Sharif, H. Neumann, H. Junge, R. Jackstell, B. U. W. Maes, M. Beller, *Nat. Commun.* **2022**, *13*, 4432; c) S. Sengupta, A. Jha, P. Shende, R. Maskara, A. K. Das, *J. Env. Chem. Eng.* **2019**, *7*, 102911; d) V. Hosseinpour, M. Kazemeini, A. Mohammadrezaee, *Chem. Eng. Sci.* **2011**, *66*, 4798-4806.
- [8] M. Gaudeau, M. Zhang, M. Tatouliau, C. Lescot, S. Ognier, *React. Chem. Eng.* **2020**, *5*, 1981-1991.
- [9] X. He, Y. Cao, X. D. Lang, N. Wang, L. N. He, *ChemSusChem* **2018**, *11*, 3382-3387.
- [10] M. T. Jensen, M. H. Ronne, A. K. Ravn, R. W. Juhl, D. U. Nielsen, X. M. Hu, S. U. Pedersen, K. Daasbjerg, T. Skrydstrup, *Nat. Commun.* **2017**, *8*, 489.
- [11] S. Nitopi, E. Bertheussen, S. B. Scott, X. Liu, A. K. Engstfeld, S. Horch, B. Seger, I. E. L. Stephens, K. Chan, C. Hahn, J. K. Nørskov, T. F. Jaramillo, I. Chorkendorff, *Chem. Rev.* **2019**, *119*, 7610-7672.
- [12] a) R. Küngas, *J. Electrochem. Soc.* **2020**, *167*; b) A. Hauch, R. Küngas, P. Blennow, A. B. Hansen, J. B. Hansen, B. V. Mathiesen, M. B. Mogensen, *Science* **2020**, *370*, eaba6118.
- [13] P. Holtappels, J. T. S. Irvine, S. Wang, in *High-Temperature Electrolysis*, IOP Publishing, **2023**, pp. 4-1-4-24.
- [14] Y. Tao, S. D. Ebbesen, M. B. Mogensen, *J. Electrochem. Soc.* **2014**, *161*, F337-F343.
- [15] a) A. Nanning, M. Holzmann, J. Fleig, A. K. Opitz, *Mater. Adv.* **2021**, *2*, 5422-5431; b) W. C. Chueh, Y. Hao, W. Jung, S. M. Haile, *Nat. Mater.* **2012**, *11*, 155-161; c) Z. A. Feng, M. L. Machala, W. C. Chueh, *Phys. Chem. Chem. Phys.* **2015**, *17*, 12273-12281; d) S. C. DeCaluwe, M. E. Grass, C. Zhang, F. E. Gabaly, H. Bluhm, Z. Liu, G. S. Jackson, A. H. McDaniel, K. F. McCarty, R. L. Farrow, M. A. Linne, Z. Hussain, B. W. Eichhorn, *J. Phys. Chem. C* **2010**, *114*, 19853-19861.
- [16] T. L. Skafte, Z. Guan, M. L. Machala, C. B. Gopal, M. Monti, L. Martinez, E. Stamate, S. Sanna, J. A. Garrido Torres, E. J. Crumlin, M. García-Melchor, M. Bajdich, W. C. Chueh, C. Graves, *Nat. Energy* **2019**, *4*, 846-855.

- [17] R. Sang, Y. Hu, R. Razzaq, R. Jackstell, R. Franke, M. Beller, *Org. Chem. Front.* **2021**, *8*, 799-811.
- [18] a) C. Bolm, M. Beller, *Transition metals for organic synthesis, Vol. 1*, Wiley-VCH: Weinheim, **2004**, ; b) K. Bauer, D. Garbe, H. Surburg, *Common fragrance and flavor materials: preparation, properties and uses*, John Wiley & Sons, **2008**, ; c) L. Kollár, *Modern carbonylation methods*, John Wiley & Sons, **2008**,
- [19] C. Jimenez Rodriguez, D. F. Foster, G. R. Eastham, D. J. Cole-Hamilton, *Chem. Commun.* **2004**, 1720-1721.
- [20] a) T. G. Solomons, C. B. Fryhle, *Organic chemistry*, John Wiley & Sons, **2008**, ; b) P. Gautam, P. Kathe, B. M. Bhanage, *Green Chem.* **2017**, *19*, 823-830; c) X. Zhu, L. Yu, M. Zhang, Z. Xu, Z. Yao, Q. Wu, X. Du, J. Li, *Chem. Cent. J.* **2018**, *12*, 111.
- [21] a) K. V. Nikitin, N. P. Andryukhova, N. A. Bumagin, I. P. Beletskaya, *Mendeleev Commun.* **1991**, *1*, 129-131; b) M. V. Khedkar, T. Sasaki, B. M. Bhanage, *ACS Catal.* **2013**, *3*, 287-293.
- [22] P. Losch, A.-S. Felten, P. Pale, *Adv. Synth. Catal.* **2015**, *357*, 2931-2938.
- [23] J. Friedland, R. Güttel, *J. Flow Chem.* **2021**, *11*, 625-640.
- [24] a) F. Toriyama, J. Cornella, L. Wimmer, T. G. Chen, D. D. Dixon, G. Creech, P. S. Baran, *J. Am. Chem. Soc.* **2016**, *138*, 11132-11135; b) S. Murarka, *Adv. Synth. Catal.* **2018**, *360*, 1735-1753; c) T. Cao, T. Xu, R. Xu, X. Shu, S. Liao, *Nat. Commun.* **2020**, *11*, 5340; d) S. Karmakar, A. Silamkoti, N. A. Meanwell, A. Mathur, A. K. Gupta, *Adv. Synth. Catal.* **2021**, *363*, 3693-3736.
- [25] C. L. Hypolite, T. L. McLernon, D. N. Adams, K. E. Chapman, C. B. Herbert, C. C. Huang, M. D. Distefano, W.-S. Hu, *Bioconjug. Chem.* **1997**, *8*, 658-663.
- [26] G. Sengle, A. Jenne, P. S. Arora, B. Seelig, J. S. Nowick, A. Jäschke, M. Famulok, *Bioorg. Med. Chem.* **2000**, *8*, 1317-1329.
- [27] R. Lou, M. VanAlstine, X. Sun, M. P. Wentland, *Tetrahedron Lett.* **2003**, *44*, 2477-2480.
- [28] a) S. I. Lee, S. U. Son, Y. K. Chung, *Chem. Commun.* **2002**, 1310-1311; b) R. Grigg, S. P. Mutton, *Tetrahedron* **2010**, *66*, 5515-5548; c) P. Hermange, A. T. Lindhardt, R. H. Taaning, K. Bjerglund, D. Lupp, T. Skrydstrup, *J. Am. Chem. Soc.* **2011**, *133*, 6061-6071; d) S. W. Robinson, A. M. Afzal, D. P. Leader, in *Handbook of Pharmacogenomics and Stratified Medicine* (Ed.: S. Padmanabhan), Academic Press, San Diego, **2014**, pp. 259-287; e) J. Liu, H. Li, A. Spannenberg, R. Franke, R. Jackstell, M. Beller, *Angew. Chem. Int. Ed.* **2016**, *55*, 13544-13548.
- [29] C. Herzig, J. Frank, A. Nennung, M. Gerstl, A. Bumberger, J. Fleig, A. K. Opitz, A. Limbeck, *J. Mater. Chem. A* **2022**, *10*, 1840-1851.

7. Conclusions

The thesis presents the successful application of continuous-flow technologies for synthesising ionic liquids, performing allylic aminations, and valorising carbon dioxide. The developed strategies result in a significant decrease in reaction time and provide excellent yields.

The first part of the thesis focused on the halide-free continuous synthesis of hydrophobic ionic liquids. The simple, two-step procedure gave straightforward access to a plethora of NTf₂-based ILs with excellent yields and purities. The quaternisation step could be carried out under solvent-free conditions and provided high atom efficiency without forming additional waste. The reported method is intrinsically halide-free, which offers many benefits for the development of new ionic liquid-based technologies that are sensitive to halide content. The overall process is significantly less time-consuming than most reported halide-free methods, and due to the reaction's homogeneous nature, it could be successfully performed in continuous-flow operation mode. This provided an even more fast and safe synthesis of these ILs, allowing them to be obtained in high yields (86-99%) and productivity, with a residence time of 7.5 minutes only. The high purity renders this process safe and efficient and makes the IL products suitable for a significantly broader application range, especially for material sciences (**Figure 52**).

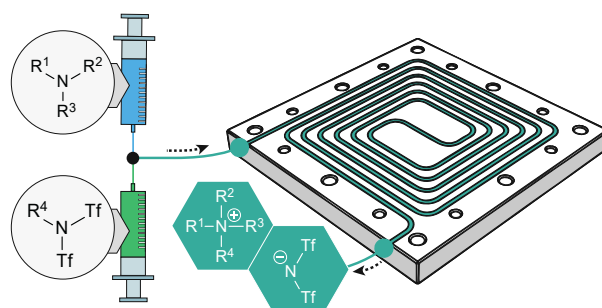


Figure 52. Halide-free continuous synthesis of NTf₂-based ionic liquids

In the second sub-project, hydrophobic ionic liquids were employed for depositing transition metal complexes on silica. The supported catalyst frameworks were utilised in continuous allylic aminations. Apart from the fast and straightforward catalyst immobilisation, the developed approach requires neither an additional base nor an inert atmosphere for efficient *N*-allylations. Furthermore, the reactions could be carried out under mild conditions in benign reaction media. The optimal SILP catalyst could provide easy access to *N*-allylation products within short reaction times (30 minutes). By extending the reaction time to 3.5 hours, such a SILP catalyst could maintain stable conversions, whereas only a marginal (0.7 wt%) ionic liquid- and no palladium complex leaching could be observed. Furthermore, this approach could be used for the simple immobilisation of chiral palladium complexes,

enabling asymmetric *N*-allylation reactions in continuous flow with good yields and enantioselectivities (Figure 53).

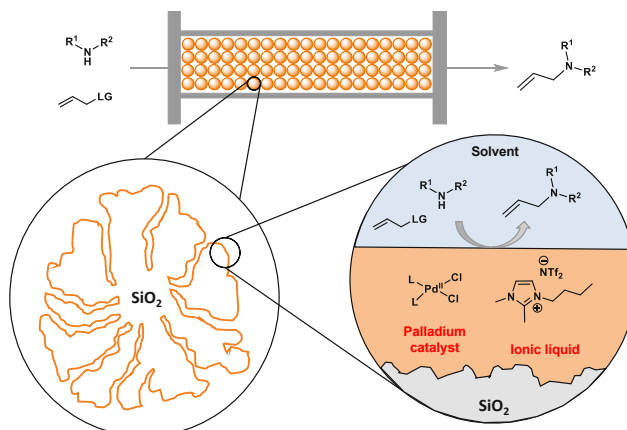


Figure 53. SILP-assisted continuous allylic aminations

The third part of the thesis was dedicated to the continuous carbon dioxide-based synthesis of carbamates was examined. We reported an approach for continuously utilising CO_2 without employing any catalyst or additive. To the best of our knowledge, this is the first continuous methodology that employs amines and alkyl halides in the presence of DBU and CO_2 to form urethanes. The process provides a faster and safer alternative for synthesising carbamates from both primary and secondary amines. The desired compounds were obtained in just 50 minutes, with good to excellent yields. Column chromatography could be avoided in many cases since an acidic treatment proved sufficient to obtain the products in high purities. Moreover, the modified method was tested in the aziridine-based synthesis of oxazolidinones and demonstrated high selectivity toward the desired compounds (Figure 54).

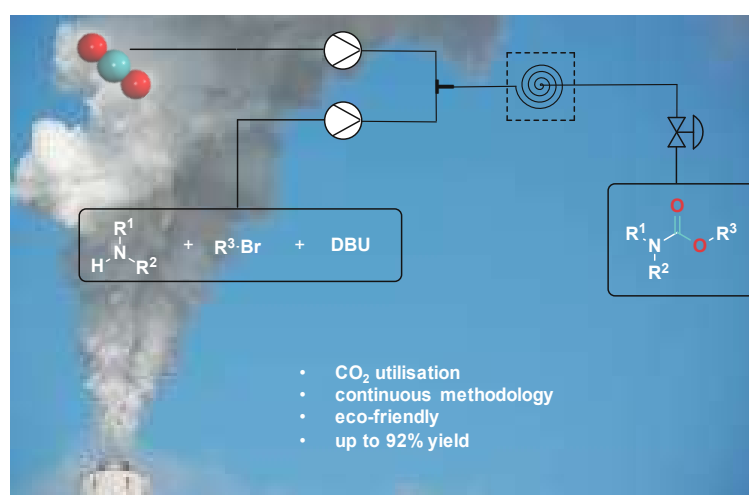


Figure 54. CO_2 -based continuous synthesis of urethanes

In the last part of the thesis, the continuous utilisation of carbon dioxide in carbonylation reactions. A synthetic method relying on the utilisation of CO/CO₂ mixtures in carbonylation reactions has been established. The developed process demonstrated widespread applicability in amino-, alkoxy-, and phenoxy-carbonylations, in synthesising redox-active esters, and in carbonylative Sonogashira couplings. The strategy utilises gas mixtures with low (15-30%) CO content, thus providing a safer alternative. The application of flow chemistry technologies renders the overall process less time-consuming and provides a safer, more rapid, and easily scalable synthesis of these carbonyl compounds. Combining the solid-oxide electrochemical cell with the flow chemistry device allowed for the direct utilisation of carbon dioxide in continuous carbonylations. The developed methodology gave access to the desired products with excellent yields (up to 93%) in just 40 minutes (**Figure 55**).

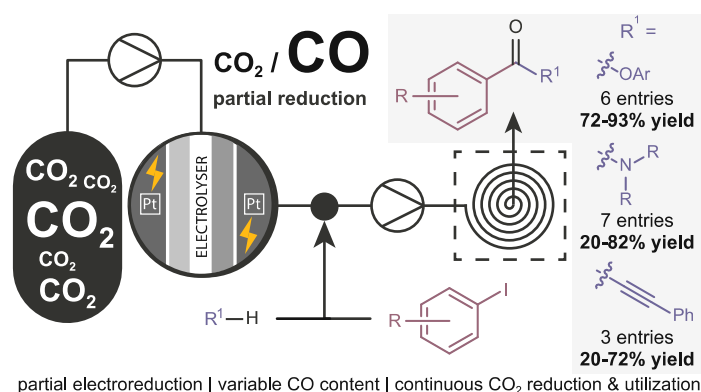


Figure 55. Continuous carbonylations with CO/CO₂ mixtures

8. Appendix A

Supporting Information

Halide-free Continuous Synthesis of Hydrophobic Ionic Liquids

Kristof Stagel,^a Andrea Szpecht,^b Dawid Zielinski,^{b,c} Marcin Smiglak,^b Michael Schnürch^a and Katharina Bica-Schröder^{a,}*

^aInstitute of Applied Synthetic Chemistry, TU Wien, Getreidemarkt 9/163, Vienna, 1060, Austria

^bPoznan Science and Technology Park, Adam Mickiewicz University Foundation, ul. Rubiez 46, 61-612 Poznan, Poland

^cFaculty of Chemistry, Adam Mickiewicz University in Poznan, st. Uniwersytetu Poznanskiego 8, 61-614 Poznan, Poland

*Corresponding author: Katharina Bica-Schröder. E-mail: katharina.schroeder@tuwien.ac.at, Tel.: +43 1 58801 163601

8.1 General remarks

All commercially available chemicals were used without further purification, unless otherwise specified. Dry CH_2Cl_2 was pre-distilled and desiccated on aluminum oxide columns (PURESOLV, Innovative Technology).

^1H -, ^{13}C - and ^{19}F NMR spectra were recorded from CDCl_3 solutions on a Bruker Avance UltraShield 200 MHz (^1H : 200 MHz, ^{13}C : 50 MHz) or 400 MHz (^1H : 400 MHz, ^{13}C : 101 MHz, ^{19}F : 376 MHz) NMR instrument. Chemical shifts are reported in parts per million (ppm) and were calibrated to the residual solvent signal (CDCl_3 , ^1H : 7.26 ppm). Coupling constants are reported in hertz. The assignments are based on the comparison with reported spectra.

GC analysis was performed on a Thermo Scientific Focus, on a BGB5 column, using an FID detector. A linear temperature program was used, starting with a temperature of 50 °C, followed by a ramp rate of 15°C/min up to a final temperature of 240 °C. For the optimisation of the bistriflimide synthesis, the conversion has been determined by using *n*-dodecane as an internal standard.

HRMS analysis was performed using a TC PAL system autosampler, an Agilent 1100/1200 HPLC, and an Agilent 6230 AJS ESI-TOF mass spectrometer. The spectra were recorded from methanolic solutions ($c = 3 \times 10^{-5} \text{ mol dm}^{-3}$). The cations ($[\text{C}]^+$) of the ILs ($[\text{C}]^+[\text{A}]^-$) were detected in positive-ion mode.

Infrared spectra were recorded on a Perkin Elmer Spectrum 65 FTIR spectrometer equipped with a Specac MK II Golden Gate Single Reflection ATR unit.

Water content analysis has been performed using a semi-automatic, coulometric Mitsubishi CA-21 Moisture Meter titrator.

Continuous-flow experiments were performed in a 1000 μl CAP DISC reactor. The nucleophile and the reagent were supplied with the aid of one-one New Era NE-1000 syringe pumps, respectively.

8.2 Representative protocol for the synthesis of alkyl bistriflimides

After 40 mmol (1.00 eq.) of the corresponding amine and *N,N*-diisopropylethylamine (82 mmol, 2.05 eq.) were transferred to a 3-neck round-bottom flask, 90 mL anhydrous dichloromethane were added under argon atmosphere. The mixture was stirred and cooled down *via* NaCl/ice bath. Then, trifluoromethanesulfonic anhydride (82 mmol, 2.05 eq.) was dissolved in 20 mL anhydrous dichloromethane and it was added to the mixture dropwise, while the temperature was maintained below 5 °C. Once the triflic anhydride was added, the NaCl/ice bath was removed and the mixture was stirred at room temperature for 1 hour. After that, the mixture was washed once with saturated NaHCO₃ solution, once with 2 N HCl solution, and once with distilled water. The aqueous phases were back-extracted with dichloromethane. The combined organic layers were dried over Na₂SO₄, filtered, and concentrated. The residuals were transferred in a round-bottom flask and distilled under vacuum (20 mbar) using a Vigreux-column. The products were obtained as colourless to slightly yellowish liquids.

8.3 General procedure for the batch-wise synthesis of ionic liquids

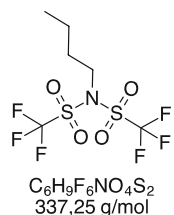
2 mmol (1.00 eq.) of the corresponding nucleophile was transferred to an 8-mL vial, then it was heated up to 80 °C. Once the temperature reached 80 °C, 2 mmol (1.00 eq.) alkyl bistriflimide was added, and the mixture was stirred for 24 hours. Then, the mixture was transferred into a glass round-bottom flask and it was dried under high vacuum at elevated temperature overnight (0.3 bar, 90 °C).

8.4 General procedure for the continuous-flow synthesis of ionic liquids

The continuous-flow experiments were performed in a 1000 μl reactor. The nucleophile and the reagent were supplied with the aid of one-one syringe pumps, respectively. The reactor was heated up to the desired temperature with the aid of a magnetic hotplate stirrer and the syringes were filled with the reagents (7.00 mmol from both the nucleophiles and the alkyl bistriflimides). After setting the pumps into operation, the dead volume of the reactor was allowed to pass. The products were then collected into tared round-bottom flasks for a specific amount of time. The unreacted starting materials were removed under high vacuum (0.3 mbar) at 90 °C overnight.

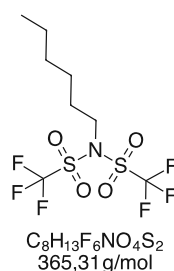
8.5 Analysis of alkyl bistriflimides

N-Butyl-1,1,1-trifluoro-*N*-((trifluoromethyl)sulfonyl)methanesulfonamide (**1a**)



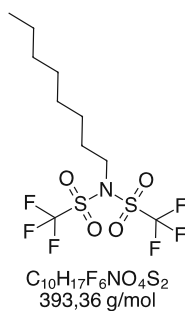
Product **1a** was obtained as colourless liquid (9.94 g, 74% yield). Boiling point at 24 mbar: 83-85 °C, density: 1.500 g cm⁻¹.^[155] ¹H NMR (200 MHz, CDCl₃) δ 4.10 – 3.73 (m, 2H, NCH₂(CH₂)₂CH₃), 1.80 (ddd, *J* = 15.7, 8.8, 6.4 Hz, 2H, NCH₂CH₂CH₂CH₃), 1.48 – 1.17 (m, 2H, N(CH₂)₂CH₂CH₃), 0.96 (t, *J* = 7.3 Hz, 3H, N(CH₂)₃CH₃). ¹³C NMR (101 MHz, CDCl₃) δ 123.94, 120.71, 117.48, 114.26, 54.12, 31.73, 19.57, 13.42. ¹⁹F NMR (376 MHz, CDCl₃) δ -72.10. IR (ν_{max}/cm⁻¹): 2970, 2883, 1429, 1214, 119, 855, 605, 504.

N-Hexyl-1,1,1-trifluoro-*N*-((trifluoromethyl)sulfonyl)methanesulfonamide (**1b**)



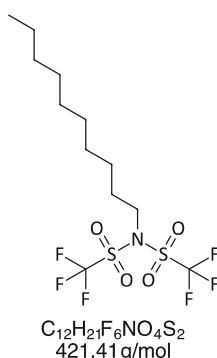
Product **1b** was obtained as colourless liquid (11.79 g, 81% yield). Boiling point at 18 mbar: 104-107 °C, density: 1.413 g cm⁻¹.^[155] ¹H NMR (400 MHz, CDCl₃) δ 3.92 (dd, *J* = 9.4, 6.9 Hz, 2H, NCH₂(CH₂)₄CH₃), 1.81 (p, *J* = 7.2 Hz, 2H, NCH₂CH₂(CH₂)₃CH₃), 1.42 – 1.23 (m, 6H, NCH₂CH₂(CH₂)₃CH₃), 0.96 – 0.82 (m, 3H, N(CH₂)₅CH₃). ¹³C NMR (101 MHz, CDCl₃) δ 123.94, 120.71, 117.48, 114.26, 54.35, 31.05, 29.74, 25.92, 22.50, 13.99. ¹⁹F NMR (376 MHz, CDCl₃) δ -72.09. IR (ν_{max}/cm⁻¹): 2935, 2864, 1429, 1214, 1120, 844, 605, 503.

N-Octyl-1,1,1-trifluoro-*N*-((trifluoromethyl)sulfonyl)methanesulfonamide (**1c**)



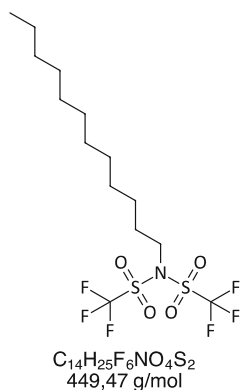
Product **1c** was obtained as colourless liquid (11.63 g, 74% yield). Boiling point at 0.30 mbar: 80-82 °C, density: 1.310 g cm⁻¹.^[156] ¹H NMR (200 MHz, CDCl₃) δ 4.04 – 3.76 (m, 2H, NCH₂CH₂(CH₂)₅CH₃), 1.81 (p, *J* = 7.0 Hz, 2H, NCH₂CH₂(CH₂)₅CH₃), 1.30 (h, *J* = 4.6, 4.0 Hz, 10H, NCH₂CH₂(CH₂)₅CH₃), 1.05 – 0.66 (m, 3H, N(CH₂)₇CH₃). ¹³C NMR (101 MHz, CDCl₃) δ 123.94, 120.71, 117.48, 114.26, 54.35, 31.77, 29.78, 29.11, 28.88, 26.25, 22.71, 14.17. ¹⁹F NMR (376 MHz, CDCl₃) δ -72.05. IR (ν_{max}/cm⁻¹): 2930, 2861, 1429, 1216, 1120, 855, 606, 504.

N-Decyl-1,1,1-trifluoro-*N*-((trifluoromethyl)sulfonyl)methanesulfonamide (**1d**)



Product **1d** was obtained as colourless liquid (14.95 g, 89% yield). Boiling point at 0.31 mbar: 92-95 °C, density: 1.22 g cm⁻¹.^[156] ¹H NMR (400 MHz, CDCl₃) δ 3.97 – 3.83 (m, 2H, NCH₂CH₂(CH₂)₇CH₃), 1.88 – 1.73 (m, 2H, NCH₂CH₂(CH₂)₇CH₃), 1.39 – 1.14 (m, 14H, NCH₂CH₂(CH₂)₇CH₃), 0.95 – 0.81 (m, 3H, N(CH₂)₉CH₃). ¹³C NMR (101 MHz, CDCl₃) δ 123.93, 120.71, 117.48, 114.25, 54.35, 31.98, 29.78, 29.53, 29.44, 29.36, 28.92, 26.25, 22.80, 14.23. ¹⁹F NMR (376 MHz, CDCl₃) δ -72.08. IR (ν_{max}/cm⁻¹): 2928, 2858, 1429, 1216, 1120, 855, 606, 504.

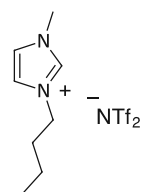
N-Dodecyl-1,1,1-trifluoro-N-((trifluoromethyl)sulfonyl)methanesulfonamide (1e)



Product **1e** was obtained as slightly yellowish liquid (15.40 g, 86% yield). Boiling point at 0.35 mbar: 110-115 °C, density: 1.22 gcm⁻¹.^[156] **¹H NMR** (400 MHz, CDCl₃) δ 4.01 – 3.76 (m, 2H, NCH₂CH₂(CH₂)₉CH₃), 1.81 (t, *J* = 8.1 Hz, 2H, NCH₂CH₂(CH₂)₉CH₃), 1.29 (d, *J* = 18.4 Hz, 18H, NCH₂CH₂(CH₂)₉CH₃), 0.99 – 0.77 (m, 3H, N(CH₂)₁₁CH₃). **¹³C NMR** (101 MHz, CDCl₃) δ 123.93, 120.70, 117.48, 114.25, 54.35, 32.05, 29.78, 29.72, 29.70, 29.57, 29.46, 29.44, 28.92, 26.25, 22.83, 14.25. **¹⁹F NMR** (376 MHz, CDCl₃) δ -72.07. **IR** (ν_{max}/cm⁻¹): 2926, 2857, 1429, 1217, 1121, 855, 606, 506.

8.6 Analysis of bis(trifluoromethanesulfonyl)imide-based ionic liquids

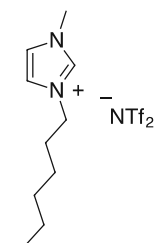
1-Butyl-3-methylimidazolium bis(trifluoromethylsulfonyl)imide (2a)



$C_{10}H_{15}F_6N_3O_4S_2$
419,36 g/mol

Product **2a** was obtained as yellowish liquid (743 mg, 89% yield). 1H NMR (400 MHz, $CDCl_3$) δ 8.74 (q, $J = 2.0$ Hz, 1H, NCHN), 7.30 (dt, $J = 4.8, 1.9$ Hz, 2H, NCHCHN), 4.16 (t, $J = 7.5$ Hz, 2H, $NCH_2(CH_2)_2CH_3$), 3.93 (d, $J = 1.2$ Hz, 3H, NCH_3), 1.84 (tt, $J = 8.3, 6.9$ Hz, 2H, $NCH_2CH_2CH_2CH_3$), 1.35 (dt, $J = 14.7, 7.5$ Hz, 2H, $NCH_2CH_2CH_2CH_3$), 0.95 (t, $J = 7.3$ Hz, 3H, $NCH_2CH_2CH_2CH_3$). ^{13}C NMR (101 MHz, $CDCl_3$) δ 136.24, 123.79, 122.36, 121.52, 118.33, 50.09, 36.45, 32.04, 19.45, 13.32. ^{19}F NMR (376 MHz, $CDCl_3$) δ -79.09. HRMS [C^+] calc. 139.1230, found 139.1235.

1-Hexyl-3-methylimidazolium bis(trifluoromethylsulfonyl)imide (2b)

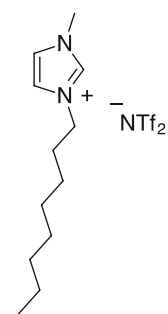


$C_{12}H_{19}F_6N_3O_4S_2$
447,41 g/mol

Product **2b** was obtained as yellowish liquid (811 mg, 91% yield). 1H NMR (400 MHz, $CDCl_3$) δ 8.77 (d, $J = 7.0$ Hz, 1H, NCHN), 7.30 (dq, $J = 9.1, 1.8$ Hz, 2H, NCHCHN), 4.31 – 4.13 (m, 2H, $NCH_2(CH_2)_4CH_3$), 3.94 (d, $J = 1.8$ Hz, 3H, NCH_3), 1.95 – 1.79 (m, 2H, $NCH_2CH_2(CH_2)_3CH_3$), 1.31 (q, $J = 4.1, 2.9$ Hz, 6H, $NCH_2CH_2(CH_2)_3CH_3$), 0.98 – 0.77 (m, 3H, $N(CH_2)_5CH_3$). ^{13}C NMR (101 MHz, $CDCl_3$) δ 136.26, 123.80, 122.32, 121.52, 118.33, 50.36, 36.47, 31.05, 30.12, 25.86, 22.40, 13.93. ^{19}F NMR (376 MHz, $CDCl_3$) δ -79.05.

HRMS [C^+] calc. 167.1543, found 167.1544.

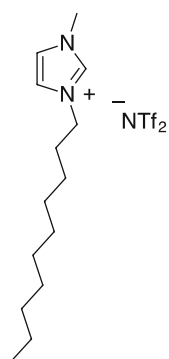
1-Octyl-3-methylimidazolium bis(trifluoromethylsulfonyl)imide (2c)



$C_{14}H_{23}F_6N_3O_4S_2$
475,47 g/mol

Product **2c** was obtained as slightly yellowish liquid (843 mg, 89% yield). 1H NMR (400 MHz, $CDCl_3$) δ 8.76 (s, 1H, NCHN), 7.29 (dt, $J = 11.1, 1.7$ Hz, 2H, NCHCHN), 4.29 – 4.07 (m, 2H, $NCH_2(CH_2)_6CH_3$), 3.94 (d, $J = 1.6$ Hz, 3H, NCH_3), 1.94 – 1.78 (m, 2H, $NCH_2CH_2(CH_2)_5CH_3$), 1.43 – 1.12 (m, 10H, $NCH_2CH_2(CH_2)_5CH_3$), 0.92 – 0.78 (m, 3H, $N(CH_2)_7CH_3$). ^{13}C NMR (101 MHz, $CDCl_3$) δ 124.72, 123.80, 122.29, 121.53, 118.34, 50.41, 36.52, 31.74, 30.19, 29.05, 28.92, 26.24, 22.67, 14.14. ^{19}F NMR (376 MHz, $CDCl_3$) δ -79.04. HRMS [C^+] calc. 195.1856, found 195.1860.

1-Decyl-3-methylimidazolium bis(trifluoromethylsulfonyl)imide (2d)



$C_{16}H_{27}F_6N_3O_4S_2$
503,52 g/mol

Product **2d** was obtained as yellowish liquid (883 mg, 88% yield). 1H NMR (400 MHz, $CDCl_3$) δ 8.78 (s, 1H, NCHN), 7.32 – 7.26 (m, 2H, NCHCHN), 4.16 (td, $J = 7.6, 2.4$ Hz, 2H, $NCH_2(CH_2)_8CH_3$), 3.95 (d, $J = 2.9$ Hz, 3H, NCH_3), 1.86 (h, $J = 6.4, 5.9$ Hz, 2H, $NCH_2CH_2(CH_2)_7CH_3$), 1.28 (d, $J = 26.6$ Hz, 14H, $NCH_2CH_2(CH_2)_7CH_3$), 0.87 (t, $J = 6.8$ Hz, 3H, $N(CH_2)_9CH_3$). ^{13}C NMR (101 MHz, $CDCl_3$) δ 136.37, 123.76, 122.25, 121.53, 118.34, 50.43, 36.55, 31.95, 30.20, 29.52, 29.41, 29.34, 28.98, 26.26, 22.78, 14.21. ^{19}F NMR (376 MHz, $CDCl_3$) δ -79.01. HRMS [C^+] calc. 223.2169, found 223.2175.

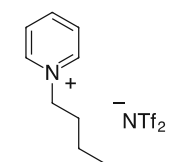
1-Dodecyl-3-methylimidazolium bis(trifluoromethylsulfonyl)imide (2e)



$C_{18}H_{31}F_6N_3O_4S_2$
531,57 g/mol

Product **2e** was obtained as yellowish liquid (879 mg, 83% yield). 1H NMR (400 MHz, $CDCl_3$) δ 8.77 (d, $J = 1.9$ Hz, 1H, NCHN), 7.29 (dt, $J = 12.5, 1.9$ Hz, 2H, NCHCHN), 4.16 (dd, $J = 8.2, 6.8$ Hz, 2H, $NCH_2(CH_2)_{10}CH_3$), 3.94 (s, 3H, NCH_3), 1.86 (p, $J = 7.4$ Hz, 2H, $NCH_2CH_2(CH_2)_9CH_3$), 1.36 – 1.11 (m, 18H, $NCH_2CH_2(CH_2)_9CH_3$), 0.94 – 0.80 (m, 3H, $N(CH_2)_{11}CH_3$). ^{13}C NMR (101 MHz, $CDCl_3$) δ 136.34, 123.77, 122.26, 121.52, 118.33, 50.41, 36.52, 32.03, 30.20, 29.71, 29.70, 29.58, 29.45, 29.42, 28.99, 26.26, 22.81, 14.23. ^{19}F NMR (376 MHz, $CDCl_3$) δ -79.02. HRMS [C^+] calc. 251.2482, found 251.2485.

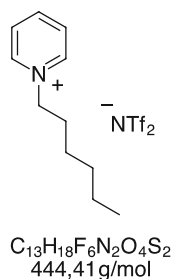
1-Butylpyridinium bis(trifluoromethylsulfonyl)imide (3a)



$C_{11}H_{14}F_6N_2O_4S_2$
416,36 g/mol

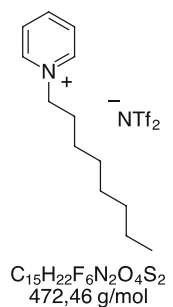
Product **3a** was obtained as slightly yellowish liquid (764 mg, 92% yield). 1H NMR (400 MHz, $CDCl_3$) δ 9.02 – 8.69 (m, 2H, 2 x $CH(CH)(CH)N$, *H*-arom), 8.47 (tt, $J = 7.8, 1.4$ Hz, 1H, $CH(CH)(CH)N$, *H*-arom), 8.06 (t, $J = 7.0$ Hz, 2H, 2 x $CH(CH)(CH)N$, *H*-arom), 4.74 – 4.41 (m, 2H, $NCH_2(CH_2)_2CH_3$), 1.99 (tt, $J = 9.4, 6.8$ Hz, 2H, $NCH_2CH_2CH_2CH_3$), 1.40 (dq, $J = 14.9, 7.4$ Hz, 2H, $NCH_2CH_2CH_2CH_3$), 0.98 (t, $J = 7.4$ Hz, 3H, $N(CH_2)_2CH_3$). ^{13}C NMR (101 MHz, $CDCl_3$) δ 145.53, 144.54, 128.80, 121.52, 118.33, 62.62, 33.53, 19.40, 13.34. ^{19}F NMR (376 MHz, $CDCl_3$) δ -78.92. HRMS [C^+] calc. 136.1121, found 136.1127.

1-Hexylpyridinium bis(trifluoromethylsulfonyl)imide (3b)



Product **3b** was obtained as slightly yellowish liquid (814 mg, 92% yield). 1H NMR (400 MHz, $CDCl_3$) δ 8.90 – 8.72 (m, 2H, 2 x $CH(CH)(CH)N$, *H*-arom), 8.47 (tt, $J = 7.8, 1.4$ Hz, 1H, $CH(CH)(CH)N$, *H*-arom), 8.18 – 7.93 (m, 2H, 2 x $CH(CH)(CH)N$, *H*-arom), 4.60 (t, $J = 7.6$ Hz, 2H, $NCH_2(CH_2)_4CH_3$), 2.09 – 1.88 (m, 2H, $NCH_2CH_2(CH_2)_3CH_3$), 1.44 – 1.18 (m, 6H, $NCH_2CH_2(CH_2)_3CH_3$), 0.93 – 0.76 (m, 3H, $N(CH_2)_5CH_3$). ^{13}C NMR (101 MHz, $CDCl_3$) δ 145.56, 144.52, 124.72, 121.53, 118.33, 62.76, 31.63, 31.01, 25.69, 22.35, 13.89. ^{19}F NMR (376 MHz, $CDCl_3$) δ -78.93. HRMS [C^+] calc. 164.1434, found 164.1437.

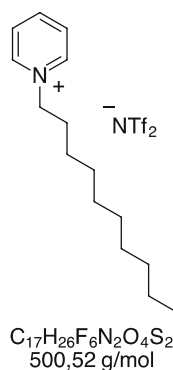
1-Octylpyridinium bis(trifluoromethylsulfonyl)imide (3c)



Product **3c** was obtained as colourless liquid (817 mg, 87% yield). 1H NMR (400 MHz, $CDCl_3$) δ 8.89 – 8.74 (m, 2H, 2x $CH(CH)(CH)N$, *H*-arom), 8.47 (tt, $J = 7.8, 1.4$ Hz, 1H, $CH(CH)(CH)N$, *H*-arom), 8.15 – 7.95 (m, 2H, 2 x $CH(CH)(CH)N$, *H*-arom), 4.59 (td, $J = 7.5, 1.3$ Hz, 2H, $NCH_2(CH_2)_6CH_3$), 1.99 (q, $J = 7.5$ Hz, 2H, $NCH_2CH_2(CH_2)_5CH_3$), 1.46 – 1.09 (m, 10H, $NCH_2CH_2(CH_2)_5CH_3$), 0.91 – 0.79 (m, 3H, $N(CH_2)_7CH_3$). ^{13}C NMR (101 MHz, $CDCl_3$) δ 145.54, 144.52, 128.80, 121.53, 118.33, 62.84, 31.69, 28.99, 28.90, 26.07, 22.65, 14.12.

^{19}F NMR (376 MHz, $CDCl_3$) δ -78.93. HRMS [C^+] calc. 192.1747, found 192.1751.

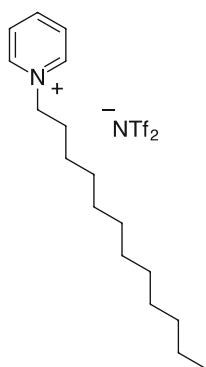
1-Decylpyridinium bis(trifluoromethylsulfonyl)imide (3d)



Product **3d** was obtained as slightly brownish, viscous liquid (910 mg, 91% yield). 1H NMR (400 MHz, $CDCl_3$) δ 8.89 – 8.69 (m, 2H, 2 x $CH(CH)(CH)N$, *H*-arom), 8.48 (d, $J = 7.9$ Hz, 1H, $CH(CH)(CH)N$, *H*-arom), 8.06 (t, $J = 7.0$ Hz, 2H, 2 x $CH(CH)(CH)N$, *H*-arom), 4.69 – 4.49 (m, 2H, $NCH_2(CH_2)_8CH_3$), 2.00 (t, $J = 7.4$ Hz, 2H, $NCH_2CH_2(CH_2)_7CH_3$), 1.29 (d, $J = 37.9$ Hz, 14H, $NCH_2CH_2(CH_2)_7CH_3$), 0.87 (t, $J = 6.8$ Hz, 3H, $N(CH_2)_9CH_3$). ^{13}C NMR (101 MHz, $CDCl_3$) δ 145.54, 144.52, 128.81, 121.53, 118.34, 62.87, 31.94, 31.71, 29.49, 29.36, 29.32, 28.96, 26.10, 22.77, 14.21. ^{19}F NMR (376 MHz, $CDCl_3$) δ -78.91.

HRMS [C^+] calc. 220.2060, found 220.2064.

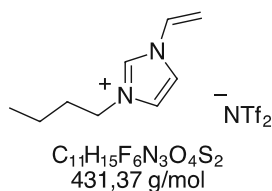
1-Dodecylpyridinium bis(trifluoromethylsulfonyl)imide (3e)



$C_{19}H_{30}F_6N_2O_4S_2$
528,57 g/mol

Product **3e** was obtained as slightly yellowish, viscous liquid (887 mg, 84% yield). 1H NMR (400 MHz, $CDCl_3$) δ 8.87 – 8.74 (m, 2H, 2 x CH(CH)(CH)N, *H*-arom), 8.47 (tt, J = 7.8, 1.4 Hz, 1H, CH(CH)(CH)N, *H*-arom), 8.11 – 8.00 (m, 2H, 2 x CH(CH)(CH)N, *H*-arom), 4.59 (t, J = 7.6 Hz, 2H, $NCH_2(CH_2)_{10}CH_3$), 1.99 (m, 2H, $NCH_2CH_2(CH_2)_9CH_3$), 1.38 – 1.18 (m, 18H, $NCH_2CH_2(CH_2)_9CH_3$), 0.93 – 0.77 (m, 3H, $N(CH_2)_{11}CH_3$). ^{13}C NMR (101 MHz, $CDCl_3$) δ 145.54, 144.51, 128.80, 121.52, 118.32, 62.86, 32.02, 31.70, 29.69, 29.67, 29.54, 29.44, 29.37, 28.97, 26.10, 22.80, 14.23. ^{19}F NMR (376 MHz, $CDCl_3$) δ -78.92. HRMS [C^+] calc. 248.2373, found 248.2370.

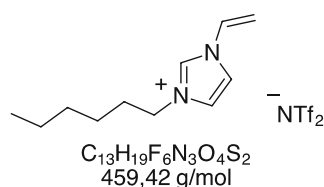
1-Butyl-3-vinylimidazolium bis(trifluoromethylsulfonyl)imide (5a)



$C_{11}H_{15}F_6N_3O_4S_2$
431,37 g/mol

Product **5a** was obtained as yellowish liquid (767 mg, 89% yield). 1H NMR (400 MHz, $CDCl_3$) δ 9.03 (d, J = 1.9 Hz, 1H, NCHN), 7.62 (d, J = 1.9 Hz, 1H, NCHCHN), 7.44 (d, J = 1.9 Hz, 1H, NCHCH), 7.13 (dd, J = 15.6, 8.6 Hz, 1H, NCHCH₂), 5.78 (dd, J = 15.6, 3.1 Hz, 1H, NCHCH₂), 5.43 (dd, J = 8.7, 3.1 Hz, 1H, NCHCH₂), 4.23 (t, J = 7.5 Hz, 2H, $NCH_2(CH_2)_2CH_3$), 1.87 (tt, J = 9.3, 6.9 Hz, 2H, $NCH_2CH_2CH_2CH_3$), 1.37 (dt, J = 14.8, 7.4 Hz, 2H, $NCH_2CH_2CH_2CH_3$), 0.96 (t, J = 7.4 Hz, 3H, $N(CH_2)_3CH_3$). ^{13}C NMR (101 MHz, $CDCl_3$) δ 134.60, 128.10, 123.22, 121.51, 119.39, 118.32, 110.42, 50.47, 31.99, 19.44, 13.31. ^{19}F NMR (376 MHz, $CDCl_3$) δ -79.02. HRMS [C^+] calc. 151.1230, found 151.1235.

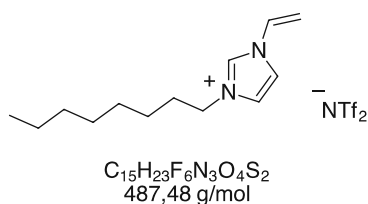
1-Hexyl-3-vinylimidazolium bis(trifluoromethylsulfonyl)imide (5b)



$C_{13}H_{19}F_6N_3O_4S_2$
459,42 g/mol

Product **5b** was obtained as yellow liquid (889 mg, 97% yield). 1H NMR (400 MHz, $CDCl_3$) δ 9.09 (q, J = 1.6 Hz, 1H, NCHN), 7.60 (t, J = 2.0 Hz, 1H, NCHCHN), 7.41 (d, J = 2.0 Hz, 1H, NCHCHN), 7.15 (dd, J = 15.6, 8.6 Hz, 1H, NCHCH₂), 5.78 (dd, J = 15.6, 3.1 Hz, 1H, NCHCH₂), 5.45 (dd, J = 8.6, 3.1 Hz, 1H, NCHCH₂), 4.30 – 4.15 (m, 2H, $NCH_2(CH_2)_4CH_3$), 1.97 – 1.80 (m, 2H, $NCH_2CH_2(CH_2)_3CH_3$), 1.33 (tdt, J = 8.5, 5.6, 3.5 Hz, 6H, $NCH_2CH_2(CH_2)_3CH_3$), 0.97 – 0.78 (m, 3H, $N(CH_2)_5CH_3$). ^{13}C NMR (101 MHz, $CDCl_3$) δ 134.73, 128.12, 123.13, 121.52, 119.32, 118.33, 110.43, 50.75, 31.05, 30.09, 25.84, 22.40, 13.93. ^{19}F NMR (376 MHz, $CDCl_3$) δ -78.96. HRMS [C^+] calc. 179.1543, found 179.1547.

1-Octyl-3-vinylimidazolium bis(trifluoromethylsulfonyl)imide (5c)

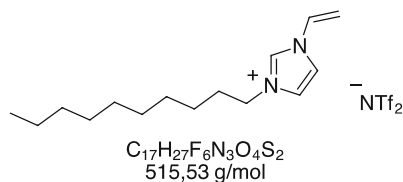


$C_{15}H_{23}F_6N_3O_4S_2$
487,48 g/mol

Product **5c** was obtained as yellowish liquid (906 mg, 93% yield). 1H NMR (400 MHz, $CDCl_3$) δ 9.06 (s, 1H, NCHN), 7.65 – 7.56 (m, 1H, NCHCHN), 7.45 – 7.35 (m, 1H, NCHCHN), 7.20 – 7.08 (m, 1H, NCHCH₂), 5.78 (dt, J = 15.5, 2.5 Hz, 1H, NCHCH₂), 5.49 – 5.30 (m, 1H, NCHCH₂), 4.24 (dt, J = 11.5, 5.9 Hz, 2H, $NCH_2(CH_2)_6CH_3$), 1.87 (s, 2H, $NCH_2CH_2(CH_2)_5CH_3$), 1.50 – 1.13 (m,

10H, NCH₂CH₂(CH₂)₅CH₃), 0.94 – 0.77 (m, 3H, N(CH₂)₇CH₃). **¹³C NMR** (101 MHz, CDCl₃) δ 128.14, 124.72, 123.11, 121.53, 119.33, 118.33, 110.47, 50.79, 31.73, 30.16, 29.04, 28.92, 26.21, 22.67, 14.14. **¹⁹F NMR** (376 MHz, CDCl₃) δ -78.97. **HRMS** [C⁺] calc. 207.1856, found 207.1862.

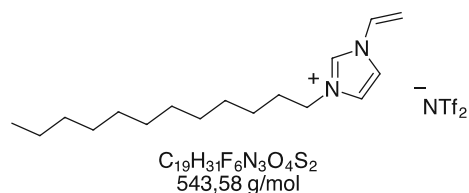
1-Decyl-3-vinylimidazolium bis(trifluoromethylsulfonyl)imide (5d)



Product **5d** was obtained as yellowish liquid (883 mg, 93% yield).

¹H NMR (400 MHz, CDCl₃) δ 9.10 (s, 1H, NCHN), 7.64 – 7.55 (m, 1H, NCHCHN), 7.39 (d, *J* = 1.9 Hz, 1H, NCHCHN), 7.16 (dd, *J* = 15.6, 8.7 Hz, 1H, NCHCH₂), 5.77 (dd, *J* = 15.6, 3.1 Hz, 1H, NCHCH₂), 5.45 (dd, *J* = 8.6, 3.1 Hz, 1H, NCHCH₂), 4.29 – 4.13 (m, 2H, NCH₂(CH₂)₈CH₃), 1.90 (q, *J* = 6.7, 6.1 Hz, 2H, NCH₂CH₂(CH₂)₇CH₃), 1.41 – 1.10 (m, 14H, NCH₂CH₂(CH₂)₇CH₃), 0.93 – 0.77 (m, 3H, N(CH₂)₉CH₃). **¹³C NMR** (101 MHz, CDCl₃) δ 134.99, 128.15, 122.96, 121.53, 119.16, 118.34, 110.50, 50.82, 31.95, 30.17, 29.52, 29.40, 29.34, 28.98, 26.23, 22.78, 14.21. **¹⁹F NMR** (376 MHz, CDCl₃) δ -78.93. **HRMS** [C⁺] calc. 235.2169, found 235.2174.

1-Dodecyl-3-vinylimidazolium bis(trifluoromethylsulfonyl)imide (5e)



Product **5e** was obtained as brownish, viscous liquid (984

mg, 91% yield). **¹H NMR** (400 MHz, CDCl₃) δ 9.11 – 9.00 (m, 1H, NCHN), 7.61 (d, *J* = 1.9 Hz, 1H, NCHCHN), 7.40 (t, *J* = 1.9 Hz, 1H, NCHCHN), 7.15 (dd, *J* = 15.6, 8.7 Hz, 1H, NCHCH₂), 5.78 (dd, *J* = 15.6, 3.1 Hz, 1H, NCHCH₂), 5.44 (dd, *J* = 8.6, 3.1 Hz, 1H, NCHCH₂), 4.23 (t, *J* = 7.5 Hz, 2H, NCH₂(CH₂)₁₀CH₃), 1.89 (p, *J* = 7.8 Hz, 2H, NCH₂CH₂(CH₂)₉CH₃), 1.42 – 1.15 (m, 18H, NCH₂CH₂(CH₂)₉CH₃), 0.93 – 0.79 (m, 3H, N(CH₂)₉CH₃). **¹³C NMR** (101 MHz, CDCl₃) δ 134.80, 128.14, 123.05, 121.51, 119.27, 118.32, 110.47, 50.79, 32.03, 30.17, 29.71, 29.69, 29.57, 29.45, 29.41, 28.99, 26.23, 22.81, 14.23. **¹⁹F NMR** (376 MHz, CDCl₃) δ -78.96. **HRMS** [C⁺] calc. 263.2482, found 263.2497.

8.7 Kinetic analysis of ionic liquid formation

For the kinetic analysis of the ionic liquid formation, 2 mmol substrate (in the given example: 1-methylimidazole, 164 mg, 159 μl) were heated up to 80 $^{\circ}\text{C}$ in a glass vial, then 1.30 equivalent (2.60 mmol, 878 mg) butyl-bistriflimide were added. Subsequently, samples (20 μl) were taken at the following intervals: 0.5 min, 5 min, 10 min, 15 min, 20 min, 25 min, 30 min, 45 min, 60 min, 90 min, 120 min, 180 min, and 1440 min. The collected samples were immediately cooled down to room temperature and diluted with 0.6 mL CDCl_3 . The conversion was calculated using the following equation:

$$\frac{\int \text{product}}{(\int \text{product} + \int \text{educt})} \times 100 = \text{conversion} [\%]$$

An example for determining the conversion *via* ^1H NMR spectroscopy can be seen in **Figure 56** and **Figure 57**.

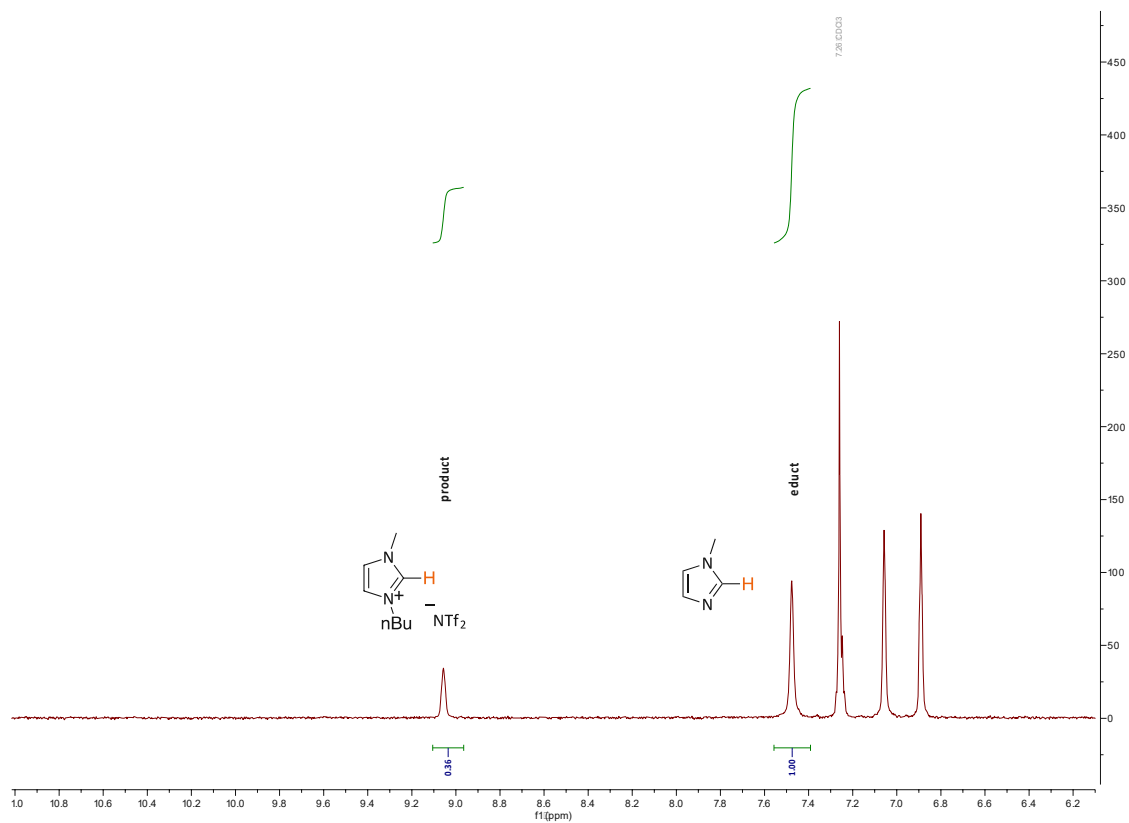


Figure 56. Calculation of conversion for the batch-wise synthesis of IL **2a** (sample taken after 0.5 minutes)

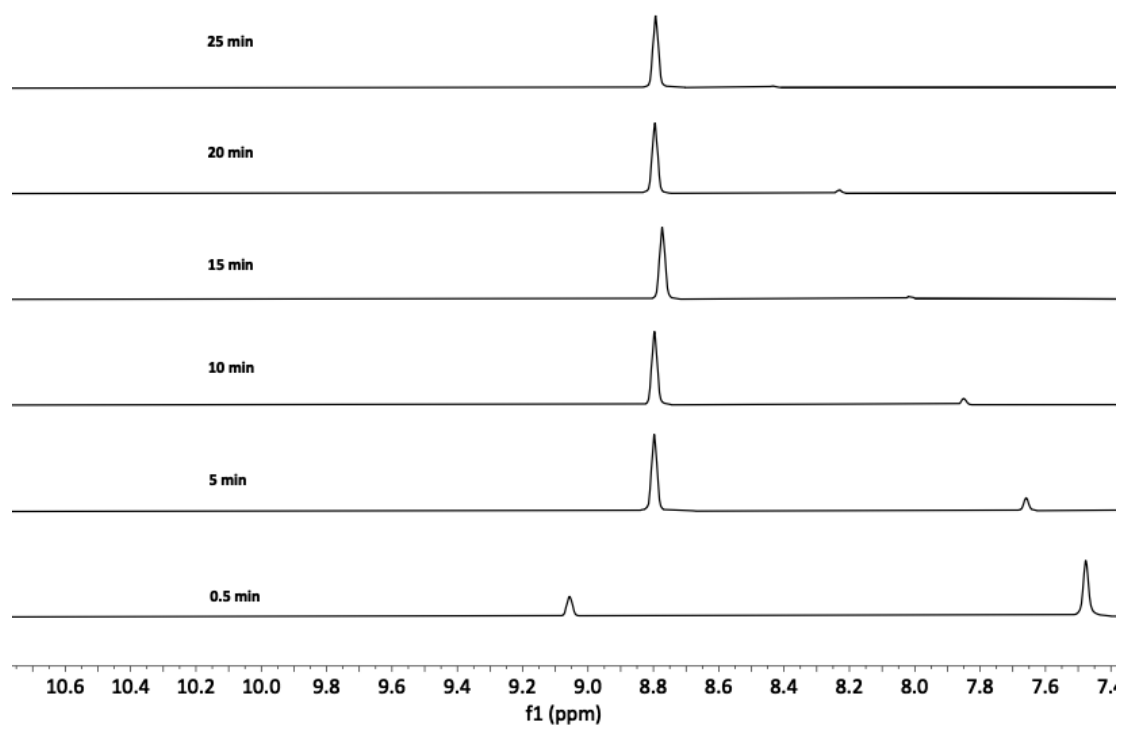


Figure 57. IL formation monitored by ^1H NMR spectroscopy over time

8.8 Optimisation of the alkyl bistriflimide synthesis

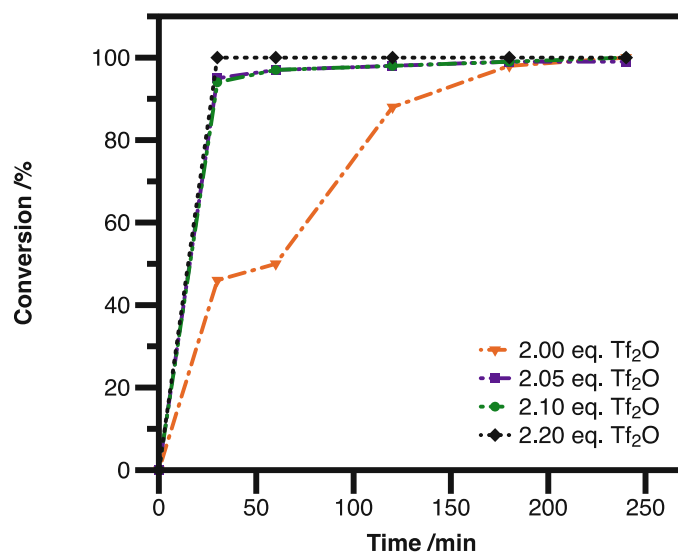


Figure 58. Varying the triflic anhydride ratio by using 1.00 eq. *n*-butylamine as substrate

8.9 Batch and continuous-flow synthesis of 2b

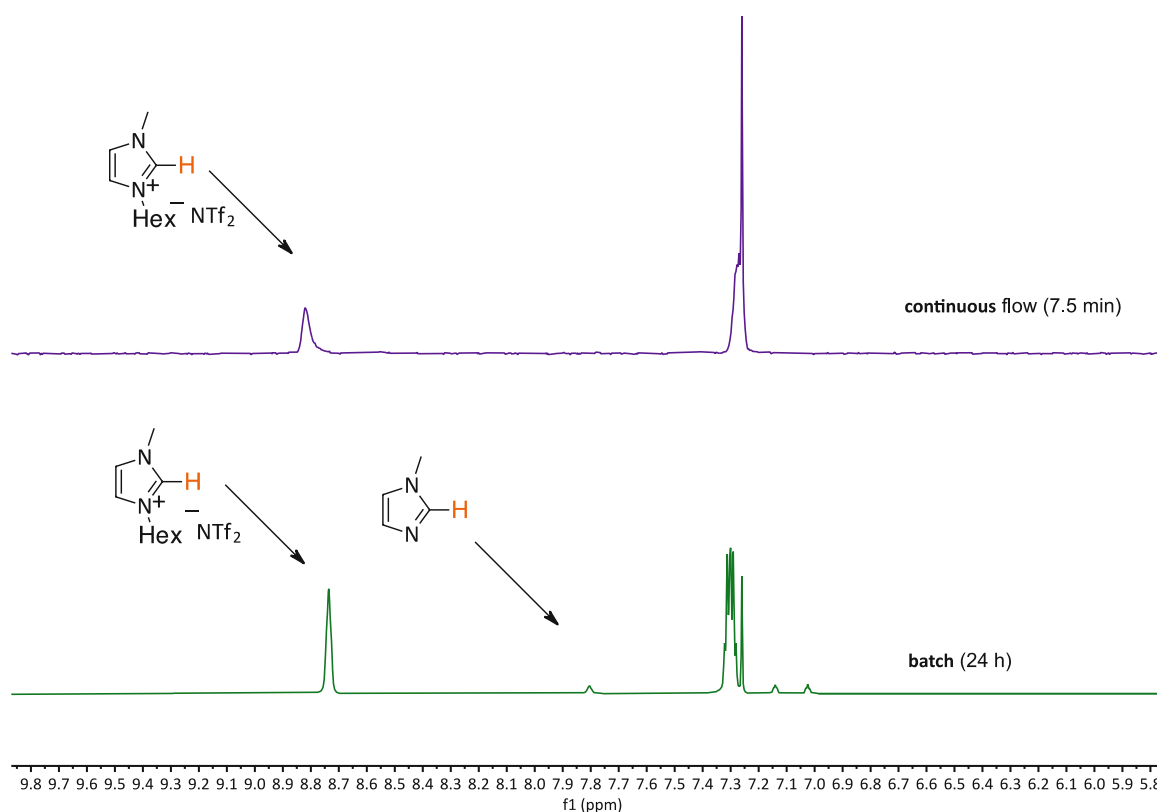


Figure 59. Conversion obtained under batch-wise and continuous-flow conditions at 120 °C

Both the batch-wise and the continuous-flow experiments were carried out at 120 °C. As it can be seen, IL **2b** has not yielded full conversion after 24 hours under batch-wise conditions (green), whereas full conversion could be reached in 7.5 minutes when the continuous-flow reactor (purple) was employed.

8.10 Ion chromatography measurement parameters, halide- and water content

Ion chromatography experiments were carried out using a Metrohm Eco IC system (Metrohm, Herisau, Switzerland) equipped with 863 Compact IC Autosampler, 10.0 μL injection loop, and conductometric detector (maintained at room temperature). Self-regenerating Suppressor Module (MSM) (Metrohm, Herisau, Switzerland), regenerated with distilled water and sulfuric acid, was used to separate and determine anions in ionic liquids. All data were recorded by Metrohm software. Anion ion chromatograph apparatus was equipped with a Metrosep A Supp. 5 ion exchange column (150×4.0 mm) coupled with Metrosep A Supp. Guard. A flow rate of 0.9 mL min^{-1} was used in both systems. Anion separation was performed with eluent composed of a 30:70 ratio of acetonitrile and an aqueous solution containing 3.2mM of sodium bicarbonate and 1.0 mM of sodium carbonate (Merck). All aqueous solutions were prepared carefully using distilled water ($\sigma = 0.05 \mu\text{S cm}^{-1}$). During anion separation, average pressure in the analytical system was maintained at the level of 13.5 MPa. Samples for anion analysis were first dissolved in 1 mL of acetone (HPLC grade, Merck), then the sample was taken for analysis (200 μL) and then complemented in a vial with 5 mL of the eluent.

Table 2. Halide- and water content of the produced ionic liquids

Entry	[Cl ⁻] content /ppm ^[a]	Water content /ppm ^[b]
2a	150	356
2b	140	359
2c	140	386
2d	490	312
2e	120	376
3a	450	132
3b	100	154
3c	220	267
3d	260	112
3e	340	121
4a	N/A	268
4b	160	198
4c	310	182
4d	490	239
4e	445	288

[a] Determined by IC analysis. [b] Determined by Karl Fischer-titration, the given value is the average of 3 consecutive measurements, samples were measured after they were dried on high vacuum (0.3 mbar) at 90 °C overnight.

8.11 E-factor calculations

State-of-the-art method

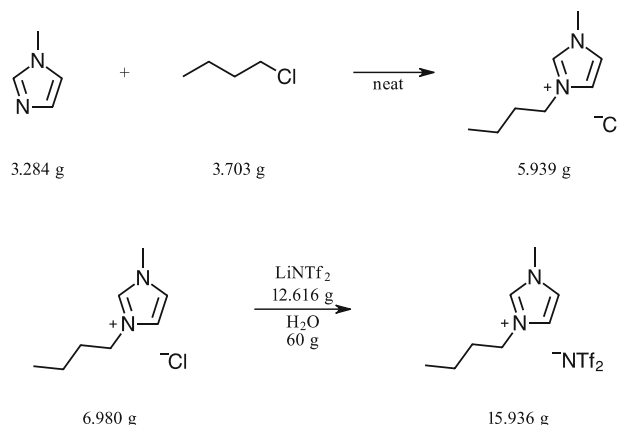


Figure 60. State-of-the-art synthesis of NTf_2^- -based ionic liquids

Working on a 40 mmolar scale, assuming the use of 3 x 10 g ethyl acetate for washing the formed IL, 30 g ethyl acetate: acetonitrile (1:1) mixture for the recrystallisation of the chloride IL and 85% yield, the calculated E-factor for the first step:

$$E - factor = \frac{3.284 + 3.703 + 3 \times 10.00 + 30.00 - 5.939}{5.939} = 10.279$$

Working on a 40 mmolar scale, assuming the use of 3 x 30 g dichloromethane for extraction of the formed IL, 10 x 40 g distilled water for the washing of the IL, 5 g of Na_2SO_4 for drying and 95% yield, the calculated E-factor for the second step:

$$E - factor = \frac{6.980 + 12.616 + 60.00 + 3 \times 30.00 + 10 \times 40.00 + 5.00 - 15.936}{15.936} = 35.056$$

The cumulative E-factor over 2 steps:

$$\sum E - factor = 45.335$$

Halide-free alkyl bistriflimide-based method

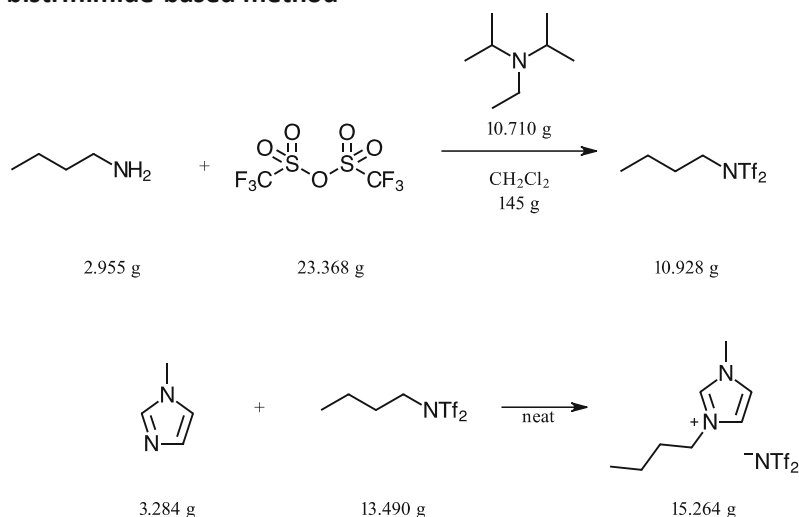


Figure 61. Halide-free synthesis of NTf₂⁻-based ionic liquids

Working on a 40 mmolar scale, assuming the use of 40 g sat. NaHCO₃ solution, 40 g 1M HCl solution and 40 g water for the washing of the alkyl bistriflimide containing crude mixture, 3 x 10 g dichloromethane for the back-extraction of the aqueous phases, 5 g Na₂SO₄ for drying and 81% yield, the calculated E-factor for the first step: (plus by-product: 31.78)

$$E - factor = \frac{2.96 + 23.37 + 10.71 + 145.00 + 3 \times 40.00 + 3 \times 10.00 + 5.00 - 10.93}{10.928} = 29.84$$

Working on a 40 mmolar scale, assuming no use of any further chemicals and 91% yield, the calculated E-factor for the second step:

$$E - factor = \frac{3.28 + 13.49 - 15.26}{15.26} = 0.01$$

The summarized E-factor over 2 steps:

$$\sum E - factor = 29.85$$

Based on the comparison of the calculated E-factor values, our bistriflimide-based method generates approximately 15 kg less waste per kg product.

8.12 NMR spectra of alkyl bistriflimides

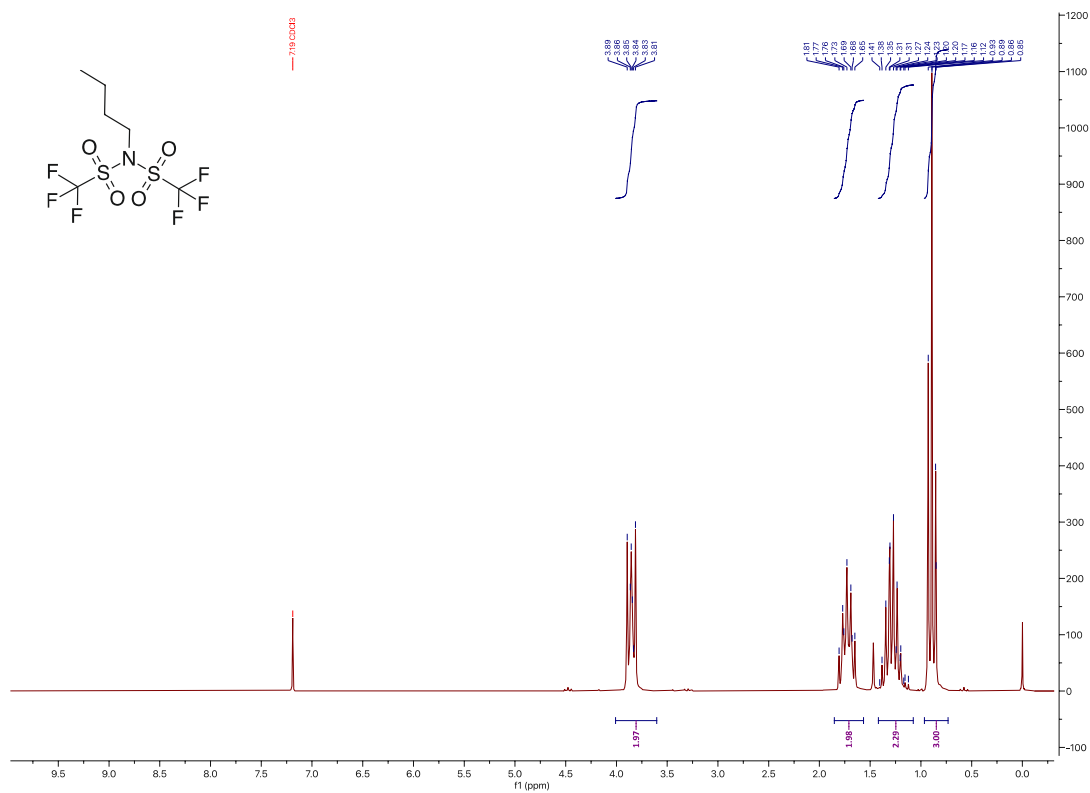


Figure 62. ¹H NMR spectrum of 1a

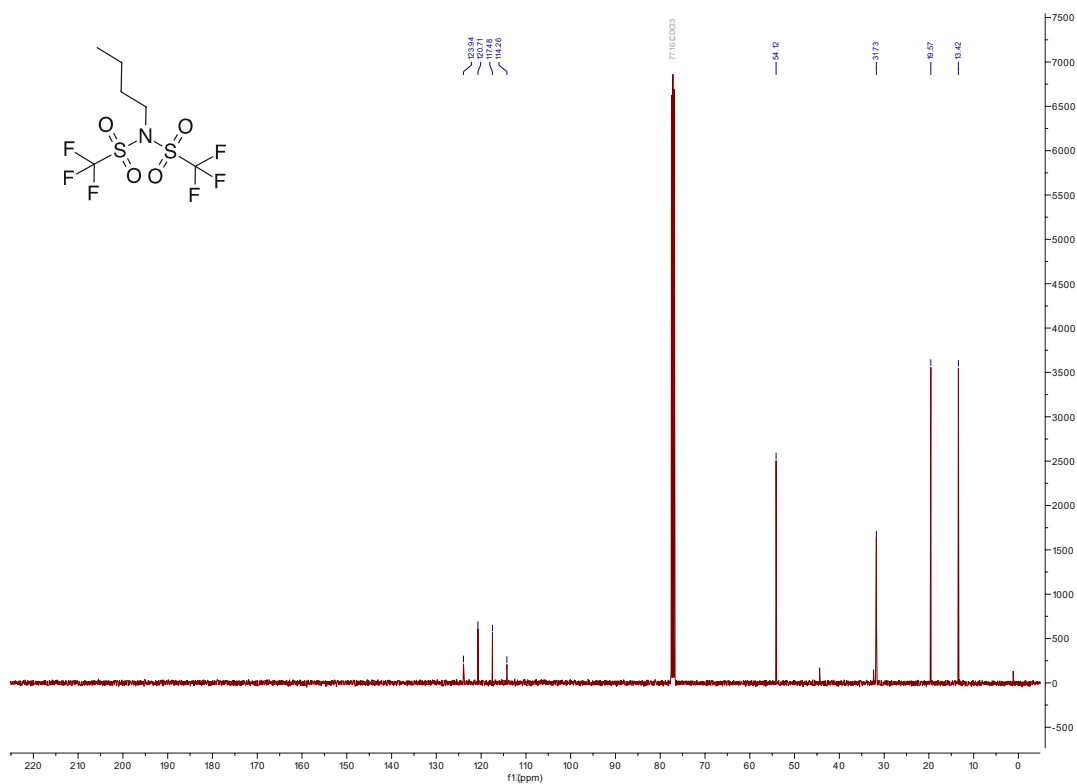


Figure 63. ¹³C NMR spectrum of 1a

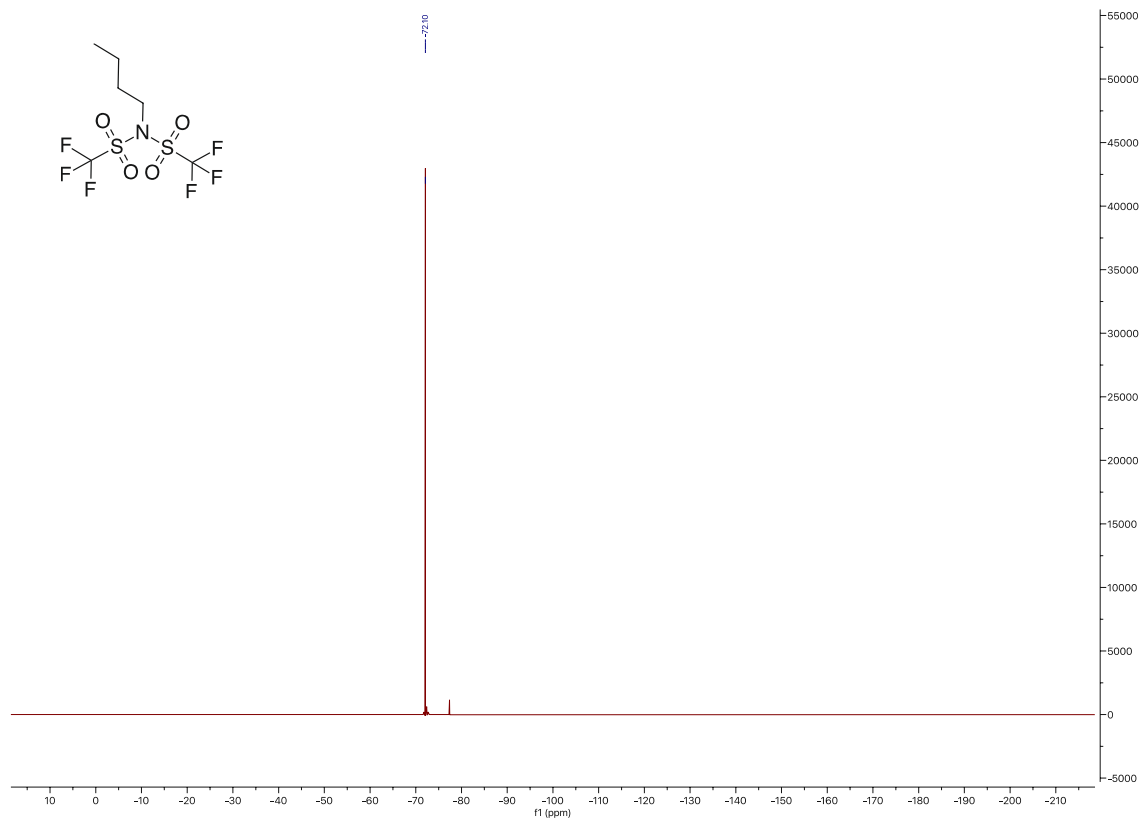


Figure 64. ^{19}F NMR spectrum of 1a

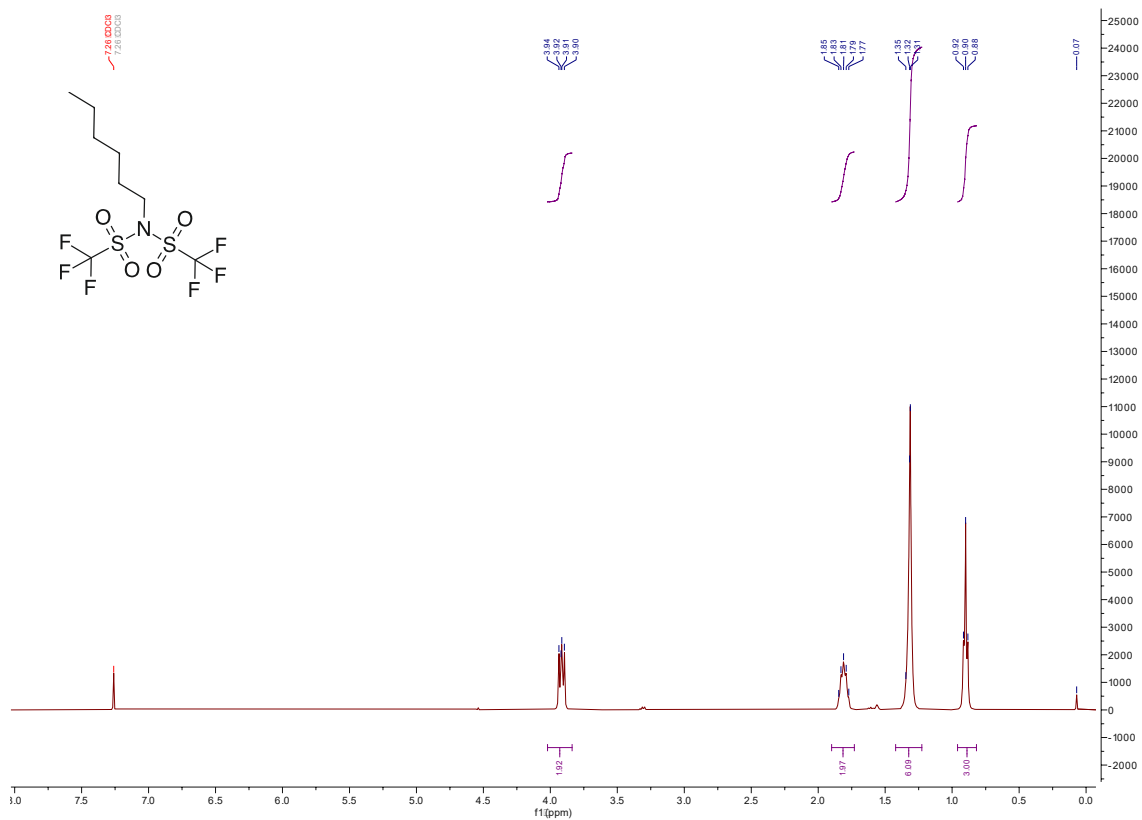


Figure 65. ^1H NMR spectrum of 1b

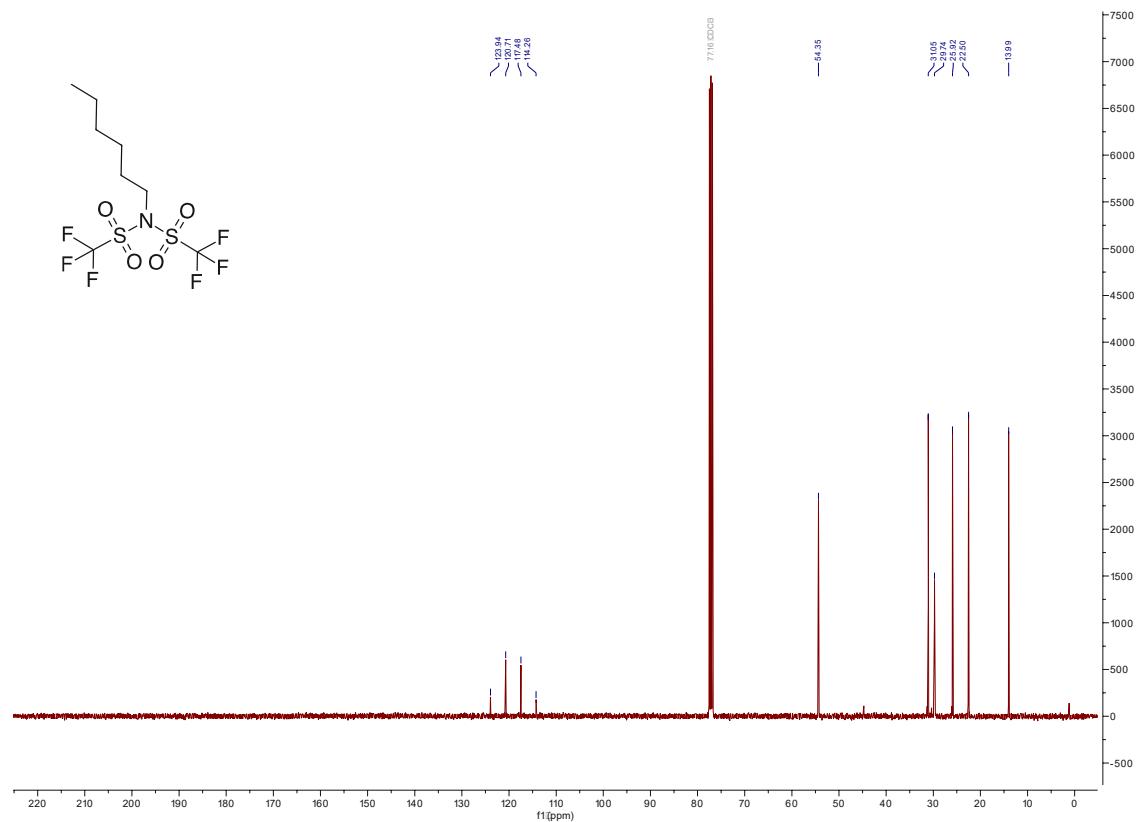


Figure 66. ¹³C NMR spectrum of 1b

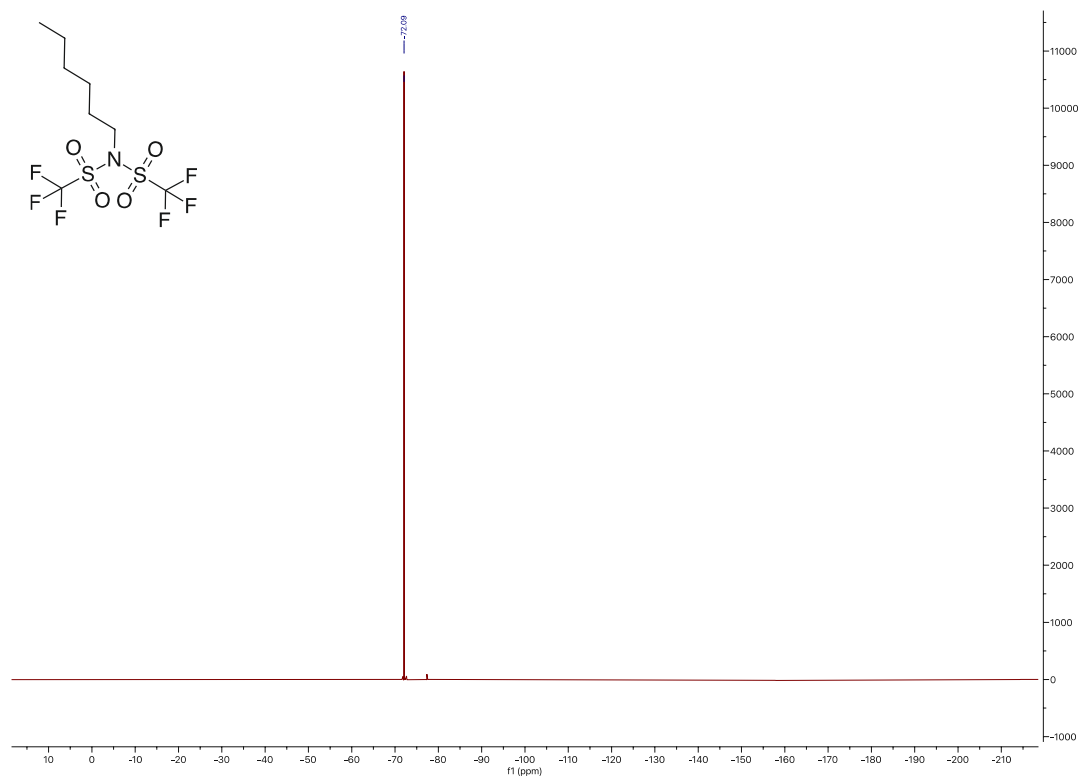


Figure 67. ¹⁹F NMR spectrum of 1b

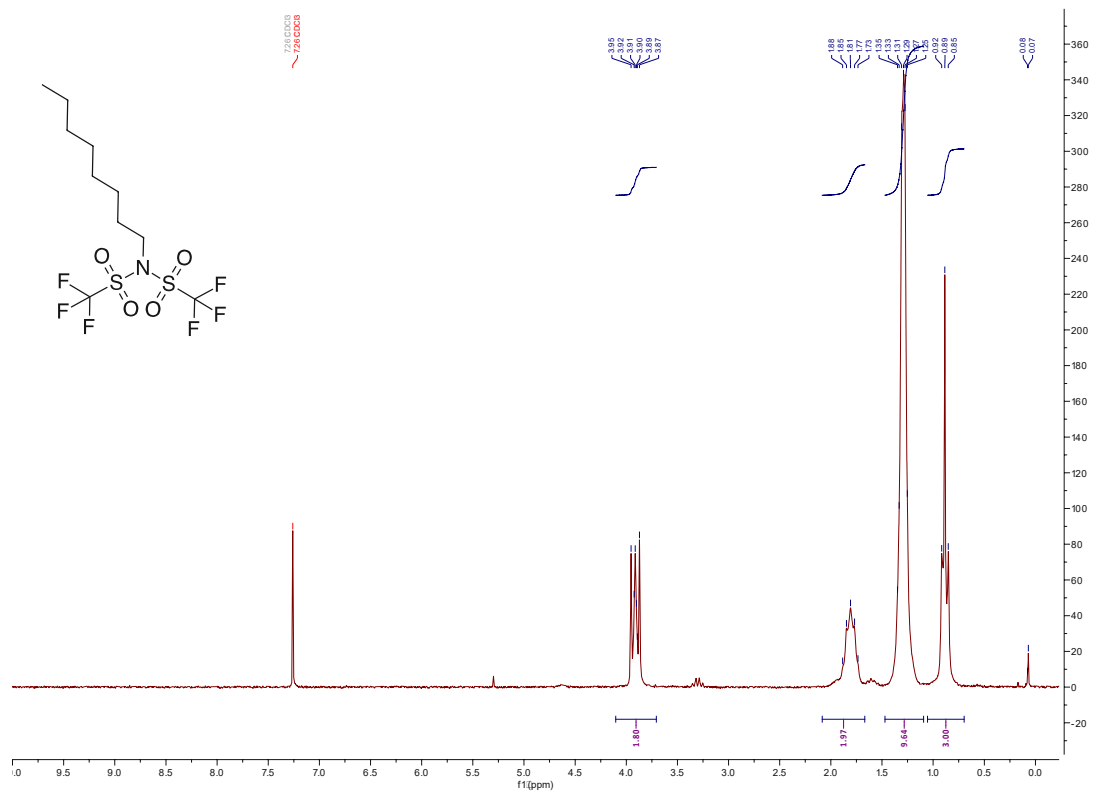


Figure 68. ^1H NMR spectrum of 1c

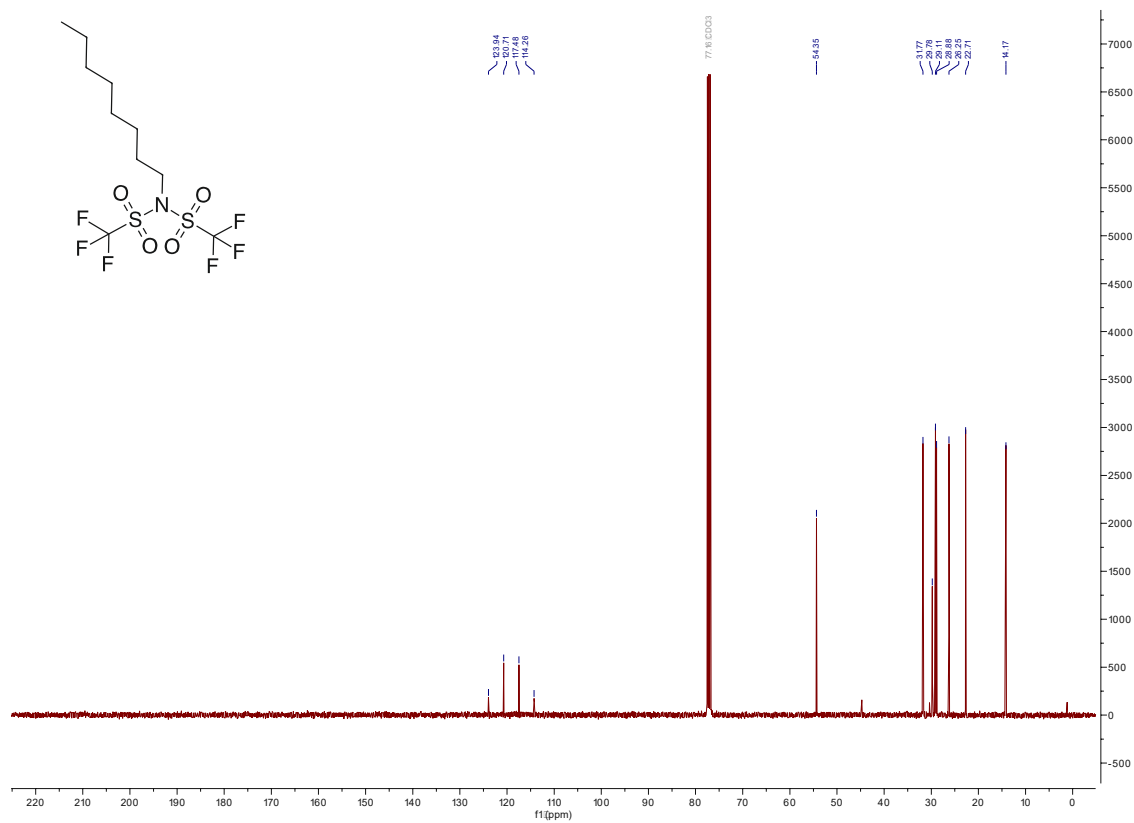


Figure 69. ^{13}C NMR spectrum of 1c

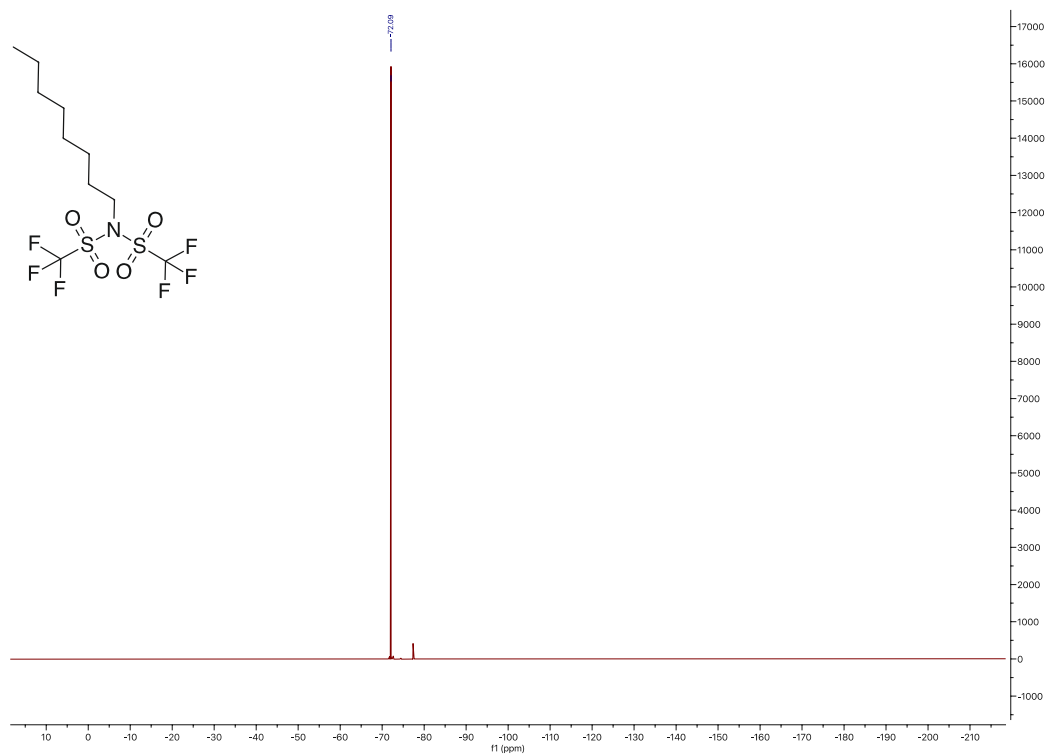


Figure 70. ^{19}F NMR spectrum of **1c**

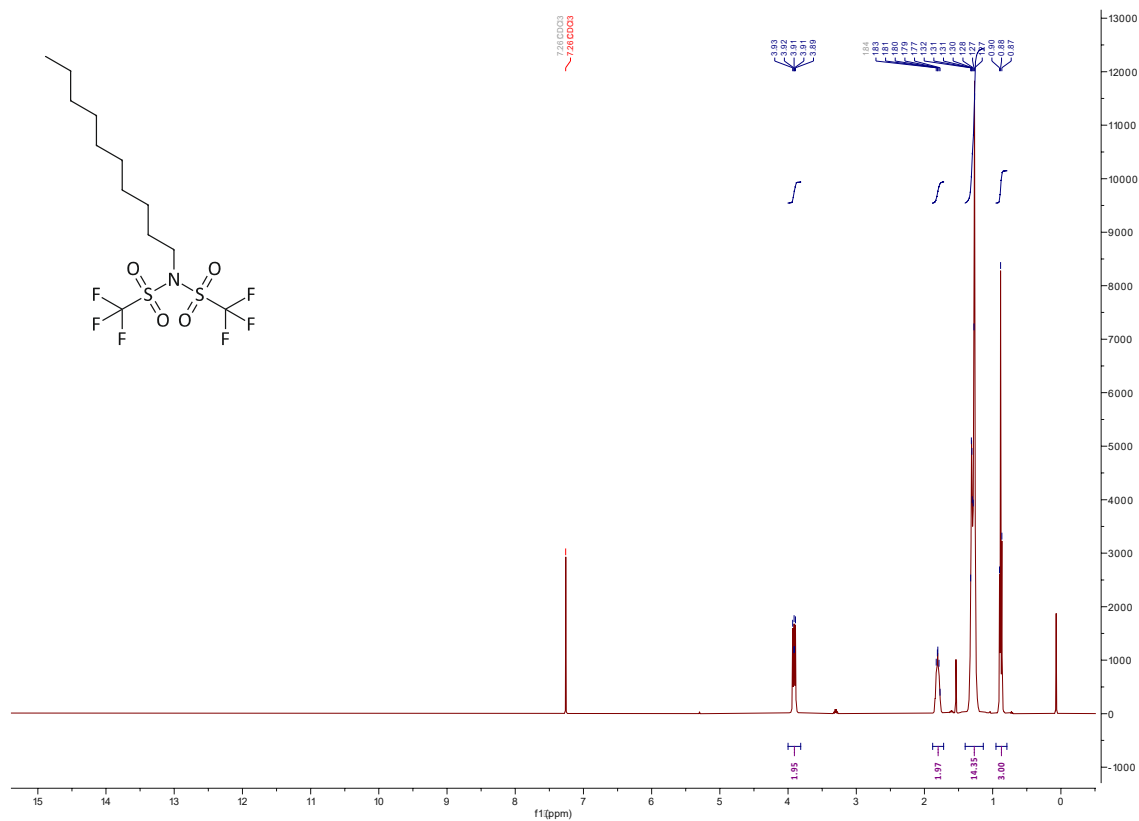


Figure 71. ^1H NMR spectrum of **1d**

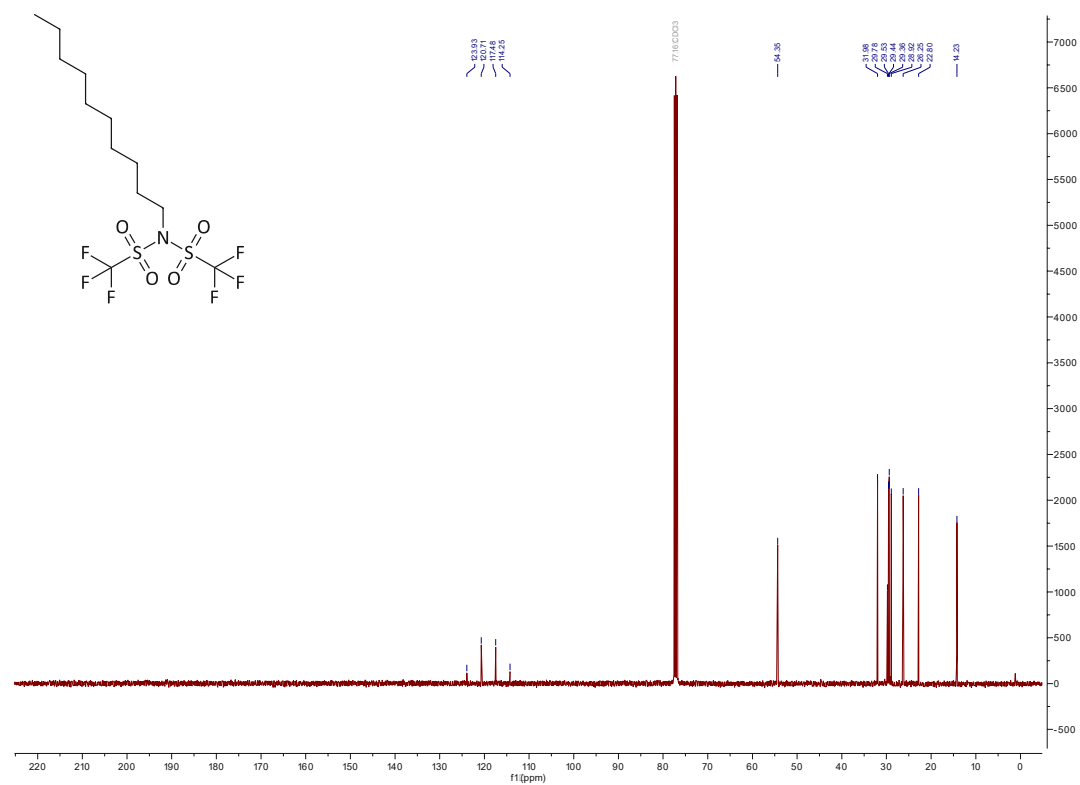


Figure 72. ¹³C NMR spectrum of 1d

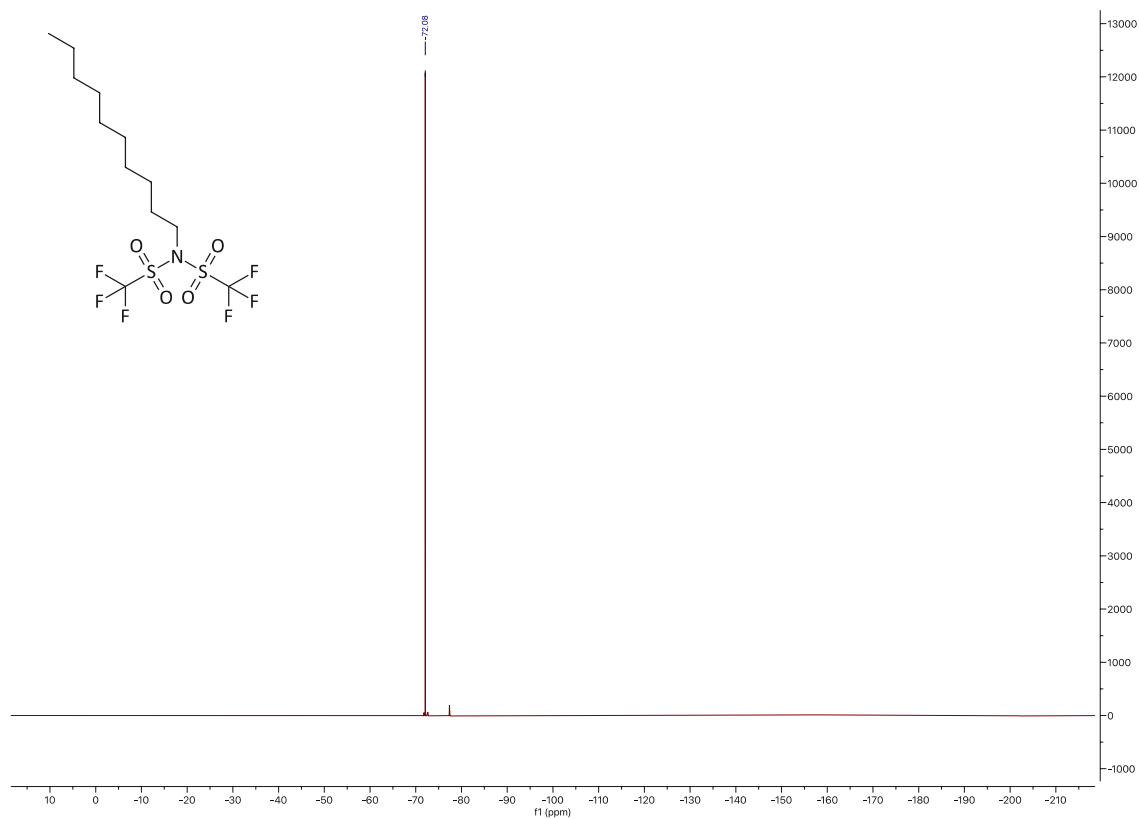


Figure 73. ¹⁹F NMR spectrum of 1d

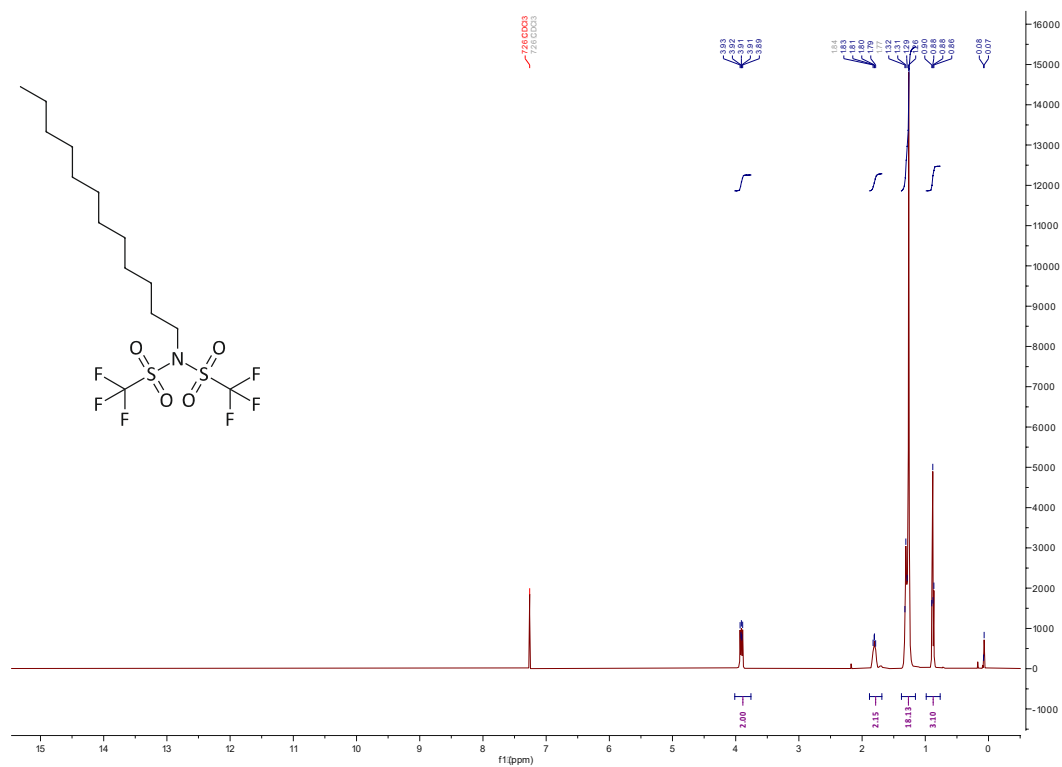


Figure 74. ¹H NMR spectrum of 1e

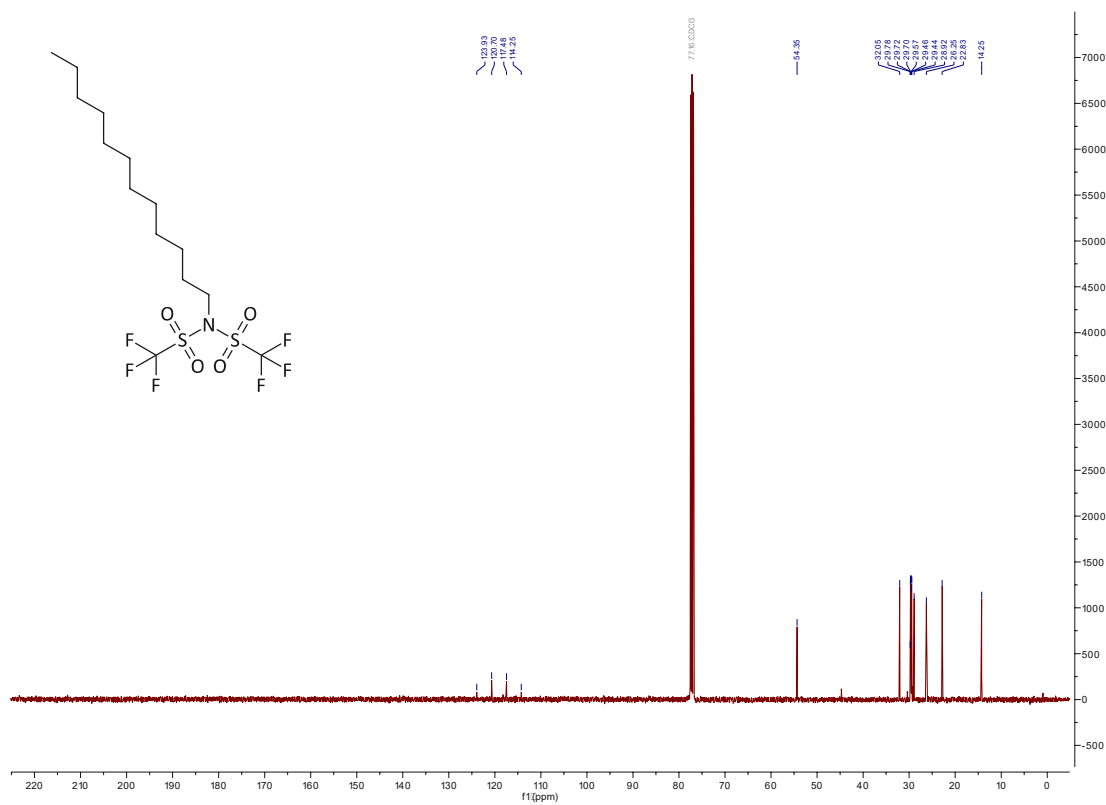


Figure 75. ¹³C NMR spectrum of 1e

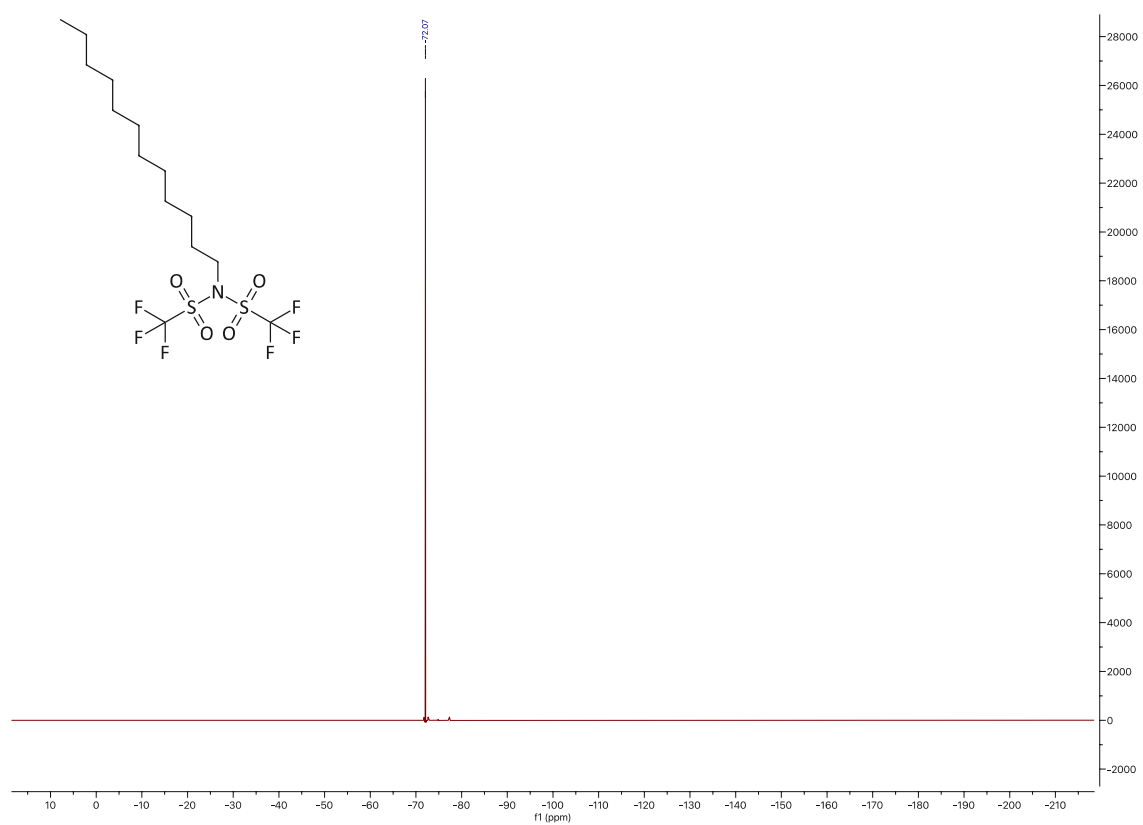


Figure 76. ^{19}F NMR spectrum of **1e**

8.13 NMR spectra of ionic liquids

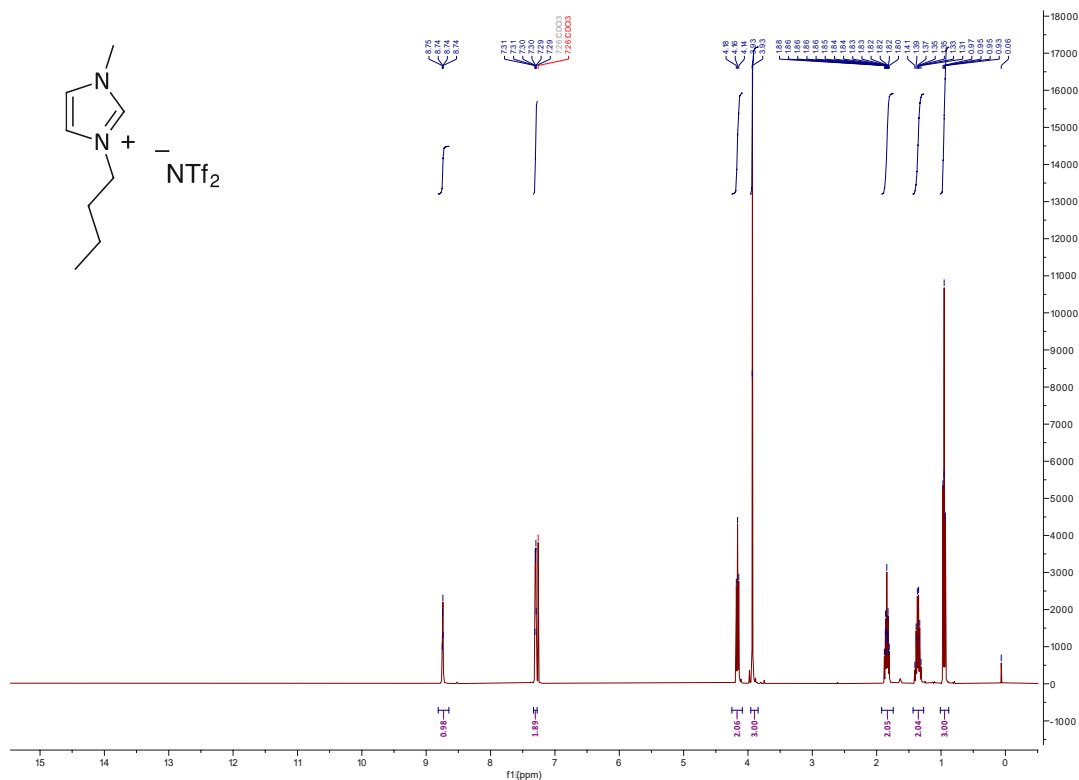


Figure 77. ^1H NMR spectrum of 2a

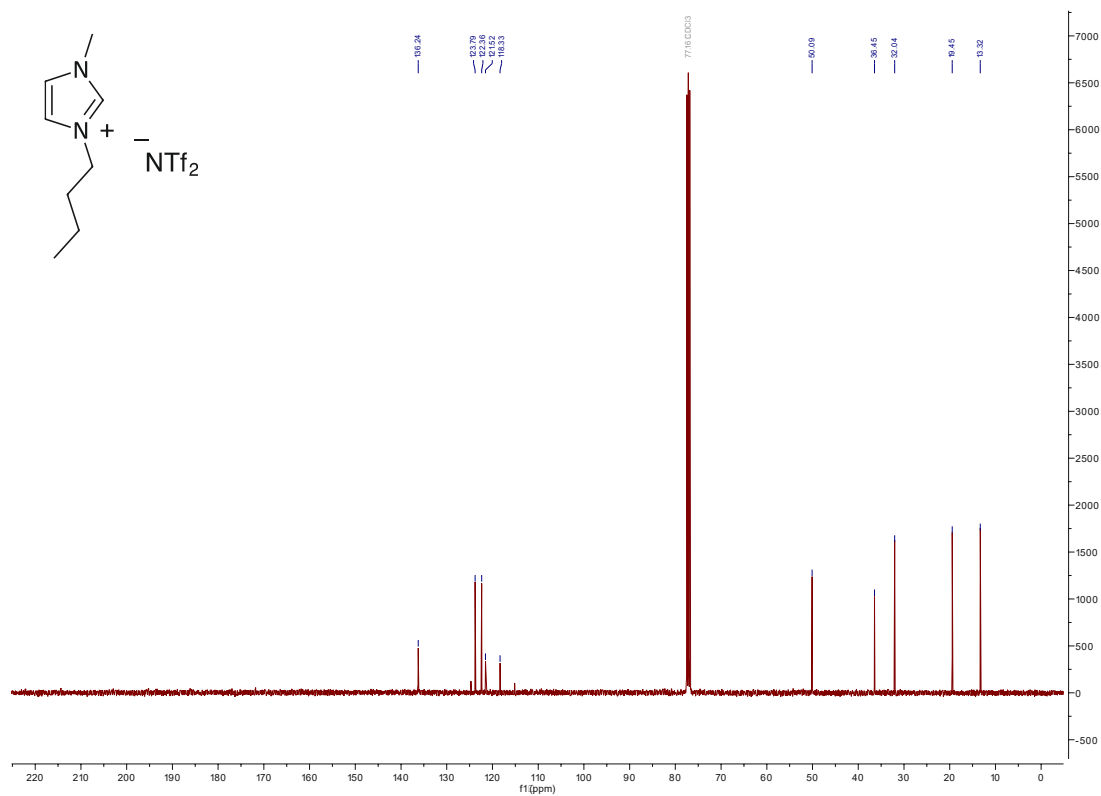


Figure 78. ^{13}C NMR spectrum of 2a

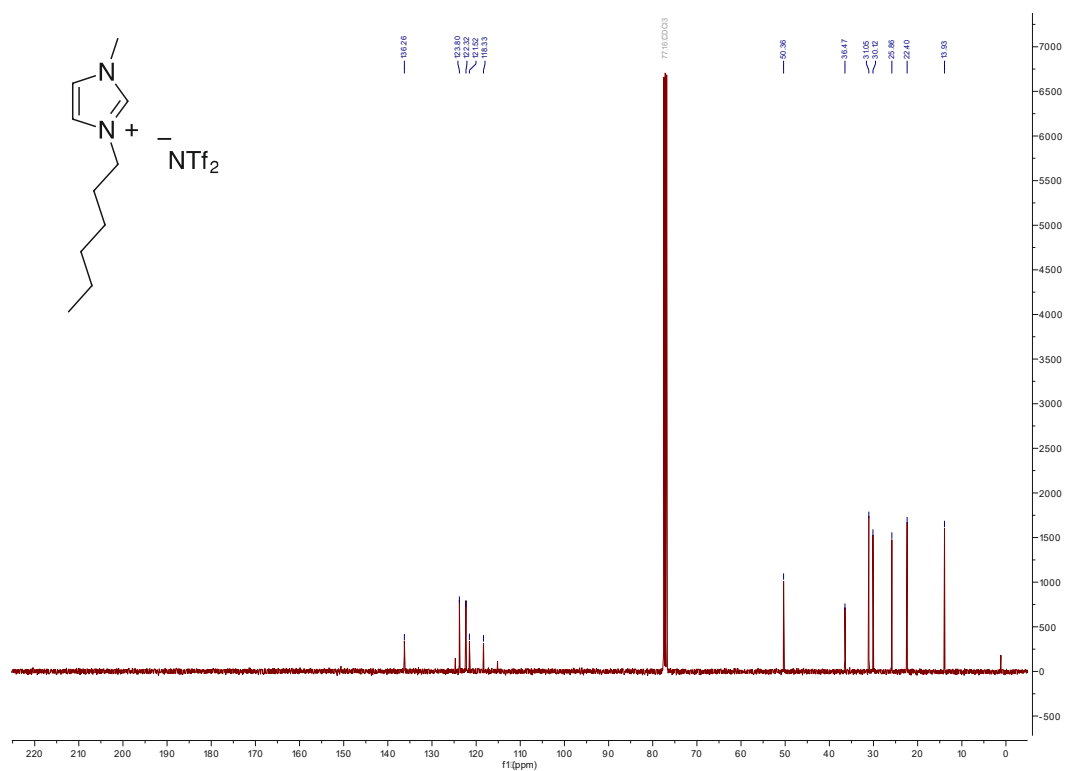


Figure 81. ¹³C NMR spectrum of 2b

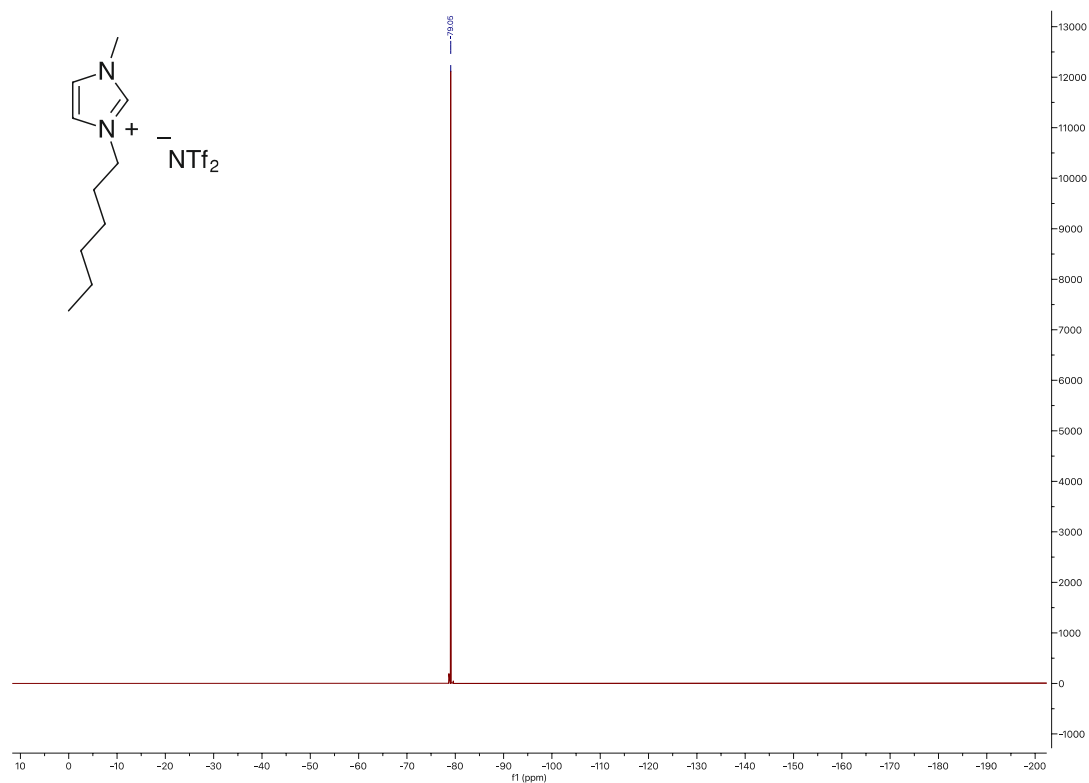
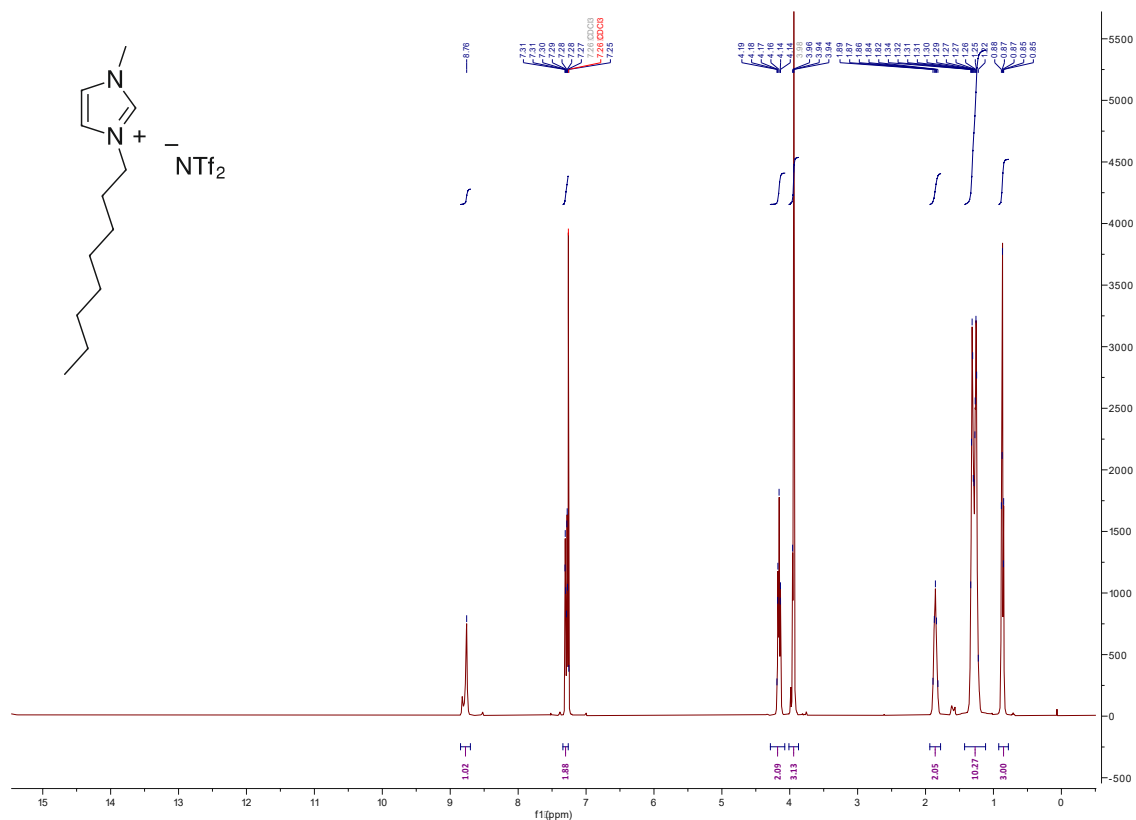


Figure 82. ¹⁹F NMR spectrum of 2b



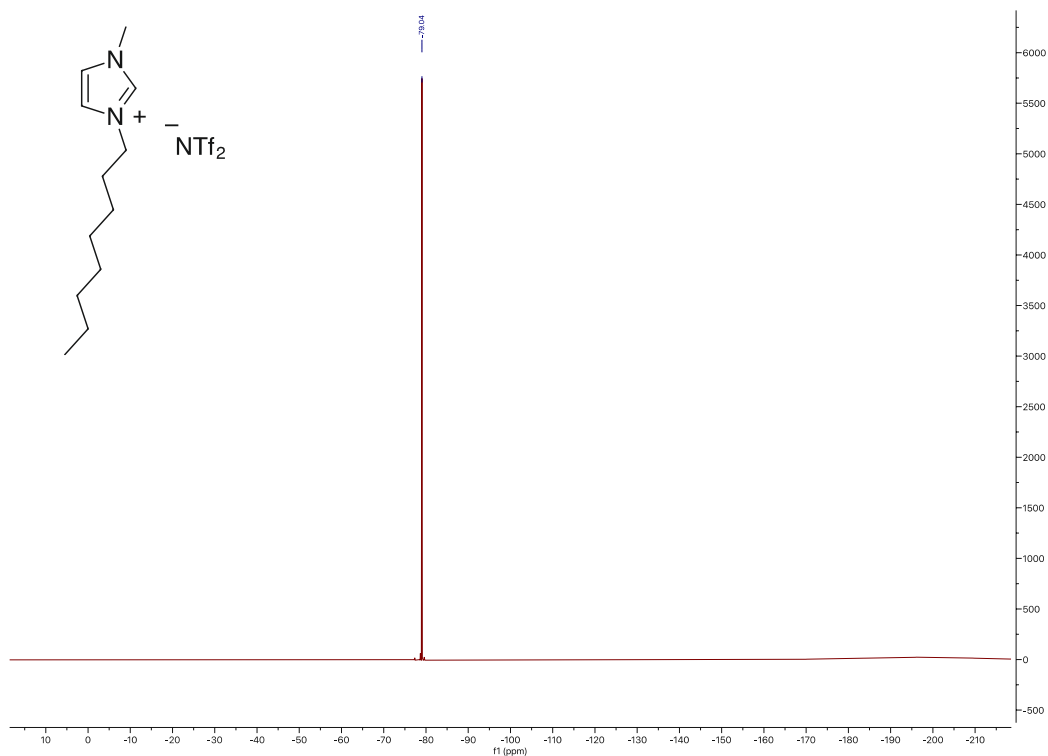


Figure 85. ^{19}F NMR spectrum of 2c

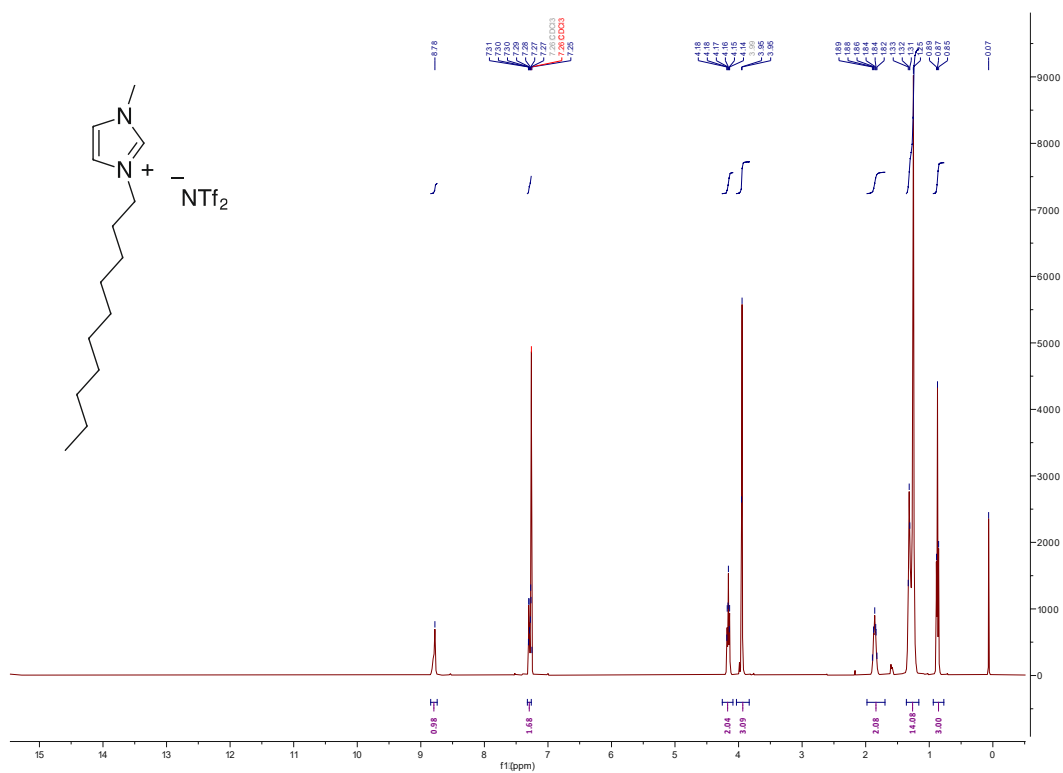


Figure 86. 1H NMR spectrum of 2d

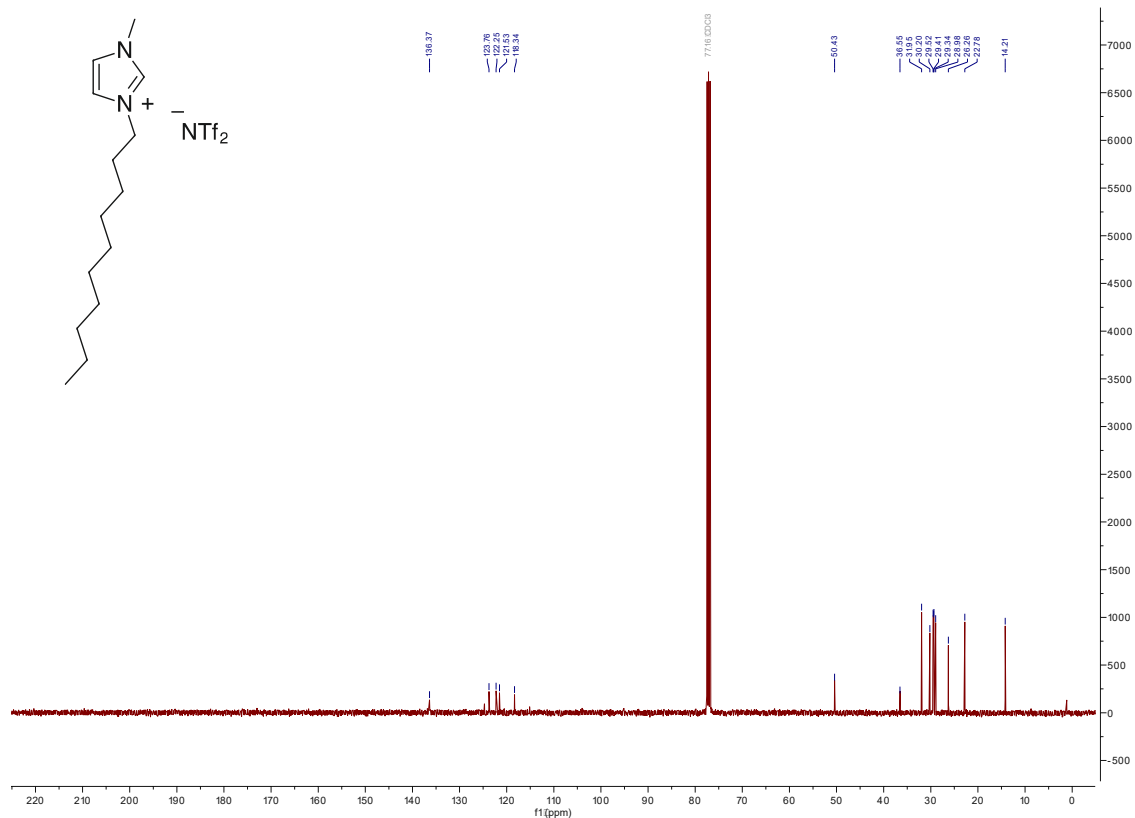


Figure 87. ¹³C NMR spectrum of 2d

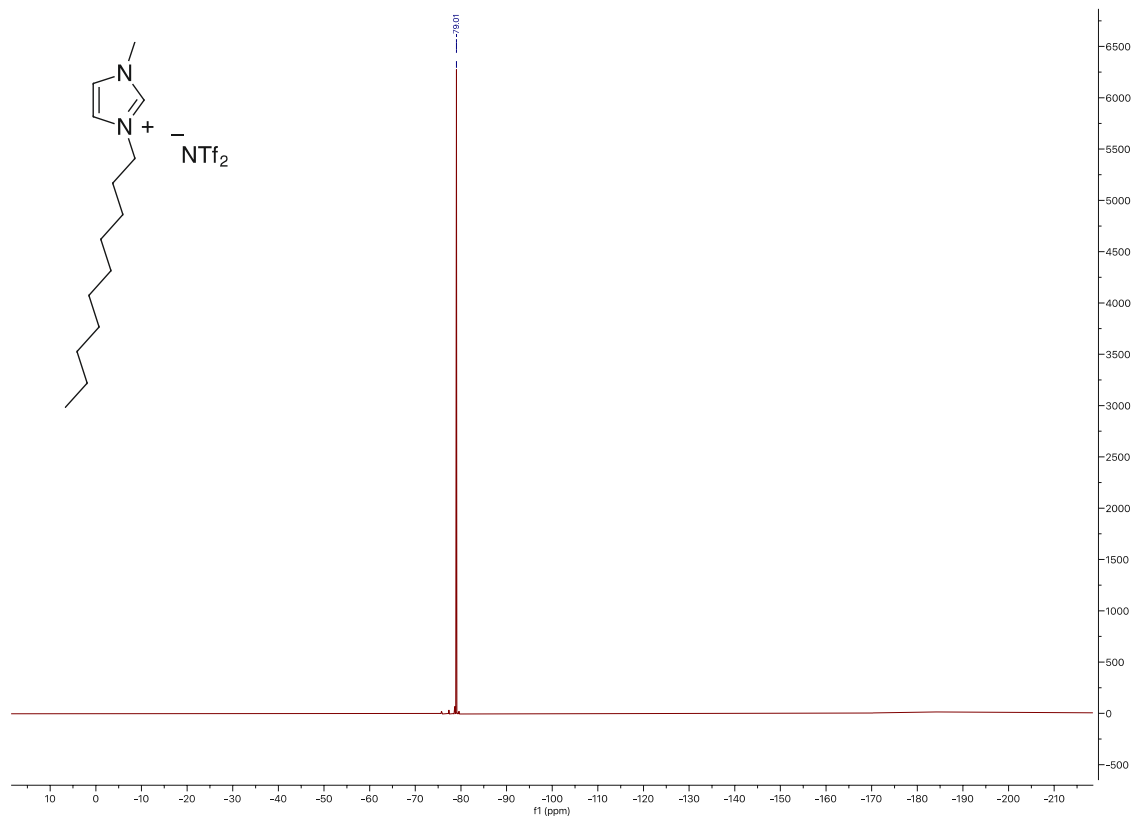


Figure 88. ¹⁹F NMR spectrum of 2d

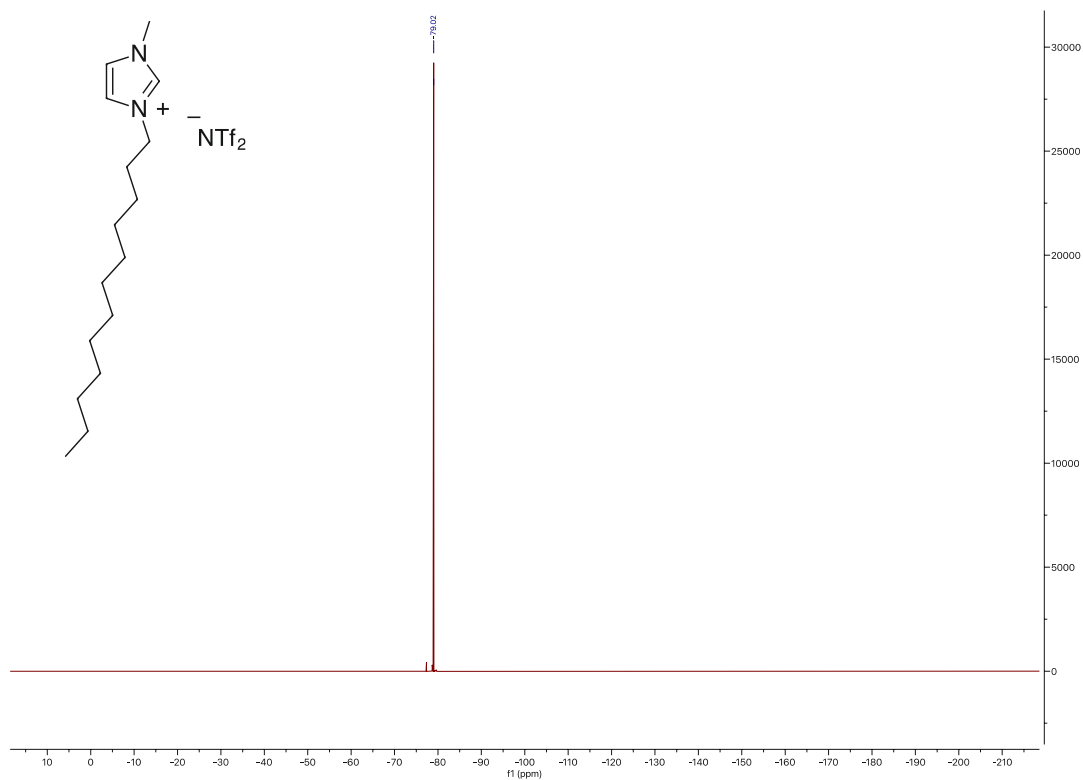
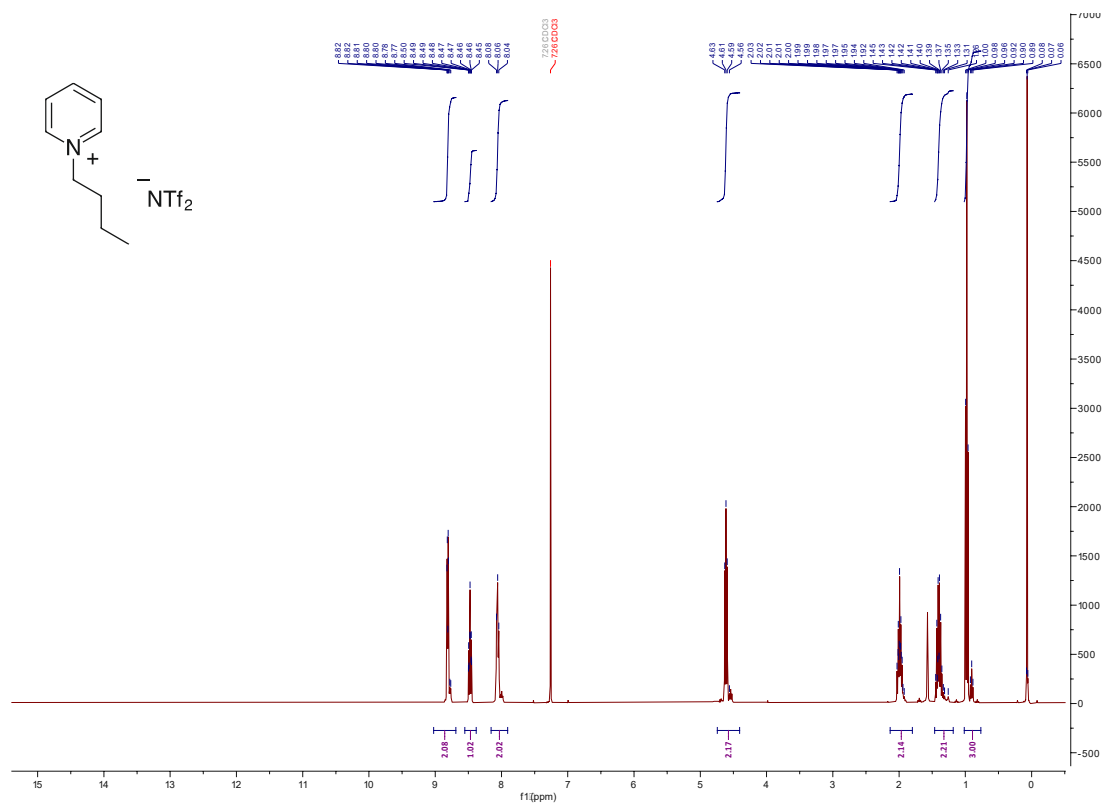
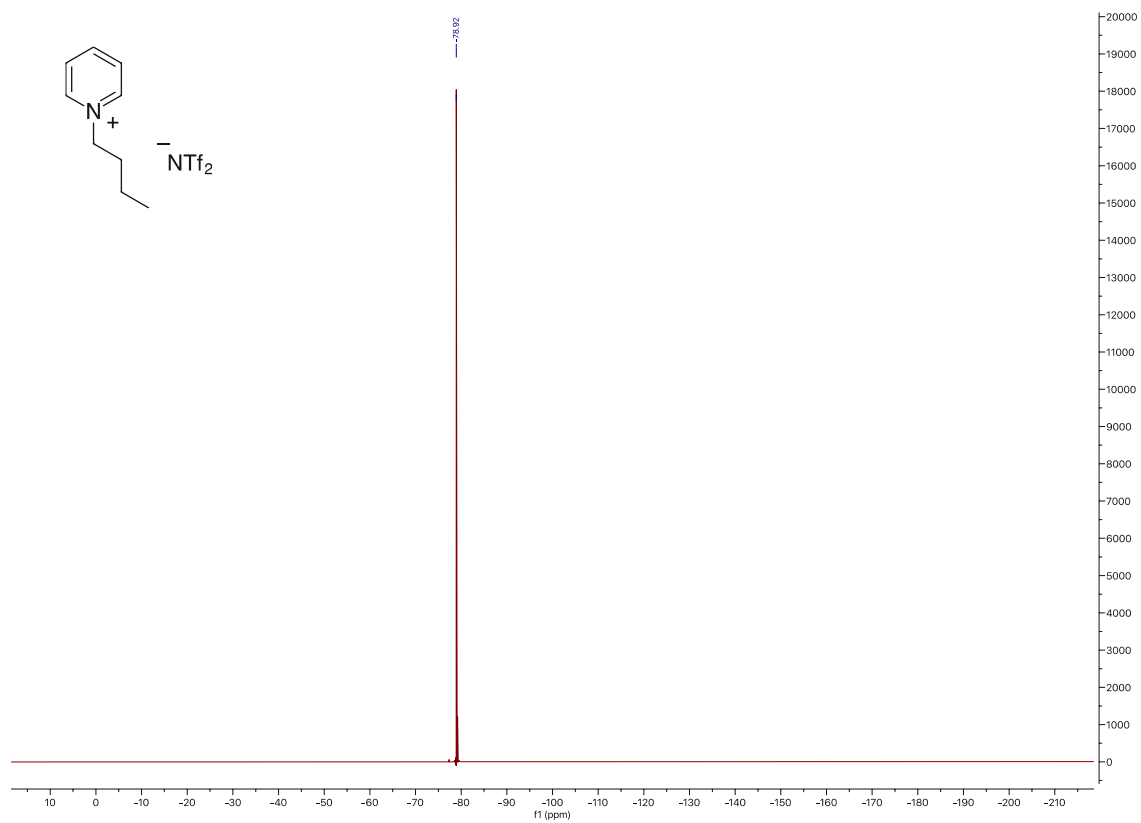
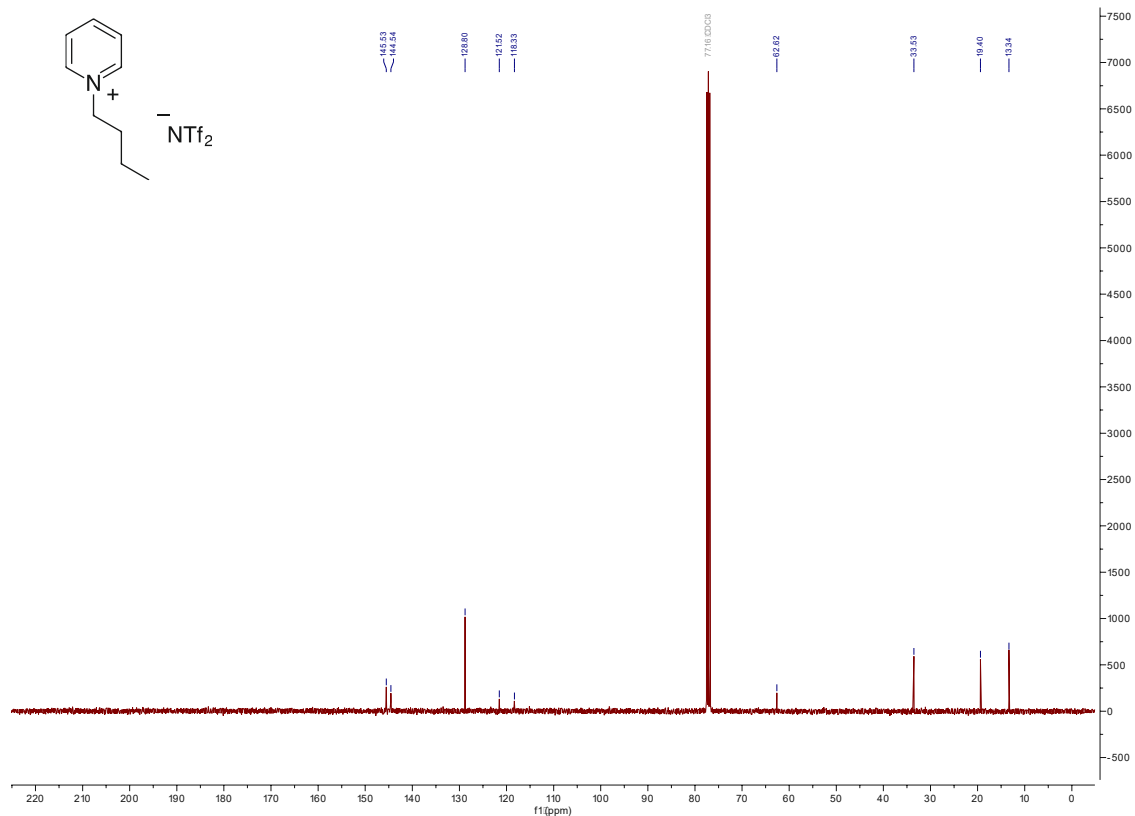


Figure 91. ^{19}F NMR spectrum of 2e





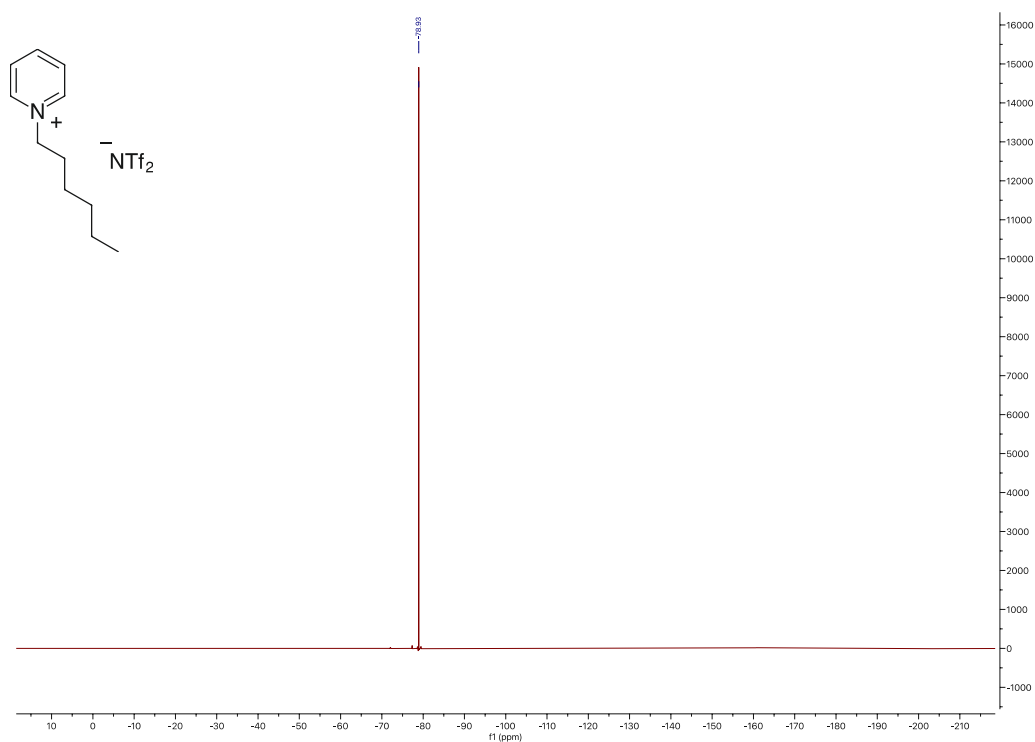


Figure 97. ^{19}F NMR spectrum of 3b

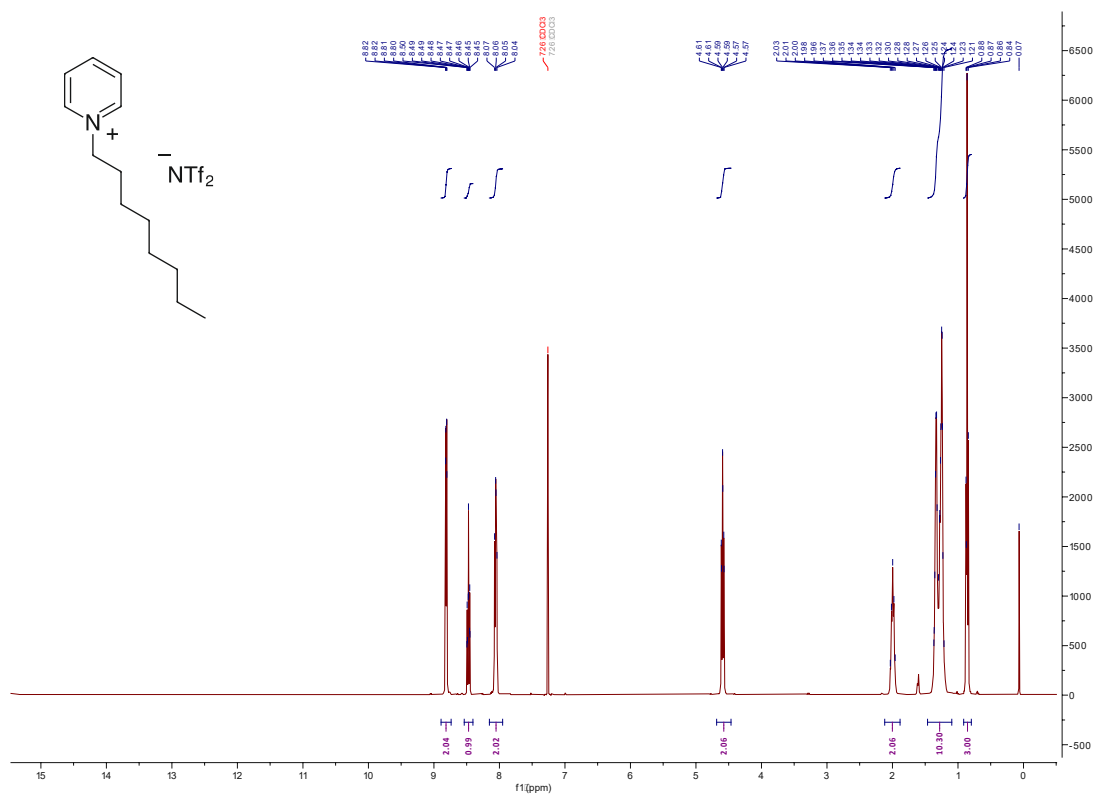


Figure 98. ^1H NMR spectrum of 3c

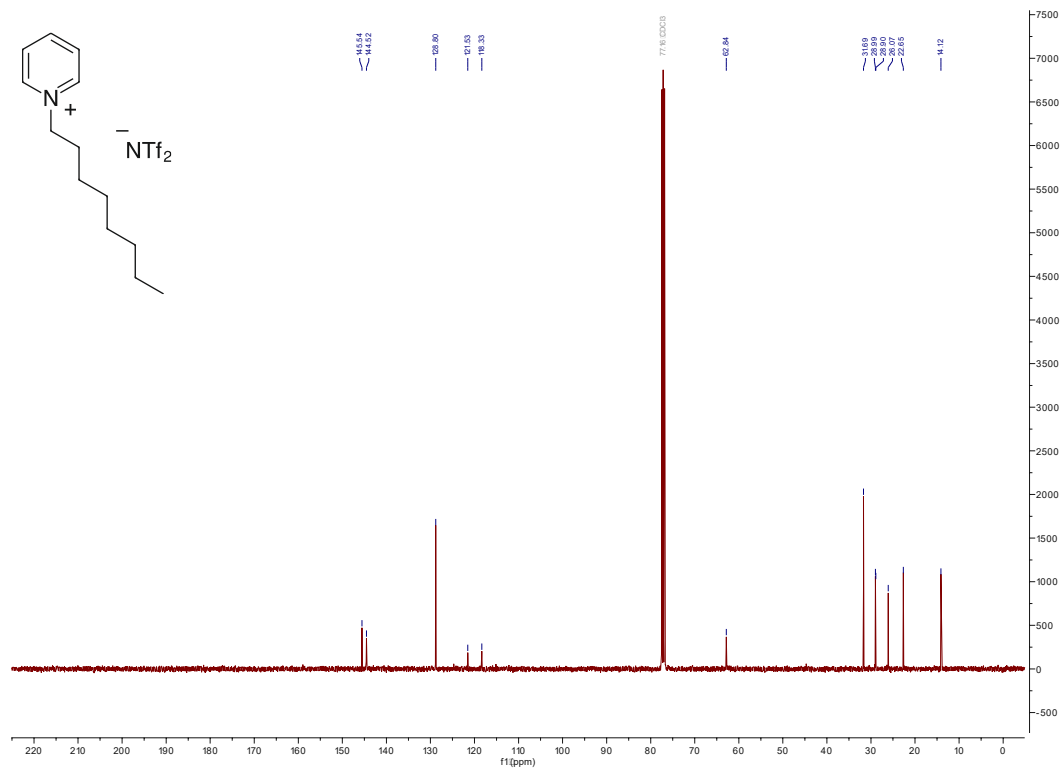


Figure 99. ^{13}C NMR spectrum of **3c**

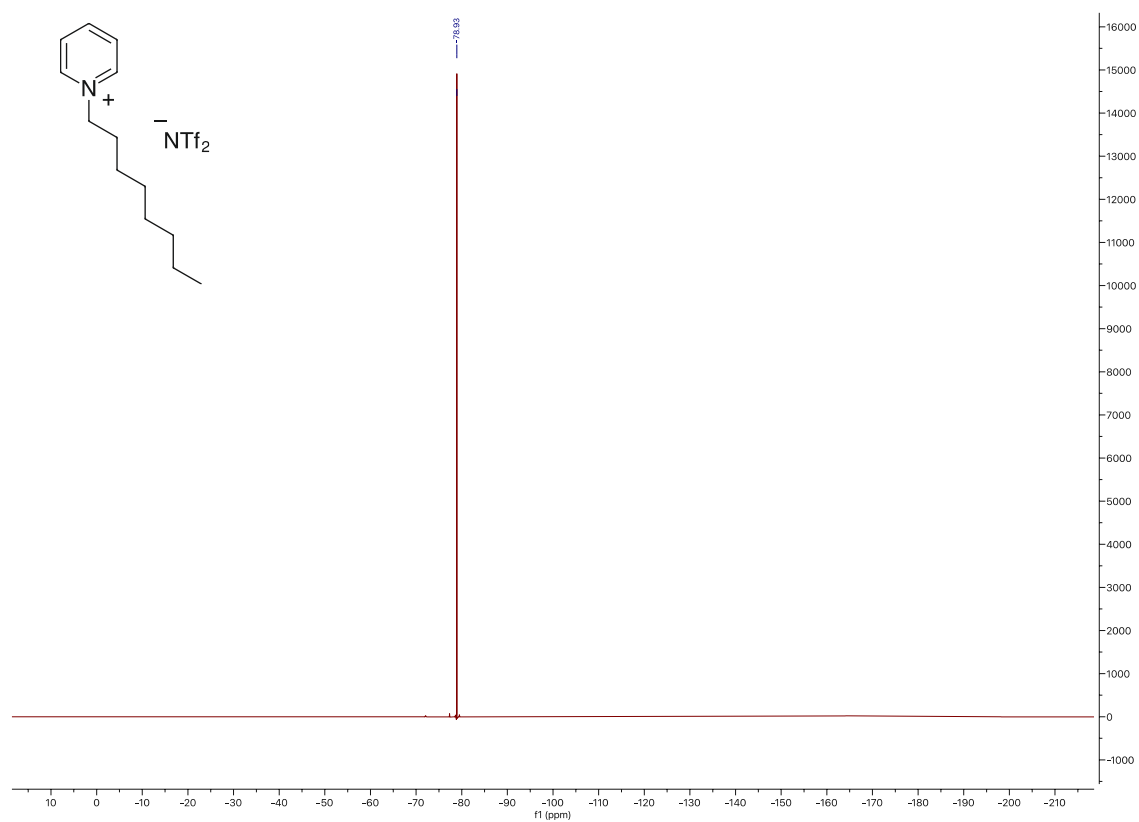


Figure 100. ^{19}F NMR spectrum of **3c**

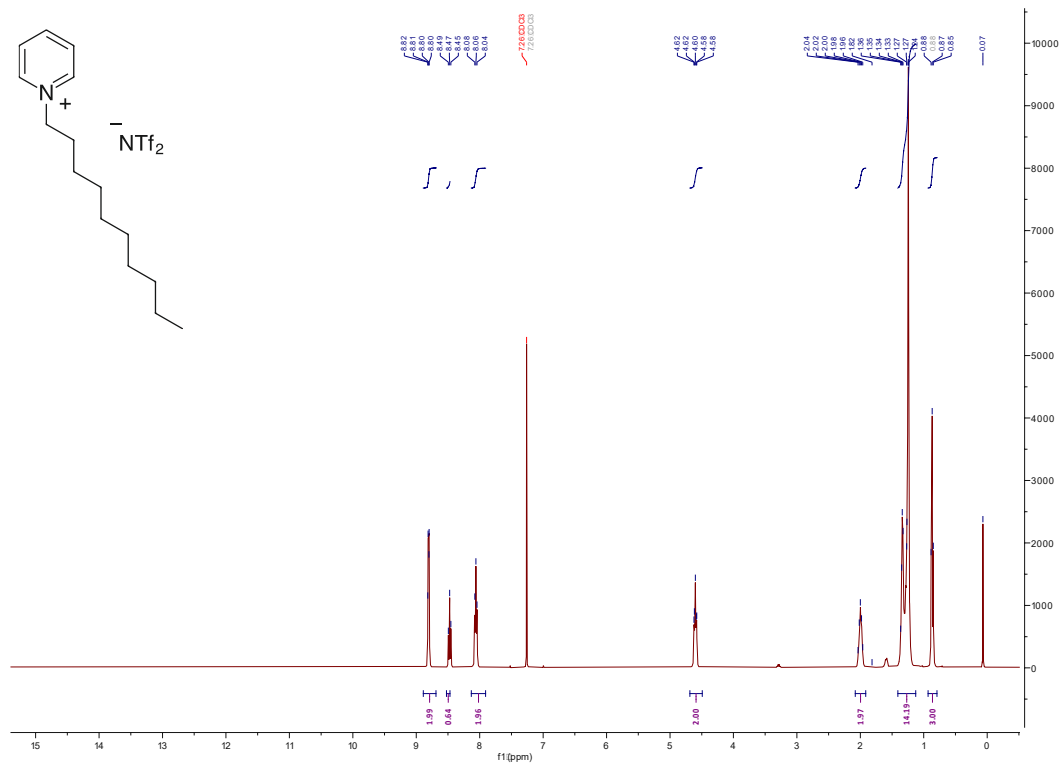


Figure 101. ^1H NMR spectrum of **3d**

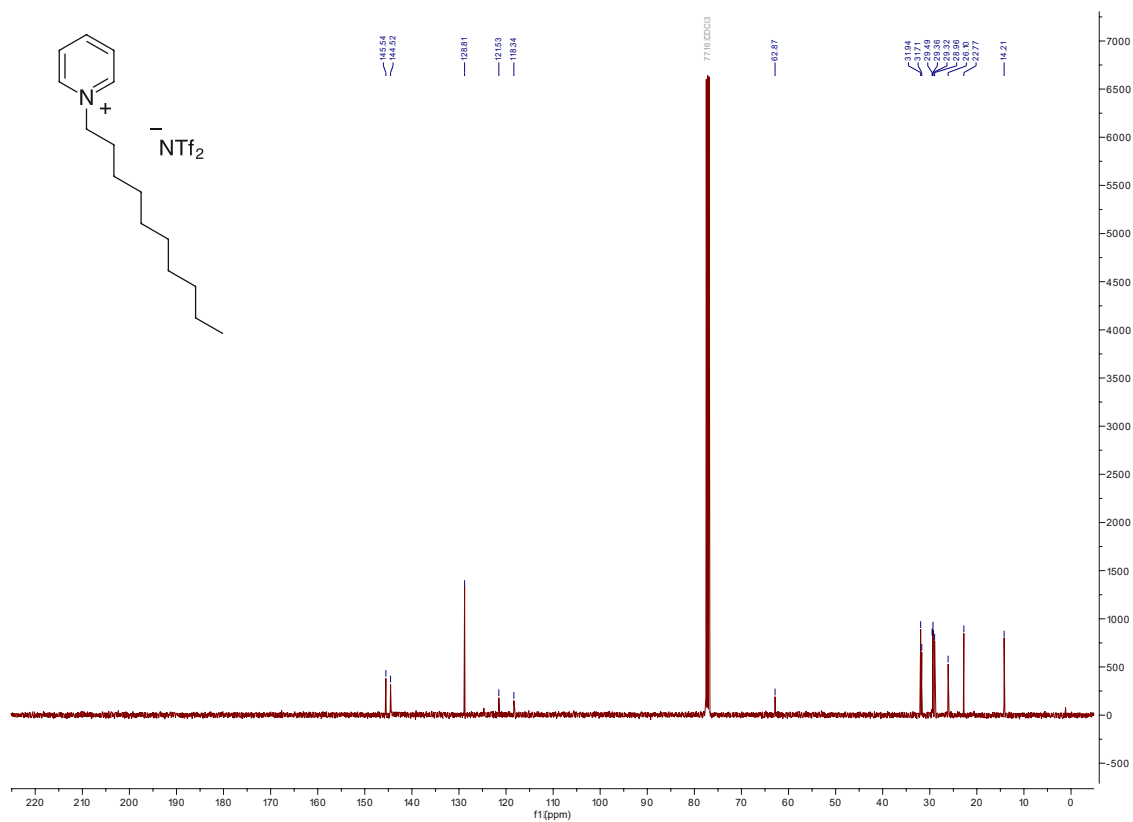


Figure 102. ^{13}C NMR spectrum of **3d**

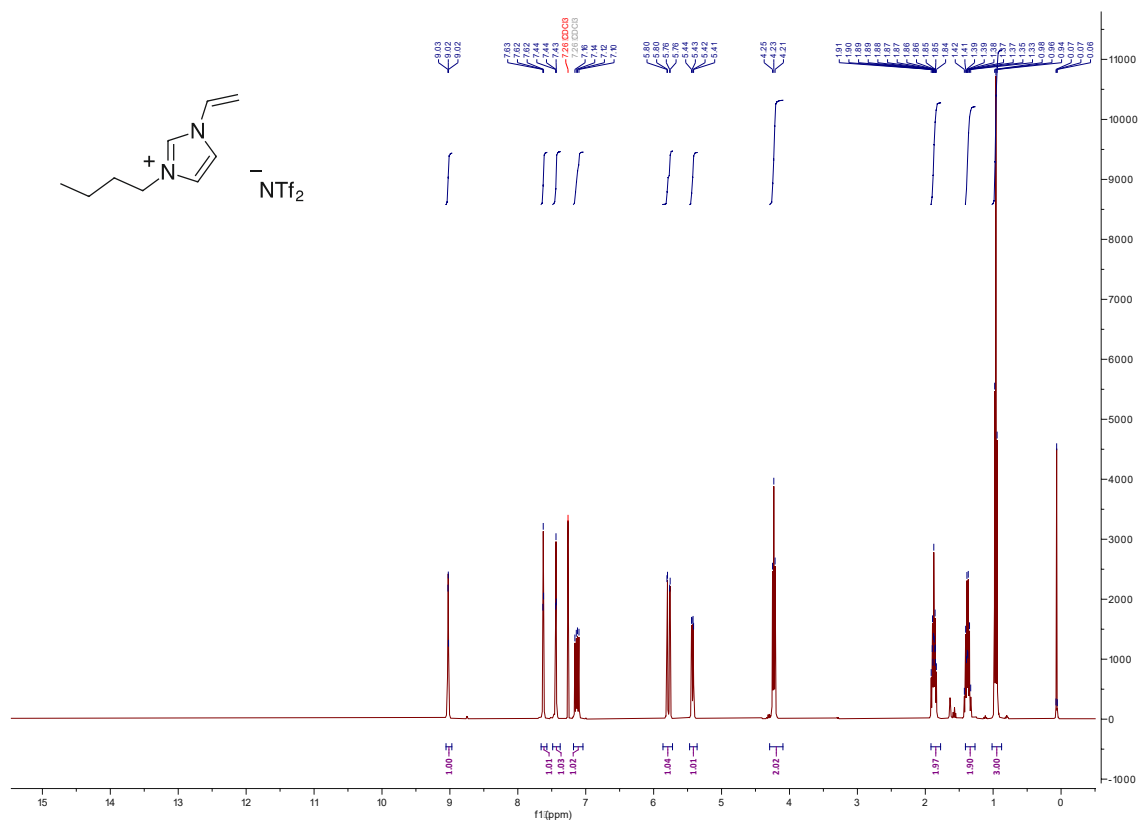


Figure 107. ^1H NMR spectrum of 4a

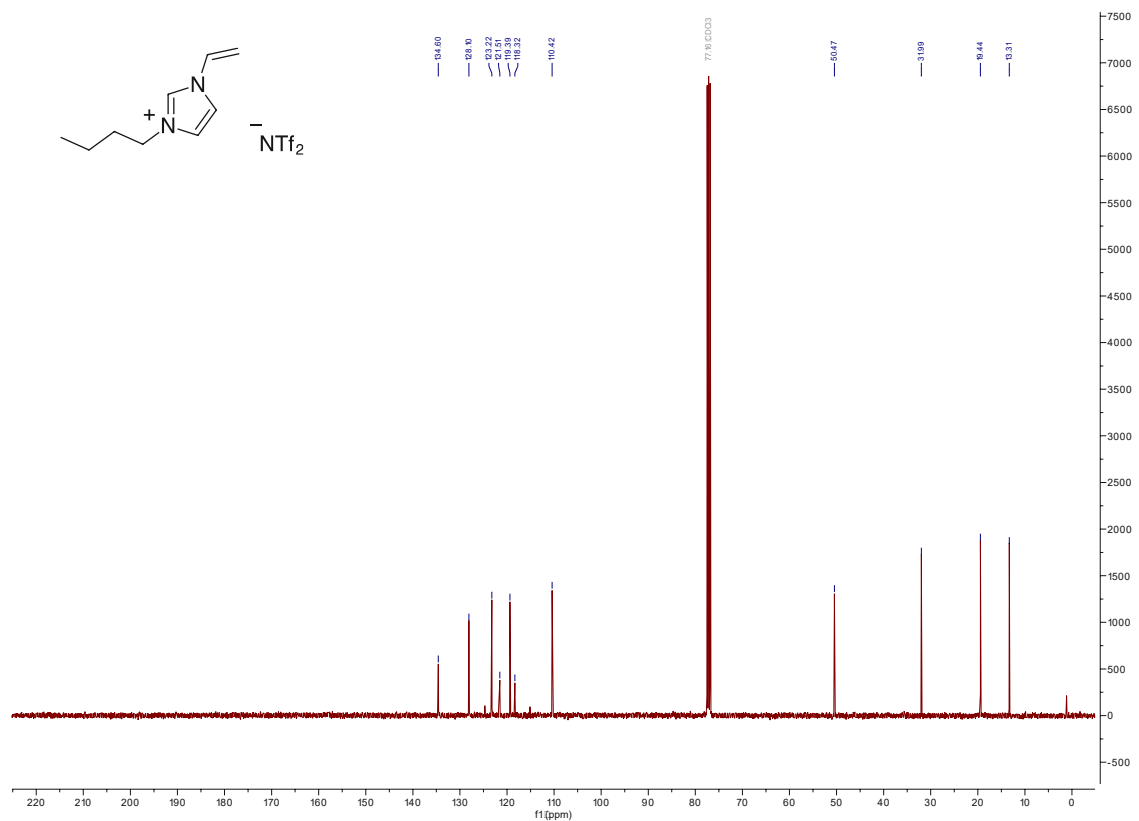


Figure 108. ^{13}C NMR spectrum of 4a

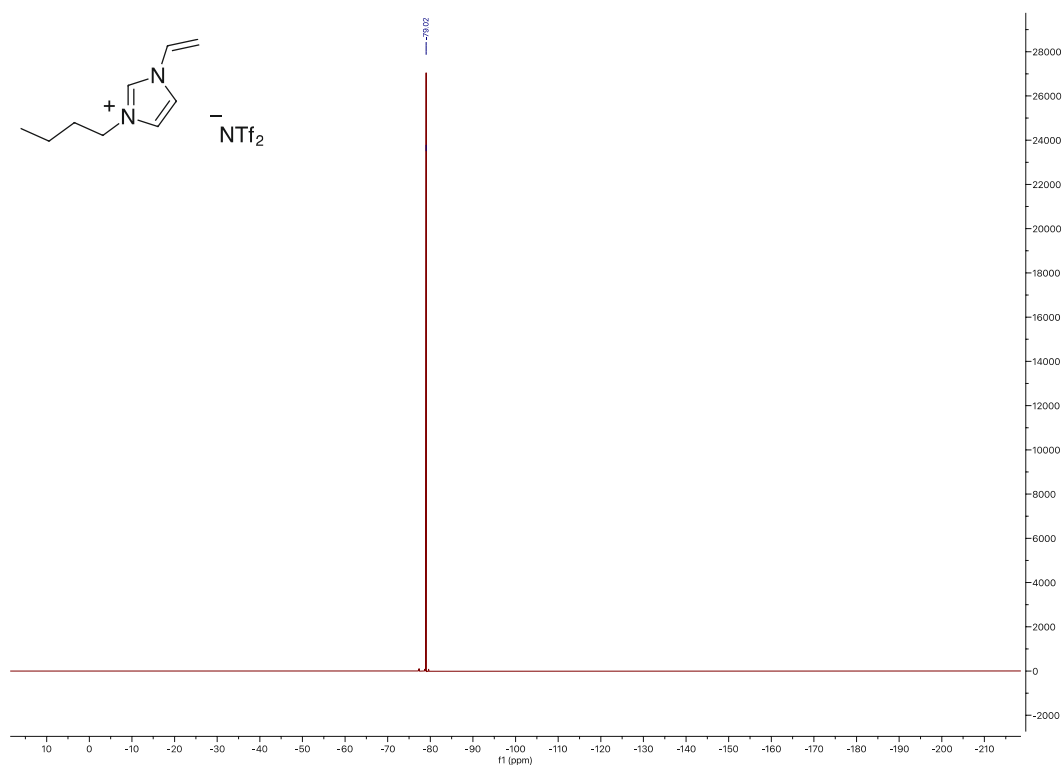


Figure 109. ¹⁹F NMR spectrum of 4a

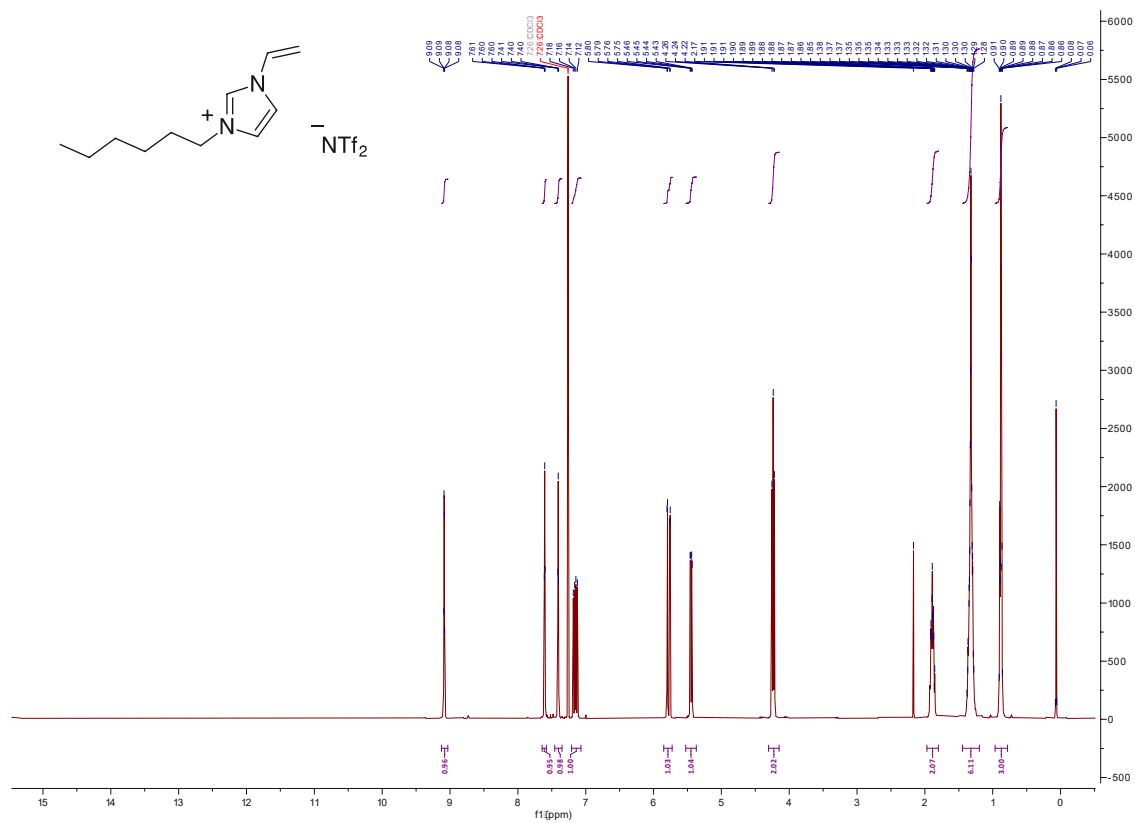


Figure 110. ¹H NMR spectrum of 4b

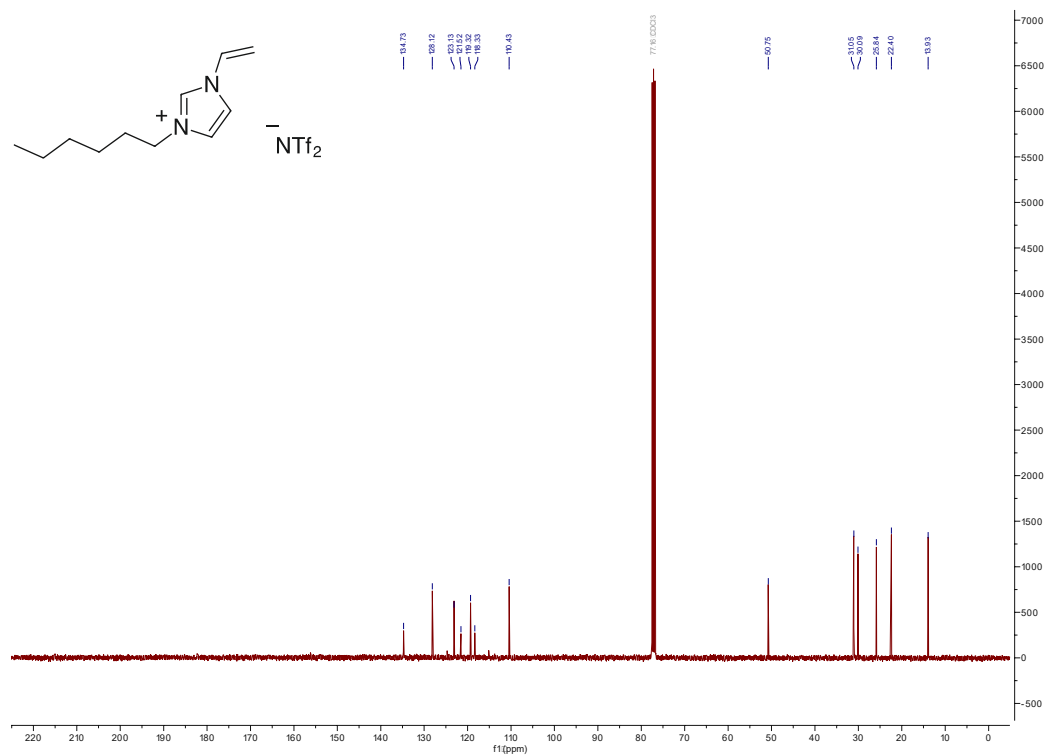


Figure 111. ¹³C NMR spectrum of 4b

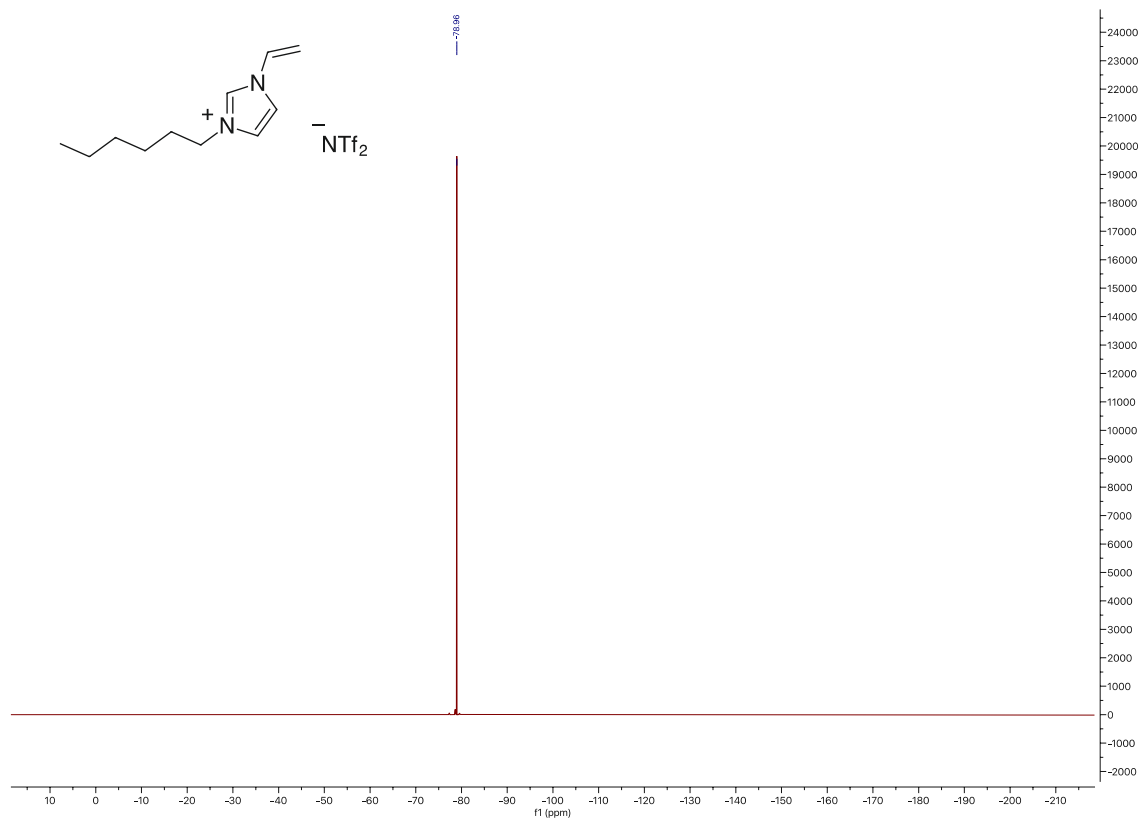


Figure 112. ¹⁹F NMR spectrum of 4b

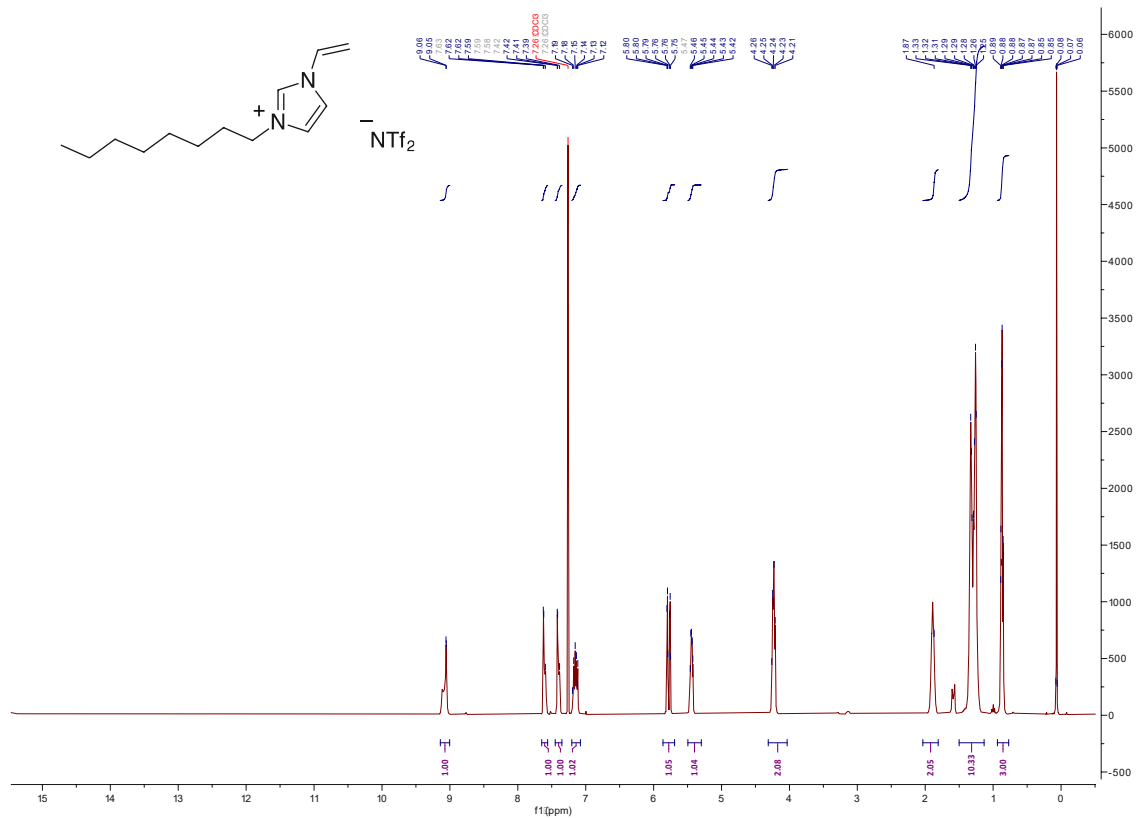


Figure 113. ^1H NMR spectrum of 4c

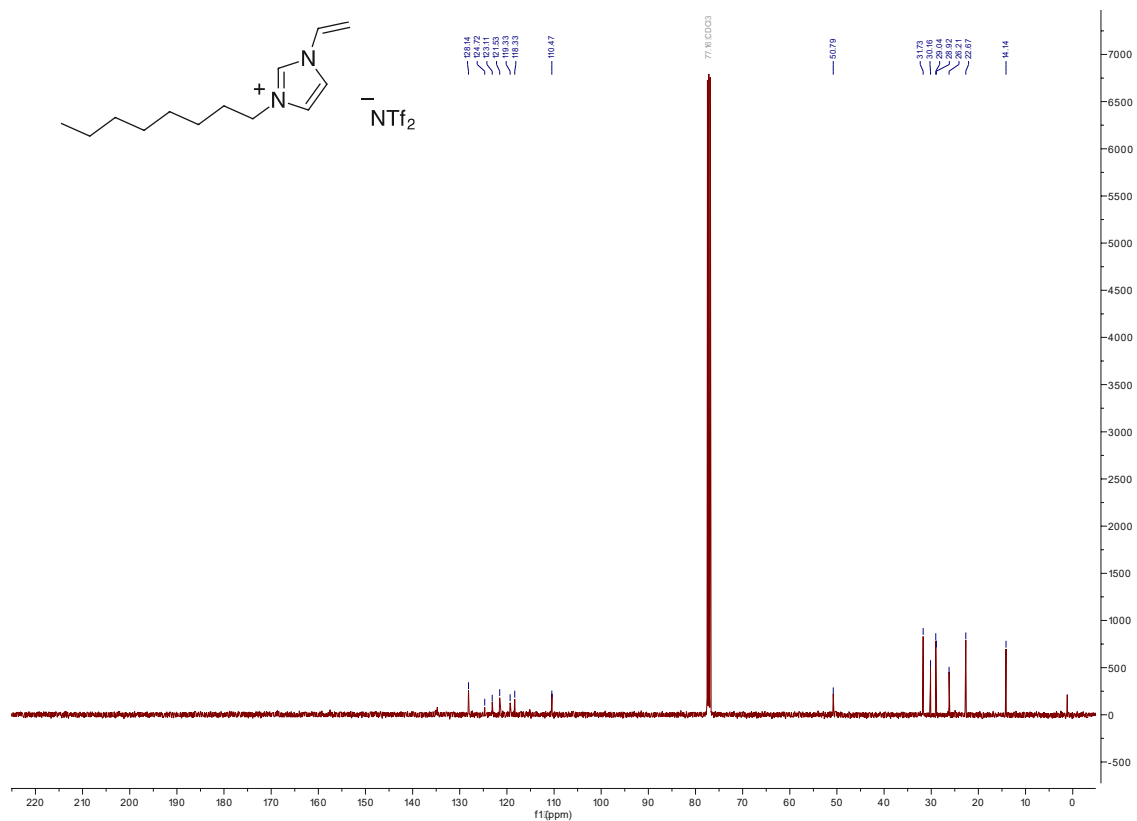


Figure 114. ^{13}C NMR spectrum of 4c

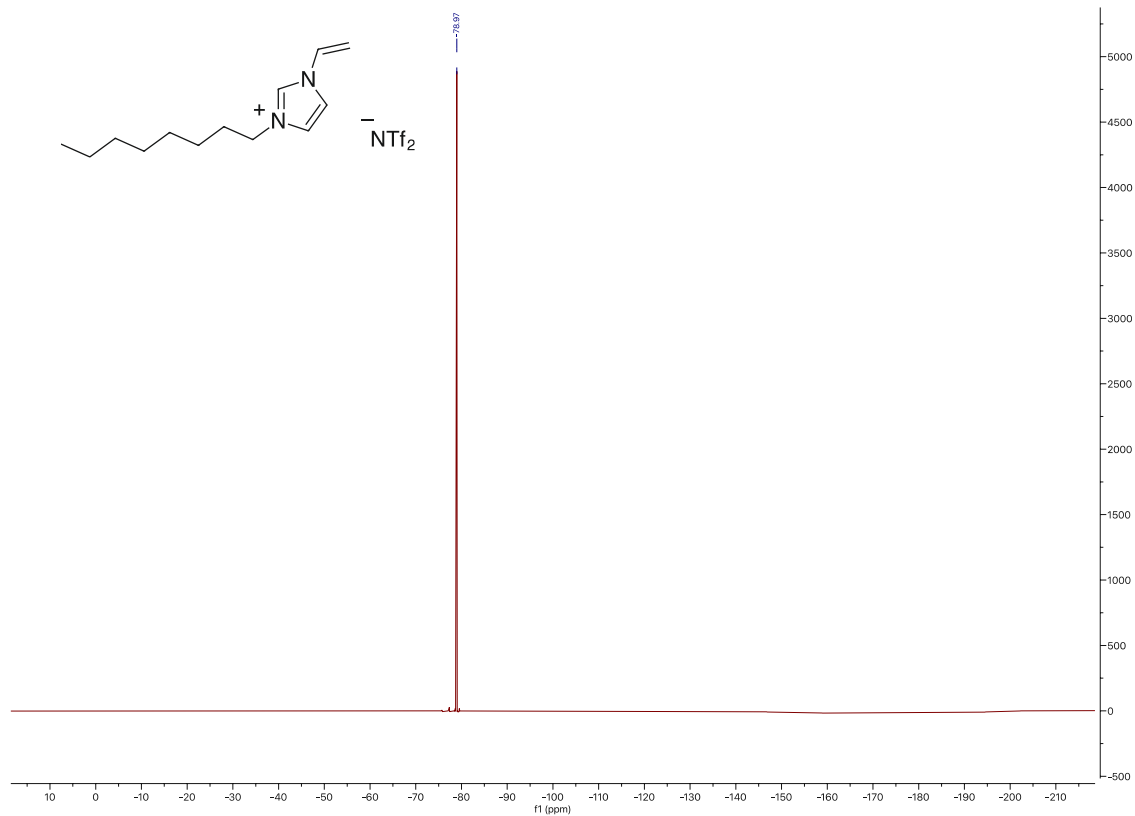


Figure 115. ^{19}F NMR spectrum of 4c

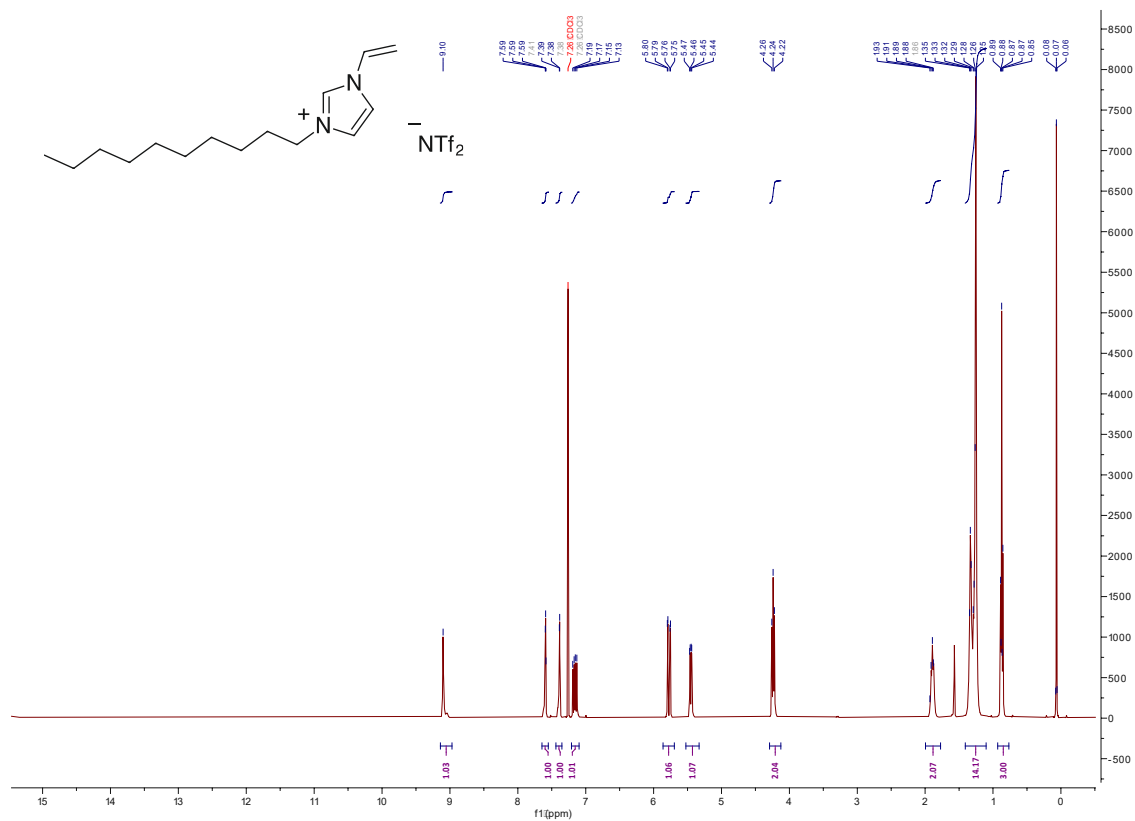


Figure 116. ^1H NMR spectrum of 4d

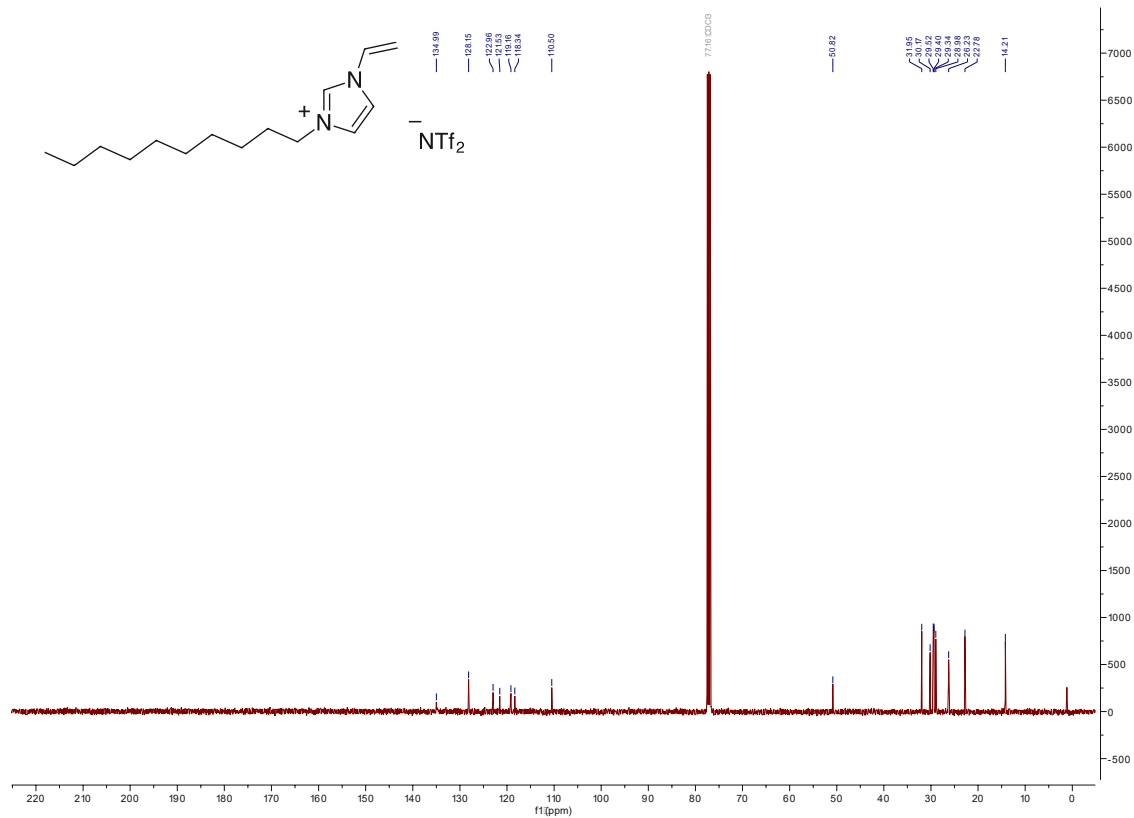


Figure 117. ¹³C NMR spectrum of 4d

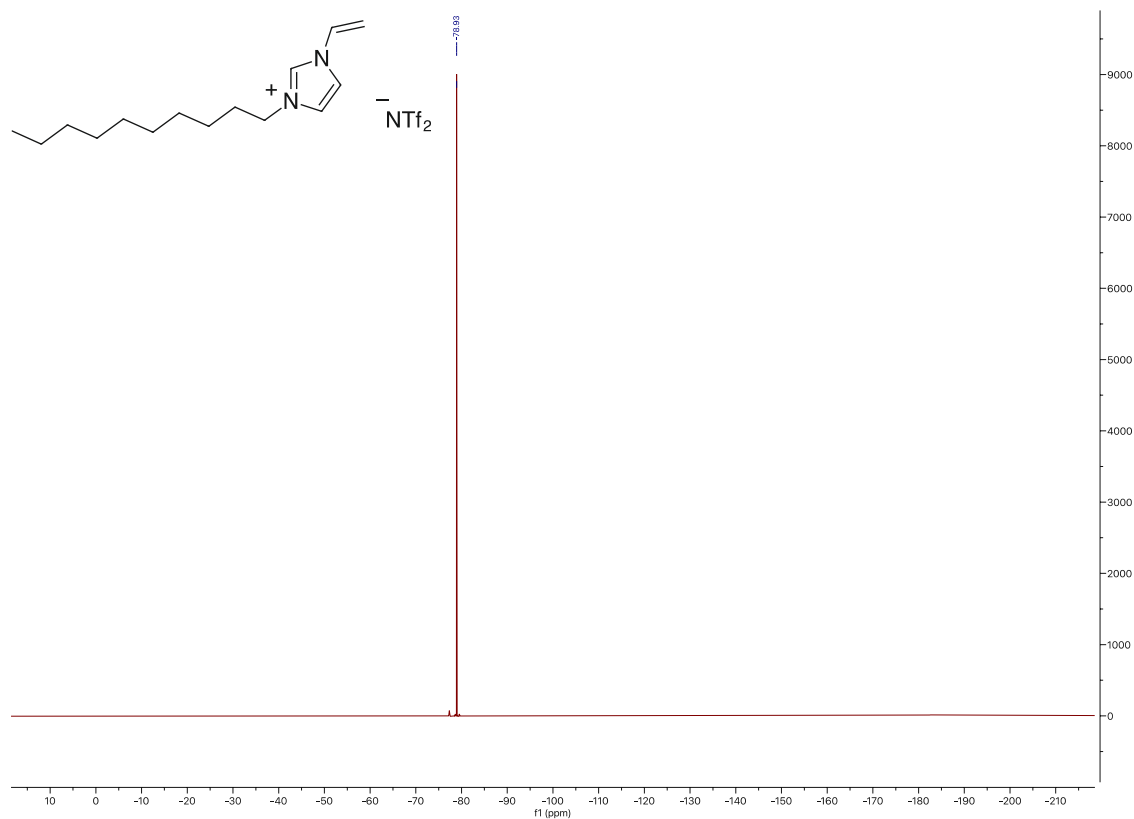


Figure 118. ¹⁹F NMR spectrum of 4d

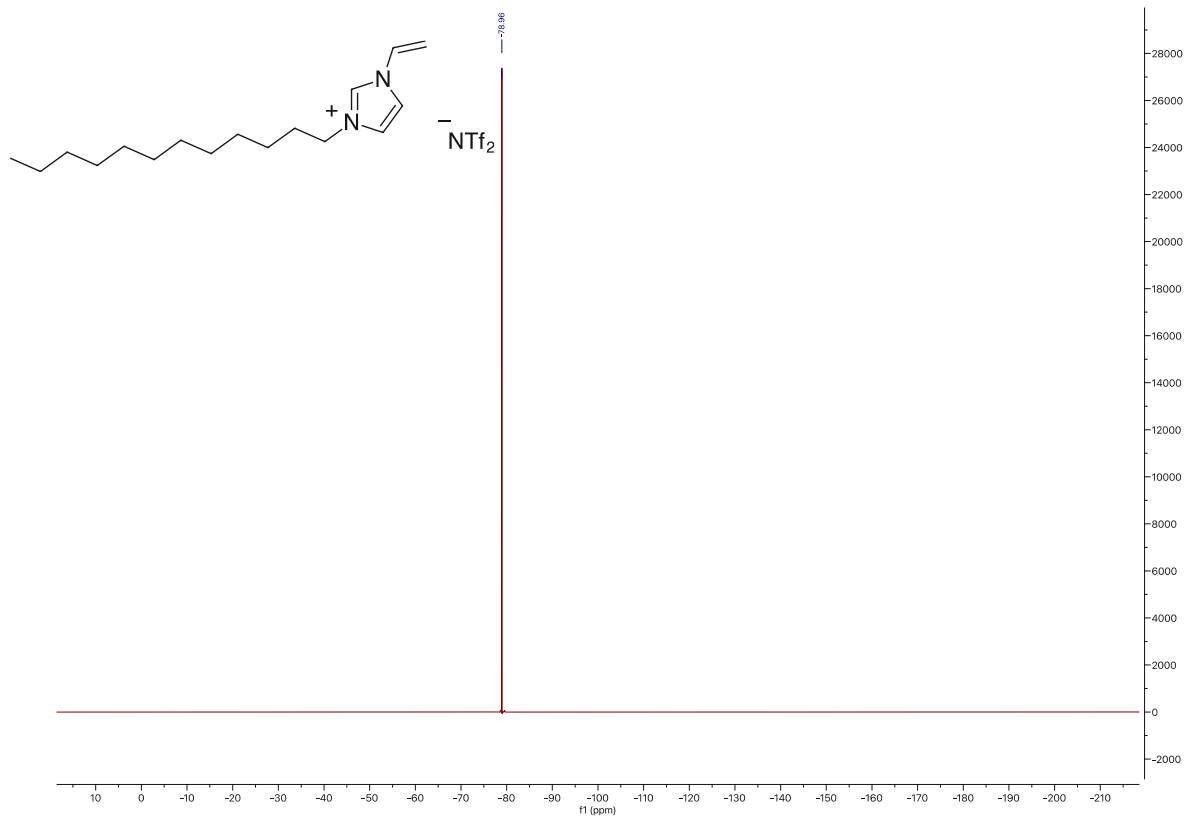


Figure 121. ¹⁹F NMR spectrum of **4e**

9.1 General remarks

All commercially supplied chemicals were used without further purification, unless otherwise noted. Dry CH_2Cl_2 was pre-distilled and desiccated on aluminum oxide columns (PURESOLV, Innovative Technology).

Column chromatography was performed on standard glass columns using Merck (40-60 μm) silica with pre-distilled solvents. For TLC analysis, pre-coated aluminium-backed plates were used (Merck, silica 60 F₂₅₄). All compounds were detected at 254 nm.

^1H -, ^{13}C -, ^{19}F - and ^{31}P NMR spectra were recorded from CDCl_3 solutions on a Bruker Avance UltraShield 200 MHz (^1H : 200 MHz, ^{13}C : 50 MHz) or 400 MHz (^1H : 400 MHz, ^{13}C : 101 MHz, ^{19}F : 376 MHz) NMR instrument. Chemical shifts are reported in parts per million (ppm) and were calibrated to the residual solvent signal (e.g., CDCl_3 , ^1H : 7.26 ppm, ^{13}C : 77.0 ppm). Coupling constants are reported in hertz (Hz). The assignments are based on comparison with reported spectra.

Chiral HPLC measurements were carried out on a DIONEX UPLC equipped with a photoiodode array (PDA) plus detector (190-360 nm), using either a Daicel Chiralpak® IA-3 column (250 × 4.6 mm, 3 μm) or a Chiralcel® OD column (250 × 4.6 mm, 10 μm).

Optical rotation was measured on an Anton Paar MCP500 polarimeter at the specific conditions and the results were compared to literature values. Concentrations are given in g/100 mL.

HRMS analysis was performed using a TC PAL system auto sampler, an Agilent 1100/1200 HPLC and an Agilent 6230 AJS ESI-TOF mass spectrometer. The spectra were recorded from methanolic solutions ($c = 3 - 50 \times 10^{-5} \text{ mol dm}^{-3}$). The compounds were detected both in negative- and positive-ion mode.

Melting points were measured on an automated melting point system OPTI MELT of Stanford Research System and are uncorrected.

Continuous-flow experiments were performed with the aid of an Omnifit cartridge (bed length 10 cm). The reaction mixture was supplied with the aid of a New Era NE-1000 syringe pump.

9.2 Substrate synthesis for the non-enantioselective allylic alkylations (1a-d)

Cinnamyl acetate (**1a**) was purchased from commercial provider. Compounds **1c**^[157] and **1d**^[158] were synthesised according to literature procedures, respectively.

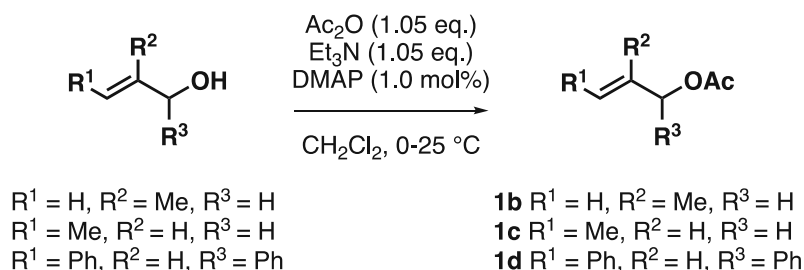
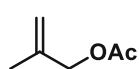


Figure 122. Synthesis of compounds **1a-d**

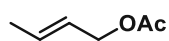
To a solution of the corresponding allylic alcohol (29.50 mmol, 1.00 eq.) in dry CH_2Cl_2 (3.0 mL), acetic anhydride (2.52 mL, 30.94 mmol, 1.05 eq.) and *N,N*-dimethylaminopyridine (36.2 mg, 0.295 mmol, 1.0 mol%) were added at 0 °C. Subsequently, a solution of Et_3N (4.30 mL, 30.94 mmol, 1.05 eq.) in 4.0 mL dry CH_2Cl_2 was added dropwise at the same temperature and it was then allowed to warm up to room temperature. After 3 hours, the reaction mixture was poured onto 2M HCl/icewater and it was extracted with Et_2O (3 × 25 mL). The combined organic phases were washed with NaHCO_3 (1 × 20 mL) and brine (1 × 20 mL), dried over Na_2SO_4 , filtered and concentrated *in vacuo*.

2-Methallyl acetate (**1b**)^[157]



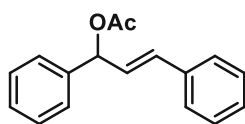
Prepared according to the general procedure using β -methallyl alcohol (2.50 mL, 29.50 mmol, 1.0 eq.). It was only concentrated to a pressure of 200 mbar on the rotavapor, as the product is volatile. *Kugelrohr* distillation (b.p. = 72 °C at 220 mBar) afforded **1b** as a colourless oil (2.43 g, 80% yield). $^1\text{H NMR}$ (400 MHz, CDCl_3) δ 4.99 – 4.84 (m, 2H, $\text{CH}_3\text{C}(\text{CH}_2)\text{CH}_2\text{OAc}$), 4.49 (s, 2H, $\text{CH}_3\text{C}(\text{CH}_2)\text{CH}_2\text{OAc}$), 2.09 (s, 3H, $\text{C}(\text{O})\text{CH}_3$), 1.75 (d, $J = 1.2$ Hz, 3H, $\text{CH}_3\text{C}(\text{CH}_2)\text{CH}_2\text{OAc}$). $^{13}\text{C NMR}$ (101 MHz, CDCl_3) δ 170.91, 140.07, 113.02, 67.88, 21.03, 19.62.

(*E*)-But-2-en-1-yl acetate (**1c**)^[159]



Prepared according to the general procedure using crotyl alcohol (3.41 mL, 40.0 mmol, 1.0 eq.). It was only concentrated to a pressure of 200 mbar on the rotavapor, as the product is volatile. *Kugelrohr* distillation (b.p. = 72 °C at 220 mBar) afforded **1c** as a colourless oil (3.11 g, 76% yield). $^1\text{H NMR}$ (400 MHz, CDCl_3) δ 5.79 (dqt, $J = 15.3, 6.4, 1.2$ Hz, 1H, $\text{CH}_3\text{CHCHCH}_2\text{OAc}$), 5.58 (dtq, $J = 16.3, 6.5, 1.6$ Hz, 1H, $\text{CH}_3\text{CHCHCH}_2\text{OAc}$), 4.49 (dp, $J = 6.5, 1.1$ Hz, 2H, $\text{CH}_3\text{CHCHCH}_2\text{OAc}$), 2.05 (s, 3H, $\text{C}(\text{O})\text{CH}_3$), 1.76 – 1.68 (m, 3H, $\text{CH}_3\text{CHCHCH}_2\text{OAc}$). $^{13}\text{C NMR}$ (101 MHz, CDCl_3) δ 171.02, 131.60, 125.21, 65.37, 21.14, 17.89.

(E)-1,3-Diphenylallyl acetate (1d)^[158]



Prepared according to the general procedure using (*E*)-1,3-diphenylallyl alcohol (2.86 g, 28.0 mmol, 1.0 eq.). *Kugelrohr* distillation (b.p. 165-170 °C at 0.4 mBar) afforded **1d** as yellowish, viscous oil (3.08 g, 87% yield). ¹H NMR (400 MHz,

CDCl₃) δ 7.33 – 7.10 (m, 10H, *H*-arom), 6.58 – 6.47 (m, 1H, Ar-CH=CH-CHO-Ar), 6.36 – 6.30 (m, 1H, Ar-CH=CH-CHO-Ar), 6.23 (dd, *J* = 15.8, 6.8 Hz, 1H, Ar-CH=CH-CHO-Ar), 2.02 (s, 3H, C(O)CH₃). ¹³C NMR (101 MHz, CDCl₃) δ 170.18, 139.38, 136.31, 132.74, 128.77, 128.72, 128.32, 128.20, 127.64, 127.19, 126.84, 76.28, 21.50.

9.3 Substrate synthesis for the enantioselective allylic alkylations (1e-i)

Compounds **1e-i** were prepared according the three-step procedure as follows:

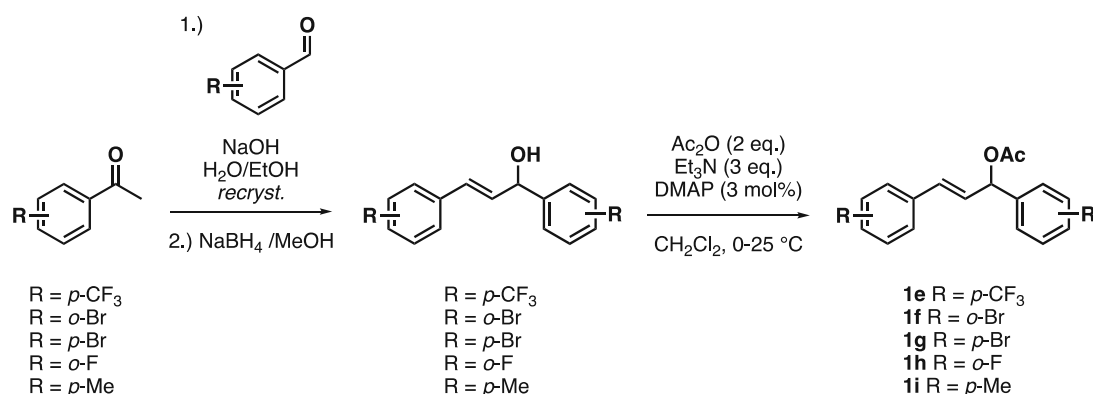
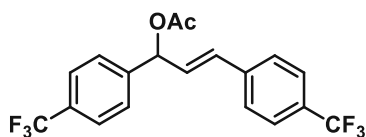


Figure 123. Synthesis of compounds **1e-i**

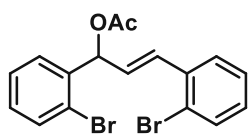
The corresponding chalcone derivatives^[160] and alcohols^[161] were prepared according to the literature procedures. Allylic acetates were prepared according to the modified literature procedure.^[158] The corresponding alcohol (1.00 eq.), Et₃N (3.00 eq.) and *N,N*-dimethylaminopyridine (0.036 eq.) were transferred to a one-neck round-bottom flask and they were dissolved in anhydrous CH₂Cl₂ (0.25 M) under argon atmosphere. The mixture was cooled down with an ice bath, and it was stirred for 5 minutes at 0 °C. Then, acetic anhydride (2.00 eq.) was added dropwise to the mixture with the aid of a syringe pump over 1 hour. After the addition was complete, the mixture was allowed to warm to room temperature and it was stirred overnight at room temperature. The reaction mixture was then quenched with water, and the aqueous phase was extracted with CH₂Cl₂ (2×). The combined organic extracts were washed with saturated NaHCO₃ solution (3×) and brine (1×), dried over anhydrous Na₂SO₄ and it was concentrated *in vacuo*. The residue was either used without further purification, purified *via* flash column chromatography, or distilled by *Kugelrohr* distillation.

(*E*)-1,3-Bis[*p*-(trifluoromethyl)phenyl]-2-propenyl acetate (**1e**)



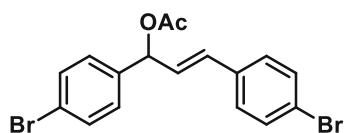
Prepared according to the general procedure from the corresponding alcohol (3.79 g, 11.0 mmol, 1.0 eq.). Flash column chromatography (petroleum ether/EtOAc 10:1) afforded the product as colourless, viscous oil (3.56 g, 84% yield). ¹H NMR (400 MHz, CDCl₃) δ 7.68 – 7.44 (m, 8H, *H*-arom), 6.68 (d, *J* = 15.8 Hz, 1H, Ar-CH=CH-CHO-Ar), 6.48 (d, *J* = 6.7 Hz, 1H, Ar-CH=CH-CHO-Ar), 6.39 (dd, *J* = 15.8, 6.6 Hz, 1H, Ar-CH=CH-CHO-Ar), 2.17 (s, 3H, C(O)CH₃). ¹³C NMR (101 MHz, CDCl₃) δ 169.93, 142.84, 139.43, 131.90, 129.45, 127.46, 127.06, 125.95, 125.92, 125.88, 125.84, 125.82, 125.78, 125.74, 75.24, 21.33. ¹⁹F NMR (376 MHz, CDCl₃) δ -62.63 – -62.66 (d, *J* = 11.0 Hz). IR (ν_{max}/cm⁻¹): 1742, 1323, 1229, 1120, 1066, 1016, 535. HRMS (ESI): calc. for C₁₇H₁₅F₆ [M - OAc + H]⁺: 333.1072; found: 333.1101.

(E)-1,3-Bis(o-bromophenyl)-2-propenyl acetate (1f)



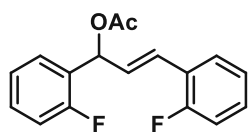
Prepared according to the general procedure from the corresponding alcohol (5.39 g, 14.0 mmol, 1.0 eq.). Flash column chromatography (petroleum ether/EtOAc 30:1) afforded the product as colourless, viscous oil (4.79 g, 81% yield). $^1\text{H NMR}$ (400 MHz, CDCl_3) δ 7.60 – 7.10 (m, 8H, *H*-arom), 7.04 – 6.97 (m, 1H, Ar-CH=CH-CHO-Ar), 6.79 (dd, J = 6.2, 1.4 Hz, 1H, Ar-CH=CH-CHO-Ar), 6.24 (dd, J = 15.8, 6.2 Hz, 1H, Ar-CH=CH-CHO-Ar), 2.18 (s, 3H, C(O)CH₃). $^{13}\text{C NMR}$ (101 MHz, CDCl_3) δ 169.68, 138.45, 136.30, 133.23, 133.09, 133.00, 131.72, 130.50, 129.73, 129.43, 128.94, 128.37, 127.94, 127.59, 127.34, 127.09, 124.10, 122.98, 122.23, 74.78, 74.51, 35.54, 32.45, 21.28, 21.26. IR ($\nu_{\text{max}}/\text{cm}^{-1}$): 1736, 1563, 1370, 1226, 962, 776, 632, 535. HRMS (ESI): calc. for C₁₅H₁₁Br₂ [M - OAc - H]⁺: 348.9225; found: 348.9221.

(E)-1,3-Bis(p-bromophenyl)-2-propenyl acetate (1g)



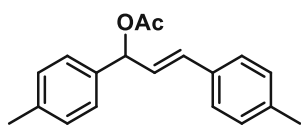
Prepared according to the general procedure from the corresponding alcohol (1.86 g, 5.0 mmol, 1.0 eq.). Flash column chromatography (petroleum ether/EtOAc 10:1) afforded the product as yellow, viscous oil (1.56 g, 75% yield). $^1\text{H NMR}$ (400 MHz, CDCl_3) δ 7.55 – 7.16 (m, 8H, *H*-arom), 6.58 – 6.51 (m, 1H, Ar-CH=CH-CHO-Ar), 6.38 – 6.34 (m, 1H, Ar-CH=CH-CHO-Ar), 6.28 (dd, J = 15.7, 6.6 Hz, 1H, Ar-CH=CH-CHO-Ar), 2.13 (s, 3H, C(O)CH₃). $^{13}\text{C NMR}$ (101 MHz, CDCl_3) δ 169.87, 138.02, 134.91, 131.85, 131.77, 131.76, 131.57, 130.08, 128.78, 128.24, 127.75, 122.31, 122.11, 75.30, 37.47, 31.18, 21.28. IR ($\nu_{\text{max}}/\text{cm}^{-1}$): 2786, 1490, 1116, 962, 919, 747, 690, 613, 545, 520. HRMS (ESI): calc. for C₁₅H₁₁Br₂ [M - OAc - H]⁺: 348.9242; found: 348.9249.

(E)-1,3-Bis(o-fluorophenyl)-2-propenyl acetate (1h)



Prepared according to the general procedure from the corresponding alcohol (2.01 g, 8.0 mmol, 1.0 eq.). Flash column chromatography (petroleum ether/EtOAc 8:1) afforded the product as colourless, viscous oil (1.65 g, 70% yield). $^1\text{H NMR}$ (400 MHz, CDCl_3) δ 7.50 – 6.95 (m, 8H, *H*-arom), 6.80 (d, J = 16.1 Hz, 1H, Ar-CH=CH-CHO-Ar), 6.70 (d, J = 6.6 Hz, 1H, Ar-CH=CH-CHO-Ar), 6.47 (ddd, J = 16.1, 6.7, 0.9 Hz, 1H, Ar-CH=CH-CHO-Ar), 2.15 (s, 3H, C(O)CH₃). $^{13}\text{C NMR}$ (101 MHz, CDCl_3) δ 169.85, 161.82, 158.96, 130.09, 130.00, 129.60, 129.51, 128.89, 128.45, 127.96, 125.38, 124.50, 124.23, 116.05, 115.83, 70.78, 21.33. $^{19}\text{F NMR}$ (376 MHz, CDCl_3) δ -117.21, -117.26 (d, J = 19.1 Hz). IR ($\nu_{\text{max}}/\text{cm}^{-1}$): 1740, 1488, 1456, 1371, 1222, 1019, 965, 753, 536, 521. HRMS (ESI): calc. for C₁₅H₁₁F₂ [M - OAc - H]⁺: 229.0912; found: 229.0909.

(E)-1,3-Bis(p-tolyl)-2-propenyl acetate (1i)



Prepared according to the general procedure from the corresponding alcohol (2.25 g, 22.0 mmol, 1.0 eq.). Product was obtained as orange, viscous oil (2.72 g, 88% yield) and was used without further purification. **¹H**

NMR (400 MHz, CDCl₃) δ 7.35 – 7.06 (m, 8H, *H*-arom), 6.65 – 6.55 (m, 1H, Ar-CH=CH-CHO-Ar), 6.41 (d, *J* = 6.9 Hz, 1H, Ar-CH=CH-CHO-Ar), 6.30 (dd, *J* = 15.8, 6.8 Hz, 1H, Ar-CH=CH-CHO-Ar), 2.34 (d, *J* = 10.4 Hz, 6H, 2 × Ar-CH₃), 2.12 (s, 3H, C(O)CH₃). **¹³C NMR** (101 MHz, CDCl₃) δ 170.23, 138.08, 138.03, 136.56, 133.60, 132.48, 129.42, 129.39, 127.21, 126.73, 126.72, 76.32, 21.54, 21.36, 21.32. **IR** (ν_{max}/cm⁻¹): 1736, 1514, 1369, 1229, 1017, 963, 632, 536, 516, 502. **HRMS (ESI)**: calc. for C₁₇H₁₇ [M - OAc]⁻: 222.1403; found: 222.1373.

9.4 Continuous-flow synthesis of allylic amines (3a-h)

9.4.1 Synthesis of non-chiral supported ionic liquid phases (SILPs)

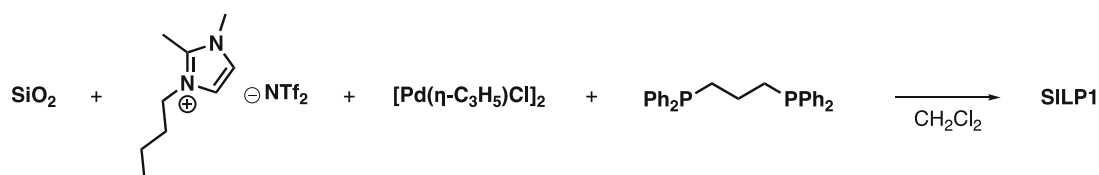


Figure 124. Synthesis of non-chiral SILPs

The catalytically active supported ionic liquid phase (SILP) was prepared as follows:

Allylpalladium(II)-chloride dimer (0.055 mmol, 20 mg, 0.5 wt%), 1,3-Bis(diphenylphosphino)propane (0.22 mmol, 2.75 wt%) and 1-butyl-2,3-dimethylimidazolium bis(trifluoro-methylsulfonyl)imide ([C₄mim][NTf₂], 1.38 mmol, 600 mg, 15 wt%) were dissolved in anhydrous CH₂Cl₂ (1 mL) under argon atmosphere in a screw-cap vial (8 mL, VWR). The mixture was stirred for 30 minutes, and it was poured into a silica (Merck silica 60 Mesh, 3270 mg, 81.75 wt%) containing flask and it was rinsed with CH₂Cl₂. The suspension was shaken for 30 minutes (mechanical shaker, 700 rpm) and stirred for 24 hours at room temperature under inert atmosphere. Then, the solvent was removed *in vacuo*, and the resulting fine powder was dried on high vacuum (0.4 mbar) at room temperature for several hours.

9.4.2 General procedure for the synthesis of allylamines 3a-h

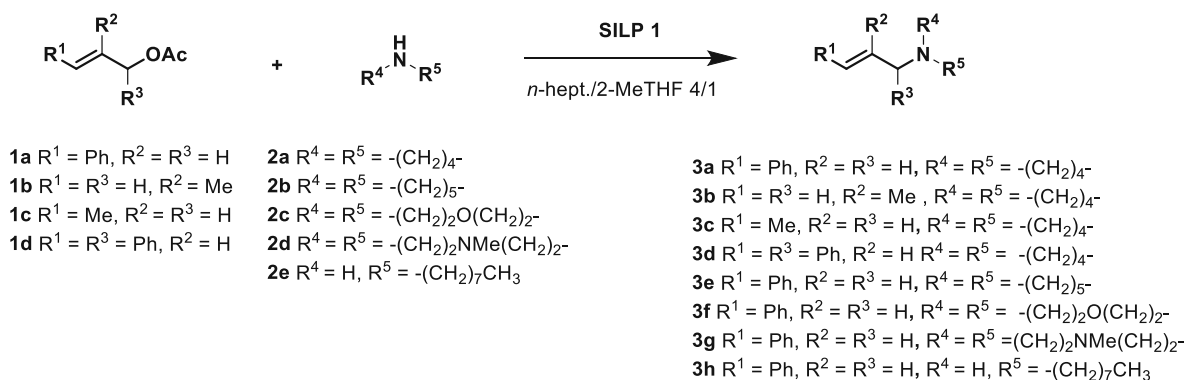


Figure 125. Synthesis of compounds 3a-h

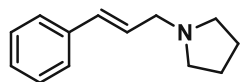
The corresponding allylic acetate (1.00 eq.) and amine (2.00 eq.) were dissolved in a mixture of *n*-heptane: 2-methyltetrahydrofuran (4:1; 5 mL) and it was stirred for 15 minutes. A cartridge (100 × 3 mm, glass column) was filled with the solid supported catalyst (450 mg) and it was equilibrated with the same solvent mixture. The reaction mixture was taken up with a syringe (5 mL) and pumped through the cartridge with the aid of a syringe pump. A flow rate which corresponds to 30 min residence time was chosen. The product was collected in a vial. After the mixture was pumped through,

the column was washed with the same solvent mixture again. The collected mixture was concentrated *in vacuo* and purified by flash column chromatography.



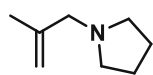
Figure 126. Set-up of the continuous-flow experiments

1-[(*E*)-3-Phenyl-2-propenyl]pyrrolidine (**3a**)^[162]



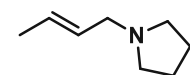
Following the general procedure (0.62 mmolar scale), purification by flash column chromatography (petroleum ether/ EtOAc/Et₃N 10:1:0.4), afforded the product as a yellow liquid (89 mg, 77% yield). ¹H NMR (400 MHz, CDCl₃) δ 7.41 – 7.19 (m, 5H, *H*-arom), 6.54 (dt, *J* = 15.7, 1.4 Hz, 1H, ArCH=CH), 6.34 (dt, *J* = 15.8, 6.7 Hz, 1H, ArCH=CH), 3.27 (dd, *J* = 6.7, 1.4 Hz, 2H, ArCH=CHCH₂), 2.62 – 2.51 (m, 4H, N(CH₂CH₂)₂), 1.88 – 1.73 (m, 4H, N(CH₂CH₂)₂). ¹³C NMR (101 MHz, CDCl₃) δ 137.30, 131.95, 128.66, 127.92, 127.47, 126.43, 58.56, 54.23, 23.62.

1-(2-Methylallyl)pyrrolidine (**3b**)



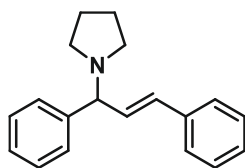
Due to its volatile nature, the product has not been isolated. GC-MS conversion: 67% (no by-product formation was observed).

(*E*)-1-(But-2-en-1-yl)pyrrolidine (**3c**)



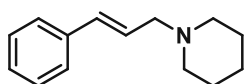
Due to its volatile nature, the product has not been isolated. GC-MS conversion: 51% (no by-product formation was observed).

1-[(*E*)-1,3-Diphenyl-2-propenyl]pyrrolidine (**3d**)^[163]



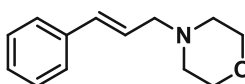
Following the general procedure (0.61 mmolar scale), purification by flash column chromatography (petroleum ether/EtOAc 5:1) afforded the product as a pale yellow solid (108 mg, 67% yield). ¹H NMR (400 MHz, CDCl₃) δ 7.48 – 7.15 (m, 10H, *H*-arom), 6.62 – 6.52 (m, 1H, ArCH=CHCHNAr), 6.47 – 6.37 (m, 1H, ArCH=CHCHNAr), 3.82 – 3.70 (m, 1H ArCH=CHCHNAr), 2.65 – 2.35 (m, 4H, N(CH₂CH₂)₂), 1.79 (ddt, *J* = 7.1, 5.6, 2.6 Hz, 4H, N(CH₂CH₂)₂). ¹³C NMR (101 MHz, CDCl₃) δ 143.28, 137.22, 133.29, 129.96, 128.66, 128.61, 127.82, 127.49, 127.23, 126.53, 74.52, 53.27, 23.50.

1-[(*E*)-3-Phenyl-2-propenyl]piperidine (**3e**)^[164]



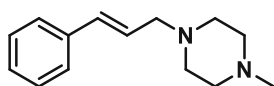
Following the general procedure (0.66 mmolar scale), purification by flash column chromatography (petroleum ether/ EtOAc/Et₃N 10:1:0.4) afforded the product as a yellow liquid (102 mg, 77% yield). ¹H NMR (400 MHz, CDCl₃) δ 7.42 – 7.14 (m, 5H, *H*-arom), 6.50 (dt, *J* = 15.8, 1.4 Hz, 1H, ArCH=CH), 6.31 (dt, *J* = 15.9, 6.8 Hz, 1H, ArCH=CH), 3.12 (dd, *J* = 6.8, 1.3 Hz, 2H, ArCH=CHCH₂), 2.44 (s, 4H, N(CH₂CH₂)₂CH₂), 1.61 (p, *J* = 5.6 Hz, 4H, N(CH₂CH₂)₂CH₂), 1.45 (h, *J* = 5.4, 4.6 Hz, 2H, N(CH₂CH₂)₂CH₂). ¹³C NMR (101 MHz, CDCl₃) δ 137.23, 132.74, 128.66, 127.48, 127.41, 126.41, 62.04, 54.76, 26.13, 24.48.

4-[(*E*)-3-Phenyl-2-propenyl]morpholine (**3f**)^[165]



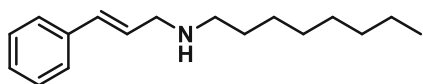
Following the general procedure (0.64 mmolar scale), purification by flash column chromatography (petroleum ether/ EtOAc/Et₃N 8:1:0.4) afforded the product as a yellow liquid (101 mg, 78% yield). ¹H NMR (400 MHz, CDCl₃) δ 7.39 – 7.23 (m, 5H, *H*-arom), 6.54 (dt, *J* = 15.8, 1.5 Hz, 1H, ArCH=CH), 6.26 (dt, *J* = 15.9, 6.8 Hz, 1H, ArCH=CH), 3.75 (t, *J* = 4.7 Hz, 4H, N(CH₂CH₂)₂O), 3.17 (dd, *J* = 6.7, 1.4 Hz, 2H, ArCH=CHCH₂), 2.52 (t, *J* = 4.8 Hz, 4H, N(CH₂CH₂)₂O). ¹³C NMR (101 MHz, CDCl₃) δ 136.93, 133.61, 128.73, 127.74, 126.48, 67.11, 61.62, 53.83.

1-[(*E*)-3-Phenyl-2-propenyl]-4-methylpiperazine (**3g**)^[166]



Following the general procedure (0.64 mmolar scale), purification by flash column chromatography (petroleum ether/ EtOAc/Et₃N 2.5:1:0.4) afforded the product as a yellow liquid (98 mg, 71% yield). ¹H NMR (400 MHz, CDCl₃) δ 7.40 – 7.20 (m, 5H, *H*-arom), 6.53 (dt, *J* = 15.9, 1.4 Hz, 1H, ArCH=CH), 6.27 (dt, *J* = 15.9, 6.8 Hz, 1H, ArCH=CH), 3.17 (dt, *J* = 6.9, 1.4 Hz, 2H, ArCH=CHCH₂), 2.51 (s, 8H, N(CH₂CH₂)₂NCH₃), 2.30 (d, *J* = 2.1 Hz, 3H, N(CH₂CH₂)₂NCH₃). ¹³C NMR (101 MHz, CDCl₃) δ 137.05, 133.25, 128.69, 127.62, 126.71, 126.45, 61.18, 55.25, 53.31, 46.16.

[(*E*)-3-Phenyl-2-propenyl]octylamine (**3h**)^[167]



Following the general procedure (0.64 mmolar scale), purification by flash column chromatography (petroleum ether/EtOAc/Et₃N 10:1:0.4) afforded the product as a yellowish oil (86 mg, 55% yield). ¹H NMR (400 MHz, CDCl₃) δ 7.40 – 7.20 (m, 5H, *H*-arom), 6.53 (dt, *J* = 15.7, 1.6 Hz, 1H, ArCH=CH), 6.31 (dt, *J* = 15.9, 6.3 Hz, 1H, ArCH=CH), 3.42 (dd, *J* = 6.3, 1.4 Hz, 2H, ArCH=CHCH₂), 2.65 (t, *J* = 7.3 Hz, 2H, NCH₂(CH₂)₆CH₃), 1.52 (p, *J* = 7.2 Hz, 3H, NCH₂CH₂(CH₂)₅CH₃, NH), 1.35 – 1.23 (m, 10H, NCH₂CH₂(CH₂)₅CH₃), 0.94 – 0.83 (m, 3H, N(CH₂)₇CH₃). ¹³C NMR (101 MHz, CDCl₃) δ 137.32, 131.34, 128.67, 127.46, 126.40, 52.12, 49.70, 31.98, 30.29, 29.69, 29.42, 27.55, 22.81, 14.25.

9.5 Procedures for the synthesis of chiral ligands L1-L4

N-((1*R*,2*R*)-2-[*o*-(Diphenylphosphino)benzylamino]cyclohexyl)*o*-(diphenyl-phosphino)benzamide (L1)

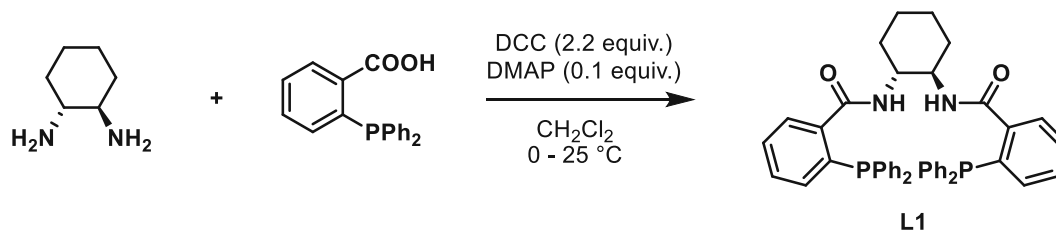


Figure 127. Synthesis of compound L1

According to the literature procedure,^[168] (1*R*,2*R*)-1,2-cyclohexanediamine (0.53 g, 4.68 mmol, 1.00 eq.), *o*-(diphenylphosphino)-benzoic acid (3.02 g, 9.38 mmol, 2.10 eq.), DCC (2.13 g, 10.3 mmol, 2.20 eq.) and DMAP (61 mg, 0.5 mmol, 0.10 eq.) were dissolved in anhydrous CH₂Cl₂ (0.16 M) under argon atmosphere. The mixture was stirred at room temperature overnight. After completion, the majority of the formed DCU was removed *via* filtration, and the filter cake was washed with CH₂Cl₂. Then, the filtrate was washed with 10% HCl (3×), water (1×), saturated NaHCO₃ (3×), water (1×) and brine (1×). The organic phase was dried over Na₂SO₄, concentrated *in vacuo*, and the residue was purified by column chromatography (30% EtOAc in petroleum ether). The product was obtained as slightly yellowish solid (2.12 g, 66% yield). ¹H NMR (400 MHz, CDCl₃) δ 7.57 (ddd, *J* = 5.5, 3.8, 2.1 Hz, 2H, *H*-arom), 7.41 – 7.13 (m, 24H, *H*-arom), 6.91 (ddd, *J* = 6.5, 3.9, 2.0 Hz, 2H, *H*-arom), 6.32 (d, *J* = 7.4, 2H, 2 × NH), 3.77 (ddt, *J* = 8.6, 5.8, 2.5 Hz, 2H, 2 × CHNH), 1.85 (d, *J* = 13.8 Hz, 2H, NHCHCH₂), 1.68 – 1.60 (m, 2H, NHCHCH₂), 1.37 – 1.15 (m, 2H, NHCHCH₂CH₂), 1.01 (t, *J* = 11.4 Hz, 2H, NHCHCH₂CH₂). ¹³C NMR (101 MHz, CDCl₃) δ 169.41, 141.05, 140.81, 137.91, 137.84, 137.80, 137.73, 136.80, 136.59, 134.42, 134.10, 133.90, 130.31, 128.92, 128.75, 128.69, 128.66, 128.62, 128.59, 128.52, 127.70, 127.65, 54.02, 32.12, 24.75. ³¹P NMR (162 MHz, CDCl₃) δ -9.66. HRMS (ESI): calc. for C₄₄H₄₁N₂O₂P₂ [M + H]⁺: 691.2638; found: 691.2638.

(1*R*,2*R*)-2-[*o*-(Diphenylphosphino)benzylamino]cyclohexylamino-*tert*-butyl-formylate (L3)

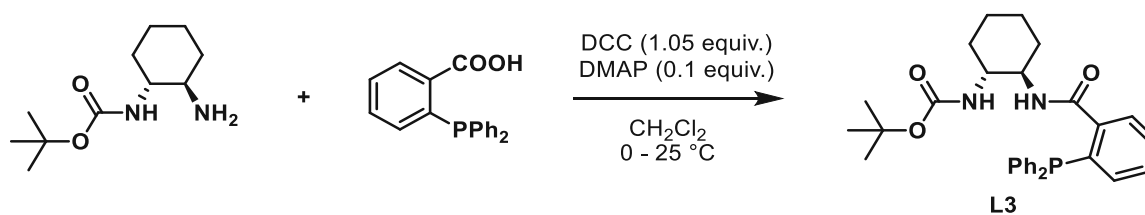


Figure 128. Synthesis of compound L3

According to the literature procedure,^[169] *o*-(diphenylphosphino)benzoic acid (1.50 g, 4.9 mmol, 1.05 eq.) was dissolved in 20 mL anhydrous CH₂Cl₂ at 0 °C. Then, *N,N*-dicyclohexylcarbodiimide (DCC, 1.01 g, 4.9 mmol, 1.05 eq.) was added to the mixture and it was stirred for 15 minutes at 0 °C. To this, the solution of (1*R*,2*R*)-2-aminocyclohexylamino-*tert*-butylformylate (1.00 g, 4.7 mmol, 1.00 eq.) and DMAP (57 mg, 0.47 mmol, 0.10 eq.) in 25 mL anhydrous CH₂Cl₂ was slowly added. The mixture was allowed to warm up to room temperature and it was stirred overnight. After completion, the majority of the formed dicyclohexyl urea by-product (DCU) was removed *via* filtration, and the filter cake was washed with cold CH₂Cl₂. Then, the filtrate was washed with 0.5 M HCl (3×), saturated NaHCO₃ (3×) and water (2×). The organic phase was dried over Na₂SO₄ and concentrated *in vacuo*. Flash column chromatography (petroleum ether/EtOAc 4:1) afforded the product as a white solid (1.72 g, 73% yield). ¹H NMR (400 MHz, CDCl₃) δ 7.64 – 7.58 (m, 1H, NHC(O)Ar), 7.40 – 7.19 (m, 12H, *H*-arom), 6.95 (dd, *J* = 7.9, 4.6 Hz, 1H, *H*-arom), 6.48 (s, 1H, *H*-arom), 4.81 (d, *J* = 8.6 Hz, 1H, NHC(O)O), 3.67 (tdd, *J* = 11.6, 8.1, 4.0 Hz, 1H, CHNHC(O)), 3.35 (d, *J* = 8.7 Hz, 1H, CHNHC(O)O), 2.05 – 1.96 (m, 1H, CH_{2*a*}CH), 1.95 – 1.88 (m, 1H, CH_{2*b*}CH), 1.72 (s, 1H, CH_{2*a*}CH), 1.64 (d, *J* = 10.6 Hz, 1H, CH_{2*b*}CH), 1.38 (s, 9H, C(CH₃)₃), 1.25 – 1.16 (m, 3H, CH₂CH_{2*a*}), 1.01 – 0.88 (m, 1H, CH₂CH_{2*b*}). ¹³C NMR (101 MHz, CDCl₃) δ 169.08, 156.80, 141.06, 140.83, 137.80, 134.38, 134.15, 134.12, 133.95, 133.92, 130.25, 128.74, 128.68, 128.61, 128.58, 128.54, 127.49, 127.45, 79.61, 65.99, 55.00, 54.20, 32.92, 32.28, 28.53, 25.09, 24.65, 15.41. ³¹P NMR (162 MHz, CDCl₃) δ -9.01. HRMS (ESI): calc. for C₃₀H₃₆N₂O₃P [M + H]⁺: 503.2458; found: 503.2464.

(S)-2-([(S)-4-Isopropyl-4,5-dihydro-1,3-oxazol-2-yl]methyl)-4-isopropyl-4,5-dihydro-1,3-oxazole (L4)

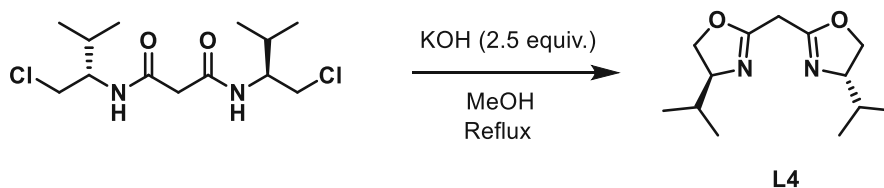


Figure 129. Synthesis of compound L4

According to the literature procedure,^[170] *N,N*-di[(*S*)-1-(chloromethyl)-2-methylpropyl]malonamide (3.66 g, 12.0 mmol, 1.00 eq.) and potassium hydroxide (1.62 g, 3.0 mmol, 2.50 eq.) were dissolved in anhydrous methanol (0.12 M). The mixture was refluxed for 3 hours, then it was cooled down and poured onto water. It was extracted with CH₂Cl₂, washed with brine, dried over anhydrous Na₂SO₄ and concentrated *in vacuo*. Flash column chromatography (CH₂Cl₂/MeOH 20:1) afforded the product as a yellow gel (1.46 g, 52% yield). ¹H NMR (400 MHz, CDCl₃) δ 4.31 – 4.23 (m, 2H, 2 × NCH), 4.06 – 3.89 (m, 4H, 2 × OCH₂C), 3.34 (s, *J* = 1.1 Hz, 2H, CCH₂C), 1.84 – 1.66 (m, 2H, 2 × CH(CH₃)₂), 1.02 – 0.84 (m, 12H, 2 × CH(CH₃)₂). ¹³C NMR (101 MHz, CDCl₃) δ 161.67, 72.34, 70.69, 32.19, 28.53, 18.80, 18.15. HRMS (ESI): calc. for C₁₃H₂₂N₂O₂ [M + H]⁺: 239.1754; found: 239.1759.

9.6 General procedure for the continuous-flow asymmetric allylation – synthesis of allylic amines 3d, 3i-m

9.6.1 General procedure for the synthesis of racemic diphenyl-propenyl pyrrolidine derivatives

1,3-Bis(diphenylphosphino)propane (0.02 eq.) and allylpalladium(II) chloride dimer (0.01 eq.) were dissolved in dichloromethane and the mixture was stirred for 15 minutes. Then, the corresponding diphenyl-propenyl acetate derivative (1.00 eq.) dissolved in CH_2Cl_2 (0.5 M) was added to the mixture and stirred for further 15 minutes. Finally, pyrrolidine (2.00 eq.) was added to the mixture and it was stirred at room temperature overnight. The mixture was concentrated *in vacuo* and purified by flash column chromatography, and they were used as racemic control for determining the enantioselectivity.

9.6.2 Synthesis of chiral supported ionic liquid phases (chiral SILPs)

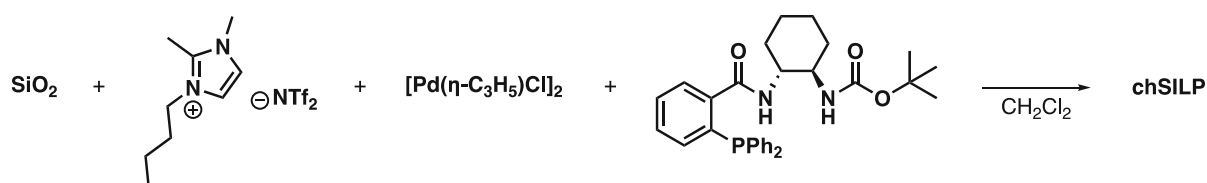


Figure 130. Synthesis of chiral SILPs (chSILP)

The catalytically active supported ionic liquid phase (SILP) was prepared as follows: Allylpalladium(II)-chloride dimer (0.055 mmol, 20 mg, 0.5 wt%), the corresponding chiral ligand (0.22 mmol, 2.75 wt%) and 1-butyl-2,3-dimethylimidazolium bis(trifluoromethylsulfonyl)imide ($[\text{C}_4\text{mim}][\text{NTf}_2]$, 1.38 mmol, 600 mg, 15 wt%) were dissolved in anhydrous CH_2Cl_2 (1 mL) in a screw-cap vial (8 mL, VWR). The mixture was stirred for 30 minutes, and it was poured into a silica (Merck silica 60 Mesh, 3270 mg, 81.75 wt%) containing flask, and it was rinsed with CH_2Cl_2 . The suspension was shaken for 30 minutes (mechanical shaker, 700 rpm) and stirred for 24 hours at room temperature under argon atmosphere. Then, the solvent was removed *in vacuo*, and the resulting fine powder was dried on high vacuum (0.4 mbar) at room temperature for several hours.

9.6.3 General procedure for the synthesis of allylamines 3a, 3i-m

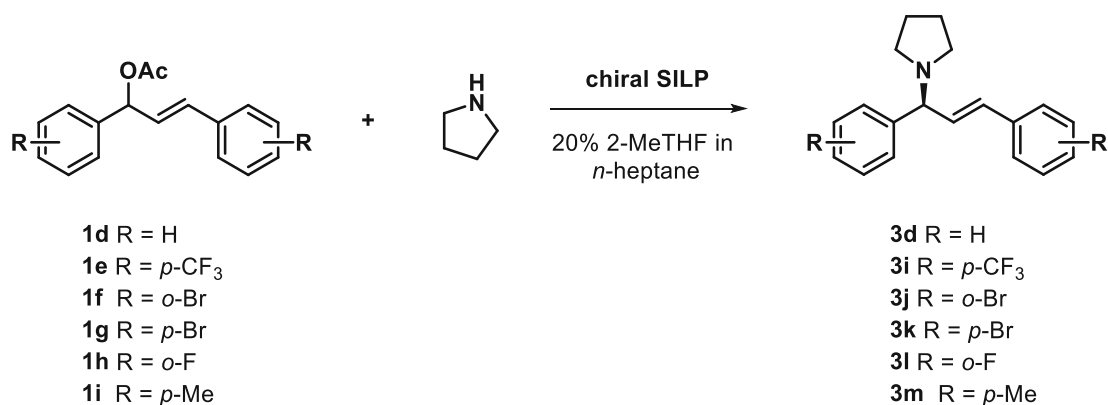
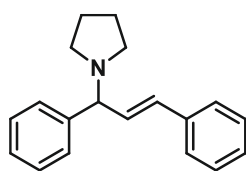


Figure 131. Synthesis of compounds **3d**, **3i-m**

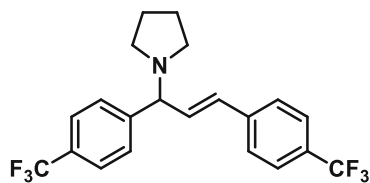
The corresponding diphenyl-propenyl acetate derivative (1.00 eq.) and pyrrolidine (2.00 eq.) were dissolved in a mixture of *n*-heptane: 2-methyltetrahydrofuran (4:1) and stirred for 15 minutes. A cartridge was filled with the solid supported catalyst (chiral SILP 15) and was equilibrated with the same solvent mixture. The reaction mixture was taken up with a syringe and pumped through the cartridge with the aid of a syringe pump. A flow rate which corresponds to 30 min residence time was chosen. The product was collected in a vial. The flow reaction setup was the same as described before. After the mixture was pumped through, the column was washed with the same solvent mixture again. The collected mixture was concentrated *in vacuo* and purified by flash column chromatography.

1-[(*E*)-1,3-Diphenyl-2-propenyl]pyrrolidine (**3d**)



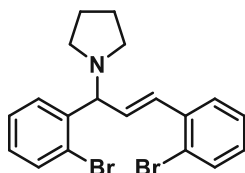
Following the general procedure (0.52 mmolar scale), purification by flash column chromatography (petroleum ether/EtOAc 5:1) afforded the product as a pale yellow solid (111 mg, 81% yield, 74% ee). $[\alpha]_{20}^D$: -3.57 (*c* = 1.0, CH₂Cl₂); ¹H NMR (400 MHz, CDCl₃) δ 7.48 – 7.15 (m, 10H, *H*-arom), 6.62 – 6.52 (m, 1H, ArCH=CHCHNAr), 6.47 – 6.37 (m, 1H, ArCH=CHCHNAr), 3.82 – 3.70 (m, 1H ArCH=CHCHNAr), 2.65 – 2.35 (m, 4H, N(CH₂CH₂)₂), 1.79 (ddt, *J* = 7.1, 5.6, 2.6 Hz, 4H, N(CH₂CH₂)₂). ¹³C NMR (101 MHz, CDCl₃) δ 143.28, 137.22, 133.29, 129.96, 128.66, 128.61, 127.82, 127.49, 127.23, 126.53, 74.52, 53.27, 23.50. IR (*v*_{max}/cm⁻¹): 2957, 2786, 1490, 1451, 1275, 1139, 1027, 986, 962, 896, 747, 690, 613, 545. HRMS (ESI): calc. for C₁₉H₂₂N [M + H]⁺: 264.1747; found: 264.1752. Chiral HPLC: Chiralpak® IA-3 column, *n*-heptane: ethanol 95:5, 0.35 mL/min, 25 °C, UV 220 nm, *t*_R (minor) = 12.8 min, *t*_R (major) = 13.2 min.

1-[(E)-1,3-Bis(p-(trifluoromethyl)phenyl)-2-propenyl]pyrrolidine (3i)



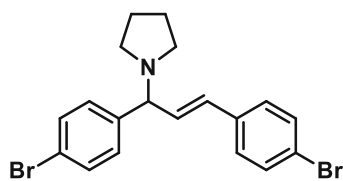
Following the general procedure (0.66 mmolar scale), purification by flash column chromatography (petroleum ether/EtOAc 7:1) afforded the product as an orange viscous liquid (177 mg, 67% yield, 58% ee). $[\alpha]_{20}^D$: +1.4 (c = 1.0, CH₂Cl₂); ¹H NMR (400 MHz, CDCl₃) δ 7.84 – 7.14 (m, 8H, *H*-arom), 6.62 (d, *J* = 15.8 Hz, 1H, ArCH=CHCHNAr), 6.45 (dd, *J* = 15.6, 8.2 Hz, 1H, ArCH=CHCHNAr), 3.87 (d, *J* = 8.5 Hz, 1H, ArCH=CHCHNAr), 2.50 (d, *J* = 35.2 Hz, 4H, N(CH₂CH₂)₂), 1.81 (d, *J* = 6.1 Hz, 4H, N(CH₂CH₂)₂). ¹³C NMR (101 MHz, CDCl₃) δ 140.27, 131.79, 128.12, 126.74, 125.83, 125.79, 125.71, 125.68, 125.64, 125.60, 122.92, 73.86, 53.19, 23.51. ¹⁹F NMR (376 MHz, CDCl₃) δ -62.44, -62.55. IR (ν_{max}/cm⁻¹): 2964, 2795, 1616, 1417, 1322, 1163, 1121, 1066, 1017, 969, 835, 645, 632, 607, 551, 544, 535, 515. HRMS (ESI): calc. for C₂₁H₂₀F₆N [M + H]⁺: 400.1557; found: 400.1558. Chiral HPLC: Chiralpak® IA-3 column, *n*-heptane: ethanol 99.5:0.5, 0.35 mL/min, 25 °C, UV 220 nm, t_R (minor) = 19.1 min, t_R (major) = 22.6 min.

1-[(E)-1,3-Bis(m-bromophenyl)-2-propenyl]pyrrolidine (3j)



Following the general procedure (0.65 mmolar scale), purification by flash column chromatography (petroleum ether/EtOAc 5:1) afforded the product as a colourless viscous liquid (191 mg, 70% yield, 48% ee). $[\alpha]_{20}^D$: -6.2 (c = 1.0, CH₂Cl₂); ¹H NMR (400 MHz, CDCl₃) δ 7.78 – 7.02 (m, 9H, *H*-arom, ArCH=CHCHNAr), 6.12 (dd, *J* = 15.7, 8.8 Hz, 1H, ArCH=CHCHNAr), 4.43 (d, *J* = 8.8 Hz, 1H, ArCH=CHCHNAr), 2.73 – 2.42 (m, 4H, N(CH₂CH₂)₂), 1.81 (d, *J* = 6.3 Hz, 4H, N(CH₂CH₂)₂). ¹³C NMR (101 MHz, CDCl₃) δ 137.08, 134.55, 133.08, 132.99, 129.76, 128.87, 128.47, 127.95, 127.50, 127.27, 123.83, 123.79, 71.48, 53.09, 23.57. IR (ν_{max}/cm⁻¹): 2964, 2789, 1464, 1437, 1138, 1022, 965, 900, 748, 632, 540, 528, 521, 503. HRMS (ESI): calc. for C₁₉H₂₀Br₂N [M + H]⁺: 419.9963; found: 419.9957. Chiral HPLC: Chiralcel® OD column, *n*-hexane: isopropanol: Et₂NH 99.8:0.2:0.2, 0.5 mL/min, 25 °C, UV 220 nm, t_R (major) = 13.3 min, t_R (minor) = 16.3 min.

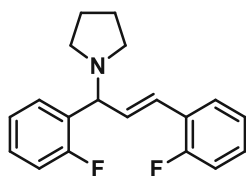
1-[(E)-1,3-Bis(p-bromophenyl)-2-propenyl]pyrrolidine (3k)



Following the general procedure (0.65 mmolar scale), purification by flash column chromatography (petroleum ether/EtOAc 7:1) afforded the product as a yellow solid (208 mg, 76% yield, 64% ee). **M.p.** 108-113 °C. $[\alpha]_{20}^D$: -17.2 (c=1.0, CH₂Cl₂); ¹H NMR (400 MHz, CDCl₃) δ 7.56 – 7.14 (m, 8H, *H*-arom), 6.49 (d, *J* = 15.8 Hz, 1H, ArCH=CHCHNAr), 6.33 (dd, *J* = 15.8, 8.5 Hz, 1H, ArCH=CHCHNAr), 3.73 (d, *J* = 8.5 Hz, 1H, ArCH=CHCHNAr), 2.47 (d, *J* = 34.4 Hz, 4H, N(CH₂CH₂)₂), 1.79 (d, *J* = 6.3 Hz, 4H, N(CH₂CH₂)₂). ¹³C NMR (101 MHz, CDCl₃) δ 131.80, 131.64, 129.38, 127.98, 73.54,

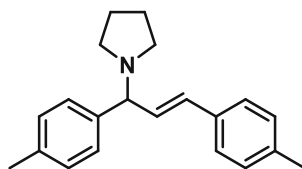
53.04, 31.60, 23.36, 22.67, 14.14. **IR** ($\nu_{\max}/\text{cm}^{-1}$): 2961, 2877, 2792, 1485, 1070, 1007, 982, 814, 565. **HRMS (ESI)**: calc. for $\text{C}_{19}\text{H}_{20}\text{Br}_2\text{N}$ [$\text{M} + \text{H}$] $^+$: 419.9848; found: 419.9854. **Chiral HPLC**: Chiralpak[®] IA-3 column, *n*-heptane: ethanol 95:5, 0.35 mL/min, 25 °C, UV 220 nm, t_{R} (minor) = 14.3 min, t_{R} (major) = 15.3 min.

1-[(*E*)-1,3-Bis(*o*-fluorophenyl)-2-propenyl]pyrrolidine (3l)



Following the general procedure (0.64 mmolar scale), purification by flash column chromatography (petroleum ether/EtOAc 7:1) afforded the product as yellow viscous liquid (144 mg, 75% yield, 70% ee). $[\alpha]_{20}^{\text{D}}$: +1.5 ($c = 1.0$, CH_2Cl_2); $^1\text{H NMR}$ (400 MHz, CDCl_3) δ 7.68 – 6.93 (m, 8H, *H*-arom), 6.80 (d, $J = 15.9$ Hz, 1H, $\text{ArCH}=\text{CHCHNAr}$), 6.48 (dd, $J = 15.9, 8.7$ Hz, 1H, $\text{ArCH}=\text{CHCHNAr}$), 4.24 (d, $J = 8.7$ Hz, 1H, $\text{ArCH}=\text{CHCHNAr}$), 2.81 – 2.32 (m, 4H, $\text{N}(\text{CH}_2\text{CH}_2)_2$), 1.90 – 1.69 (m, 4H, $\text{N}(\text{CH}_2\text{CH}_2)_2$). $^{13}\text{C NMR}$ (101 MHz, CDCl_3) δ 161.61, 159.17, 159.13, 129.33, 129.29, 128.91, 128.83, 128.55, 128.47, 127.53, 127.49, 124.49, 124.46, 124.16, 124.12, 123.05, 115.91, 115.77, 115.69, 115.55, 66.06, 66.05, 53.14, 23.49. $^{19}\text{F NMR}$ (376 MHz, CDCl_3) δ -118.06, -118.66. **IR** ($\nu_{\max}/\text{cm}^{-1}$): 1966, 2791, 1486, 1456, 1268, 1229, 968, 753, 632, 535, 514, 503. **HRMS (ESI)**: calc. for $\text{C}_{19}\text{H}_{20}\text{F}_2\text{N}$ [$\text{M} + \text{H}$] $^+$: 300.1558; found: 300.1566. **Chiral HPLC**: Chiralpak[®] IA-3 column, *n*-heptane: ethanol 99.5:0.5, 0.35 mL/min, 25 °C, UV 220 nm, t_{R} (minor) = 14.3 min, t_{R} (major) = 15.5 min.

1-[(*E*)-1,3-Bis(*p*-tolyl)-2-propenyl]pyrrolidine (3m)



Following the general procedure (0.66 mmolar scale), purification by flash column chromatography (petroleum ether/EtOAc 5:1) afforded the product as a pale yellow solid (193 mg, 76% yield, 74% ee). **M.p.** 87-91 °C. $[\alpha]_{20}^{\text{D}}$: -8.8 ($c = 1.0$, CH_2Cl_2); $^1\text{H NMR}$ (400 MHz, CDCl_3) δ 7.40 – 7.00 (m, 8H, *H*-arom), 6.52 (d, $J = 15.8$ Hz, 1H, $\text{ArCH}=\text{CHCHNAr}$), 6.36 (dd, $J = 15.7, 8.6$ Hz, 1H, $\text{ArCH}=\text{CHCHNAr}$), 3.71 (d, $J = 8.5$ Hz, 1H, $\text{ArCH}=\text{CHCHNAr}$), 2.49 (dtd, $J = 43.9, 7.8, 6.9, 3.2$ Hz, 4H, $\text{N}(\text{CH}_2\text{CH}_2)_2$), 2.32 (d, $J = 8.4$ Hz, 6H, $2 \times \text{Ar-CH}_3$), 1.91 – 1.73 (m, 4H, $\text{N}(\text{CH}_2\text{CH}_2)_2$). $^{13}\text{C NMR}$ (101 MHz, CDCl_3) δ 140.42, 137.18, 136.74, 134.49, 132.40, 129.67, 129.32, 129.26, 127.70, 126.43, 74.24, 53.26, 23.48, 21.29, 21.23. **IR** ($\nu_{\max}/\text{cm}^{-1}$): 2973, 2874, 2780, 1509, 1122, 987, 906, 901, 589, 520. $\text{C}_{21}\text{H}_{26}\text{N}$ **HRMS (ESI)**: calc. for $\text{C}_{21}\text{H}_{26}\text{N}$ [$\text{M} + \text{H}$] $^+$: 292.2267; found: 292.2285. **Chiral HPLC**: Chiralpak[®] IA-3 column, *n*-hexane: ethanol 99.6:0.4, 0.35 mL/min, 25 °C, UV 220 nm, t_{R} (minor) = 20.9 min, t_{R} (major) = 24.0 min.

9.7 TGA measurements of the SILP catalysts

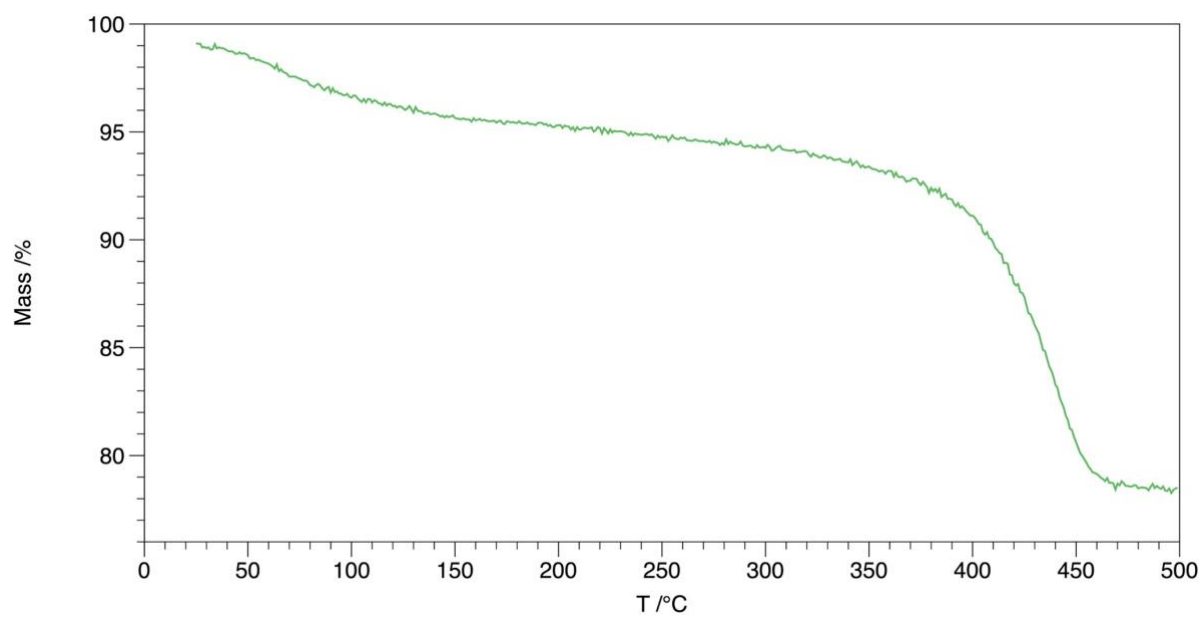


Figure 132. Thermogravimetric analysis of SILP1

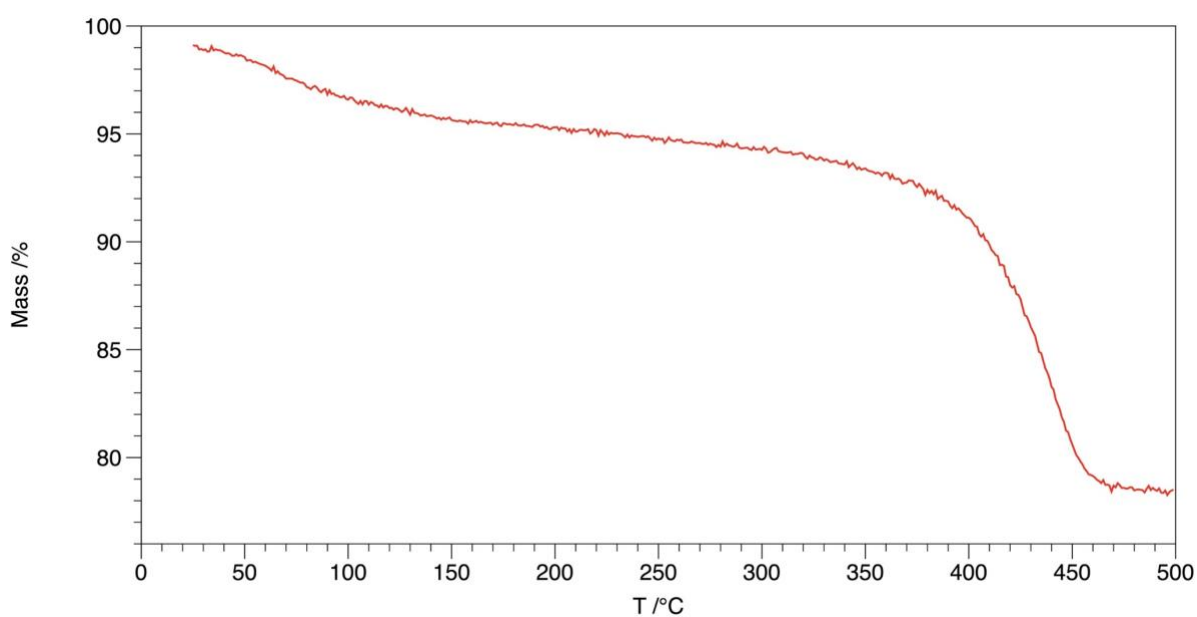


Figure 133. Thermogravimetric analysis of chSILP with chiral ligand L1

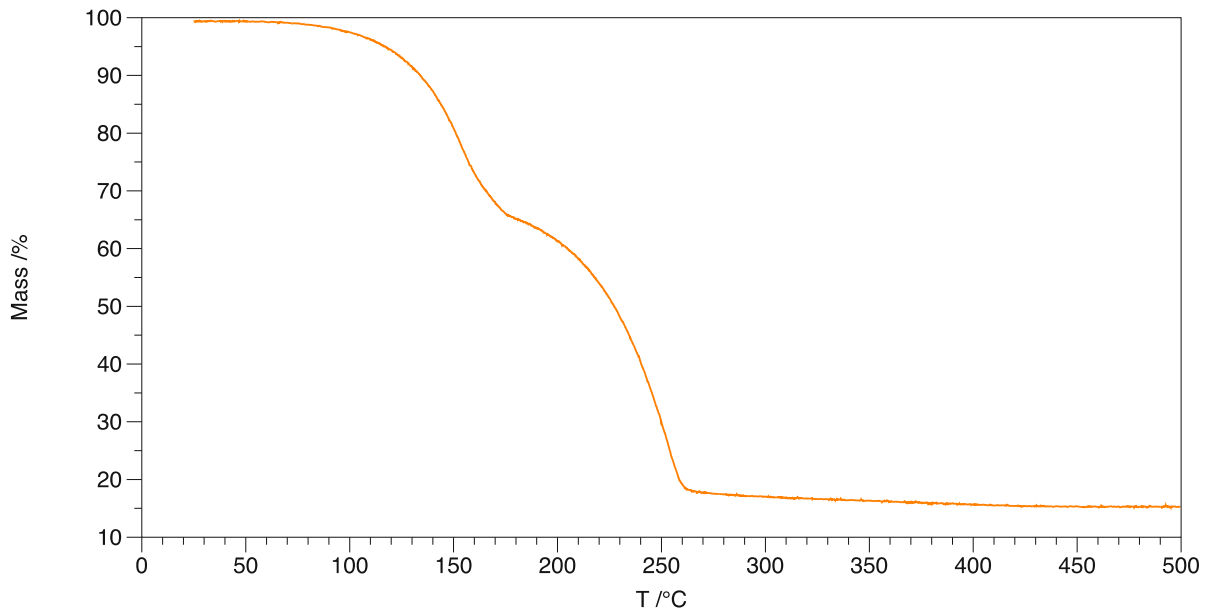


Figure 134. Thermogravimetric analysis of **3e**

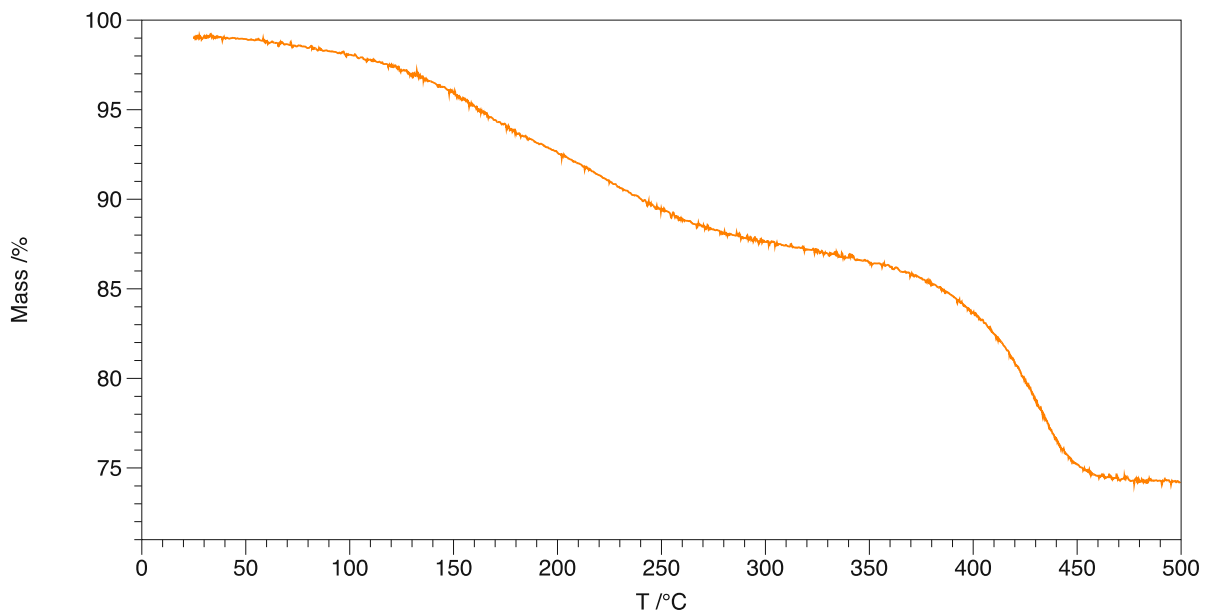


Figure 135. Thermogravimetric analysis of **SILP1** after the long-term experiment

9.8 SEM images of the chiral SILP catalyst

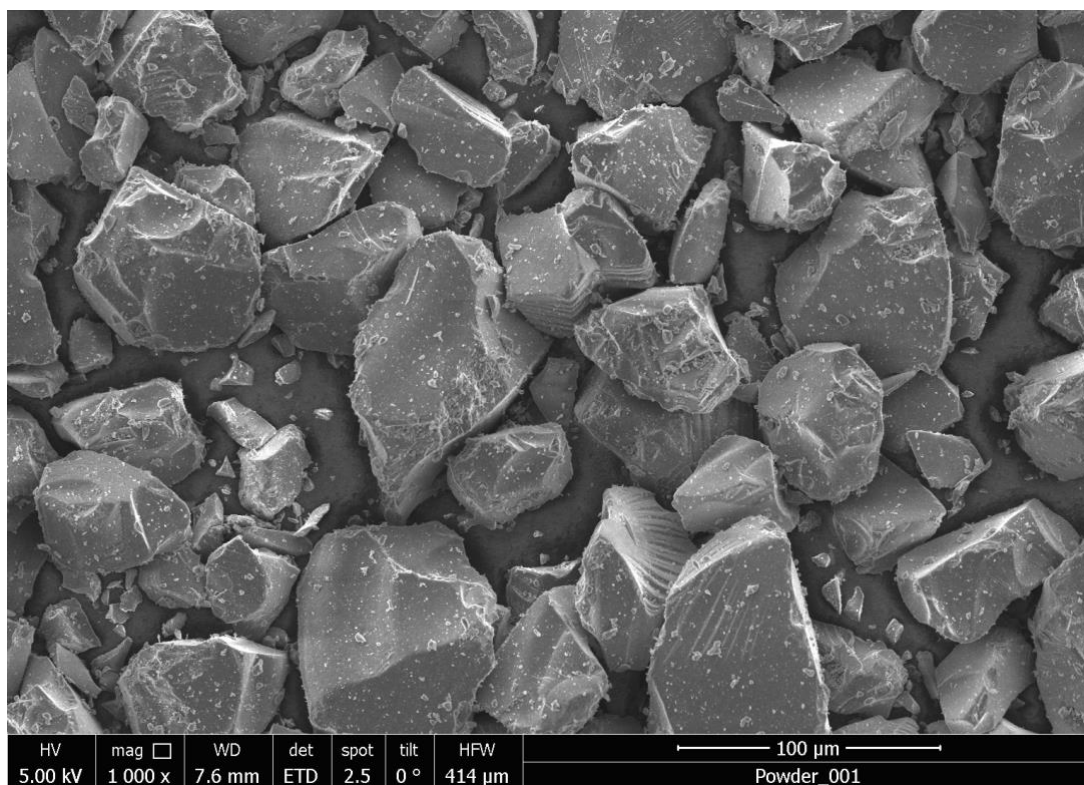


Figure 136. Scanning electron microscope image of chSILP with chiral ligand L1

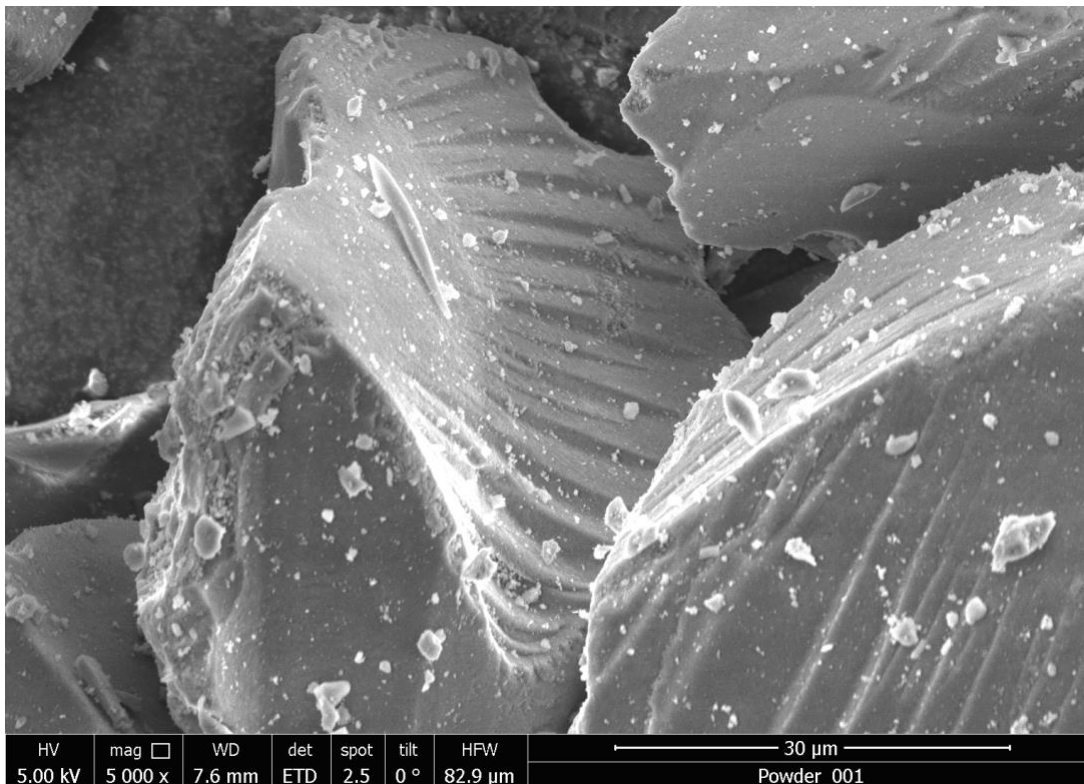
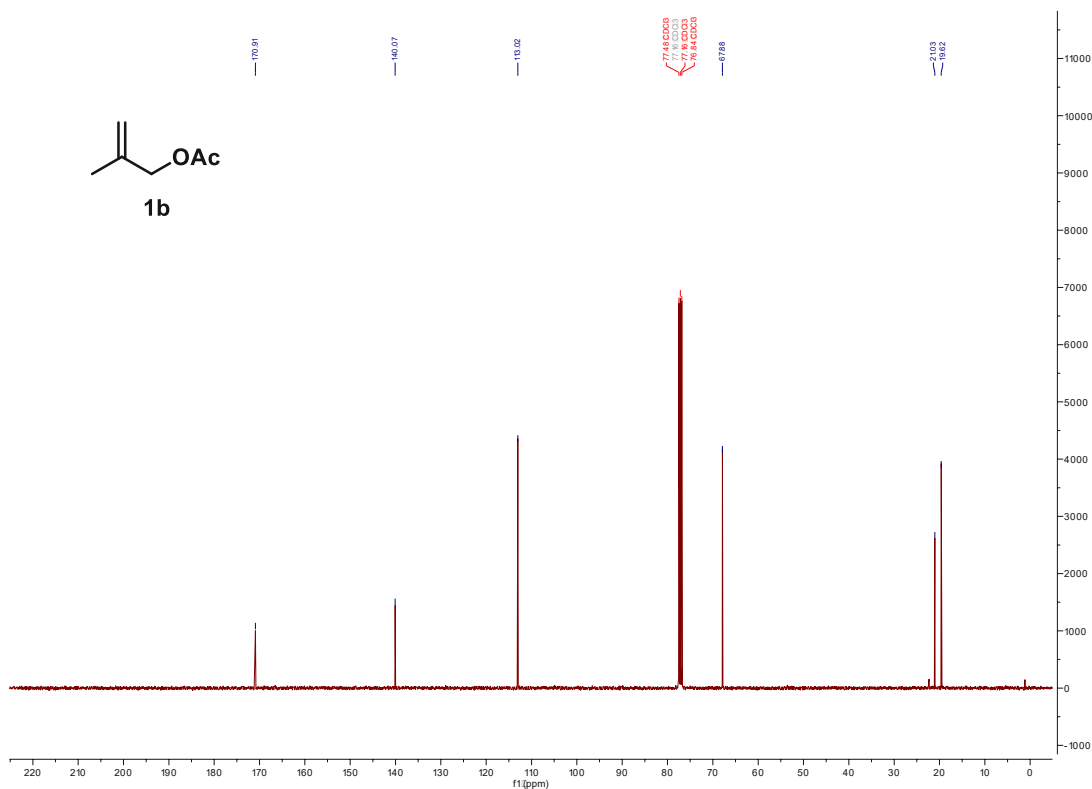
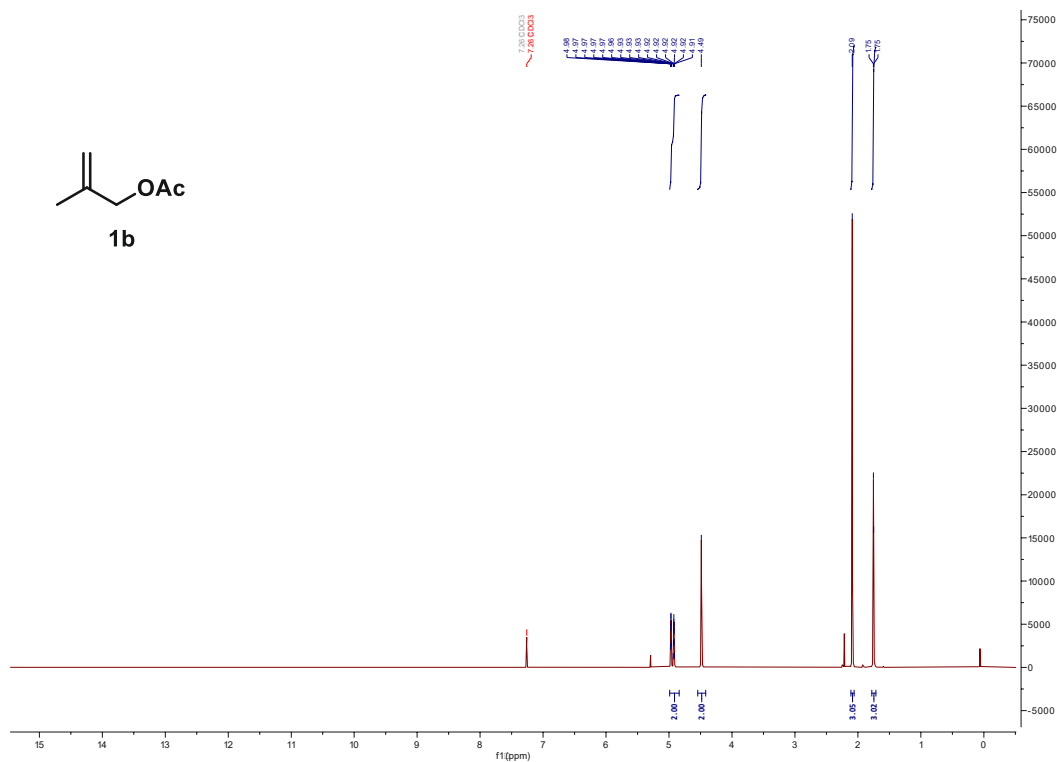


Figure 137. Scanning electron microscope image of chSILP with chiral ligand L1

9.9 NMR spectra of allyl acetate derivatives



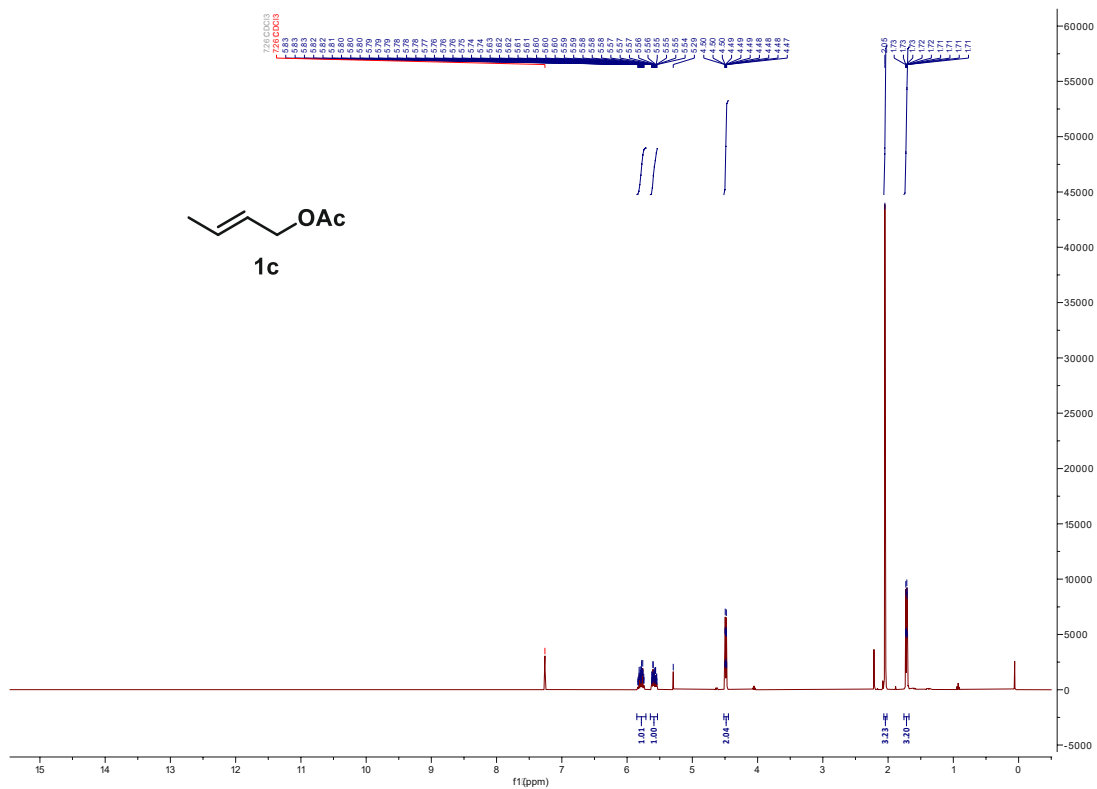


Figure 140. ^1H NMR spectrum of **1c**

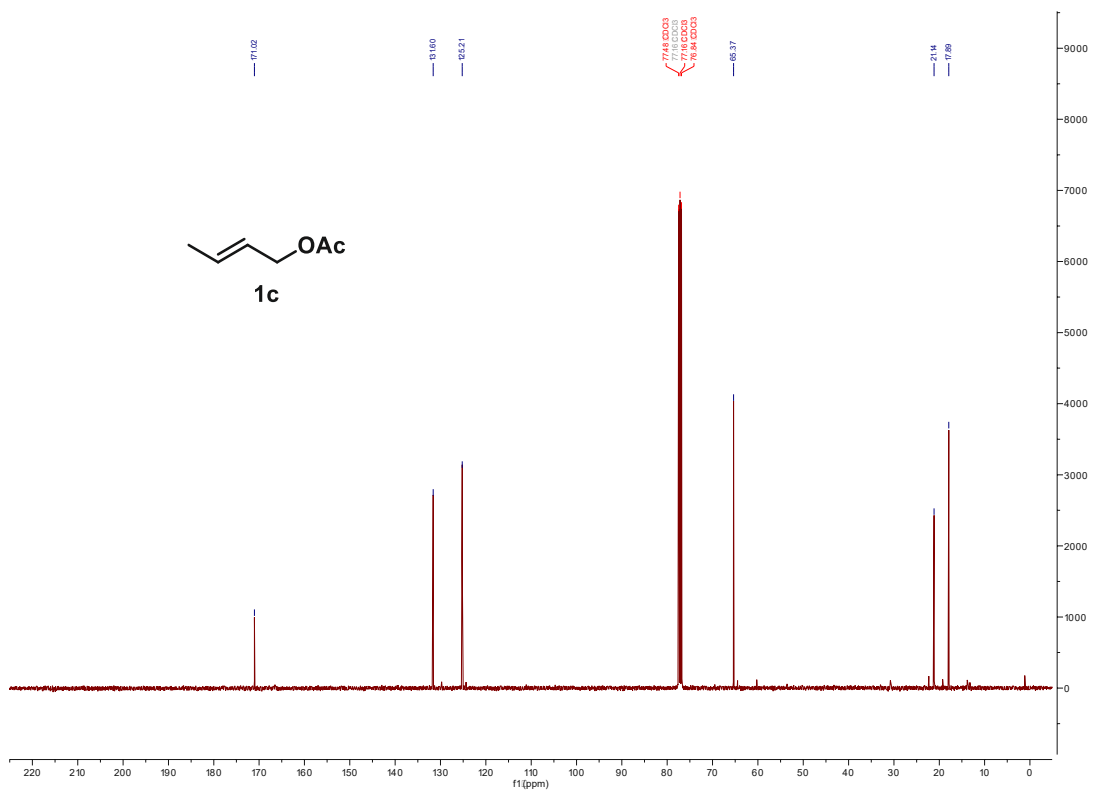


Figure 141. ^{13}C NMR spectrum of **1c**

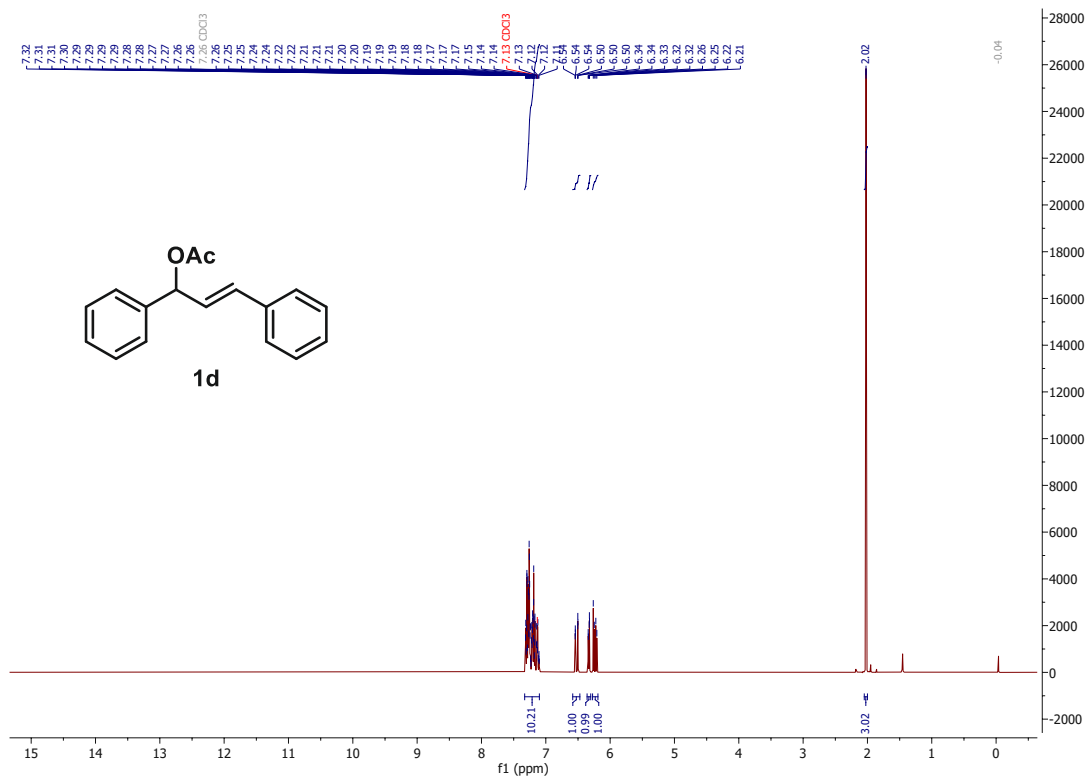


Figure 142. ¹H NMR spectrum of 1d

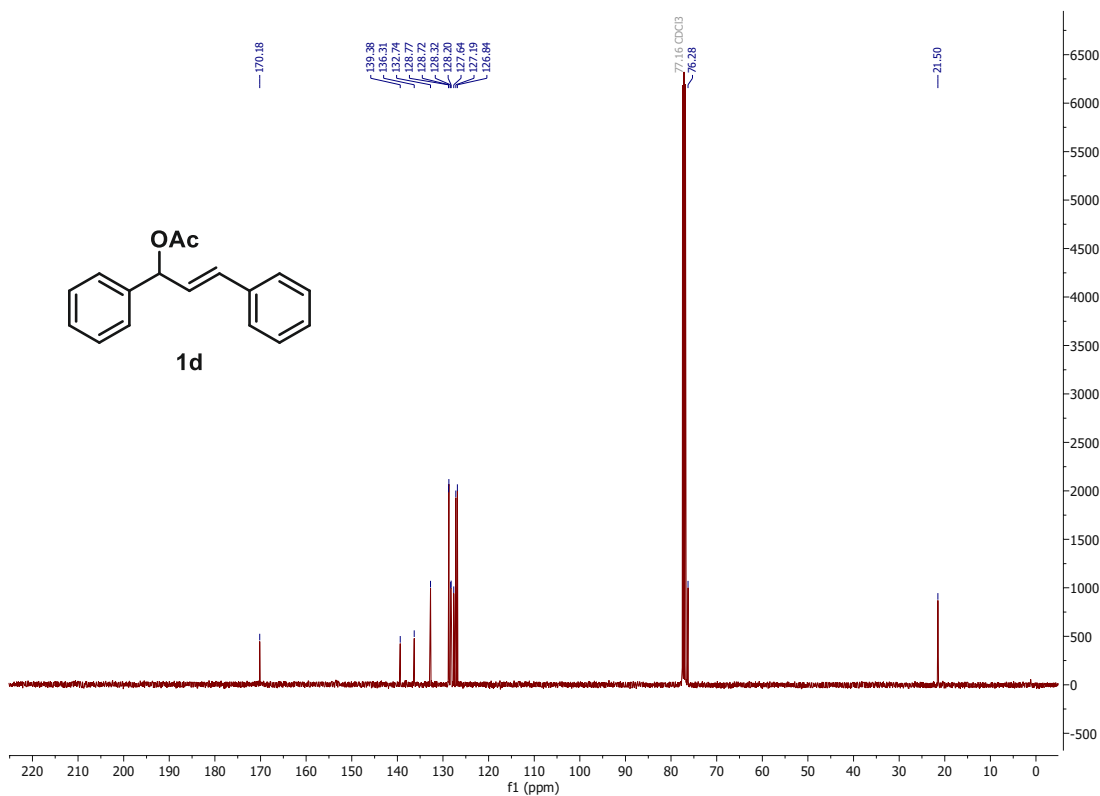


Figure 143. ¹³C NMR spectrum of 1d

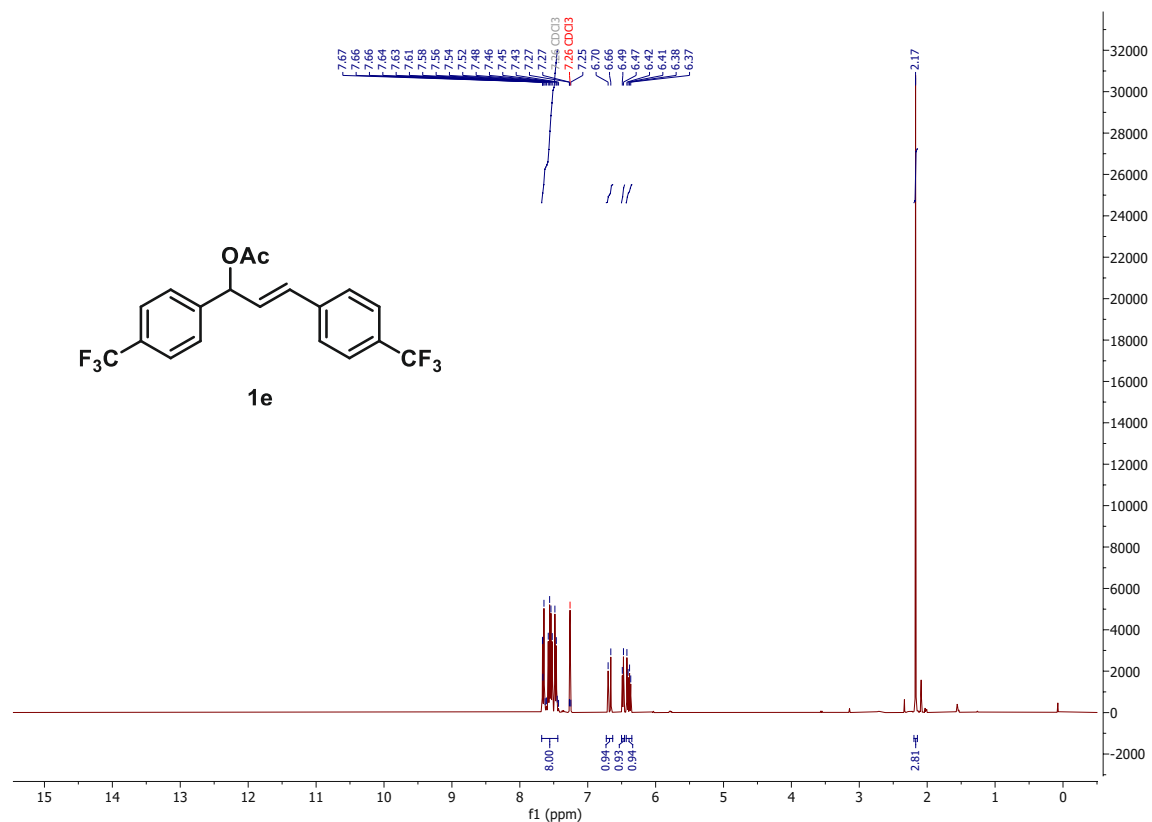


Figure 144. ^1H NMR spectrum of **1e**

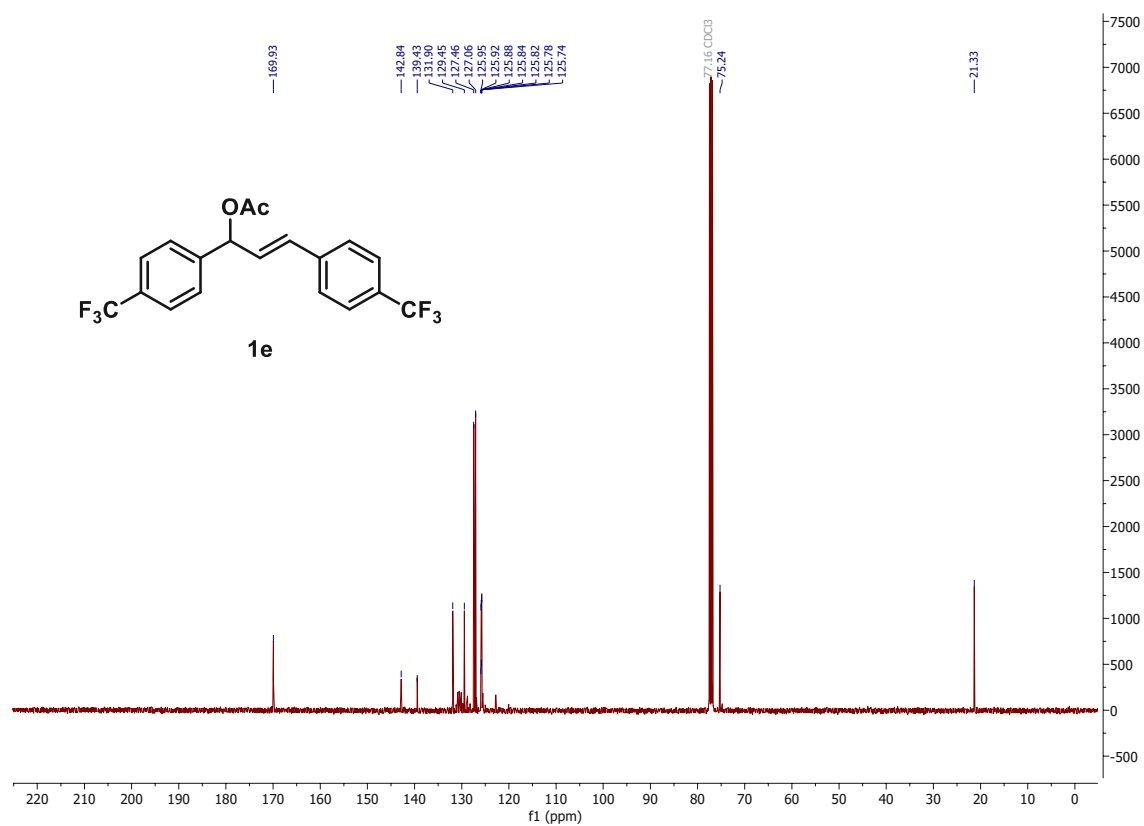
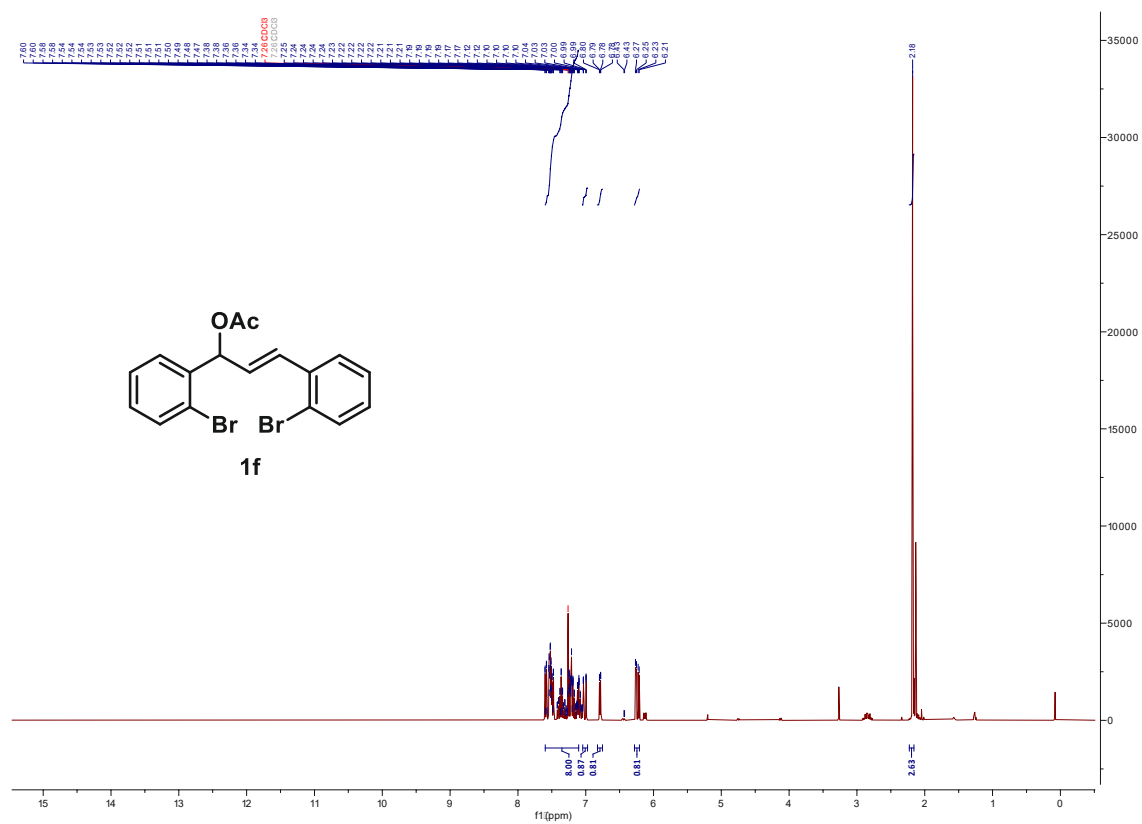
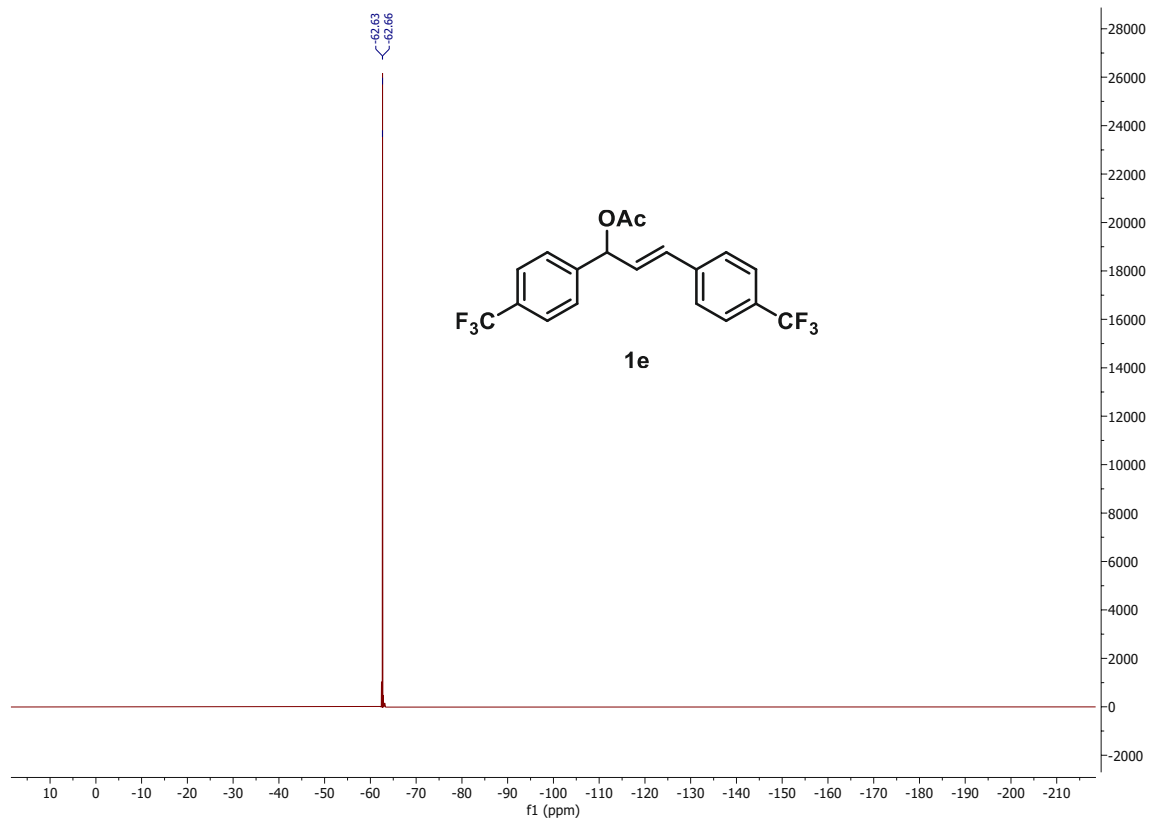
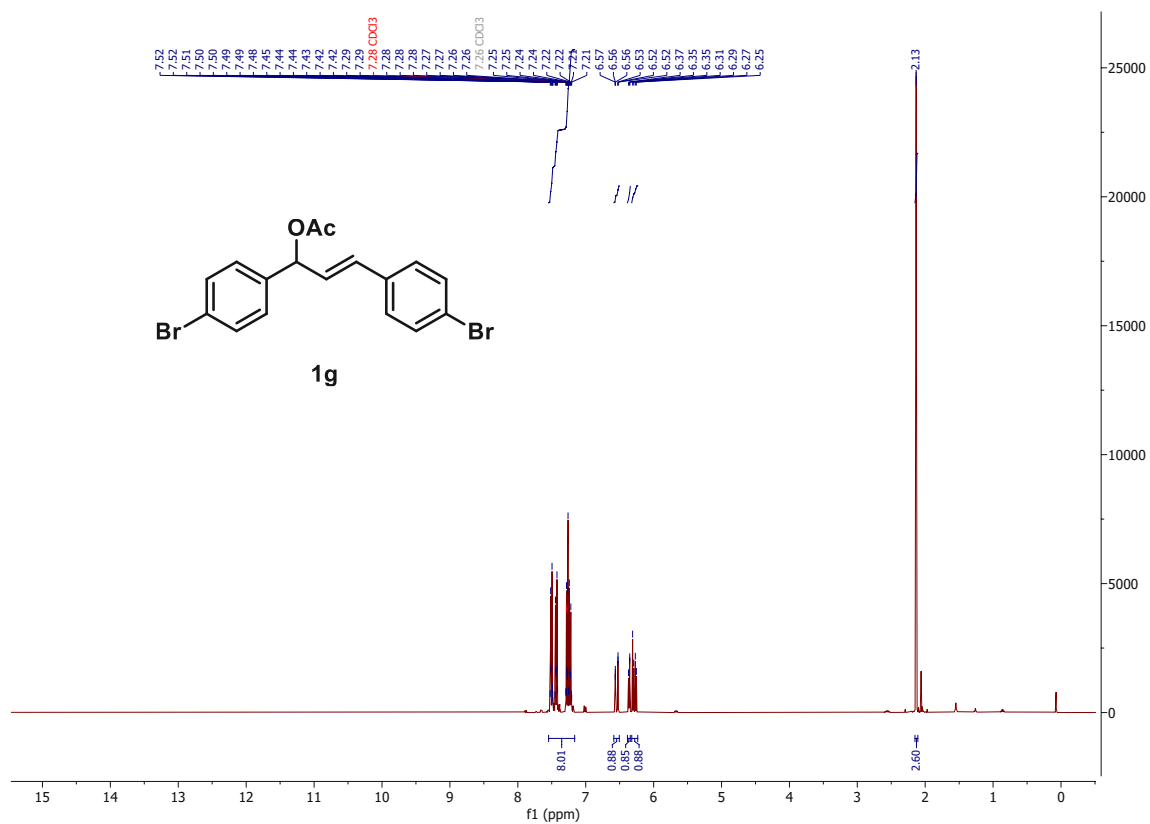
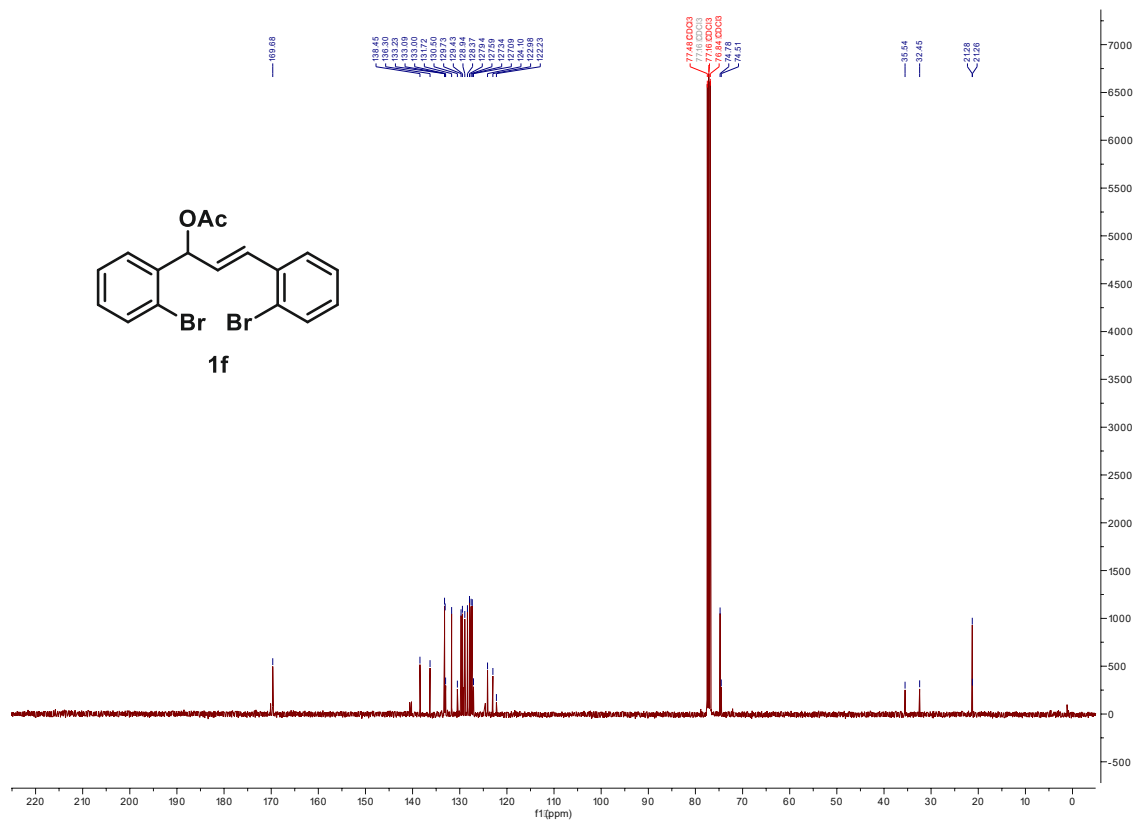


Figure 145. ^{13}C NMR spectrum of **1e**





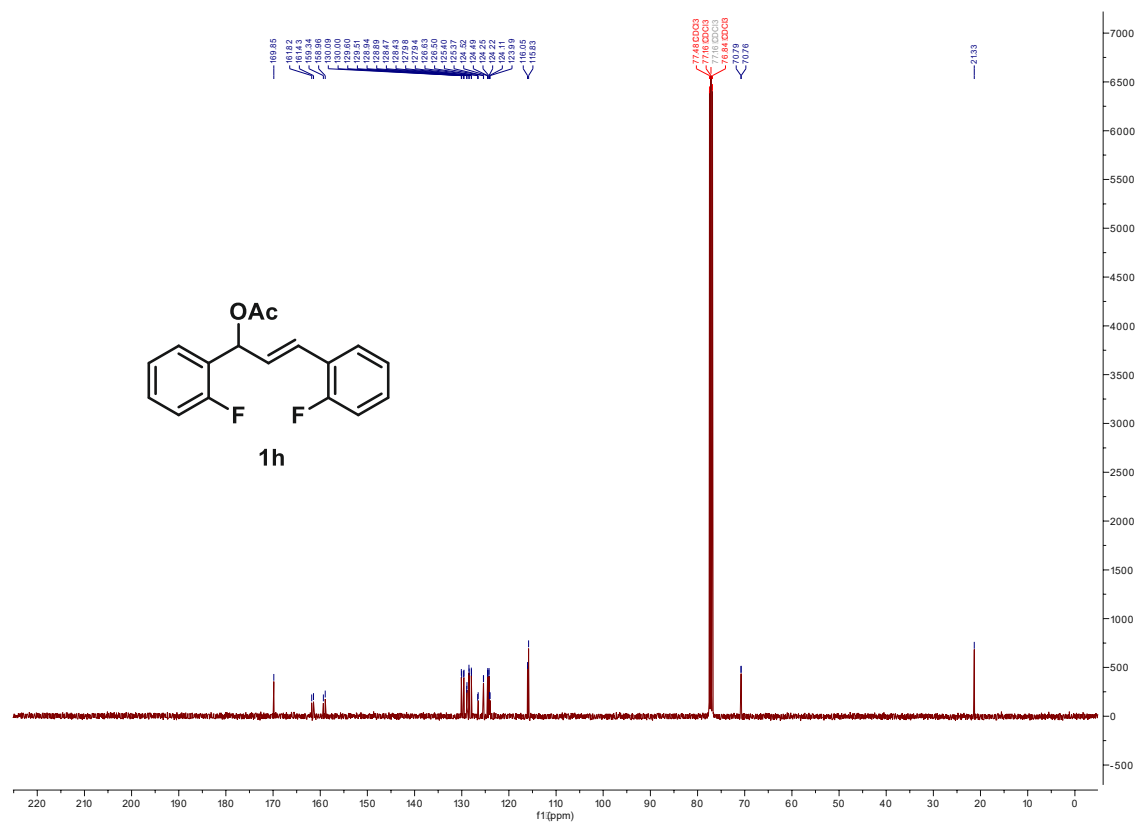


Figure 152. ¹³C NMR spectrum of 1h

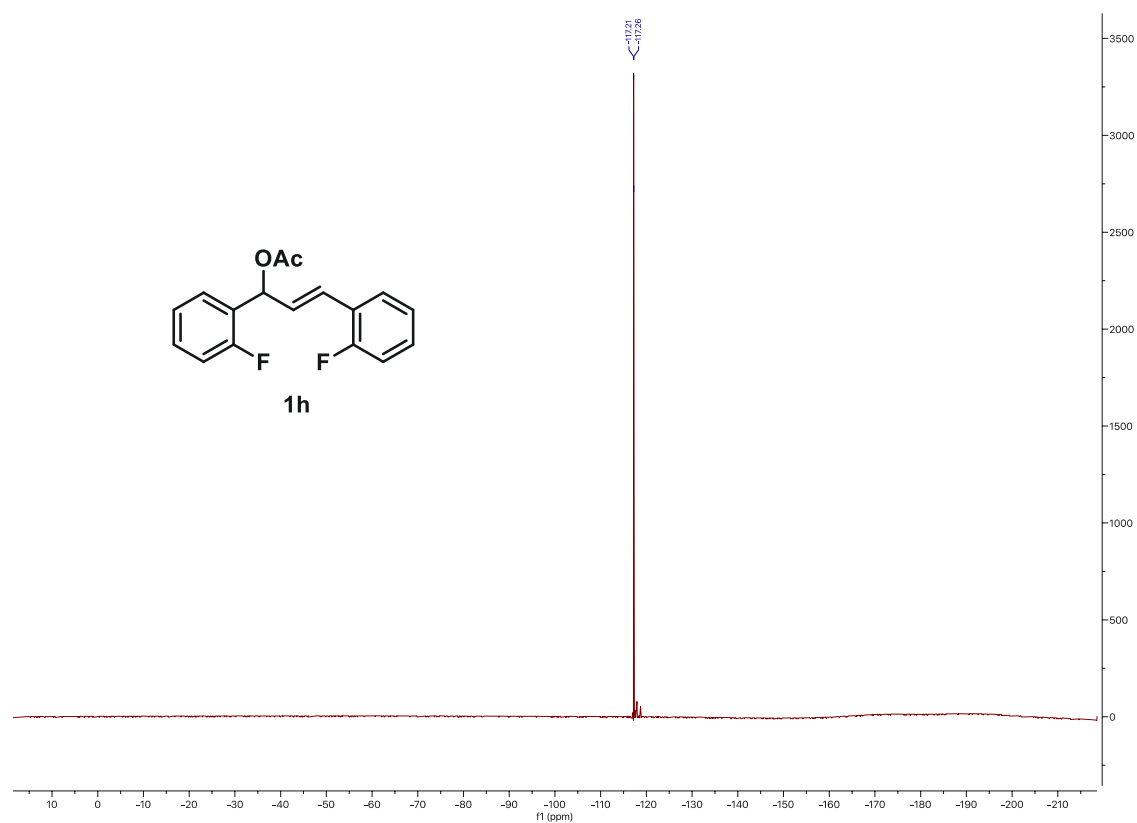


Figure 153. ¹⁹F NMR spectrum of 1h

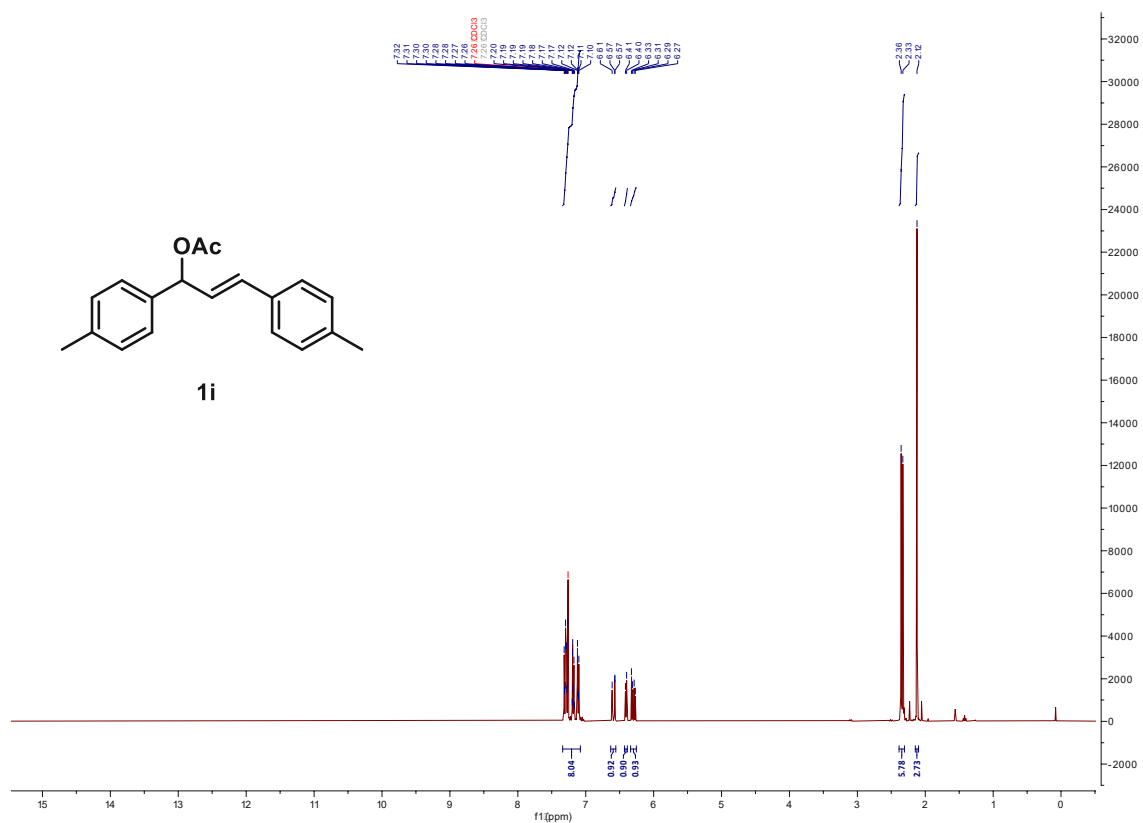


Figure 154. ¹H NMR spectrum of 1i

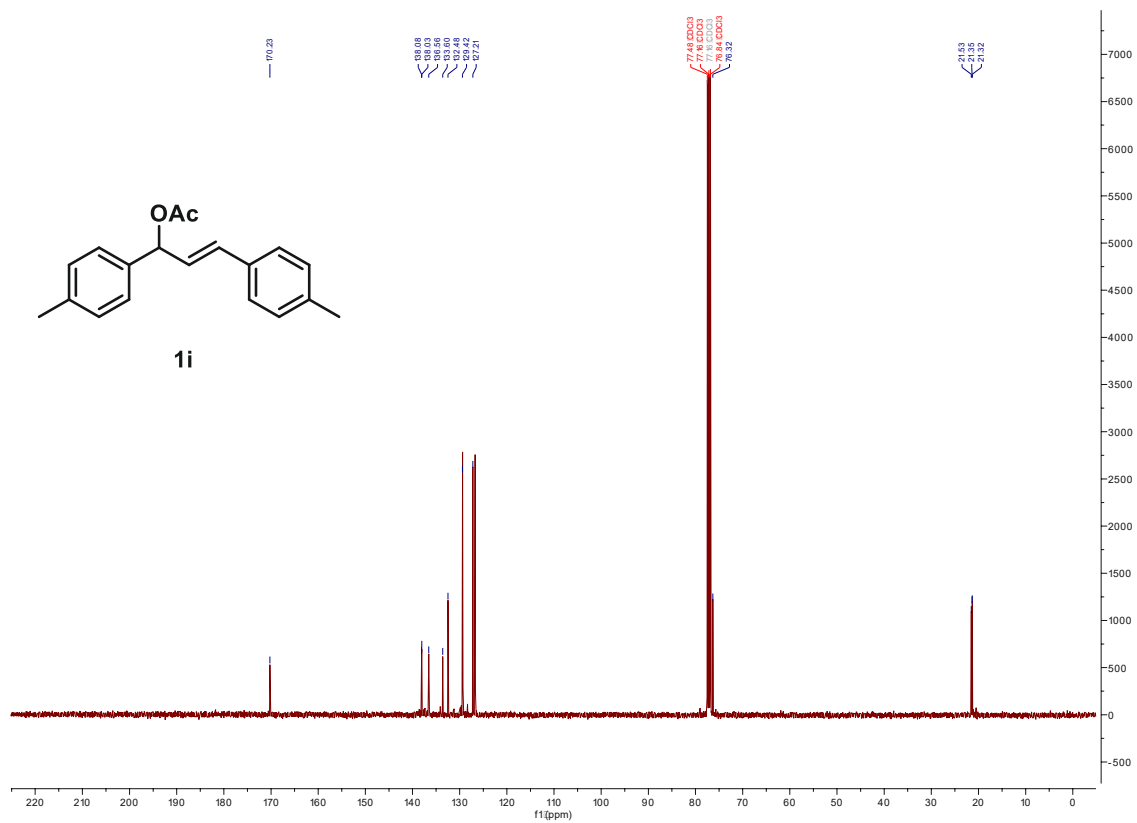


Figure 155. ¹³C NMR spectrum of 1i

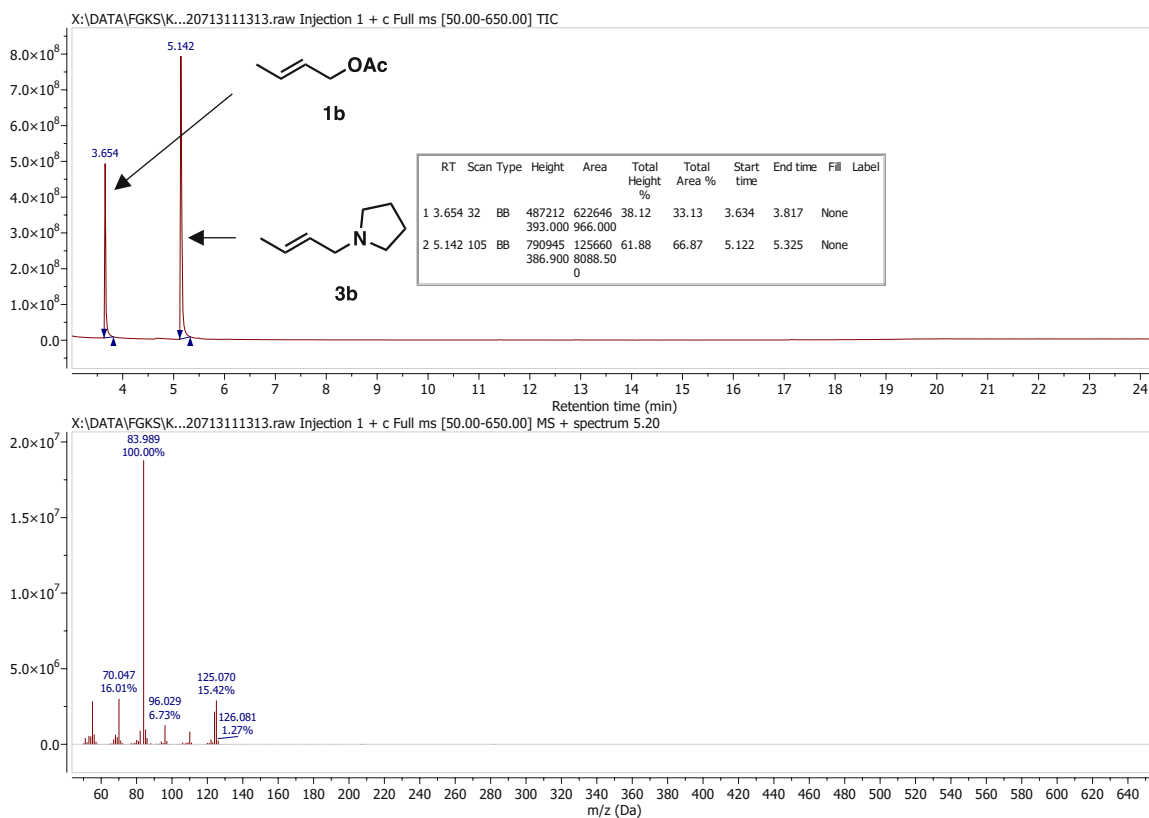


Figure 158. GC-MS chromatogram of **3b**

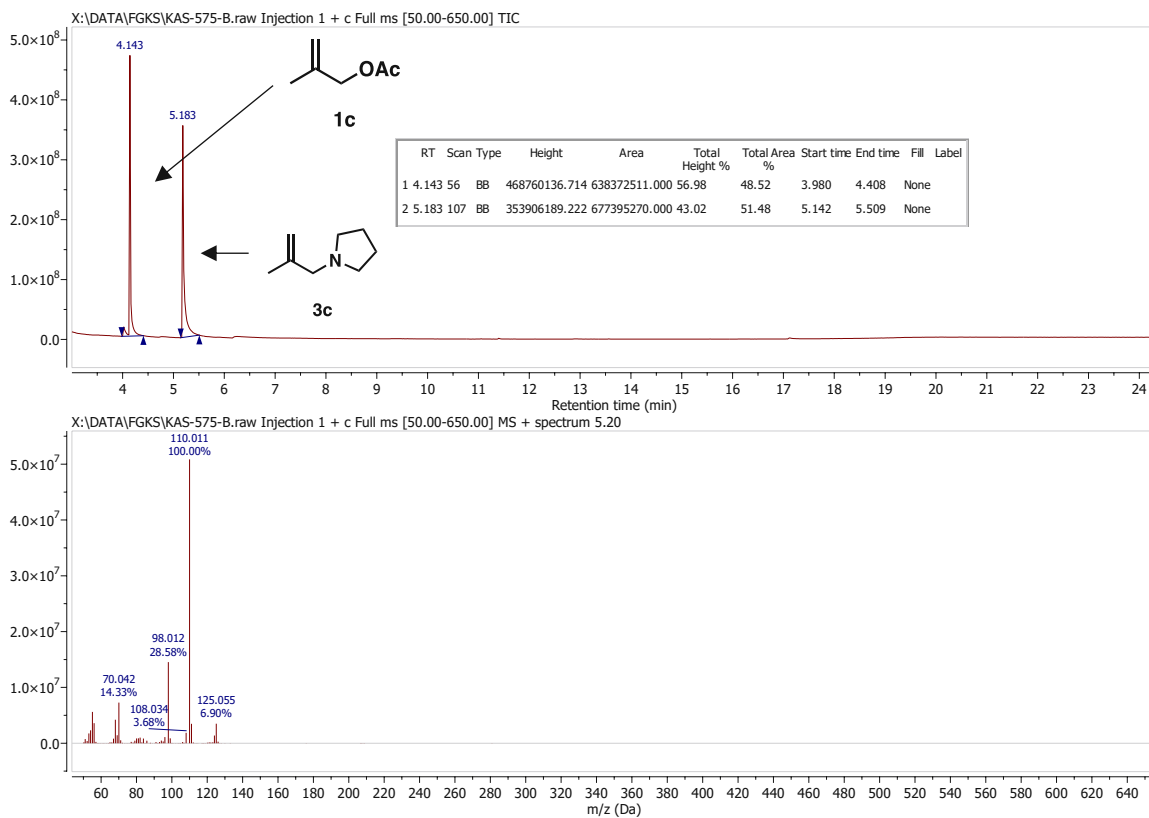


Figure 159. GC-MS chromatogram of **3c**

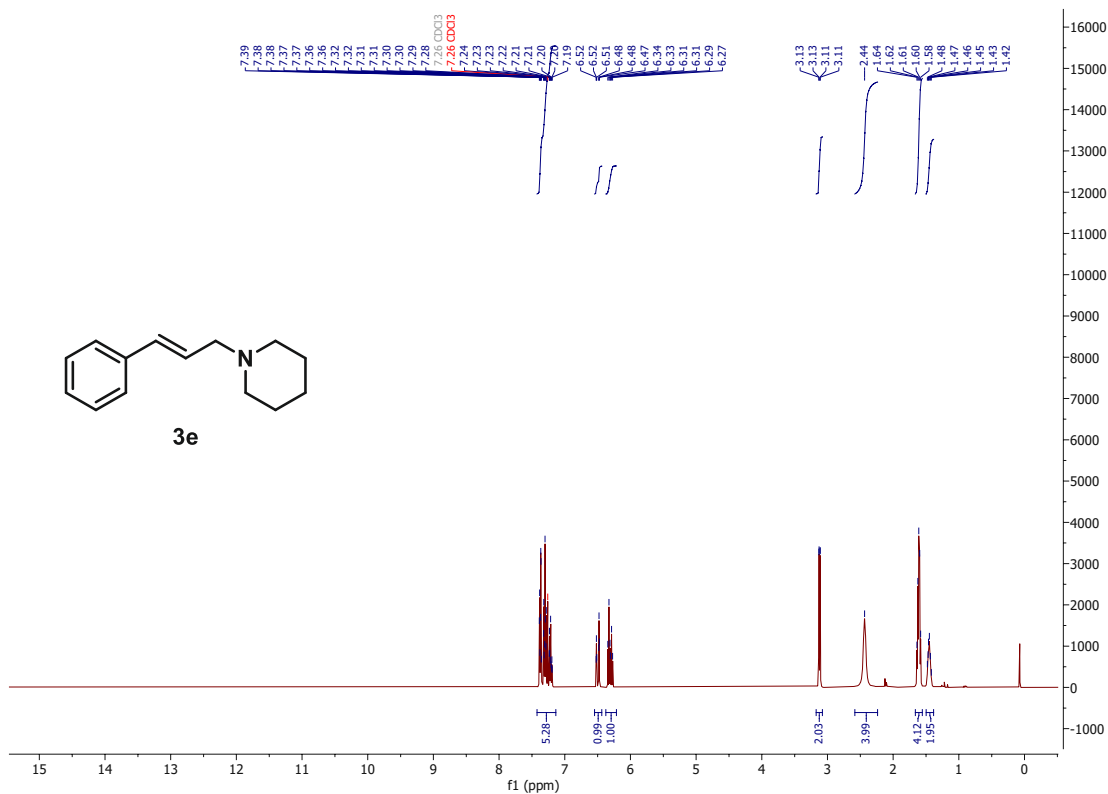


Figure 162. ¹H NMR spectrum of 3e

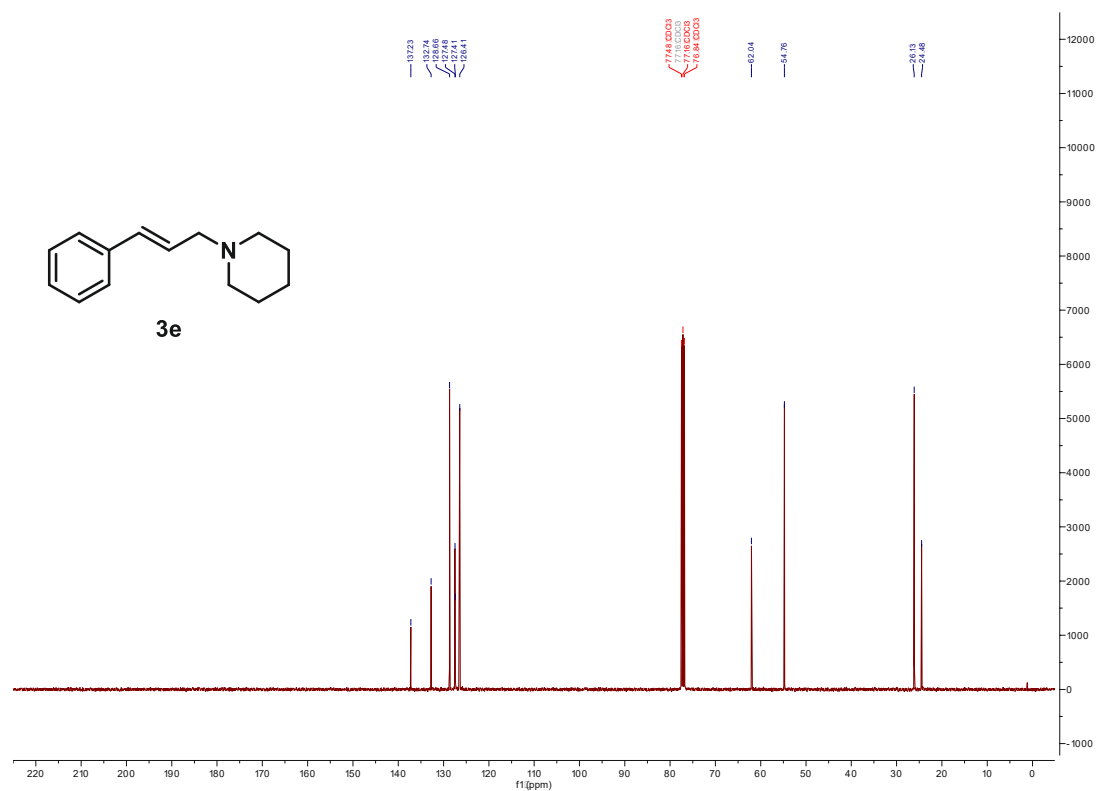


Figure 163. ¹³C NMR spectrum of 3e

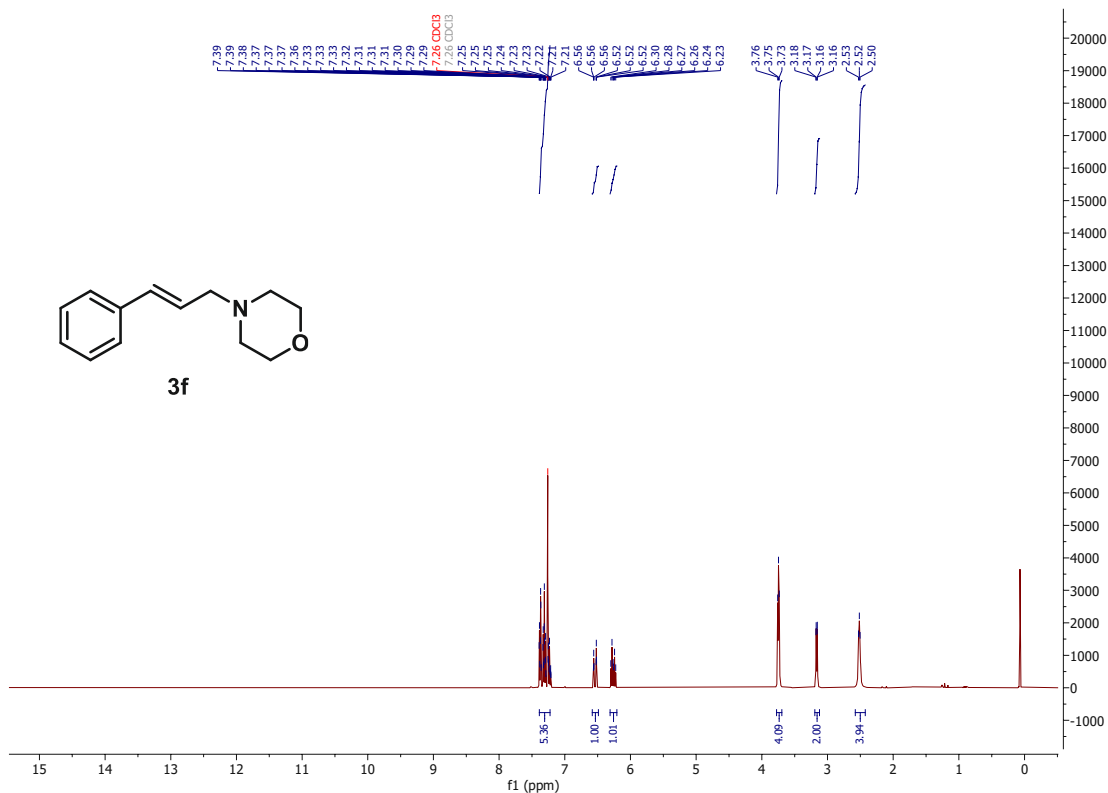


Figure 164. ^1H NMR spectrum of **3f**

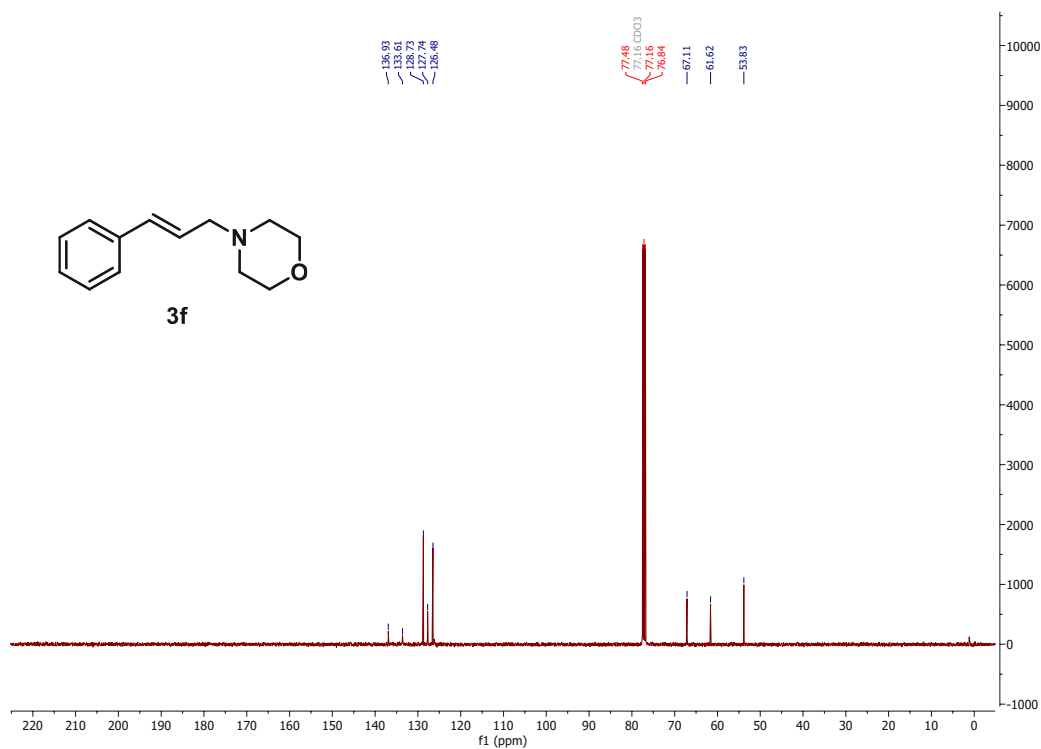


Figure 165. ^{13}C NMR spectrum of **3f**

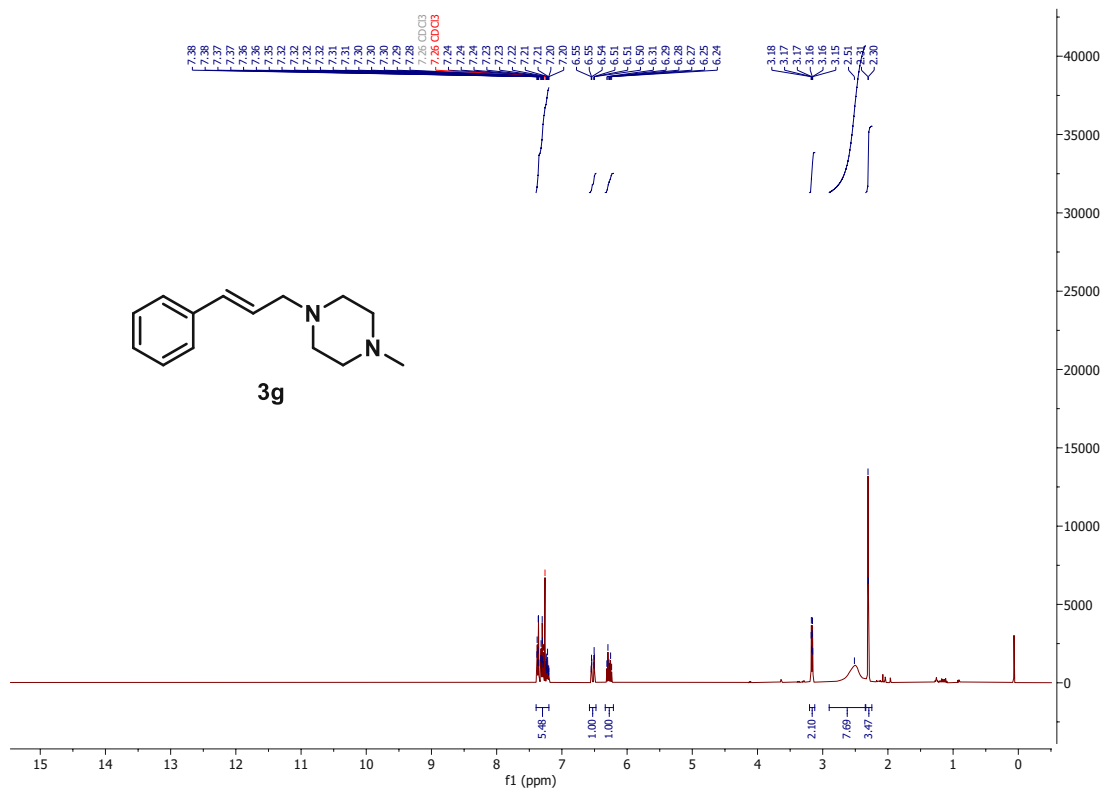


Figure 166. ¹H NMR spectrum of 3g

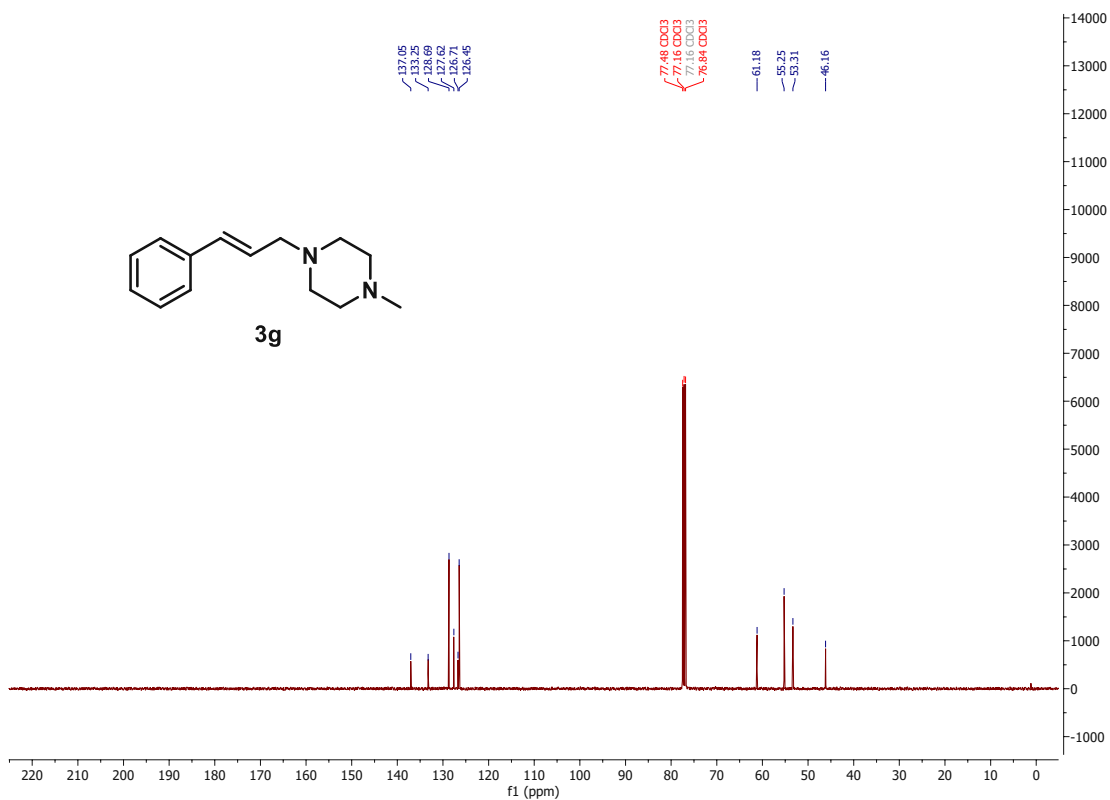


Figure 167. ¹³C NMR spectrum of 3g

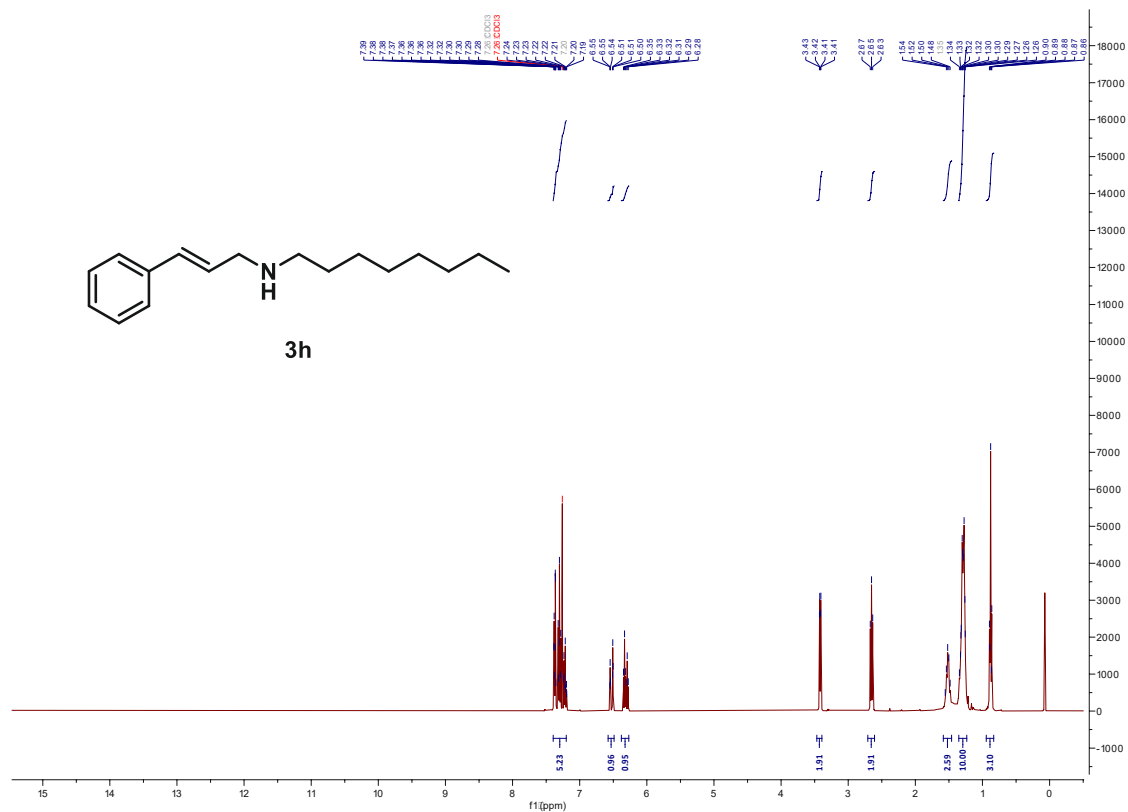


Figure 168. ^1H NMR spectrum of **3h**

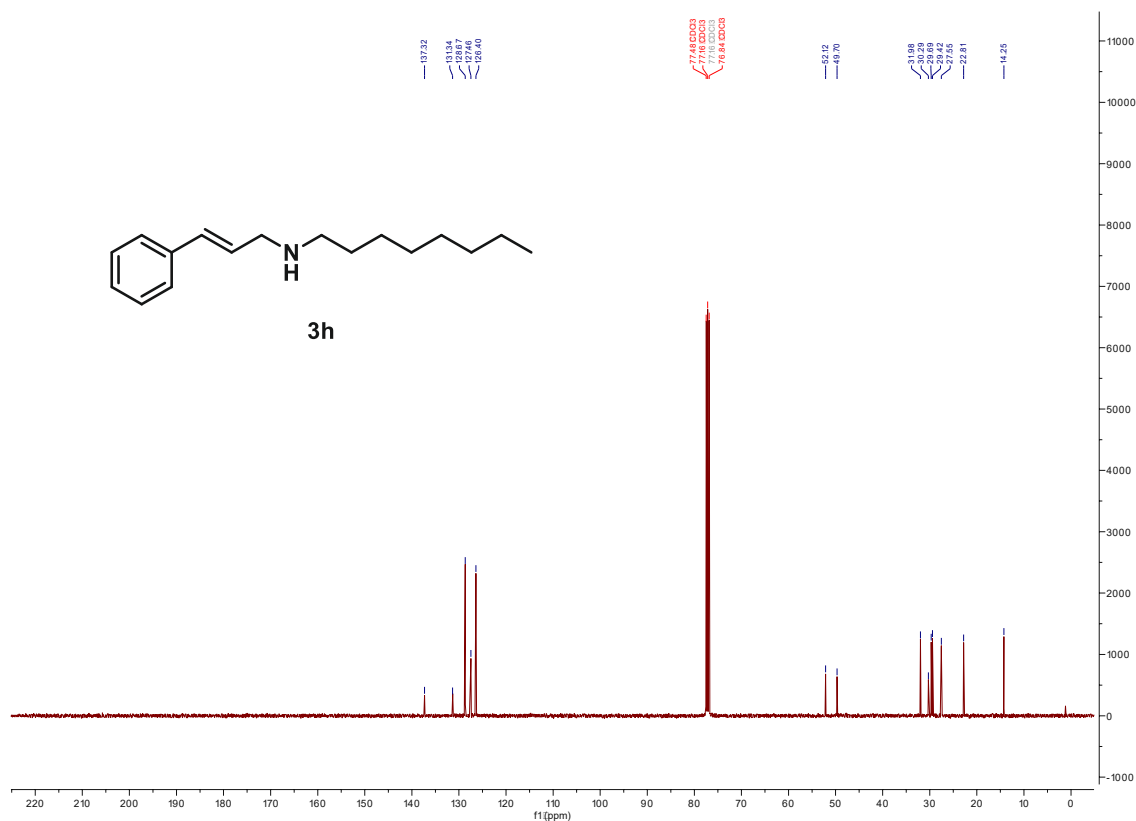


Figure 169. ^{13}C NMR spectrum of **3h**

9.11 NMR spectra of chiral ligands

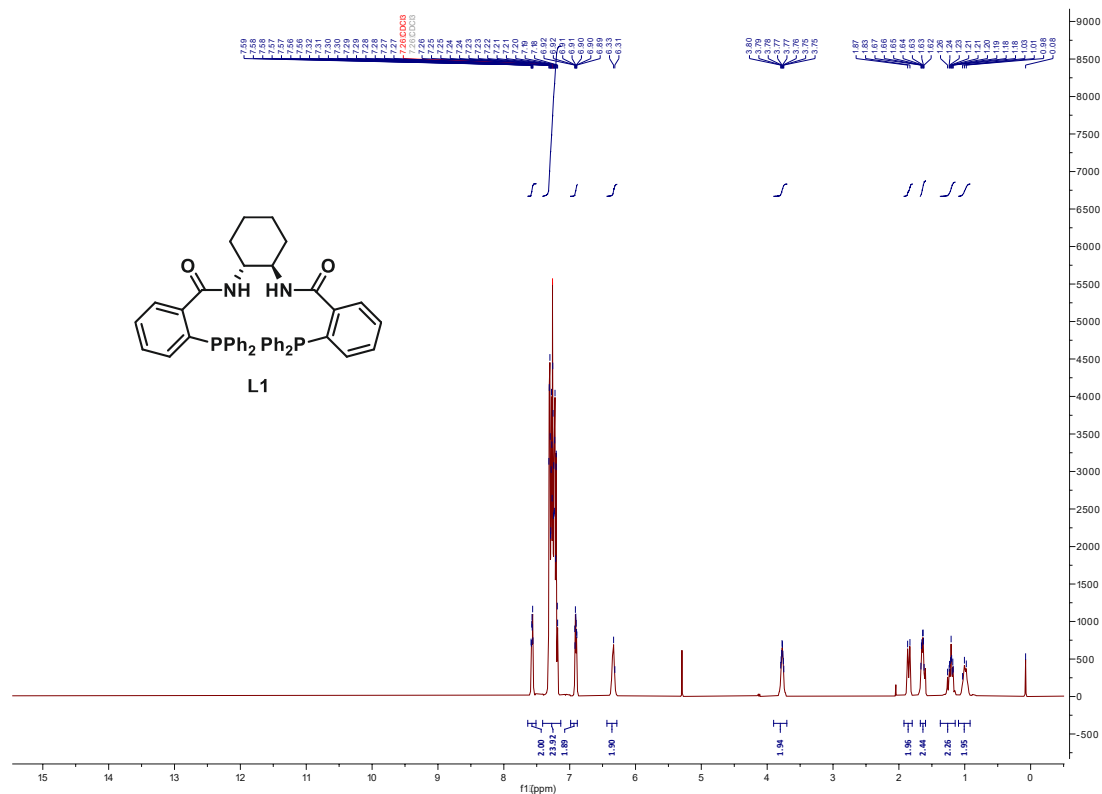
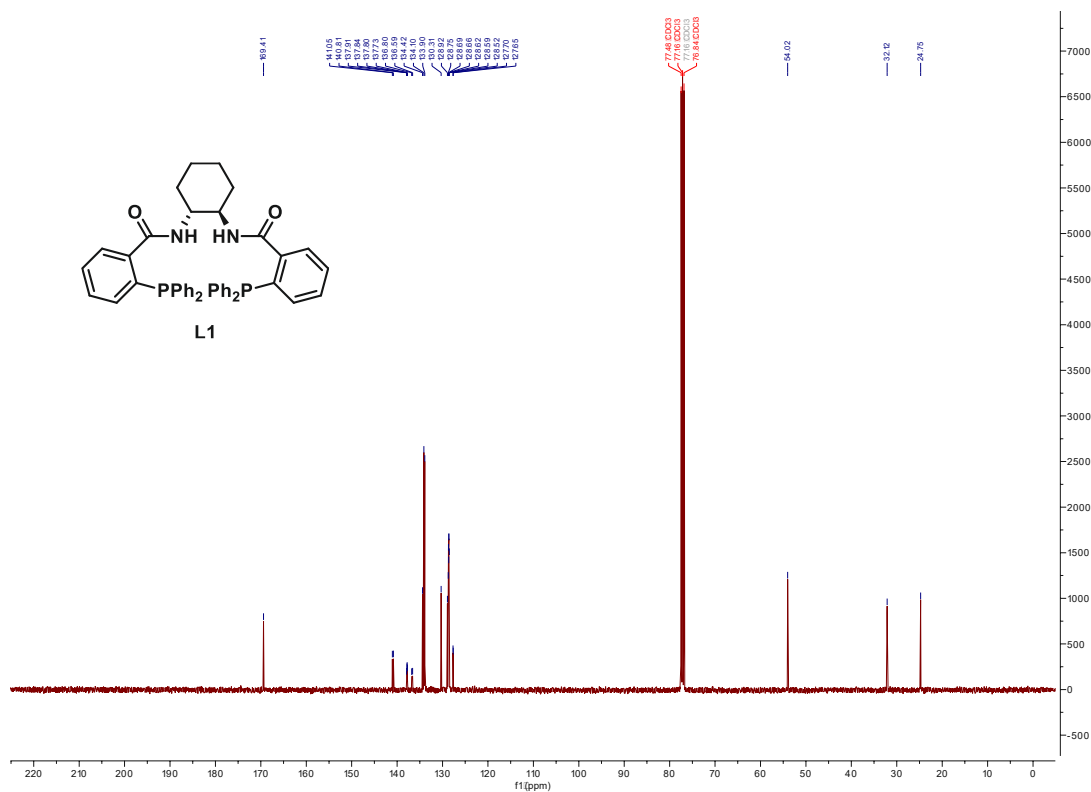
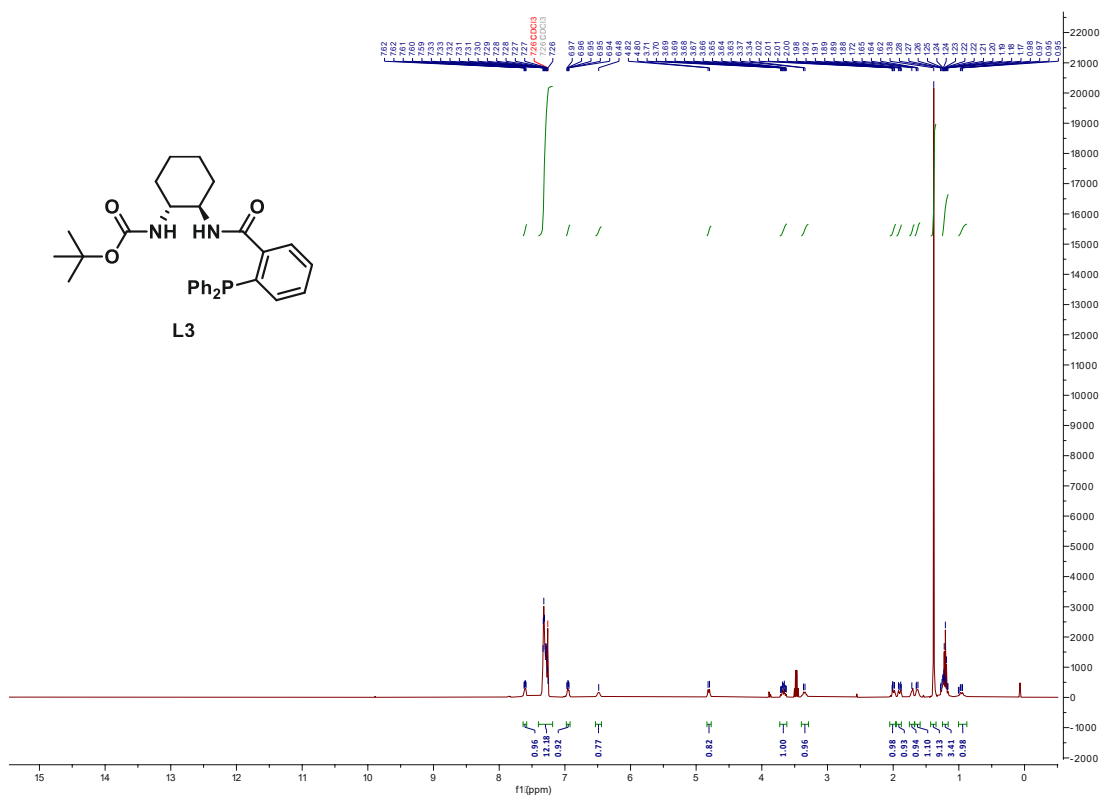
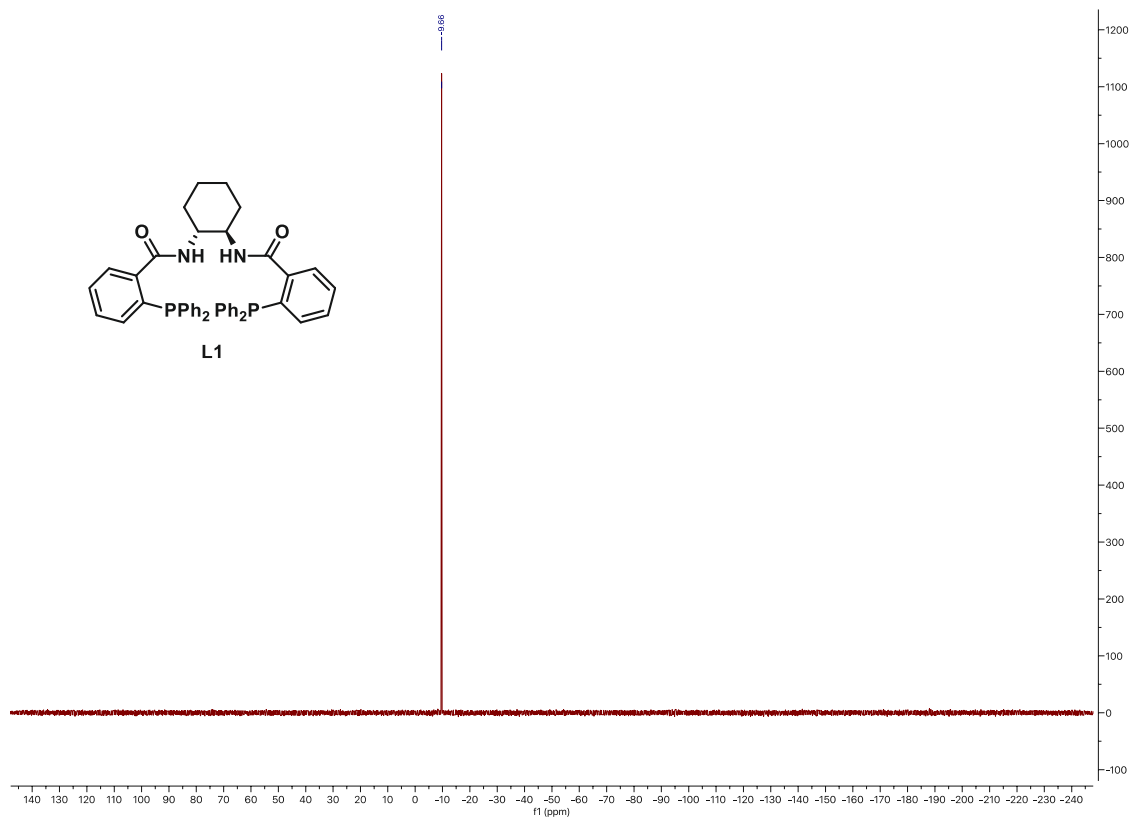


Figure 170. ^1H NMR spectrum of L1





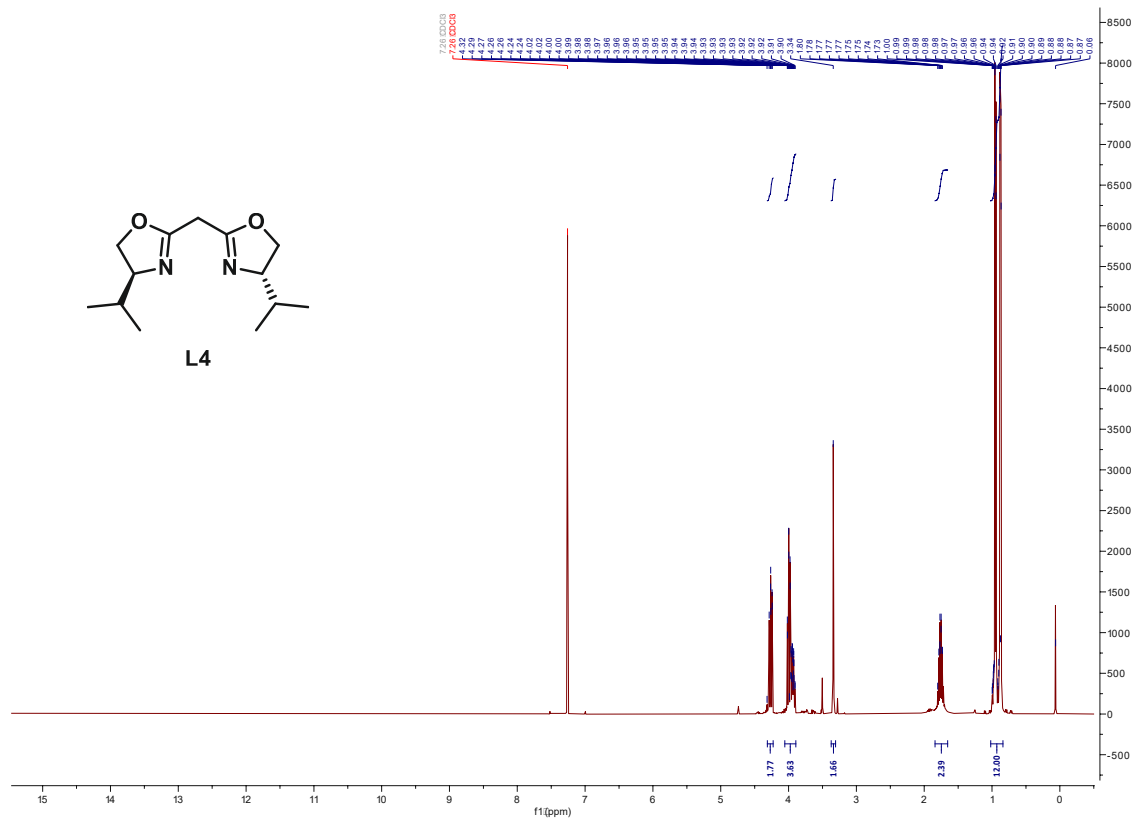


Figure 176. ^1H NMR spectrum of L4

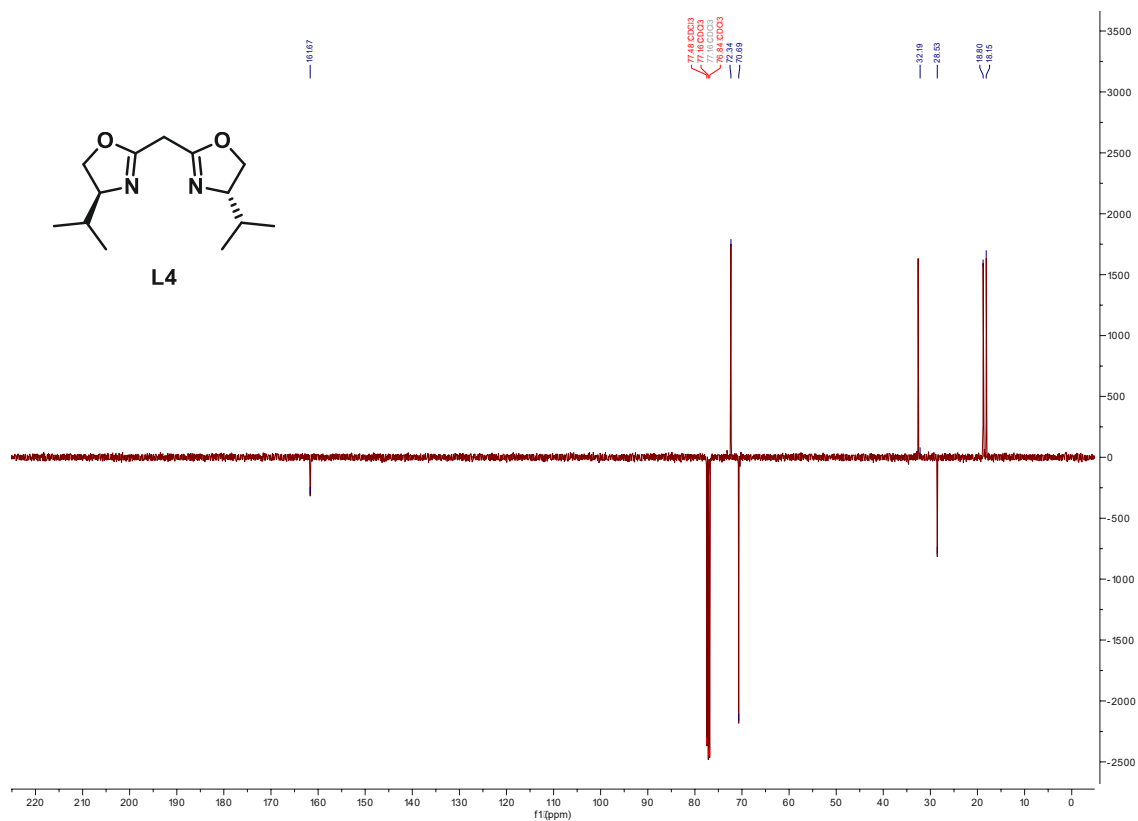


Figure 177. ^{13}C NMR of L4 (APT)

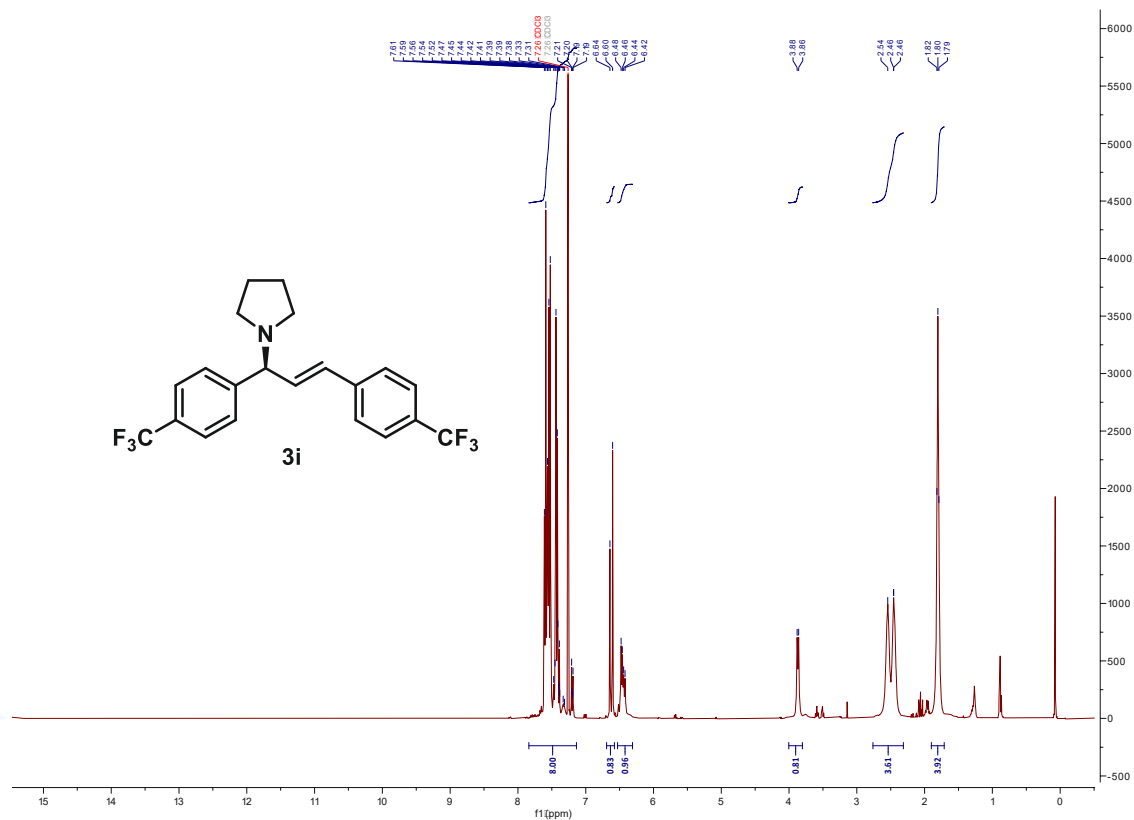


Figure 180. ^1H NMR spectrum of **3i**

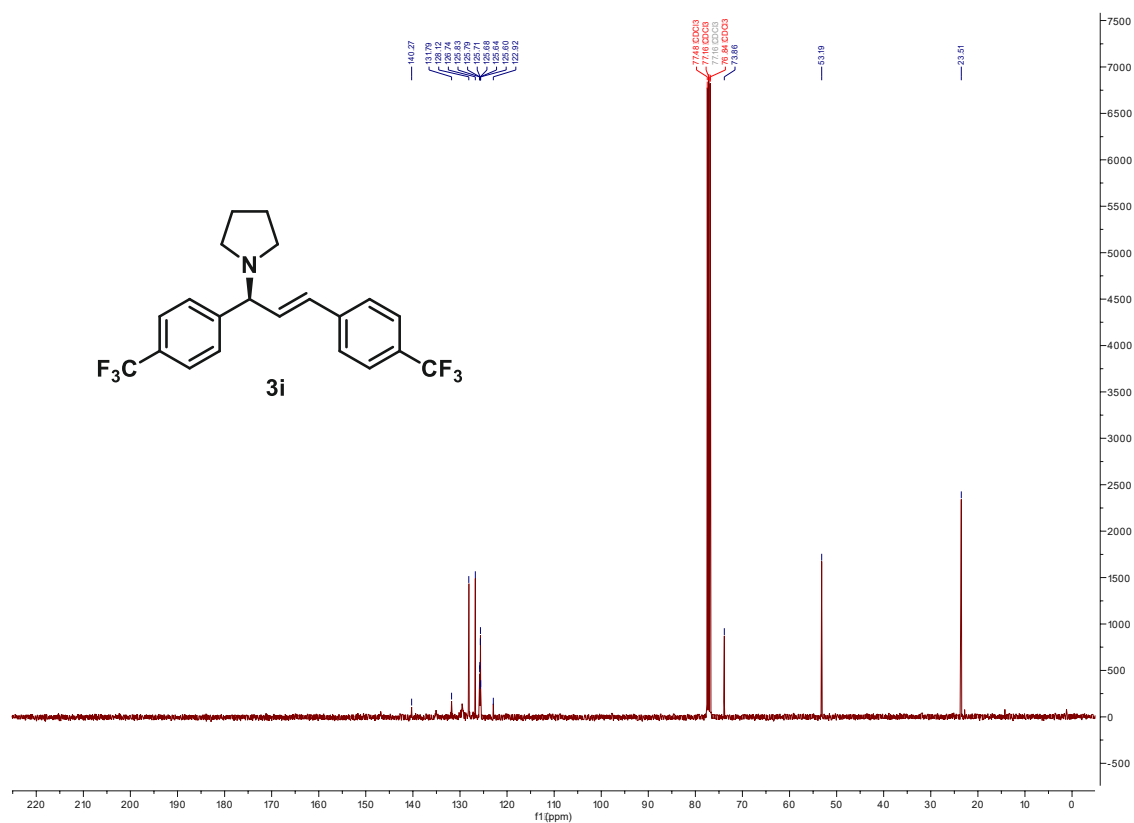
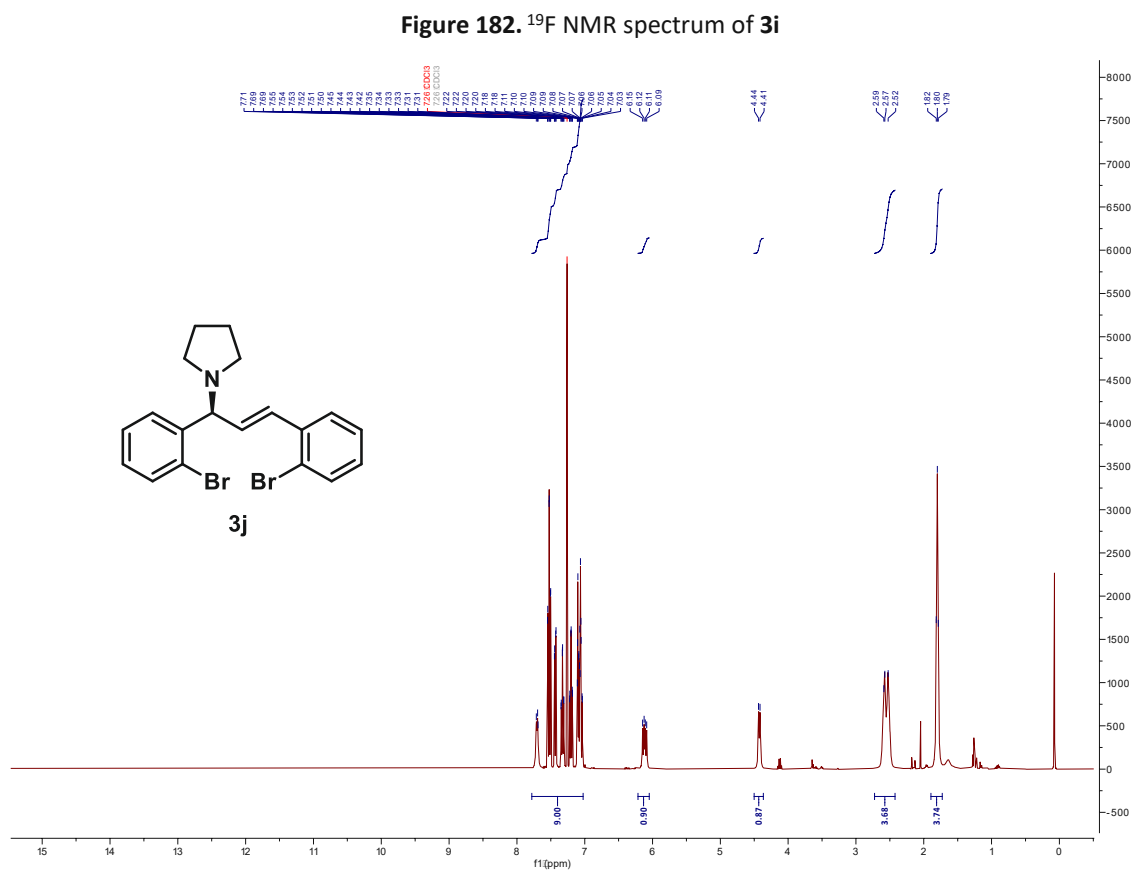
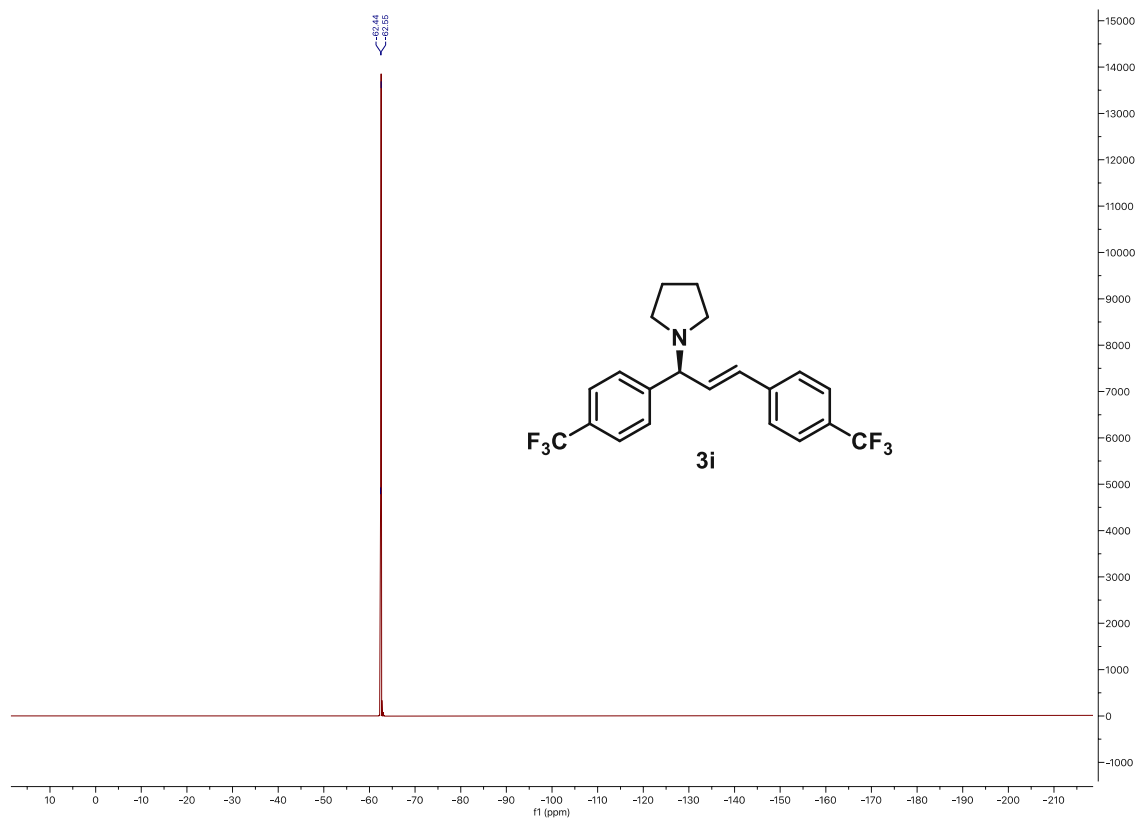


Figure 181. ^{13}C NMR spectrum of **3i**



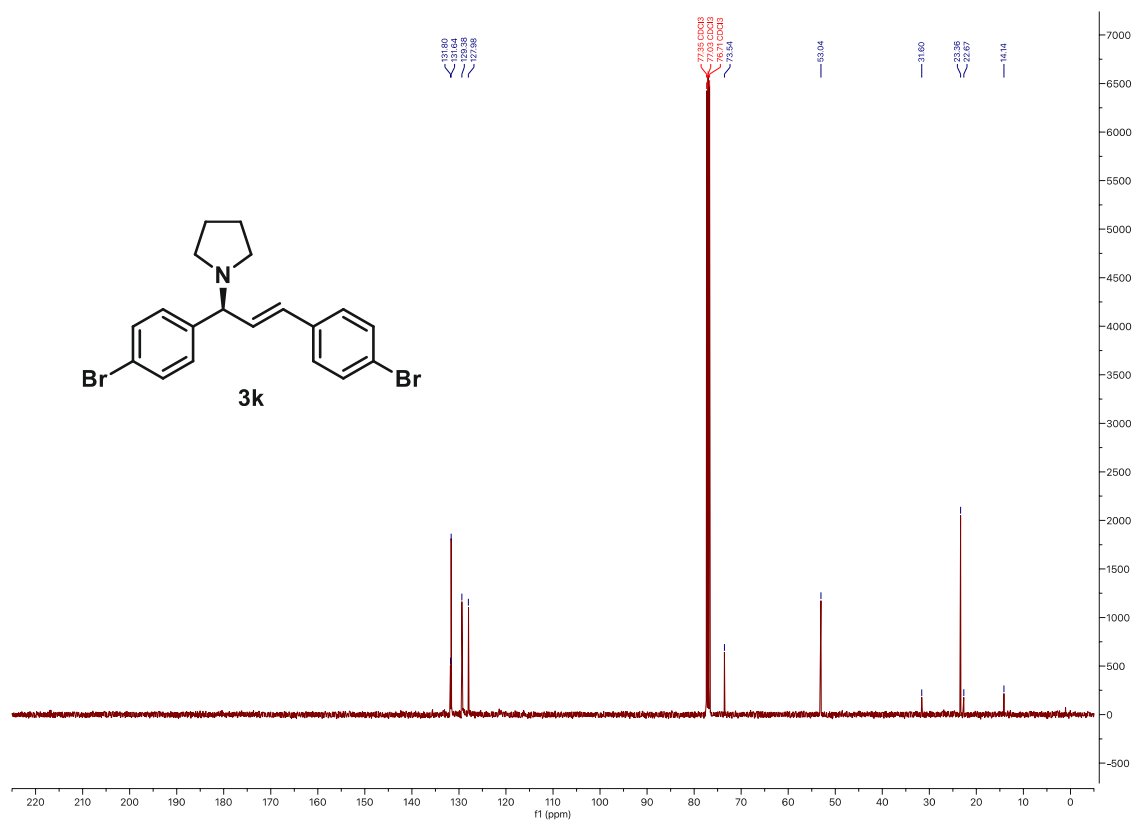


Figure 186. ¹³C NMR spectrum of **3k**

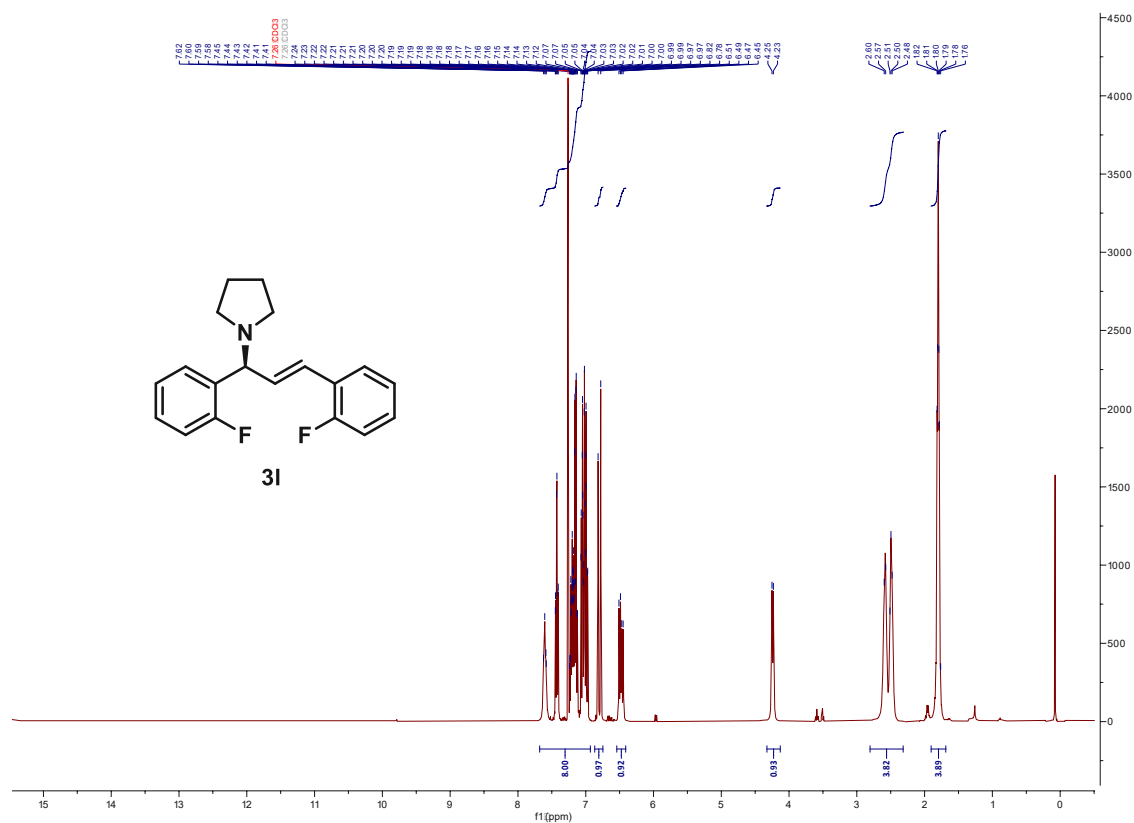


Figure 187. ¹H NMR spectrum of **3l**

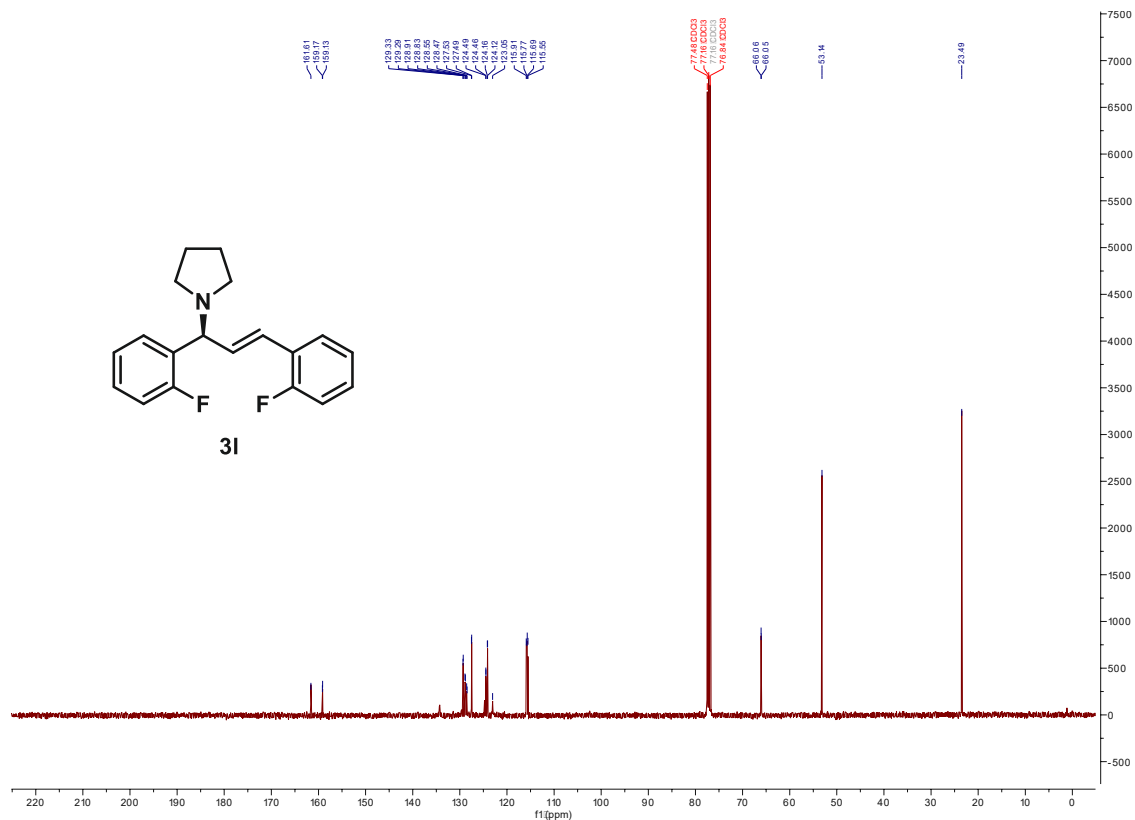


Figure 188. ¹³C NMR spectrum of 3I

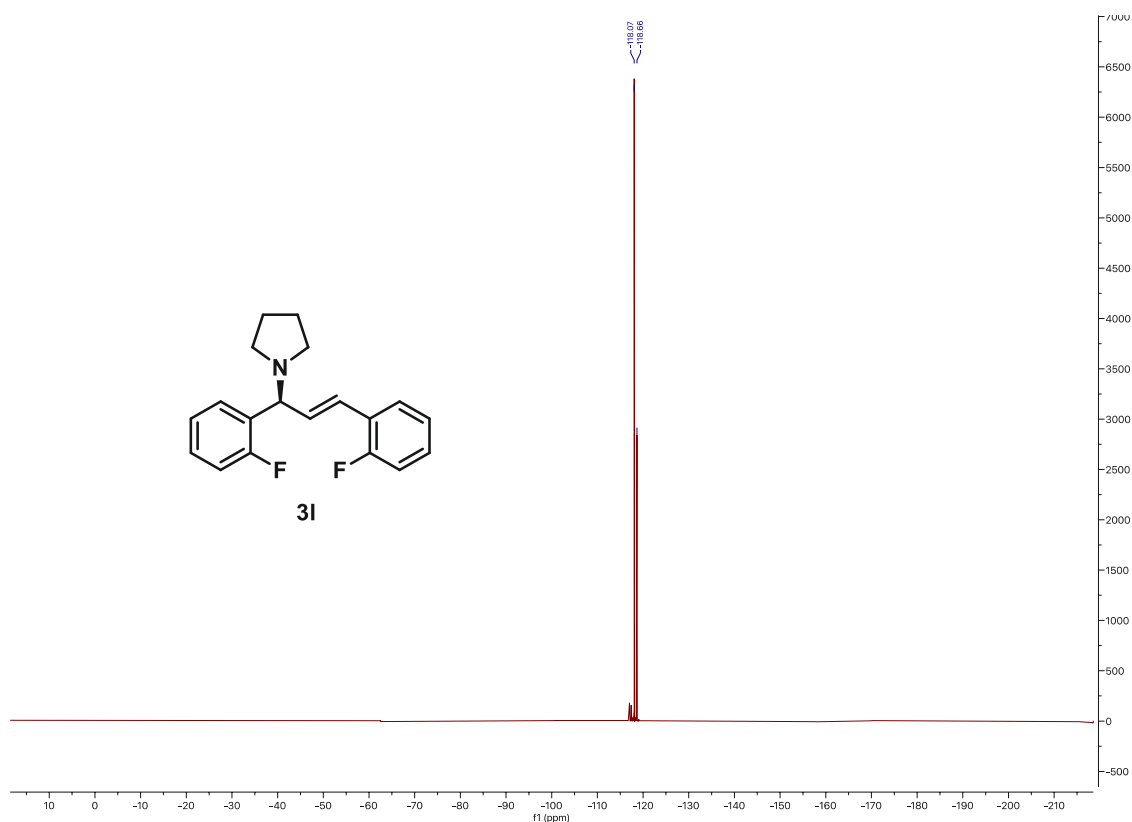


Figure 189. ¹⁹F NMR spectrum of 3I

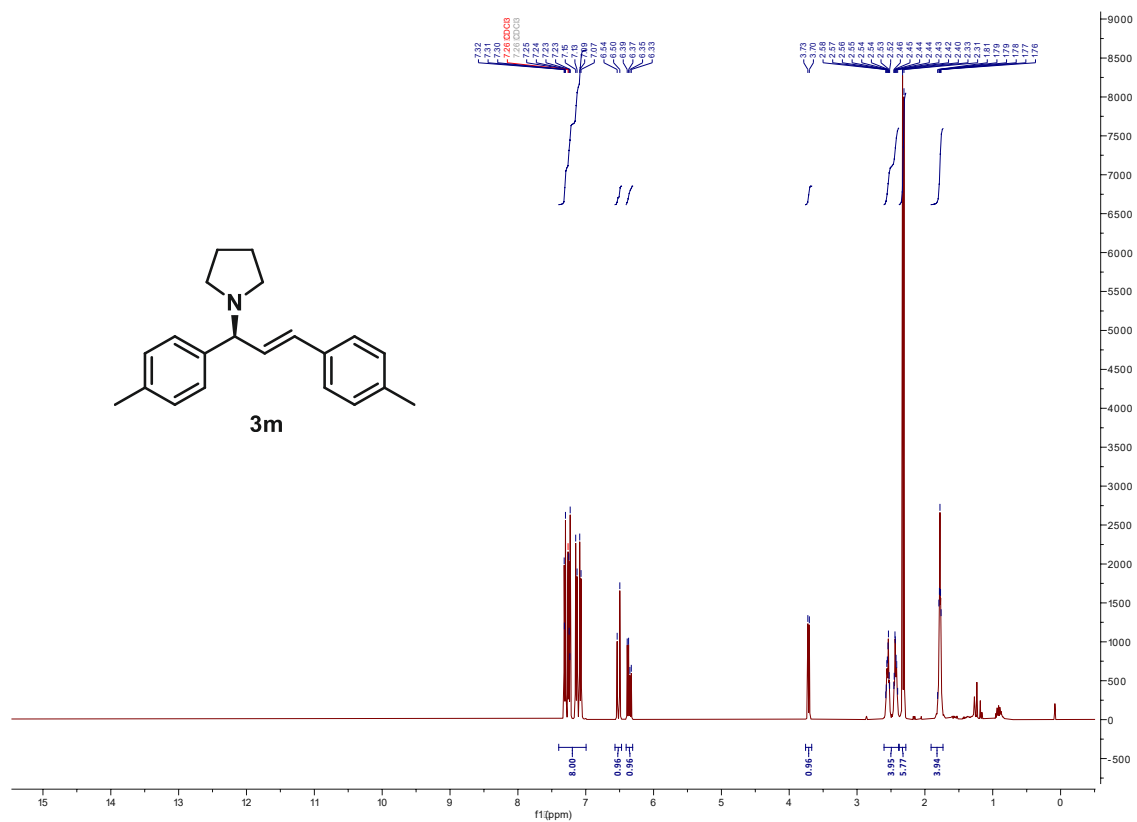


Figure 190. ¹H NMR spectrum of 3m

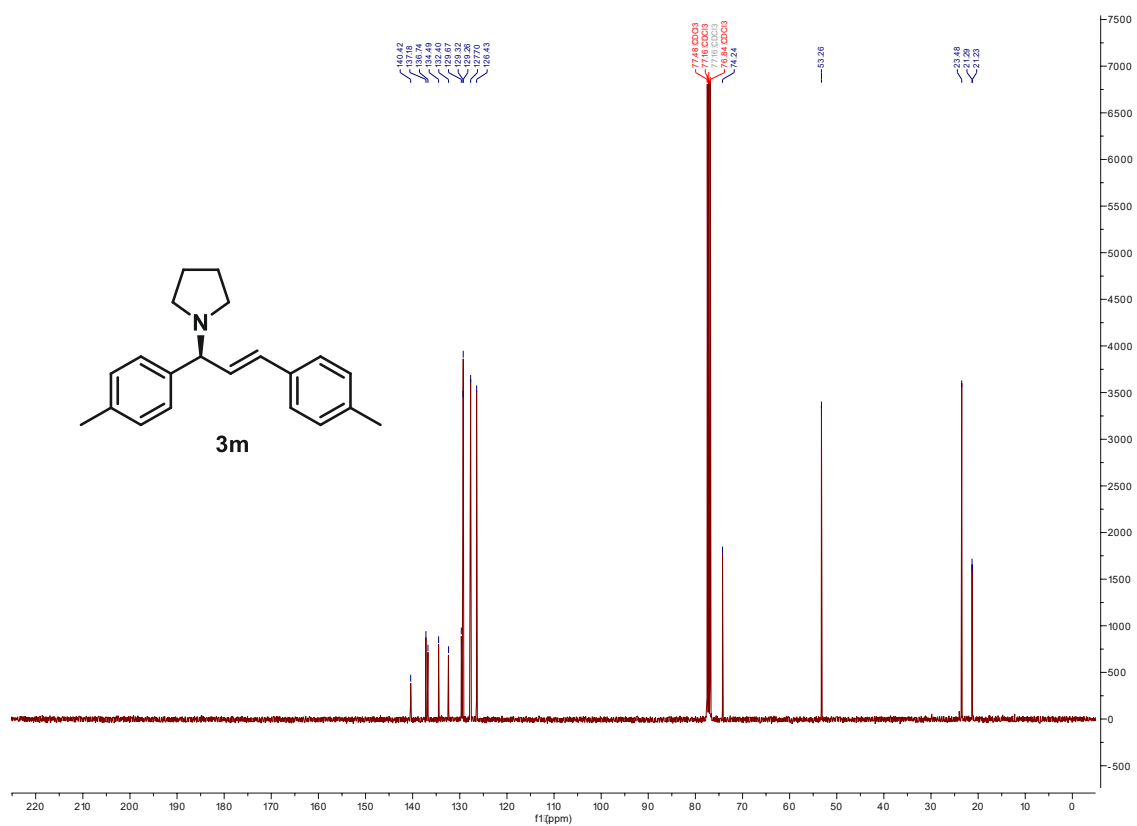
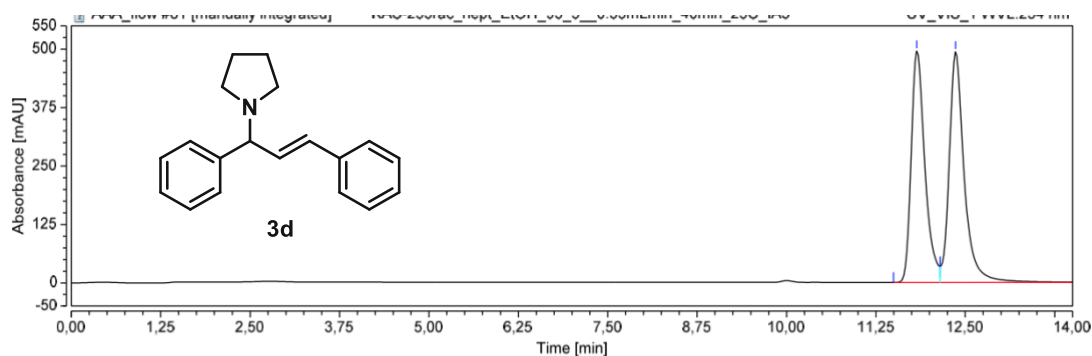


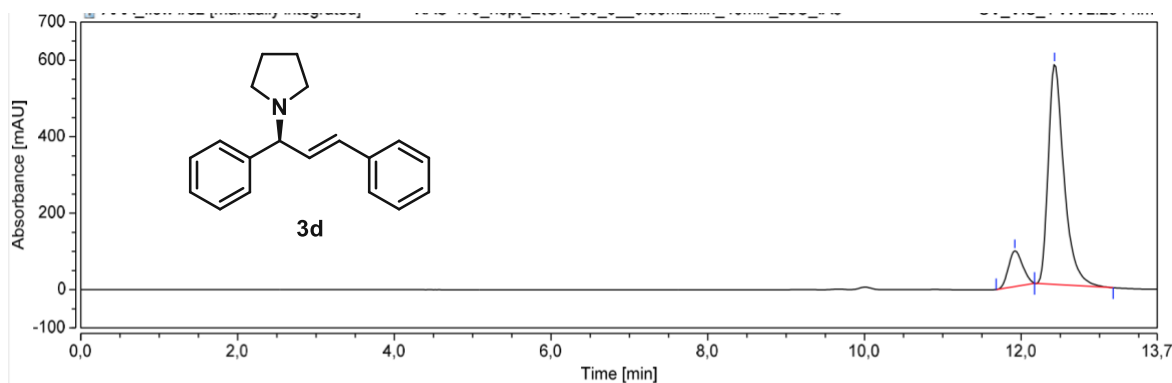
Figure 191. ¹³C NMR spectrum of 3m

9.13 Chiral HPLC traces



Integration Results							
No.	Peak Name	Retention Time min	Area mAU*min	Height mAU	Relative Area %	Relative Height %	Amount n.a.
1		11,823	109,371	495,556	47,63	50,09	n.a.
2		12,363	120,237	493,708	52,37	49,91	n.a.
Total:			229,608	989,264	100,00	100,00	

Figure 192. Chiral HPLC chromatogram of **3d** (racemic)



Integration Results							
No.	Peak Name	Retention Time min	Area mAU*min	Height mAU	Relative Area %	Relative Height %	Amount n.a.
1		11,920	19,557	93,447	12,68	13,94	n.a.
2		12,427	134,709	576,750	87,32	86,06	n.a.
Total:			154,267	670,197	100,00	100,00	

Figure 193. Chiral HPLC chromatogram of **3d** (enantioenriched)

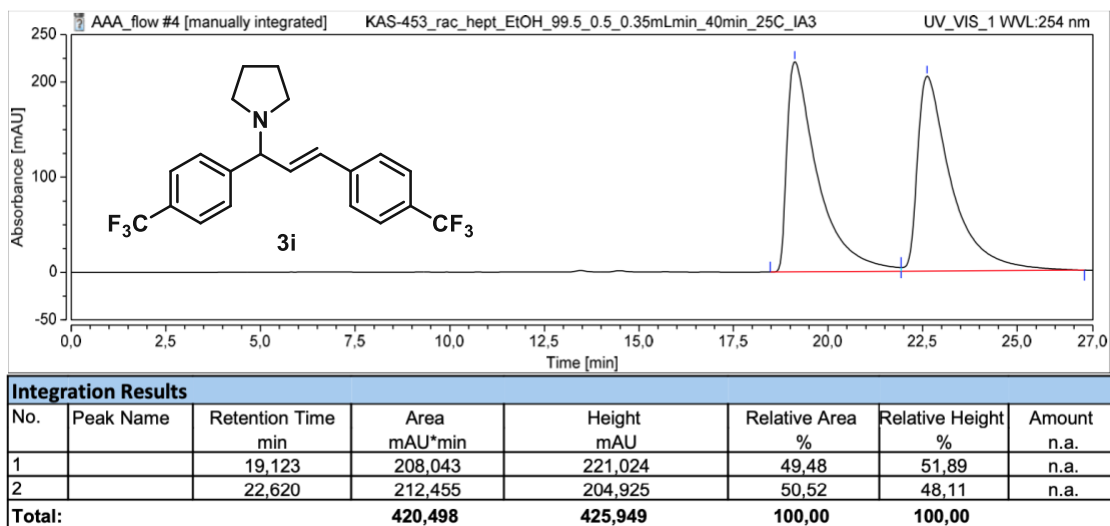


Figure 194. Chiral HPLC chromatogram of **3i** (racemic)

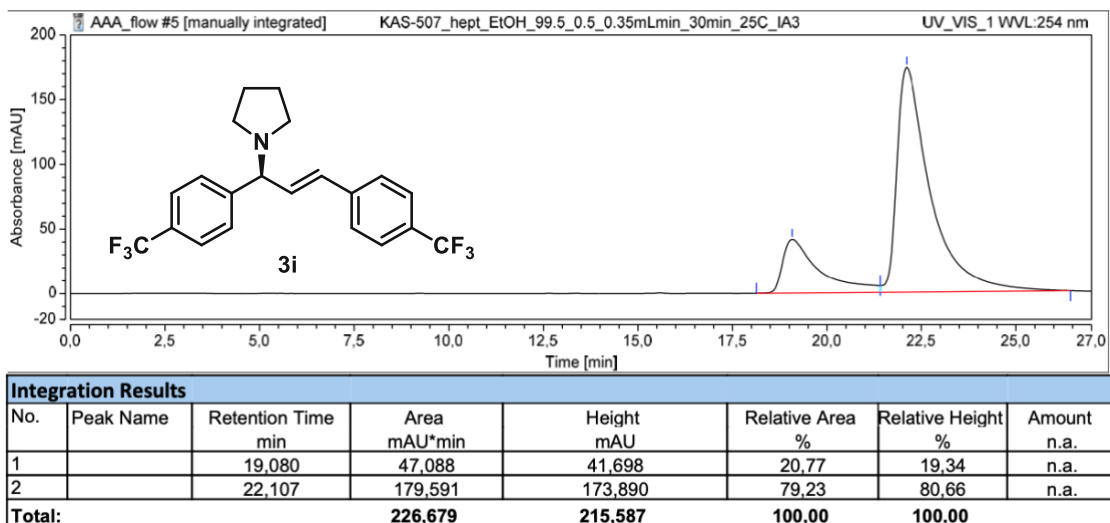


Figure 195. Chiral HPLC chromatogram of **3i** (enantioenriched)

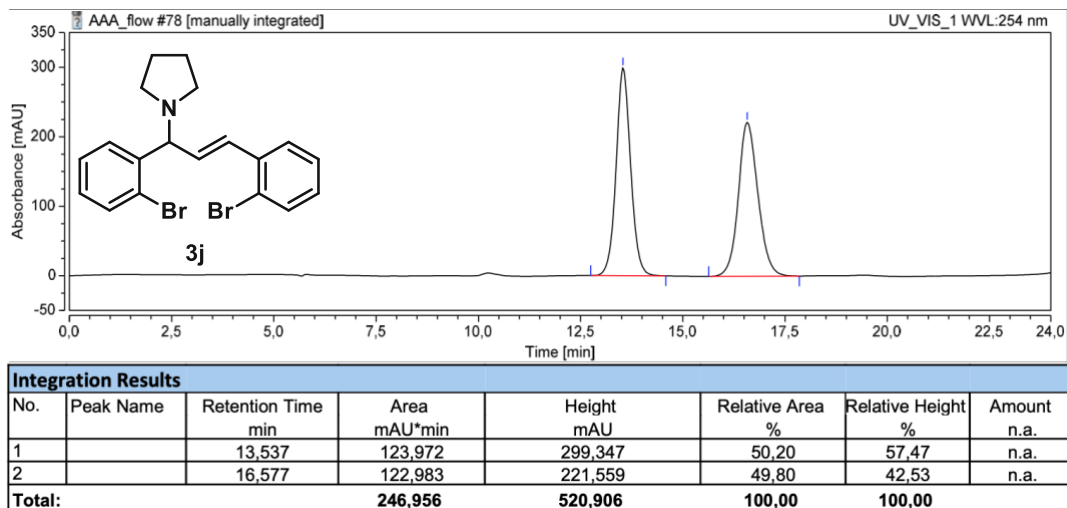


Figure 196. Chiral HPLC chromatogram of **3j** (racemic)

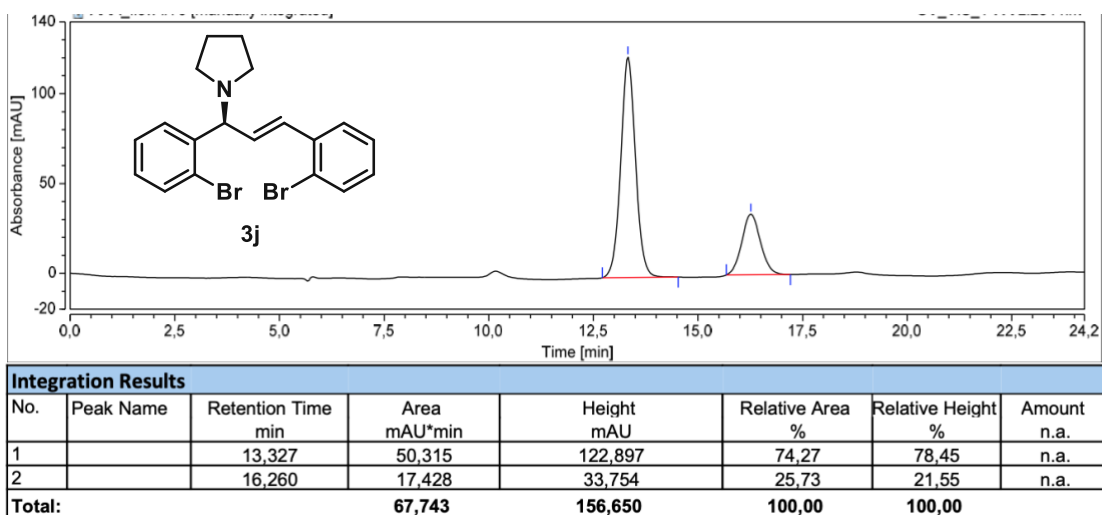


Figure 197. Chiral HPLC chromatogram of **3j** (enantioenriched)

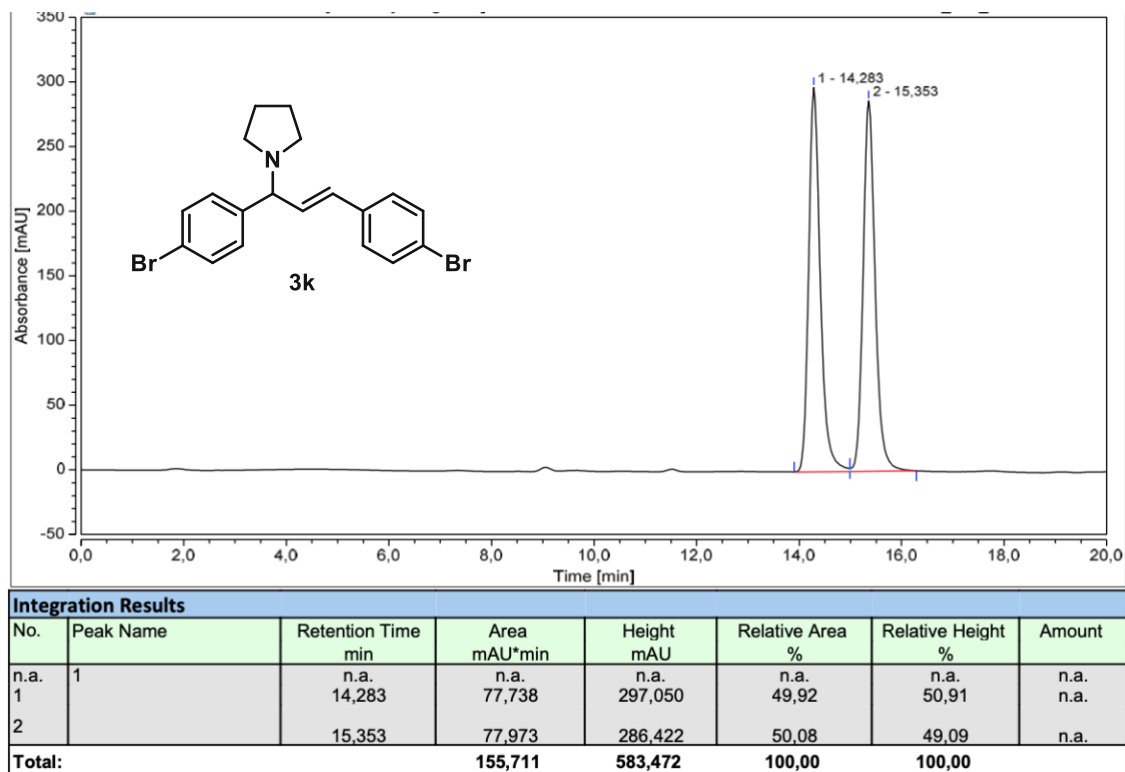


Figure 198. HPLC chromatogram of **3k** (racemic)

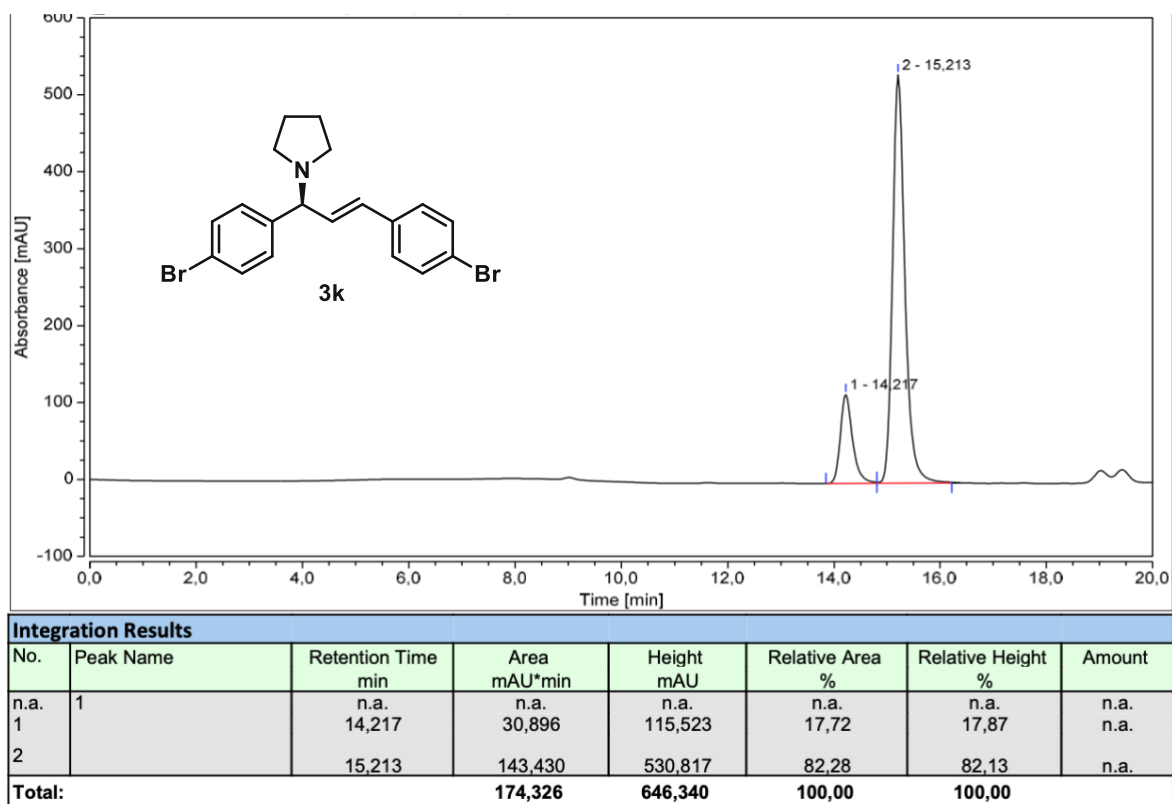


Figure 199. HPLC chromatogram of **3k** (enantiomeriched)

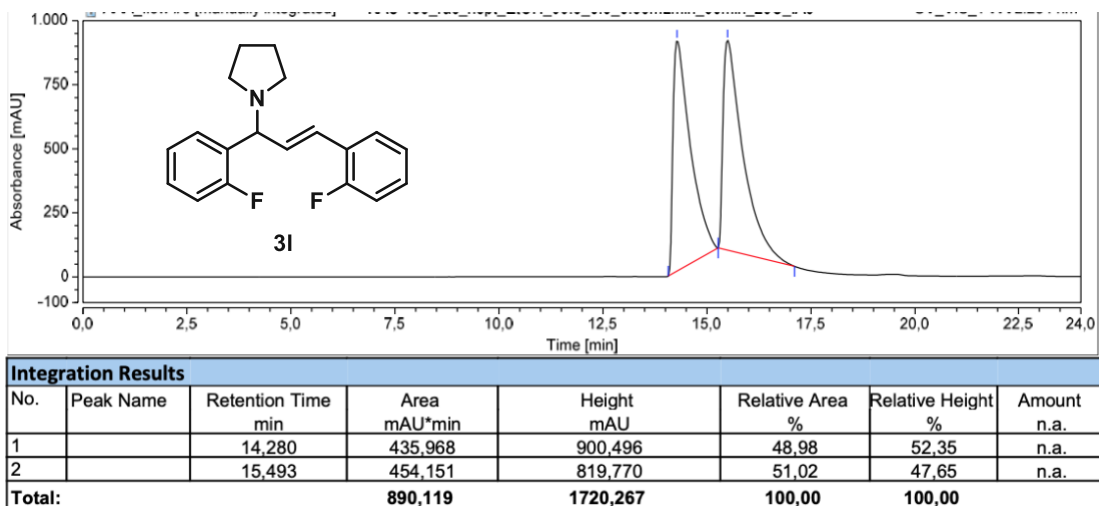


Figure 200. Chiral HPLC chromatogram of **3I** (racemic)

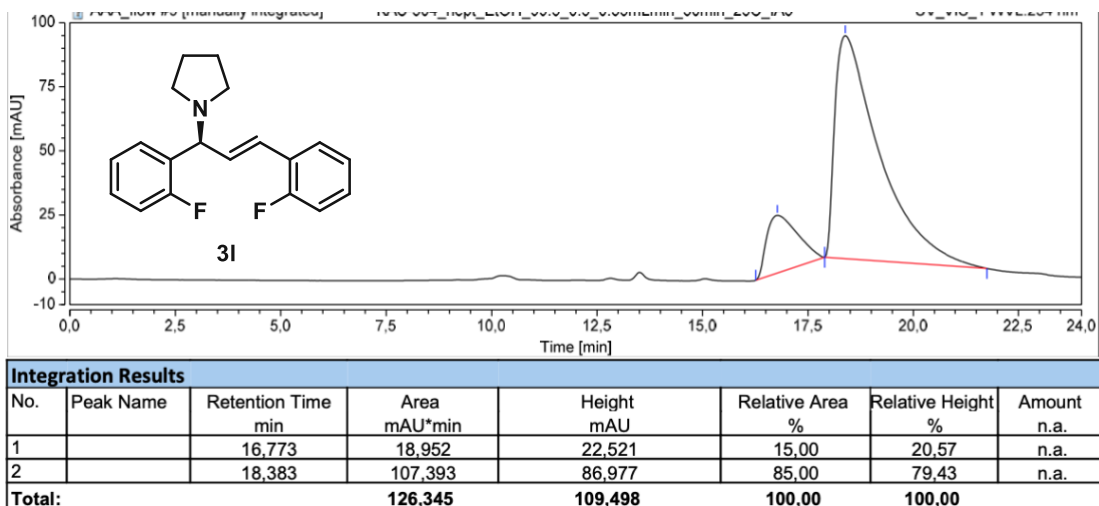


Figure 201. Chiral HPLC chromatogram of **3I** (enantioenriched)

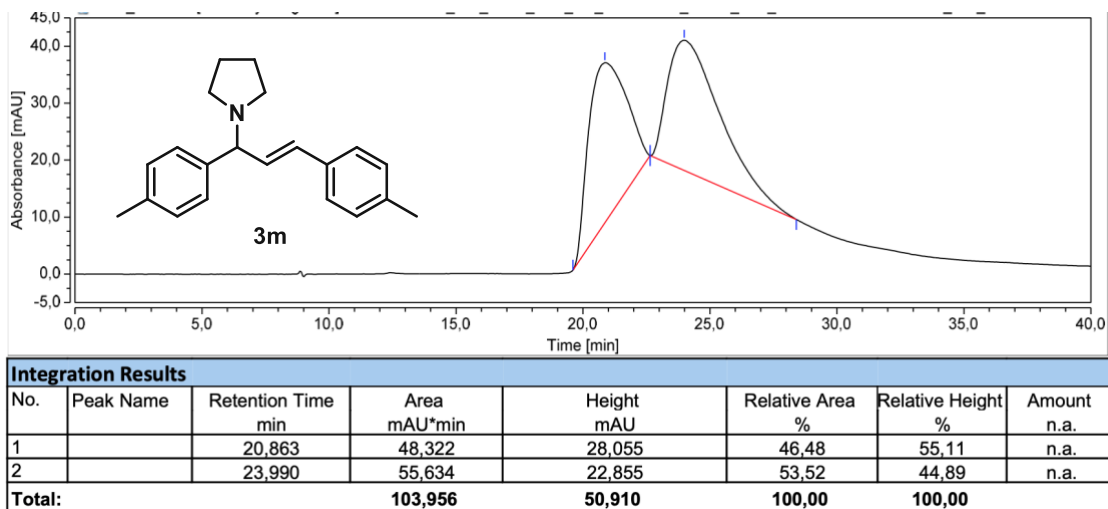


Figure 202. HPLC chromatogram of **3m** (racemic)

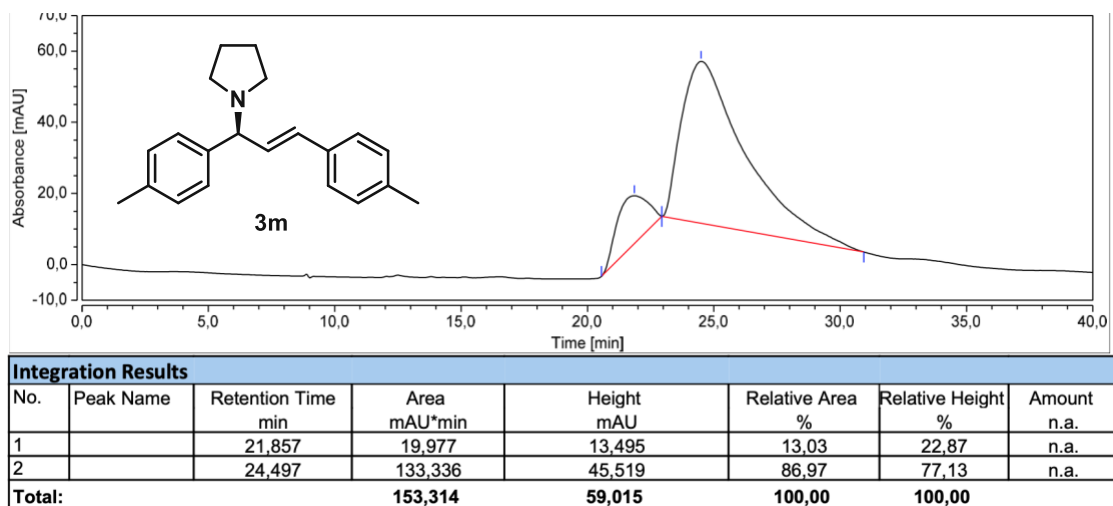


Figure 203. HPLC chromatogram of **3m** (enantioenriched)

10. Appendix C

Supporting Information

Continuous Synthesis of Carbamates from CO₂ and Amines

Kristof Stigel,^a Laura Ielo,^{a,b} Michael Schnürch,^a and Katharina Bica-Schröder^a*

^aInstitute of Applied Synthetic Chemistry, TU Wien, Getreidemarkt 9/163, Vienna, 1060, Austria

^bDepartment of Chemistry, University of Turin, Via P. Giuria 7, Torino, 10125, Italy

*Corresponding author: Katharina Bica-Schröder. E-mail: katharina.schroeder@tuwien.ac.at, Tel.: +43 1 58801 163601

10.1 General remarks

Unless otherwise noted, all commercially supplied chemicals were used without further purification. Petroleum ether is 40-60 bp unless stated otherwise.

Column chromatography was performed on standard glass columns using either Merck (40-60 μm) silica or Thermo Scientific (58 angstroms) neutral aluminum oxide with pre-distilled solvents. Analytical thin-layer chromatography (TLC) was performed on pre-coated, aluminum-backed plates (Merck, silica 60 F₂₅₄ or Merck, aluminum oxide 60 F₂₅₄ neutral). All compounds were visualized at 254 nm unless otherwise mentioned.

¹H-, ¹³C- and ¹⁹F spectra were recorded from CDCl₃ solutions on a Bruker Avance UltraShield 400 MHz (¹H: 400 MHz, ¹³C: 101 MHz, ¹⁹F: 376 MHz) NMR instrument. Chemical shifts are reported in parts per million (ppm) from Me₄Si and were calibrated to the residual solvent signal (e.g., CDCl₃, ¹H: 7.26 ppm, ¹³C: 77.0 ppm). Coupling constants are reported in hertz (Hz). The assignments are based on the comparison with reported spectra.

High-resolution mass spectrometry (HRMS) was carried out using an Agilent 1100/1200 HPLC with a 6230 AJS ESI-TOF MS. GC-MS was carried out using a Thermo Scientific DSQ II with a BGB5 column.

Infrared (IR) spectra were recorded with the aid of a Perkin-Elmer Spectrum65 FT IS Spectrometer with absorption maxima (ν_{max}) quoted in wavenumbers (cm⁻¹).

Continuous-flow experiments were performed using a Vapourtec® E-Series flow chemistry device using a standard 10-mL coil reactor.

10.2 Set-up of the continuous-flow experiments

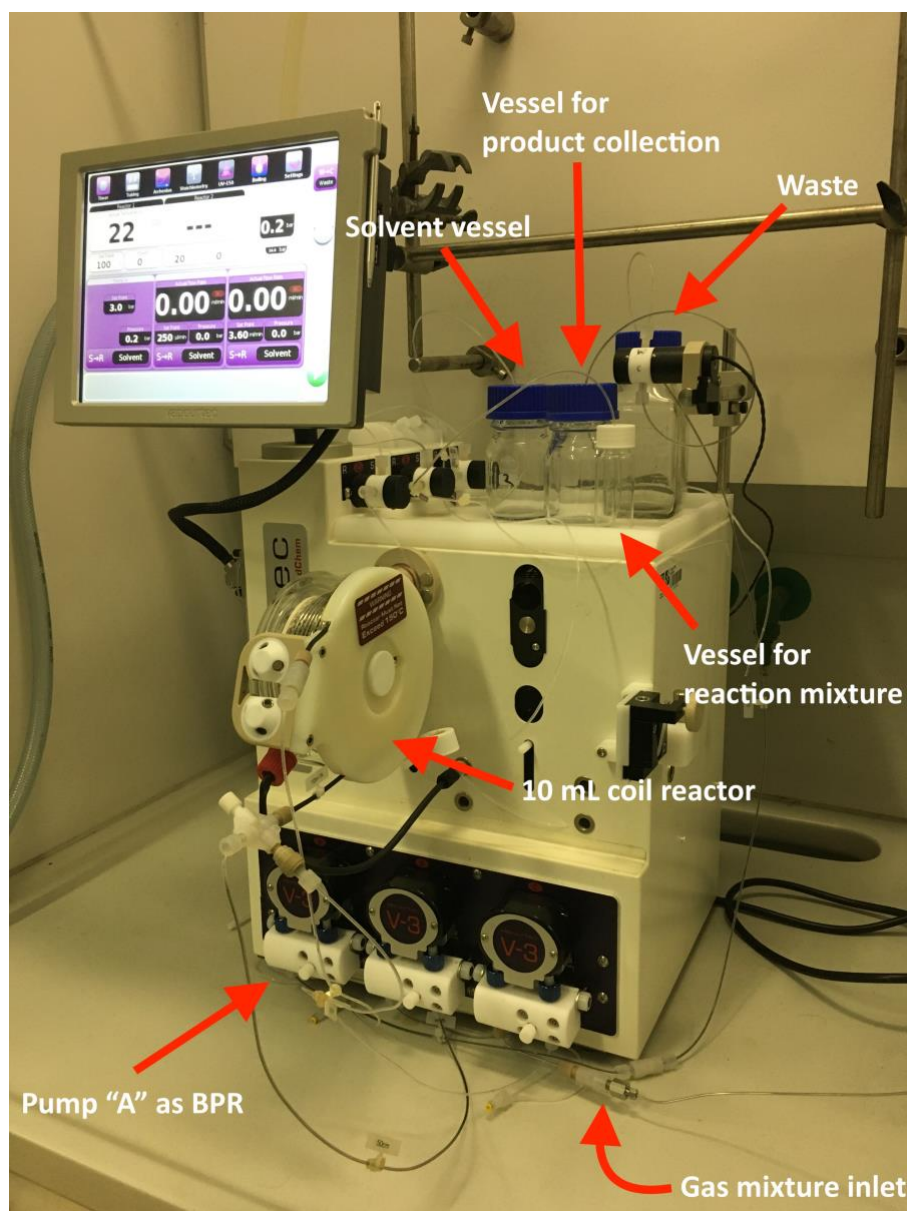


Figure 204. Set-up of the device operating in continuous mode

10.3 General procedure for the continuous synthesis of carbamates

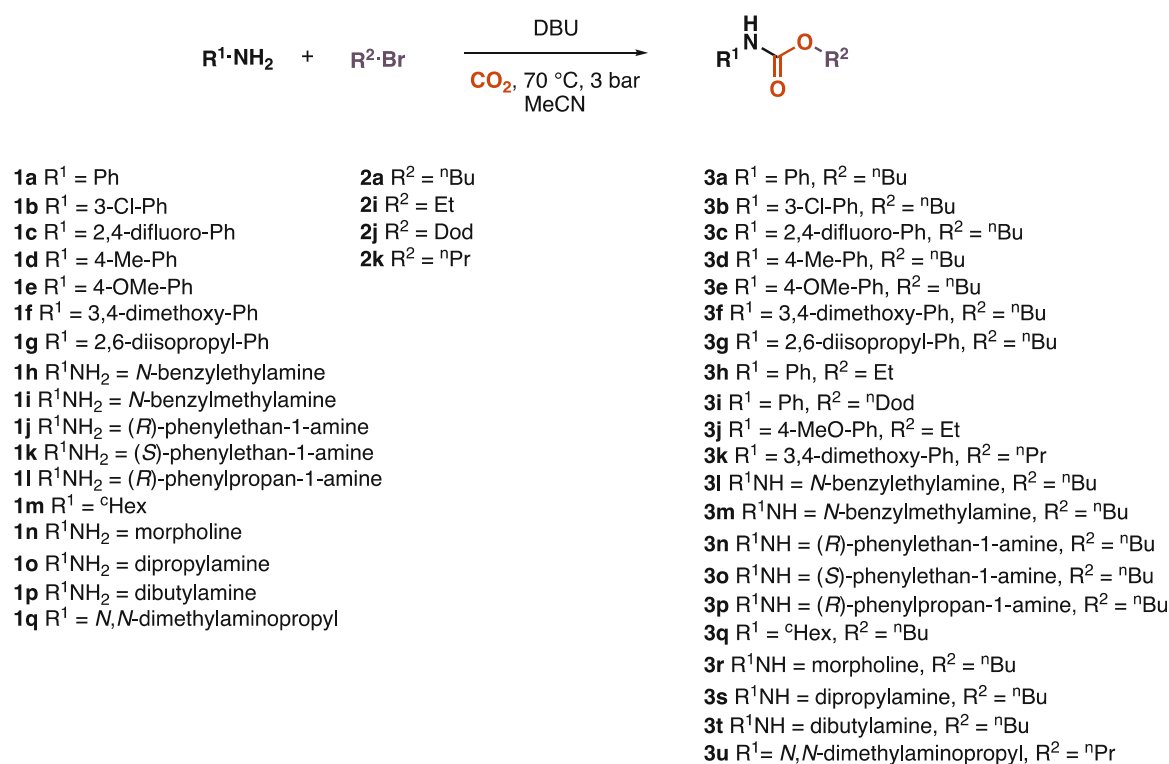
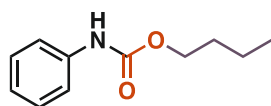


Figure 205. Continuous synthesis of carbamates

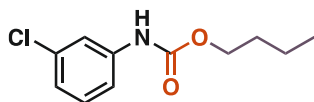
A 30-mL vial with septum was charged with the corresponding amine (1.00 eq., 4.29 mmol), the corresponding alkyl bromide (2.00 eq., 8.58 mmol), and DBU (2.00 eq., 8.58 mmol). The reactants were dissolved in 5 mL acetonitrile. The solvent bottle was charged with MeCN. The reactor was heated up to the desired temperature (70 °C). Pump A was used as a back-pressure regulator (BPR, 3 bar). Pump B was connected to the vial with the reaction mixture and pump C was connected to the gas tube, where the CO₂ was introduced. Carbon dioxide was supplied from a cylinder, the gas flow rate was set with the aid of a mass flow controller (6 mL/min). The reactor (10-mL coil reactor) was initially rinsed by a CO₂/MeCN flow for several minutes. Then, the reaction mixture was supplied to the reactor (pump B: 0.25 mL/min; pump C: 6 mL/min). After the whole volume of the reaction mixture was pumped through the reactor, the vial was rinsed with pure MeCN, and the residue was pumped through the reactor. The product was collected for 50 minutes. Rotary evaporation of the solvent gave the crude product, which was bound to silica and subjected to column chromatography. Alternatively, the products could be purified *via* acidic treatment: the crude residue was dissolved in dichloromethane, was washed thrice with 1.5 M HCl solution, dried over anhydrous Na₂SO₄, filtered and concentrated.

Butyl phenylcarbamate (3a)^[171]



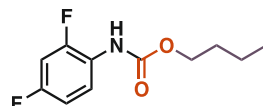
Acidic treatment afforded the product as slightly yellowish white solid (657 mg, 79%). **¹H NMR** (400 MHz, CDCl₃) δ 7.38 (d, *J* = 8.0 Hz, 2H), 7.34 – 7.27 (m, 2H), 7.12 – 7.00 (m, 1H), 6.63 (s, 1H), 4.17 (t, *J* = 6.7 Hz, 2H), 1.76 – 1.56 (m, 2H), 1.54 – 1.32 (m, 2H), 0.96 (t, *J* = 7.4 Hz, 3H). **¹³C NMR** (101 MHz, CDCl₃) δ 153.87, 138.12, 129.17, 123.46, 118.76, 65.26, 31.11, 19.21, 13.86.

Butyl (3-chlorophenyl)carbamate (3b)^[172]



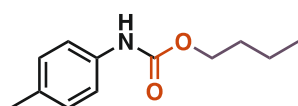
Acidic treatment afforded the product as slightly orange oil (564 mg, 58%). **¹H NMR** (400 MHz, CDCl₃) δ 7.59 – 7.43 (m, 1H), 7.24 – 7.14 (m, 2H), 7.10 – 6.98 (m, 1H), 6.60 (s, 1H), 4.15 (dt, *J* = 17.3, 6.7 Hz, 2H), 1.70 – 1.61 (m, 2H), 1.48 – 1.36 (m, 2H), 0.96 (t, *J* = 7.4 Hz, 3H). **¹³C NMR** (101 MHz, CDCl₃) δ 153.53, 139.34, 134.92, 130.15, 123.50, 118.77, 116.65, 65.53, 31.05, 19.20, 13.85

Butyl (2,4-difluorophenyl)carbamate (3c)



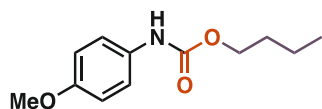
Flash column chromatography (petroleum ether/Et₂O 10:1, *R_f* = 0.44) afforded the product as colourless oil (440 mg, 45%). **¹H NMR** (400 MHz, CDCl₃) δ 8.02 (s, 1H), 6.85 (qt, *J* = 8.8, 2.8 Hz, 2H), 6.68 (s, 1H), 4.18 (t, *J* = 6.7 Hz, 2H), 1.66 (ddt, *J* = 8.8, 8.0, 6.5 Hz, 2H), 1.51 – 1.32 (m, 2H), 0.96 (t, *J* = 7.4 Hz, 3H). **¹³C NMR** (101 MHz, CDCl₃) δ 153.53, 139.34, 134.92, 130.15, 123.50, 118.77, 116.65, 65.53, 31.05, 19.20, 13.85. **¹⁹F NMR** (376 MHz, CDCl₃) δ -116.99, -127.95. **HRMS (ESI)**: calc. For C₁₁H₁₄F₂NO₂ [M + H]⁺: 230.987; found: 230.0989. **IR** (ν_{max}/cm⁻¹): 2961, 1717, 1612, 1529, 1432, 1287, 1222, 1194, 1141, 1099, 1068, 962, 846, 727.

Butyl *p*-tolylcarbamate (3d)^[173]



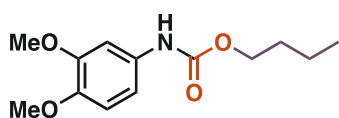
Acidic treatment afforded the product as yellowish brown oil (689 mg, 78%). **¹H NMR** (400 MHz, CDCl₃) δ 7.26 (d, *J* = 8.2 Hz, 2H), 7.10 (d, *J* = 8.2 Hz, 2H), 6.53 (s, 1H), 4.16 (t, *J* = 6.7 Hz, 2H), 2.30 (s, 3H), 1.65 (ddt, *J* = 8.8, 7.8, 6.5 Hz, 2H), 1.48 – 1.32 (m, 2H), 0.95 (t, *J* = 7.4 Hz, 3H). **¹³C NMR** (101 MHz, CDCl₃) δ 153.98, 135.51, 133.03, 129.66, 118.66, 65.18, 31.13, 20.87, 19.23, 13.87.

Butyl (4-methoxyphenyl)carbamate (3e)^[174]



Acidic treatment afforded the product as black oil (797 mg, 83%). **¹H NMR** (400 MHz, CDCl₃) δ 7.28 (d, *J* = 8.3 Hz, 2H), 6.90 – 6.79 (m, 2H), 6.49 (s, 1H), 4.15 (t, *J* = 6.7 Hz, 2H), 3.78 (s, 3H), 1.64 (ddt, *J* = 8.9, 8.0, 6.5 Hz, 2H), 1.50 – 1.34 (m, 2H), 0.95 (t, *J* = 7.4 Hz, 3H). **¹³C NMR** (101 MHz, CDCl₃) δ 156.05, 154.26, 131.18, 120.75, 114.37, 65.17, 55.64, 31.14, 19.22, 13.87.

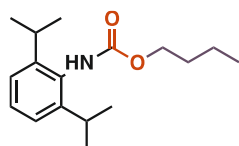
Butyl (3,4-dimethoxyphenyl)carbamate (3f)



Acidic treatment afforded the product as black solid (897 mg, 83%).

M.p. 56-58 °C. $^1\text{H NMR}$ (400 MHz, CDCl_3) δ 7.19 (s, 1H), 6.83 – 6.70 (m, 2H), 6.50 (s, 1H), 4.15 (t, $J = 6.7$ Hz, 2H), 3.86 (dd, $J = 11.4, 0.9$ Hz, 6H), 1.65 (dtd, $J = 8.3, 6.9, 5.9$ Hz, 2H), 1.47 – 1.32 (m, 2H), 0.99 – 0.88 (m, 3H). $^{13}\text{C NMR}$ (101 MHz, CDCl_3) δ 154.14, 149.37, 145.43, 131.72, 111.67, 65.20, 56.31, 56.00, 31.13, 19.23, 13.86. **HRMS (ESI)**: calc. For $\text{C}_{13}\text{H}_{20}\text{NO}_4$ $[\text{M} + \text{H}]^+$: 254.1387; found: 254.1388. **IR** ($\nu_{\text{max}}/\text{cm}^{-1}$): 2959, 1689, 1604, 1534, 1455, 1419, 1290, 1267, 1230, 1171, 1138, 1075, 1023, 956, 848, 805, 756, 737.

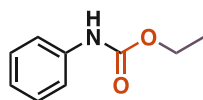
Butyl (2,6-diisopropylphenyl)carbamate (3g)



Flash column chromatography (petroleum ether/ Et_2O 10:1, $R_f = 0.28$) afforded

the product as white solid (636 mg, 53%). **M.p.** 76-79 °C. $^1\text{H NMR}$ (400 MHz, CDCl_3) δ 7.33 – 7.24 (m, 1H), 7.16 (d, $J = 7.7$ Hz, 2H), 5.93 (s, 1H), 4.12 (dt, $J = 40.5, 6.8$ Hz, 2H), 3.19 (dt, $J = 14.6, 7.9$ Hz, 2H), 1.67 (q, $J = 7.5$ Hz, 2H), 1.45 (dt, $J = 15.3, 7.6$ Hz, 2H), 1.21 (d, $J = 7.4$ Hz, 12H), 1.04 – 0.90 (m, 2H), 0.83 (q, $J = 6.2, 5.5$ Hz, 1H). $^{13}\text{C NMR}$ (101 MHz, CDCl_3) δ 155.74, 146.96, 128.42, 123.59, 65.25, 31.30, 28.74, 24.11, 23.77, 23.34, 19.17, 13.91. **HRMS (ESI)**: calc. For $\text{C}_{17}\text{H}_{28}\text{NO}_2$ $[\text{M} + \text{H}]^+$: 278.2115; found: 278.2119. **IR** ($\nu_{\text{max}}/\text{cm}^{-1}$): 2959, 1695, 1509, 1474, 1245, 1204, 1074, 1052, 799.

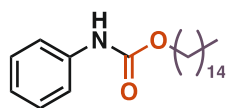
Ethyl phenylcarbamate (3h)^[175]



Acidic treatment afforded the product as orange oil (420 mg, 59%). $^1\text{H NMR}$ (400

MHz, CDCl_3) δ 7.43 – 7.34 (m, 2H), 7.34 – 7.27 (m, 2H), 7.09 – 7.02 (m, 1H), 6.63 (s, 1H), 4.23 (q, $J = 7.1$ Hz, 2H), 1.31 (t, $J = 7.1$ Hz, 3H). $^{13}\text{C NMR}$ (101 MHz, CDCl_3) δ 153.74, 138.09, 129.17, 123.48, 118.79, 61.34, 14.68.

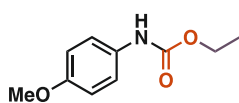
Tetradecyl phenylcarbamate (3i)^[176]



Flash column chromatography (petroleum ether/ Et_2O 15:1, $R_f = 0.45$, *p*-

anisaldehyde stain) afforded the product as white solid (997 mg, 76%). $^1\text{H NMR}$ (400 MHz, CDCl_3) δ 7.46 – 7.23 (m, 4H), 7.12 – 6.96 (m, 1H), 6.58 (s, 1H), 4.16 (t, $J = 6.7$ Hz, 2H), 1.75 – 1.60 (m, 2H), 1.45 – 1.18 (m, 18H), 0.88 (t, $J = 6.8$ Hz, 3H). $^{13}\text{C NMR}$ (101 MHz, CDCl_3) δ 153.84, 138.12, 129.18, 123.47, 118.75, 65.59, 32.06, 29.79, 29.77, 29.72, 29.69, 29.49, 29.43, 29.09, 26.02, 22.83, 14.26.

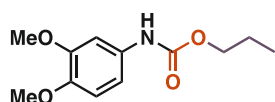
Ethyl (4-methoxyphenyl)carbamate (3j)^[177]



Acidic treatment afforded the product as black solid (475 mg, 57%). $^1\text{H NMR}$

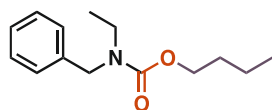
(400 MHz, CDCl_3) δ 7.28 (d, $J = 8.5$ Hz, 2H), 6.91 – 6.79 (m, 2H), 6.56 (s, 1H), 4.26 – 4.15 (m, 2H), 3.78 (d, $J = 1.1$ Hz, 3H), 1.29 (tt, $J = 7.1, 1.2$ Hz, 3H). $^{13}\text{C NMR}$ (101 MHz, CDCl_3) δ 156.05, 154.17, 131.16, 120.82, 114.36, 61.23, 55.62, 14.71.

Propyl (3,4-dimethoxyphenyl)carbamate (3k)



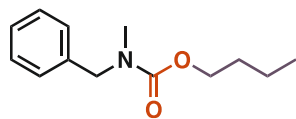
Acidic treatment afforded the product as black solid (900 mg, 88%). **M.p.** 55-58 °C. **¹H NMR** (400 MHz, CDCl₃) δ 7.19 (s, 1H), 6.75 (dd, *J* = 10.9, 8.5 Hz, 2H), 6.54 (s, 1H), 4.11 (t, *J* = 6.7 Hz, 2H), 3.87 (t, *J* = 0.8 Hz, 3H), 3.84 (d, *J* = 0.7 Hz, 3H), 1.76 – 1.62 (m, 2H), 0.97 (t, *J* = 7.4 Hz, 3H). **¹³C NMR** (101 MHz, CDCl₃) δ 154.14, 149.35, 145.41, 131.72, 111.66, 66.92, 56.30, 55.99, 22.43, 10.48. **HRMS (ESI)**: calc. For C₁₂H₁₈NO₄ [M + H]⁺: 240.1230; found: 240.1231. **IR** (ν_{max}/cm⁻¹): 2966, 1689, 1604, 1516, 1447, 1326, 1291, 1223, 1169, 1137, 1070, 1022, 957, 847, 804, 755.

Butyl benzyl(ethyl)carbamate (3l)



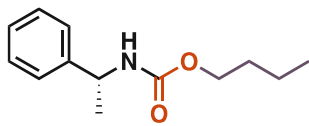
Acidic treatment afforded the product as yellow oil (768 mg, 76%). **¹H NMR** (400 MHz, CDCl₃) δ 7.40 – 7.02 (m, 5H), 4.47 (s, 2H), 4.13 (t, *J* = 6.5 Hz, 2H), 3.41 – 3.11 (m, 2H), 1.64 (dt, *J* = 16.9, 11.3 Hz, 2H), 1.45 – 1.25 (m, 2H), 1.07 (s, 3H), 1.01 – 0.84 (m, 3H). **¹³C NMR** (101 MHz, CDCl₃) δ 138.42, 128.61, 127.33, 65.38, 31.29, 19.33, 13.90. **HRMS (ESI)**: calc. For C₁₄H₂₂NO₂ [M + H]⁺: 236.1645; found: 236.1647. **IR** (ν_{max}/cm⁻¹): 2959, 1694, 1470, 1422, 1256, 1142, 1081, 980, 733.

Butyl benzyl(methyl)carbamate (3m)



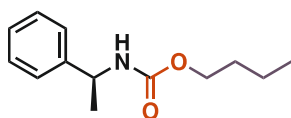
Acidic treatment afforded the product as yellow oil (681 mg, 72%). **¹H NMR** (400 MHz, CDCl₃) δ 7.42 – 7.15 (m, 5H), 4.47 (s, 2H), 4.13 (t, *J* = 6.6 Hz, 2H), 2.85 (s, 3H), 1.72 – 1.59 (m, 2H), 1.50 – 1.28 (m, 2H), 0.99 – 0.82 (m, 3H). **¹³C NMR** (101 MHz, CDCl₃) δ 137.79, 128.69, 127.44, 65.56, 52.48, 31.28, 19.30, 13.89. **HRMS (ESI)**: calc. For C₁₃H₁₉NO₂ [M + H]⁺: 222.1489; found: 222.1491. **IR** (ν_{max}/cm⁻¹): 2959, 1692, 1647, 1620, 1456, 1325, 747.

Butyl (*R*)-(1-phenylethyl)carbamate (3n)^[178]



Flash column chromatography (petroleum ether/Et₂O 5:1, *R_f* = 0.20) afforded the product as slightly yellowish oil (875 mg, 92%). **¹H NMR** (400 MHz, CDCl₃) δ 7.42 – 7.20 (m, 5H), 4.87 (d, *J* = 22.9 Hz, 2H), 4.04 (td, *J* = 6.7, 4.7 Hz, 2H), 1.56 (q, *J* = 7.4, 6.8 Hz, 2H), 1.48 (d, *J* = 6.7 Hz, 3H), 1.30 (td, *J* = 20.6, 19.9, 6.2 Hz, 2H), 0.92 (dt, *J* = 11.2, 7.4 Hz, 3H). **¹³C NMR** (101 MHz, CDCl₃) δ 156.11, 128.76, 127.41, 126.06, 64.92, 50.69, 31.19, 22.65, 19.19, 13.87. **Chiral HPLC**: Chiralpak[®] AS-H column, *n*-hexane: isopropanol 90:10, 1 mL/min, 25 °C, UV 220 nm, *t_R* = 8.3 min.

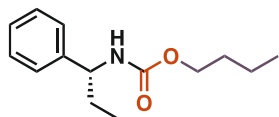
Butyl (*S*)-(1-phenylethyl)carbamate (3o)^[178]



Flash column chromatography (petroleum ether/Et₂O 5:1, *R_f* = 0.20) afforded the product as slightly yellowish oil (774 mg, 82%). **¹H NMR** (400 MHz, CDCl₃) δ 7.40 – 7.18 (m, 5H), 4.87 (d, *J* = 22.9 Hz, 2H), 4.04 (td, *J* = 6.7, 4.7 Hz, 2H), 1.56 (q, *J* = 7.4, 6.8 Hz, 2H), 1.48 (d, *J* = 6.7 Hz, 3H), 1.32 (dq, *J* = 19.2, 12.9, 10.3 Hz, 2H),

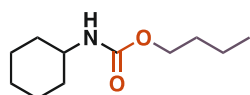
0.92 (q, $J = 7.3, 5.6$ Hz, 3H). $^{13}\text{C NMR}$ (101 MHz, CDCl_3) δ 156.11, 128.76, 127.41, 126.06, 64.92, 50.71, 31.19, 22.65, 19.19, 13.87. **Chiral HPLC:** Chiralpak[®] AS-H column, *n*-hexane: isopropanol 90:10, 1 mL/min, 25 °C, UV 220 nm, $t_R = 6.2$ min.

Butyl (*R*)-(1-phenylpropyl)carbamate (3p)



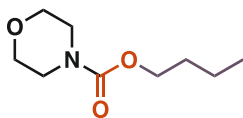
Flash column chromatography (petroleum ether/ Et_2O 5:1, $R_f = 0.23$, KMnO_4 stain) afforded the product as slightly yellowish oil (726 mg, 72%). $^1\text{H NMR}$ (400 MHz, CDCl_3) δ 7.40 – 7.17 (m, 5H), 4.91 (s, 1H), 4.58 (s, 1H), 4.12 – 3.93 (m, 2H), 1.83 – 1.75 (m, 2H), 1.56 (s, 2H), 1.35 (s, 2H), 0.90 (t, $J = 7.4$ Hz, 6H). $^{13}\text{C NMR}$ (101 MHz, CDCl_3) δ 128.69, 127.37, 126.53, 64.92, 56.88, 31.19, 29.84, 19.19, 13.87, 10.82. **HRMS (ESI):** calc. For $\text{C}_{14}\text{H}_{22}\text{NO}_2$ [$\text{M} + \text{H}$]⁺: 236.1645; found: 236.1645. **IR** ($\nu_{\text{max}}/\text{cm}^{-1}$): 2961, 1688, 1529, 1455, 1232, 1084, 1041, 756.

Butyl cyclohexylcarbamate (3q)^[179]



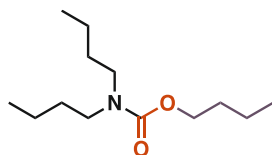
Flash column chromatography (petroleum ether/ Et_2O 5:1, $R_f = 0.32$, KMnO_4 stain) afforded the product as white solid (578 mg, 68%). $^1\text{H NMR}$ (400 MHz, CDCl_3) δ 4.51 (s, 1H), 4.04 (t, $J = 6.6$ Hz, 2H), 3.46 (s, 1H), 1.93 (dt, $J = 12.4, 4.2$ Hz, 2H), 1.69 (dq, $J = 12.0, 3.9$ Hz, 2H), 1.64 – 1.48 (m, 3H), 1.45 – 1.25 (m, 4H), 1.21 – 1.03 (m, 3H), 0.92 (t, $J = 7.4$ Hz, 3H). $^{13}\text{C NMR}$ (101 MHz, CDCl_3) δ 156.23, 64.71, 49.94, 33.61, 31.26, 25.64, 24.93, 19.25, 13.90.

Butyl morpholine-4-carboxylate (3r)^[180]



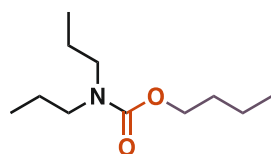
Acidic treatment afforded the product as yellow oil (492 mg, 61%). $^1\text{H NMR}$ (400 MHz, CDCl_3) δ 4.09 (t, $J = 6.6$ Hz, 2H), 3.64 (t, $J = 4.8$ Hz, 4H), 3.52 – 3.32 (m, 4H), 1.61 (dq, $J = 8.5, 6.7$ Hz, 2H), 1.45 – 1.29 (m, 2H), 0.93 (t, $J = 7.4$ Hz, 3H). $^{13}\text{C NMR}$ (101 MHz, CDCl_3) δ 155.78, 66.75, 65.57, 44.14, 31.17, 19.30, 13.88.

Butyl dibutylcarbamate (3s)^[133b]



Acidic treatment afforded the product as slightly yellowish oil (725 mg, 74%). $^1\text{H NMR}$ (400 MHz, CDCl_3) δ 4.05 (t, $J = 6.6$ Hz, 2H), 3.18 (s, 4H), 1.60 (ddt, $J = 8.7, 7.9, 6.4$ Hz, 2H), 1.49 (p, $J = 7.5$ Hz, 4H), 1.43 – 1.36 (m, 2H), 1.28 (dt, $J = 14.7, 7.4$ Hz, 4H), 0.92 (q, $J = 7.2$ Hz, 9H). $^{13}\text{C NMR}$ (101 MHz, CDCl_3) δ 156.71, 64.95, 46.99, 31.31, 30.71, 20.17, 19.38, 14.00.

Butyl dipropylcarbamate (3t)



Acidic treatment afforded the product as yellow oil (665 mg, 77%). $^1\text{H NMR}$ (400 MHz, CDCl_3) δ 4.05 (t, $J = 6.6$ Hz, 2H), 3.19 – 3.11 (m, 4H), 1.65 – 1.46 (m, 6H), 1.43 – 1.32 (m, 2H), 0.93 (t, $J = 7.4$ Hz, 3H), 0.86 (t, $J = 7.4$ Hz, 6H). $^{13}\text{C NMR}$ (101 MHz, CDCl_3) δ 156.78, 64.96, 48.99, 31.31, 21.74, 19.37, 13.90, 11.37. **HRMS (ESI):** calc. For $\text{C}_{11}\text{H}_{24}\text{NO}_2$ [$\text{M} + \text{H}$]⁺: 202.1802; found: 202.1803. **IR** ($\nu_{\text{max}}/\text{cm}^{-1}$): 2959, 1695, 1509, 1474, 1245, 1204, 1074, 1052, 799.

10.4 General procedure for the synthesis of aziridines

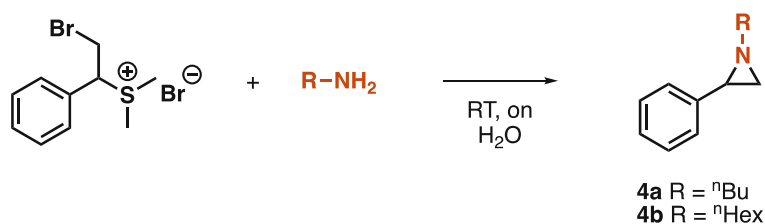
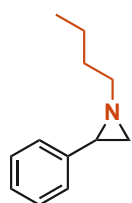


Figure 206. Synthesis of aziridines

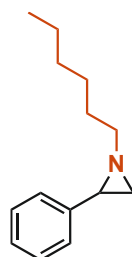
(2-bromo-1-phenylethyl)dimethylsulfonium bromide was prepared according to the standard literature procedure.^[181] Aziridines were prepared according to the literature procedure;^[182] the alkylsulfonium bromide (1.0 eq., 10.0 mmol) was dissolved in 20 mL distilled water. To this, the solution of the corresponding amine (3.0 eq., 30.0 mmol) in 10 mL water was added dropwise. The reaction mixture was stirred overnight at room temperature. After completion, the mixture was quenched with 20 mL brine, extracted with diethyl ether (3 x 20 mL), dried over anhydrous Na₂SO₄, and concentrated *in vacuo*. The crude products were subjected to column chromatography on neutral aluminum oxide (Brockmann Grade IV).

1-Butyl-2-phenylaziridine (**4a**)^[183]



Column chromatography (petroleum ether/Et₂O 20:1, R_f = 0.61) afforded the product as colourless liquid (1.56 g, 89%). ¹H NMR (400 MHz, CDCl₃) δ 7.35 – 7.18 (m, 5H), 2.51 (dt, J = 11.5, 7.3 Hz, 1H), 2.38 – 2.27 (m, 2H), 1.89 (dd, J = 3.4, 0.8 Hz, 1H), 1.68 – 1.64 (m, 1H), 1.64 – 1.55 (m, 2H), 1.47 – 1.33 (m, 2H), 0.93 (t, J = 7.3 Hz, 3H). ¹³C NMR (101 MHz, CDCl₃) δ 140.70, 128.38, 126.87, 126.31, 61.71, 41.39, 37.92, 32.13, 20.74, 14.25.

1-Hexyl-2-phenylaziridine (**4b**)^[184]



Column chromatography (petroleum ether/Et₂O 20:1, R_f = 0.69) afforded the product as colourless liquid (1.97 g, 97%). ¹H NMR (400 MHz, CDCl₃) δ 7.48 – 7.16 (m, 5H), 2.49 (dt, J = 11.5, 7.4 Hz, 1H), 2.38 – 2.27 (m, 2H), 1.90 (dd, J = 3.3, 0.7 Hz, 1H), 1.69 – 1.55 (m, 3H), 1.44 – 1.22 (m, 6H), 0.97 – 0.81 (m, 3H). ¹³C NMR (101 MHz, CDCl₃) δ 140.69, 128.38, 126.87, 126.32, 62.05, 41.39, 37.91, 31.96, 29.93, 27.27, 22.73, 14.18.

10.5 General procedure for the continuous synthesis of oxazolidinones

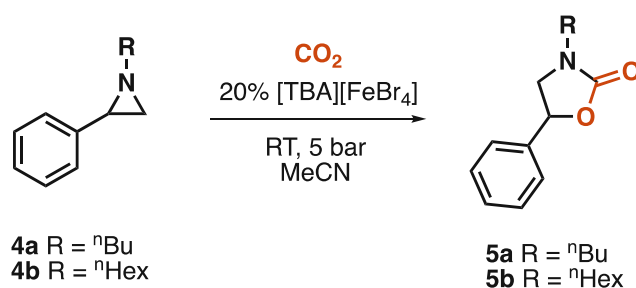
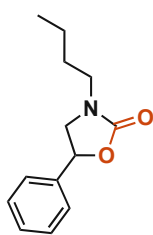


Figure 207. Synthesis of oxazolidinones

A 30-mL vial with septum was charged with the corresponding aziridine (1.00 eq., 0.73 mmol), FeBr₃ (20 mol%, 0.146 mmol), and TBAB (20 mol%, 0.146 mmol). The reactants were dissolved in 5 mL acetonitrile. The solvent bottle was charged with MeCN. Pump A was used as a back-pressure regulator (BPR, 5 bar). Pump B was connected to the vial with the reaction mixture; pump C was connected to the gas tube, where the CO₂ was introduced. Carbon dioxide was supplied from a cylinder. The gas flow rate was set with a mass flow controller (8 mL/min). The reactor (10-mL coil reactor) was initially rinsed by a CO₂/MeCN flow for several minutes. Then, the reaction mixture was supplied to the reactor (pump B: 0.25 mL/min; pump C: 8 mL/min). After the entire volume of the reaction mixture was pumped through the reactor, the vial was rinsed with pure MeCN, and the residue was pumped through the reactor. The product was collected for 50 minutes. Rotary evaporation of the solvent afforded the crude product, which was bound to silica and subjected to column chromatography on silica.

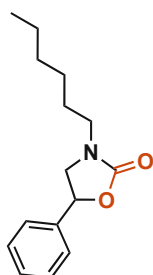
3-Butyl-5-phenyloxazolidin-2-one (5a)^[183]



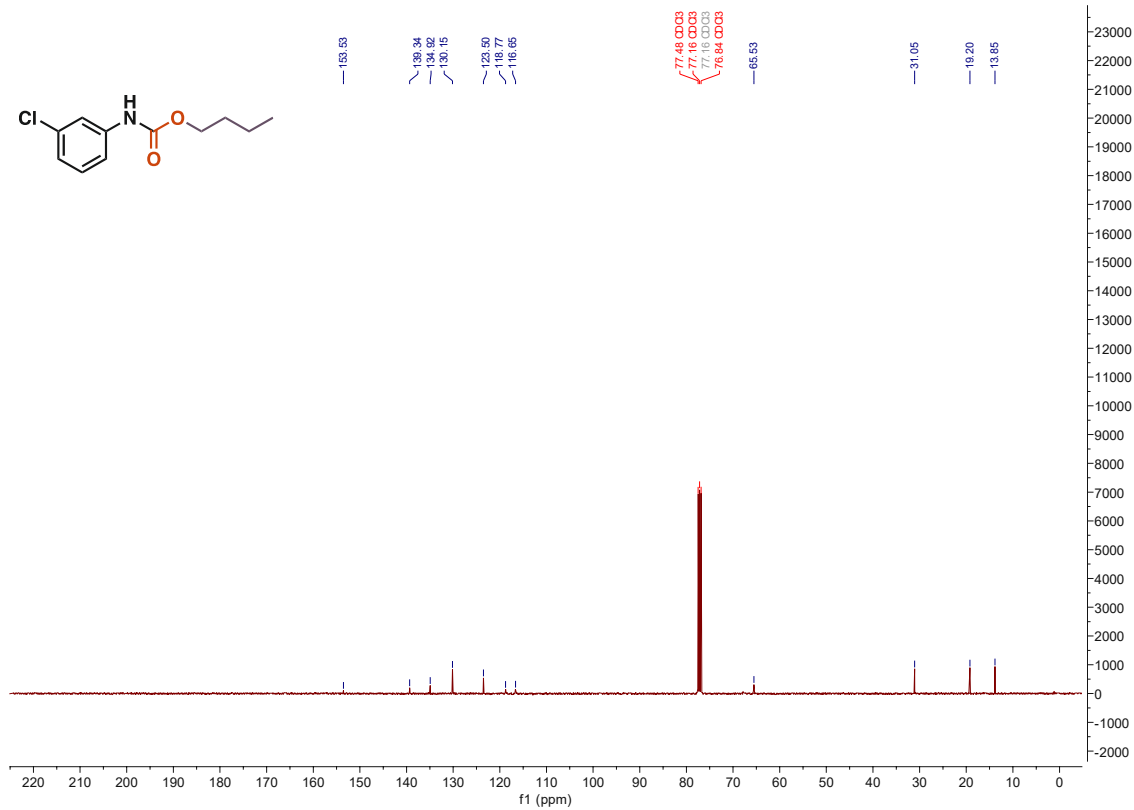
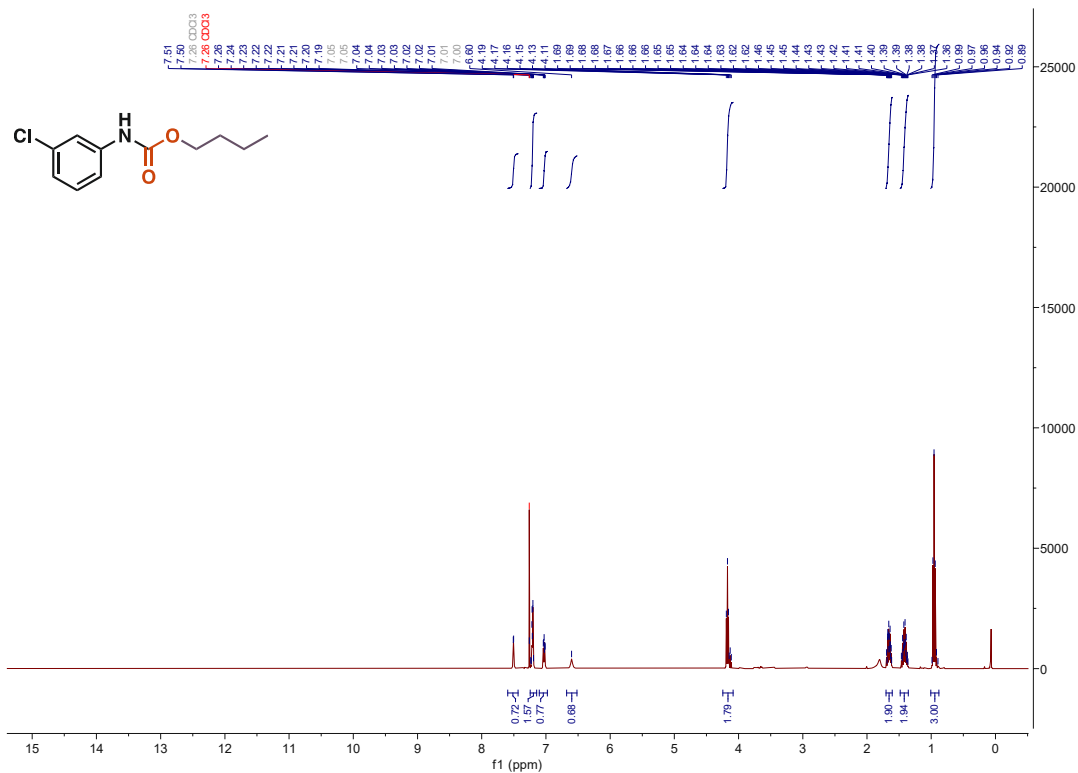
19.98, 13.83.

Column chromatography (petroleum ether/Et₂O 2:1, *R_f* = 0.55) afforded the product as colourless liquid (101 mg, 63%). ¹H NMR (400 MHz, CDCl₃) δ 7.46 – 7.29 (m, 5H), 5.48 (t, *J* = 8.1 Hz, 1H), 3.91 (t, *J* = 8.7 Hz, 1H), 3.42 (ddd, *J* = 8.2, 7.4, 0.7 Hz, 1H), 3.39 – 3.21 (m, 2H), 1.60 – 1.47 (m, 2H), 1.43 – 1.29 (m, 2H), 0.94 (t, *J* = 7.3 Hz, 3H). ¹³C NMR (101 MHz, CDCl₃) δ 158.06, 139.05, 129.04, 128.90, 125.63, 74.45, 52.32, 44.07, 29.56,

3-Hexyl-5-phenyloxazolidin-2-one (5b)^[185]



Column chromatography (petroleum ether/Et₂O 2:1, *R_f* = 0.61) afforded the product as colourless liquid (114 mg, 63%). ¹H NMR (400 MHz, CDCl₃) δ 7.49 – 7.28 (m, 5H), 5.48 (dd, *J* = 8.8, 7.4 Hz, 1H), 3.91 (t, *J* = 8.7 Hz, 1H), 3.42 (dd, *J* = 8.6, 7.4 Hz, 1H), 3.30 (ddp, *J* = 21.1, 14.0, 7.1 Hz, 2H), 1.55 (p, *J* = 7.4 Hz, 2H), 1.39 – 1.15 (m, 6H), 0.88 (q, *J* = 4.0, 3.2 Hz, 3H). ¹³C NMR (101 MHz, CDCl₃) δ 158.03, 139.08, 129.02, 128.89, 125.62, 74.42, 52.31, 44.35, 31.53, 27.46, 26.41, 22.65, 14.11.



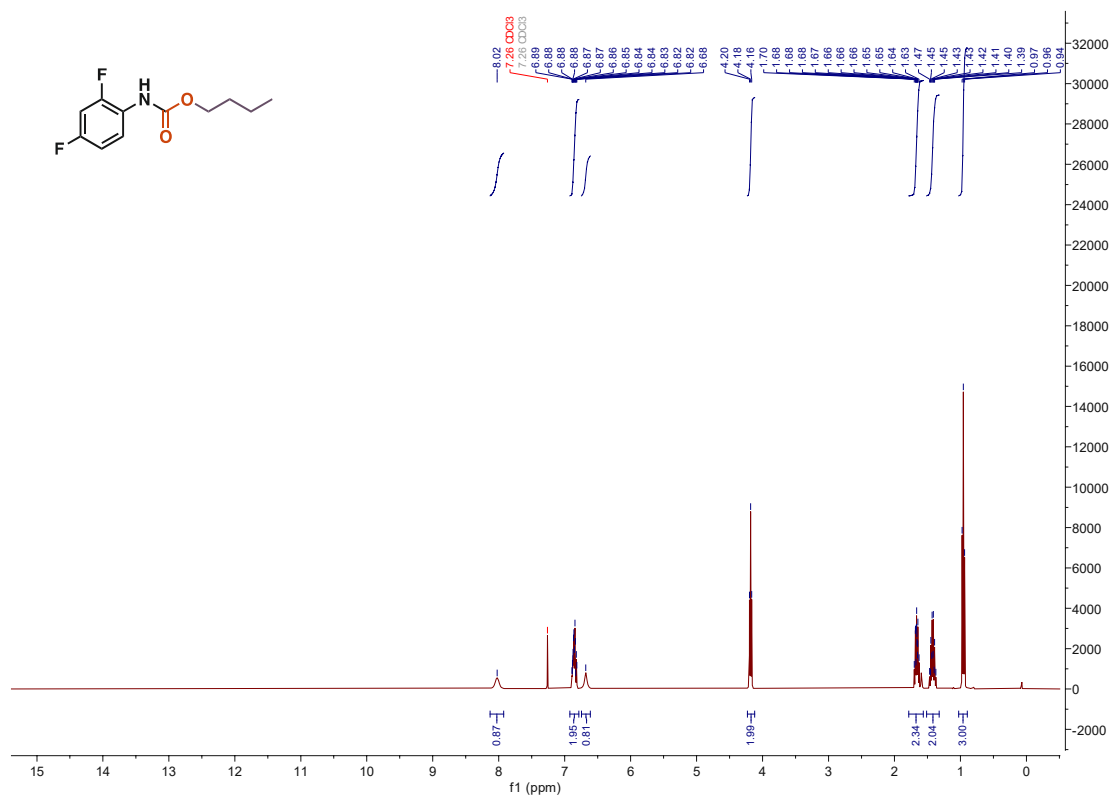


Figure 212. ¹H NMR of 3c

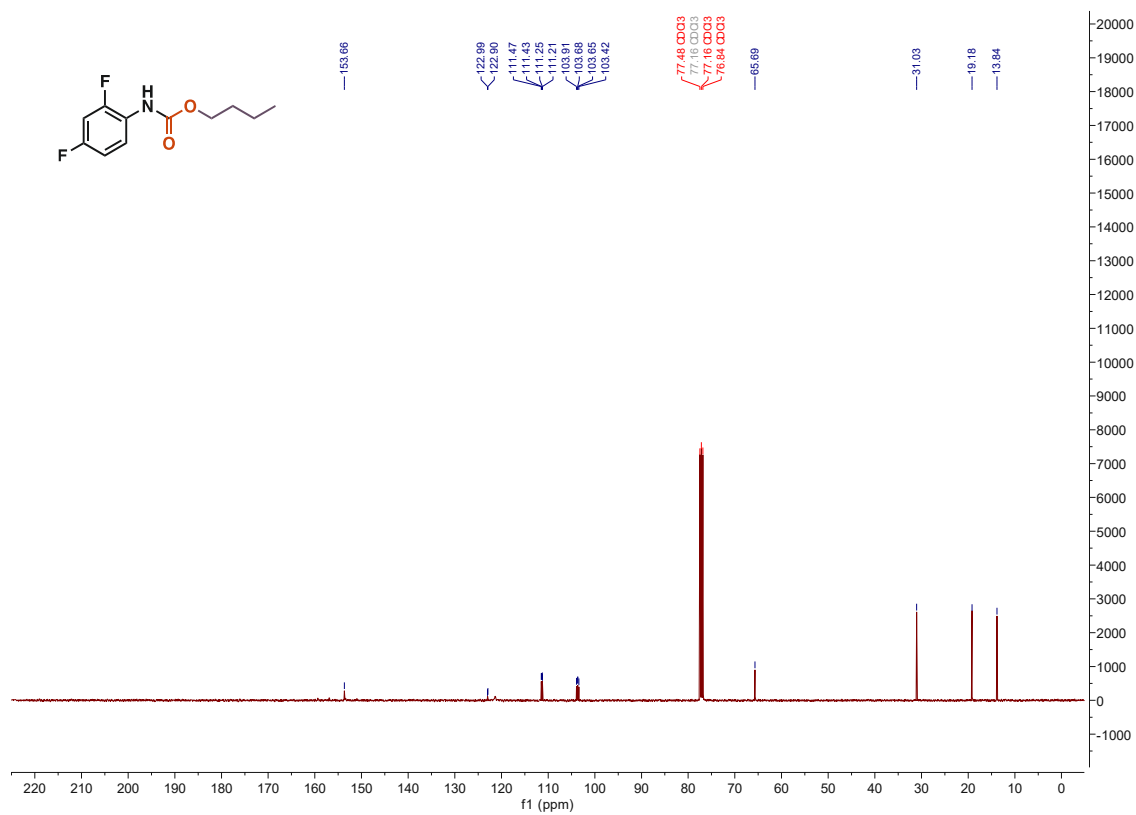


Figure 213. ¹³C NMR of 3c

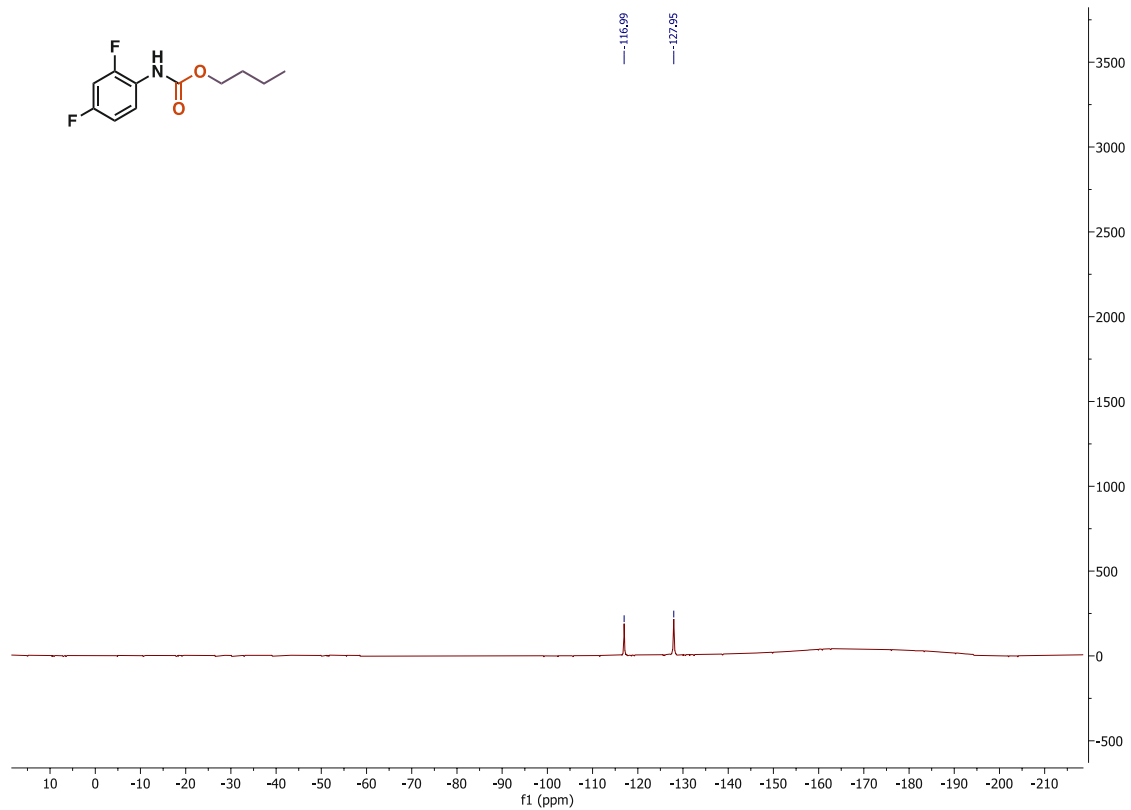


Figure 214. ¹⁹F NMR of 3c

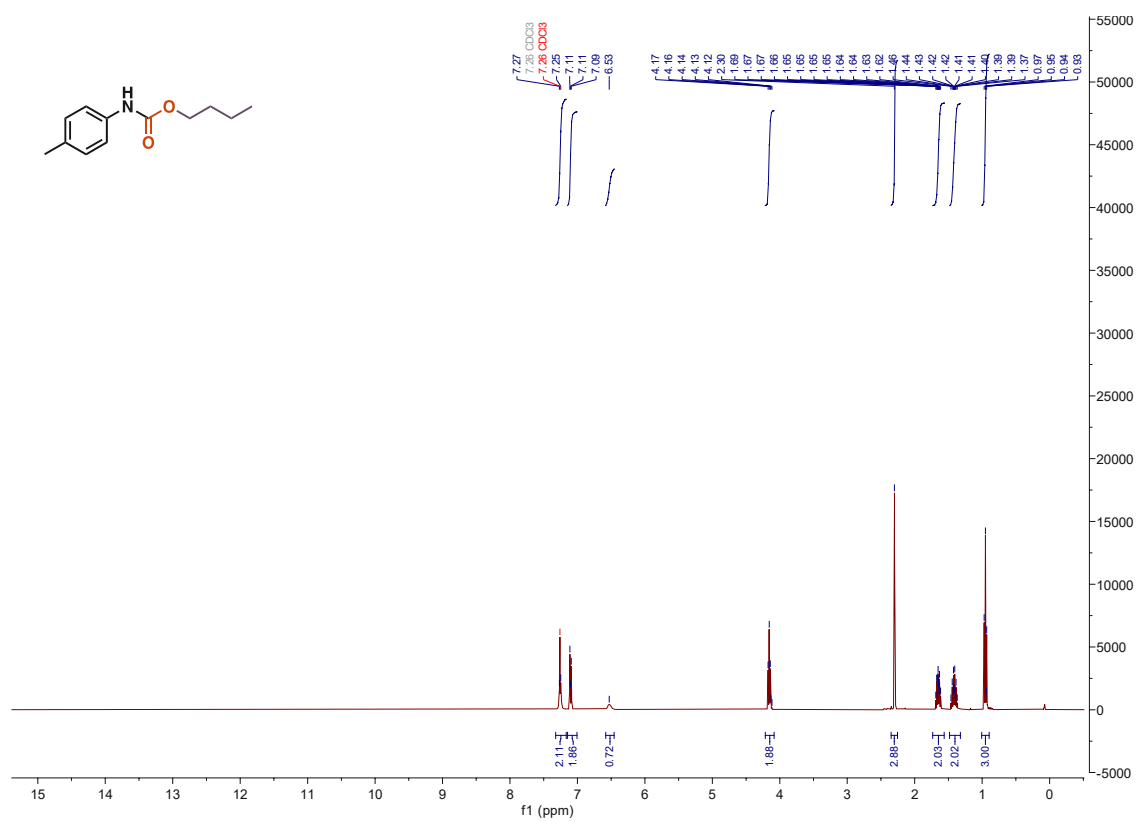
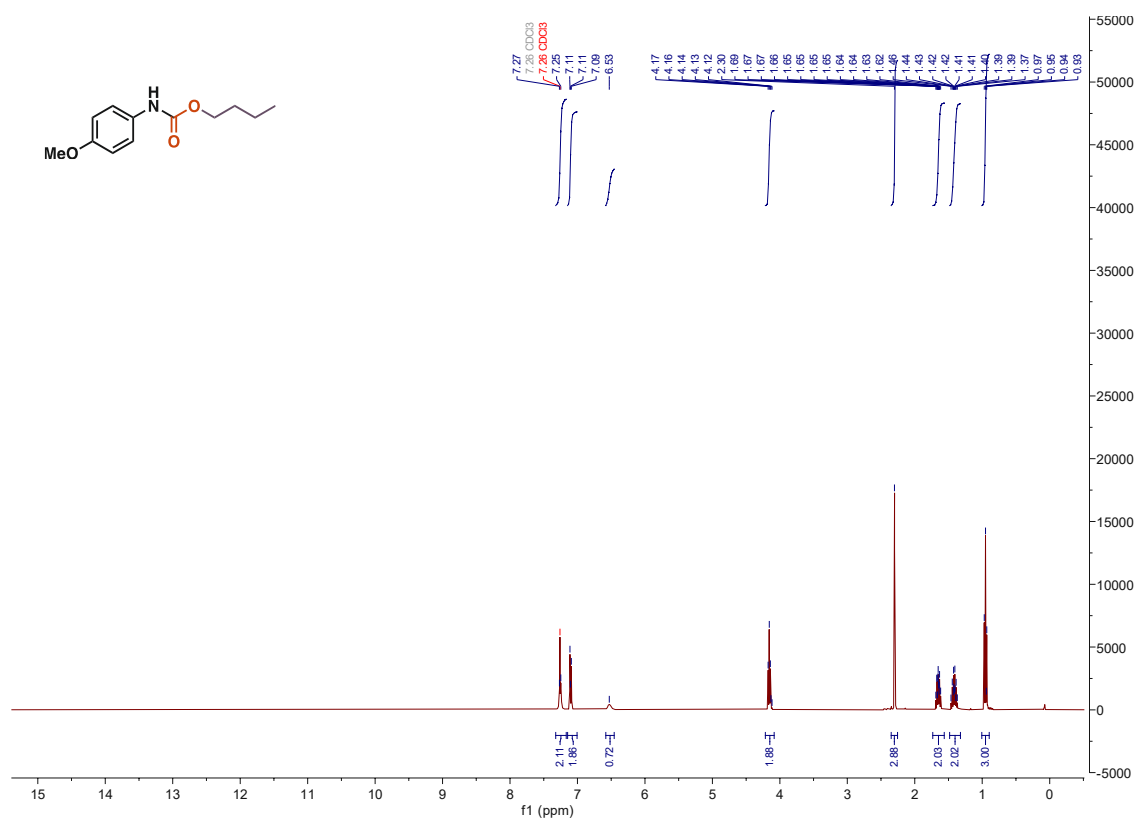
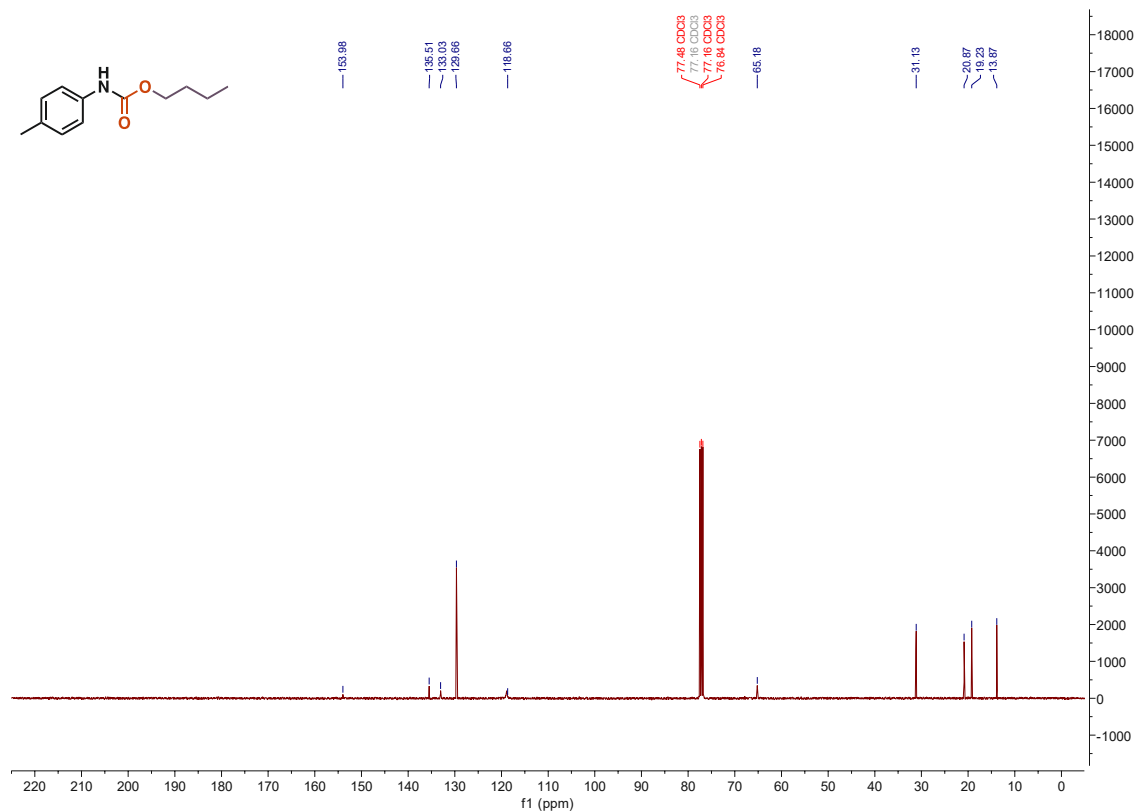


Figure 215. ¹H NMR of 3d



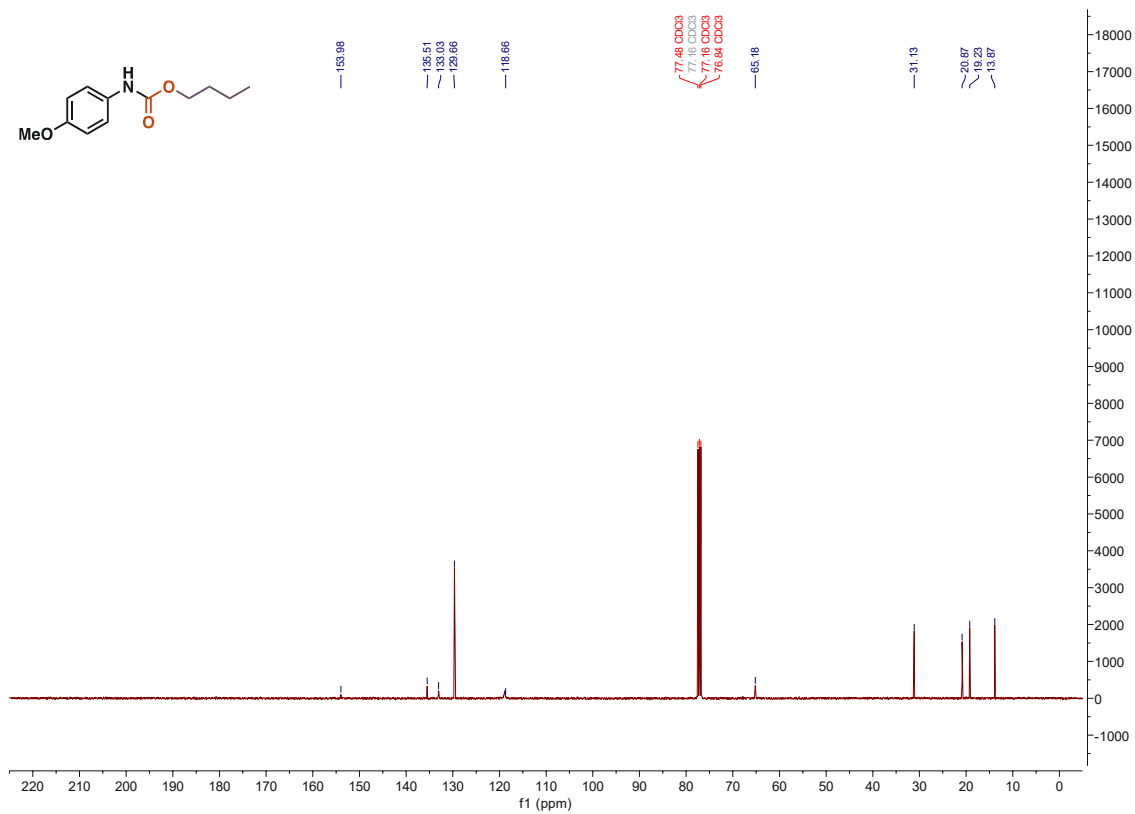


Figure 218. ^{13}C NMR of 3e

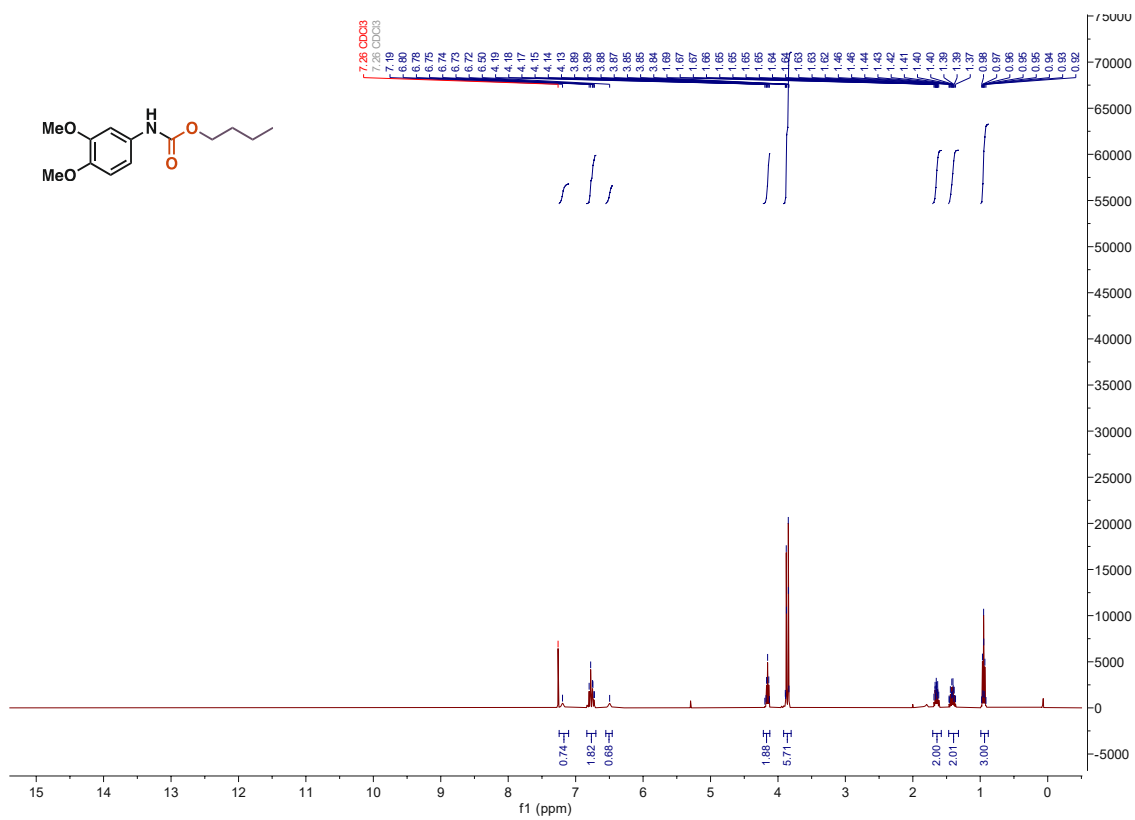


Figure 219. ^1H NMR of 3f

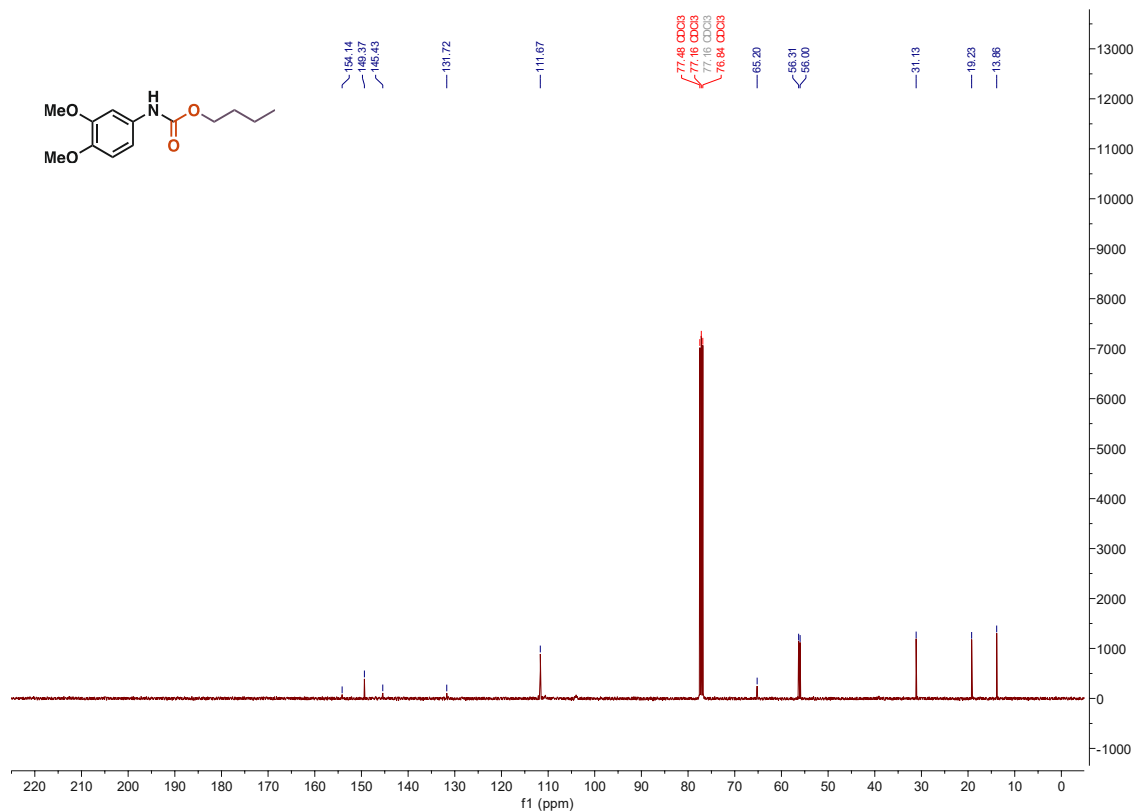


Figure 220. ^{13}C NMR of 3f

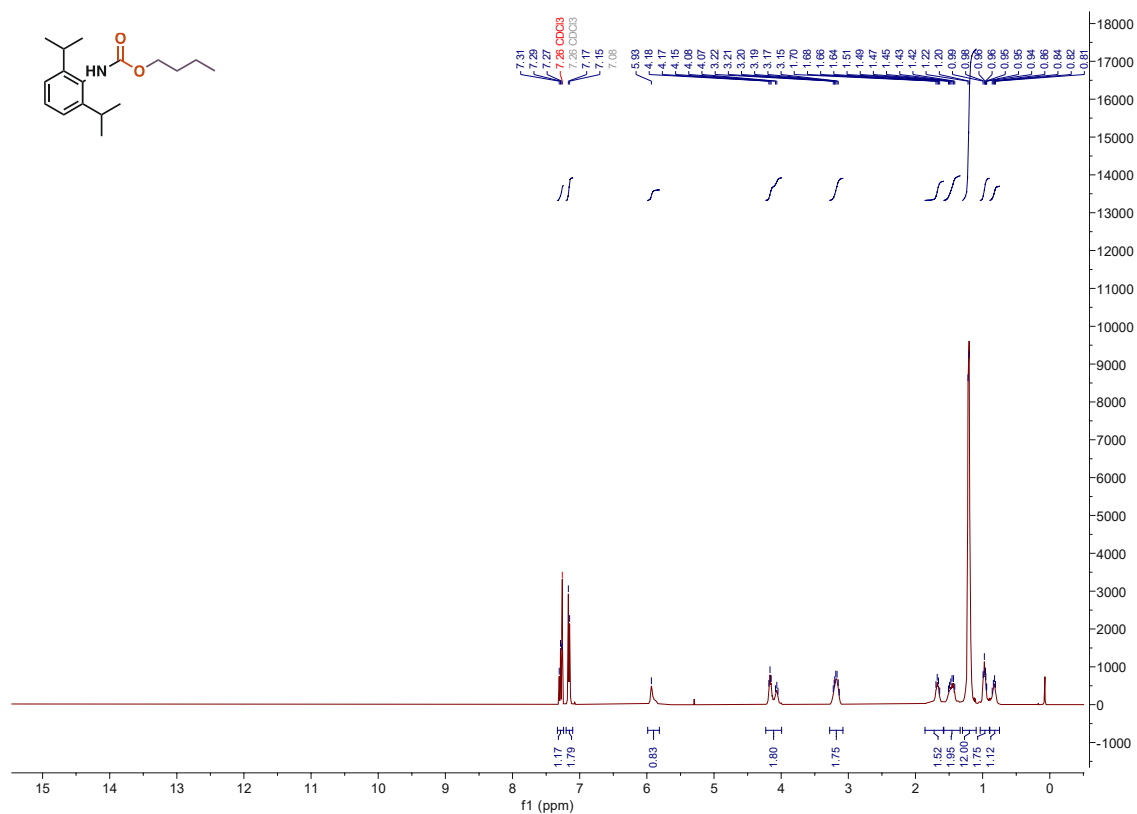


Figure 221. ^1H NMR of 3g

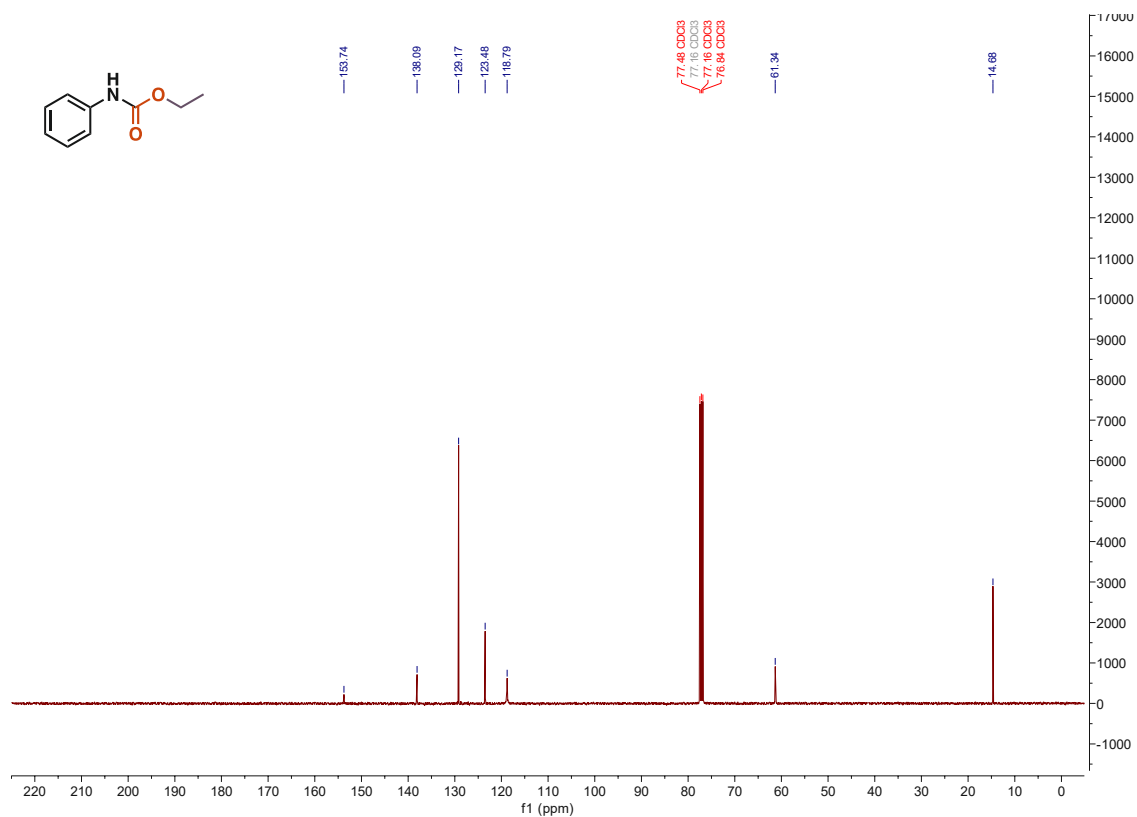


Figure 224. ^{13}C NMR of 3h

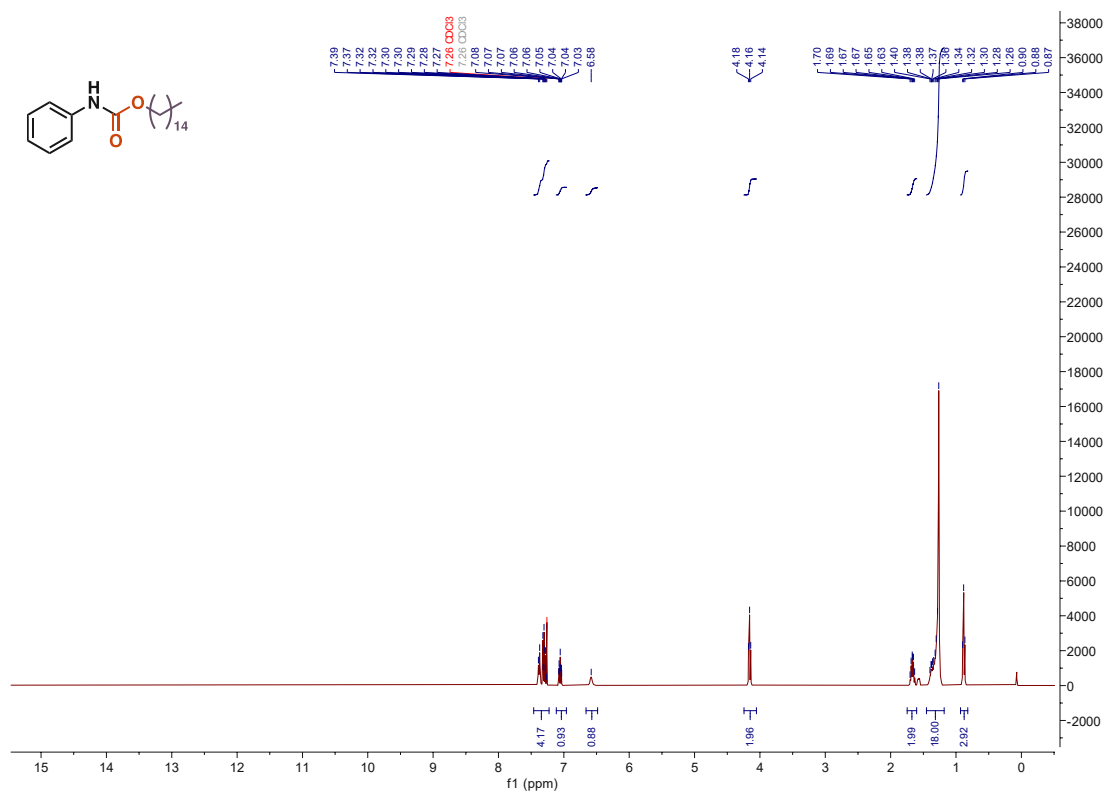
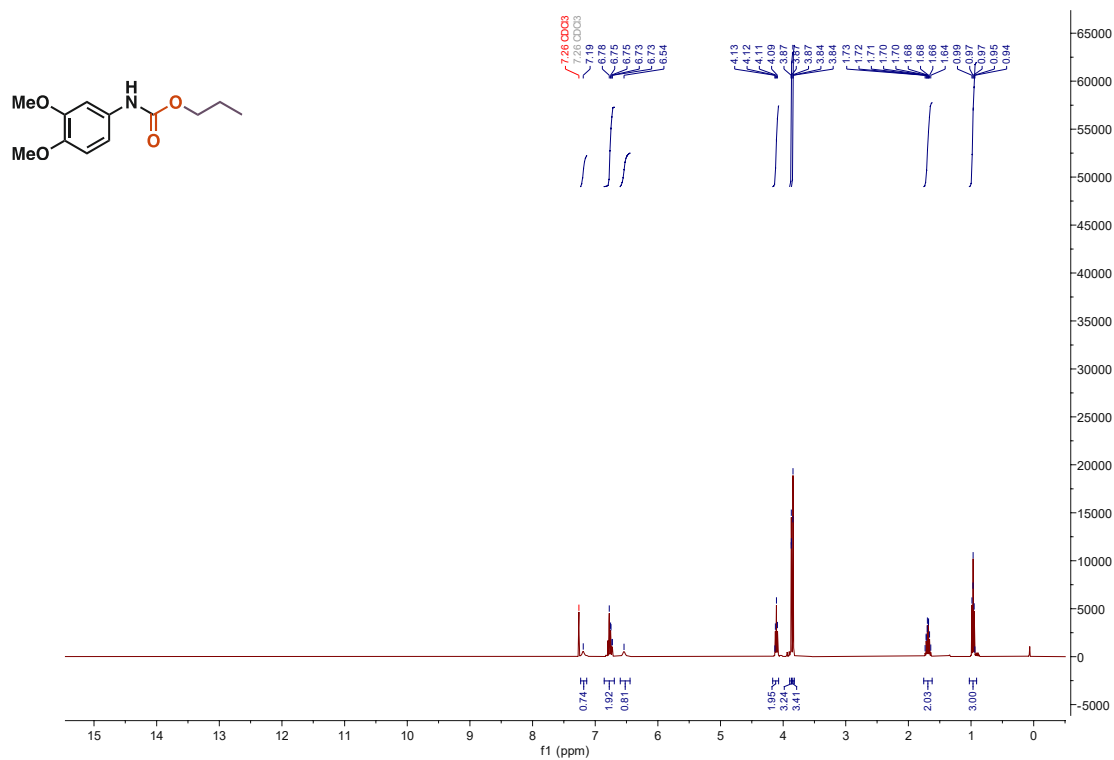
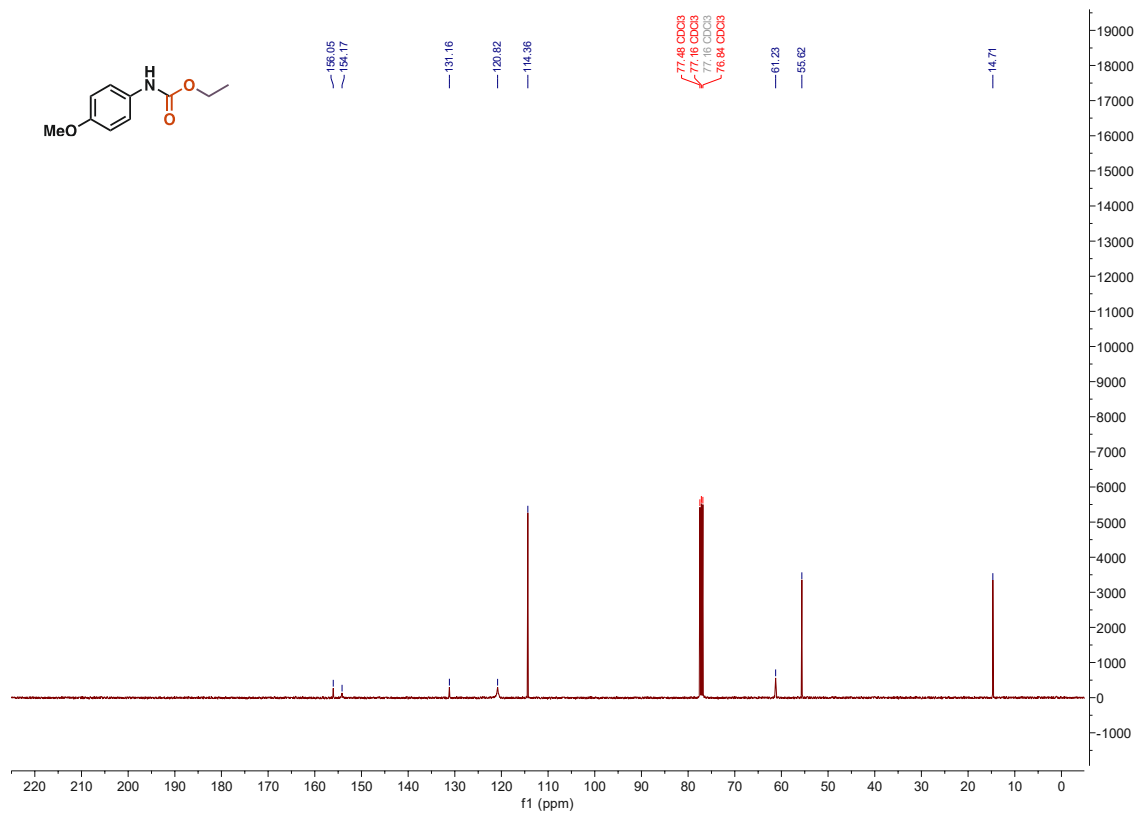


Figure 225. ^1H NMR of 3i



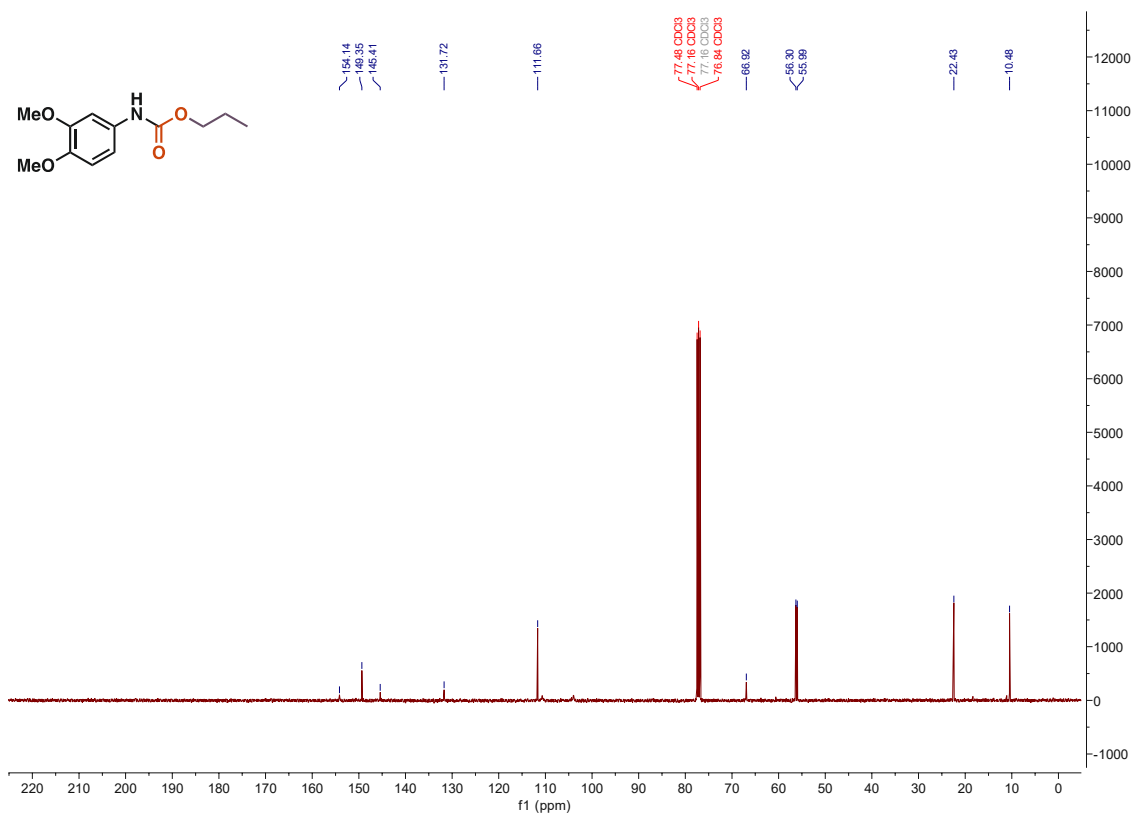


Figure 230. ¹³C NMR of 3k

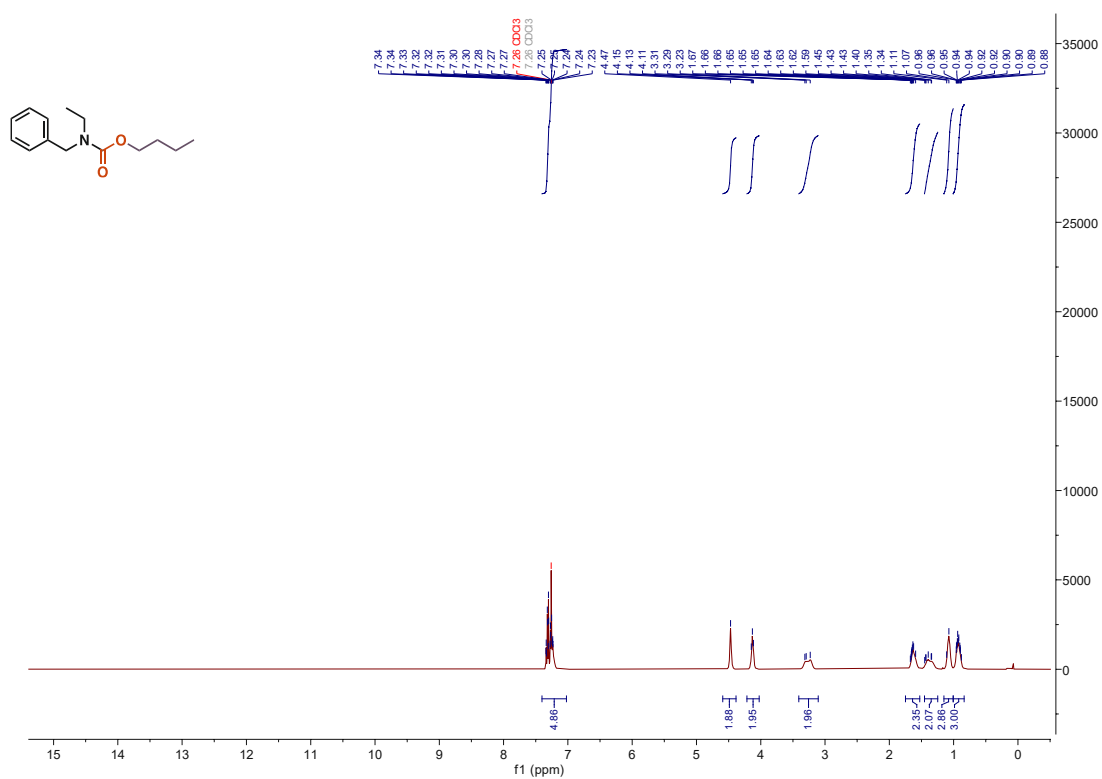
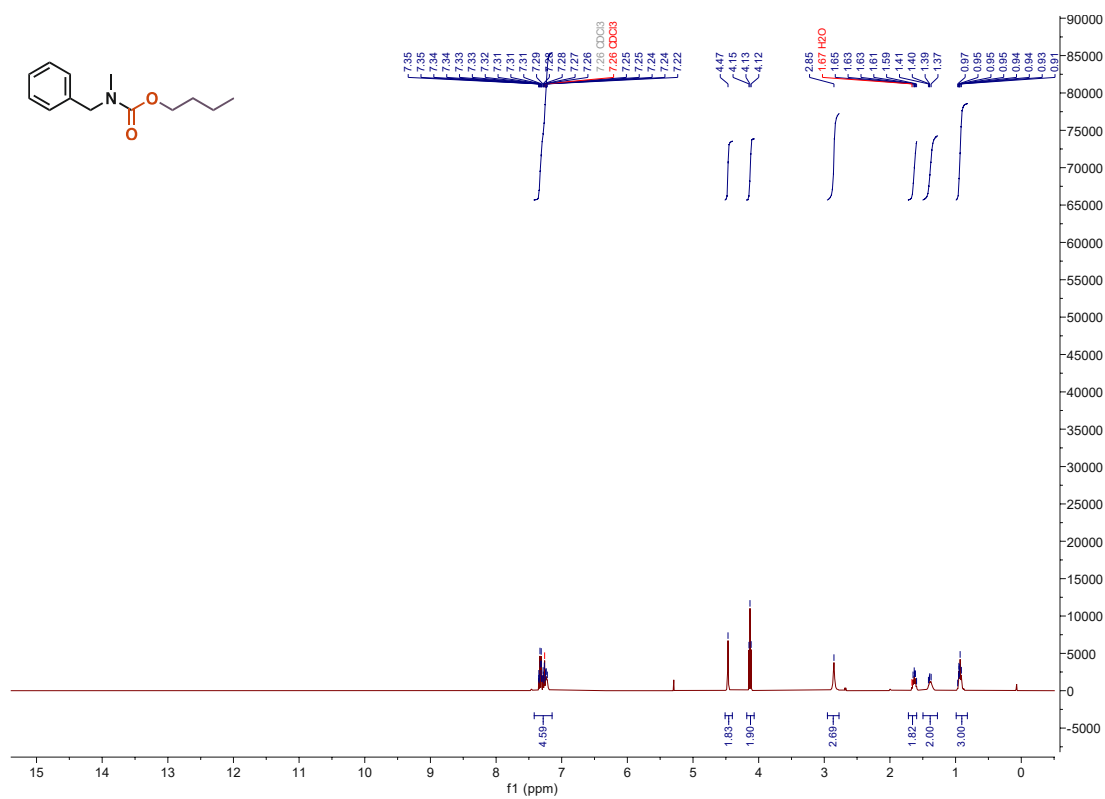
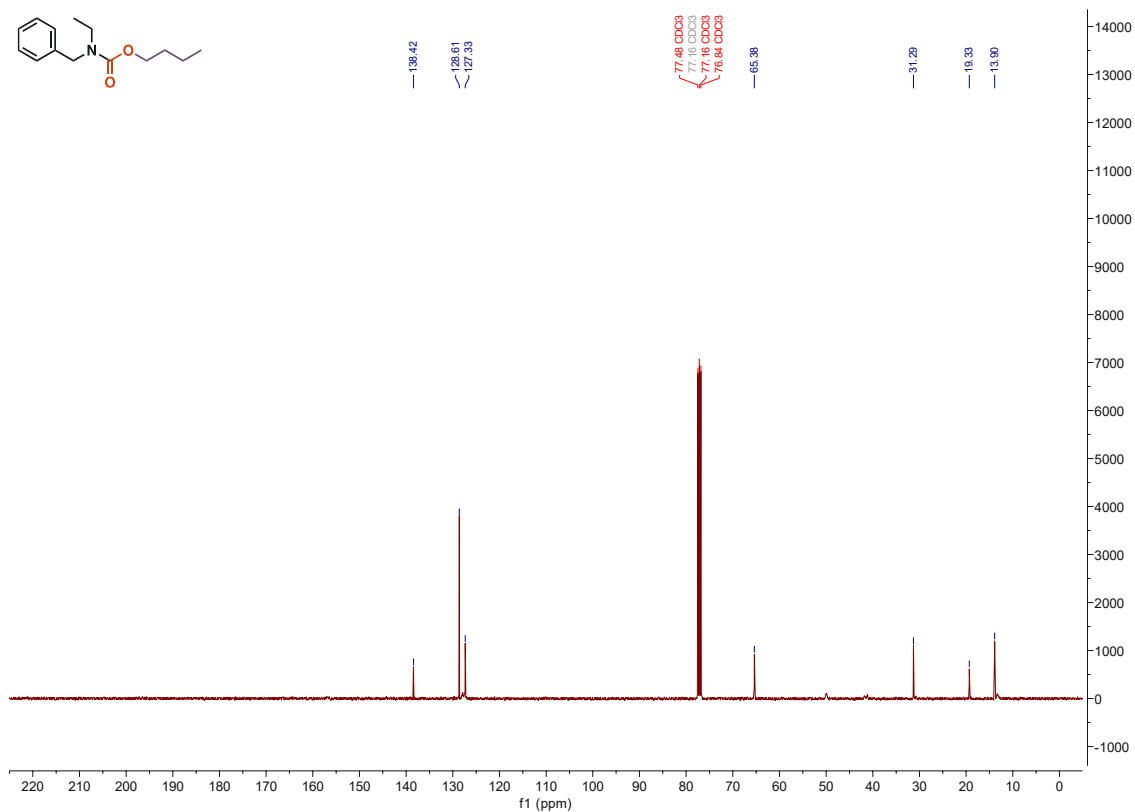


Figure 231. ¹H NMR of 3l



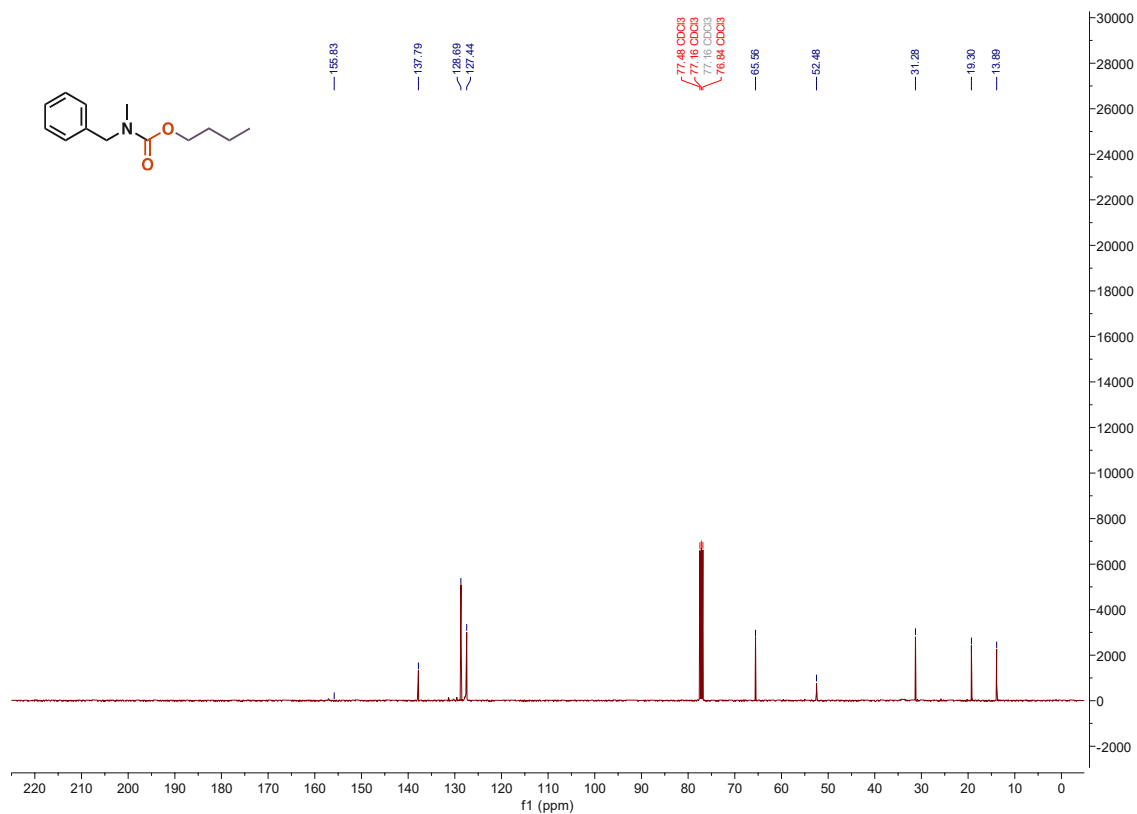


Figure 234. ^{13}C NMR of 3m

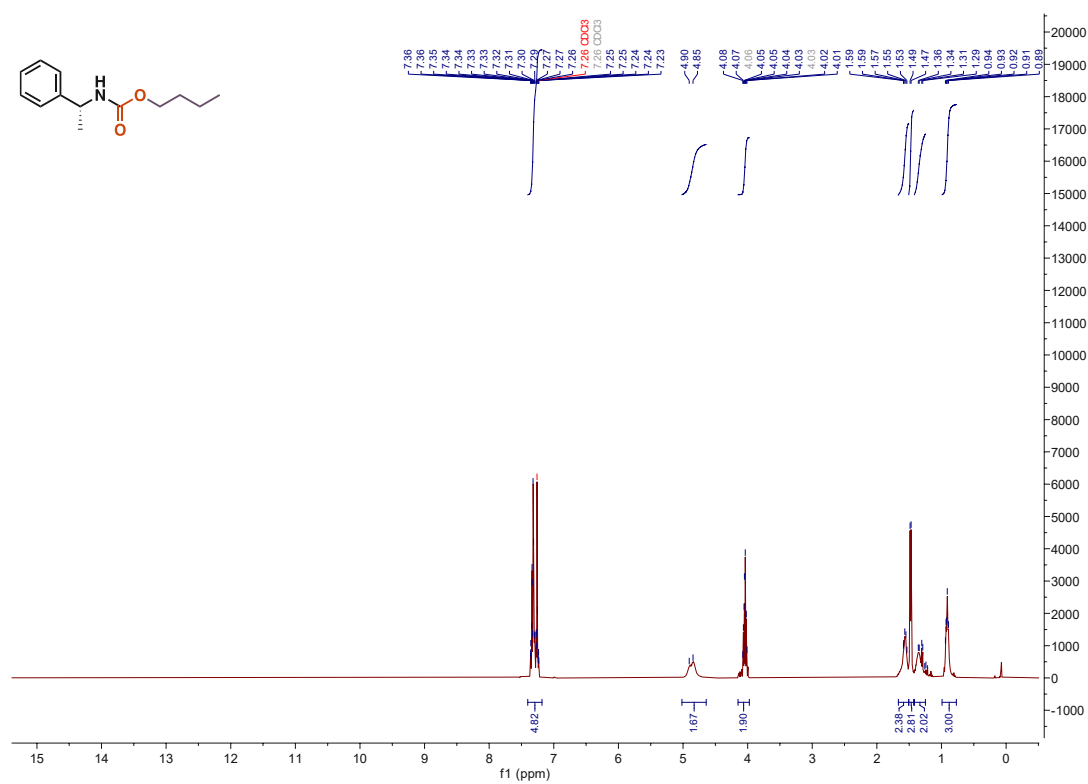


Figure 235. ^1H NMR of 3n

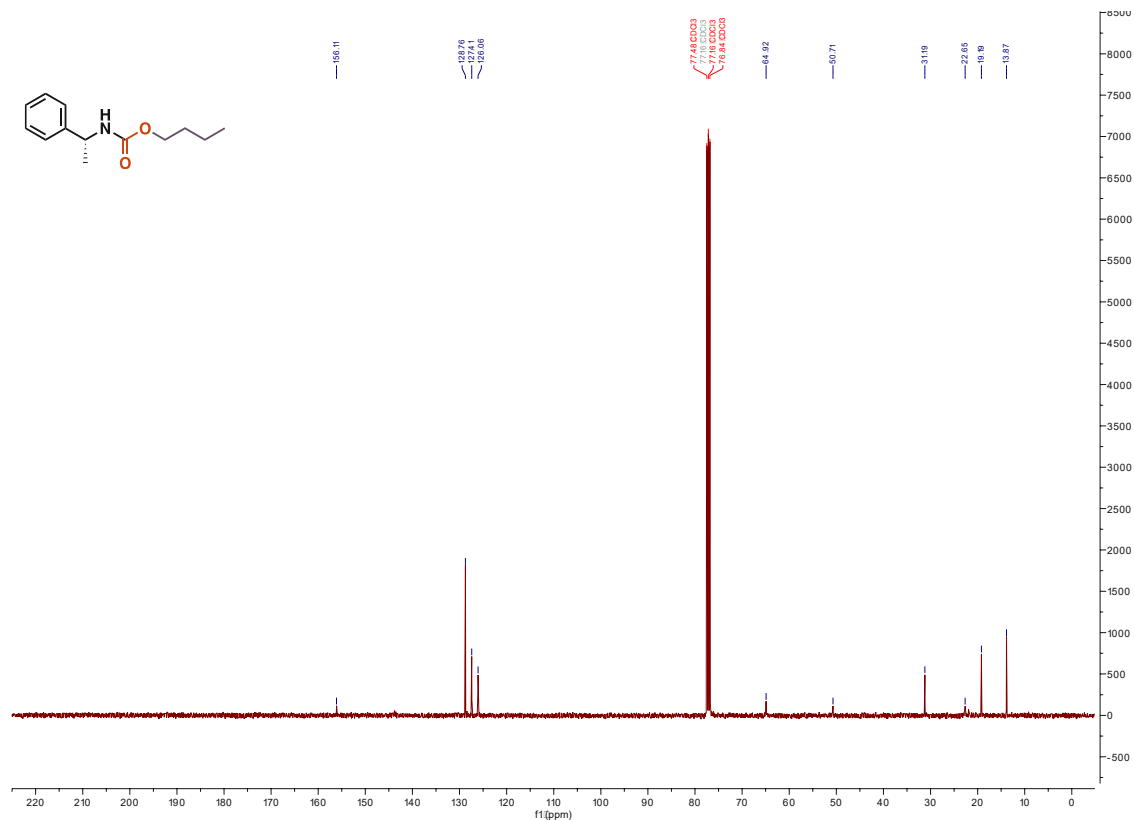


Figure 236. ^{13}C NMR of 3n

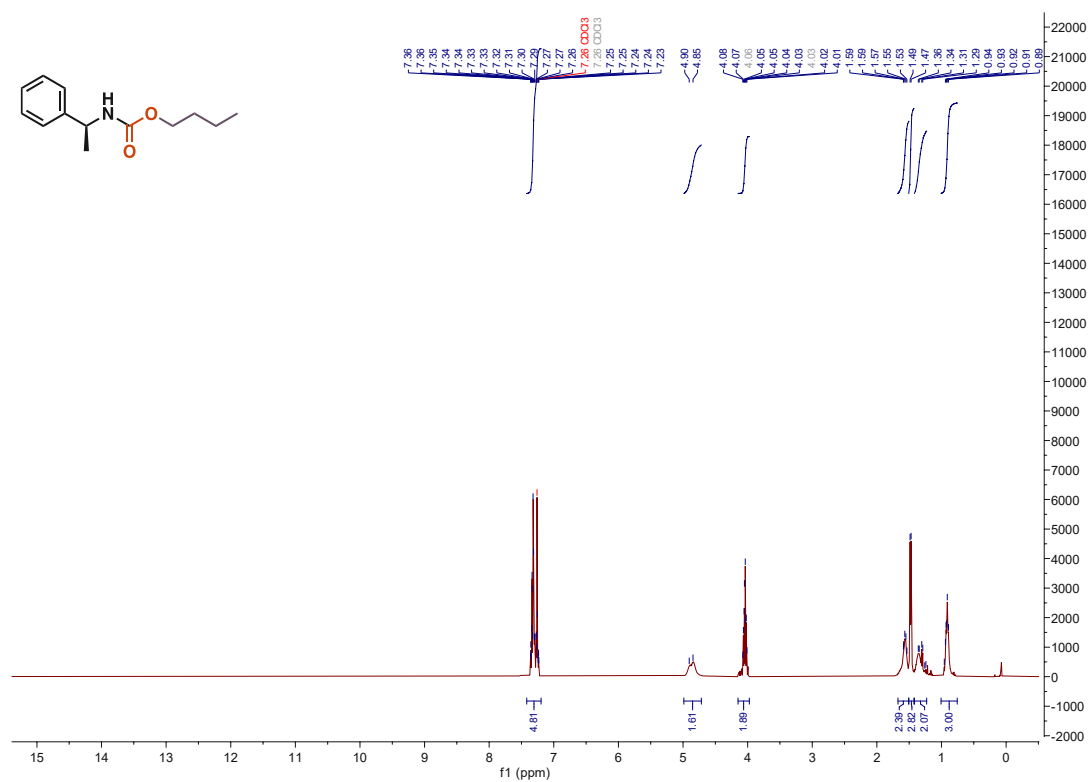


Figure 237. ^1H NMR of 3o

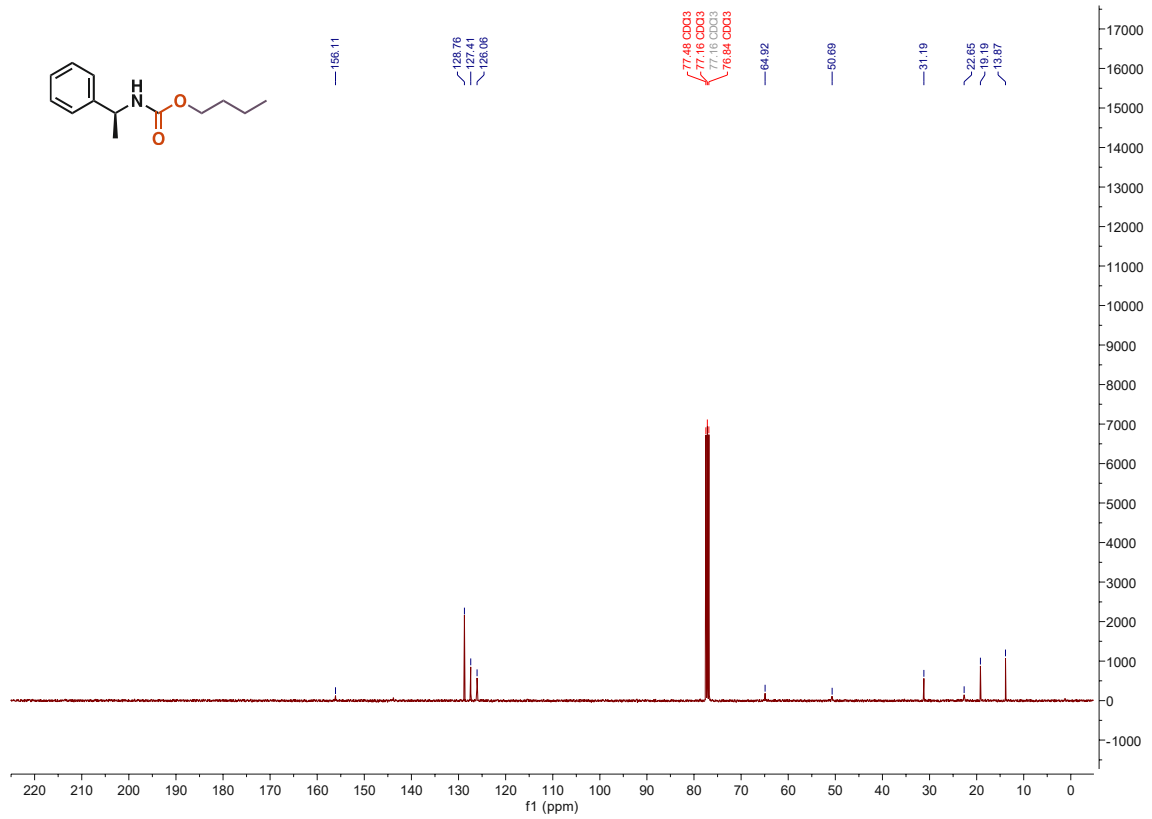


Figure 238. ¹³C NMR of 3o

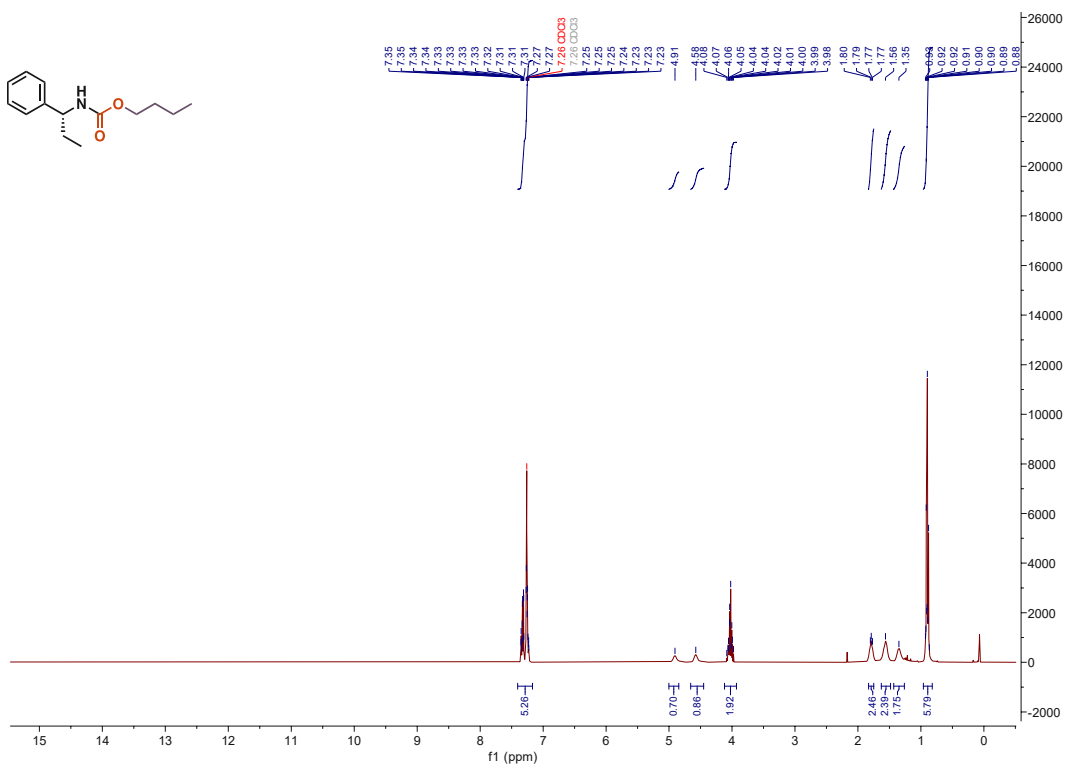


Figure 239. ¹H NMR of 3p

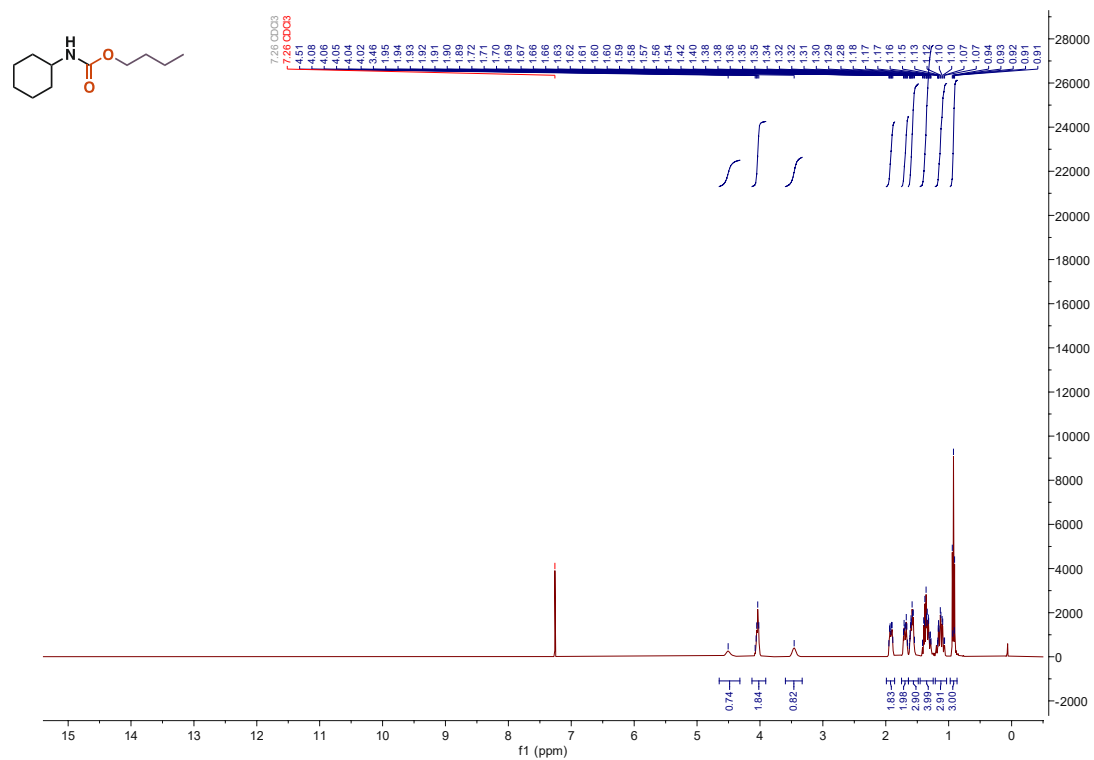
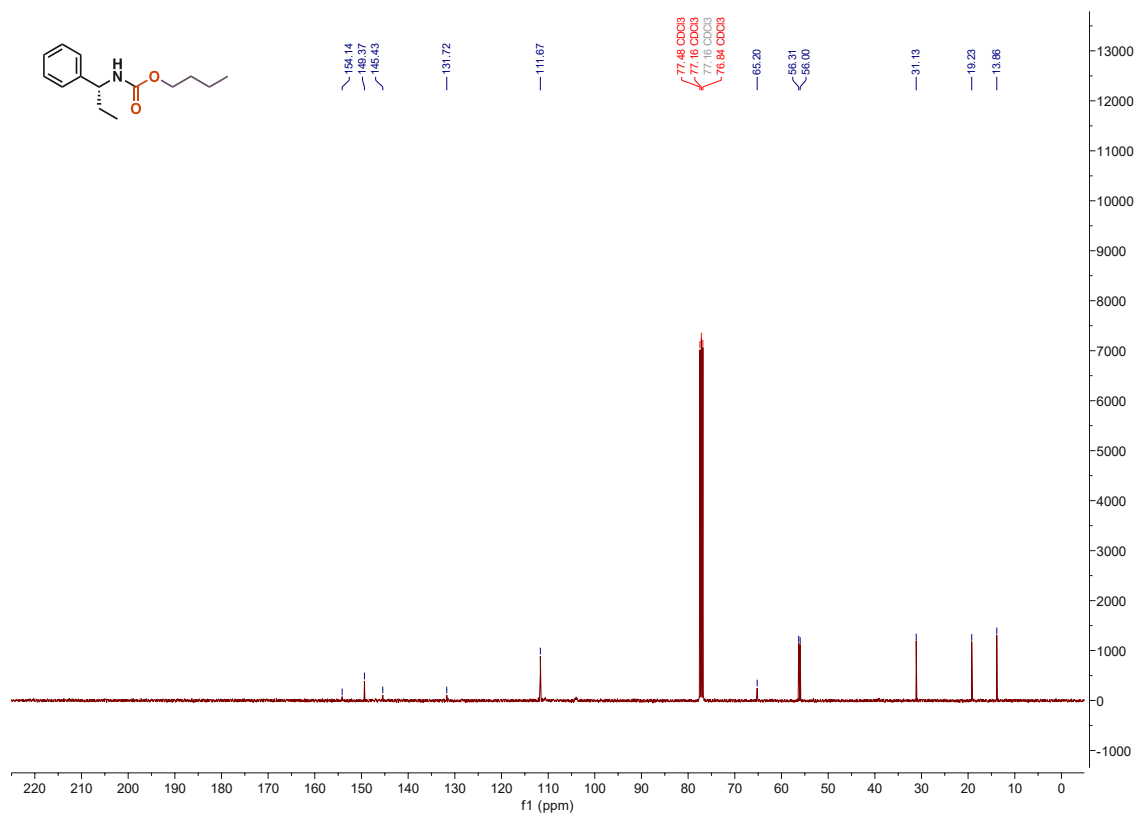


Figure 241. ¹H NMR of 3q

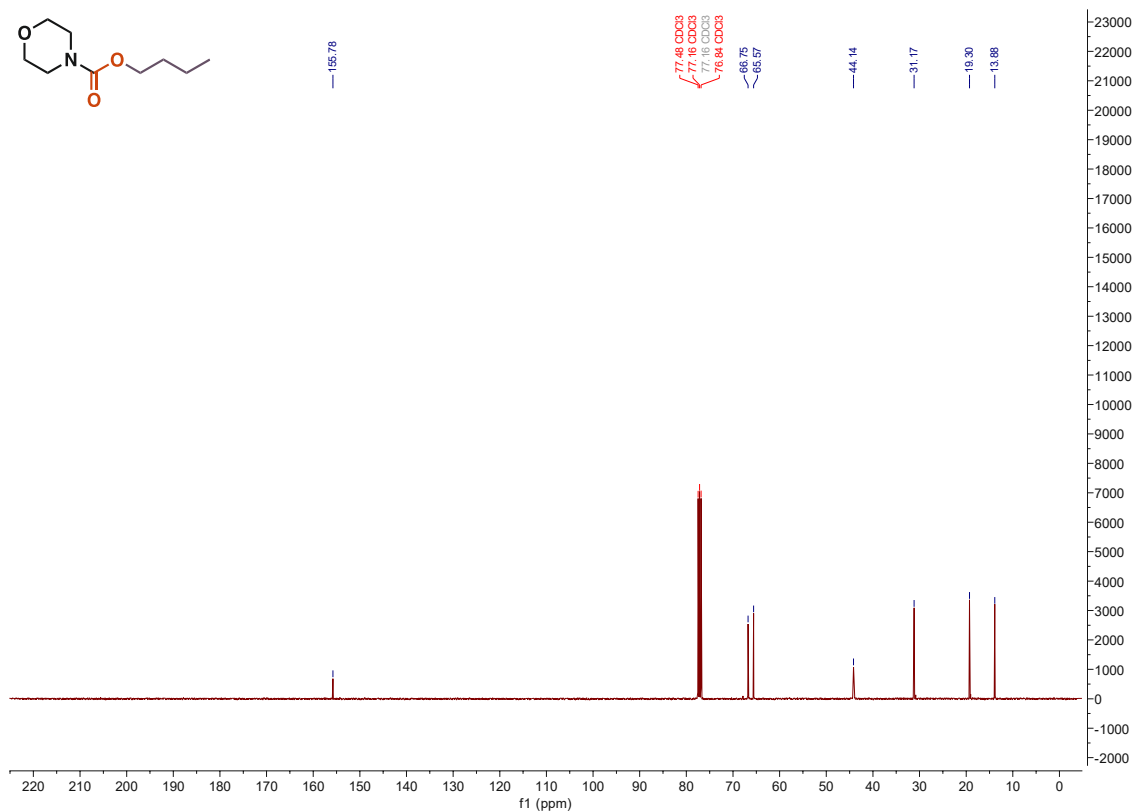


Figure 244. ^{13}C NMR of **3r**

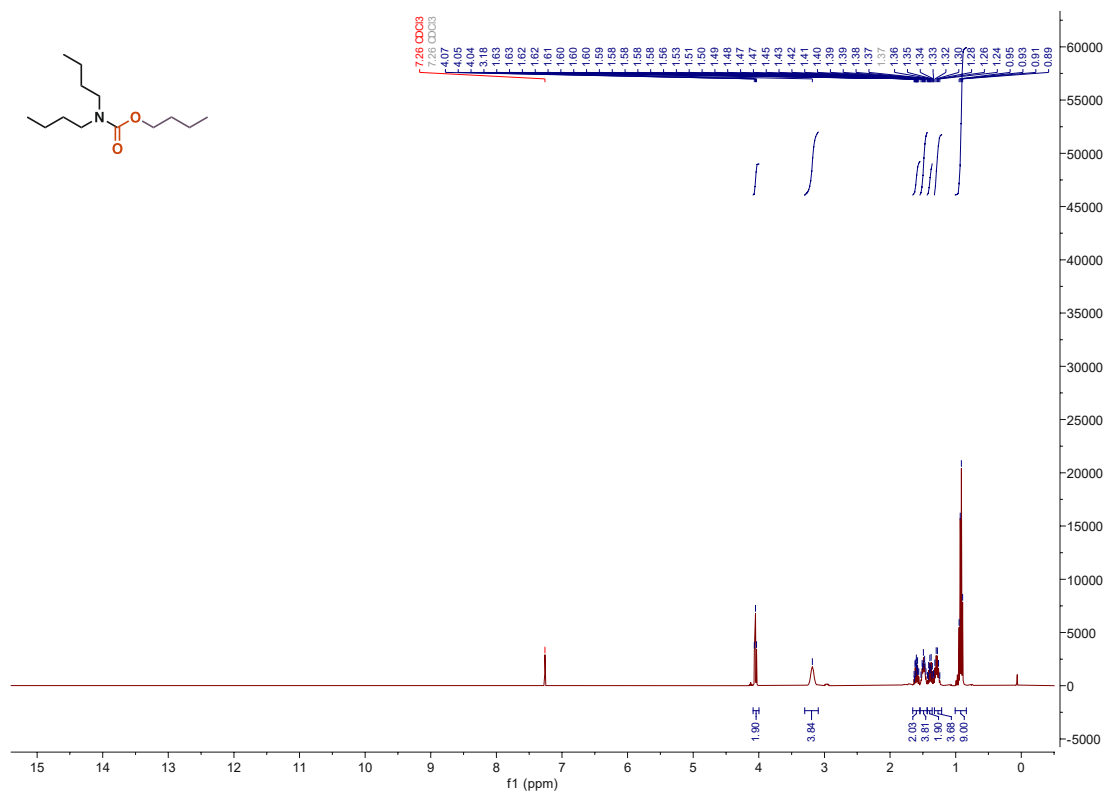


Figure 245. ^1H NMR of **3s**

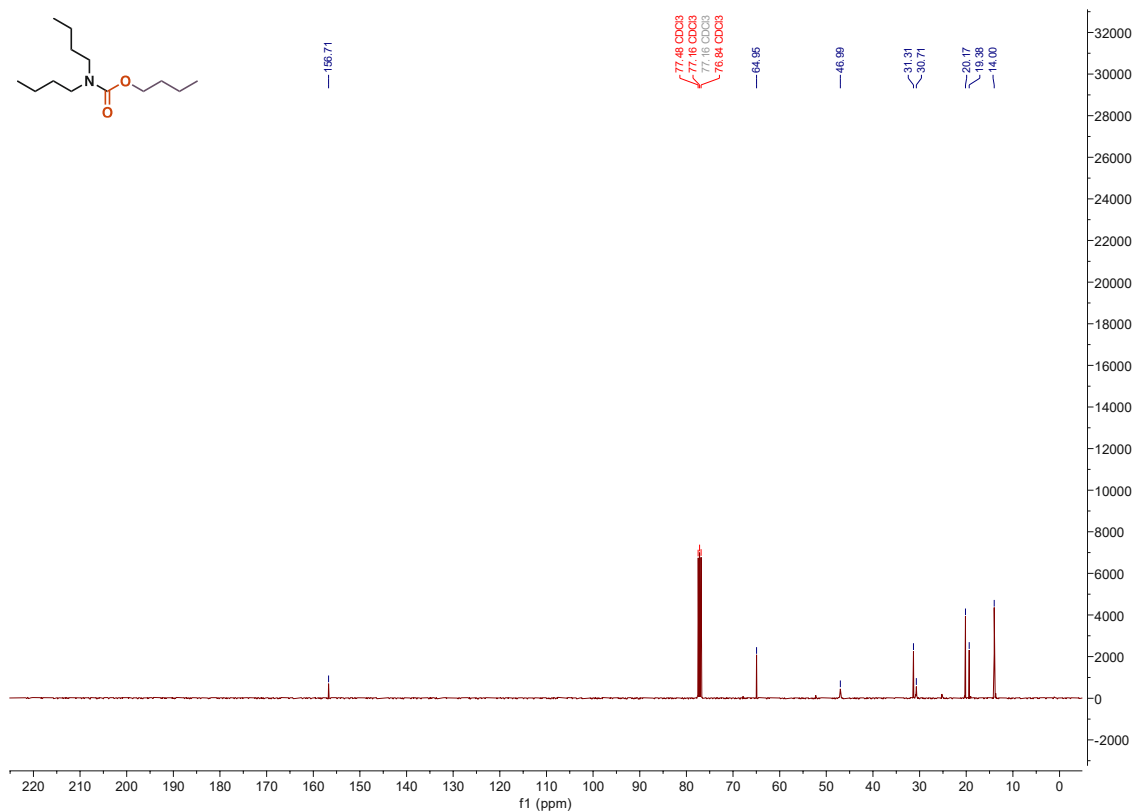


Figure 246. ^{13}C NMR of 3s

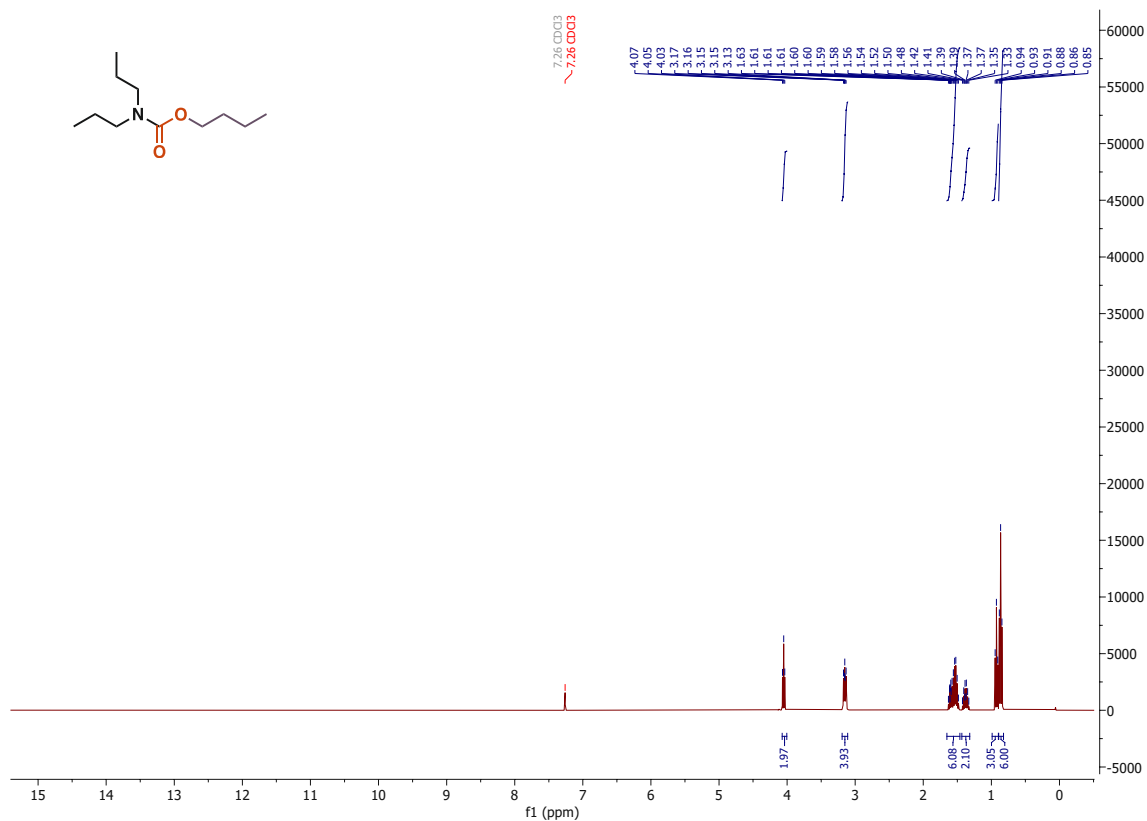


Figure 247. ^1H NMR of 3t

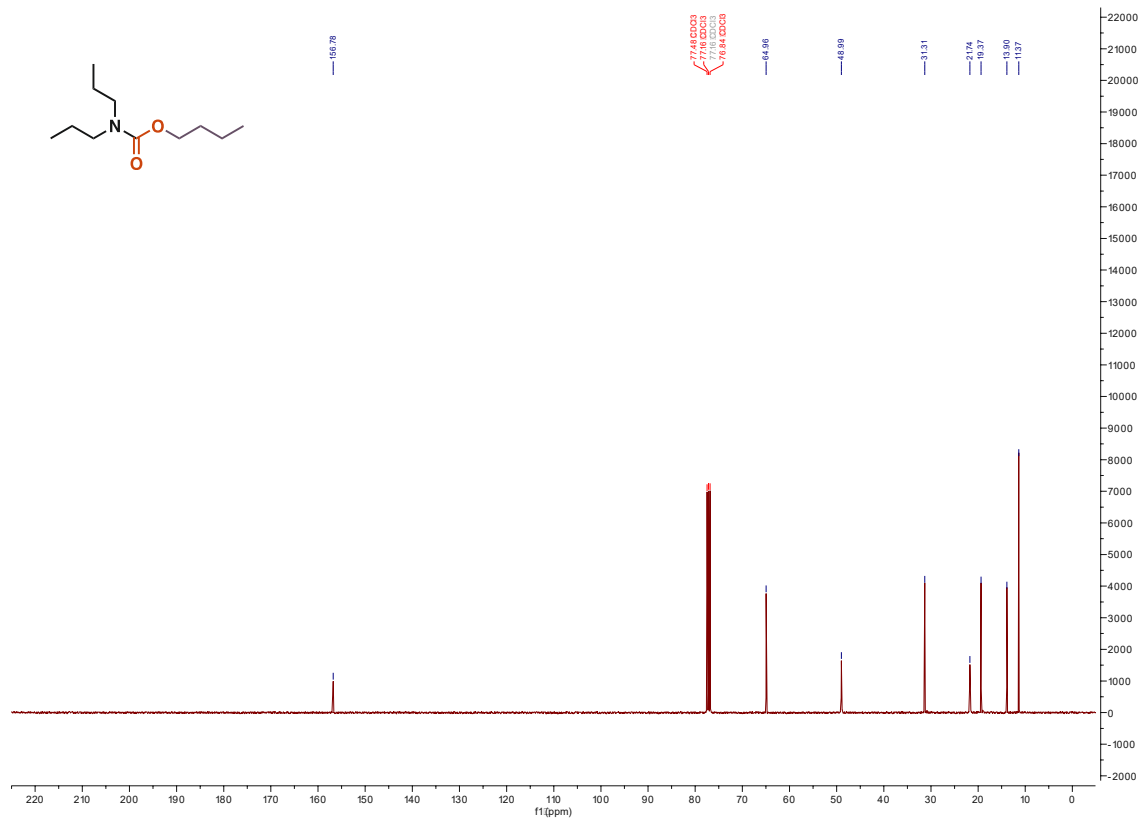


Figure 248. ^{13}C NMR of 3t

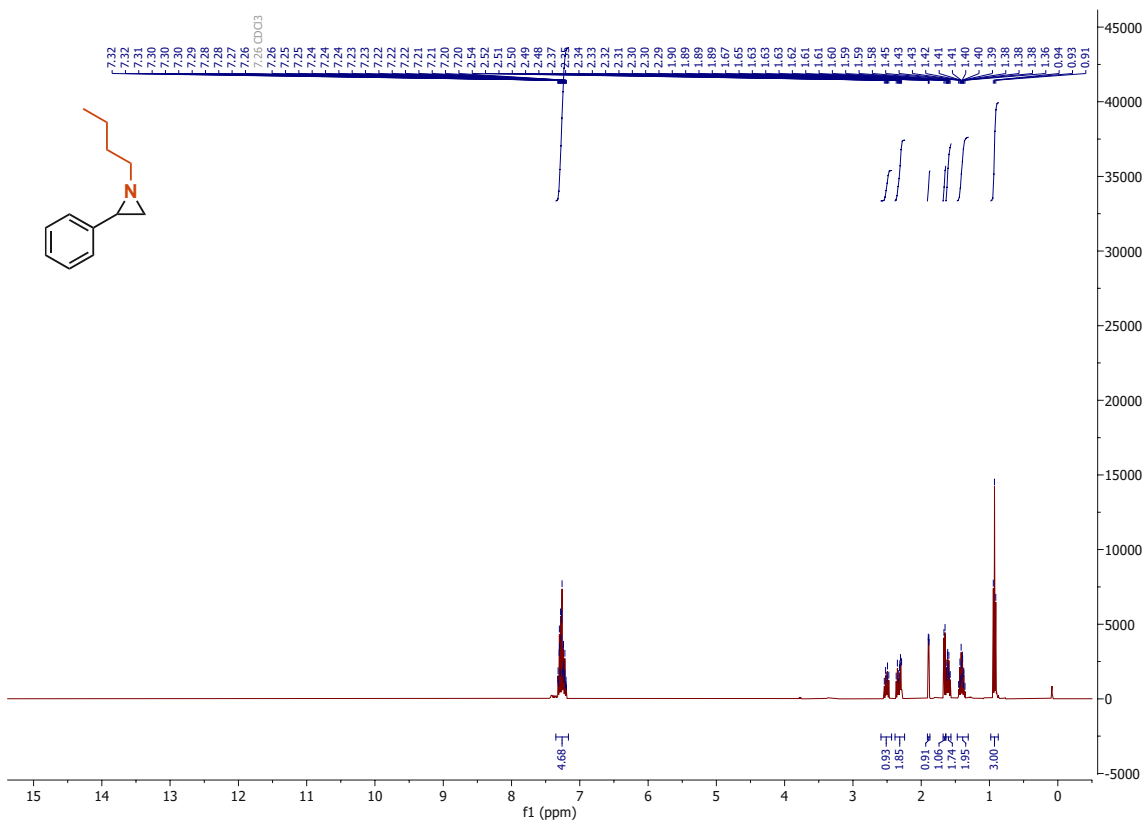
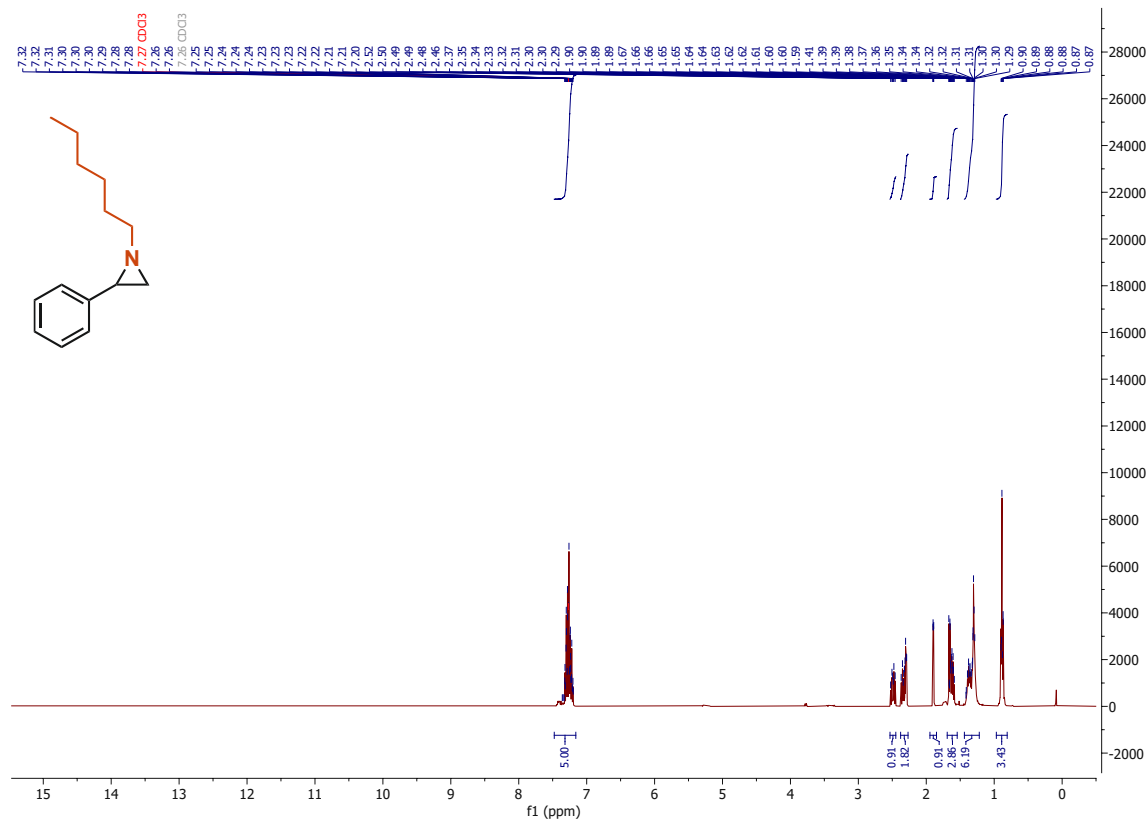
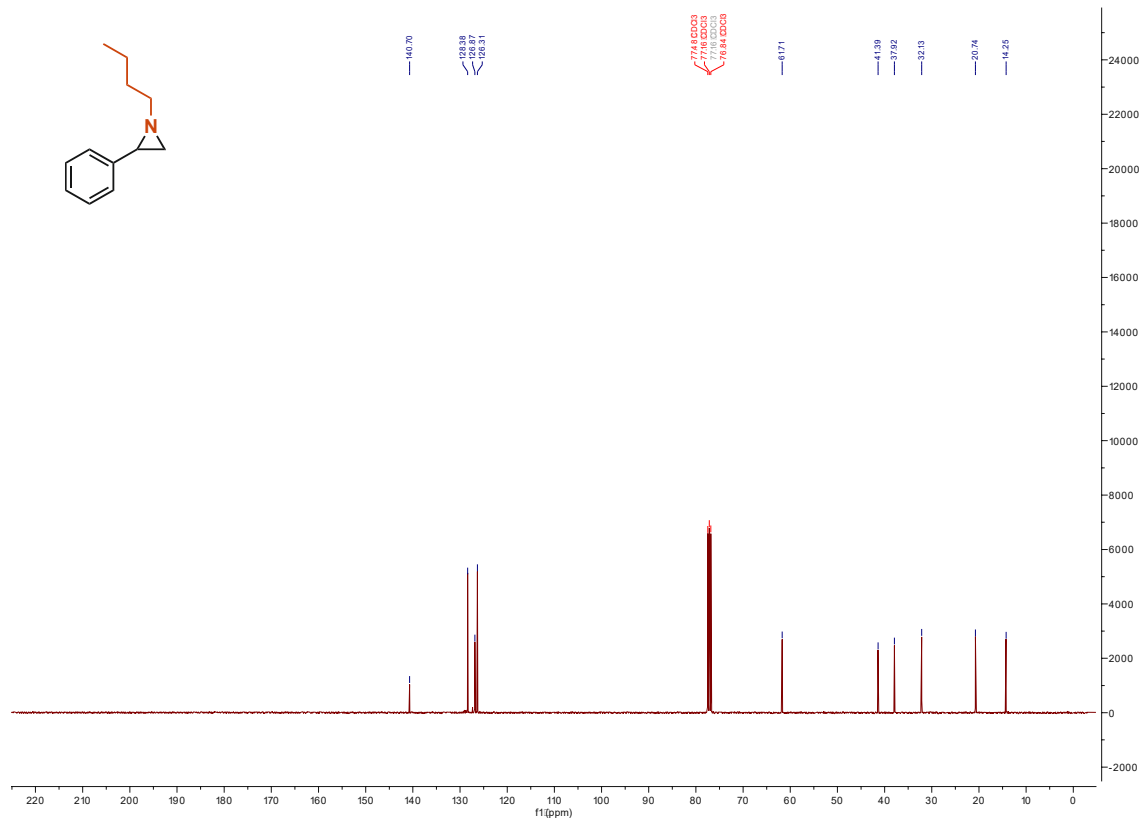


Figure 249. ^1H NMR of 4a



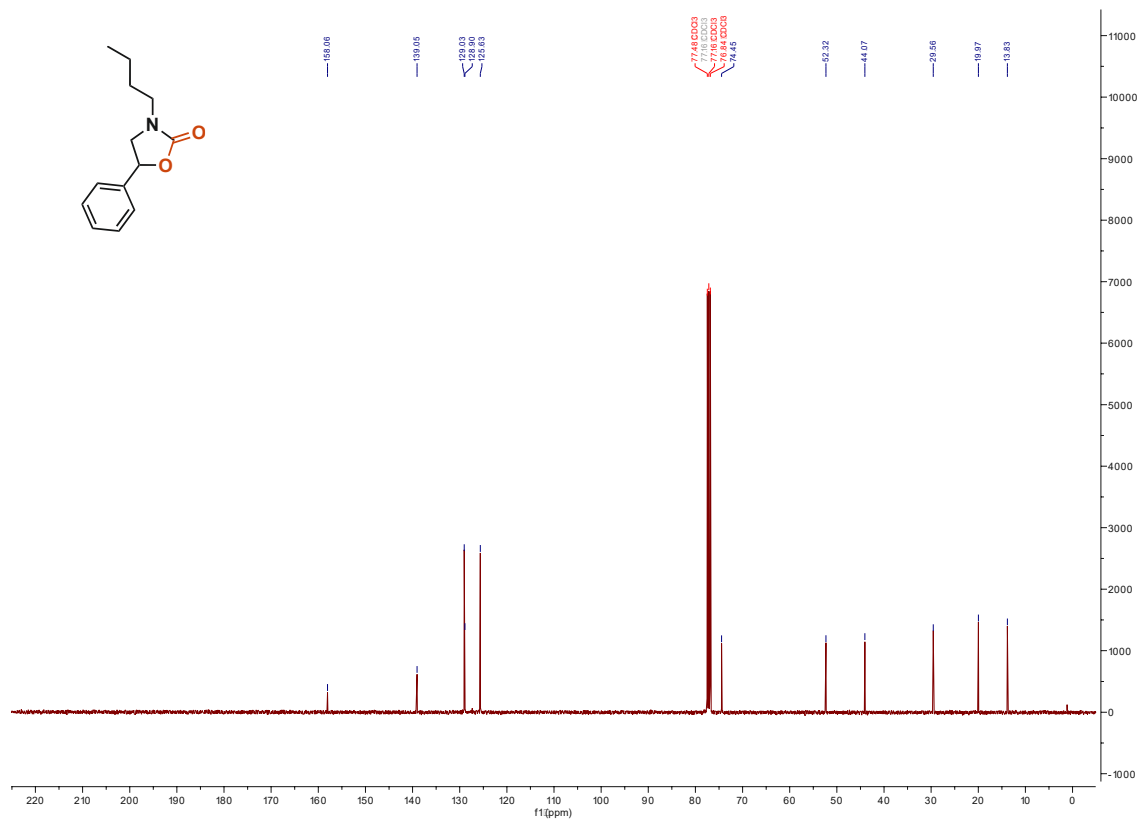


Figure 254. ^{13}C NMR of 5a

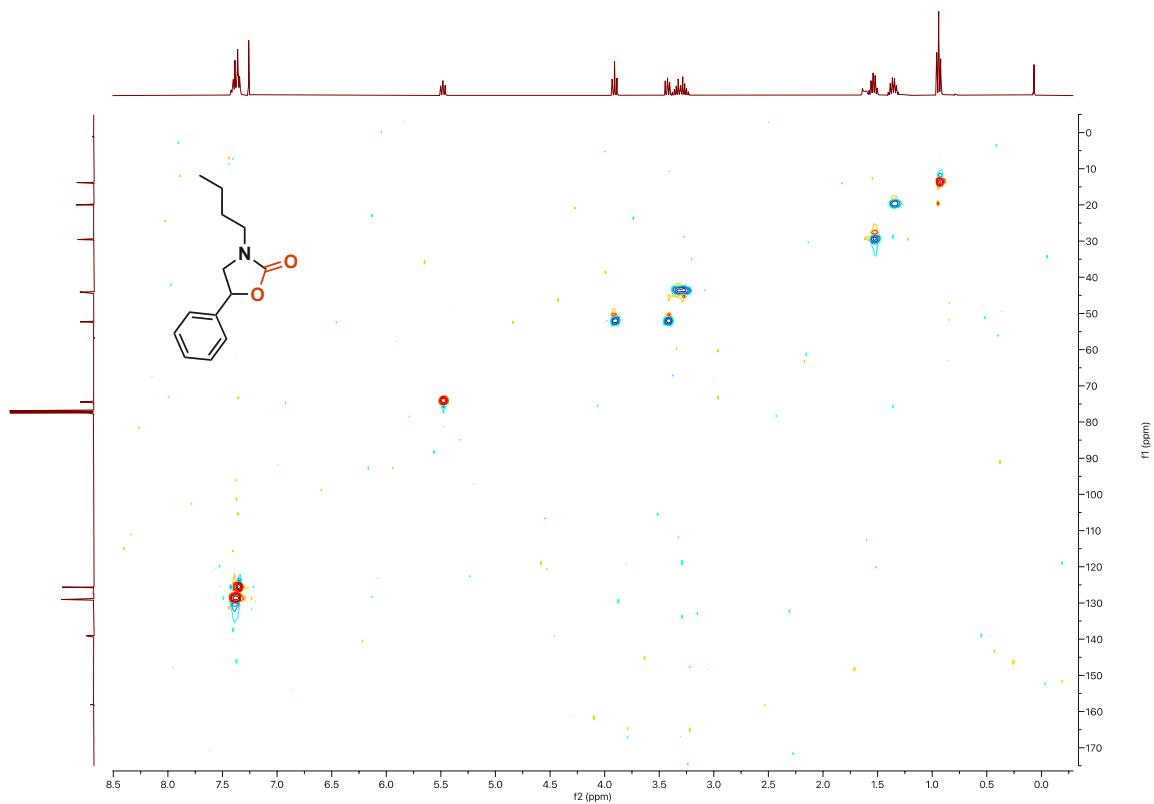


Figure 255. HSQC NMR of 5a

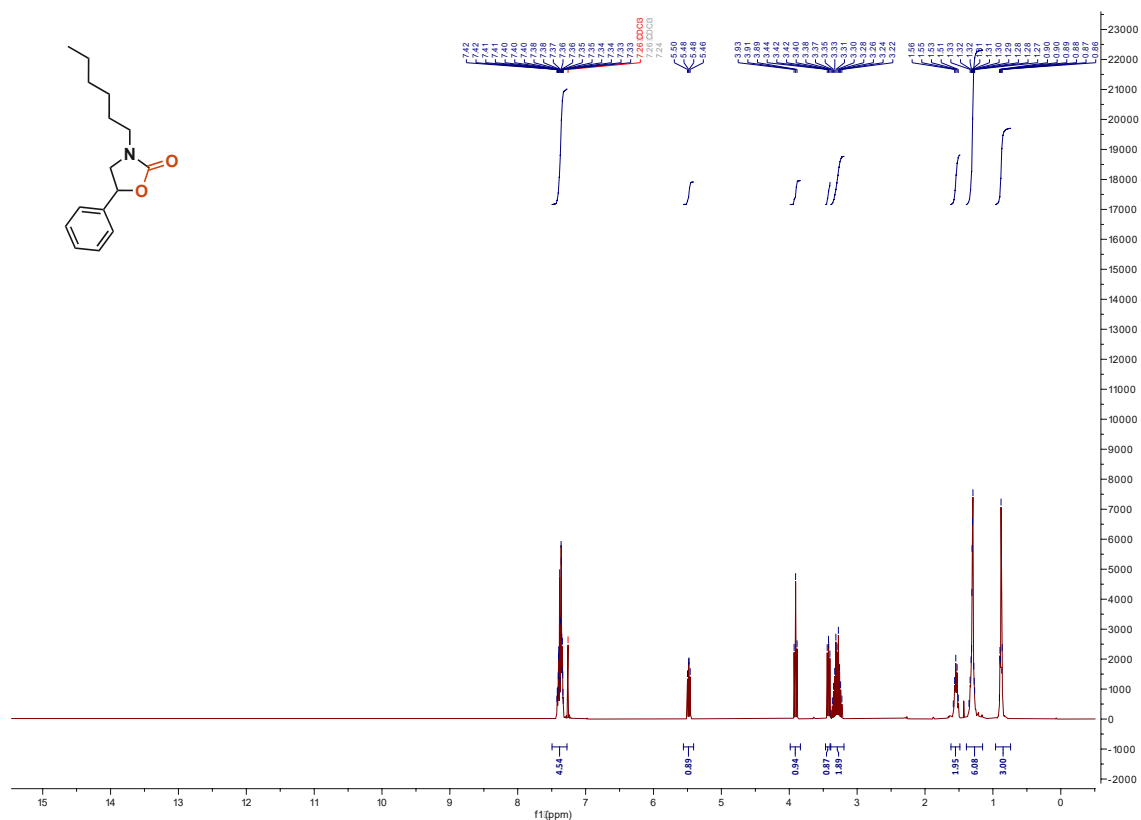


Figure 256. ¹H NMR of 5b

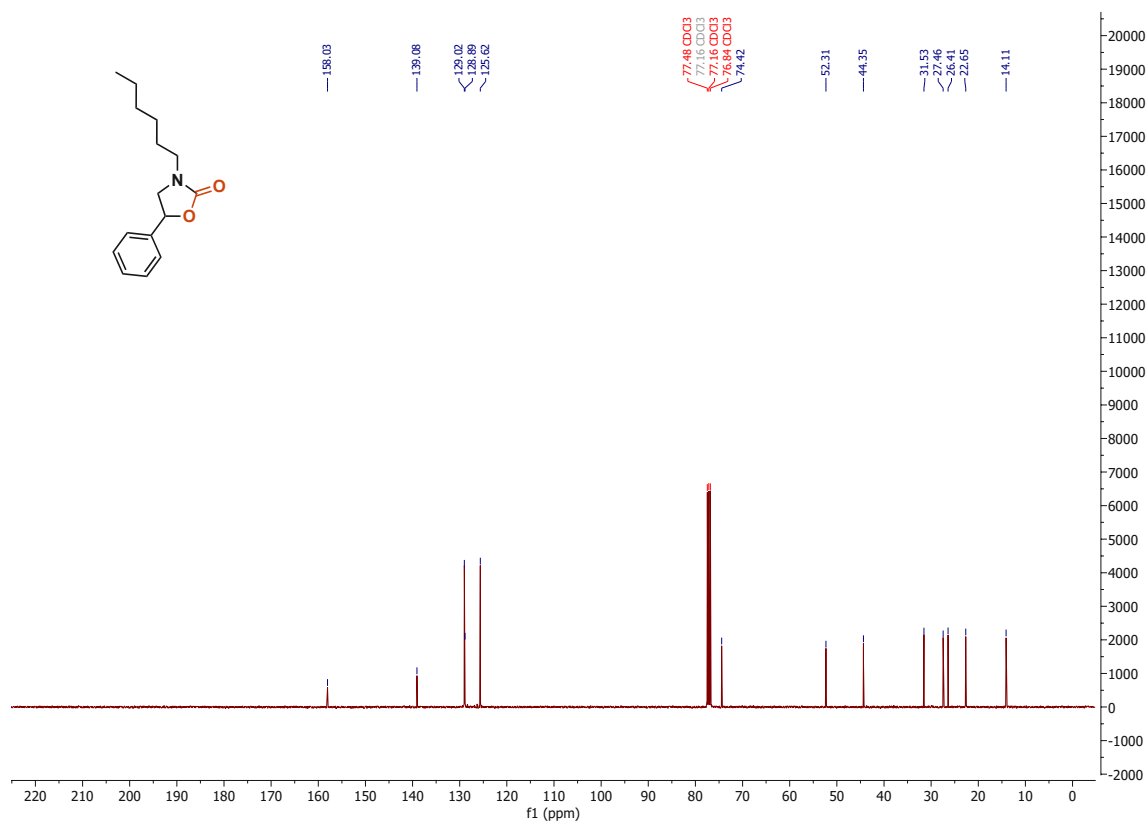


Figure 257. ¹³C NMR of 5b

10.7 Chiral HPLC traces

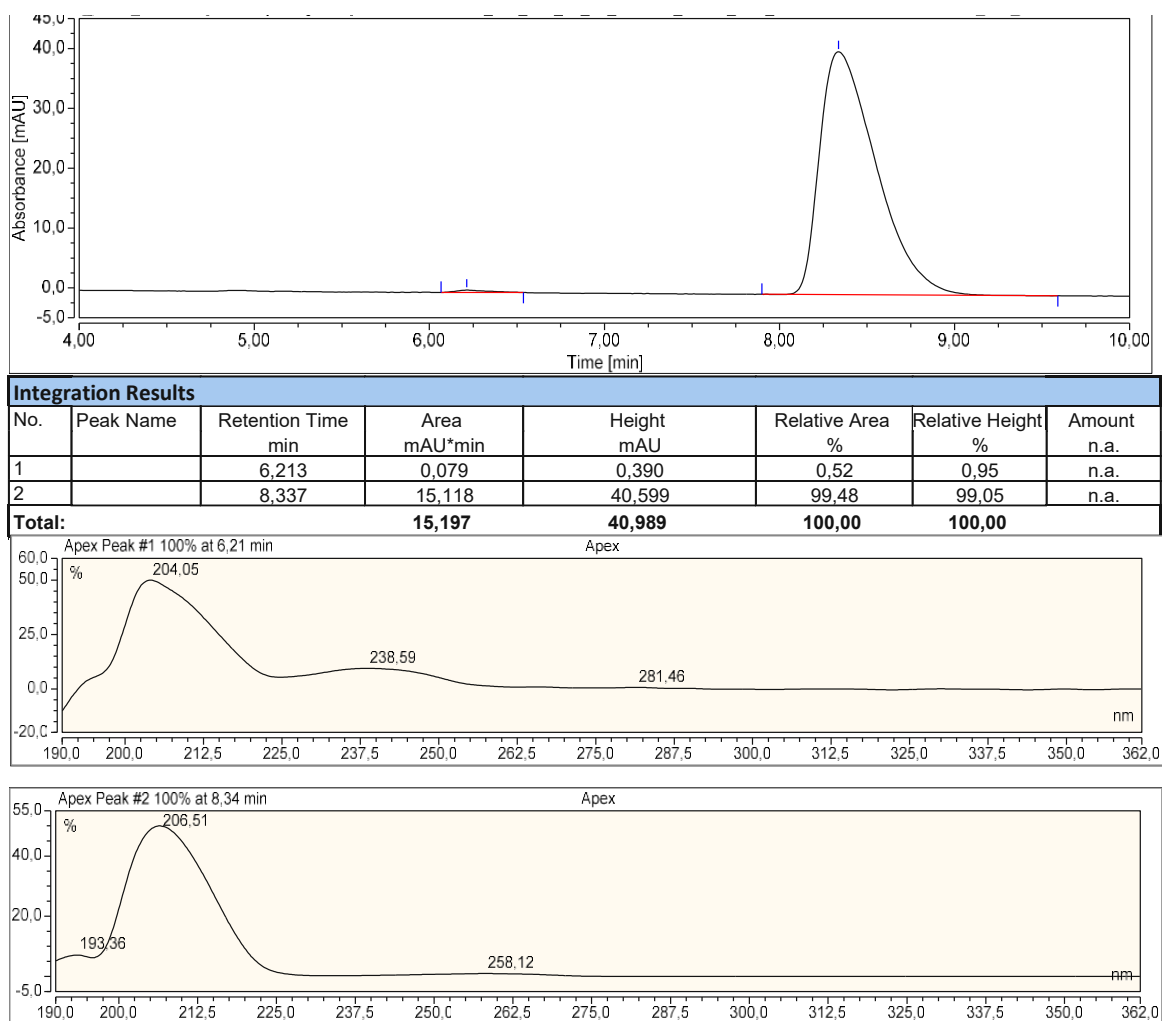


Figure 258. Chiral HPLC chromatogram of 3n

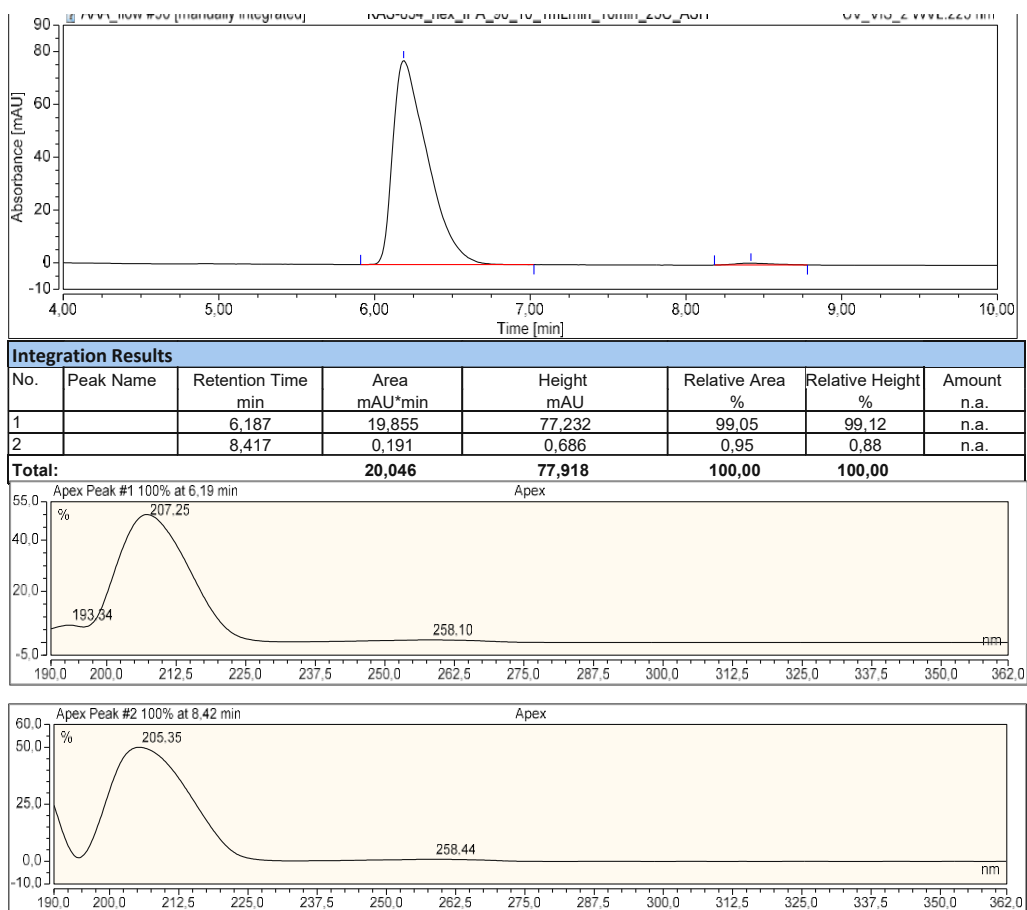


Figure 259. Chiral HPLC chromatogram of **3o**

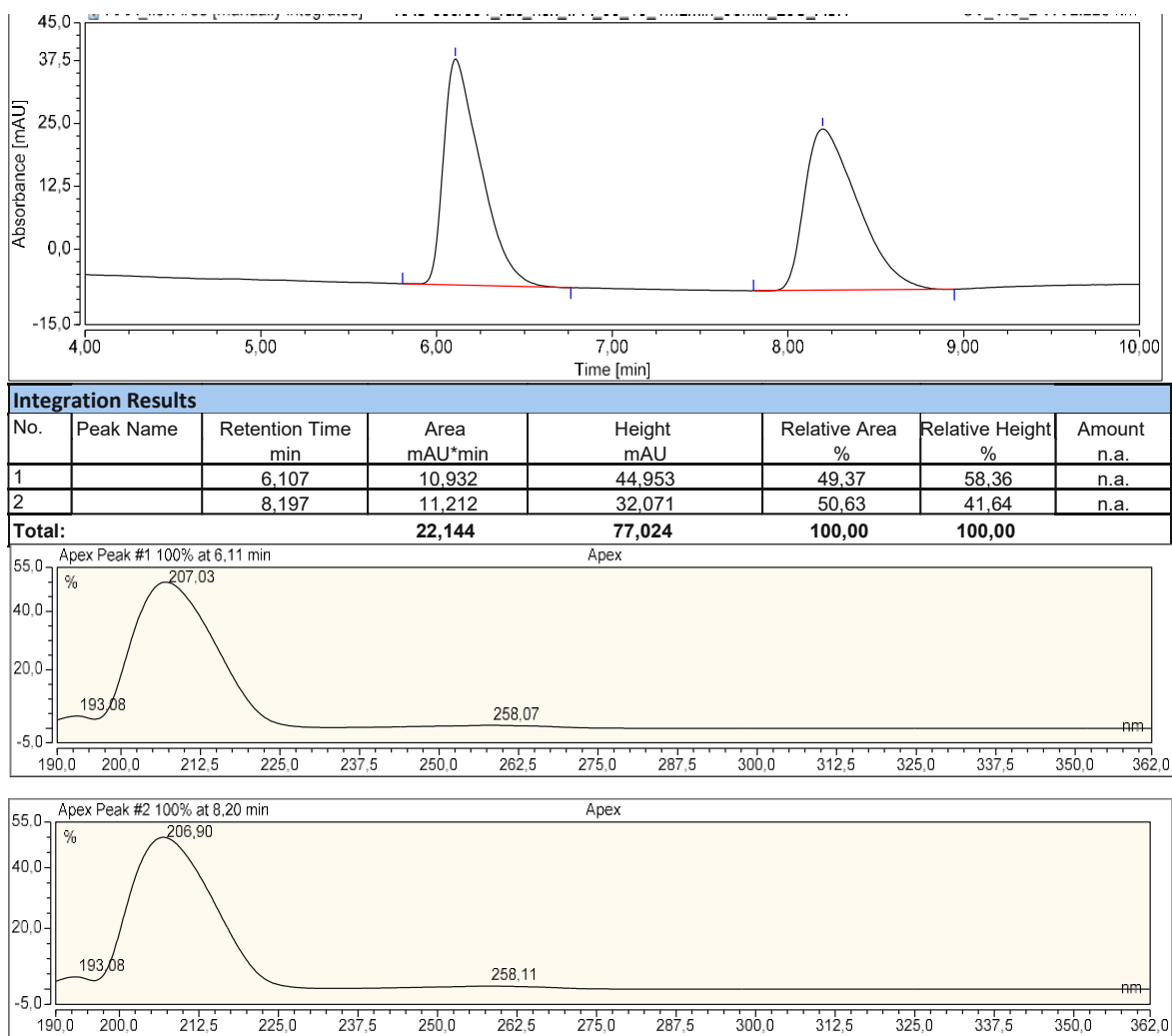


Figure 260. Chiral HPLC chromatogram of **3n-3o** (racemic)

11. Appendix D

Supporting Information

Online Coupling High-Temperature Electrolysis with Carbonylation Reactions: A Powerful Method for Continuous Carbon Dioxide Utilisation

Kristof Stigel,^[a] Kirsten Rath,^[b] Prasad M. Kathe,^[a] Alexander K. Opitz,^{,[b]} Michael Schnürch,^[a] and Katharina Bica-Schröder^{*,[a]}*

^aInstitute of Applied Synthetic Chemistry, TU Wien, Getreidemarkt 9/163, Vienna, 1060, Austria

^bInstitute of Chemical Technologies and Analytics, TU Wien, Getreidemarkt 9/164, Vienna, 1060, Austria

*Corresponding authors:

Katharina Bica-Schröder, E-mail: katharina.schroeder@tuwien.ac.at

Alexander Karl Opitz, E-mail: alexander.opitz@tuwien.ac.at

11.1 General remarks

Unless otherwise noted, commercially supplied chemicals were used without further purification.

Column chromatography was performed on standard glass columns using Merck (40-60 μm) silica with pre-distilled solvents. For TLC analysis, pre-coated aluminum-backed plates were used (Merck, silica 60 F₂₅₄). All compounds were detected at 254 nm.

¹H-, ¹³C- and ¹⁹F spectra were recorded from CDCl₃ or (CD₃)₂SO solutions on a Bruker Avance UltraShield 400 MHz (¹H: 400 MHz, ¹³C: 101 MHz, ¹⁹F: 376 MHz) NMR instrument. Chemical shifts are reported in parts per million (ppm) and were calibrated to the residual solvent signal (e.g., CDCl₃, ¹H: 7.26 ppm, ¹³C: 77.0 ppm). Coupling constants are reported in hertz (Hz). The assignments are based on the comparison with reported spectra.

GC analysis was performed on a Thermo Scientific Focus, employing a BGB5 column using an FID detector. A linear temperature program was used, starting with a temperature of 50 °C, followed by a ramp rate of 15°C/min up to a final temperature of 240 °C. For optimising the synthesis of ethyl nonanoate, the yield was determined by using *n*-dodecane as internal standard.

Continuous-flow experiments were performed with the aid of a Vapourtec® E-Series flow chemistry device.

Mass flow controllers were purchased from Brooks Instruments; SLA5850 series with four channel secondary electronics (Model 0254). The MFCs were purchased with a configuration that allowed a maximum inlet pressure of 7.5 atm. and an outlet pressure of 1 atm. Carbon monoxide and carbon dioxide were provided from the respective cylinders equipped with a low-pressure regulator, constantly outputting 5 bar (2 bar when the electrochemical cell was employed). For the continuous-flow experiments, the gases were introduced using a V-3 pump after passing through the gas mixer.

11.2 Set-up of the continuous-flow experiments

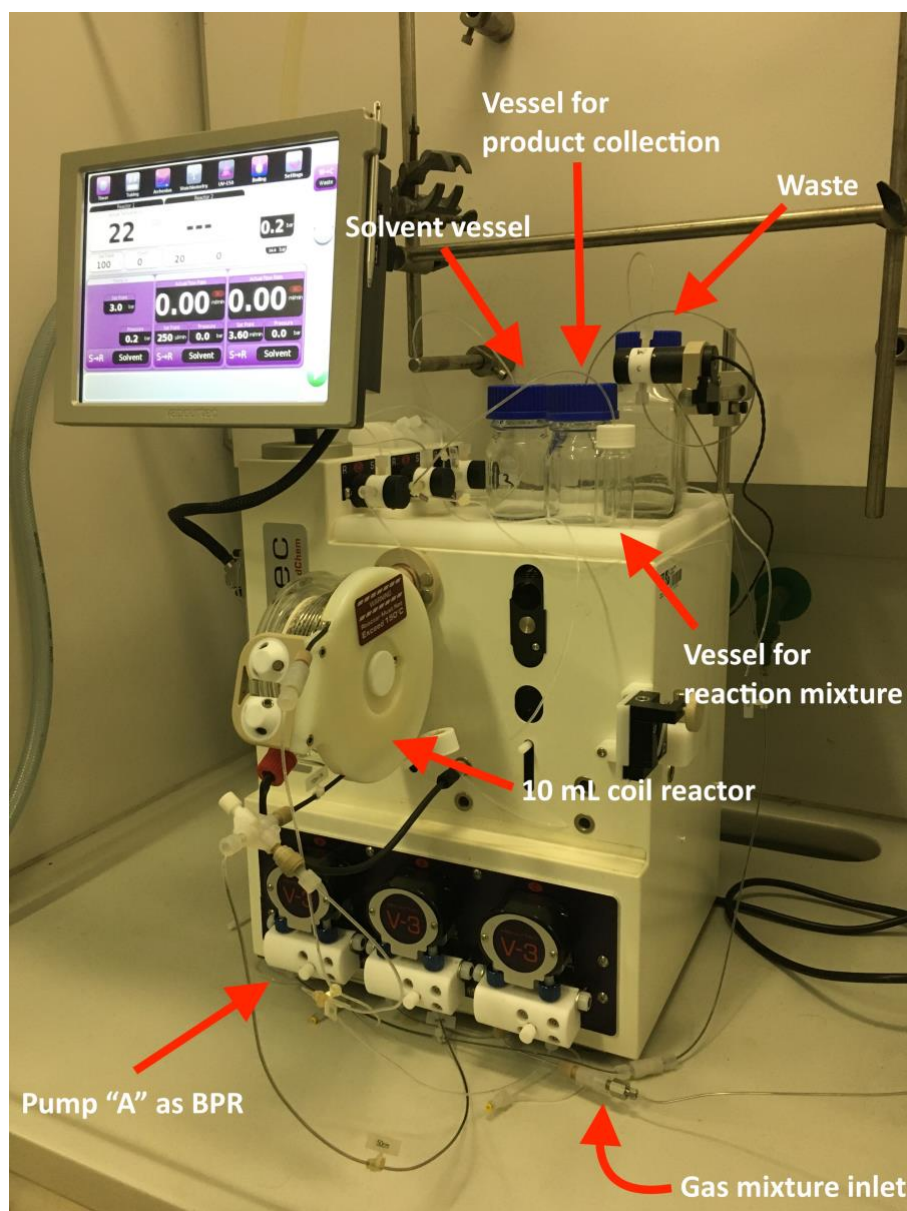


Figure 261. Set-up of the device operating in continuous mode

11.3 Solid-oxide electrochemical cell

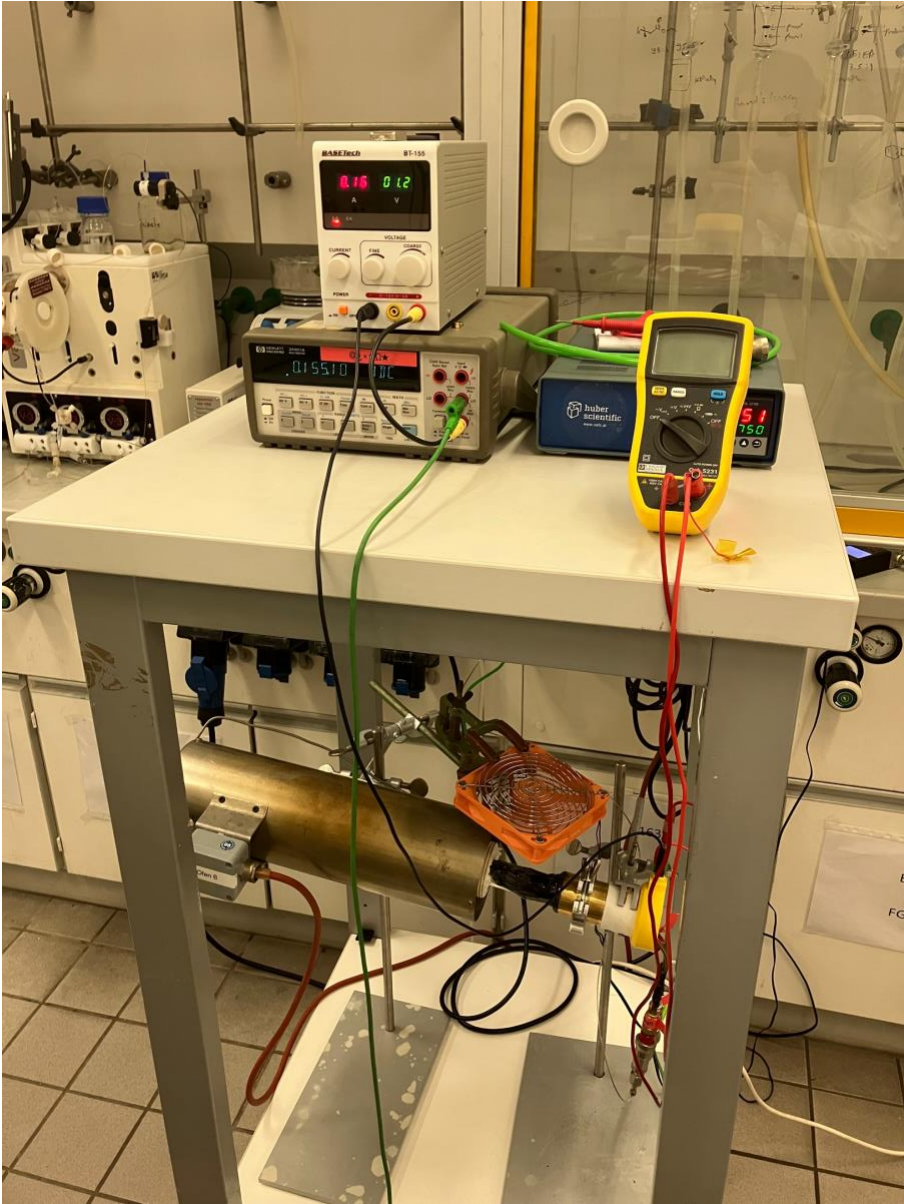


Figure 262. Solid-oxide electrochemical cell for partial CO₂ reduction

Die approbierte gedruckte Originalversion dieser Dissertation ist an der TU Wien Bibliothek verfügbar.
The approved original version of this doctoral thesis is available in print at TU Wien Bibliothek.

11.4 Optimisation of the aminocarbonylation reactions in continuous mode

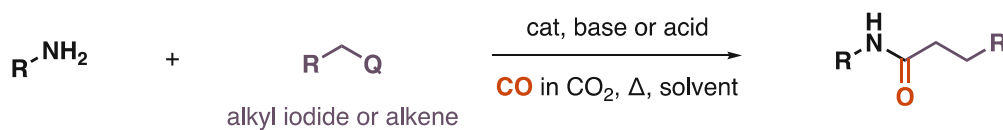


Figure 263. Aminocarbonylation parameter screening

Table 3. Parameter screening of aminocarbonylations

Entry	Reactants	CO amount /%	Temperature, reaction time, catalyst, base/acid, additive, solvent	Conversion ^[e] /%
1 ^{[a][186]}	Pyrrole, iodobenzene	50	90 °C, 24 h, Pd(PPh ₃) ₄ , K ₃ PO ₄ , DMF	66 ^[f]
2 ^[a]	Pyrrole, iodobenzene	15	90 °C, 24 h, Pd(PPh ₃) ₄ , DBU, DMF	0
3 ^[a]	Pyrrole, iodobenzene	15	90 °C, 24 h, Pd(PPh ₃) ₄ , Et ₃ N, DMF	33 ^[f]
4 ^[a]	Pyrrole, iodobenzene	15	90 °C, 24 h, Pd(PPh ₃) ₄ , Et ₃ N, toluene	0
5 ^{[a][187]}	Pyrrole, iodobenzene	15	100 °C, 24 h, Pd(OAc) ₂ , cataCXium [®] A, TMEDA, DMF	0
6 ^{[b][186]}	Pyrrole, iodobenzene	15	60 °C, 24 h, Pd(OAc) ₂ , PPh ₃ , Et ₃ N, THF	0
7 ^{[b][188]}	Aniline, iodobenzene	15	100 °C, 24 h, Pd(OAc) ₂ , [C ₄ mim]Cl, KO ^t Bu, Et ₃ N, MeCN	0
8 ^[b]	Pyrrole, iodobenzene	15-50	90 °C, 40 min, Pd(PPh ₃) ₄ , Et ₃ N, toluene	0
9 ^{[b][189]}	Aniline, 1-octene	15	150 °C, 40 min, Pd(OAc) ₂ , dtbpx, MeSO ₃ H, NaI, β-naphthol, toluene	0
10 ^[b]	Aniline, 1-octene	15	100 °C, 40 min, Pd(OAc) ₂ , Xantphos, MeSO ₃ H, NaI, β-naphthol, toluene	0
11 ^{[b][c]}	Aniline, iodobenzene	15	100 °C, 40 min, Pd(OAc) ₂ , Xantphos, Et ₃ N, MeCN	0
12 ^{[b][d]}	Aniline, iodobenzene	15	100 °C, 40 min, Pd(OAc) ₂ , Xantphos, Et ₃ N, MeCN	0
13 ^{[b][c]}	Aniline, iodobenzene	50	120 °C, 40 min, Pd(OAc) ₂ , Xantphos, Et ₃ N, MeCN	>99 (57) ^[f]
14 ^{[b][c]}	Aniline, iodobenzene	30	110 °C, 40 min, Pd(OAc) ₂ , Xantphos, Et ₃ N, MeCN	91
15 ^[b]	Aniline, iodobenzene	30	110 °C, 40 min, Pd(OAc) ₂ , Et ₃ N, MeCN	94 (71) ^[f]
16 ^[b]	Aniline, iodobenzene	30	110 °C, 40 min, Pd(OAc) ₂ , MeCN	0

[a] Performed under batch-wise conditions. [b] Performed in continuous mode. [c] Performed with 5 mol% Pd(OAc)₂ and 10 mol% Xantphos. [d] Performed with 3 mol% Pd(OAc)₂ and 6 mol% Xantphos. [e] Determined by GC-MS analysis. [f] Isolated yields.

11.5 Procedure for the synthesis of ethyl nonanoate

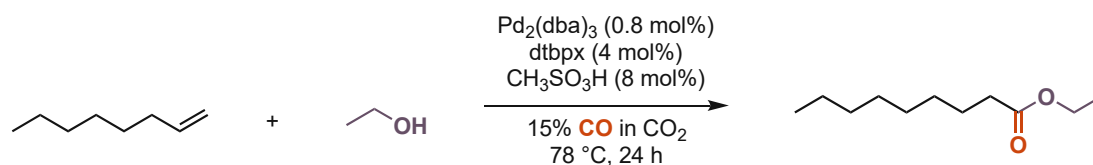


Figure 264. Synthesis of ethyl nonanoate

In a 3-neck round-bottom flask equipped with a stir bar, tris(dibenzylideneacetone)dipalladium (51 mg, 0.8 mol%) was added, followed by 1,2-bis((di-tert-butylphosphanyl)methyl)benzene (110 mg, 4 mol%) inside a glove box. Dry ethanol (6 mL) was then added. Following this, the substrate 1-octene (1.1 mL) was added. Finally, methanesulfonic acid (36 μL , 8 mol%) was added to the reaction vessel. The flask was then disconnected from the argon line, and a quick-fit fitted with a septum, through which a 1/8" steel tubing was passed, was connected. The reaction vessel was then connected to a cooled cryostat (cooled to a temperature below $-5\text{ }^\circ\text{C}$) condenser. The tubing at the gas outlet from the CO_2 electrolysis setup (155 mA corresponding to 15% CO content) was attached to the 1/8" steel tubing. The 1/8" steel tubing was dipped in the reaction vessel in a manner that constant bubbling was observed, and there was no hindrance to the stirring bar. A stirring rate of 200 rpm was employed. The 3-neck round-bottom flask was then placed in a preheated oil bath (at $78\text{ }^\circ\text{C}$). After 24 h, the reaction mixture was cooled down to room temperature and transferred to a round-bottom flask for bulb-to-bulb distillation. Initially, at a vacuum of 900 mBar, the round-bottom flask was heated to $90\text{ }^\circ\text{C}$ to remove the ethanol. After the complete removal of ethanol, the vacuum was slowly increased to 100 mBar and finally to 25 mBar. Thereafter increasing the temperature to $125\text{ }^\circ\text{C}$ resulted in the product ethyl nonanoate being distilled off. The product was obtained as a colourless oil (82%, 1.06 g) and was analytically confirmed to be pure. The spectral data matches the one reported in the literature.^[190]

Ethyl nonanoate (1a)

The chemical structure of ethyl nonanoate (1a) is shown as a skeletal structure of a 9-carbon chain with an ethyl ester group at the end. The NMR data is provided as follows:

$^1\text{H NMR}$ (400 MHz, CDCl_3) δ 4.11 (q, $J = 7.1\text{ Hz}$, 2H), 2.27 (t, $J = 7.6\text{ Hz}$, 2H), 1.61 (t, $J = 7.3\text{ Hz}$, 2H), 1.26 (dt, $J = 14.2, 6.4\text{ Hz}$, 13H), 0.92 – 0.82 (m, 3H). $^{13}\text{C NMR}$ (101 MHz, CDCl_3) δ 174.05, 60.26, 34.53, 31.94, 29.36, 29.29, 29.25, 25.13, 22.77, 14.38, 14.21.

11.6 Procedure for the batch-wise synthesis of phenyl benzoate

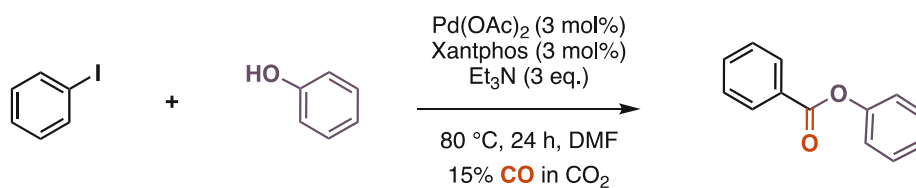


Figure 265. Synthesis of phenyl benzoate

Pd(OAc)₂ (3 mol%, 13,4 mg) followed by Xantphos (3 mol%, 52 mg) and iodobenzene (3.0 mmol, 612 mg), phenol (570 mg, 6.0 mmol) were added to a 3-neck round-bottom flask under argon flow. This was immediately followed by the addition of dry DMF (6 mL). Finally, the base triethylamine (9.0 mmol, 1.25 mL) was added, and the flask containing the reaction mixture was immediately attached to the steel tubing of the electrochemical cell (155 mA corresponding to 15% CO content). Upon equipping the reaction flask with a condenser and ensuring a constant gas flow, the reaction vessel was immersed into a pre-heated oil bath at 80 °C and maintained at this temperature for 24 h. A stirring rate of 200 rpm was employed. The reaction mixture was diluted with 10 mL ethyl acetate and transferred to a separating funnel. The reaction mixture was swirled to ensure that the product was well distributed in ethyl acetate/DMF. Following this, the organic phases were washed with 5-6 mL of water 4 to 5 times till no more emulsion resulting from DMF in the aqueous phase was visible. The aqueous phase was then re-extracted to ensure that product remained behind. The organic phase was dried with MgSO₄ and filtered. Rotary evaporation of the solvent afforded the crude product, which was bound to silica and subjected to column chromatography with PE/Et₂O 95:5. The final pure product was isolated as a white solid (309 mg, 52%).

11.7 General procedure for the continuous synthesis of benzoic acid ester derivatives

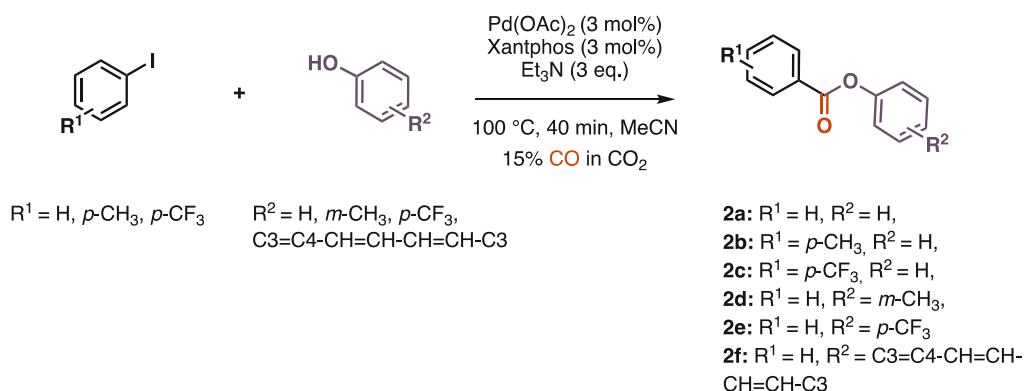
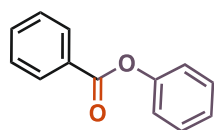


Figure 266. Synthesis of compounds **2a-f**

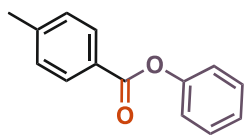
A 30-mL vial with septum was charged with the corresponding aryl iodide (1.0 eq., 1.0 mmol), the corresponding phenol-derivative (2.0 eq., 2.0 mmol), Pd(OAc)₂ (3 mol%, 0.03 mmol, 6.74 mg), Xantphos (3 mol%, 0.03 mmol, 17.4 mg), and triethylamine (3.0 eq., 3.0 mmol, 418 μL). The reactants were dissolved in 10 mL acetonitrile. The solvent bottle was charged with MeCN. The reactor was heated up to the desired temperature (100 $^{\circ}\text{C}$). Pump A was used as a back-pressure regulator (BPR, 3 bar). Pump B was connected to the vial with the reaction mixture; subsequently, pump C was connected to the gas tube, where the pre-mixed gas mixture was introduced. The gases were supplied from the respective cylinders and were pre-mixed with the aid of two mass flow controllers (CO: 0.64 mL/min and CO₂: 3.6 mL/min). Alternatively, pump C was connected to the solid-oxide electrochemical cell (155 mA, corresponding to 15% CO content, employing a flow rate of 8.0 mL/min. The reactor (10-mL coil reactor) was initially rinsed by a CO/CO₂/MeCN flow for several minutes. Then, the reaction mixture was supplied to the reactor (pump B: 0.25 mL/min; pump C: 3.6 mL/min (or 8.0 mL/min if the electrochemical cell was employed)). After the whole volume of the reaction mixture was pumped through the reactor, the vial was rinsed with pure MeCN, and the residue was pumped through the reactor. The product was collected for 50 minutes. Rotary evaporation of the solvent gave the crude product, which was bound to silica and subjected to column chromatography.

Phenyl benzoate (**2a**)^[191]



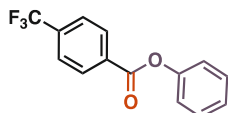
Flash column chromatography (petroleum ether/Et₂O 20:1, $R_f = 0.65$) afforded the product as white solid (174 mg, 88%). ¹H NMR (400 MHz, CDCl₃) δ 8.27 – 8.17 (m, 2H), 7.69 – 7.61 (m, 1H), 7.56 – 7.49 (m, 2H), 7.48 – 7.40 (m, 2H), 7.33 – 7.19 (m, 3H). ¹³C NMR (101 MHz, CDCl₃) δ 165.53, 151.11, 133.72, 130.32, 129.75, 129.64, 128.71, 126.03, 121.86.

Phenyl 4-methylbenzoate (2b)^[192]



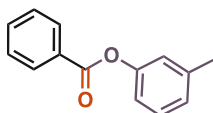
Flash column chromatography (petroleum ether/Et₂O 20:1, *R_f* = 0.59) afforded the product as white solid (186 mg, 88%). ¹H NMR (400 MHz, CDCl₃) δ 8.12 – 8.05 (m, 2H), 7.47 – 7.38 (m, 2H), 7.34 – 7.19 (m, 6H), 2.46 (s, 3H). ¹³C NMR (101 MHz, CDCl₃) δ 165.39, 151.18, 144.54, 130.36, 129.60, 129.43, 126.98, 125.92, 121.91, 21.90.

Phenyl 4-(trifluoromethyl)benzoate (2c)^[193]



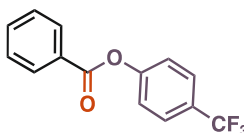
Flash column chromatography (petroleum ether/Et₂O 20:1, *R_f* = 0.67) afforded the product as crystalline white solid (192 mg, 72%). ¹H NMR (400 MHz, CDCl₃) δ 8.33 (dp, *J* = 7.7, 0.9 Hz, 2H), 7.83 – 7.75 (m, 2H), 7.50 – 7.42 (m, 2H), 7.34 – 7.28 (m, 1H), 7.25 – 7.20 (m, 2H). ¹³C NMR (101 MHz, CDCl₃) δ 164.14, 150.81, 135.02, 132.99, 130.72, 129.76, 126.37, 125.79, 125.75, 122.36, 121.68. ¹⁹F NMR (376 MHz, CDCl₃) δ -63.15.

m-Tolyl benzoate (2d)^[194]



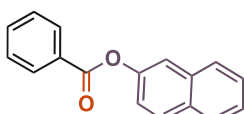
Flash column chromatography (petroleum ether/Et₂O 20:1, *R_f* = 0.61) afforded the product as colourless liquid (194 mg, 91%). ¹H NMR (400 MHz, CDCl₃) δ 8.24 – 8.16 (m, 2H), 7.64 (ddt, *J* = 8.7, 6.9, 1.4 Hz, 1H), 7.56 – 7.47 (m, 2H), 7.32 (t, *J* = 7.8 Hz, 1H), 7.13 – 6.99 (m, 3H), 2.40 (d, *J* = 0.8 Hz, 3H). ¹³C NMR (101 MHz, CDCl₃) δ 165.44, 151.06, 139.83, 133.66, 130.30, 129.82, 129.35, 128.69, 126.84, 122.45, 118.78, 21.49.

4-(Trifluoromethyl)phenyl benzoate (2e)^[195]



Flash column chromatography (petroleum ether/Et₂O 20:1, *R_f* = 0.67) afforded the product as crystalline, white solid (247 mg, 93%). ¹H NMR (400 MHz, CDCl₃) δ 8.24 – 8.18 (m, 2H), 7.76 – 7.64 (m, 3H), 7.58 – 7.50 (m, 2H), 7.39 – 7.33 (m, 2H). ¹³C NMR (101 MHz, CDCl₃) δ 164.81, 153.63, 134.12, 130.42, 128.85, 128.18, 127.03, 122.41. ¹⁹F NMR (376 MHz, CDCl₃) δ -62.20.

Naphtalen-2-yl benzoate (2f)^[196]



Flash column chromatography (petroleum ether/Et₂O 10:1, *R_f* = 0.68) afforded the product as crystalline, white solid (214 mg, 86%). ¹H NMR (400 MHz, CDCl₃) δ 8.27 (dt, *J* = 8.4, 1.3 Hz, 2H), 7.95 – 7.82 (m, 3H), 7.73 – 7.70 (m, 1H), 7.70 – 7.63 (m, 1H), 7.58 – 7.46 (m, 4H), 7.38 (ddd, *J* = 8.9, 2.4, 1.2 Hz, 1H). ¹³C NMR (101 MHz, CDCl₃) δ 165.51, 148.75, 133.97, 133.79, 131.67, 130.37, 129.72, 129.61, 128.76, 127.95, 127.83, 126.73, 125.88, 121.39, 118.84.

11.8 Procedure for the batch-wise synthesis of *N*-(benzoyloxy)-succinimide

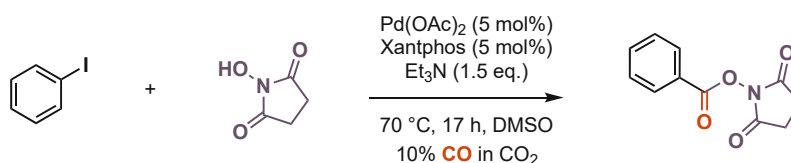


Figure 267. Synthesis of *N*-(benzoyloxy)-succinimide

In a dry 3-neck round-bottom flask (25 mL) was added Pd(OAc)₂ (33,6 mg, 5 mol%), Xantphos (86 mg, 5 mol%), iodobenzene (3.0 mmol, 612 mg) and *N*-hydroxysuccinimide (4.2 mmol, 482 mg). The contents of the reaction vessel were dissolved in DMSO (6 mL). This was followed by the addition of triethylamine (4.5 mmol, 627 μ l). A mixture of CO and CO₂ was then bubbled through this mixture for 17 hours. After reaction completion, the reaction mixture was diluted with 10 mL ethyl acetate and stirred for 10 mins. The mixture was then transferred to a separating funnel. The organic phase was washed with H₂O (5 x 7 mL) and brine (1 x 1 mL). The organic phase was then dried over dry MgSO₄. The residue was bound to silica and subjected to column chromatography with PE/EtOAc 3:1 to obtain the product as a crystalline solid (552 mg, 84 %).

11.9 General procedure for the continuous synthesis of redox-active esters

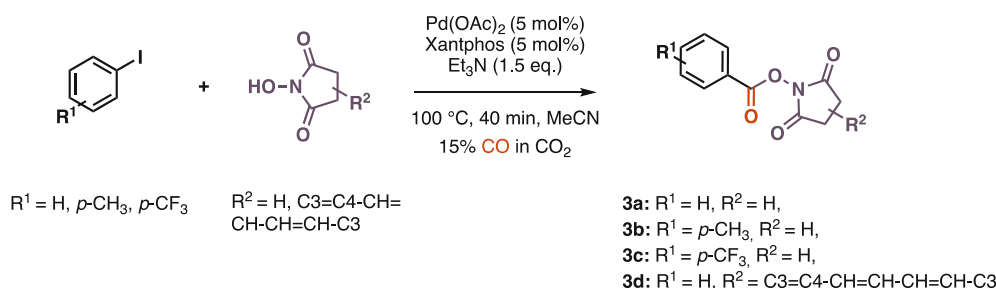
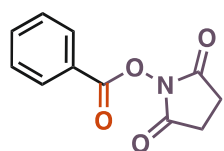


Figure 268. Synthesis of compounds **3a-d**

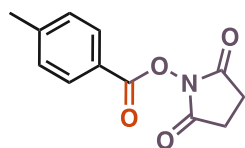
A 30-mL vial with septum was charged with the corresponding aryl iodide (1.0 eq., 1.0 mmol), the corresponding *N*-hydroxyimide (1.4 eq., 1.4 mmol), Pd(OAc)₂ (5 mol%, 0.05 mmol, 11.2 mg), Xantphos (5 mol%, 0.05 mmol, 28.9 mg) and triethylamine (1.5 eq., 1.5 mmol, 209 μL), and the reactants were dissolved in 10 mL acetonitrile. The solvent bottle was charged with MeCN. The reactor was heated up to the desired temperature (100 °C). Pump A was used as a back-pressure regulator (BPR, 3 bar). Pump B was connected to the vial with the reaction mixture; subsequently, pump C was connected to the gas tube, where the pre-mixed gas mixture was introduced. The gases were supplied from the respective cylinders and were pre-mixed with the aid of two mass flow controllers (CO: 0.64 mL/min; and CO₂: 3.6 mL/min). Alternatively, pump C was connected to the solid-oxide electrochemical cell (155 mA, corresponding to 15% CO content, employing a flow rate of 8.0 mL/min. The reactor (10-mL coil reactor) was initially rinsed by a CO/CO₂/MeCN flow for several minutes. Then, the reaction mixture was supplied to the reactor (pump B: 0.25 mL/min; pump C: 3.6 mL/min (or 8.0 mL/min if the electrochemical cell was employed)). After the whole volume of the reaction mixture was pumped through the reactor, the vial was rinsed with pure MeCN, and the residue was pumped through the reactor. The product was collected for 50 minutes. Rotary evaporation of the solvent gave the crude product, which was bound to silica and subjected to column chromatography.

2,5-Dioxopyrrolidin-1-yl benzoate (**3a**)^[197]



Flash column chromatography (petroleum ether/EtOAc 3:1, $R_f = 0.34$) afforded the product as crystalline, brownish-white solid (180 mg, 82%). ¹H NMR (400 MHz, DMSO) δ 8.11 – 8.04 (m, 2H), 7.87 – 7.78 (m, 1H), 7.68 – 7.60 (m, 2H), 2.88 (s, 4H). ¹³C NMR (101 MHz, DMSO) δ 170.34, 161.80, 135.60, 129.99, 129.57, 124.51, 25.56.

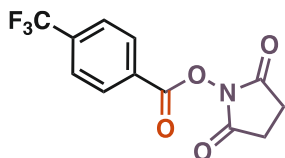
2,5-Dioxopyrrolidin-1-yl 4-methylbenzoate (3b)^[198]



Flash column chromatography (petroleum ether/EtOAc 3:1, R_f = 0.34) afforded the product as crystalline, pinkish solid (182 mg, 78%). $^1\text{H NMR}$ (400 MHz, DMSO) δ 8.02 – 7.96 (m, 2H), 7.46 (d, J = 8.0 Hz, 2H), 2.89 (s, 4H), 2.44 (s, 3H).

$^{13}\text{C NMR}$ (101 MHz, DMSO) δ 170.41, 161.74, 146.46, 130.10, 130.03, 121.71, 25.55, 21.40.

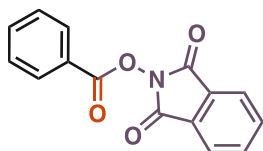
2,5-Dioxopyrrolidin-1-yl 4-(trifluoromethyl)benzoate (3c)^[198]



Flash column chromatography (petroleum ether/EtOAc 3:1, R_f = 0.37) afforded the product as crystalline, brownish-white solid (187 mg, 65%). $^1\text{H NMR}$ (400 MHz, DMSO) δ 8.31 (d, J = 8.1 Hz, 2H), 8.04 (d, J = 8.3 Hz, 2H), 2.91 (s, 4H). $^{13}\text{C NMR}$ (101 MHz, DMSO) δ 170.14, 160.96, 134.81, 130.99,

128.32, 126.56, 124.77, 25.59. $^{19}\text{F NMR}$ (376 MHz, DMSO) δ -62.03.

1,3-Dioxoisindolin-2-yl benzoate (3d)^[199]



Flash column chromatography (petroleum ether/EtOAc 7:1, R_f = 0.51) afforded the product as white solid (206 mg, 77%). $^1\text{H NMR}$ (400 MHz, CDCl_3) δ 8.23 – 8.17 (m, 2H), 7.93 (dd, J = 5.5, 3.1 Hz, 2H), 7.82 (dd, J = 5.5, 3.1 Hz, 2H), 7.70 (ddt, J = 7.9, 7.1, 1.3 Hz, 1H), 7.58 – 7.50 (m, 2H). $^{13}\text{C NMR}$ (101 MHz,

CDCl_3) δ 162.96, 162.21, 135.03, 134.93, 130.80, 129.18, 129.02, 125.45, 124.17.

11.10 Procedure for the batch-wise synthesis of diphenylpropynone

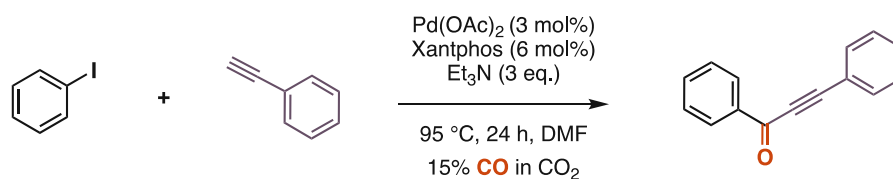


Figure 269. Synthesis of diphenylpropynone

Pd(OAc)₂ (3 mol%, 13,4 mg) followed by Xantphos (6 mol%, 70 mg) and iodobenzene (2.0 mmol, 222 μ L), phenylacetylene (3.5 mmol, 384 μ L) were added to a 3-neck round-bottom flask under argon counterflow. This was immediately followed by the addition of dry DMF (6 mL). Finally, the base triethylamine (6.0 mmol, 831 μ L) was added, and the flask containing the reaction mixture was immediately attached to the steel tubing coming from the electrochemical cell (155 mA, corresponding to 15% CO content). Upon equipping the reaction flask with a condenser and ensuring a constant gas flow, the reaction vessel was immersed into a pre-heated oil bath at 95 °C and maintained at this temperature for 24 h. A stirring rate of 200 rpm was employed. The reaction mixture was diluted with 10 mL ethyl acetate and transferred to a separating funnel. The reaction mixture was swirled to ensure that the product is well distributed in ethyl acetate/DMF. Following this, the organic phases were washed with 5-6 mL of water 4 to 5 times till no more emulsion resulting from DMF in the aqueous phase was observed. The aqueous phase was then re-extracted to ensure that no product remained behind. The organic phase was dried with MgSO₄ and filtered. Rotary evaporation of the solvent afforded the crude product, which was bound to silica and subjected to column chromatography with PE/Et₂O 95:5. The final pure product was isolated as a yellow oil (194 mg, 47%).

11.11 General procedure for the continuous carbonylative Sonogashira coupling

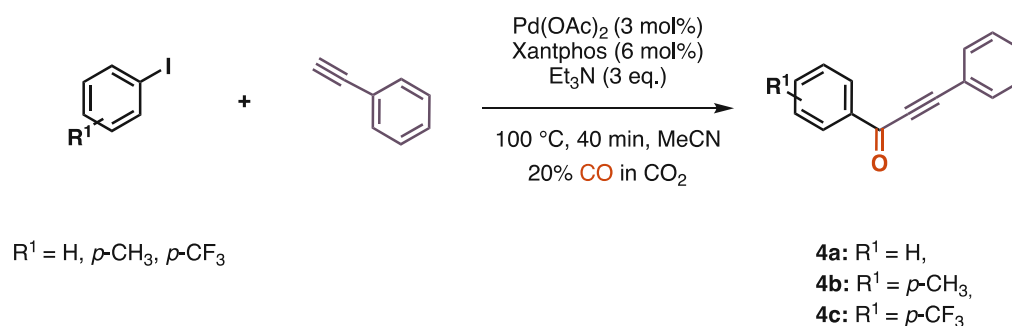
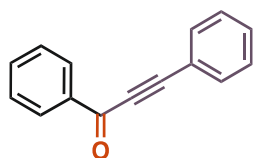


Figure 270. Synthesis of compounds **4a-c**

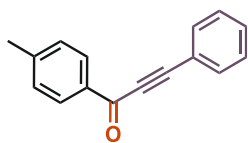
A 30-mL vial with septum was charged with the corresponding aryl iodide (1.00 eq., 1.00 mmol), phenylacetylene (1.75 eq., 1.75 mmol, 192 μL), $\text{Pd}(\text{OAc})_2$ (3 mol%, 0.03 mmol, 6.74 mg), Xantphos (6 mol%, 0.06 mmol, 34.7 mg) and triethylamine (3.00 eq., 3.00 mmol, 418 μL), and the reactants were dissolved in 10 mL acetonitrile. The solvent bottle was charged with MeCN. The reactor was heated up to the desired temperature (100 $^\circ\text{C}$). Pump A was used as a back-pressure regulator (BPR, 3 bar). Pump B was connected to the vial with the reaction mixture; subsequently, pump C was connected to the gas tube, where the pre-mixed gas mixture was introduced. The gases were supplied from the respective cylinders and were pre-mixed with the aid of two mass flow controllers (CO: 0.9 mL/min; and CO_2 : 3.6 mL/min). Alternatively, pump C was connected to the solid-oxide electrochemical cell (207 mA, corresponding to 20% CO content, employing a flow rate of 8.0 mL/min. The reactor (10-mL coil reactor) was initially rinsed by a $\text{CO}/\text{CO}_2/\text{MeCN}$ flow for several minutes. Then, the reaction mixture was supplied to the reactor (pump B: 0.25 mL/min; pump C: 3.6 mL/min (or 8.0 mL/min if the electrochemical cell was employed)). After the entire volume of the reaction mixture was pumped through the reactor, the vial was rinsed with pure MeCN, and the residue was pumped through the reactor. The product was collected for 50 minutes. Rotary evaporation of the solvent gave the crude product, which was bound to silica and subjected to column chromatography.

1,3-Diphenylprop-2-yn-1-one (**4a**)^[200]



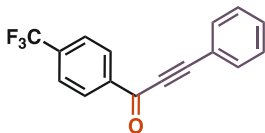
Flash column chromatography (petroleum ether/ Et_2O 20:1, $R_f = 0.50$) afforded the product as yellow oil (159 mg, 77%). $^1\text{H NMR}$ (400 MHz, CDCl_3) δ 8.27 – 8.20 (m, 2H), 7.73 – 7.67 (m, 2H), 7.67 – 7.61 (m, 1H), 7.56 – 7.46 (m, 3H), 7.46 – 7.39 (m, 2H). $^{13}\text{C NMR}$ (101 MHz, CDCl_3) δ 178.18, 137.05, 134.27, 133.23, 130.94, 129.73, 128.84, 128.78., 120.30, 93.25, 87.04.

3-Phenyl-1-(*p*-tolyl)prop-2-yn-1-one (**4b**)^[201]



Flash column chromatography (petroleum ether/Et₂O 20:1, R_f = 0.54) afforded the product as yellow solid (167 mg, 76%). ¹H NMR (400 MHz, CDCl₃) δ 8.15 – 8.09 (m, 2H), 7.71 – 7.65 (m, 2H), 7.55 – 7.38 (m, 3H), 7.36 – 7.28 (m, 2H), 2.45 (s, 3H). ¹³C NMR (101 MHz, CDCl₃) δ 177.88, 145.38, 134.78, 133.17, 130.81, 129.87, 129.49, 128.81, 120.43, 92.47, 87.12, 21.99.

3-Phenyl-1-(4-(trifluoromethyl)phenyl)prop-2-yn-1-one (4c)^[202]



Flash column chromatography (petroleum ether/Et₂O 25:1, R_f = 0.41) afforded the product as yellow solid (55 mg, 20%). ¹H NMR (400 MHz, CDCl₃) δ 8.33 (dq, J = 7.7, 0.9 Hz, 2H), 7.82 – 7.76 (m, 2H), 7.73 – 7.67 (m, 2H), 7.55 – 7.49 (m, 1H), 7.48 – 7.42 (m, 2H). ¹³C NMR (101 MHz, CDCl₃) δ 176.88, 139.54, 135.52, 135.19, 133.36, 131.36, 129.96, 128.96, 125.93, 125.89, 125.85, 125.82, 125.05, 122.34, 119.83, 94.64, 86.73. ¹⁹F NMR (376 MHz, CDCl₃) δ -63.13.

11.12 General procedure for the continuous aminocarbonylations

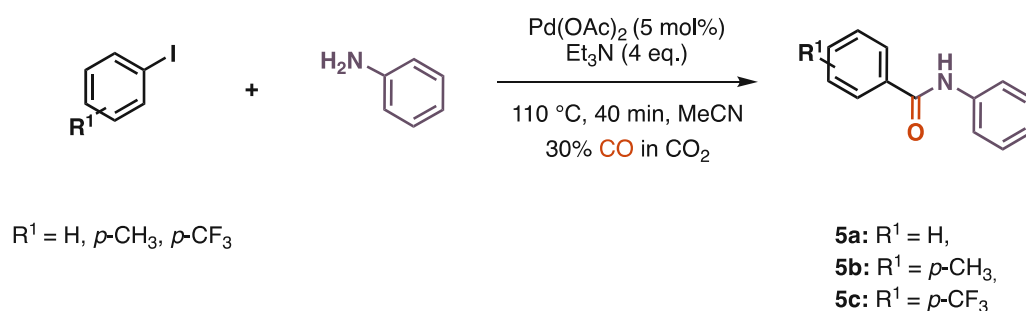
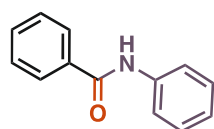


Figure 271. Synthesis of compounds **5a-c**

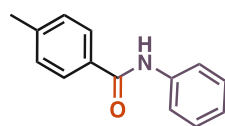
A 30-mL vial with septum was charged with the corresponding aryl iodide (1.0 eq., 1.0 mmol), aniline (3.0 eq., 3.0 mmol), Pd(OAc)₂ (5 mol%, 0.05 mmol, 11.2 mg), and triethylamine (4.0 eq., 4.0 mmol, 557 μL), and the reactants were dissolved in 10 mL acetonitrile. The solvent bottle was charged with MeCN. The reactor was heated up to the desired temperature (110 $^{\circ}\text{C}$). Pump A was used as a back-pressure regulator (BPR, 4 bar). Pump B was connected to the vial with the reaction mixture; pump C was connected to the gas tube, where the pre-mixed gas mixture was introduced. The gases were supplied from the respective cylinders and were pre-mixed with the aid of two mass flow controllers (CO: 1.55 mL/min; and CO₂: 3.6 mL/min). The reactor (10-mL coil reactor) was initially rinsed by a CO/CO₂/MeCN flow for several minutes. Then, the reaction mixture was supplied to the reactor (pump B: 0.25 mL/min; pump C: 3.6 mL/min). After the entire volume of the reaction mixture was pumped through the reactor, the vial was rinsed with pure MeCN, and the residue was pumped through the reactor. The product was collected for 50 minutes. After evaporation of the solvent, the residue was dissolved in 20 mL DCM and was washed thrice with 1 N HCl solution. The organic phases were collected and dried over anhydrous Na₂SO₄. After removing the solvent, the crude product was bound to silica and subjected to column chromatography.

N-Phenylbenzamide (5a)^[203]



Flash column chromatography (petroleum ether/EtOAc 7:1, $R_f = 0.42$) afforded the product as yellowish-white, crystalline solid (139 mg, 71%). ¹H NMR (400 MHz, DMSO) δ 10.25 (s, 1H), 7.98 – 7.93 (m, 2H), 7.80 – 7.75 (m, 2H), 7.62 – 7.50 (m, 3H), 7.40 – 7.30 (m, 2H), 7.10 (tt, $J = 7.3, 1.2$ Hz, 1H). ¹³C NMR (101 MHz, DMSO) δ 165.61, 139.18, 135.01, 131.57, 128.63, 128.41, 127.67, 123.70, 120.40.

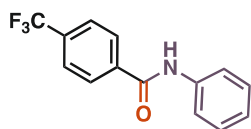
4-Methyl-N-phenylbenzamide (5b)^[204]



Flash column chromatography (petroleum ether/EtOAc 3:1, $R_f = 0.47$) afforded the product as yellowish-white, crystalline solid (134 mg, 63%). ¹H NMR (400 MHz, DMSO) δ 10.14 (s, 1H), 7.91 – 7.82 (m, 2H), 7.81 – 7.71 (m, 2H), 7.33 (t, $J =$

7.9 Hz, 4H), 7.08 (tt, $J = 7.2, 1.2$ Hz, 1H), 2.38 (s, 3H). ^{13}C NMR (101 MHz, DMSO) δ 165.34, 141.53, 139.24, 132.08, 128.89, 128.56, 127.68, 123.53, 120.34, 21.00.

***N*-Phenyl-4-(trifluoromethyl)benzamide (5c)**^[204]



Flash column chromatography (petroleum ether/EtOAc 7:1, $R_f = 0.44$) afforded the product as yellowish, crystalline solid (105 mg, 40%). ^1H NMR (400 MHz, DMSO) δ 10.46 (s, 1H), 8.14 (d, $J = 8.1$ Hz, 2H), 7.91 (d, $J = 8.2$ Hz, 2H), 7.78 (d, $J = 8.0$ Hz, 2H), 7.41 – 7.29 (m, 2H), 7.12 (td, $J = 7.3, 1.2$ Hz, 1H). ^{13}C NMR (101 MHz, DMSO) δ 164.39, 138.82, 131.51, 131.19, 128.67, 128.59, 125.39, 125.36, 124.02, 120.45. ^{19}F NMR (376 MHz, DMSO) δ -61.34.

11.13 NMR spectra of 1a-5c

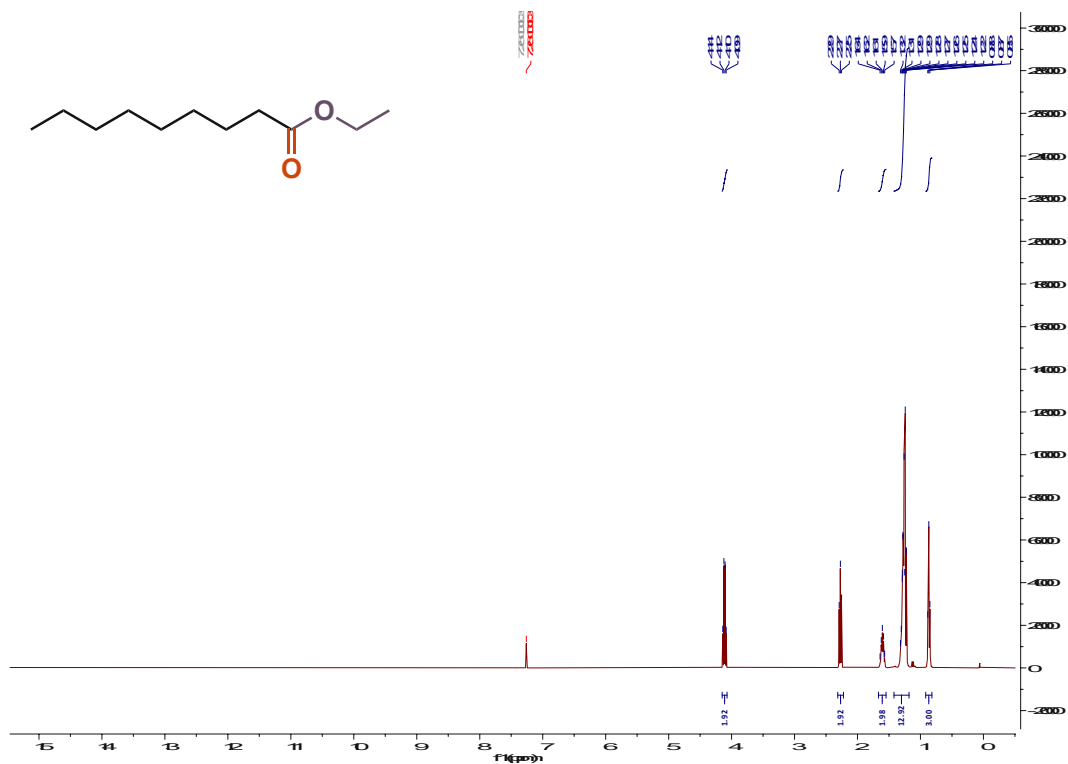


Figure 272. ^1H NMR of 1a

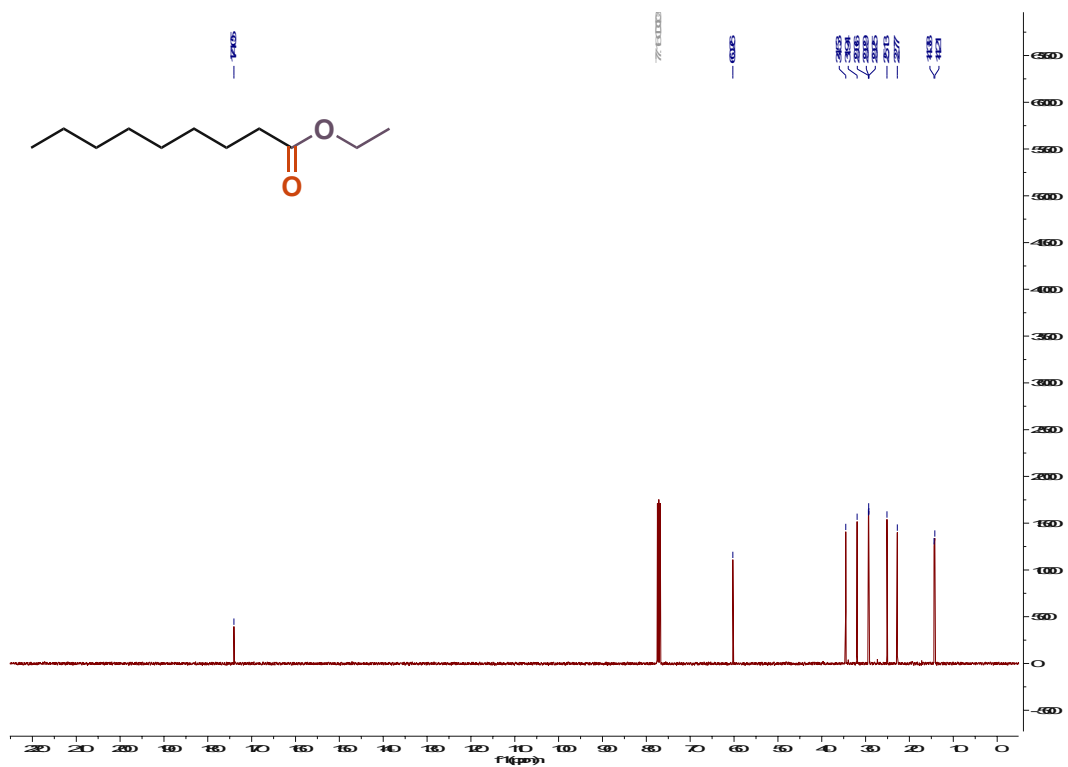
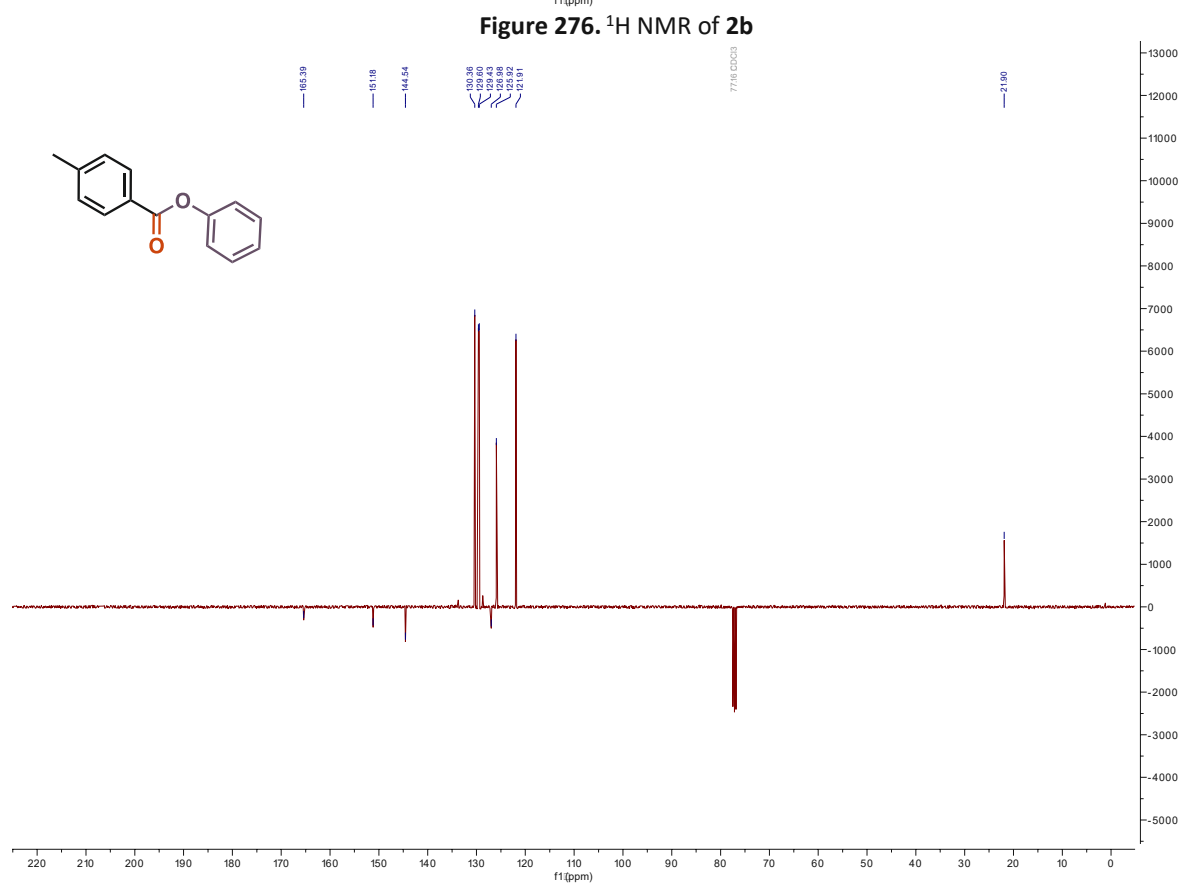
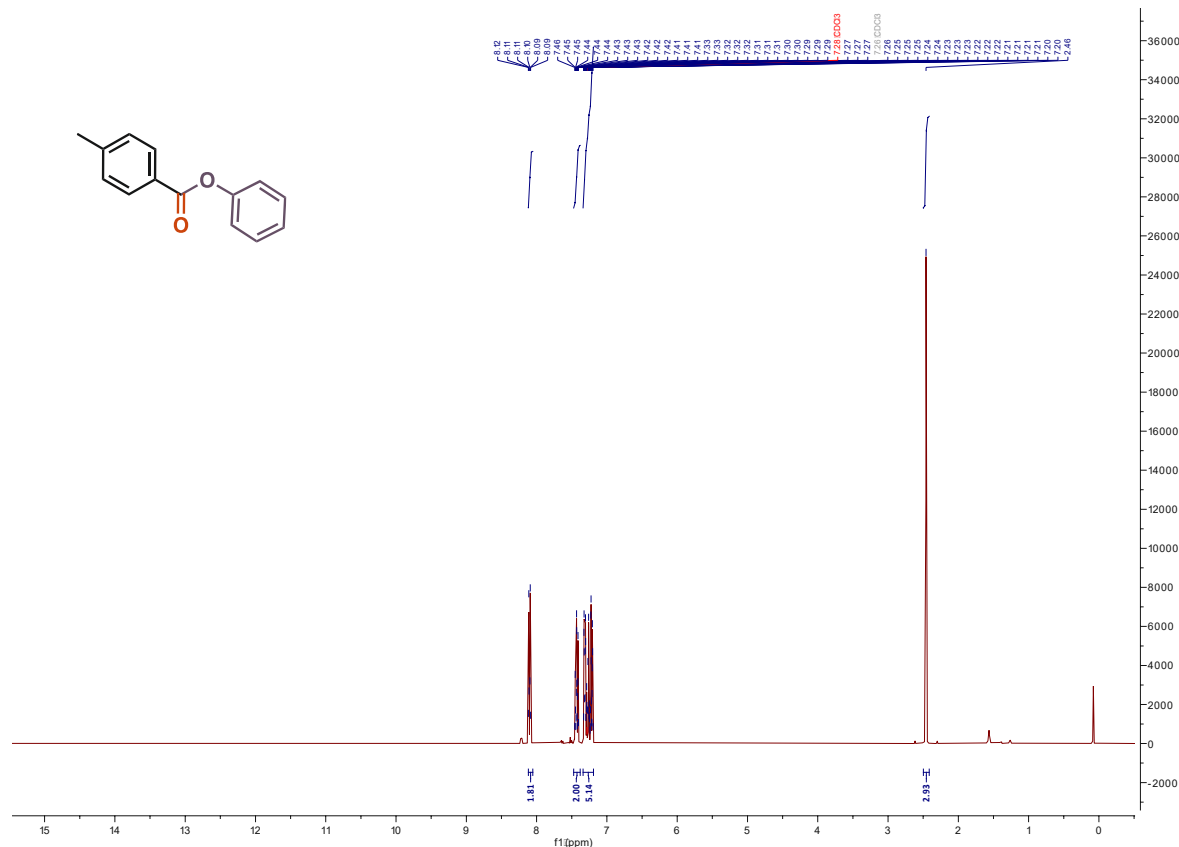
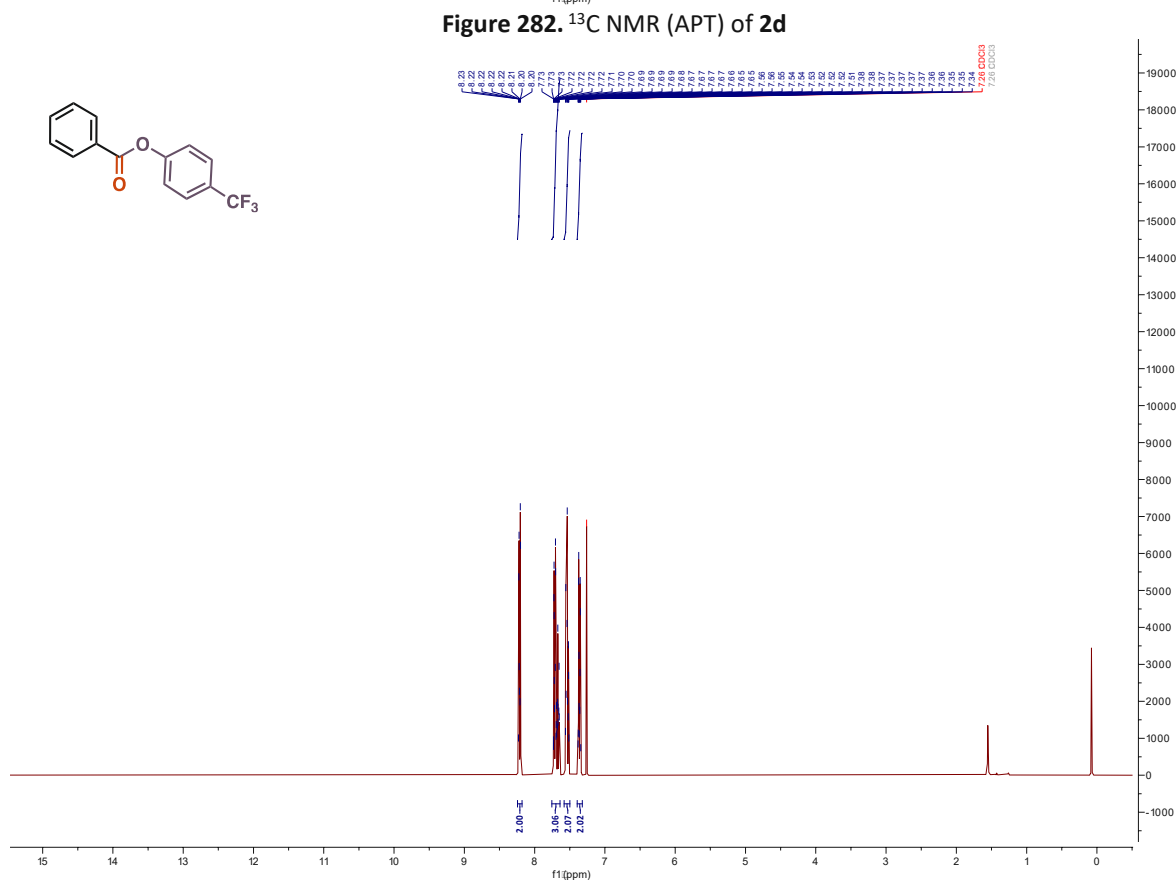
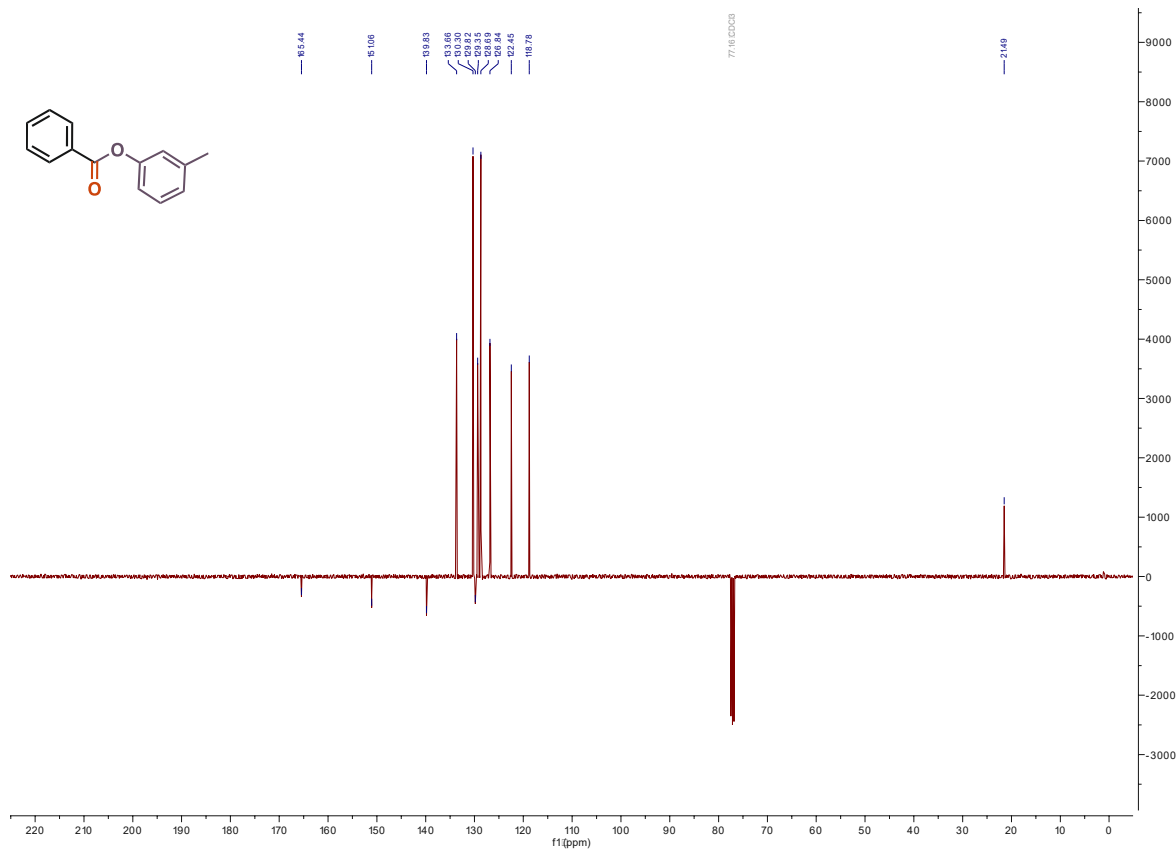


Figure 273. ^{13}C NMR of 1a





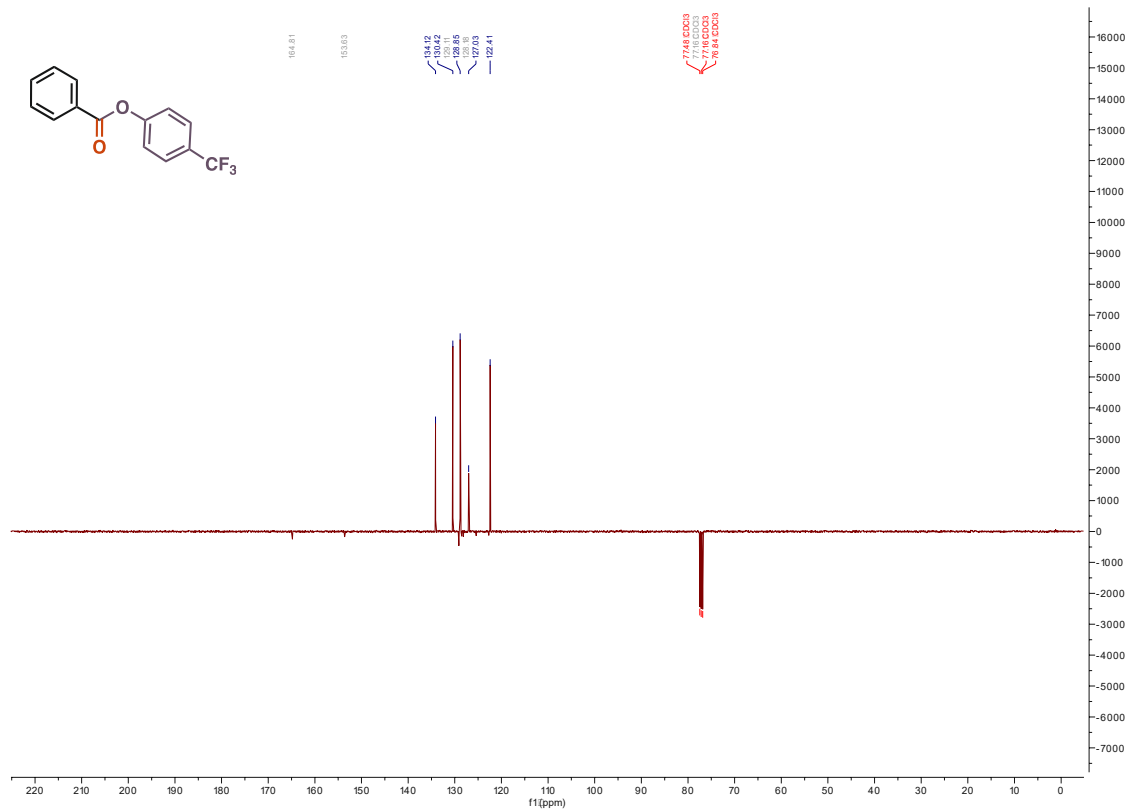


Figure 284. ¹³C NMR (APT) of 2e

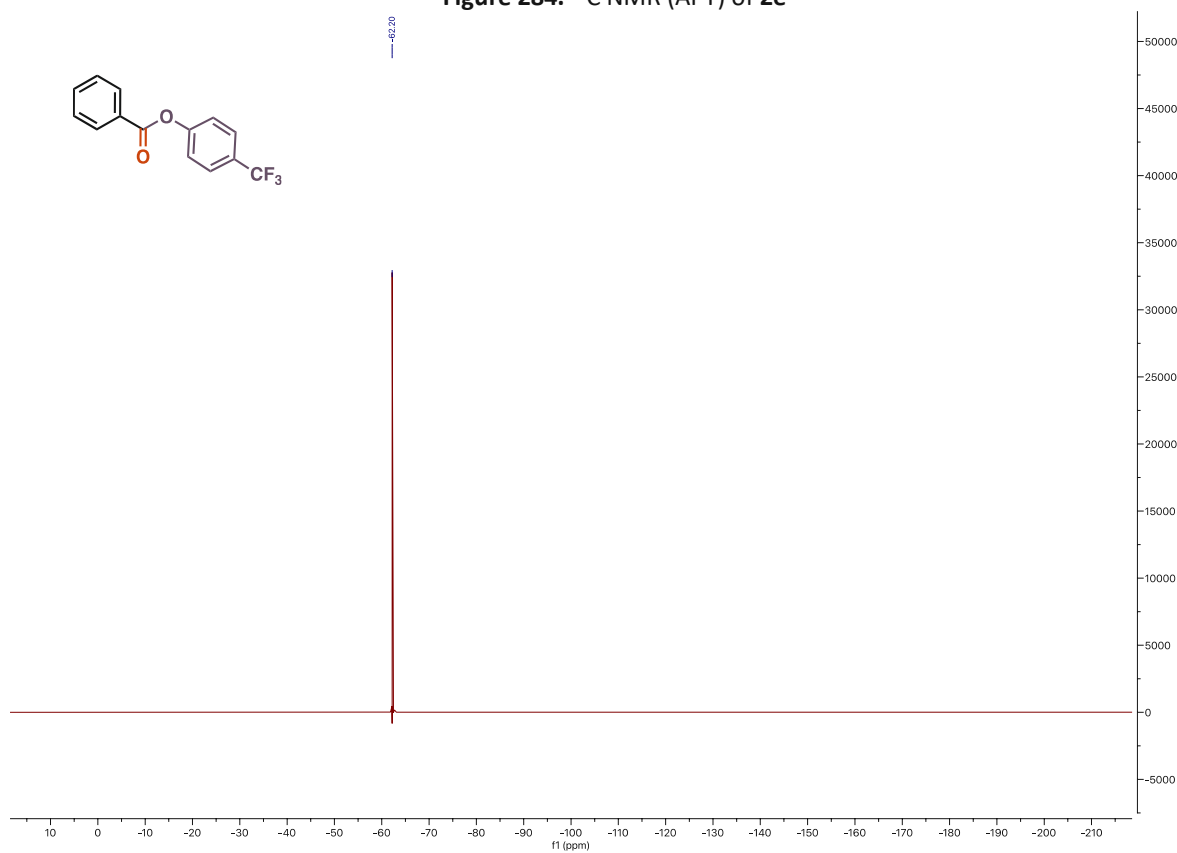


Figure 285. ¹⁹F NMR of 2e

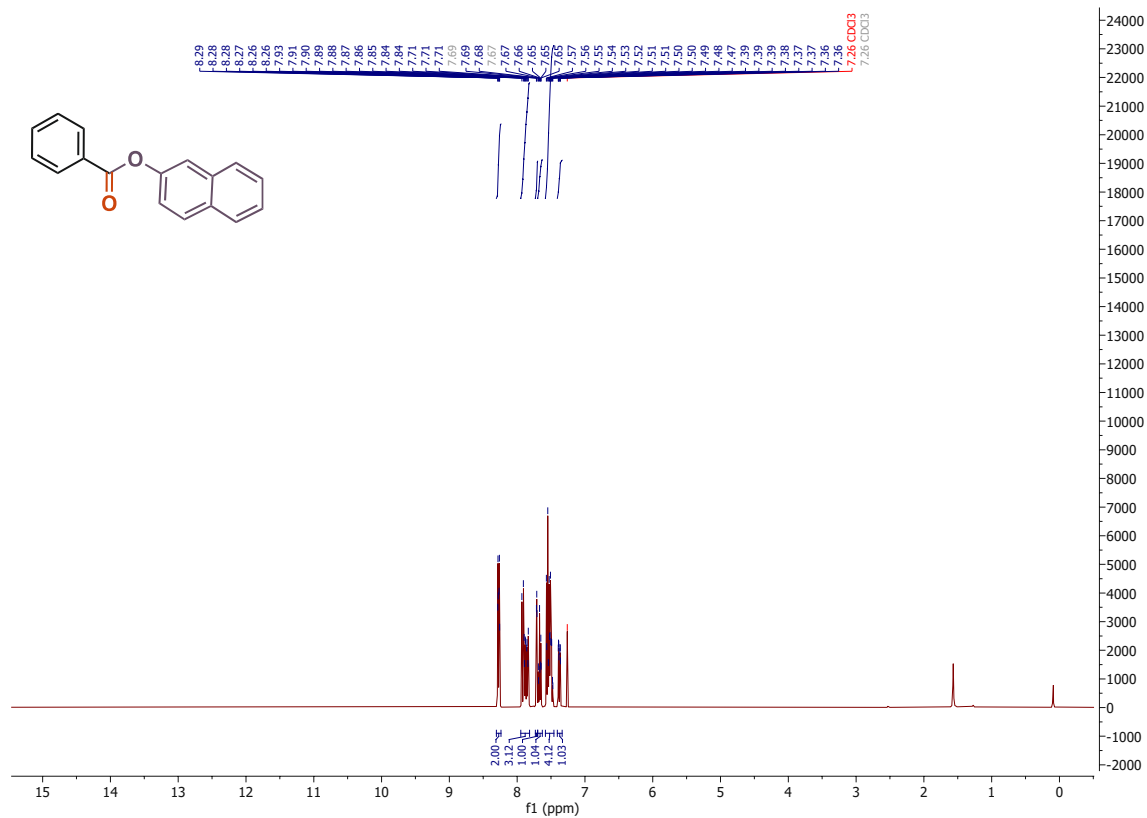


Figure 286. ¹H NMR of 2f

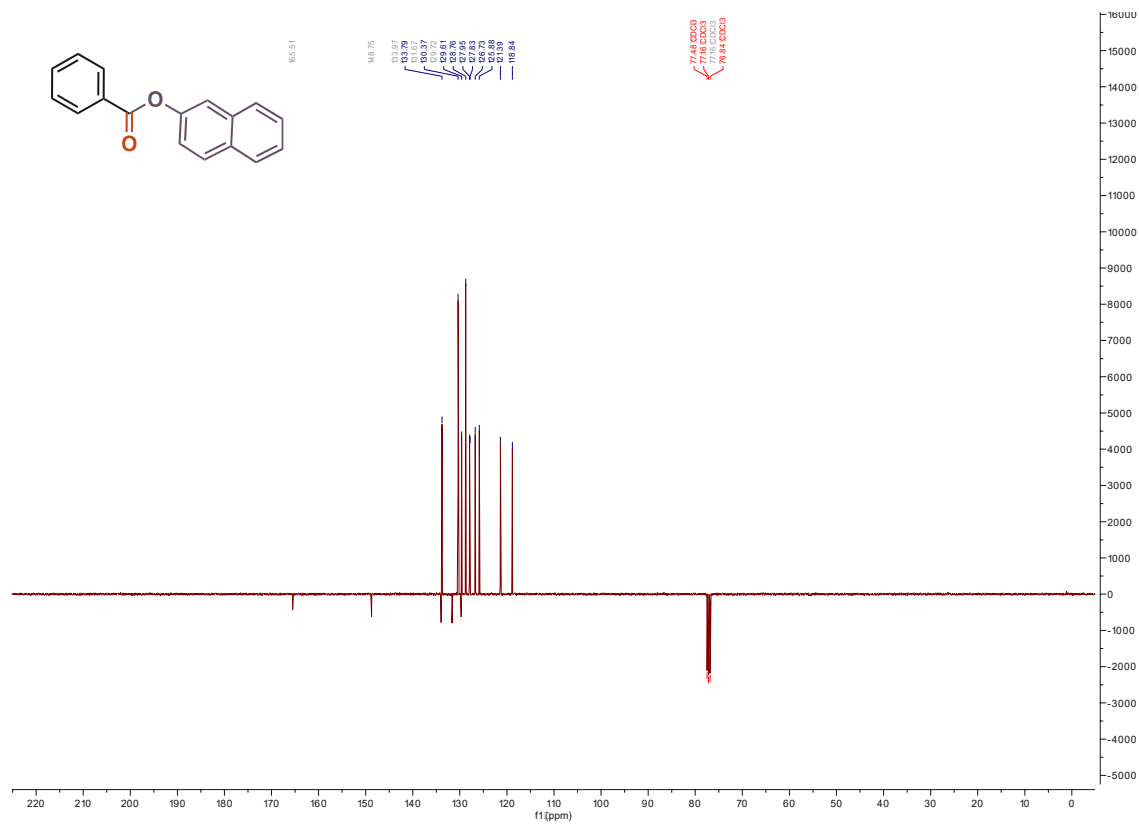


Figure 287. ¹³C NMR (APT) of 2f

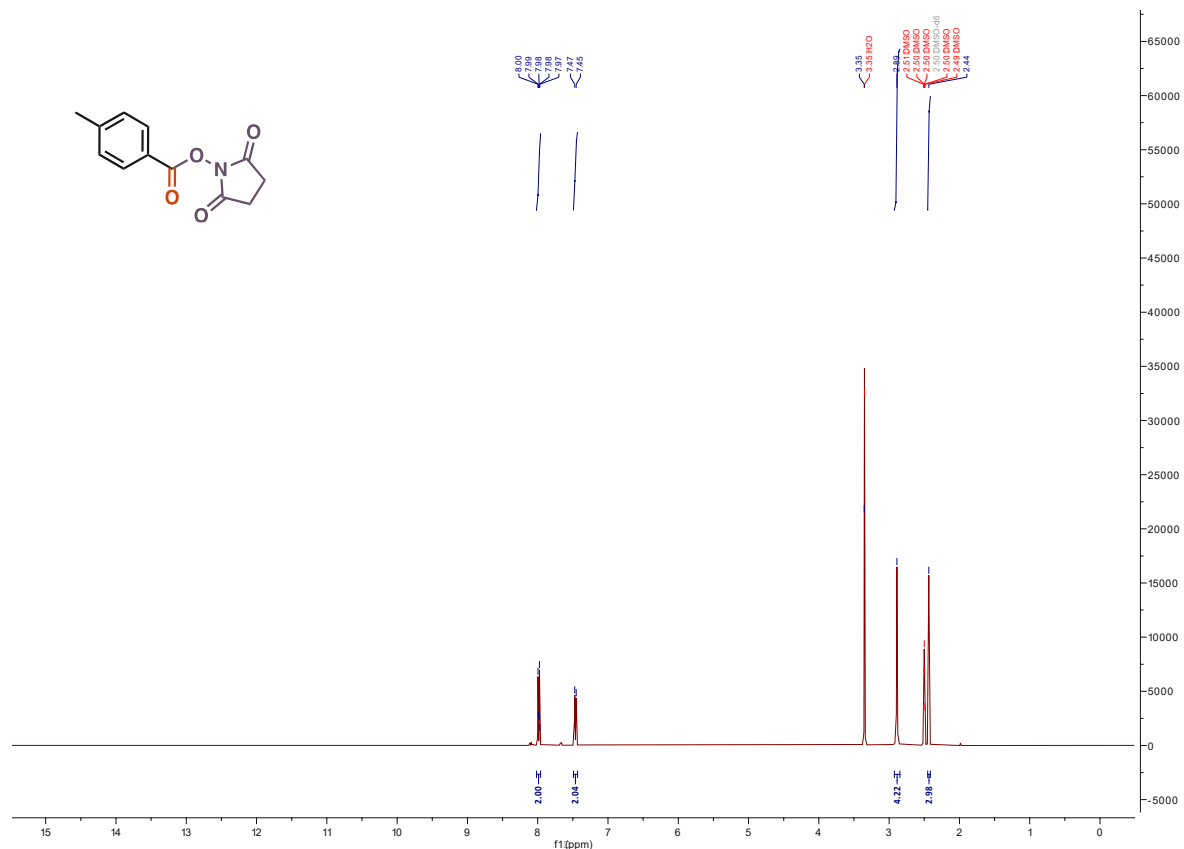


Figure 290. ¹H NMR of 3b

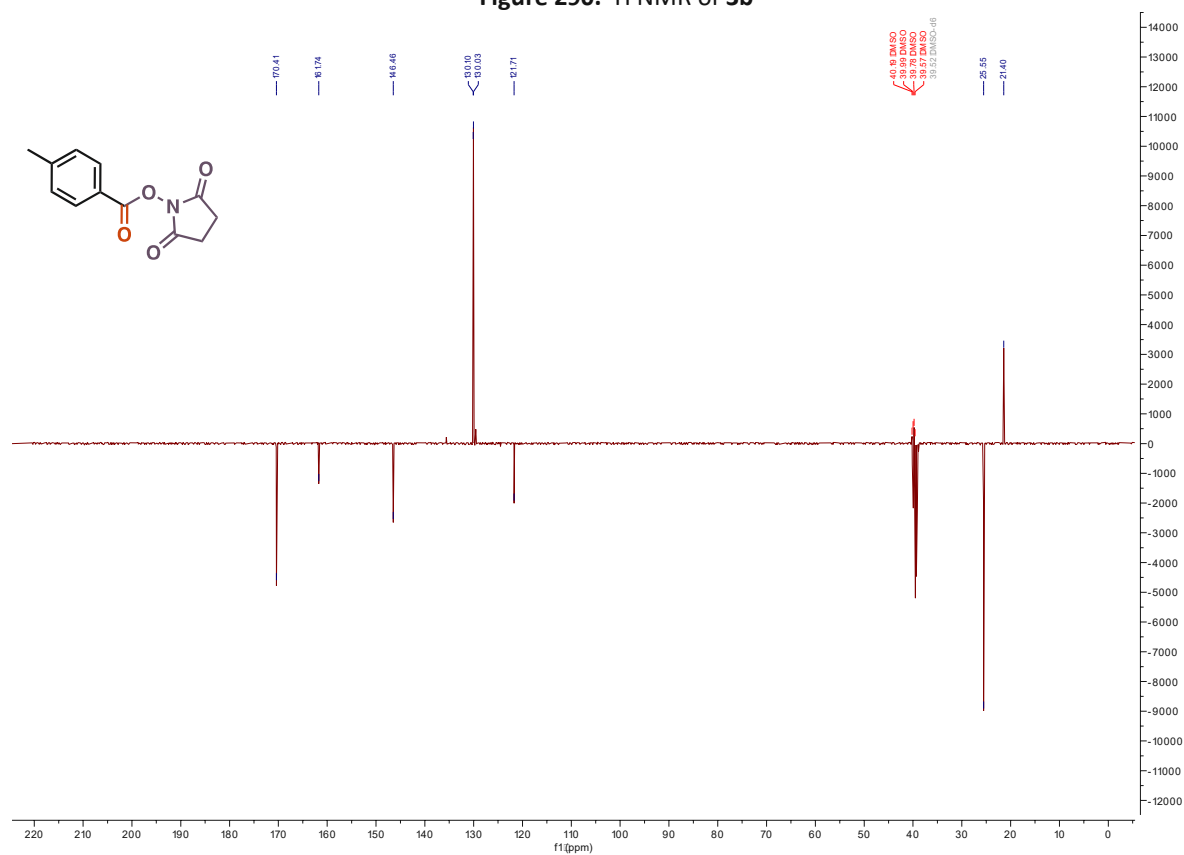
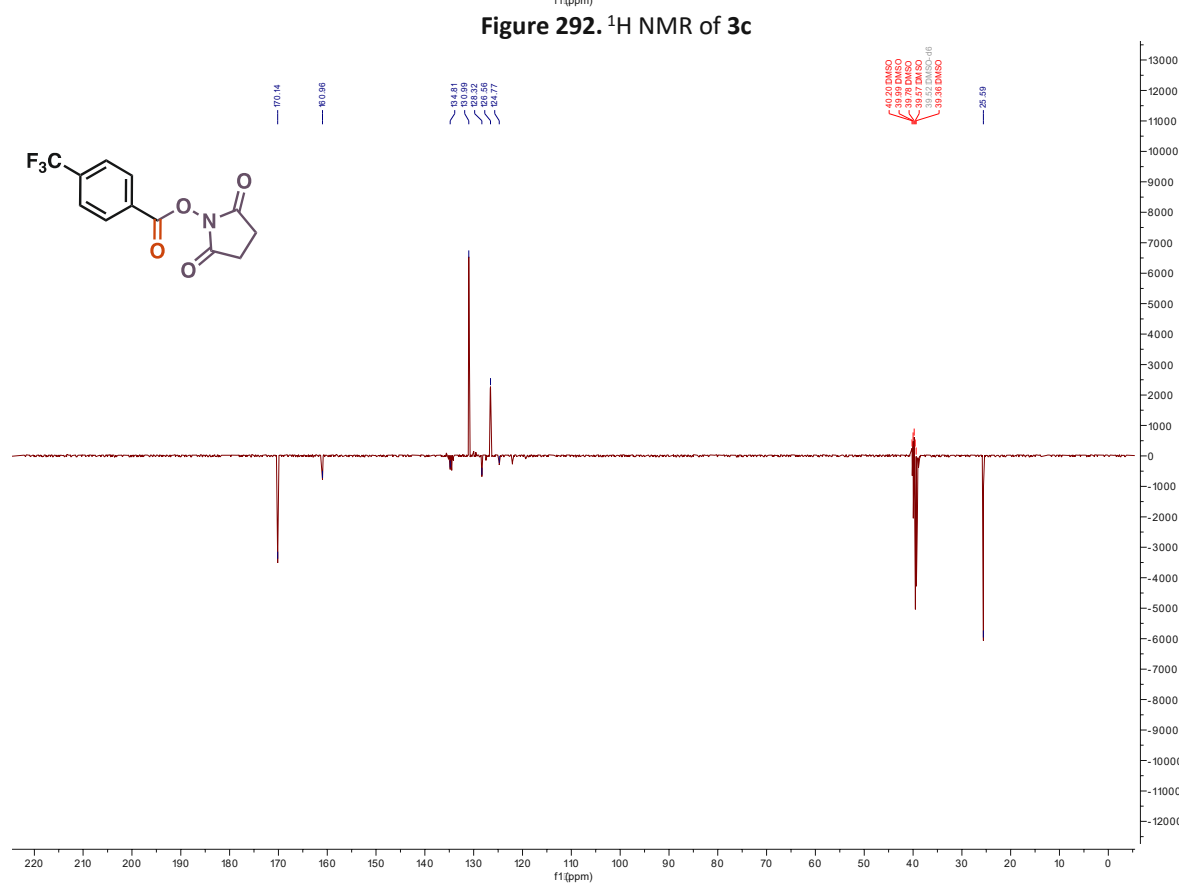
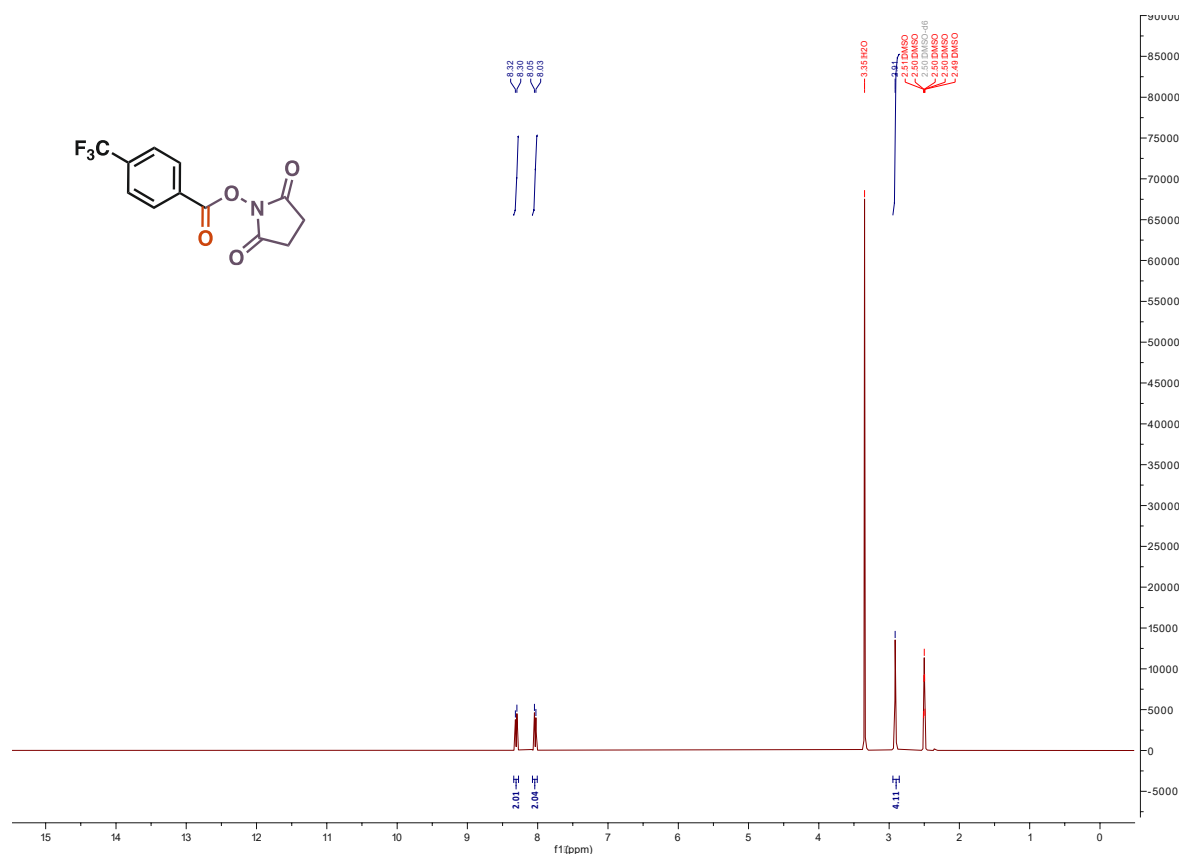
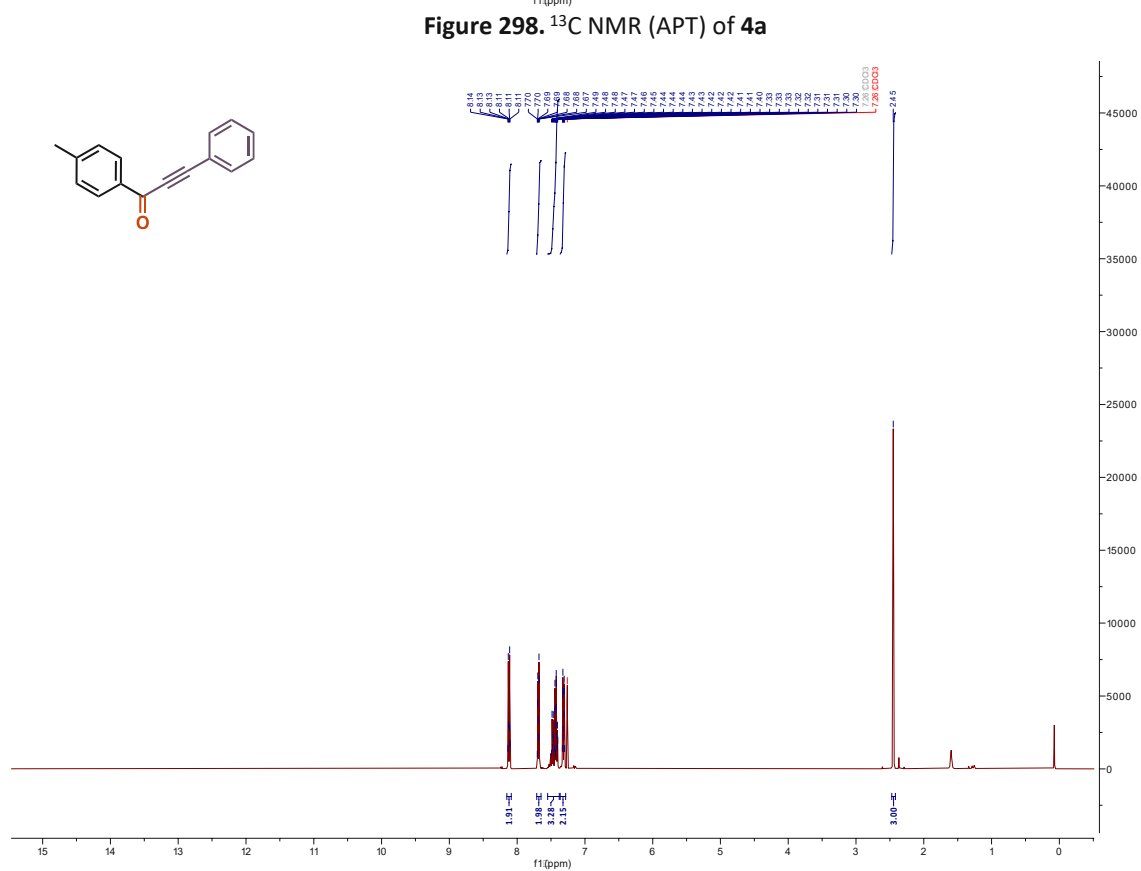
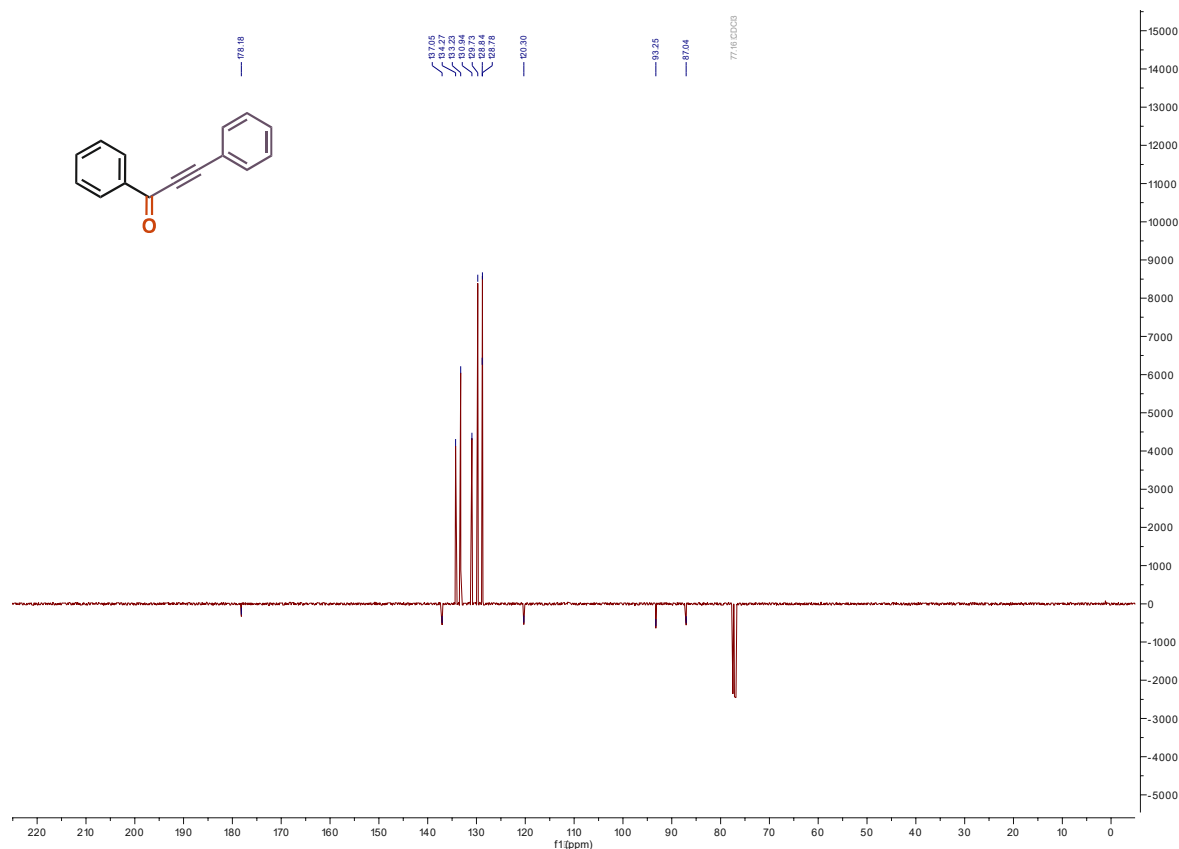
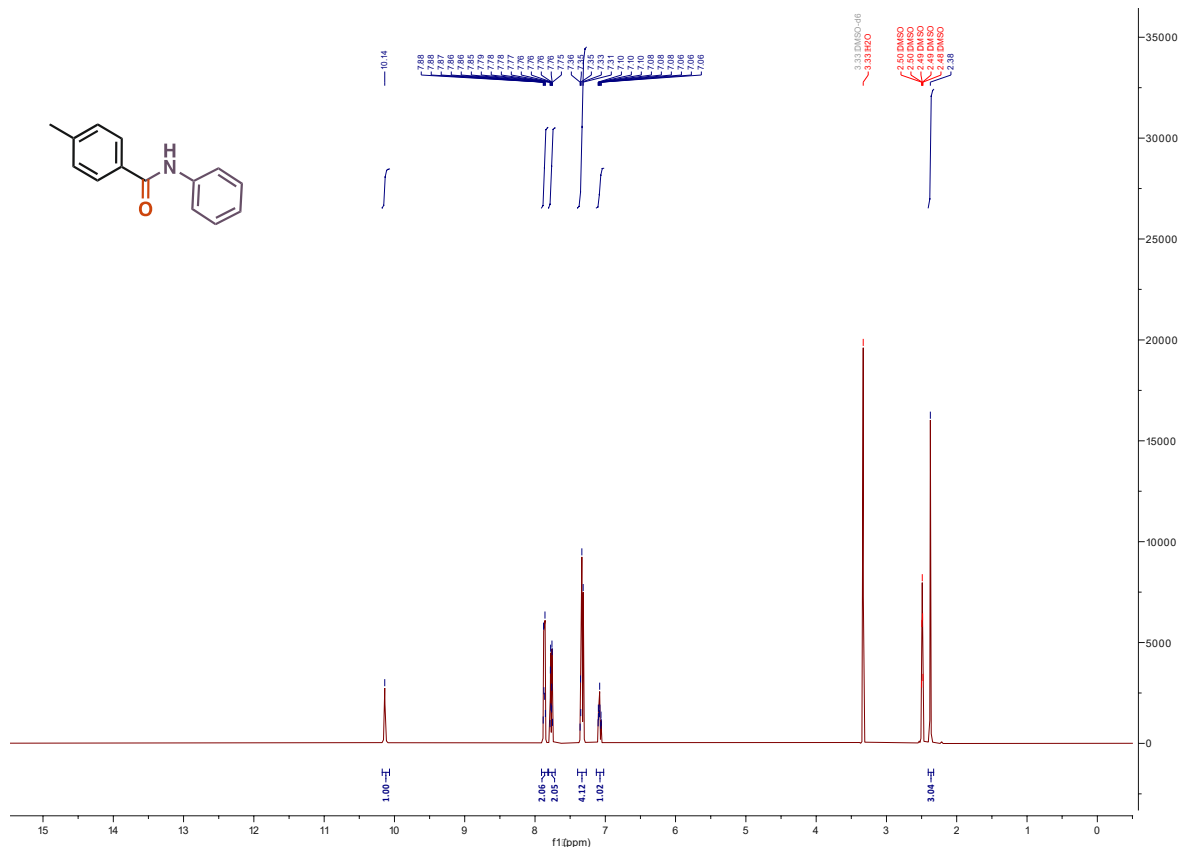


Figure 291. ¹³C NMR (APT) of 3b







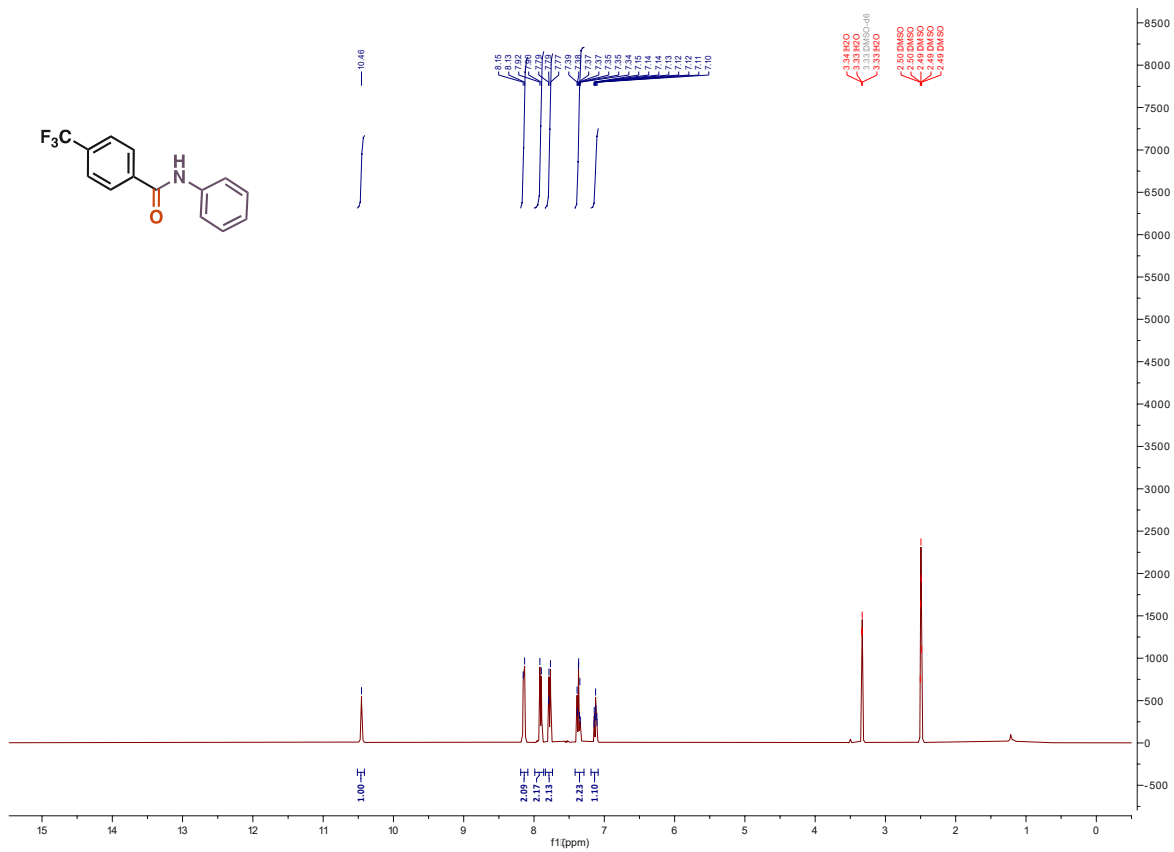


Figure 308. ¹H NMR of 5c

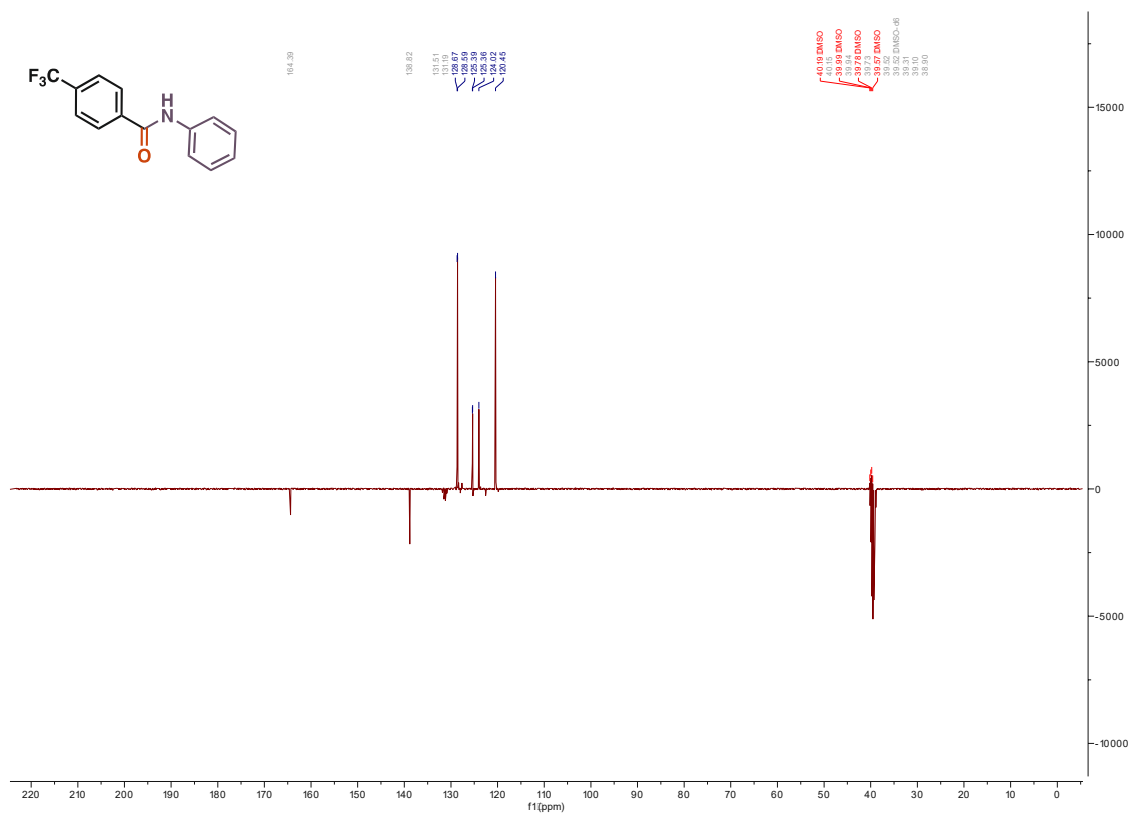


Figure 309. ¹³C NMR (APT) of 5c



Figure 310. ^{19}F NMR of 5c

12. Bibliography

- [1] A. Hermann, *Phys. Bl.* **1965**, *21*, 168-171.
- [2] A. Kalsi, N. Balani, in *Physics for the Anaesthetic Viva*, Cambridge University Press, Cambridge, **2016**, pp. 27-28.
- [3] a) N. E. Leadbeater, *An Introduction to Flow Chemistry: A Practical Laboratory Course*, U. o. Connecticut, USA, **2013**; b) J. M. Souza, R. Galaverna, A. A. N. Souza, T. J. Brocksom, J. C. Pastre, R. Souza, K. T. Oliveira, *An. Acad. Bras. Cienc.* **2018**, *90*, 1131-1174; c) M. Guidi, P. H. Seeberger, K. Gilmore, *Chem. Soc. Rev.* **2020**, *49*, 8910-8932; d) C. A. Hone, C. O. Kappe, *Chemistry-Methods* **2021**, *1*, 454-467; e) E. M. Purcell, *Am. J. Phys.* **1977**, *45*, 3-11; f) F. M. Akwi, P. Watts, *Chem. Commun.* **2018**, *54*, 13894-13928.
- [4] P. Walden, *Bull. Acad. Imper. Sci. (St. Petersburg)* **1914**, *8*, 405-422.
- [5] S. Gabriel, J. Weiner, *Ber. Dtsch. Chem. Ges.* **1888**, *21*, 2669-2679.
- [6] C. Schröder, in *Analytical Applications of Ionic Liquids* (Ed.: M. Koel), World Scientific Publishing Europe Ltd., London, Great Britain, **2016**, pp. 2-6.
- [7] J. Yuan, M. Antonietti, *Polymer* **2011**, *52*, 1469-1482.
- [8] C. Li, J. Patra, J. Li, P. C. Rath, M.-H. Lin, J.-K. Chang, *Adv. Funct. Mater.* **2020**, *30*, 1909565.
- [9] L. C. Brown, J. M. Hogg, M. Swadźba-Kwaśny, *Top. Curr. Chem.* **2017**, *375*, 78.
- [10] J. Qi, Y. Hu, Y. Zhao, J. Li, *Chin. J. Chem. Eng.* **2015**, *23*, 1565-1571.
- [11] X. Wang, Y. Chi, T. Mu, *J. Mol. Liq.* **2014**, *193*, 262-266.
- [12] E. Kianfar, S. Mafi, *Fine Chem. Eng.* **2020**, *2*, 22-31.
- [13] a) C. Jork, M. Seiler, Y.-A. Beste, W. Arlt, *J. Chem. Eng. Data* **2004**, *49*, 852-857; b) X. Zhao, P. Cai, C. Sun, Y. Pan, *Trends Anal. Chem.* **2019**, *111*, 148-162; c) M. Koel, *Crit. Rev. Anal. Chem.* **2005**, *35*, 177-192; d) T. D. Ho, C. Zhang, L. W. Hantao, J. L. Anderson, *Anal. Chem.* **2014**, *86*, 262-285.
- [14] a) C. Kornpointner, A. Sainz Martinez, M. Schnürch, H. Halbwirth, K. Bica-Schröder, *Green Chem.* **2021**, *23*, 10079-10089; b) S. P. M. Ventura, F. A. e Silva, M. V. Quental, D. Mondal, M. G. Freire, J. A. P. Coutinho, *Chem. Rev.* **2017**, *117*, 6984-7052.
- [15] a) J. Brünig, Z. Csendes, S. Weber, N. Gorgas, R. W. Bittner, A. Limbeck, K. Bica, H. Hoffmann, K. Kirchner, *ACS Catal.* **2018**, *8*, 1048-1051; b) H.-P. Steinrück, P. Wasserscheid, *Catal. Lett.* **2015**, *145*, 380-397.
- [16] a) H. Xiao, *Tribol. Trans.* **2017**, *60*, 20-30; b) A. Anifa Mohamed Faruck, P. G. Grützmaier, C.-J. Hsu, D. Dworschak, H.-W. Cheng, M. Valtiner, K. Stagel, P. Mikšovský, A. R. Sahoo, A. Sainz Martinez, K. Bica-Schröder, M. Weigand, C. Gachot, *Friction* **2022**.
- [17] a) R. Kawano, H. Matsui, C. Matsuyama, A. Sato, M. A. B. H. Susan, N. Tanabe, M. Watanabe, *J. Photochem. Photobiol. A.* **2004**, *164*, 87-92; b) F. Endres, S. Zein El Abedin, *Phys. Chem. Chem. Phys.* **2006**, *8*, 2101-2116; c) H. Zhang, J. Liang, B. Xia, Y. Li, S. Du, *Front. Chem. Sci. Eng.* **2019**, *13*, 695-701.
- [18] a) K. Binnemans, *Chem. Rev.* **2005**, *105*, 4148-4204; b) K. Goossens, K. Lava, C. W. Bielawski, K. Binnemans, *Chem. Rev.* **2016**, *116*, 4643-4807.
- [19] a) A. A. Minea, *Int. J. Thermophys.* **2020**, *41*, 151; b) J. Wang, X. Tang, Z. Qi, T. Xu, T. Zou, Y. Bie, D. Wang, Y. Liu, *ACS Sustain. Chem. Eng.* **2022**, *10*, 2248-2261.
- [20] T. Welton, *Chem. Rev.* **1999**, *99*, 2071-2084.
- [21] T. Welton, *Biophys. Rev.* **2018**, *10*, 691-706.
- [22] G. W. Parshall, *J. Am. Chem. Soc.* **1972**, *94*, 8716-8719.
- [23] K. S. Rosenthal, D. R. Storm, W. T. Ford, *Antimicrob. Agents Chemother.* **1975**, *8*, 510-512.

- [24] W. T. Ford, R. J. Hauri, S. G. Smith, *J. Am. Chem. Soc.* **1974**, *96*, 4316-4318.
- [25] C. L. Hussey, T. M. Laher, *Inorg. Chem.* **1981**, *20*, 4201-4206.
- [26] D. K. Magnuson, J. W. Bodley, D. F. Evans, *J. Solution Chem.* **1984**, *13*, 583-587.
- [27] F. Pacholec, H. T. Butler, C. F. Poole, *Anal. Chem.* **1982**, *54*, 1938-1941.
- [28] J. S. Wilkes, J. A. Levisky, R. A. Wilson, C. L. Hussey, *Inorg. Chem.* **1982**, *21*, 1263-1264.
- [29] a) G. P. Smith, A. S. Dworkin, R. M. Pagni, S. P. Zingg, *J. Am. Chem. Soc.* **1989**, *111*, 525-530; b) M. Misono, T. Okuhara, *Chemtech* **1993**, *23*.
- [30] T. V. Harris, M. Driver, S. Elomari, H.-K. C. Timken, *Alkylation process using an alkyl halide promoted ionic liquid catalyst*, U.S. Patent No. 7,531,707, **2009**.
- [31] J. A. Boon, J. A. Levisky, J. L. Pflug, J. S. Wilkes, *J. Org. Chem.* **1986**, *51*, 480-483.
- [32] J. S. Wilkes, M. J. Zaworotko, *J. Chem. Soc., Chem. Commun.* **1992**, 965-967.
- [33] P. Bonhôte, A.-P. Dias, N. Papageorgiou, K. Kalyanasundaram, M. Grätzel, *Inorg. Chem.* **1996**, *35*, 1168-1178.
- [34] J. Fuller, R. T. Carlin, H. C. De Long, D. Haworth, *J. Chem. Soc., Chem. Commun.* **1994**, 299-300.
- [35] J. Sun, D. R. MacFarlane, M. Forsyth, *Ionics* **1997**, *3*, 356-362.
- [36] a) A. Brandt, J. Gräsvik, J. P. Hallett, T. Welton, *Green Chem.* **2013**, *15*, 550-583; b) Z. Zhang, J. Song, B. Han, *Chem. Rev.* **2017**, *117*, 6834-6880.
- [37] a) L.-L. Fan, H.-J. Li, Q.-H. Chen, *Int. J. Mol. Sci.* **2014**, *15*, 12196-12216; b) T. Itoh, *Chem. Rev.* **2017**, *117*, 10567-10607.
- [38] a) D. R. MacFarlane, N. Tachikawa, M. Forsyth, J. M. Pringle, P. C. Howlett, G. D. Elliott, J. H. Davis, M. Watanabe, P. Simon, C. A. Angell, *Energy Environ. Sci.* **2014**, *7*, 232-250; b) M. Watanabe, M. L. Thomas, S. Zhang, K. Ueno, T. Yasuda, K. Dokko, *Chem. Rev.* **2017**, *117*, 7190-7239.
- [39] T. D. Ho, A. J. Canestraro, J. L. Anderson, *Anal. Chim. Acta* **2011**, *695*, 18-43.
- [40] a) M. Díaz, A. Ortiz, I. Ortiz, *J. Membr. Sci.* **2014**, *469*, 379-396; b) A. Eftekhari, *Energy Storage Mater.* **2017**, *9*, 47-69.
- [41] M. J. Salar-García, V. M. Ortiz-Martínez, F. J. Hernández-Fernández, A. P. de los Ríos, J. Quesada-Medina, *J. Hazard. Mater.* **2017**, *321*, 484-499.
- [42] a) D. L. Davies, S. K. Kandola, R. K. Patel, *Tetrahedron: Asymmetry* **2004**, *15*, 77-80; b) K. S. Egorova, E. G. Gordeev, V. P. Ananikov, *Chem. Rev.* **2017**, *117*, 7132-7189.
- [43] Y. Chauvin, B. Gilbert, I. Guibard, *J. Chem. Soc., Chem. Commun.* **1990**, 1715-1716.
- [44] a) N. V. Plechkova, K. R. Seddon, *Chem. Soc. Rev.* **2008**, *37*, 123-150; b) H. Olivier-Bourbigou, F. Favre, A. Forestière, F. Hugues, in *Handbook of Green Chemistry* (Ed.: P. T. Anastas), Wiley-VCH, Weinheim, **2010**, pp. 101-126.
- [45] B. Gilbert, H. Olivier-Bourbigou, F. Favre, *Oil Gas Sci. Techn.– Rev. IFP* **2007**, *62*, 745-759.
- [46] M. Volland, V. Seitz, M. Maase, M. Flores, R. Papp, K. Massonne, V. Stegmann, K. Halbritter, R. Noe, M. Bartsch, *Method for the separation of acids from chemical reaction mixtures by means of ionic fluids*, U.S. Patent No. 7,767,852, **2010**.
- [47] a) P. Berton, N. Abidi, J. L. Shamshina, *Curr. Opin. Green Sustain. Chem.* **2022**, *35*, 100625; b) G. Liu, G. Wu, Y. Liu, R. Hu, G. Gao, *Fuel* **2022**, *310*, 122379.
- [48] H. K. Timken, H. Luo, B.-K. Chang, E. Carter, M. Cole, in *Commercial Applications of Ionic Liquids* (Ed.: M. B. Shiflett), Springer International Publishing, Cham, **2020**, pp. 33-47.
- [49] R. Franke, H. Hahn, *Evonik Ind.* **2015**, *2*, 18-23.
- [50] M. Abai, M. P. Atkins, A. Hassan, J. D. Holbrey, Y. Kuah, P. Nockemann, A. A. Oliferenko, N. V. Plechkova, S. Rafeen, A. A. Rahman, R. Ramli, S. M. Shariff, K. R. Seddon, G. Srinivasan, Y. Zou, *Dalton Trans.* **2015**, *44*, 8617-8624.

- [51] a) P. Wasserscheid, W. Keim, *Angew. Chem. Int. Ed.* **2000**, *39*, 3772-3789; b) C. M. Gordon, M. J. Muldoon, M. Wagner, C. Hilgers, J. H. Davis Jr, P. Wasserscheid, in *Ionic Liquids in Synthesis*, John Wiley & Sons, Ltd, **2007**, pp. 7-55.
- [52] a) R. S. Varma, V. V. Namboodiri, *Chem. Commun.* **2001**, 643-644; b) M. Deetlefs, K. R. Seddon, *Green Chem.* **2003**, *5*, 181-186; c) K. Madgula, S. Dandu, S. Kasula, P. Halady, *Inorg. Chem. Commun.* **2022**, *138*, 109218.
- [53] a) V. V. Namboodiri, R. S. Varma, *Org. Lett.* **2002**, *4*, 3161-3163; b) J. D. Oxley, T. Prozorov, K. S. Suslick, *J. Am. Chem. Soc.* **2003**, *125*, 11138-11139.
- [54] a) C. Maton, N. De Vos, C. V. Stevens, *Chem. Soc. Rev.* **2013**, *42*, 5963-5977; b) S. D. Chambreau, A. C. Schenk, A. J. Sheppard, G. R. Yandek, G. L. Vaghjiani, J. Maciejewski, C. J. Koh, A. Golan, S. R. Leone, *J. Phys. Chem. A* **2014**, *118*, 11119-11132.
- [55] a) J.-M. Lévêque, J. Estager, M. Draye, G. Cravotto, L. Boffa, W. Bonrath, *Monatsh. Chem.* **2007**, *138*, 1103-1113; b) M. J. Earle, C. M. Gordon, N. V. Plechkova, K. R. Seddon, T. Welton, *Anal. Chem.* **2007**, *79*, 758-764; c) R. E. Del Sesto, T. M. McCleskey, C. Macomber, K. C. Ott, A. T. Koppisch, G. A. Baker, A. K. Burrell, *Thermochim. Acta* **2009**, *491*, 118-120.
- [56] J. L. Ferguson, J. D. Holbrey, S. Ng, N. V. Plechkova, K. R. Seddon, A. A. Tomaszowska, D. F. Wassell, *Pure Appl. Chem.* **2011**, *84*, 723-744.
- [57] K. R. Seddon, A. Stark, M.-J. Torres, *Pure Appl. Chem.* **2000**, *72*, 2275-2287.
- [58] J. D. Holbrey, W. M. Reichert, R. P. Swatloski, G. A. Broker, W. R. Pitner, K. R. Seddon, R. D. Rogers, *Green Chem.* **2002**, *4*, 407-413.
- [59] E. Kuhlmann, S. Himmler, H. Giebelhaus, P. Wasserscheid, *Green Chem.* **2007**, *9*, 233-242.
- [60] A. Westerholt, M. Weschta, A. Bösmann, S. Tremmel, Y. Korth, M. Wolf, E. Schlücker, N. Wehrum, A. Lennert, M. Uerdingen, W. Holweger, S. Wartzack, P. Wasserscheid, *ACS Sustain. Chem. Eng.* **2015**, *3*, 797-808.
- [61] a) M. Ue, M. Takeda, T. Takahashi, M. Takehara, *Electrochem. Solid-State Lett.* **2002**, *5*, A119; b) M. Smiglak, J. D. Holbrey, S. T. Griffin, W. M. Reichert, R. P. Swatloski, A. R. Katritzky, H. Yang, D. Zhang, K. Kirichenko, R. D. Rogers, *Green Chem.* **2007**, *9*, 90-98.
- [62] J. D. Holbrey, W. M. Reichert, I. Tkatchenko, E. Bouajila, O. Walter, I. Tommasi, R. D. Rogers, *Chem. Commun.* **2003**, 28-29.
- [63] R. S. Kalb, E. N. Stepurko, V. N. Emel'yanenko, S. P. Verevkin, *Phys. Chem. Chem. Phys.* **2016**, *18*, 31904-31913.
- [64] J. Zhang, G. R. Martin, D. D. DesMarteau, *Chem. Commun.* **2003**, 2334-2335.
- [65] K. Takao, Y. Ikeda, *Chem. Lett.* **2008**, *37*, 682-683.
- [66] N. W. Smith, S. P. Gourisankar, J.-L. Montchamp, S. V. Dzyuba, *New J. Chem.* **2011**, *35*, 909-914.
- [67] D. J. Kim, K. H. Oh, J. K. Park, *Green Chem.* **2014**, *16*, 4098-4101.
- [68] V. Hessel, H. Löwe, F. Schönfeld, *Chem. Eng. Sci.* **2005**, *60*, 2479-2501.
- [69] A. Große Böwing, A. Jess, P. Wasserscheid, *Chem. Ing. Tech.* **2005**, *77*, 1430-1439.
- [70] D. A. Waterkamp, M. Heiland, M. Schlüter, J. C. Sauvageau, T. Beyersdorff, J. Thöming, *Green Chem.* **2007**, *9*, 1084-1090.
- [71] H. Löwe, R. D. Axinte, D. Breuch, C. Hofmann, *Chem. Eng. J.* **2009**, *155*, 548-550.
- [72] D. Wilms, J. Klos, A. F. M. Kilbinger, H. Löwe, H. Frey, *Org. Process. Res. Dev.* **2009**, *13*, 961-964.
- [73] M. A. Gonzalez, J. T. Ciszewski, *Org. Process. Res. Dev.* **2009**, *13*, 64-66.
- [74] J. Zimmermann, B. Ondruschka, A. Stark, *Org. Process. Res. Dev.* **2010**, *14*, 1102-1109.

- [75] T. Nokami, K. Matsumoto, T.-a. Itoh, Y. Fukaya, T. Itoh, *Org. Process. Res. Dev.* **2014**, *18*, 1367-1371.
- [76] L. Cao, H. W. Kim, Y. J. Jeong, S. C. Han, J. K. Park, *Org. Process. Res. Dev.* **2022**, *26*, 207-214.
- [77] R. S. Kalb, M. Damm, S. P. Verevkin, *React. Chem. Eng.* **2017**, *2*, 432-436.
- [78] V. I. Pârvulescu, C. Hardacre, *Chem. Rev.* **2007**, *107*, 2615-2665.
- [79] E. García-Verdugo, B. Altava, M. I. Burguete, P. Lozano, S. V. Luis, *Green Chem.* **2015**, *17*, 2693-2713.
- [80] P. Wasserscheid, *J. Ind. Eng. Chem.* **2007**, *13*, 325-338.
- [81] S. Liu, T. Fukuyama, M. Sato, I. Ryu, *Org. Process. Res. Dev.* **2004**, *8*, 477-481.
- [82] L. Xu, W. Chen, J. Xiao, *Organometallics* **2000**, *19*, 1123-1127.
- [83] T. Fukuyama, M. T. Rahman, Y. Sumino, I. Ryu, *Synlett* **2012**, *23*, 2279-2283.
- [84] G. W. Phillips, S. N. Falling, S. A. Godleski, J. R. Monnier, *Continuous process for the manufacture of 2, 5-dihydrofurans from γ , δ -epoxybutenes*, US Patent No. 5,315,019, **1994**.
- [85] T. N. Glasnov, J. D. Holbrey, C. O. Kappe, K. R. Seddon, T. Yan, *Green Chem.* **2012**, *14*, 3071-3076.
- [86] D. Horii, T. Fuchigami, M. Atobe, *J. Am. Chem. Soc.* **2007**, *129*, 11692-11693.
- [87] A. Blanco, G. Blanco, in *Medical Biochemistry* (Eds.: A. Blanco, G. Blanco), Academic Press, **2017**, pp. 153-175.
- [88] J. Wang, S.-S. Gu, H.-S. Cui, X.-Y. Wu, F.-A. Wu, *Bioresour. Technol.* **2014**, *158*, 39-47.
- [89] L. Gubicza, K. Bélafi-Bakó, E. Fehér, T. Fráter, *Green Chem.* **2008**, *10*, 1284-1287.
- [90] F. Jutz, J.-M. Andanson, A. Baiker, *Chem. Rev.* **2011**, *111*, 322-353.
- [91] L. A. Blanchard, D. Hancu, E. J. Beckman, J. F. Brennecke, *Nature* **1999**, *399*, 28-29.
- [92] S. Keskin, D. Kayrak-Talay, U. Akman, Ö. Hortaçsu, *J. Supercrit. Fluids* **2007**, *43*, 150-180.
- [93] P. B. Webb, M. F. Sellin, T. E. Kunene, S. Williamson, A. M. Z. Slawin, D. J. Cole-Hamilton, *J. Am. Chem. Soc.* **2003**, *125*, 15577-15588.
- [94] M. F. Sellin, P. B. Webb, D. J. Cole-Hamilton, *Chem. Commun.* **2001**, 781-782.
- [95] J. Theuerkauf, G. Franciò, W. Leitner, *Adv. Synth. Catal.* **2013**, *355*, 209-219.
- [96] M. T. Rahman, T. Fukuyama, N. Kamata, M. Sato, I. Ryu, *Chem. Commun.* **2006**, 2236-2238.
- [97] O. Bartlewicz, I. Dąbek, A. Szymańska, H. Maciejewski, *Catalysts* **2020**, *10*, 1227.
- [98] R. Castro-Amoedo, Z. Csendes, J. Brünig, M. Sauer, A. Foelske-Schmitz, N. Yigit, G. Rupprechter, T. Gupta, A. M. Martins, K. Bica, H. Hoffmann, K. Kirchner, *Catal. Sci. Technol.* **2018**, *8*, 4812-4820.
- [99] A. Riisager, P. Wasserscheid, R. van Hal, R. Fehrmann, *J. Catal.* **2003**, *219*, 452-455.
- [100] A. Riisager, B. Jørgensen, P. Wasserscheid, R. Fehrmann, *Chem. Commun.* **2006**, 994-996.
- [101] M. J. Schneider, M. Haumann, P. Wasserscheid, *J. Mol. Catal. A Chem.* **2013**, *376*, 103-110.
- [102] M. J. Schneider, M. Lijewski, R. Woelfel, M. Haumann, P. Wasserscheid, *Angew. Chem. Int. Ed.* **2013**, *52*, 6996-6999.
- [103] M. J. Schneider, M. Haumann, M. Stricker, J. Sundermeyer, P. Wasserscheid, *J. Catal.* **2014**, *309*, 71-78.
- [104] J. Joni, M. Haumann, P. Wasserscheid, *Appl. Catal. A: Gen.* **2010**, *372*, 8-15.
- [105] F. T. U. Kohler, K. Gärtner, V. Hager, M. Haumann, M. Sternberg, X. Wang, N. Szesni, K. Meyer, P. Wasserscheid, *Catal. Sci. Technol.* **2014**, *4*, 936-947.

- [106] U. Hintermair, Z. Gong, A. Serbanovic, M. J. Muldoon, C. C. Santini, D. J. Cole-Hamilton, *Dalton Trans.* **2010**, 39, 8501-8510.
- [107] U. Hintermair, T. Höfener, T. Pullmann, G. Franciò, W. Leitner, *ChemCatChem* **2010**, 2, 150-154.
- [108] P. Lozano, T. De Diego, T. Sauer, M. Vaultier, S. Gmouh, J. L. Iborra, *J. Supercrit. Fluids* **2007**, 40, 93-100.
- [109] A. Sainz Martinez, C. Hauzenberger, A. R. Sahoo, Z. Csendes, H. Hoffmann, K. Bica, *ACS Sustain. Chem. Eng.* **2018**, 6, 13131-13139.
- [110] C. P. Mehnert, R. A. Cook, N. C. Dispenziere, M. Afeworki, *J. Am. Chem. Soc.* **2002**, 124, 12932-12933.
- [111] B. Urbán, D. Srankó, G. Sáfrán, L. Üрге, F. Darvas, J. Bakos, R. Skoda-Földes, *J. Mol. Catal. A Chem.* **2014**, 395, 364-372.
- [112] S. Martín, R. Porcar, E. Peris, M. I. Burguete, E. García-Verdugo, S. V. Luis, *Green Chem.* **2014**, 16, 1639-1647.
- [113] M. I. Burguete, H. Erythropel, E. Garcia-Verdugo, S. V. Luis, V. Sans, *Green Chem.* **2008**, 10, 401-407.
- [114] a) B. M. Trost, D. L. Van Vranken, *Chem. Rev.* **1996**, 96, 395-422; b) B. M. Trost, M. L. Crawley, *Chem. Rev.* **2003**, 103, 2921-2944.
- [115] J. Tsuji, H. Takahashi, M. Morikawa, *Tetrahedron Lett.* **1965**, 6, 4387-4388.
- [116] B. M. Trost, T. J. Fullerton, *J. Am. Chem. Soc.* **1973**, 95, 292-294.
- [117] O. Pàmies, J. Margalef, S. Cañellas, J. James, E. Judge, P. J. Guiry, C. Moberg, J.-E. Bäckvall, A. Pfaltz, M. A. Pericàs, M. Diéguez, *Chem. Rev.* **2021**, 121, 4373-4505.
- [118] R.-D. Gao, Q.-L. Xu, L.-X. Dai, S.-L. You, *Org. Biomol. Chem.* **2016**, 14, 8044-8046.
- [119] B. M. Trost, T. Zhang, J. D. Sieber, *Chem. Sci.* **2010**, 1, 427-440.
- [120] a) A. Armstrong, *Org. Process. Res. Dev.* **2001**, 5, 457-457; b) T. C. Nugent, M. El-Shazly, *Adv. Synth. Catal.* **2010**, 352, 753-819.
- [121] a) R. A. Kerr, *Science* **2005**, 309, 100-100; b) S. A. Montzka, E. J. Dlugokencky, J. H. Butler, *Nature* **2011**, 476, 43-50.
- [122] C. Bettenhausen, *C&EN* **2022**, 100, 22-24.
- [123] a) M. Aresta, in *Carbon dioxide as chemical feedstock* (Ed.: M. Aresta), John Wiley & Sons, **2010**, p. 394; b) M. Bertau, H. Offermanns, G. Menges, W. Keim, F. Effenberger, *Chem. Ing. Tech.* **2010**, 82, 2055-2058; c) A. Saravanan, P. Senthil kumar, D.-V. N. Vo, S. Jeevanantham, V. Bhuvanewari, V. Anantha Narayanan, P. R. Yaashikaa, S. Swetha, B. Reshma, *Chem. Eng. Sci.* **2021**, 236, 116515; d) C. Kim, C.-J. Yoo, H.-S. Oh, B. K. Min, U. Lee, *J. CO2 Util.* **2022**, 65, 102239.
- [124] a) I. Ghiat, T. Al-Ansari, *J. CO2 Util.* **2021**, 45, 101432; b) A. Dubey, A. Arora, *J. Clean. Prod.* **2022**, 373, 133932; c) H. Chen, H. Dong, Z. Shi, A. K. SenGupta, *Sci. Adv.* **2023**, 9, eadg1956.
- [125] T. E. Müller, W. Leitner, *Beilstein J. Org. Chem.* **2015**, 11, 675-677.
- [126] M. Peters, B. Köhler, W. Kuckshinrichs, W. Leitner, P. Markewitz, T. E. Müller, *ChemSusChem* **2011**, 4, 1216-1240.
- [127] C.-K. Ran, L.-L. Liao, T.-Y. Gao, Y.-Y. Gui, D.-G. Yu, *Curr. Opin. Green Sustain. Chem.* **2021**, 32, 100525.
- [128] a) D. S. Marlin, E. Sarron, Ó. Sigurbjörnsson, *Front. Chem.* **2018**, 6; b) F. Zeng, C. Mebrahtu, X. Xi, L. Liao, J. Ren, J. Xie, H. J. Heeres, R. Palkovits, *App. Catal. B: Environ.* **2021**, 291, 120073.
- [129] T. Sakakura, K. Kohno, *Chem. Commun.* **2009**, 1312-1330.
- [130] a) W. McGhee, D. Riley, K. Christ, Y. Pan, B. Parnas, *J. Org. Chem.* **1995**, 60, 2820-2830; b) M. Yoshida, N. Hara, S. Okuyama, *Chem. Commun.* **2000**, 151-152.
- [131] Y. Yu, L.-M. Fang, Y. Liu, X.-B. Lu, *ACS Catal.* **2021**, 11, 8349-8357.

- [132] a) L. Wang, C. Qi, W. Xiong, H. Jiang, *Chinese J. Catal.* **2022**, *43*, 1598-1617; b) A. K. Ghosh, M. Brindisi, *J. Med. Chem.* **2015**, *58*, 2895-2940.
- [133] a) R. Srivastava, M. D. Manju, D. Srinivas, P. Ratnasamy, *Catal. Lett.* **2004**, *97*, 41-47; b) D.-L. Kong, L.-N. He, J.-Q. Wang, *Synth. Commun.* **2011**, *41*, 3298-3307; c) I. Dindarloo Inaloo, S. Majnooni, *New J. Chem.* **2019**, *43*, 11275-11281.
- [134] J.-B. Peng, H.-Q. Geng, X.-F. Wu, *Chem* **2019**, *5*, 526-552.
- [135] L. Gattermann, J. A. Koch, *Ber. Dtsch. Chem. Ges.* **1897**, *30*, 1622-1624.
- [136] a) R. Skoda-Földes, K. Kollár, *Curr. Org. Chem.* **2002**, *6*, 1097-1119; b) A. Brennführer, H. Neumann, M. Beller, *Angew. Chem. Int. Ed.* **2009**, *48*, 4114-4133; c) S. Sumino, A. Fusano, T. Fukuyama, I. Ryu, *Acc. Chem. Res.* **2014**, *47*, 1563-1574.
- [137] M. Beller, B. Cornils, C. D. Frohning, C. W. Kohlpaintner, *J. Mol. Catal. A Chem.* **1995**, *104*, 17-85.
- [138] M. Beller, X.-F. Wu, in *Transition Metal Catalyzed Carbonylation Reactions*, Springer Berlin, Heidelberg, **2013**, pp. 1-11.
- [139] G. L. Miessler, D. A. Tarr, in *Inorg. Chem.*, 2 ed., Prentice Hall, **1999**, p. 338.
- [140] a) X.-F. Wu, H. Neumann, *ChemCatChem* **2012**, *4*, 447-458; b) X.-F. Wu, X. Fang, L. Wu, R. Jackstell, H. Neumann, M. Beller, *Acc. Chem. Res.* **2014**, *47*, 1041-1053.
- [141] J.-B. Peng, F.-P. Wu, X.-F. Wu, *Chem. Rev.* **2019**, *119*, 2090-2127.
- [142] J.-B. Peng, X.-F. Wu, *Angew. Chem. Int. Ed.* **2018**, *57*, 1152-1160.
- [143] R. Franke, D. Selent, A. Börner, *Chem. Rev.* **2012**, *112*, 5675-5732.
- [144] a) S. Ahrland, J. Chatt, N. R. Davies, *Q. Rev. Chem. Soc.* **1958**, *12*, 265-276; b) W. A. Herrmann, C. W. Kohlpaintner, H. Bahrmann, W. Konkol, *J. Mol. Catal.* **1992**, *73*, 191-201; c) H. Bahrmann, H. Bach, C. D. Frohning, H. J. Kleiner, P. Lappe, D. Peters, D. Regnat, W. A. Herrmann, *J. Mol. Catal. A Chem.* **1997**, *116*, 49-53; d) A. Fukuoka, W. Kosugi, F. Morishita, M. Hirano, S. Komiya, L. McCaffrey, W. Henderson, *Chem. Commun.* **1999**, 489-490.
- [145] a) M. Dessoudeix, M. Urrutigoity, P. Kalck, *Eur. J. Inorg. Chem.* **2001**, *2001*, 1797-1800; b) S. Tilloy, E. Genin, F. Hapiot, D. Landy, S. Fourmentin, J. P. Genêt, V. Michelet, E. Monflier, *Adv. Synth. Catal.* **2006**, *348*, 1547-1552.
- [146] T. Fukuyama, M. T. Rahman, N. Kamata, I. Ryu, *Beilstein J. Org. Chem.* **2009**, *5*, 34.
- [147] U. Gross, P. Koos, M. O'Brien, A. Polyzos, S. V. Ley, *Eur. J. Org. Chem.* **2014**, *2014*, 6418-6430.
- [148] M. T. Jensen, M. H. Ronne, A. K. Ravn, R. W. Juhl, D. U. Nielsen, X. M. Hu, S. U. Pedersen, K. Daasbjerg, T. Skrydstrup, *Nat. Commun.* **2017**, *8*, 489.
- [149] X. He, Y. Cao, X.-D. Lang, N. Wang, L.-N. He, *ChemSusChem* **2018**, *11*, 3382-3387.
- [150] S. Fu, S. Yao, S. Guo, G.-C. Guo, W. Yuan, T.-B. Lu, Z.-M. Zhang, *J. Am. Chem. Soc.* **2021**, *143*, 20792-20801.
- [151] Y.-S. Xia, M. Tang, L. Zhang, J. Liu, C. Jiang, G.-K. Gao, L.-Z. Dong, L.-G. Xie, Y.-Q. Lan, *Nat. Commun.* **2022**, *13*, 2964.
- [152] L. Song, Y.-X. Jiang, Z. Zhang, Y.-Y. Gui, X.-Y. Zhou, D.-G. Yu, *Chem. Commun.* **2020**, *56*, 8355-8367.
- [153] R. Sang, Y. Hu, R. Razzaq, G. Mollaert, H. Atia, U. Bentrup, M. Sharif, H. Neumann, H. Junge, R. Jackstell, B. U. W. Maes, M. Beller, *Nat. Commun.* **2022**, *13*, 4432.
- [154] M. Gaudeau, M. Zhang, M. Tatoulian, C. Lescot, S. Ognier, *React. Chem. Eng.* **2020**, *5*, 1981-1991.
- [155] K. Bica, M. Schön, P. Gärtner, M. Mihovilovic, *Method for producing ionic liquids*, WO 2017/112972 AI, **2017**.
- [156] R. Kawai, S. Yada, T. Yoshimura, *Phys. Chem. Chem. Phys.* **2019**, *21*, 25065-25071.
- [157] M. Nascimento de Oliveira, S. Arseniyadis, J. Cossy, *Chem. Eur. J.* **2018**, *24*, 4810-4814.

- [158] A.-M. Carroll, M. McCarthy, P. M. Lacey, C. P. Saunders, D. J. Connolly, A. Farrell, B. V. Rokade, R. Goddard, P. Fristrup, P.-O. Norrby, P. J. Guiry, *Tetrahedron* **2020**, *76*, 130780.
- [159] N. Boufroua, E. Dunach, F. Fontaine-Vive, S. Achouche-Bouzroua, S. Poulain-Martini, *New J. Chem.* **2020**, *44*, 6042-6052.
- [160] H. Jin, X. Jiang, H. Yoo, T. Wang, C. G. Sung, U. Choi, C. R. Lee, H. Yu, S. Koo, *ChemistrySelect* **2020**, *5*, 12421-12424.
- [161] P.-S. Gao, F. Ye, X.-Y. Dong, Y. Chen, Z.-W. Gao, W.-Q. Zhang, L.-W. Xu, *RSC Adv.* **2015**, *5*, 33818-33822.
- [162] J. Jing, X. Huo, J. Shen, J. Fu, Q. Meng, W. Zhang, *Chem. Commun.* **2017**, *53*, 5151-5154.
- [163] K. N. Gavrilov, S. V. Zheglov, M. N. Gavrilova, I. M. Novikov, M. G. Maksimova, N. N. Groshkin, E. A. Rastorguev, V. A. Davankov, *Tetrahedron* **2012**, *68*, 1581-1589.
- [164] T. H. West, D. S. B. Daniels, A. M. Z. Slawin, A. D. Smith, *J. Am. Chem. Soc.* **2014**, *136*, 4476-4479.
- [165] D. Krishnan, M. Wu, M. Chiang, Y. Li, P.-H. Leung, S. A. Pullarkat, *Organometallics* **2013**, *32*, 2389-2397.
- [166] T. Ohshima, Y. Miyamoto, J. Ipposhi, Y. Nakahara, M. Utsunomiya, K. Mashima, *J. Am. Chem. Soc.* **2009**, *131*, 14317-14328.
- [167] D. Banerjee, R. V. Jagadeesh, K. Junge, H. Junge, M. Beller, *ChemSusChem* **2012**, *5*, 2039-2044.
- [168] B. M. Trost, D. L. Van Vranken, C. Bingel, *J. Am. Chem. Soc.* **1992**, *114*, 9327-9343.
- [169] Y. K. Kim, S. J. Lee, K. H. Ahn, *J. Org. Chem.* **2000**, *65*, 7807-7813.
- [170] M. Marinova, M. Torres-Werlé, G. Taupier, A. Maise-François, T. Achard, A. Boeglin, K. D. H. Dorkenoo, S. Bellemin-Laponnaz, *ACS Omega* **2019**, *4*, 2676-2683.
- [171] K. Takeuchi, M.-Y. Chen, H.-Y. Yuan, H. Koizumi, K. Matsumoto, N. Fukaya, Y.-K. Choe, S. Shigeyasu, S. Matsumoto, S. Hamura, J.-C. Choi, *Chem. Eur. J.* **2021**, *27*, 18066-18073.
- [172] X. Yang, Y. Zhang, D. Ma, *Adv. Synth. Catal.* **2012**, *354*, 2443-2446.
- [173] J. Helberg, T. Ampßler, H. Zipse, *J. Org. Chem.* **2020**, *85*, 5390-5402.
- [174] S. V. Kumar, D. Ma, *J. Org. Chem.* **2018**, *83*, 2706-2713.
- [175] B. Zhang, W. Deng, Z.-Y. Xu, *Organometallics* **2023**, *42*, 588-596.
- [176] S. Roy, K. K. Majumdar, *Synth. Commun.* **1994**, *24*, 333-340.
- [177] C. Ghiazza, L. Wagner, S. Fernández, M. Leutzsch, J. Cornella, *Angew. Chem. Int. Ed.* **2023**, *62*, e202212219.
- [178] M. S. de Castro, P. Domínguez, J. V. Sinisterra, *Tetrahedron* **2000**, *56*, 1387-1391.
- [179] I. M. Ogbu, J. Lusseau, G. Kurtay, F. Robert, Y. Landais, *Chem. Commun.* **2020**, *56*, 12226-12229.
- [180] V. Gómez-Parra, F. Sánchez, T. Torres, *Synthesis (Stuttgart)* **1985**, 282-285.
- [181] J. V. Matlock, S. P. Fritz, S. A. Harrison, D. M. Coe, E. M. McGarrigle, V. K. Aggarwal, *J. Org. Chem.* **2014**, *79*, 10226-10239.
- [182] V. B. Saptal, B. M. Bhanage, *ChemSusChem* **2016**, *9*, 1980-1985.
- [183] Z.-Z. Yang, Y.-N. Li, Y.-Y. Wei, L.-N. He, *Green Chem.* **2011**, *13*, 2351-2353.
- [184] Y. Shi, B. Tang, X.-L. Jiang, Y.-E. Jiao, H. Xu, B. Zhao, *J. Mater. Chem. A* **2022**, *10*, 4889-4894.
- [185] R. A. Watile, D. B. Bagal, Y. P. Patil, B. M. Bhanage, *Tetrahedron Lett.* **2011**, *52*, 6383-6387.
- [186] S. Ho, G. Bondarenko, D. Rosa, B. Dragisic, A. Orellana, *J. Org. Chem.* **2012**, *77*, 2008-2012.

- [187] M. Haumann, K. Dentler, J. Joni, A. Riisager, P. Wasserscheid, *Adv. Synth. Catal.* **2007**, 349, 425-431.
- [188] B. Urbán, M. Papp, D. Srankó, R. Skoda-Földes, *J. Mol. Catal. A Chem.* **2015**, 397, 150-157.
- [189] C. Jiménez-Rodríguez, A. A. Núñez-Magro, T. Seidensticker, G. R. Eastham, M. R. L. Furst, D. J. Cole-Hamilton, *Catal. Sci. Technol.* **2014**, 4, 2332-2339.
- [190] A. Fusano, S. Sumino, S. Nishitani, T. Inouye, K. Morimoto, T. Fukuyama, I. Ryu, *Chem. Eur. J.* **2012**, 18, 9415-9422.
- [191] P. Losch, A.-S. Felten, P. Pale, *Adv. Synth. Catal.* **2015**, 357, 2931-2938.
- [192] V. V. Gaikwad, B. M. Bhanage, *Appl. Organomet. Chem.* **2019**, 33, e4741.
- [193] X. Pu, J. Hu, Y. Zhao, Z. Shi, *ACS Catal.* **2016**, 6, 6692-6698.
- [194] H. Mei, S. Xiao, T. Zhu, Y. Lei, G. Li, *Trans. Met. Chem.* **2014**, 39, 443-450.
- [195] R. S. Reddy, J. N. Rosa, L. F. Veiros, S. Caddick, P. M. P. Gois, *Org. Biomol. Chem.* **2011**, 9, 3126-3129.
- [196] C.-T. Chen, Y. S. Munot, *J. Org. Chem.* **2005**, 70, 8625-8627.
- [197] G. Wang, Q.-Y. Yu, J. Wang, S. Wang, S.-Y. Chen, X.-Q. Yu, *RSC Adv.* **2013**, 3, 21306-21310.
- [198] J. Dussart-Gautheret, J. Deschamp, M. Monteil, O. Gager, T. Legigan, E. Migianu-Griffoni, M. Lecouvey, *J. Org. Chem.* **2020**, 85, 14559-14569.
- [199] G. Li, M. Arisawa, M. Yamaguchi, *Asian J. Org. Chem.* **2013**, 2, 983-988.
- [200] A. S. Levashov, D. S. Buryi, V. V. Konshin, V. V. Dotsenko, N. A. Aksenov, I. V. Aksenova, *Russ. J. Gen. Chem.* **2017**, 87, 1627-1630.
- [201] S. Karabiyikoglu, Y. Kelgokmen, M. Zora, *Tetrahedron* **2015**, 71, 4324-4333.
- [202] C. Bai, S. Jian, X. Yao, Y. Li, *Catal. Sci. Technol.* **2014**, 4, 3261-3267.
- [203] R. S. Mane, T. Sasaki, B. M. Bhanage, *RSC Adv.* **2015**, 5, 94776-94785.
- [204] Q. Hu, L. Wang, C. Wang, Y. Wu, Z. Ding, R. Yuan, *RSC Adv.* **2017**, 7, 37200-37207.